OBSERVATIONAL ASSESSMENTS OF GLACIER MASS CHANGES AT REGIONAL AND GLOBAL LEVEL

EDITED BY: Michael Zemp, Matthias Holger Braun, Fanny Brun and Laura Thomson
PUBLISHED IN: Frontiers in Earth Science

frontiers Research Topics

frontiers

ISSN 1664-8714
ISBN 978-2-88966-579-2
DOI 10.3389/978-2-88966-579-2

About Frontiers

Frontiers is more than just an open-access publisher of scholarly articles: it is a pioneering approach to the world of academia, radically improving the way scholarly research is managed. The grand vision of Frontiers is a world where all people have an equal opportunity to seek, share and generate knowledge. Frontiers provides immediate and permanent online open access to all its publications, but this alone is not enough to realize our grand goals.

Frontiers Journal Series

The Frontiers Journal Series is a multi-tier and interdisciplinary set of open-access, online journals, promising a paradigm shift from the current review, selection and dissemination processes in academic publishing. All Frontiers journals are driven by researchers for researchers; therefore, they constitute a service to the scholarly community. At the same time, the Frontiers Journal Series operates on a revolutionary invention, the tiered publishing system, initially addressing specific communities of scholars, and gradually climbing up to broader public understanding, thus serving the interests of the lay society, too.

Dedication to Quality

Each Frontiers article is a landmark of the highest quality, thanks to genuinely collaborative interactions between authors and review editors, who include some of the world's best academicians. Research must be certified by peers before entering a stream of knowledge that may eventually reach the public - and shape society; therefore, Frontiers only applies the most rigorous and unbiased reviews.
Frontiers revolutionizes research publishing by freely delivering the most outstanding research, evaluated with no bias from both the academic and social point of view. By applying the most advanced information technologies, Frontiers is catapulting scholarly publishing into a new generation.

What are Frontiers Research Topics?

Frontiers Research Topics are very popular trademarks of the Frontiers Journals Series: they are collections of at least ten articles, all centered on a particular subject. With their unique mix of varied contributions from Original Research to Review Articles, Frontiers Research Topics unify the most influential researchers, the latest key findings and historical advances in a hot research area! Find out more on how to host your own Frontiers Research Topic or contribute to one as an author by contacting the Frontiers Editorial Office: frontiersin.org/about/contact

OBSERVATIONAL ASSESSMENTS OF GLACIER MASS CHANGES AT REGIONAL AND GLOBAL LEVEL

Topic Editors:
Michael Zemp, University of Zurich, Switzerland
Matthias Holger Braun, University of Erlangen Nuremberg, Germany
Fanny Brun, Université Grenoble Alpes, France
Laura Thomson, Queen's University, Canada

Citation: Zemp, M., Braun, M. H., Brun, F., Thomson, L., eds. (2021). Observational Assessments of Glacier Mass Changes at Regional and Global Level. Lausanne: Frontiers Media SA. doi: 10.3389/978-2-88966-579-2

Table of Contents

frontiers in Earth Science

EDITORIAL
published: 01 February 2021
doi: 10.3389/feart.2020.641710

Editorial: Observational Assessments of Glacier Mass Changes at Regional and Global Level

Laura Thomson[1]*, *Fanny Brun*[2], *Matthias Braun*[3] and *Michael Zemp*[4]

[1]Department of Geography and Planning, Queen's University, Kingston, ON, Canada, [2]Department of Physical Geography, Université Grenoble Alpes, Saint Martin d'Hères, France, [3]Department of Geography and Geosciences, Friedrich-Alexander-University of Erlangen-Nuremberg, Erlangen, Germany, [4]Department of Geography, University of Zurich, Zurich, Switzerland

Keywords: glaciers, mass change, climate change, cryosphere, sea-level rise

Editorial on the Research Topic

Observational Assessments of Glacier Mass Changes at Regional and Global Level.

Glaciers represent a measurable indicator of the spatial and temporal patterns of global climate variability. Those distinct from the Greenland and Antarctic Ice Sheets cover an area of approximately 706,000 km^2 globally (RGI Consortium, 2017), with an estimated total volume of $170 \pm 21 \times 10^3$ km^3, or 0.43 ± 0.06 m of potential sea-level rise equivalent (Huss and Farinotti, 2012). Retreating and thinning glaciers are icons of climate change and affect the local hazard scenario, regional water resources and glacier runoff as well as changes in global sea level.

Techniques for measuring and monitoring changes to glaciers over the last century have expanded from *in situ* point measurements of snow accumulation and ice ablation to large regional- and global-scale surveys employing remote sensing and modeling approaches, which have shaped our understanding of world-wide glacier changes. Today, the Gravity Recovery and Climate Experiment (GRACE) mission can be used to derive monthly regional mass changes (Wouters et al.) and has proven to be particularly effective in detecting glacier mass changes over regions with extensive ice cover (Alaska, Canadian Arctic, Russian Arctic, Svalbard, Iceland, the Southern Andes, and High Mountain Asia). However, Wouters et al. note that GRACE cannot resolve the signal from peripheral glaciers of the Greenland and Antarctic ice sheets and struggles to detect statistically significant signals in mountain ranges with smaller glacier covers due to weaker signals and relatively greater background noise and uncertainty.

Increasingly, geodetic mass-balance records are filling the spatial-scale gap between coarse-resolution gravimetry and point-based glaciological mass-balance records. Advances in digital elevation model creation, automation, and analysis from historic and contemporary sources are driving a notable increase in the availability of geodetic mass-balance records from around the world. Indeed, original works within this Research Topic alone represent 9,908 new geodetic mass balance contributions to the World Glacier Monitoring Service (WGMS) and the IPCC AR6, notably from regions of Greenland (Huber et al.), the European Alps (Davaze et al.), Iceland (Belart et al.), Northern Tien Shan (Kapitsa et al.) and the Patagonian Andes (Falashi et al.), as well as ~8,000 updated geodetic records from the Central Andes (Ferri et al.). Advances in digital photogrammetry and improved accuracies in the 3D alignment of elevation models have rekindled the scientific value inherent to historical maps, aerial photography and declassified spy satellite imagery as exemplified by Falashi et al., Huber et al., Belart et al., and Kapitsa et al. These advances extend the temporal reach

OPEN ACCESS

Edited and reviewed by:
Michael Lehning,
École Polytechnique Fédérale de Lausanne, Switzerland

***Correspondence:**
Laura Thomson
L.Thomson@queensu.ca

Specialty section:
This article was submitted to Cryospheric Sciences, a section of the journal Frontiers in Earth Science

Received: *14 December 2020*
Accepted: *23 December 2020*
Published: *01 February 2021*

Citation:
Thomson L, Brun F, Braun M and Zemp M (2021) Editorial: Observational Assessments of Glacier Mass Changes at Regional and Global Level. Front. Earth Sci. 8:641710. doi: 10.3389/feart.2020.641710

of geodetic mass-balance estimates, offering new life to early imagery and resulting in notably reduced uncertainties in geodetic mass-balance estimates. However, issues persist in high-elevation, snow-covered regions where low contrast between images results in data voids, leading researchers to devise strategies for void-filling (Huber et al., McNabb et al., 2019; Seehaus et al., 2020).

The global collection of glaciological (*in situ*) mass-balance records available through WGMS and national monitoring programs provide important cross-validation for gravimetry (Wouters et al.) and geodetic mass-balance methods (Kapitsa et al., Davaze et al., Schuler et al.). Furthermore, these glaciological mass-balance records capture interannual and seasonal mass balance amplitudes and expand our understanding of the regional climatologies (Braithewaite and Hughes) and glacier morphologies (Davaze et al.) responsible for the global and regional variability in glacier response.

While the collection of glaciological mass-balance measurements can be logistically demanding, new potential exists for continuous, remote monitoring of surface mass-balance components (accumulation and ablation) given advances in automated field instrumentation and data telemetry. This was demonstrated over a 10-year period (2009–2019) by Fausto et al. using a pressure transducer assembly complemented by sonic ranging systems as part of the Program for Monitoring of the Greenland ice sheet (PROMICE). In the time of COVID-19 and restrictions on field-related travel, the automated measurement and remote-delivery of mass balance measurements and related climate variables is likely to become increasingly popular.

Creative approaches that bring together the more abundant geodetic mass-balance estimates, spanning multiple years, and the relatively small sample of glaciological mass-balance records, providing interannual variability, has also enabled the modeling of annual mass balances for glaciers lacking field observations (e.g. Belart et al.). It was demonstrated by Davaze et al. that annual snowline altitudes in combination with multi-year geodetic records may alternatively provide the annual temporal variability signal required for the estimation of annual mass balances of unmonitored glaciers in the Alps. Aðalgeirsdóttir et al. revealed that the combination of multiple data sources can even support the estimation of mass-balance conditions dating back to the Little Ice Age (estimated as ~1890 for Iceland).

Despite these advances, challenges remain regarding the estimation of glacier mass changes. While glaciological mass balances remain an invaluable indicator of temporal variability and important ground-validation for remote sensing and modeling techniques, several studies acknowledge the need for caution using these records. For instance, a slight negative bias has been found to be associated with glaciological records that may be attributed to the relatively shallower slopes of monitored glaciers (Davaze et al.), or due to bias in stake distribution across elevations (Kapitsa et al.). Schuler et al. also highlight the need to extend glaciological mass-balance efforts into under-sampled, often logistically challenging areas to reduce regional biases. In high-latitude and highly glacierized regions, the greater potential for surge dynamics, calving, as well as internal accumulation by melt and refreezing in cold accumulation zones adds uncertainty to mass balance estimates (Schuler et al.). In low-latitude and arid regions, challenges associated with the monitoring of debris-covered ice and rock glaciers persist (Ferri et al.), however the consideration and inclusion of these features in glacier inventories have proven to be particularly valuable in drought-susceptible regions where ice-rock complexes serve as important water resources (Schaffer et al., 2019).

Independent of technique, the original works presented in this Research Topic indicate mass loss to be the dominant signal observed from glaciers distinct from the ice sheets through the 19th, 20th and early twenty-first centuries. Ice mass changes detected by GRACE over regions with extensive ice coverage confirm widespread losses but cannot detect an acceleration in these losses over the period of record (2002–2016; Wouters et al.). Geodetic mass-balance surveys spanning multiple epochs, including the pre-satellite era, generally demonstrate greater thinning rates toward the end of the 20th century (Falaschi et al., Davaze et al., Aðalgeirsdóttir et al., Braithwaite and Hughes, Schuler et al.), with the exception of northern Tien Shan where very little difference in change rates was observed between 1958–1998 and 1998–2016 periods (Kapitsa et al.). Interestingly, in some instances these studies note a slight decline in thinning rates since ~2010, including in regions of the Patagonian Andes (Falaschi et al.) and Iceland (Belart et al.). The large variability observed in the seasonal and annual mass-balance signal (Braithwaite and Hughes; Wouters et al.) highlights the need for persistent efforts at all scales of glacier monitoring and continued "openness and generosity with hard-won data" within the glaciological community (Braithwaite and Hughes).

AUTHOR CONTRIBUTIONS

The editorial was drafted by LT, with contributions from MZ, MB, and FB. The scope and contents of the editorial were discussed among all authors.

ACKNOWLEDGMENTS

The present Research Topic is a contribution to the working group on Regional Assessments of Glacier Mass Change (RAGMAC) of the International Association of Cryospheric Sciences (IACS; https://cryosphericsciences.org/activities/wg-ragmac/). It was enabled by support from the Federal Office of Meteorology and Climatology MeteoSwiss within the framework of the Global Climate Observing System (GCOS) Switzerland for MZ.

REFERENCES

Huss, M., and Farinotti, D. (2012). Distributed ice thickness and volume of all glaciers around the globe. *J. Geophys. Res.* 117, F04010. doi:10.1029/2012JF002523

McNabb, R., Nuth, C., Kääb, A., and Girod, L. (2019). Sensitivity of glacier volume change estimation to DEM void interpolation. *Cryosphere* 13, 895–910. doi:10.5194/tc-13-895-2019

RGI Consortium (2017). Randolph glacier inventory (v.6.0). A dataset of global glacier outlines. Global land ice measurements from space. doi:10.7265/N5-RGI-60

Schaffer, N., MacDonell, S., Réveillet, M., Yáñez, E., and Valois, R. (2019). Rock glaciers as a water resource in a changing climate in the semiarid Chilean Andes. *Reg. Environ. Change* 19, 1263. doi:10.1007/s10113-018-01459-3

Seehaus, T., Morgenshtern, V. I., Hübner, F., Bänsch, E., and Braun, M. H. (2020). Novel techniques for void filling in glacier elevation change data sets. *Rem. Sens.* 12, 3917. doi:10.3390/rs12233917

Conflict of Interest: The authors declare that the research was conducted in the absence of any commercial or financial relationships that could be construed as a potential conflict of interest.

frontiers in Earth Science

ORIGINAL RESEARCH
published: 21 May 2019
doi: 10.3389/feart.2019.00096

Global Glacier Mass Loss During the GRACE Satellite Mission (2002-2016)

Bert Wouters[1,2]*, *Alex S. Gardner*[3] *and Geir Moholdt*[4]

[1] Department of Physics, Institute for Marine and Atmospheric Research, Utrecht University, Utrecht, Netherlands, [2] Faculty of Civil Engineering and Geosciences, Delft University of Technology, Delft, Netherlands, [3] Jet Propulsion Laboratory, California Institute of Technology, Pasadena, CA, United States, [4] Norwegian Polar Institute, Fram Centre, Tromsø, Norway

Glaciers outside of the ice sheets are known to be important contributors to sea level rise. In this work, we provide an overview of changes in the mass of the world's glaciers, excluding those in Greenland and Antarctica, between 2002 and 2016, based on satellite gravimetry observations of the Gravity Recovery and Climate Experiment (GRACE). Glaciers lost mass at a rate of 199 ± 32 Gt yr^{-1} during this 14-yr period, equivalent to a cumulative sea level contribution of 8 mm. We present annual mass balances for 17 glacier regions, that show a qualitatively good agreement with published estimates from *in situ* observations. We find that annual mass balance varies considerably from year to year, which can in part be attributed to changes in the large-scale circulation of the atmosphere. These variations, combined with the relatively short observational record, hamper the detection of acceleration of glacier mass loss. Our study highlights the need for continued observations of the Earth's glacierized regions.

Keywords: GRACE, glaciers, ice caps, sea level, mass balance

OPEN ACCESS

Edited by:
Matthias Holger Braun, University of Erlangen Nuremberg, Germany

Reviewed by:
Roelof Rietbroek, University of Bonn, Germany
Horst Machguth, Université de Fribourg, Switzerland

***Correspondence:**
Bert Wouters
b.wouters@uu.nl

Specialty section:
This article was submitted to Cryospheric Sciences, a section of the journal Frontiers in Earth Science

Received: *15 October 2018*
Accepted: *18 April 2019*
Published: *21 May 2019*

Citation:
Wouters B, Gardner AS and Moholdt G (2019) Global Glacier Mass Loss During the GRACE Satellite Mission (2002-2016). Front. Earth Sci. 7:96. doi: 10.3389/feart.2019.00096

1. INTRODUCTION

Compared to the much larger ice sheets, glaciers tend to be located in more temperate environments with a majority of their surface experiencing ablation each year. This makes glaciers particularly sensitive to changes in climate and one of the most visible indicators of global warming. Even though their total potential contribution to sea level rise of about 324 ± 8 mm (Farinotti et al., 2019) is orders of magnitude lower than that of the ice sheets of Greenland and Antarctica, they have been the single largest mass contributor to sea level rise in the twentieth century, responsible for 0.5–0.6 mm yr^{-1} (IPCC, 2013). Model predictions indicate that glaciers will continue to play an important role in the coming decades, with a projected mass loss equivalent to 5–17 cm sea level rise by the end of the century (Huss and Hock, 2015; Marzeion et al., 2018). The impact of rising sea levels is global, but shrinking of these frozen freshwater compounds will also have profound local societal and environmental effects. Disappearance and degradation of habitat, and changes in water supply, for example, may strongly affect local communities (Huss et al., 2017; Wester et al., 2019). The release of freshwater into the ocean may not only disturb marine ecosystems (Slemmons et al., 2013), but future accumulation of glacial freshwater in key areas of deep convection also has the potential to interfere with the thermohaline circulation (Yang et al., 2016; Bamber et al., 2018).

Before the advent of satellite gravimetry and altimetry, estimates of global glacier mass change were based on analysis of non-continuous direct and geodetic mass-balance measurements of a few hundred glaciers. Most of these glaciers are small and located in maritime climate regions, with an uneven distribution between different types of glaciers. This, together with the fragmented records of *in-situ* mass balance, called for extrapolation of the data, with results varying between studies,

depending on the statistical approach used. Kaser et al. (2006) reported an increase in glacier mass loss from 137 ± 68 Gt yr^{-1} for 1961–1990 to 353 ± 68 Gt yr^{-1} for 2001–2004, whereas Meier et al. (2007) estimated a 2006 mass loss of 402±95 Gt yr^{-1}. Both these estimates were significantly lower than the 508 ± 72 Gt yr^{-1} mass loss for 2001–2005 put forward in Cogley (2009). It should be noted that all these estimates included mass losses from the peripheral glaciers to the Antarctic and Greenland ice sheets that are not included in this study.

Satellite platforms provide near-complete coverage at regular intervals of the Earth's cryosphere, which led to a leap forward in our understanding of the state of the cryosphere. Using GRACE observations, Jacob et al. (2012) estimated the mass loss of 148 ± 30 Gt yr^{-1} for 2003–2010, excluding the peripheral glaciers on Antarctica and Greenland. Combining GRACE, altimetry and *in situ* measurements, Gardner et al. (2013) showed that glaciers lost 215 ± 26 Gt yr^{-1} between 2003 and 2009, with the peripheral glaciers adding another 44 ± 12 Gt yr^{-1}. This is about three times the contribution of the Antarctic ice sheet during that period, and similar to that of the Greenland Ice Sheet (Shepherd et al., 2012). Furthermore, subsampling the altimetry data in the regions around the locations of the *in situ* data used in Cogley (2009) showed that the local mass balance measurements are generally more negative than the regional mean, implying that *in situ* based estimates of regional glacier loss are likely biased too negative. Using a least-squares inversion based on sea-level fingerprints of regional mass anomalies, Rietbroek et al. (2016) reported an mean annual glacier mass deficit of 141 ± 26 Gt yr^{-1} for 2002-2014, but this estimate did not include some key contributors such as the southern part of the Canadian Arctic. Schrama et al. (2014), estimated a mass loss of 162 ± 10 Gt yr^{-1} between 2003 and 2013, based on GRACE observations, and Reager et al. (2016) estimated a mass loss of 253 Gt yr^{-1} for the period 2002–2014 using an updated methodology to Gardner et al. (2013). In all these studies, ice loss was particularly pronounced in the North Atlantic Arctic region but also in Alaska and more temperate, mid-latitude regions such as the High Mountain Asia and the Patagonian ice fields.

Motivated by completion of the GRACE mission in 2017, and recent improvements of the data quality, we present an update of the status of the world's glaciers. In contrast to earlier studies, we provide estimates of annual mass balances for all regions defined in the Randolph Glacier Inventory (RGI; RGI Consortium, 2017)-except for the peripheral glaciers of Greenland and Antarctica, which are too closely positioned to the ice sheet to be isolated by the ∼350 km horizontal resolution of GRACE.

2. DATA AND METHODS

Our analysis is based on monthly GRACE Stokes coefficients from the latest releases, from three different processing centers: CSR RL06 from the Center for Space Research (Bettadpur, 2018), JPL RL06 from the Jet Propulsion Laboratory (Yuan, 2018) and ITSG-Grace2018 from TU Graz Mayer-Gürr et al. (2018). These solutions use updated parameters and processing algorithms, and improved models to estimate background gravity signals, such as high-frequency ocean and atmosphere mass fluctuations. Compared to earlier releases, noise in the time series is reduced by 20–50%, with the highest reduction at lower latitudes, where groundtrack separation between passes is generally larger. Although the GRACE satellites were in operation until mid-2017, we only use data spanning April 2002 to August 2016. Stokes coefficients from later months are heavily affected by the loss of the accelerometer on the GRACE-B satellite in October 2016 and are too noisy to retrieve mass changes at scales typical for the glacier regions considered in this study (PO.DAAC, 2018). We use coefficients up to degree and order 60, and apply the common post-corrections to the Level-2 data: inclusion of the degree-1 coefficients—which are not observed by the twin satellites—using the estimates of Swenson et al. (2008); and replacement of the poorly constrained C_{20} coefficients by values obtained from satellite laser ranging (Cheng et al., 2013). Furthermore, we remove correlated noise in the GRACE data using an adaptation of the method of Wouters and Schrama (2007): we first fit a 3rd order polynomial to the monthly time series of all Stokes coefficients, for each degree and order individually, to preserve the long-term variability. Next, we apply an empirical orthogonal function decomposition to the residuals, and filter out noise by rejecting the modes that cannot be distinguished from a white-noise process with 95% confidence. We then restore the long-term variability using the fitted polynomial function from the first step, and apply a 150 km Gaussian smoothing to the resulting Stokes coefficients to reduce remaining noise. These coefficients are then converted to maps of equivalent water height anomalies, following (Wahr et al., 1998).

To retrieve the mass changes in the 17 RGI regions considered in this study, we define global 0.5°×0.5° grid of mass concentrations ("mascons"), as in Gardner et al. (2013). These mascons are initially given a loading of one in cells where RGI 6.0 indicates a glacierized area of 100 km^2 or more, and zero elsewhere (**Figure 1**). The resulting map is then converted to synthetic GRACE observations, by applying the same degree/order cut-off in the spherical domain and applying the same Gaussian smoothing. The mascon loadings within each of the RGI subregions are adjusted in an iterative process, first in coarse steps of ±100 Gt, until the spatial root-mean-square difference with the actual GRACE observations is minimized. Next, the step size is reduced and the iteration is re-initiated, and this process is repeated until changes in all basins are smaller than 0.1 Gt. A detailed description of the method can be found in Wouters et al. (2008) and Wouters (2010). The 100 km^2 limit for the mascons is based on a trade-off between completeness and an acceptable range of uncertainty of the estimates; in cells with a smaller glacier coverage, the GRACE signal will be dominated by (non-ice) hydrological signals, which needs to be corrected for, as we will discuss later. Globally, the mascons cover approximately 90% of the total glacier area in RGI 6.0. As in Jacob et al. (2012) and Gardner et al. (2013), we also include mascons in Greenland and Antarctica, to remove signals from these ice sheets, and in the plains of the Indian subcontinent, where signals from extensive groundwater extraction may otherwise contaminate our glacier mass change

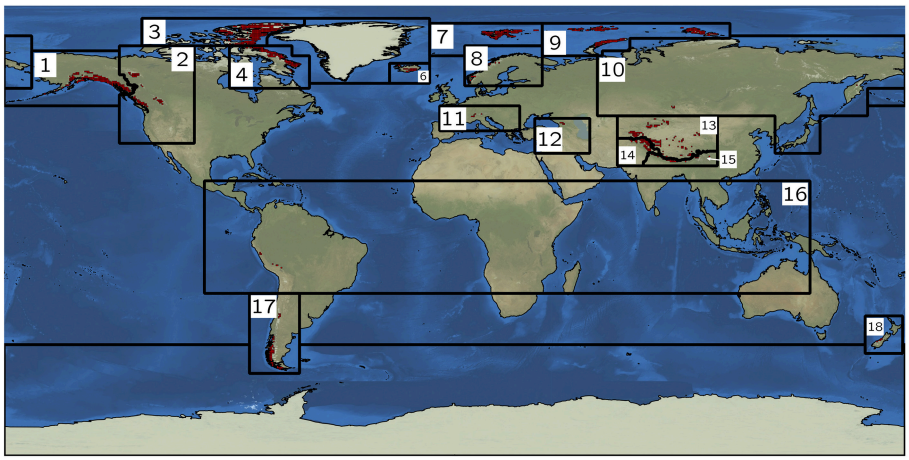

FIGURE 1 | Outlines of the RGI 6.0 regions, and location of the mascons used to retrieve the glacier mass loss from the GRACE data. Region names: 1: Alaska, 2: Western Canada and US, 3: Arctic Canada North, 4: Arctic Canada South, 6: Iceland, 7: Svalbard, 8: Scandinavia, 9: Russian Arctic, 10: North Asia, 11: Central Europe, 12: Caucasus and Middle East, 13: Central Asia, 14: South Asia West, 15: South Asia East, 16: Low Latitudes, 17: Southern Andes, 18: New Zealand.

estimates in the neighboring High Mountain Asia region (RGI regions 13–15).

We derive three time series of mass change for each RGI region, one for each processing center. Each of these processing centers uses a slightly different approach and/or background models to estimate the Stokes coefficients, and it has been shown that using the ensemble mean of the solutions suppresses noise in the time series (Sasgen et al., 2007; Sakumura et al., 2014). We use the weighted mean of the three solutions, with the monthly uncertainties in the individual time series as weights. These uncertainties are based on the reported calibrated errors, propagated for each region and scaled in such a way that the mean of the monthly uncertainties for the mid-mission period (mid 2003–mid 2015) matches the noise level estimated using the empirical approach of Wahr et al. (2006). In this approach, the time series are high-pass filtered with a cut-off period of 4 months and the standard deviation of the remaining signal is considered to represent a more realistic, yet conservative estimate of the noise level. In contrast to Sasgen et al. (2007) and Sakumura et al. (2014), we do not use the mean of the CSR, JPL, and ITSG time series, as this may introduce spurious jumps in months where data is missing in one or more of the solutions. Instead, we first compute the time derivative of the mass anomalies—i.e., the difference between successive months—and then apply the weighted-averaging. The combined time series is then obtained from the running sum of the resulting weighted mass changes, as shown in **Figure 2** . Typically, noise in the time series (computed following the method of Wahr et al., 2006 discussed earlier) is 10–20% lower than the best individual solution. Depending on the region, the CSR, ITSG, and JPL solutions contribute 40–65, 15–45, and 10–30%, respectively, to the combination. Monthly errors of the combined time series are based on the weighted-average root-square sum of the errors in the individual time series, scaled to match the empirical mid-mission noise level.

GRACE observes the integral mass change on and beneath the Earth's surface. Therefore, a number of corrections need to be applied to the data in order to isolate the glacier change signal. To account for glacial isostatic adjustment (GIA), the mass displacement in the Earth's interior in response to changes in ice mass loading since the Last Glacial Maximum, we use the model of Caron et al. (2018). This model combines vertical land rates from Global Navigation Satellite System stations and relative sea level curves in a Bayesian framework to estimate the geoid changes induced by GIA, together with an associated standard error. In the Russian Arctic (RGI region 09), we use the model of Root et al. (2015), which was specifically tailored for this region. To account for mass displacement in response to load changes since the Little Ice Age (LIA), which are not included in these GIA models, we use the LIA models of Larsen et al. (2005) for Alaska (RGI region 01), Jacob et al. (2012) High Mountain Asia (RGI region 13–15), and Ivins and James (2004) for the Southern Andes (RGI region 17). For Iceland (RGI region 06), we use the recent model of Sørensen et al. (2017). We note that our LIA correction is smaller than that reported in their study (3 vs. 5.5 Gt yr^{-1}), due to the different method to retrieve the mass changes from the GRACE data. Uncertainties for the GIA correction are based on the standard errors derived from the probability density function reported in Caron et al. (2018), an ensemble of GIA solutions with varying ice loading history for the Russian Arctic (Root et al., 2015), and varying ice loading history and earth structure models for Iceland (Sørensen et al., 2017).

To correct for hydrological signals in the GRACE observations—that can be significant at mid- and low-latitudes—we subtract monthly mass changes derived from the Global Land Data Assimilation System Version 2.1 (GLDAS V2.1; Rodell et al., 2004; Beaudoing and Rodell, 2016) from the time series. Forced with model and observation-based data sets of atmospheric circulation, precipitation and short- and longwave radiation, GLDAS V2.1 simulates land surface parameters and

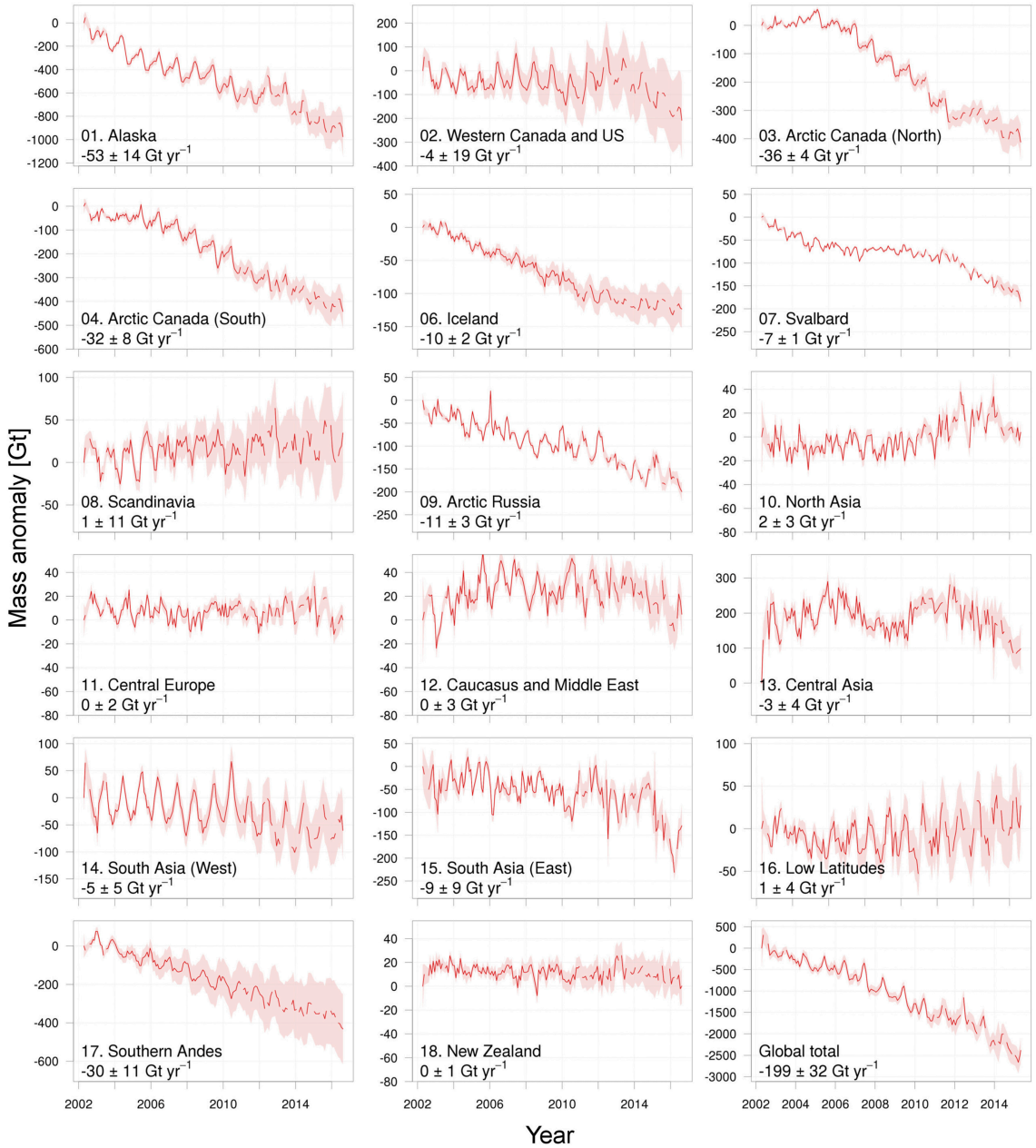

FIGURE 2 | Time series of cumulative mass anomalies for all RGI regions, except for the peripherial glaciers of Greenland and Antarctica, which cannot be resolved by GRACE. Note the difference in range on the y-axis between the different subfigures. Uncertainties grow in time due to the cumulative effect of uncertainties in the GIA correction.

fluxes at a 0.25 degree resolution from 2000 to present. Since the model shows unrealistically large variations in glacierized regions, we mask out grid points that are classified as ice in the native resolution of the models. Scanlon et al. (2018) demonstrated that long-term changes in land-storage vary considerably between different models, therefore, we include a second model to estimate the uncertainty in the hydrological correction. The PCRaster Global Water Balance 2 model (PCR-GLOBW 2; Sutanudjaja et al., 2018) provides changes in the water column at a resolution of 5 arcmin resolution and includes the effects of anthropogenic impacts, such as groundwater and surface water withdrawal, which is not included in GDLAS V2.1. PCR-GLOBW 2 data is currently available to December 2015. The uncertainty in the hydrological correction is taken as the difference between the models.

Hydrological models like GLDAS and PCR-GLOBW do not consider changes in water storage of hydropower reservoirs which are often located nearby glacierized areas. As an example

of the potential impact of this on regional GRACE signals, we estimate a time series of mass anomalies for all hydropower reservoirs in Norway based on water level statistics published by the Norwegian Water Resources and Energy Directorate (http://vannmagasinfylling.nve.no, accessed 1 March 2019). The statistics are provided as weekly percentages of total storage capacity which we estimate to 71 Gt based on upscaling of known storage volumes for 85% of the total reservoir area. The resulting reservoir mass anomalies are shown in **Figure S2** together with the GRACE signal for Scandinavia (RGI region 08).

High-frequency ocean mass signals are removed using ocean circulation models by the processing centers to avoid aliasing of these signals into the monthly Stokes coefficients. To assess the impact of this correction, we added back the removed signal and recomputed the time series. Differences are small in all regions, except for the Russian Arctic, where the model correction induces a long-term trend of –1.8 Gt yr^{-1}. This is most likely related to unphysical model drift in shallow ocean regions (personal communication H. Dobslaw). Therefore, we add back the model correction, and include 50% of this correction in the uncertainties.

To estimate the long-term mass balance of each region we apply an error-weighted least square fit to the time series. We simultaneously fit a constant, a linear trend and seasonal and semi-seasonal harmonics. We do not attempt to estimate accelerations in the time series as the results are highly affected by interannual variability. For example, in Arctic Canada North (RGI region 03), an acceleration of –9 Gt yr^{-2} is found for the period April 2002–December 2012. Extending the record to include the years between 2013 and 2016 reduces the estimate of acceleration to –2 Gt yr^{-2}, highlighting the sensitivity of the acceleration estimates to the chosen period. Trends for the full period from April 2002 to August 2016 are given in **Table 1**. Values for the 2006–2015 balance years (defined as October 2005 to September 2015 for regions in the Northern Hemisphere, and April 2005 to March 2015 for those in the Southern Hemisphere, are given in **Table S1**). The 2-sigma uncertainties account for the formal error of the fit, including propagation of the monthly errors, the uncertainties in the GIA, LIA, hydrology and ocean correction, and the exclusion of glacier areas smaller than 100 km^2, by scaling the estimated trends by the ratio of the total area reported in RGI 6.0 and the mascon area.

To assess the impact of the processing methodology on the results, we compare our trends to independent results based on JPL mascons (JPL RL06Mv1; Watkins et al., 2015). In this approach, mass variations are estimated directly from the Level-1 GRACE data, in 4551 equal-area 3° spherical caps, distributed evenly over the Earth's surface. Because a-priori information, for example from geophysical models, can be easily incorporated in the inversion process, the JPL mascon solutions suffer less from the typical North-South striping observed in spherical harmonics solutions. Furthermore, a Coastline Resolution Improvement (CRI) filter is applied to the data, to reduce leakage from land signals into the ocean caused by the limited spatial resolution of GRACE. Trends were derived using the approach described in Reager et al. (2016) and are shown in **Table S2**.

Annual mass balances are computed as the difference between the mass anomalies for October 1 and September 30 of the previous year, for regions in the Northern Hemisphere. For example, for mass balance year 2005 we take the difference of October 1 2005 and September 30 2004, where the day values are obtained through spline interpolation of the monthly time series. For regions in the Southern Hemisphere (RGI regions 16-18: Low Latitudes, Southern Andes and New Zealand), we use April 1 and March 31. As can be seen in **Figure 2**, the GRACE time series contains gaps, especially in the later phase of the mission, when no data was collected during phases when the satellites were in eclipse, to lengthen the mission's lifetime. We fill these gaps using cubic spline interpolation on the time series, using the four data points left and right of the gaps (Grund, 1979). Such an interpolation introduces two types of errors: due to measurement noise in the available months, and due to the interpolation itself. To account for the first type of error, we repeated the spline interpolation 10 000 times, while adding random noise within one standard deviation of the estimated monthly noise level to the available data points. The standard deviation of the 10 000 realizations of the interpolated points is then taken as the one-sigma uncertainty for these months. The second uncertainty arises from the fact that the spline interpolation is a mathematical procedure which connects points without knowledge of the actual climatological conditions. For example, when interpolating a missing August month, it does not take into account that local temperatures, and hence melt rates, are generally higher than in September (in the Northern Hemisphere). We address this issue using the time series between July 2003 and December 2010, when no data outages occurred. We consecutively leave out 1 months, which we then fill using the spline interpolation, and compare the interpolated and observed value. The uncertainty of the second type is then computed as the median difference of all same months of the year (e.g., the uncertainty for a missing January month is based on the median difference of all January months between 2004 and 2010). We repeat these period leaving out 2 consecutive months, to determine the uncertainties for periods with a 2-month data outage. For climatological comparison between RGI regions, we divided the annual mass balances (in unit Gt yr^{-1}) by their regional glacier areas to provide specific mass balances (in unit $kg\,m^{-2}yr^{-1}$) as shown in **Figure 3** for the major RGI regions and in **Figure S1** for the smaller RGI regions.

We compare our GRACE-based annual mass balances to measurements made in the field, based on glaciological mass balance records in the World Glacier Monitoring Service database Zemp et al. (2015); WGMS (2017). Despite the potential sampling biases in these records—as discussed in the introduction—such a comparison may provide qualitative insight into the robustness of the interannual variability captured by our GRACE analysis. A correlation analysis between GRACE and *in-situ* annual mass balances was carried out in regions where at least three *in situ* records were available, covering the full period of 2003 to 2015. An exception was made for Svalbard, where in 2003 only measurements along the western coast of Spitsbergen were available. Here, we use data from 2004 to 2015 instead, to include data from Etonbreen glacier basin of the Austfonna ice cap. To

TABLE 1 | Average GRACE mass trends and corrections for April 2002-August 2016.

RGI region number and region	Area	Glacier mass budget		GRACE only	Solid earth correction		Hydrology correction	
					GIA	LIA	GLDASV2.1	PCR-GLOBW 2*
	[km^2]	[Gt yr^{-1}]	[kg m^{-2}yr^{-1}]	[Gt yr^{-1}]	[Gt yr^{-1}]	[Gt yr^{-1}]	[Gt yr^{-1}]	[Gt yr^{-1}]
01. Alaska	86725	−53.4 ± 13.8	−620 ± 160	−44.5 ± 9.6	1.8 ± 8.6	7 ± 4	0.1 ± 3.5	1.8 ± 2.8
02. Western Canada and US	14524	−4.2 ± 19	−290 ± 1310	2.3 ± 6.4	11.3 ± 16.6	0 ± 0	−4.9 ± 3.9	1.1 ± 3.6
03. Arctic Canada North	105111	−35.8 ± 3.5	−340 ± 30	−31.6 ± 2.1	4 ± 2.8	0 ± 0	0.2 ± 0.2	0.5 ± 0.2
04. Arctic Canada South	40888	−32.5 ± 7.8	−790 ± 190	−29.3 ± 5.3	4.1 ± 5.4	0 ± 0	−0.9 ± 0.4	0.9 ± 0.6
06. Iceland	11060	−10.1 ± 2	−920 ± 180	−6.9 ± 0.9	−0.1 ± 1	3.1 ± 1.5	0.3 ± 0.2	0.2 ± 0.2
07. Svalbard	33959	−7.2 ± 1.4	−210 ± 40	−4.9 ± 1.1	1.9 ± 0.6	0 ± 0	0.3 ± 0.1	0.9 ± 0.2
08. Scandinavia	2949	1.3 ± 11.4	450 ± 3880	7.2 ± 10.9	5.9 ± 3.4	0 ± 0	0 ± 1.2	0 ± 1.6
09. Arctic Russia	51592	−10.6 ± 1.7	−210 ± 30	−7.2 ± 2.7	3.1 ± 0.6	0 ± 0	0.2 ± 0.1	1.2 ± 0.2
09.1 Novaya Zemlya	22128	−5.3 ± 1.1	−240 ± 50	−3.8 ± 0.9	1.3 ± 0.4	0 ± 0	0.2 ± 0.1	0.7 ± 0.2
09.2 Severnya Zemlya	12762	−3 ± 0.9	−230 ± 70	−2.4 ± 0.8	0.5 ± 0.2	0 ± 0	0 ± 0	0.4 ± 0
09.3 Franz Josef Land	16701	−2.3 ± 1	−140 ± 60	−1 ± 0.9	1.3 ± 0.4	0 ± 0	0 ± 0	0.1 ± 0
10. North Asia	2410	1.8 ± 3.4	730 ± 1430	0.7 ± 3.4	−1.2 ± 0.2	0 ± 0	0.1 ± 0.5	0.3 ± 0.4
11. Central Europe	2092	−0.3 ± 1.6	−160 ± 750	−0.8 ± 1.5	−0.5 ± 0.2	0 ± 0	0 ± 0.4	−0.3 ± 0.4
12. Caucasus	1307	−0.1 ± 2.9	−110 ± 2190	−2.6 ± 2.5	−0.5 ± 0.2	0 ± 0	−1.9 ± 0.5	−0.7 ± 0.4
13. Central Asia	49303	−3.2 ± 4.5	−60 ± 90	0.6 ± 3.9	2.4 ± 0.8	1 ± 0.5	0.4 ± 1.8	−1.1 ± 1.2
14. South Asia West	33568	−5.3 ± 4.9	−160 ± 150	−3.2 ± 2.6	−0.2 ± 0.2	1 ± 0.5	1.3 ± 1.4	5.3 ± 1.4
15. South Asia East	14734	−9.2 ± 9.1	−630 ± 620	−10.9 ± 3.5	0.8 ± 5.4	1 ± 0.5	−3.5 ± 1.7	2.8 ± 1.2
13.+14.+15. HMA	97606	−17.7 ± 11.3	−180 ± 120	−13.5 ± 5.8	3.0 ± 5.5	3 ± 1	−1.9 ± 2.8	7 ± 2.2
16. Low Latitudes	2341	1.2 ± 3.5	510 ± 1510	0.7 ± 2.3	−0.4 ± 0.2	0 ± 0	−0.1 ± 1.2	−2.6 ± 1.4
17. Southern Andes	29429	−30.3 ± 11	−1030 ± 370	−21.8 ± 6.2	1.5 ± 0.8	9 ± 5	−2 ± 1	−9.5 ± 1.2
18. New Zealand	1162	−0.5 ± 0.9	−420 ± 800	−0.6 ± 0.5	0.4 ± 0.2	0 ± 0	−0.6 ± 0.1	−1.3 ± 0.4
Global Total	483153	−198.5 ± 32.4	−410 ± 70	−152.8 ± 19.7	34.3 ± 20.9	22.1 ± 6.7	−11.0 ± 6.4	−0.5 ± 5.7

The "GRACE only" numbers refer to the regional mass trends as observed as observed by GRACE. Correcting for mass transport in the solid earth (GIA and LIA), and due to land hydrology, isolates the glacier mass trends. The latter are given as region totals (in Gt yr^{-1}) and per area unit (specific mass balance, in kg m^{-2}yr^{-1}). For the hydrology correction, the GLDAS V2.1 model (Rodell et al., 2004; Beaudoing and Rodell, 2016) is used, PCR-GLOBW 2 (Sutanudjaja et al., 2018) results are included to estimate the uncertainty in this correction.
∗: available to December 2015.

avoid biases due to geographical oversampling, we first average records located within 50 km of each other, and then calculate the regional mass balances by averaging all available records.

To further interpret the GRACE annual mass balances, we correlate the results to a number of climate indices: the Artic Oscillation (AO), the North Atlantic Oscillation (NAO), the Pacific Decadal Oscillation (PDO), NINO 1+2, 3, 3.4, and 4, and the Southern Oscillation index (SOI). All indices were obtained through climexp.knmi.nl. Correlation was performed using 4-month averages of the indices, at various lags ranging from October-January to June-September.

3. RESULTS AND DISCUSSION

Collectively, the 17 RGI regions show an overall mass loss of 199 ± 32 Gt yr^{-1} during the period April 2002–August 2016. Our spherical harmonics solution is consistent with the JPL mascon solution for the same period (**Table S2**) and an earlier multi-method estimate of –215±35 Gt yr^{-1} for the period 2003–2009 (Gardner et al., 2013). An apparent acceleration of the mass loss is visible in the time series (**Figure 2**), with an estimated value of 7.8 ± 3.5 Gt yr^{-2}. However, year-to-year inspection of the global specific mass balances (**Figure 3**) shows that this is largely the result of a temporary decrease in mass balance between 2005 and 2009, and the particularly negative mass balance of 2013, when the global specific mass balance reached a value of –1170 ± 620 kg m^{-2}yr^{-1}. Between 2010 and 2012, annual mass balances were less negative, and more recent years (2014–2015) were close to the long-term (2002–2016) average. The link between increasing air temperatures and glacier mass loss is well-established, but given the heterogeneous distribution across the continents, a strong correlation between deviations from the

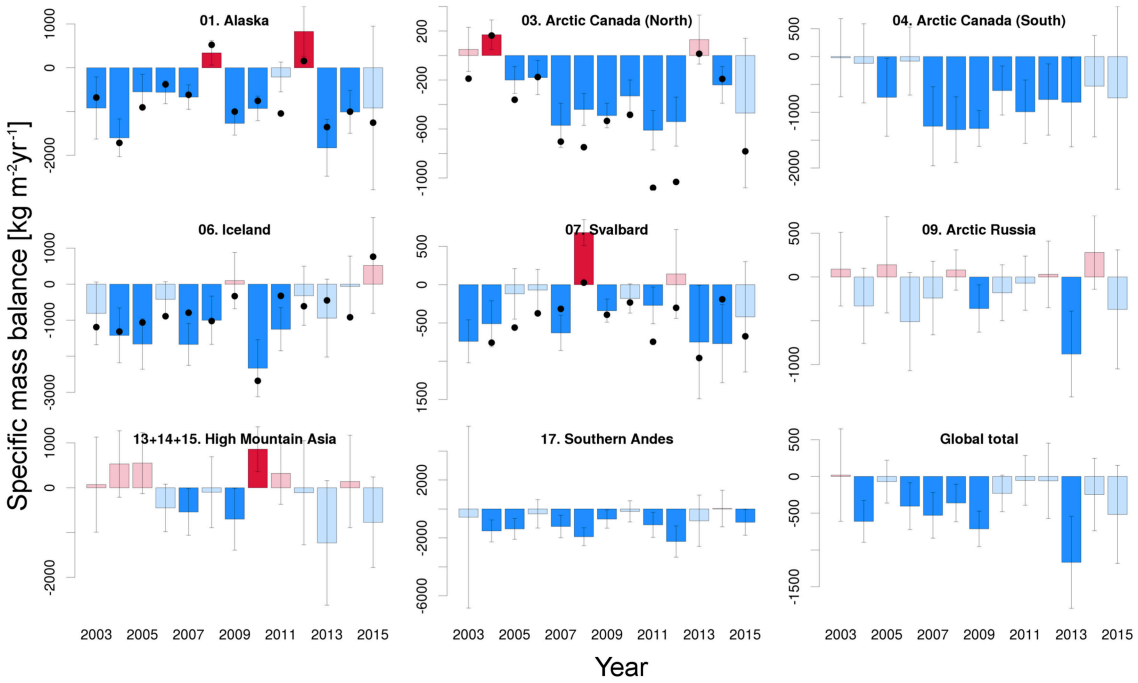

FIGURE 3 | Annual specific mass balance for the larger RGI regions in kg $m^{-2}yr^{-1}$. Mass balance years run from October 1 to September 31 for regions in the Northern Hemisphere, and April 1 to March 31 for regions in the Southern Hemisphere. Note the difference in range on the Y-axis between the different subfigures. Values which are not significantly different from zero are plotted in pale colors. Black dots indicate the annual mass balance derived taking the mean mass balance from *in-situ* observations in the region, where available (see text for details, **Figure S2** and **Table S3** for station locations).

long-term average in global air temperatures and annual mass balance should not be expected. Indeed, we find this correlation to be insignificant ($r = -0.18$ with $p = 0.56$, where a negative correlation indicates a more negative mass balance linked to positive temperate anomalies). A significant correlation is found with the May-August NAO ($r = -0.57$; $p = 0.04$), but this is merely a representation of the large degree of regional variability in the Artic associated with this mode, as we will discuss below.

The largest net contributor to the global mass loss is Alaska (when considering the RGI Arctic Canada North and South regions as separate contributors), with an average mass loss of 53 ± 14 Gt yr^{-1}, equivalent to a long-term specific mass balance of -620 ± 160 kg $m^{-2}yr^{-1}$. The most negative specific balance of -1830 ± 650 kg $m^{-2}yr^{-1}$ is observed in 2013, followed by 2004 (-1600 ± 430 kg $m^{-2}yr^{-1}$), whereas positive values are found in 2008 and 2012. Qualitatively, this is in agreement with mass balance estimates from *in situ* observations at individual glaciers in the region (Wolverine, Lemon Creek, Taku, and Gulkana), which show similar extremely negative and moderately positive mass balances in these years (**Figure 3**; $r = 0.85$;$p < 0.01$). We find that interannual variations in the mass balance are negatively correlated with the May-September PDO and May-August NAO, with correlation values of −0.56 ($p = 0.05$) and −0.77 ($p < 0.01$), respectively (Bitz and Battisti, 1999; Josberger et al., 2007; Arendt et al., 2009).

The total mass loss of the Southern Andes region (30 ± 11 Gt yr^{-1}) is only about half that of Alaska, but relative to its glacier area, this region shows the most pronounced downwasting of all regions considered. Apart from 2013, the region consistently shows negative mass balances throughout the observation period, with an average of -1030 ± 370 kg $m^{-2}yr^{-1}$. Braun et al. (2019) estimated the 2000-2011/2015 mass loss in the region at 19 ± 0.6 Gt yr^{-1} by differencing digital elevation models derived from synthetic aperture radar interferometry. This is smaller than our estimate, but not inconsistent given the different time span and overlapping uncertainty range. Both the GRACE data and the results by Braun et al. (2019) show that nearly all of the regional mass loss can be attributed to the Patagonian Ice Fields.

Similar extreme negative mass balances are observed in Iceland, where glaciers lost on average 920 ± 180 kg $m^{-2}yr^{-1}$, or 10 ± 2 Gt yr^{-1} when integrated over the area, between 2003 and 2015. Icelandic glaciers are highly sensitive to changes in near-surface air temperature because of their area altitude distribution (Hock et al., 2009), and to aerosol radiative forcing following volcanic eruptions (e.g., Flanner et al., 2014). This is reflected in the high interannual variability we find in our GRACE-based annual mass balances, with changes of up to 2400 kg $m^{-2}yr^{-1}$ between consecutive years. Our annual mass balances are in good qualitative agreement with averaged *in-situ* observations from 8 glacier locations ($r = 0.75$; $p < 0.01$). Both types of records show a reduced mass loss since the extreme melt following the eruption of the Eyjafjallajökull in the warm summer of 2010 (Björnsson et al., 2013). Such a reduction of the mass loss was also evident in the altimetry-based estimate of Foresta et al. (2016), who reported

a mass loss of 5.8 ± 0.7 Gt yr^{-1} for the period October 2010–September 2015, which compares well with the 4.8 ± 3 Gt yr^{-1} in this study (vs. 11 ± 2 Gt yr^{-1} in the preceding years).

Both the Northern and Southern regions of the Canadian Arctic showed extensive mass loss in the period 2006–2012, that can be attributed to increasing summer temperatures induced by a weak, westerly-positioned Arctic circumpolar vortex (Gardner et al., 2011, 2012). No significant increase in discharge (VanWychen et al., 2014), or decrease in precipitation has been reported (Noël et al., 2018). Near-zero mass balances are observed in the following two years, 2013 and 2014, when a positive NAO phase lead to advection of cool, wet air toward these regions (Box and Sharp, 2017). Indeed, we find a significant correlation between annual mass balance and May-August NAO in the Northern region ($r = 0.77, p < 0.01$), whereas the variations in the Southern region are better explained by the May-July AO ($r = 0.63, p = 0.03$). In the Northern region, the GRACE annual mass balances correlate well with those derived from four *in situ* records ($r = 0.92$; $p < 0.01$). No similar validation data is available for the Southern region.

In the eastern parts of the Arctic, the same atmospheric circulation patterns led to opposite glacier behavior in Svalbard and the Russian Arctic, with near zero or positive mass balance between 2004 and 2012, but large mass losses in 2013. Both regions experienced a comparable negative specific mass balance of –220 kg $m^{-2} yr^{-1}$ during the observational period, but given its larger area, the Russian Arctic showed a larger overall mass loss (7 ± 1 Gt yr^{-1} for Svalbard, vs. 11 ± 3 Gt yr^{-1} for the Russian Arctic). This is not significantly different from a previous estimate of 9.8 ± 1.9 Gt yr^{-1} for the 2003–2009 period, based on ICESat altimetry (Moholdt et al., 2012). Correlations have opposite signs to those found in the Canadian Arctic, with r= –0.64 ($p = 0.02$) and $r = -0.58$ ($p = 0.04$) for the correlation between summer NAO and annual mass balance in Svalbard and Arctic Russia, respectively. Increased mass losses on Svalbard since 2012 can partly be attributed to the surge of Basin-3 on Austfonna ice cap (Dunse et al., 2015), but most of the negative mass balance in 2013 is explained by increased surface melting (Lang et al., 2015). A reasonable correlation of $r = 0.62$ ($p = 0.03$) is found with local mass balance, where it should be kept in mind that 6 out of 7 of the measurement sites are located on the western coast of Spitsbergen. Out of the three main archipelagoes of the Russian Arctic, Novaya Zemlya (RGI subregion 09.1) accounted for about 50% of the total mass loss, although specific mass rates in Severnaya Zemlya were comparable. No *in situ* records are available from the Russian Arctic.

In the High Mountain Asia region (RGI regions 13-15; Central Asia, South Asia West and East), interannual variability in mass balance is large, due to variations in precipitation associated with changing atmospheric circulation (Yao et al., 2012). The total mass loss of 17.7±11.3 Gt yr^{-1} for 2002–2016 is in good agreement with Brun et al. (2017), who reported a mass loss of 16.3 ± 3.5 for a slightly longer period, 2000–2016. However, when looking at the individual regions, we only observe good agreement for South Asia West (5 Gt yr^{-1} mass loss in this study, vs. 6 Gt yr^{-1} in Brun et al. (2017)). These three regions are also where the spherical harmonics solution of this study deviates the most from the JPL mascons solution despite being similar for High Mountain Asia as a whole (**Supplementary Table S2**). Mass loss in Central Asia is underestimated (3 Gt yr^{-1} vs. 6 Gt yr^{-1}), and overestimated in South Asia East (9 Gt yr^{-1} vs. 4 Gt yr^{-1}). We find that annual mass balance in the Central Asia is positively correlated with all four Niño indices (November-February), with correlation values ranging from $r = 0.64$ ($p = 0.02$) for NINO4 to $r = 0.83$ ($p < 0.01$) for NINO1+2, most likely through modulation of the monsoon circulation (Shaman and Tziperman, 2005; Kumar et al., 2006).

Combined, the ten regions discussed above make up more than 99% of the total mass loss. In the remaining seven regions, where glacier areas are typically an order of magnitude smaller, no significant changes are observed, either because the glacial signal is too small to be distinguished from the background noise, or uncertainties in the GIA and hydrology corrections are large. For Scandinavia, comparison of the GRACE-derived and *in situ* annual mass balances reveals a good agreement in the year-to-year variability ($r = 0.81$; $p < 0.01$), but a too positive mean annual mass balance in the GRACE results, considering that all monitored glaciers have lost mass since year 2000 (Andreassen et al., 2016). The close resemblance between mass anomalies of GRACE and water storage variations in Norwegian hydropower reservoirs (**Figure S3**) shows that this can be an issue for several of the smaller glacier regions that have comparable reservoir areas in the vicinity, in particular Western Canada and US, and Central Europe (RGI regions 03 and 11). The uncorrected impact of reservoir storage variations can partly explain why the seasonal amplitudes in the time series of these regions (**Figure 2**) appear to be comparatively larger and shifted in time from an expected minimum glacier mass at the end of the summer melt season to an expected minimum reservoir storage at the end of the winter before onset of snowmelt runoff. This severely limits our ability to resolve seasonal and annual glacier mass changes in affected regions, but for long-term mass trends over the whole 14-year GRACE period, we expect the impact to be relatively small. Our derived glacier mass trends for Scandinavia and Central Europe are close to zero, whereas the time series for Western Canada and US (**Figure 2**) indicate small changes until 2012 and then a period of mass loss thereafter, consistent with Menounos et al. (2019) who reported an increase in mass loss from 2.9 ± 3.1 Gt yr^{-1} in 2000-2009 to 12.3 ±4.6 Gt yr^{-1}1 in 2009-2018 based on differencing of digital elevation models. No significant correlations were found between GRACE and *in situ* annual mass balances for Western Canada and US ($r = 0.49$; $p = 0.09$), and Central Europe ($r = 0.55$; $p = 0.06$). Other small RGI regions (North Asia, Caucasus, Low Latitudes and New Zealand) constitute only 1.5% of the global glacier area and are thus of minor importance in a sea level perspective despite clearly negative specific mass balances from *in-situ* records (Gardner et al., 2013).

4. CONCLUSIONS

In this study, we provide time series of glacier mass loss, together with annual estimates of specific mass balance, for all

RGI regions, excluding the peripheral glaciers of Greenland and Antarctica. For the larger regions, these annual mass balances agree well with *in situ* observations and independent estimates from altimetry. Smaller regions are hampered by a low signal-to-noise ratio and uncertainties in the necessary corrections for GIA and hydrology. Improvement of these model corrections, including anthropogenic influences as demonstrated by our case study of Norwegian hydropower reservoirs, are a prerequisite to resolve the ongoing changes in these smaller regions. In High Mountain Asia, overall agreement was found with independent observations of mass loss, but less so when looking at the three distinct regions that make up High Mountain Asia. We associate this agreement at the regional scale but disagreement at the subregions as being caused by the coarse horizontal resolution of GRACE, which causes "signal leakage" between neighboring subregions. Until a leap forward is made to a finer spatial resolution of gravimetry missions, resolving small-scale mass change signals will have to rely on combination of GRACE observations with auxiliary data, either from climate models, or other remote sensing techniques (e.g., Sasgen et al., 2019).

Variations in regional mass loss are predominantly driven by local atmospheric circulation changes, particularly those that modify summer near-surface air temperatures. We find that annual mass balance, notably in the Northern Hemisphere, correlate well with climate indices such as the AO, PDO, ENSO, and, in particular, the NAO, leading to substantial interannual variability. This—combined with the relatively large uncertainties in the current GRACE observations in some regions—hampers the detection of a possible acceleration in the mass loss, which calls for continued and improved global observations of the Earth's glaciers and ice caps. Nevertheless, it is clear that during the GRACE-era, their overall mass balance was strongly negative. Since 2003, the world's glaciers have lost about 3000 Gt, equivalent to a sea level rise of 8 mm. The average mass loss rate of 199 $\pm$ 32 Gt yr^{-1} is only slightly smaller than that of Greenland, and about twice that of Antarctica for the same period (WCRP Global Sea Level Budget Group, 2018).

AUTHOR CONTRIBUTIONS

BW designed and performed the GRACE data analysis, and wrote a first draft of the manuscript. AG carried out the analysis of the JPL mascon time series. GM examined the impact of hydropower water storage on the GRACE results in Scandinavia. All authors contributed to the analysis of the data and further writing of the manuscript.

FUNDING

BW was funded by NWO VIDI grant 016.Vidi.171.063. AG's efforts were supported by NASA's Cryosphere Science program.

ACKNOWLEDGMENTS

Jason E. Box is acknowledged for his work on correlation of climate indices that inspired part of this study, and David N. Wiese for producing the JPL mascons and commenting on the GRACE analysis. We thank Bart Root and Alexander Jarosch for providing us with the GIA corrections for the Barentz region and Iceland, respectively, and Edwin H. Sutanudjaja for the PCR-GLOBWB v2 model data. We thank Geert Jan van Oldenborgh for making the climate indices available on climexp.knmi.nl.

SUPPLEMENTARY MATERIAL

The Supplementary Material for this article can be found online at: https://www.frontiersin.org/articles/10.3389/feart.2019.00096/full#supplementary-material

REFERENCES

Andreassen, L. M., Elvehøy, H., Kjøllmoen, B., and Engeset, R. V. (2016). Reanalysis of long-term series of glaciological and geodetic mass balance for 10 Norwegian glaciers. *Cryosphere* 10, 535–552. doi: 10.5194/tc-10-535-2016

Arendt, A., Walsh, J., and Harrison, W. (2009). Changes of Glaciers and Climate in Northwestern North America during the Late Twentieth Century. *J. Clim.* 22, 4117–4134. doi: 10.1175/2009JCLI2784.1

Bamber, J. L., Tedstone, A. J., King, M. D., Howat, I. M., Enderlin, E. M., van den Broeke, M. R., et al. (2018). Land ice freshwater budget of the Arctic and North Atlantic oceans: 1. Data, methods, and results. *J. Geophys. Res. Oceans* 123, 1827–1837. doi: 10.1002/2017JC013605

Beaudoing, H., and Rodell, M. (2016). *GLDAS Noah Land Surface Model L4 Monthly 0.25 x 0.25 Degree V2.1*. doi: 10.5067/SXAVCZFAQLNO

Bettadpur, S. V. (2018). *UTCSR Level-2 Processing Standards Document for Product Release 06*. Tech. Rep. GRACE 327-742, UTCSR, Austin, TX, 17.

Bitz, C. M., and Battisti, D. S. (1999). Interannual to decadal variability in climate and the glacier mass balance in Washington, Western Canada, and Alaska. *J. Clim.* 12, 3181–3196. doi: 10.1175/1520-0442(1999)012<3181:ITDVIC>2.0.CO;2

Björnsson, H., Pàlsson, F., Gudmundsson, S., Magnúúson, E., Adalgeirsdóttir, G., Jóhannesson, T., et al. (2013). Contribution of Icelandic ice caps to sea level rise: trends and variability since the Little Ice Age. *Geophysical Research Letters* 40, 1546–1550. doi: 10.1002/grl.50278

Box, J., and Sharp, M. (2017). "Chap. Changes to Arctic land ice," in *Snow, Water, Ice and Permafrost in the Arctic (SWIPA)* (Oslo: Arctic Monitoring and Assessment Programme (AMAP), 137–168. Available online at: https://www.amap.no/documents/doc/snow-water-ice-and-permafrost-inthe-arctic-swipa-2017/1610

Braun, M. H., Malz, P., Sommer, C., Farías-Barahona, D., Sauter, T., Casassa, G., et al. (2019). Constraining glacier elevation and mass changes in South America. *Nat. Clim. Change* 9, 130–136. doi: 10.1038/s41558-018-0375-710.1038/s41558-018-0375-7

Brun, F., Berthier, E., Wagnon, P., Kääb, A., and Treichler, D. (2017). A spatially resolved estimate of High Mountain Asia glacier mass balances from 2000 to 2016. *Nat. Geosci.* 10, 668. doi: 10.1038/ngeo2999

Caron, L., Ivins, E., Larour, E., Adhikari, S., Nilsson, J., and Blewitt, G. (2018). GIA model statistics for GRACE hydrology, cryosphere, and ocean science. *Geophys. Res. Lett.* 45, 2203–2212. doi: 10.1002/2017GL076644

Cheng, M., Tapley, B. D., and Ries, J. C. (2013). Deceleration in the earth's oblateness. *J. Geophys. Res.* 118, 740–747. doi: 10.1002/jgrb.50058

Cogley, J. G. (2009). Geodetic and direct mass-balance measurements: comparison and joint analysis. *Ann. Glaciol.* 50, 96–100. doi: 10.3189/172756409787769744

Dunse, T., Schellenberger, T., Hagen, J. O., Kääb, A., Schuler, T. V., and Reijmer, C. H. (2015). Glacier surge mechanisms promoted by a hydro-thermodynamic feedback to summer melt. *Cryosphere* 9, 197–215. doi: 10.5194/tc-9-197-2015

Farinotti, D., Huss, M., Fürst, J. J., Landmann, J., Machguth, H., Maussion, F., et al. (2019). A consensus estimate for the ice thickness distribution of all glaciers on Earth. *Nat. Geosci.* 12, 168–173. doi: 10.1038/s41561-019-0300-3

Flanner, M. G., Gardner, A. S., Eckhardt, S., Stohl, A., and Perket, J. (2014). Aerosol radiative forcing from the 2010 eyjafjallajökull volcanic eruptions. *J. Geophys. Res. Atmos.* 119, 9481–9491. doi: 10.1002/2014JD021977

Foresta, L., Gourmelen, N., Pálsson, F., Nienow, P., Björnsson, H., and Shepherd, A. (2016). Surface elevation change and mass balance of Icelandic ice caps derived from swath mode CryoSat-2 altimetry. *Geophys. Res. Lett.* 43:12, 138–145. doi: 10.1002/2016GL071485

Gardner, A., Moholdt, G., Arendt, A., and Wouters, B. (2012). Accelerated contributions of Canada's Baffin and Bylot Island glaciers to sea level rise over the past half century. *The Cryosphere.* 6, 1103–1125. doi: 10.5194/tc-6-1103-2012

Gardner, A. S., Moholdt, G., Cogley, J. G., Wouters, B., Arendt, A. A., Wahr, J., et al. (2013). A reconciled estimate of Glacier contributions to sea level rise: 2003 to 2009. *Science* 340, 852–857. doi: 10.1126/science.1234532

Gardner, A. S., Moholdt, G., Wouters, B., Wolken, G. J., Burgess, D. O., Sharp, M. J., et al. (2011). Sharply increased mass loss from glaciers and ice caps in the Canadian Arctic Archipelago. *Nature* 473, 357–360. doi: 10.1038/nature10089

Grund, F. (1979). Forsythe, G. E. / Malcolm, M. A. / Moler, C. B., Computer methods for mathematical computations. Englewood Cliffs, New Jersey 07632. Prentice Hall, Inc., 1977. XI, 259 S. *ZAMM J. Appl. Math. Mech.* 59, 141–142. doi: 10.1002/zamm.19790590235

Hock, R., de Woul, M., Radiá, V., and Dyurgerov, M. (2009). Mountain glaciers and ice caps around Antarctica make a large sea-level rise contribution. *Geophys. Res. Lett.* 36:L07501. doi: 10.1029/2008GL037020

Huss, M., Bookhagen, B., Huggel, C., Jacobsen, D., Bradley, R., Clague, J., et al. (2017).Toward mountains without permanent snow and ice. *Earths Future* 5, 418–435. doi: 10.1002/2016EF000514

Huss, M., and Hock, R. (2015). A new model for global glacier change and sea-level rise. *Front. Earth Sci.* 3:54. doi: 10.3389/feart.2015.00054

Ivins, E. R., and James, T. S. (2004). Bedrock response to Llanquihue Holocene and present-day glaciation in southernmost South America. *Geophys. Res. Lett.* 31:L24613. doi: 10.1029/2004GL021500

Jacob, T., Wahr, J., Pfeffer, W. T., and Swenson, S. (2012). Recent contributions of glaciers and ice caps to sea level rise. *Nature* 482, 514–518. doi: 10.1038/nature10847

Josberger, E. G., Bidlake, W. R., March, R. S., and Kennedy, B. W. (2007). Glacier mass-balance fluctuations in the Pacific Northwest and Alaska, USA. *Ann. Glaciol.* 46, 291–296. doi: 10.3189/172756407782871314

Kaser, G., Cogley, J. G., Dyurgerov, M. B., Meier, M. F., and Ohmura, A. (2006). Mass balance of glaciers and ice caps: consensus estimates for 1961-2004. *Geophys. Res. Lett.* 33, 19501.doi: 10.1029/2006GL027511

Kumar, K. K., Rajagopalan, B., Hoerling, M., Bates, G., and Cane, M. (2006). Unraveling the mystery of Indian monsoon failure during El Niño. *Science* 314, 115–119. doi: 10.1126/science.1131152

Lang, C., Fettweis, X., and Erpicum, M. (2015). Stable climate and surface mass balance in Svalbard over 1979-2013 despite the Arctic warming. The Cryosphere 9, 83-101. doi: 10.5194/tc-9-83-2015

Larsen, C. F., Motyka, R. J., Freymueller, J. T., Echelmeyer, K. A., and Ivins, E. R. (2005). Rapid viscoelastic uplift in southeast Alaska caused by post-Little Ice Age glacial retreat. *Earth Planet. Sci. Lett.* 237, 548–560. doi: 10.1016/j.epsl.2005.06.032

Marzeion, B., Kaser, G., Maussion, F., and Champollion, N. (2018). Limited influence of climate change mitigation on short-term glacier mass loss. *Nat. Clim. Change* 8, 305–308. doi: 10.1038/s41558-018-0093-1

Mayer-Gürr, T., Behzadpour, S., Ellmer, M., Kvas, A., Klinger, B., Strasser, S., et al. (2018). *ITSG-Grace2018 - Daily and Static Gravity Field Solutions from GRACE.* GFZ Data Services. doi: 10.5880/ICGEM.2018.003

Meier, M. F., Dyurgerov, M., Rick, U. K., O'Neel, S., Pfeffer, W. T., Anderson, R., et al. (2007). Glaciers dominate eustatic sea-level rise in the 21st century. *Science* 317, 1064–1067. doi: 10.1126/science.1143906

Menounos, B., Hugonnet, R., Shean, D., Gardner, A., Howat, I., Berthier, E., et al. (2019). Heterogeneous changes in Western North American glaciers linked to decadal variability in zonal wind strength. *Geophys. Res. Lett.* 46, 200–209. doi: 10.1029/2018GL080942

Moholdt, G., Wouters, B., and Gardner, A. S. (2012). Recent mass changes of glaciers in the Russian High Arctic. *Geophys. Res. Lett.* 39:L10502. doi: 10.1029/2012GL051466

Noël, B., Berg, W. J., Lhermitte, S., Wouters, B., Schaffer, N., and Broeke, M. R. (2018). Six decades of glacial mass loss in the Canadian Arctic Archipelago. *J. Geophys. Res. Earth Surface* 123, 1430–1449. doi: 10.1029/2017JF004304

PO.DAAC (2018). *GRACE. 2001. GRACE ACC1B R3 Transplant Data. Ver. 3.* PO.DAAC. Dataset (accessed October 13, 2018)

Reager, J. T., Gardner, A. S., Famiglietti, J. S., Wiese, D. N., Eicker, A., and Lo, M.-H. (2016). A decade of sea level rise slowed by climate-driven hydrology. *Science* 351, 699–703. doi: 10.1126/science.aad8386

RGI Consortium (2017). *Randolph Glacier Inventory (RGI) - A Dataset of Global Glacier Outlines: Version 6.0.* Tech. rep., Global Land Ice Measurements from Space, Boulder, CO, USA. doi: 10.7265/N5-RGI-60

Rietbroek, R., Brunnabend, S.-E., Kusche, J., Schröter, J., and Dahle, C. (2016). Revisiting the contemporary sea-level budget on global and regional scales. *Proc. Natl. Acad. Sci. U.S.A.*113, 1504–1509. doi: 10.1073/pnas.1519132113

Rodell, M., Houser, P. R., Jambor, U., Gottschalck, J., Mitchell, K., Meng, C.-J., et al. (2004). The global land data assimilation system. *Bull. Am. Meteorol. Soc.* 85, 381–394. doi: 10.1175/BAMS-85-3-381

Root, B. C., Tarasov, L., and Wal, W. (2015). GRACE gravity observations constrain Weichselian ice thickness in the Barents Sea. *Geophys. Res. Lett.* 42, 3313–3320. doi: 10.1002/2015GL063769

Sakumura, C., Bettadpur, S., and Bruinsma, S. (2014). Ensemble prediction and intercomparison analysis of GRACE time-variable gravity field models. *Geophys. Res. Lett.* 41, 1389–1397. doi: 10.1002/2013GL058632

Sasgen, I., Konrad, H., Helm, V., and Grosfeld, K. (2019). High-resolution mass trends of the Antarctic ice sheet through a spectral combination of satellite gravimetry and radar altimetry observations. *Remote Sens.* 11:144. doi: 10.3390/rs11020144

Sasgen, I., Martinec, Z., and Fleming, K. (2007). Wiener optimal combination and evaluation of the Gravity Recovery and Climate Experiment (GRACE) gravity fields over Antarctica. *J. Geophys. Res. Solid Earth* 112:B04401. doi: 10.1029/2006JB004605

Scanlon, B. R., Zhang, Z., Save, H., Sun, A. Y., Müller Schmied, H., van Beek, L. P. H., et al. (2018). Global models underestimate large decadal declining and rising water storage trends relative to GRACE satellite data. *Proc. Natl. Acad. Sci. U.S.A.*115, E1080–E1089. doi: 10.1073/pnas.1704665115

Schrama, E. J. O., Wouters, B., and Rietbroek, R. (2014). A mascon approach to assess ice sheet and glacier mass balances and their uncertainties from grace data. *J. Geophys. Res. Solid Earth* 119, 6048–6066. doi: 10.1002/2013JB010923

Shaman, J., and Tziperman, E. (2005). The effect of enso on tibetan plateau snow depth: a stationary wave teleconnection mechanism and implications for the south asian monsoons. *J. Clim.* 18, 2067–2079. doi: 10.1175/JCLI3391.1

Shepherd, A., Ivins, E. R., Geruo, A., Barletta, V. R., Bentley, M. J., Bettadpur, S., et al. (2012). A reconciled estimate of ice-sheet mass balance. *Science* 338, 1183–1189. doi: 10.1126/science.1228102

Slemmons, K., Saros, J., and Simon, K. (2013). The influence of glacial meltwater on alpine aquatic ecosystems: a review. *Environ. Sci. Process. Impacts* 15, 1794–1806. doi: 10.1039/c3em00243h

Sørensen, L. S., Jarosch, A. H., Aðalgeirsdóttir, G., Barletta, V. R., Forsberg, R., Pálsson, F., et al. (2017). The effect of signal leakage and glacial isostatic rebound on GRACE-derived ice mass changes in Iceland. *Geophys. J. Int.* 209, 226–233. doi: 10.1093/gji/ggx008

Sutanudjaja, E. H., van Beek, R., Wanders, N., Wada, Y., Bosmans, J. H. C., Drost, N., et al. (2018). PCR-GLOBWB 2: a 5 arcmin global hydrological and water resources model. *Geosci. Model Dev.* 11, 2429–2453. doi: 10.5194/gmd-11-2429-2018

Swenson, S., Chambers, D., and Wahr, J. (2008). Estimating geocenter variations from a combination of GRACE and ocean model output. *J. Geophys. Res.* 113:B08410. doi: 10.1029/2007JB005338

VanWychen, W., Burgess, D. O., Gray, L., Copland, L., Sharp, M., Dowdeswell, J. A., et al. (2014). Glacier velocities and dynamic ice discharge from the Queen Elizabeth Islands, Nunavut, Canada. *Geophys. Res. Lett.* 41, 484–490. doi: 10.1002/2013GL058558

Wahr, J., Molenaar, M., and Bryan, F. (1998). Time variability of the earth's gravity field: Hydrological and oceanic effects and their possible detection using GRACE. *J. Geophys. Res.* 103, 30305–30229.

Wahr, J., Swenson, S., and Velicogna, I. (2006). Accuracy of GRACE mass estimates. *Geophys. Res. Lett.* 33:L06401. doi: 10.1029/2005GL025305

Watkins, M. M., Wiese, D. N., Yuan, D., Boening, C., and Landerer, F. W. (2015). Improved methods for observing Earth's time variable mass distribution with GRACE using spherical cap mascons. *J. Geophys. Res. Solid Earth* 120, 2648–2671. doi: 10.1002/2014JB011547

WCRP Global Sea Level Budget Group (2018). Global sea-level budget 1993-present. *Earth Syst. Sci. Data* 10, 1551–1590. doi: 10.5194/essd-10-1551-2018

Wester, P., Mishra, A., Mukherji, A., and Bhakta Shrestha, A. (2019). *The Hindu Kush Himalaya Assessment Mountains, Climate Change, Sustainability and People: Mountains, Climate Change, Sustainability and People*. Cham: Springer. doi: 10.1007/978-3-319-92288-1

WGMS (2017). *Global Glacier Change Bulletin No. 2 (2014-2015)*. Zurich: CSU(WDS)/IUGG(IACS)/UNEP/UNESCO/WMO, World Glacier Monitoring Service. Publication based on database version: doi: 10.5904/wgms-fog-2017-10

Wouters, B. (2010). *Identification and Modelling of Sea Level Change Contributors - On GRACE Satellite Gravity Data and Their Application to Climate Monitoring* (Ph.D. thesis). Delft University of Technology. Available online at: https://ncgeo.nl/index.php/nl/publicaties/gele-serie/item/2580-pog-73-woutersidentification-and-modeling-of-sea-levelchange-contributors

Wouters, B., Chambers, D., and Schrama, E. (2008). GRACE observes small-scale mass loss in Greenland. *Geophys. Res. Lett.* 35:L20501. doi: 10.1029/2008GL034816

Wouters, B., and Schrama, E. J. O. (2007). Improved accuracy of GRACE gravity solutions through empirical orthogonal function filtering of spherical harmonics. *Geophys. Res. Lett.* 34:23711. doi: 10.1029/2007GL032098

Yang, Q., Dixon, T. H., Myers, P. G., Bonin, J., Chambers, D., and van den Broeke, M. R. (2016). Recent increases in Arctic freshwater flux affects Labrador Sea convection and Atlantic overturning circulation. *Nat. Commun.* 7:10525. doi: 10.1038/ncomms10525

Yao, T., Thompson, L., Yang, W., Yu, W., Gao, Y., Guo, X., et al. (2012). Different glacier status with atmospheric circulations in Tibetan Plateau and surroundings. *Nat. Clim. Change* 2:663. doi: 10.1038/nclimate158010.1038/nclimate1580

Yuan, D.-N. (2018). *JPL Level-2 Processing Standards Document For Level-2 Product Release 06*. Tech. Rep. GRACE 327-745, JPL, Pasadena, CA, 17.

Zemp, M., Frey, H., Gärtner-Roer, I., Nussbaumer, S. U., Hoelzle, M., Paul, F., et al. (2015). Historically unprecedented global glacier decline in the early 21st century. *J. Glaciol.* 61, 745–762. doi: 10.3189/2015JoG15J017

Conflict of Interest Statement: The authors declare that the research was conducted in the absence of any commercial or financial relationships that could be construed as a potential conflict of interest.

frontiers in Earth Science

ORIGINAL RESEARCH
published: 11 December 2019
doi: 10.3389/feart.2019.00326

Six Decades (1958–2018) of Geodetic Glacier Mass Balance in Monte San Lorenzo, Patagonian Andes

Daniel Falaschi[1,2], María Gabriela Lenzano[1], Ricardo Villalba[1], Tobias Bolch[3], Andrés Rivera[4,5] and Andrés Lo Vecchio[1,2]*

[1] Instituto Argentino de Nivología, Glaciología y Ciencias Ambientales, CCT-Mendoza CONICET, Mendoza, Argentina, [2] Departamento de Geografía, Facultad de Filosofía y Letras, Universidad Nacional de Cuyo, Mendoza, Argentina, [3] School of Geography and Sustainable Development, University of St Andrews, St Andrews, United Kingdom, [4] Centro de Estudios Científicos, Valdivia, Chile, [5] Departamento de Geografía, Universidad de Chile, Santiago, Chile

A full understanding of glacier changes in the Patagonian Andes over decadal to century time-scales is presently limited by a lack of detailed and appropriate long-term observations. Here, we present geodetic mass and area changes of three valley glaciers from Monte San Lorenzo derived from stereo aerial photos, the Shuttle Radar Topography Mission (SRTM) and satellite imagery (SPOT5 and Pleiades) spanning four periods from 1958 to 2018. Our results indicate that net mass balance was negative throughout the six decades, with a mean mass loss of -1.35 ± 0.08 m w.e. a^{-1} and a total glacier area loss of 14.2 ± 0.7 km^2 ($23 \pm 1\%$ or $0.40 \pm 0.02\%$ a^{-1}). The period 1981–2000 had the most negative mass budget, with an area-averaged mass loss of 1.67 ± 0.11 m w.e. a^{-1} and a maximum loss of -2.23 ± 0.07 m w.e. a^{-1} at San Lorenzo Sur glacier. Over the periods of 2000–2012 and 2012–2018, the mass budget of these three glaciers remained virtually unchanged at -1.37 ± 0.06 and -1.36 ± 0.17 m w.e. a^{-1}, respectively. To place these results into a broader geographical context, the mass balance of a further 15 glaciers from around the Monte San Lorenzo massif was determined from 2000 onwards. This wider analysis reveals a period of reduced mass loss of -0.13 ± 0.21 m w.e. a^{-1} from 2012 to 2018 after a period of enhanced mass loss of -0.31 ± 0.16 m w.e. a^{-1} between 2000 and 2012. We find that increasing air temperatures coupled with diminishing precipitation across the region explains the observed patterns and are the main drivers of the negative mass budget. Furthermore, increased calving and melting into recently formed proglacial lakes has further enhanced mass loss at some lake-terminating glaciers.

Keywords: geodetic mass balance, glacier retreat, glacial lake, Monte San Lorenzo, Patagonian Andes

OPEN ACCESS

Edited by:
Alun Hubbard,
Arctic University of Norway, Norway

Reviewed by:
David Loibl,
Humboldt University of Berlin, Germany
Remco de Kok,
Utrecht University, Netherlands

****Correspondence:***
Daniel Falaschi
dfalaschi@mendoza-conicet.gov.ar

Specialty section:
This article was submitted to Cryospheric Sciences, a section of the journal Frontiers in Earth Science

Received: *01 August 2019*
Accepted: *27 November 2019*
Published: *11 December 2019*

Citation:
Falaschi D, Lenzano MG, Villalba R, Bolch T, Rivera A and Lo Vecchio A (2019) Six Decades (1958–2018) of Geodetic Glacier Mass Balance in Monte San Lorenzo, Patagonian Andes. Front. Earth Sci. 7:326. doi: 10.3389/feart.2019.00326

INTRODUCTION

A sustained trend of rapid glacier retreat and depletion has been observed in most mountain and cold regions around the Globe (Zemp et al., 2019) including the Patagonian Andes (Davies and Glasser, 2012; Paul and Mölg, 2014; Masiokas et al., 2015; Falaschi et al., 2017; Dussaillant et al., 2019). The large, temperate ice masses of Patagonia are particularly sensitive to climate change as they are close to the melting point (Schwikowski et al., 2013), and are in fact currently among the

greatest contributors to sea-level rise (Marzeion et al., 2012; Gardner et al., 2013; Foresta et al., 2018). In addition to glacier mass losses owed to climate change, the presence of glacial lakes at glacier terminus is known to boost glacier area reduction and glacier thinning through calving (Basnett et al., 2013; Brun et al., 2019). In the Patagonian Andes, proglacial lake expansion has been mostly observed in the large outlet glaciers flowing down the Patagonian Icefields (Harrison et al., 2006; Loriaux and Casassa, 2013), yet the influence of glacier-lake interactions in the shrinkage of smaller glaciers is poorly known.

Over the last five decades the investigation of glacier changes worldwide has been favored by the increased availability of systematically acquired satellite imagery and derived products such as digital elevation models (DEMs). Before the satellite era, glacier studies usually relied on aerial photographs (e.g., Corte and Espizúa, 1981; Espizúa, 1983; among others for the Andes). These, however, were most frequently not repeatedly acquired (see, e.g., Mölg et al., 2019), implied high operational costs, and were in principle hardly aimed at glaciological studies. Even more problematic, the acquisition geometry of air photographs resulted in the deformation of terrain features (e.g., glaciers), which is maximized in areas of mountain topography. This in turn made the use of specific hardware (a photo restitutor) and precise ground control points usually obtained during field surveys mandatory, resulting in a highly complex process. In some cases, glacier inventories were done without proper orthorectification of the aerial photographs (e.g., Bertone, 1960; Corte and Espizúa, 1981; Espizúa, 1983 in the Andes in particular), potentially introducing gross errors. In recent years, however, the advent of techniques such as Structure from Motion (SFM) has allowed for assessing glacier changes during the pre-satellite era without such demanding efforts (Mölg and Bolch, 2017; Vargo et al., 2017).

Whilst a number of recent studies have used declassified Corona and Hexagon imagery data to derive glacier changes in the 1960 and 1970s on several glacierised regions in the World (e.g., Bolch et al., 2008; Bhambri et al., 2011; Pieczonka and Bolch, 2015; Racoviteanu et al., 2015; Ragettli et al., 2016; Schmidt and Nüsser, 2017; Maurer et al., 2019; King et al., 2019), glaciological studies based on aerial photographs acquired in the mid 20th century are still scarce (e.g., Cox and March, 2004; Koblet et al., 2010; Pieczonka et al., 2011; Fieber et al., 2018; Farías-Barahona et al., 2019; Mölg et al., 2019).

In general terms, the understanding of glacier mass budget trends in southern Patagonia do not rely on long or numerous glaciological records. Quite the opposite, merely Martial Este (2001-ongoing; Strelin and Iturraspe, 2007; Buttstädt et al., 2009; see also WGMS, 2017) and Glaciar de los Tres (Popovnin et al., 1999, resumed in 2013 by the Instituto Argentino de Nivología y Glaciología of Argentina) have had glaciological mass balance programs recently. At a broader scale, glacier volume and mass changes been surveyed by means of the geodetic mass balance method (Rivera et al., 2007; Willis et al., 2012; Falaschi et al., 2017; Foresta et al., 2018; Braun et al., 2019; Dussaillant et al., 2019), which retrieves glacier elevation and volume changes by differencing a series of multi-temporal, often multi-sourced DEMs (Cogley, 2009). However, most of these mass balance assessments have utilized DEMs that represent the topography of glacier surface only from the year 2000 onwards (i.e., the Shuttle Radar Topography Mission, SRTM). Consequently, glacier mass changes during the earlier 20th century are hardly known. In very few cases, early 20th century DEMs have been produced by digitalization of contour maps (see Rignot et al., 2003), where uncertainties on height elevation are high.

In this study, we (1) produce a six decade (1958–2018) geodetic mass balance record for three valley glaciers in the Monte San Lorenzo massif (Río Oro, Río Lácteo, and San Lorenzo Sur), using a combination of multi-sourced DEMs (based on aerial photos, SRTM, SPOT 5, and Pleiades data) on a two-decadal to sub-decadal sale, providing this way the longest glacier mass balance record so far for the Patagonian Andes, (2) provide an updated 2000–2018 geodetic mass balance assessment for other 15 glaciers in the Monte San Lorenzo, (3) derive glacier area and length changes and (4) discuss the influence of climatic trends in the region and the formation and growth of proglacial lakes at glacier terminus that may help in giving an explanation to the observed glacier changes in the intervening years. Data presented in this paper will be made available in the WGMS and/or GLIMS database.

STUDY AREA

Monte San Lorenzo (47° 35′ S, 72° 18′ W, 3706 m a.s.l., **Figure 1**) is located in the southern Patagonian Andes, at the international border between Argentina (Santa Cruz Province) and Chile (Región de Aysén). On Argentinian territory, the massif lies within the San Lorenzo Conservation Area, and closely bounds with the Perito Moreno National Park. It is the second highest peak in Patagonia behind Monte San Valentín (3900 m a.s.l., Metzeltin Buscaini, 2005). Monte San Lorenzo forms, along with other lower mountain ranges, a heavily glaciated region in the eastern foreland of the Southern and Northern Patagonian Icefields (SPI and NPI, respectively). Wenzens (2002) showed that during the Last Glaciation in Patagonia, glaciers in the San Lorenzo area did not form a continuous ice cap encompassing also the SPI and NPI, and that glaciers in the eastern flank of Monte San Lorenzo drained eastwards independently from the icefields.

From a glaciological perspective, Monte San Lorenzo was pivotal for establishing the chronology of glacier readvances since the Late-Glacial in southern Patagonia, since radiocarbon ages obtained at Río Lácteo glacier indicated that the onset of neoglaciations did not start until the Mid-Holocene (Mercer, 1968), much in agreement with the general scheme proposed by Aniya (2013). The work of Mercer (1968) was recently resumed by Morano-Büchner and Aravena (2013); Garibotti and Villalba (2017) and Sagredo et al. (2017), providing a detailed glacier fluctuation chronology of a number of Monte San Lorenzo glaciers based on lichenometry, surface exposure dating and historical photographic documents, from the Mid-Holocene through the Little Ace Age up to the year 1945. Falaschi et al. (2013) compiled the first glacier inventory of the Monte San Lorenzo and nearby peaks, accounting for ∼207 km^2 ice in 2008, and estimated 1985–2008 glacier area reduction rates

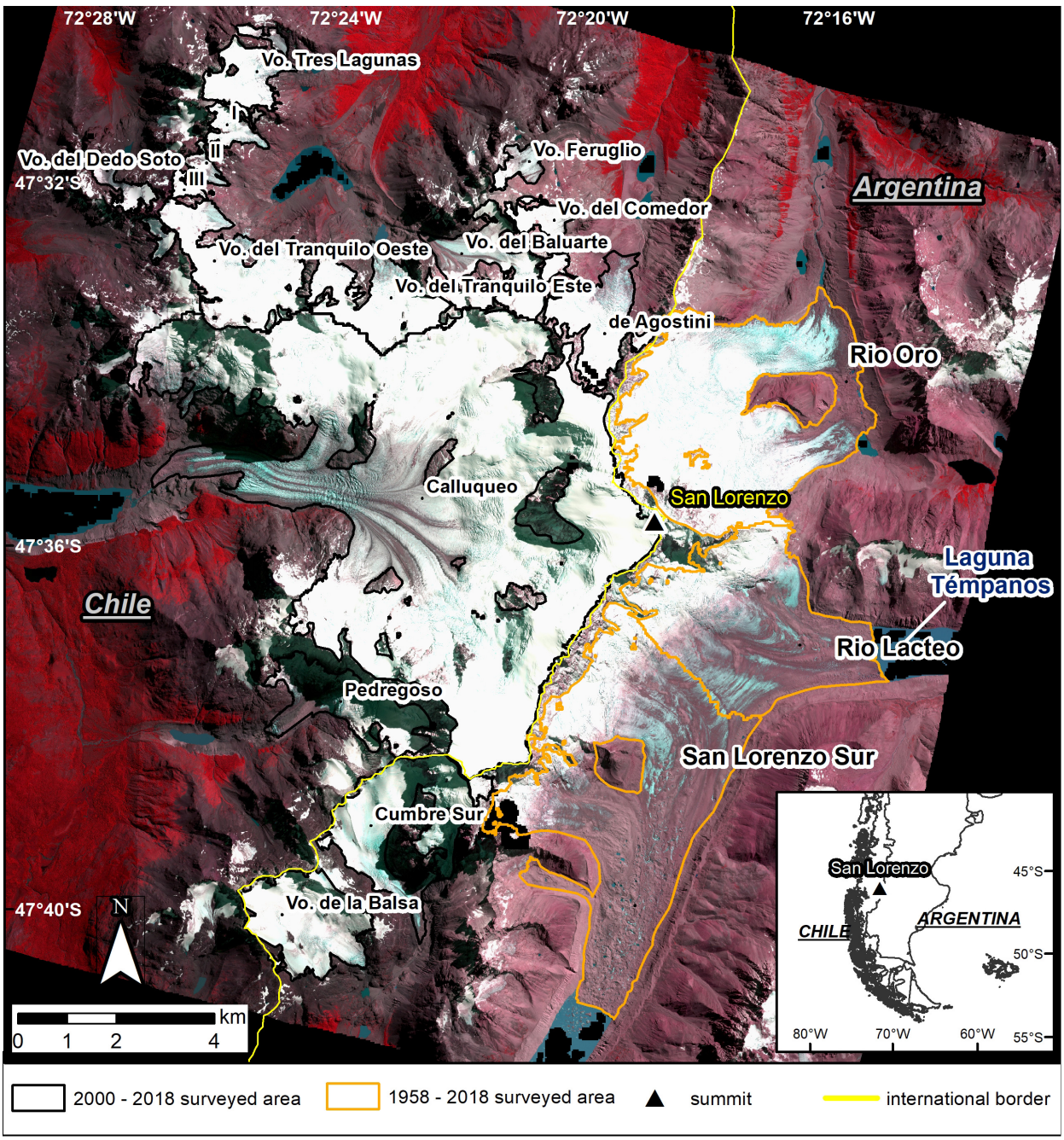

FIGURE 1 | Overview of the Monte San Lorenzo area and the investigated glaciers. I, II and II stand for three unnamed glaciers in the Tres Lagunas basin. Background image is a Pleiades RGB 432 composition. Vo, Ventisquero (lower part of a glacier in Spanish).

of ~1% a^{-1}, in agreement with the general trends observed elsewhere in Patagonia (Davies and Glasser, 2012; Paul and Mölg, 2014; Falaschi et al., 2017).

The abrupt, often intricate topography of Monte San Lorenzo results in a complex variety of cirque and valley glaciers with compound basins (Glasser and Jansson, 2008). The regenerated Río Lácteo and San Lorenzo Sur glaciers have a mostly debris-covered tongue that calve into proglacial lakes, whereas Río Oro is predominantly debris-free and has a land-terminating front (Falaschi et al., 2013). Accumulation Area Ratios (AAR) for these three glaciers are small (<0.5), which is indicative of glaciers in a disequilibrium state (Bakke and Nesje, 2011). The most reliable modern ELA determinations in the area stem from the nearby Río Tranquilo glacier at 1895 m a.s.l. (Sagredo et al., 2017).

Climate-wise, Monte San Lorenzo lies in a transitional maritime to continental area, within the strong West-East

orographic precipitation gradient that characterizes the Patagonian Andes (Garreaud et al., 2013). Whilst the temperature variations are less pronounced across the main water divide (Wolff et al., 2013), the dissimilar environmental conditions result in diverse glacier thermal regimes and sensitivity to climate perturbations. Glaciers in the drier, eastern slope of the water divide (such as Río Oro, Río Lácteo and San Lorenzo Sur), may be polythermal and probably less sensitive to rising temperatures compared to the temperate glaciers on the wetter, western flank, where a decrease in the snow/rain ratio will have a greater impact on snow accumulation and thus on mass balance as well (Sagredo and Lowell, 2012).

DATA AND METHODS

Aerial Photographs and Generation of Photogrammetric DEMs

In the historical aerial photography archive of the Instituto Geográfico Nacional of Argentina (IGN), there are few suitable photographs (no significant amounts of seasonal snow and cloud cover) for the years 1958 and 1981 (**Table 1**). These aerial photographs fully cover Río Oro, Río Lácteo and San Lorenzo Sur glaciers located in Argentinian territory (**Figure 1**). The 1958 and 1981 scenes were scanned from the negatives at 10 μm scanning resolution in a Vexcel UltraScan 5000 scanner.

The entire aerial photogrammetric processing, from the strip formation to DEM and orthophoto generation were carried out in the Photomod 4.1 software (Racurs, 2006). The basic workflow for DEM processing involves (1) *block forming* (2) *aerial triangulation* (3) *block adjustment* and (4) *block processing*. After arranging and orientating the images in strips during stage (1), block forming is used to perform interior orientation by flagging fiducial marks and relative orientation by measuring a total of 21 ground control points (Falaschi et al., 2017) on each frame. Additionally, tie points are placed within stereopairs according to the Von Gruber distribution (Kerner et al., 2016). Numerical adjustment of the model is accomplished in the block adjustment stage. A summary of ground control points and tie-point residuals after block adjustment are given in **Table 1**. Once the interior and external orientations are solved, any measured point will have *xyz* coordinates on the model.

Normally, final extraction of the photogrammetric DEM is carried out with automatic procedures, i.e., auto-correlation of homologous points on each stereopair in a photogrammetric software (Cox and March, 2004; Koblet et al., 2010). Instead of relying in automatisms, which will inevitably lead to outliers and data voids (Pieczonka et al., 2011), we materialized the DEMs by on-screen digitalization of breaklines (Lenzano, 2013) using LCD shutter stereoglasses. Breaklines represent natural terrain discontinuities such as mountain crests and valleys, slope changes, crevasses, lakes, or gullies. In general, the more complex the terrain, the denser placing of breaklines and breakline nodes will be. The area covered by the digitized breaklines covers the glaciers themselves but also part of the adjacent stable terrain, which serves for DEM coregistration and estimation of the uncertainty related to the glacier elevation changes (see section "Assessment of the Elevation Change Uncertainty"). Once the breaklines are finalized, they are converted to Triangular Irregular Networks (TINs) and ultimately DEMs are interpolated at 20 m resolution, considering the minor scale of the aerial photos (1:70.000, DEM_{1981} –see **Table 1**). Lastly, the original 1958 and 1981 aerial images are converted to orthofotos using the previously generated DEMs in the Photomod *Mosaic* module.

SRTM and Optical Satellite Imagery-Derived DEMs

Glacier surface topography for February 11–22, 2000, March 8, 2012 and February 28, 2018 were retrieved from SRTM X-band, SPOT 5 and Pleiades DEMs, respectively. These data sets encompass the whole San Lorenzo massif and cover both the Argentinian and Chilean side (**Figure 1**). The SPOT DEM was generated from a 5 m resolution stereo-pair from the SPOT5 HRS sensor and was provided by the SPIRIT project (Korona et al., 2009), whereas the SRTM X-band tiles at 1 arcsec resolution were obtained from the Deutsches Zentrum für Luft und Raumfahrt (DLR) EOWEB Portal[1]. For detailed information on SRTM and SPOT 5 generation, availability, accuracy, spatial resolution and further technical details see Falaschi et al. (2017) and references therein, as the data and processing are equivalent.

To cover the most recent period, stereo Pleiades images (spatial resolution 0.5 m), acquired on 22 February 2018, was used to generate a DEM (hereafter DEM_{2018}) using the NASA ASP stereo Pipeline (Shean et al., 2016). Pleiades data has been successfully applied for geodetic mass balance assessments in several regions, but have so far only been used on few selected sites in the Andes (Berthier et al., 2014; Ruiz et al., 2017). A comprehensive accuracy control test of the DEM_{PLE} using the terrain-surveyed ground control points in Falaschi et al. (2017) is not viable, since unfortunately only four ground control

[1]http://www.eoweb.dlr.de

TABLE 1 | Characteristics of the utilized aerial photos and derived DEMs.

Acquisition date (dd/mm/yyyy)	Camera/lens	Flight scale	Number of frames	Derived DEM name and spatial resolution	Ground control point residuals (m)				Tie points residuals (m)			
						X	Y	Z		X	Y	Z
					RMSE	5.97	8.21	6.12	RMSE	2.81	2.47	6.21
February 1958	WILD RC5/AV	1:35000	34	$DEM_{1958(20\ m)}$	Maximum	12.35	23.5	14.38	Mean	2.09	1.67	4.89
23/02/1981	WILD RC10/UAV II	1:70000	6	$DEM_{1981(20\ m)}$	Minimum	0.58	0.8	0.62	Maximum	6.61	8.36	15.24

points fall within its footprint. The mean difference between the ground control points and DEM_{2018} elevation values was 6.8 m (**Table 1**) which is in line with other Pleiades-derived DEMs where no ground control points were used, tested over a number of mountain ranges (Berthier et al., 2014).

DEM Coregistration and Calculation of Glacier Mass Budget

Determinations of glacier mass change by means of DEM differencing require a good match of the horizontal and vertical coordinates between models. We used the DEM coregistration tool developed by Berthier et al. (2007) to remove potential elevation- and slope-related biases (Nuth and Kääb, 2011).

The total 1958–2018 study period was divided into four time intervals defined by the DEM acquisition dates: 1958–1981, 1981–2000, 2000–2012, and 2012–2018. During coregistration, each DEM pair was projected to UTM Zone 18S and resampled to the coarser DEM resolution (e.g., the photogrammetric DEMS are resampled to 30 m [SRTM], and SRTM and PLE are resampled to 40 m [SPOT 5]), and each slave (later) DEM is horizontally and vertically shifted with respect to the master (earlier) DEM.

The different data acquisition dates means that there might be changeable snow conditions among the investigated time intervals. The most accurate way to determine if there are indeed differences in DEM elevation de to different snow cover would be having *in situ* measurements, which are unfortunately unavailable. Yet, the acquisition dates of all imagery from which DEMs were extracted all stem from the end of the ablation period, and any differences between them should be minimal. We are certain that any snowfall in the months of February–March is rapidly removed and has no real influence in the DEM elevation values.

We term each DEM t_x following the natural chronological order (DEM_{1958}, DEM_{1981}, DEM_{2000}, and so on). For each of them, glacier elevation changes *dh/dt* are calculated by subtracting DEM_{1981}–DEM_{1958}, DEM_{2000}–DEM_{1981}, etc. In addition, we reassess the DEM_{2012}–DEM_{2000} mass budget values of Falaschi et al. (2017), since the averaged 2000–2012 glacier size for their elevation change determinations (see, e.g., Carturan et al., 2013; Fischer et al., 2015) were not considered. Whilst Río Oro, Río Lácteo and San Lorenzo Sur glaciers are fully covered in the 1958 and 1981 aerial photographs, we have also calculated 2012–2018 *dh/dt* values for another 15 glaciers $> 0.3\ km^2$ that are in Chilean territory, and thus are not covered by the Argentinian IGN 1958 and 1981 flights. Coupled with the revised 2000–2012 analysis of Falaschi et al. (2017), this allowed for calculating improved 2000–2018 geodetic mass change values for these glaciers as well.

Because of incomplete coverage of the original frames in the case of aerial photos and low contrast areas where the optical stereo-correlation fails, DEM_{1981} (∼14%) and DEM_{2018} (6%) contain data voids on glacier area, which are transferred to the elevation change grids. The way in which data gaps in elevation change grids are handled may have considerable effects on geodetic mass balance estimations (see Berthier et al., 2018). Here we used a third-degree *polynomial fit to elevation difference by elevation bin*, a method that has proven to yield completely satisfactory results at the individual glacier scale (McNabb et al., 2019). SRTM X-band, SPOT 5, and DEM_{1958} covered the investigated glaciers in full.

The SRTM X-band elevation grids show severe artifacts on the surface of proglacial lakes, which considerably affect the elevation change values. We masked out the affected areas, replacing the original SRTM cells by calculating the mean minus 2σ elevation values and inserting them accordingly.

From the *dh/dt* glacier elevation grids, the total volume change Δv for a given glacier is calculated as:

$$\Delta v = \Delta h \cdot At_i \tag{1}$$

where Δh is the average elevation change of the glacier and At_i the larger (initial) glacier area for a given study interval (e.g., t_0 in t_1-t_0 assuming glacier retreat). Then, the area-averaged specific geodetic mass budget rate Δm in m w.e. a^{-1} can be calculated as:

$$\Delta m = \frac{\Delta v \cdot \rho}{Aa_{(ti+1)-ti}} \cdot t^{-1} \tag{2}$$

being ρ the assumed average density of the glacier, *Aa* the glacier averaged area over a given (t_{i+1})-t_1 period, and *t* the time interval in years. For all the calculations, we considered a mean density of $850 \pm 60\ kgm^{-3}$ (Huss, 2013), which adapts to a number of conditions (Sapiano et al., 1998; Fischer, 2011).

Assessment of the Elevation Change Uncertainty

The estimation of elevation change for a given glacier has an associated uncertainty, which depends on the quality of the two DEMs utilized on each time interval. To calculate this random uncertainty, we apply the same procedure and equations described in detail in Falaschi et al. (2018), which in essence comes back to the approach of Gardelle et al. (2013). Also, Koblet et al. (2010) provide the means for calculating the systematic uncertainty which, because it can have positive or negative sign, is subtracted or added to the elevation change signal.

The method of Gardelle et al. (2013) evaluates the standard deviation of the elevation changes over stable, non-glacierized terrain across 50 m altitude bands covering the glacier elevation range, considering also the degree of spatial autocorrelation of the elevation differences (see Rolstad et al., 2009; Bolch et al., 2017). Since the amount of digitized stable terrain on DEM_{1958} and DEM_{1981} is to some degree restricted, we do not calculate the standard deviation of the elevation changes in buffer areas around glaciers (e.g., Fischer et al., 2015; Falaschi et al., 2017), but rather in the total digitized stable terrain. Neither do we consider a slope threshold to exclude steep areas (which are not representative of glacier surfaces) and sharp edges where the effect of different DEM cell size is increased and reflected as artifacts in the elevation difference grids (see Gardelle et al., 2013). We nevertheless remove pixels exceeding ± 50 m in the stable terrain parts of the elevation change grids (outliers).

Overall, the uncertainty in the volumetric balance for each glacier $E\Delta v_i$ (m^3) equals the standard error $E\Delta h_i$ *(m)* of the elevation differences between DEMs over stable terrain per elevation band weighted by the glacier hypsometry:

$$E\Delta v_i = \sum_{i}^{n} E\Delta h_i * A_i \quad (3)$$

where A_i is the area of each of the elevation bands in m^2.

A further uncertainty factor is the glacier area error E_a introduced when mapping glacier ice. For this purpose, we consider an uncertainty of 5% according to Falaschi et al. (2017), which is perfectly acceptable and indeed more conservative than acknowledged glacier mapping uncertainties using similar imagery (see Paul et al., 2013). Ultimately, the overall uncertainty in the volume calculation $E\Delta v_{tot}$ (m^3) is calculated as the square root of the sum of the squares of the different uncertainty sources:

$$E\Delta v_{tot} = \sqrt{E^2\Delta v_i + E^2\rho + E^2 a} \quad (4)$$

where $E^2\rho$ is the $\pm$ 60 kg m^{-3} density assumption uncertainty (Huss, 2013).

Glacier Outlines and Length Changes

We used the Landsat-derived glacier inventory produced by Falaschi et al. (2017) for the year 2000 (i.e., matching the acquisition date of SRTM) as the basis for the necessary 1958, 1981, 2012, and 2018 glacier outlines. Glacier polygons were manually corrected by visual interpretation of the 1958 and 1981 orthophotos, the SPOT 5 2012 panchromatic scene and a false color RGB 432 composition of the Pleiades 2018 scene, and set in UTM Zone 18S projection. In relation to seasonal snow, there is general consensus that using or finding a ground-truth or reference dataset that can be used to validate glacier outlines is non-trivial (see Paul et al., 2013). Seasonal snow conditions on the images that served for glacier mapping (Landsat TM, SPOT 5 and Pleiades for the years 2000, 2012, and 2108 respectively) were cross-checked with additional Landsat and Sentinel imagery, acquired the year before and after each one of the mapping images. Elevation change grids also help with the interpretation in challenging areas such as debris-covered ice, as there is usually good contrast between the thinning glacier ice and the stable terrain off-glacier.

Quite often, glacier length changes are determined by simply measuring glacier retreat along a single flow- or centerline (see Paul et al., 2009). The Rio Oro, Río Lácteo, and San Lorenzo Sur valley glaciers do not have sharp snouts, but rather wide fronts that recede irregularly, often leaving behind a contorted silhouette. In this regard, we determined glacier length changes following Koblet et al. (2010) as the average length, measured along 50 m separated stripes that are parallel to the main glacier flow, between glacier outlines for a given period. In turn, we calculated the uncertainty in glacier length estimations $\varepsilon\Delta l$ (m) for each time interval between the corresponding pair of scenes according to Hall et al. (2003), considering the diverse pixel size of the utilized images (*ps*, in m) and the coregistration error *CE* (m) between them:

$$\varepsilon\Delta l = \sqrt{ps_1^2 + ps_2^2} + CE \quad (5)$$

As we shifted each image horizontally as per the coregistration results, there is good geolocation match among them and the *CE* term in equation (5) can be omitted.

Analysis of Climate Records in the Monte San Lorenzo Area

Meteorological data are very scarce in Patagonia, a situation that is even more serious in the southern Andean sector (Villalba et al., 2003; Garreaud, 2009), where our study area is located. Daily temperature records at San Lorenzo Sur have been recorded by IANIGLA from March 2002 to July 2009 and from February 2014 to January 2019 using HOBO dataloggers. To establish the spatial representativeness of these temperature records, the monthly temperature anomalies in San Lorenzo Sur (145 months) were compared, using KNMI facilities[2] with ERA5 modeled data over the southern region of South America and neighboring areas.

The San Lorenzo Sur temperature record shows a broad spatial correlation field with correlation coefficients greater than $r > 0.8$ all along the Andean Patagonia from approximately 45 to 53° S (**Figure 2A**). Two meteorological stations with homogeneous temperature records lie within this spatial field of high relationships: Balmaceda (45.912° S, 71.694° W, 517 m a.s.l.) (1963–2019) and Cochrane (47.243° S, 72.586° W, 204 m a.s.l.) (1970–2019), which we used to elaborate a long-term record of regional temperature deviations. We estimated the monthly temperature deviations in both records in relation to their monthly means for the common period 1975–2014 (40 years).

No precipitation records are available around Monte San Lorenzo. The closest series is from Estancia Entre Ríos (EER-48.255° S, 72.219° W, 480 m a.s.l.), located approximately 55 km to the south (**Figure 2B**). Unlike the spatial patterns of temperature, the precipitation correlation fields estimated with the ERA5 records are mostly spatially narrower, particularly on mountainous terrain (**Figure 2B**). However, the relationships are highly significant ($r > 0.6$) over the Andes from 45 to 49° S, including in this more spatially limited range the same meteorological stations used for the construction of the regional temperature record. Consequently, the regional precipitation record was based on Balmaceda (1954–2019) and Cochrane (1974–2019). Since the precipitation in Cochrane (total annual 710 mm) is substantially higher than in Balmaceda (total annual 541 mm), the monthly series were normalized and averaged to obtain the regional precipitation departures.

We compared mass balances variations of Río Oro, Río Lácteo, and San Lorenzo Sur glaciers with the seasonal and annual variations of regional temperature and precipitation. To determine the relationships between mass loss and regional climate variations, we averaged the meteorological records for each of the periods in which glacier mass balances were

[2]https://climexp.knmi.nl

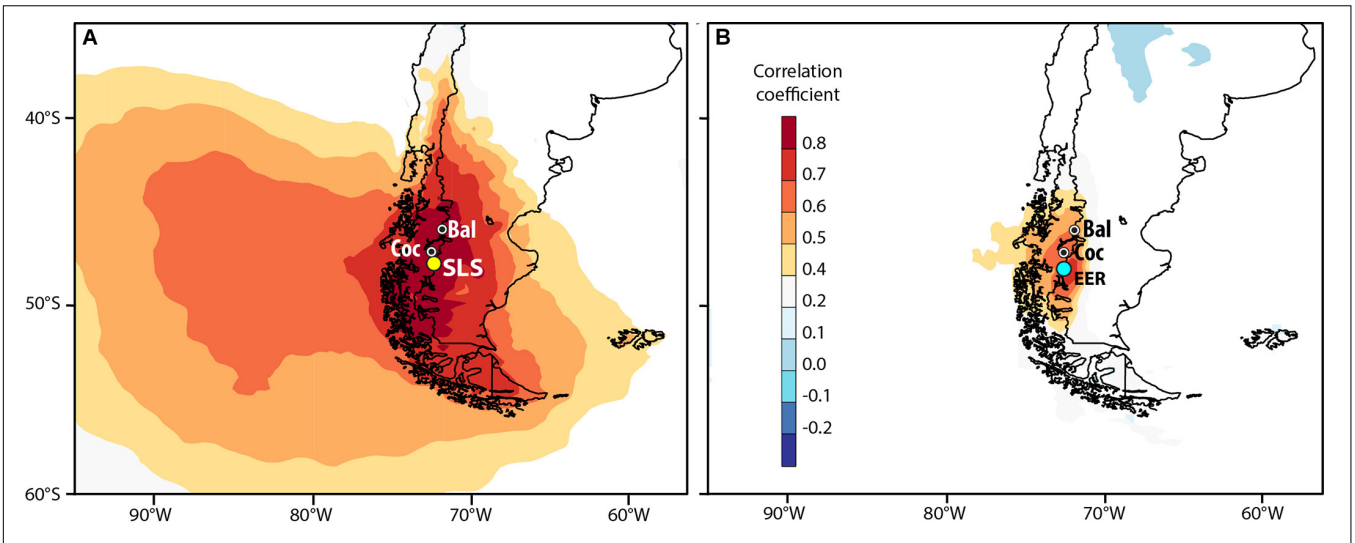

FIGURE 2 | Location of meteorological stations and spatial correlation patterns between monthly anomalies of **(A)** temperature in San Lorenzo Sur (San Lorenzo Sur), **(B)** precipitation in Estancia Entre Ríos (EER), and the corresponding anomalies in ERA5.

established and conducted comparative analyses with climate data individually for each glacier.

RESULTS

Area and Length Changes

The investigated glaciers retreated and shrunk significantly between 1958 and 2018 (**Figures 3**, **4** and **Table 2**). Río Oro, Río Lácteo, and San Lorenzo Sur lost 22 ± 1, 27 ± 1, and 22 ± 1% of their original 1958 area, respectively. This led to an overall glacier area loss rate of 0.46 ± 0.02% a^{-1} among the three glaciers. In general, the area losses and retreat rates were relatively low before 1981. Whereas Río Oro shrunk at a maximum rate of 0.08 km^2 a^{-1} during the 1981–2000 period, San Lorenzo Sur (0.13 km^2 a^{-1}) and Río Lácteo (0.11 km^2 a^{-1}) glaciers reached their maximum area loss rate between 2000 and 2012. During this later period, Río Oro and Río Lácteo had the greatest frontal retreat rates (37 and 78 m a^{-1}, respectively). In absolute terms, San Lorenzo Sur had the greatest recession between 1958 and 2018, with total recoil of ∼2762 ± 88 m.

As a whole, the Monte San Lorenzo glaciers lost ∼3% area from 2000 to 2012 and further ∼4% area between 2012 and 2018. This is equivalent to a total of 9.54 and 0.53 km^2 (about 0.4%) per year since the beginning of the 20th century. Beyond Río Oro, Río Lácteo and San Lorenzo Sur, Calluqueo was the glacier that shrunk the most (−1.16 km^2) in absolute and Ventisquero del Comedor (−26%) in relative terms.

Rio Oro, Río Lácteo, and San Lorenzo Sur 1958–2018 Mass Balance

Our results show that all three glaciers have significantly thinned and lost mass between 1958 and 2018 (**Figures 3–5** and **Table 2**). Glacier downwasting has led to negative cumulative mass balances of −47.0 ± 6.9 m w.e. [−0.78 ± 0.11 m w.e. a^{-1}] (Río Oro), −95.5 ± 4.8 m w.e. [−1.59 ± 0.08 m w.e. a^{-1}] (Río Lácteo) and −99.1 ± 4.0 m w.e. [−1.65 ± 0.07 m w.e. a^{-1}] (San Lorenzo Sur), whereas the total volume loss was around 5257.5 ± 321.5 × 10^6 m^3 a^{-1} overall (among the three glaciers) over the 1958–2018 period. Despite the variation in the glacier mass balance during the different time intervals to a certain degree, we found no positive mass balance conditions on any glacier at any investigated time span.

The altitudinal distribution of elevation changes (**Figure 5**) shows that in general thinning decreases with elevation. Steeper gradients (and more negative absolute values) for all three valley glaciers are observed from the year 1981 onwards compared with the 1958–1981 period, which had a gentler gradient (**Figure 5A**). This resulted in the least negative overall mass budget (−1.09 ± 0.07 10^6 m^3 a^{-1}) for the initial survey period. For all periods, thinning occurred also at high elevations, indicating that equilibrium line altitudes (ELAs) were rising and accumulation areas were shrinking.

Within the 60-year study period, mass balance conditions were at their most negative during the 1981–2000 time interval (**Table 2**), with the total ice volume loss reaching a maximum of 109.7 ± 5.8 × 10^6 m^3 a^{-1}. The mass losses for both Río Oro (−0.91 ± 0.11 m w.e. a^{-1}) and San Lorenzo Sur (−2.23 ± 0.07 m w.e. a^{-1}, i.e., the greatest mass loss for a given glacier) peaked during this period. Subsequently, mass loss rates at Río Oro and San Lorenzo Sur have somewhat diminished, resulting in an overall decreased annual volume loss rate of −81.3 ± 3.7 × 10^6 m^3 a^{-1} (2000–2012) and −75.4 ± 9.5 × 10^6 m^3 a^{-1} (2012–2018), which is similar to the volume loss rate before 1981 (−75.9 ± 4.8 × 10^6 m^3 a^{-1}).

In comparison with the 2000–2012 time interval, the most recent (2012–2018) mass balance assessment has shown dissimilar mass budget amongst the three valley glaciers: San Lorenzo Sur has maintained analogous conditions, Río Lácteo experienced the greatest mass losses for the whole study period

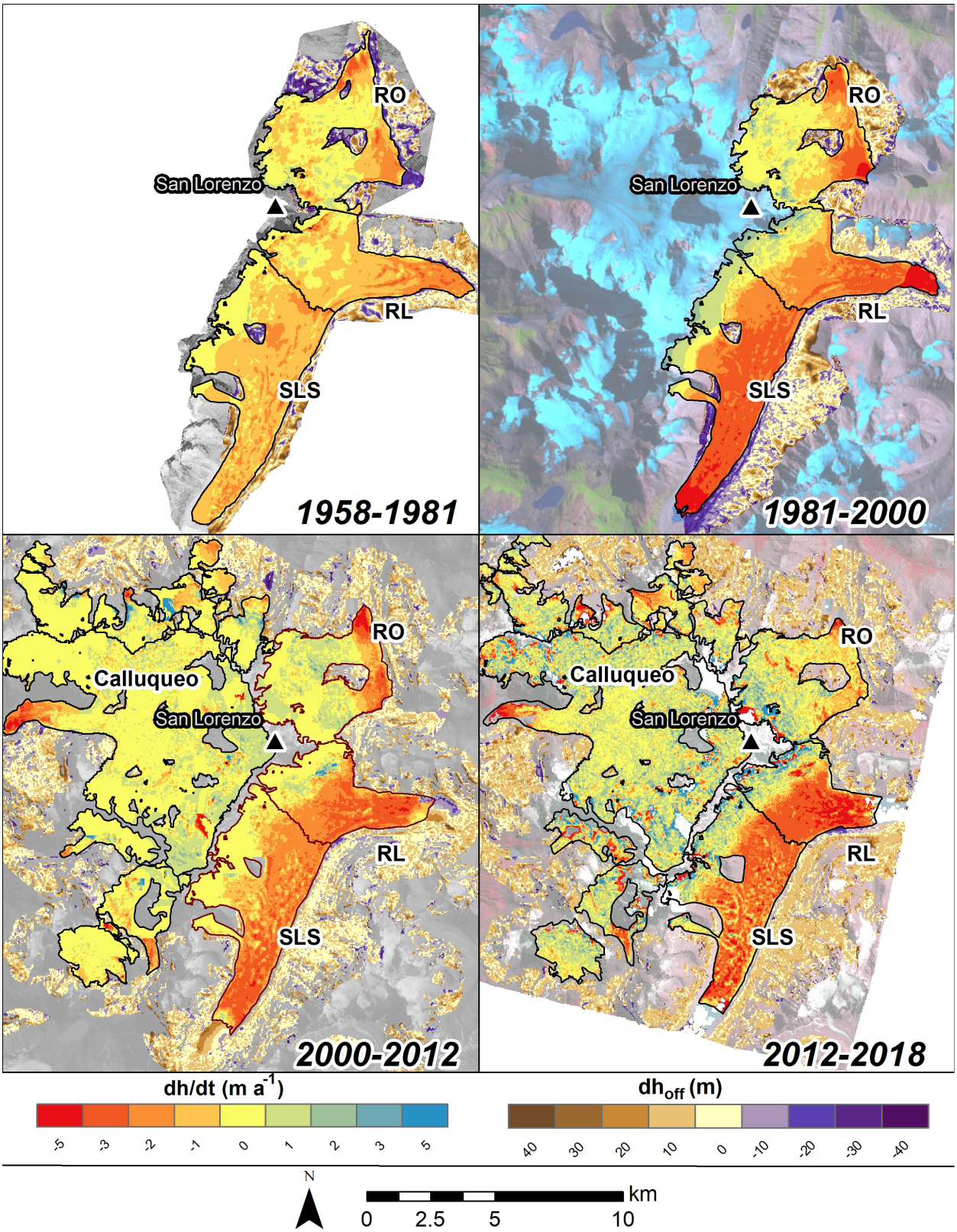

FIGURE 3 | Time-interval glacier annual elevation changes for Rio Oro, Río Lácteo, and San Lorenzo Sur (1958–2018) and the entire San Lorenzo massif (2000–2018). Also shown are elevation changes on stable terrain.

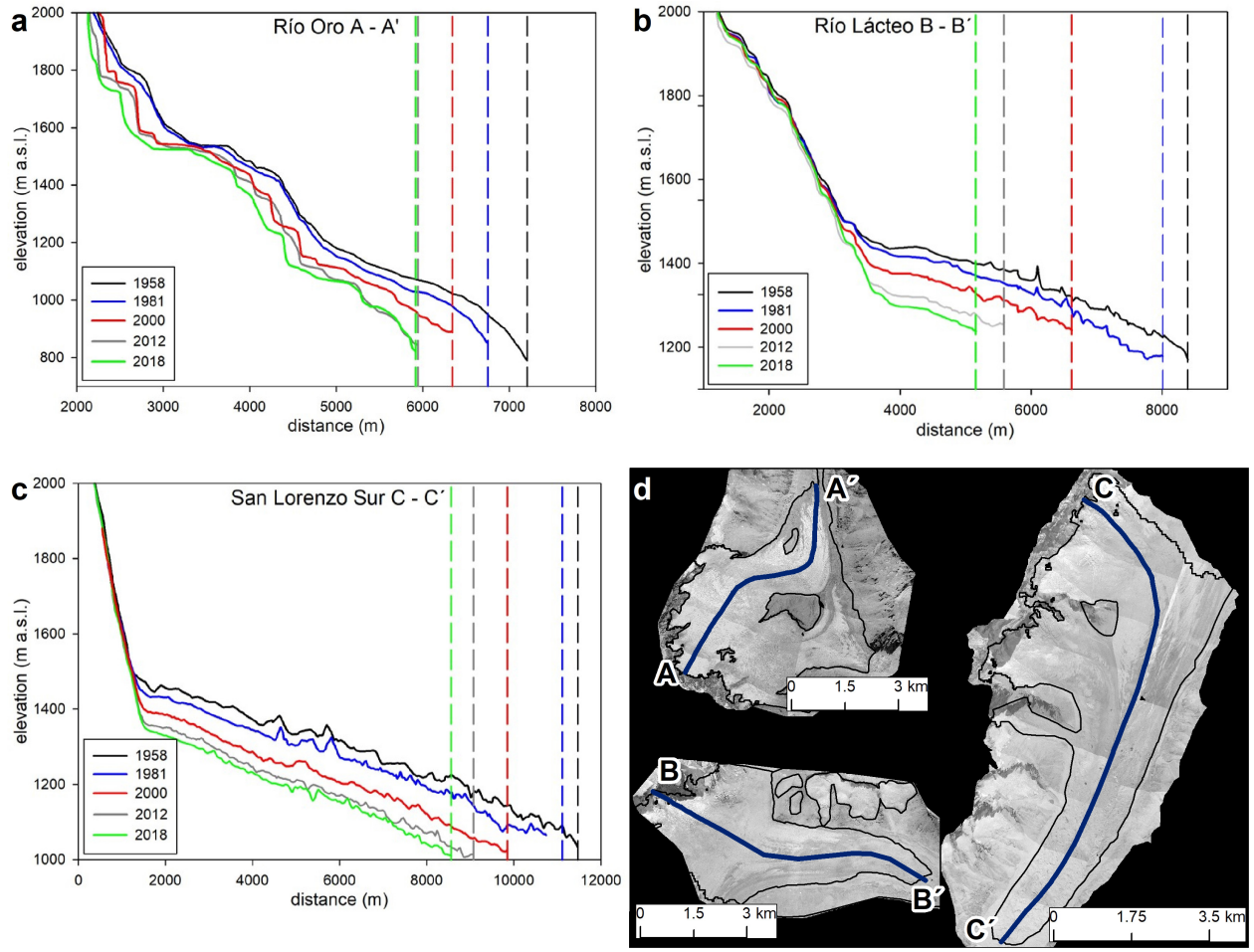

FIGURE 4 | Glacier elevation changes below 2000 m a.s.l. along longitudinal profiles **(d)** of Río Oro **(a)**, Río Lácteo **(b)** and San Lorenzo Sur **(c)**. The dashed lines represent glacier frontal positions and in the case of Río Lácteo and San Lorenzo Sur, depict the expansion of proglacial lakes.

(-2.09 ± 0.15 m w.e. a^{-1}), whilst Río Oro has thinned and lost mass at progressively diminishing rates to an absolute minimum of -0.31 ± 0.21 m w.e. a^{-1} (2012–2018) (**Table 2**).

2012–2018 Mass Balance in the Greater San Lorenzo Massif

We compared the 2012–2018 mass budget of 15 further glaciers (all land-terminating) in the greater San Lorenzo massif mass budgets against those of the 2000–2012 period. Four glaciers maintained similar values of mass balance, five glaciers had more negative mass balances, while six of them showed more positive values (**Table 3**). Overall, the mass budget has shifted to a less negative mass balance from -0.31 ± 0.18 to -0.13 ± 0.21 m w.e. a^{-1}.

At low elevations (~1500 m), these 15 mountain glaciers were thinning and losing mass at generally smaller rates when compared to the three main valley glaciers (**Figures 5B,C**) for a given elevation band, as the lack of calving activity in those smaller, land terminating glaciers results in a minor ice wastage.

Climate Trends

Comparison of the monthly deviations of the regional temperature record with those of San Lorenzo Sur shows a strong relation ($r = 0.75$, $p < 0.01$) over the 145-month common period (**Figure 6A**). A highly significant relationship ($r = 0.64$, $p < 0.01$) was also found between the monthly variations in the regional precipitation and EER records for the 204-month common period (**Figure 6B**). This suggests that the regional temperature (1963–2019) and precipitation (1954–2019) records are representative of the climatic variations in Cerro San Lorenzo, and therefore suitable for comparison with the mass balances in the surrounding glaciers.

Temporal variations in regional temperature and precipitation were analyzed seasonally for summer (October–March), winter (April–September), and yearly (April–March). Summer temperatures have increased by 0.8°C from the early 1960s to the present, at a rate of 0.14°C/decade (**Figure 6C**). In contrast, temperature increases during winter have been more moderate at a rate of 0.03°C/decade (**Figure 6C**). The summer temperature record shows a marked change from negative to

TABLE 2 | Summary of derived glacier change parameters for given time intervals.

Glacier	Volume change (10^6 m^3 a^{-1})	Mass balance (m w.e. a^{-1})	Area t_x (km^2)	Area t_{x+1} (km^2)	Area change (km^2 a^{-1})	Length change (m)
Río Oro						
1958–1981	−18.2 ± 1.9	−0.84 ± 0.09	19.6 ± 1.0	17.8 ± 0.9	−0.08 ± 0.05	−431 ± 14
1981–2000	−18.3 ± 2.3	−0.91 ± 0.11	17.8 ± 0.9	16.2 ± 0.8	−0.08 ± 0.04	−517 ± 32
2000–2012	−13.2 ± 2.2	−0.71 ± 0.12	16.2 ± 0.8	15.5 ± 0.8	−0.07 ± 0.04	−441 ± 32
2012–2018	−5.6 ± 3.7	−0.31 ± 0.21	15.5 ± 0.8	15.2 ± 0.8	−0.05 ± 0.04	−92 ± 10
AVERAGE 1958–2018	16 ± 2.3	−0.78 ± 0.11	–	–	−0.07 ± 0.04	−25 ± 1
TOTAL 1958–2018	–	–	–	–	−4.50 ± 0.22	−1481 ± 88
Río Lácteo						
1958–1981	−23.5 ± 1.2	−1.27 ± 0.07	16.1 ± 0.8	15.3 ± 0.8	−0.03 ± 0.04	−218 ± 14
1981–2000	−29.6 ± 1.6	−1.73 ± 0.09	15.3 ± 0.8	13.8 ± 0.7	−0.08 ± 0.04	−1063 ± 32
2000–2012	−26.9 ± 0.7	−1.74 ± 0.05	13.8 ± 0.7	12.4 ± 0.6	−0.11 ± 0.06	−937 ± 32
2012–2018	−30.0 ± 2.2	−2.09 ± 0.15	12.4 ± 0.6	11.7 ± 0.6	−0.06 ± 0.03	−371 ± 10
AVERAGE 1958–2018	26.8 ± 1.3	−1.59 ± 0.08	–	–	−0.07 ± 0.05	−43 ± 1
TOTAL 1958–2018	–	–	–	–	−4.40 ± 0.22	−2589 ± 88
San Lorenzo Sur						
1958–1981	−34.2 ± 1.6	−1.18 ± 0.06	25.0 ± 1.2	24.1 ± 1.2	−0.04 ± 0.06	347 ± 14
1981–2000	−61.7 ± 1.9	−2.23 ± 0.07	24.1 ± 1.2	22.9 ± 1.1	−0.06 ± 0.06	−1047 ± 32
2000–2012	−41.3 ± 0.8	−1.61 ± 0.03	22.9 ± 1.1	20.5 ± 1.0	−0.12 ± 0.05	−792 ± 32
2012–2018	−39.8 ± 3.6	−1.71 ± 0.16	20.5 ± 1.0	19.5 ± 1.0	−0.15 ± 0.05	−576 ± 10
AVERAGE 1958–2018	44.9 ± 1.7	−1.65 ± 0.07	–	–	−0.09 ± 0.06	−46 ± 1.5
TOTAL 1958–2018	–	–	–	–	−5.30 ± 0.27	−2762 ± 88

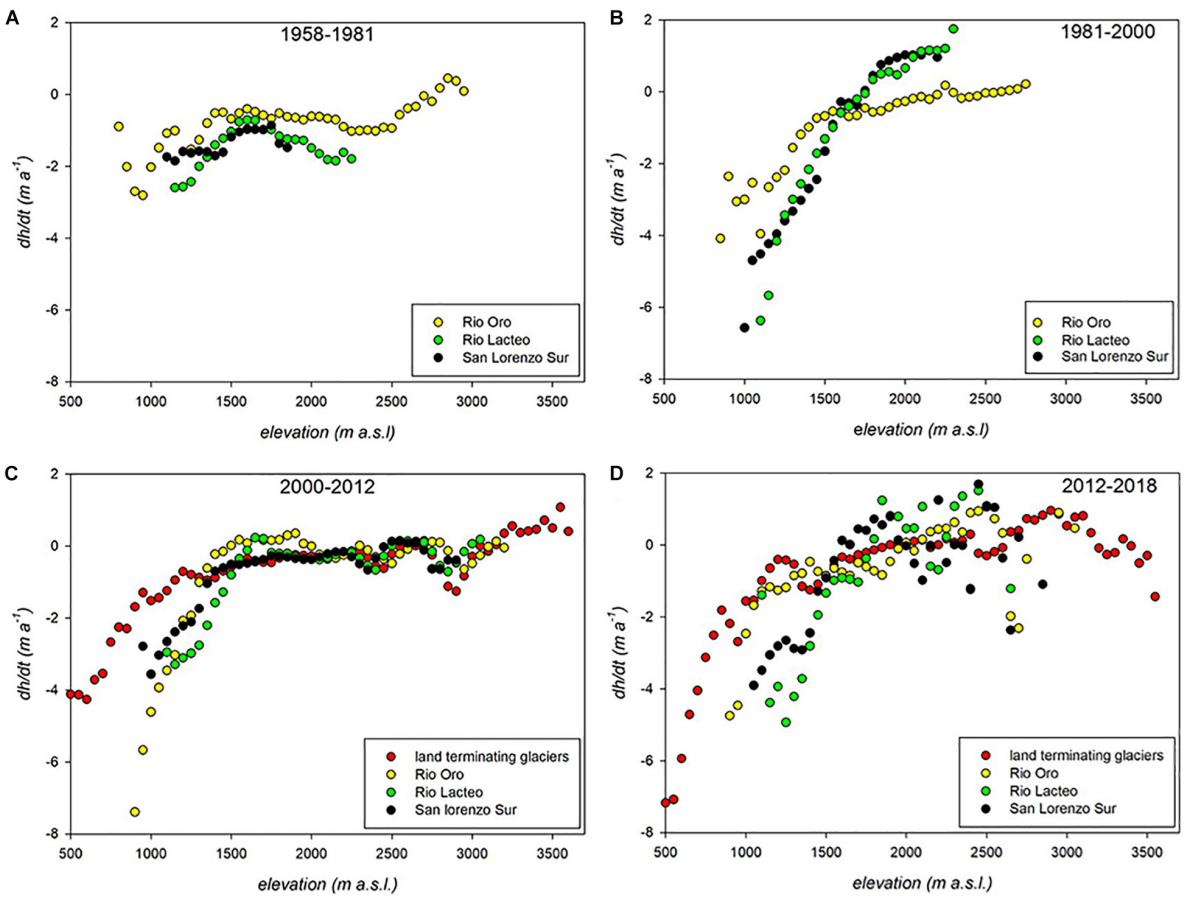

FIGURE 5 | Scatter plot showing glacier elevation change rates as a function of elevation for individual time periods **(A–D)**.

TABLE 3 | Mass budget comparison of 15 land-terminating glaciers in the western side of the main ridge and the three valley glaciers in the east flank of Monte San Lorenzo.

Glacier	$Area_{2018}$ (km^2)	Mass balance (m w.e. a^{-1})		Volume change (10^6 m^3 a^{-1})		Mass balance (m w.e. a^{-1})	Observable causes of mass balance difference between the 2000–2018 and 2000–2016 surveys			
		2000–2012	2012–2018	2000–2012	2012–2018	2000–2016*	Ice divides	Missing debris cover	DEM artifacts	Survey period
Tres Lagunas	1.48 ± 0.07	−0.45 ± 0.08	−0.07 ± 0.17	−0.6 ± 0.2	−0.1 ± 0.3	−0.55 ± 0.27	✓			✓
Tres Lagunas$_I$	0.70 ± 0.03	−0.32 ± 0.08	0.46 ± 0.19	−0.3 ± 0.1	0.4 ± 0.2	−0.39 ± 0.27			✓	
Tres Lagunas$_{II}$	0.35 ± 0.02	−0.54 ± 0.05	−0.18 ± 0.18	−0.3 ± 0.1	−0.1 ± 0.1	−0.57 ± 0.27	✓			
Tres Lagunas$_{III}$	0.30 ± 0.01	−0.19 ± 0.10	0.01 ± 0.18	−0.1 ± 0.1	0.0 ± 0.1	n/a	✓			
Del Dedo Soto	0.89 ± 0.04	−0.51 ± 0.05	−1.90 ± 0.16	−0.6 ± 0.1	−1.7 ± 0.2	−0.85 ± 0.27				✓
del Tranquilo Oeste	4.24 ± 0.21	−0.2 ± 0.15	−0.22 ± 0.20	−1.1 ± 0.1	−1.8 ± 1.0	−0.27 ± 0.27				
del Tranquilo Este	3.17 ± 0.16	−0.09 ± 0.09	−0.54 ± 0.18	−0.3 ± 0.1	−1.0 ± 0.7	−0.35 ± 0.27				✓
Feruglio	0.58 ± 0.03	−1.17 ± 0.05	−1.15 ± 0.21	−1.3 ± 0.1	−1.0 ± 0.2	−1.24 ± 0.27				
Del Comedor	0.76 ± 0.04	−0.74 ± 0.08	−0.64 ± 0.20	−0.8 ± 0.1	−0.6 ± 0.2	−0.72 ± 0.27				
de Agostini	2.91 ± 0.14	−0.06 ± 0.07	−0.37 ± 0.25	−0.3 ± 0.2	−1.3 ± 0.9	−0.08 ± 0.27	✓			✓
Del Baluarte	2.95 ± 0.15	−0.05 ± 0.10	−0.64 ± 0.20	−0.2 ± 0.1	−2.1 ± 0.7	−0.72 ± 0.27				✓
Calluqueo	49.71 ± 2.48	−0.31 ± 0.21	0.04 ± 0.21	−18.3 ± 11.4	2.0 ± 12.1	−0.18 ± 0.27	✓	✓		
Pedregoso	3.29 ± 0.16	−0.30 ± 0.12	−0.53 ± 0.25	−1.2 ± 0.1	−1.8 ± 1.0	−0.29 ± 0.27				
Cumbre Sur	5.16 ± 0.26	−0.47 ± 0.08	−0.54 ± 0.24	−3.1 ± 0.1	−2.9 ± 14	−0.68 ± 0.27	✓			
de la Balsa	3.96 ± 0.2	−0.43 ± 0.02	0.00 ± 0.18	−2.3 ± 0.1	0.0 ± 0.9	−0.51 ± 0.27			✓	
TOTAL (west flank)	80.45 ± 4.02	−0.31 ± 0.16	−0.13 ± 0.21	−30.8 ± 7.1	−12.0 ± 7.8	−0.18 ± 0.27				
Río Oro	15.27 ± 0.76	−0.71 ± 0.12	−0.31 ± 0.21	−13.1 ± 2.2	−5.6 ± 3.7	−0.34/−0.22 ± 0.27	✓	✓		
Rio Lácteo	11.69 ± 0.58	−1.74 ± 0.05	−2.09 ± 0.15	−26.9 ± 0.8	−30.0 ± 2.2	−1.75 ± 0.27	✓	✓		
San Lorenzo Sur	19.50 ± 0.98	−1.61 ± 0.03	−1.71 ± 0.16	−41.2 ± 0.8	−39.8 ± 3.6					

*The 2000–2012 mass balance and uncertainties have been recalculated from Falaschi et al. (2017). *The 2000–2016 glacier mass balance was calculated from the elevation change grids currently available from Dussaillant et al. (2019), whereas the associated uncertainty is an area-averaged value for the whole Southern Patagonan Andes.*

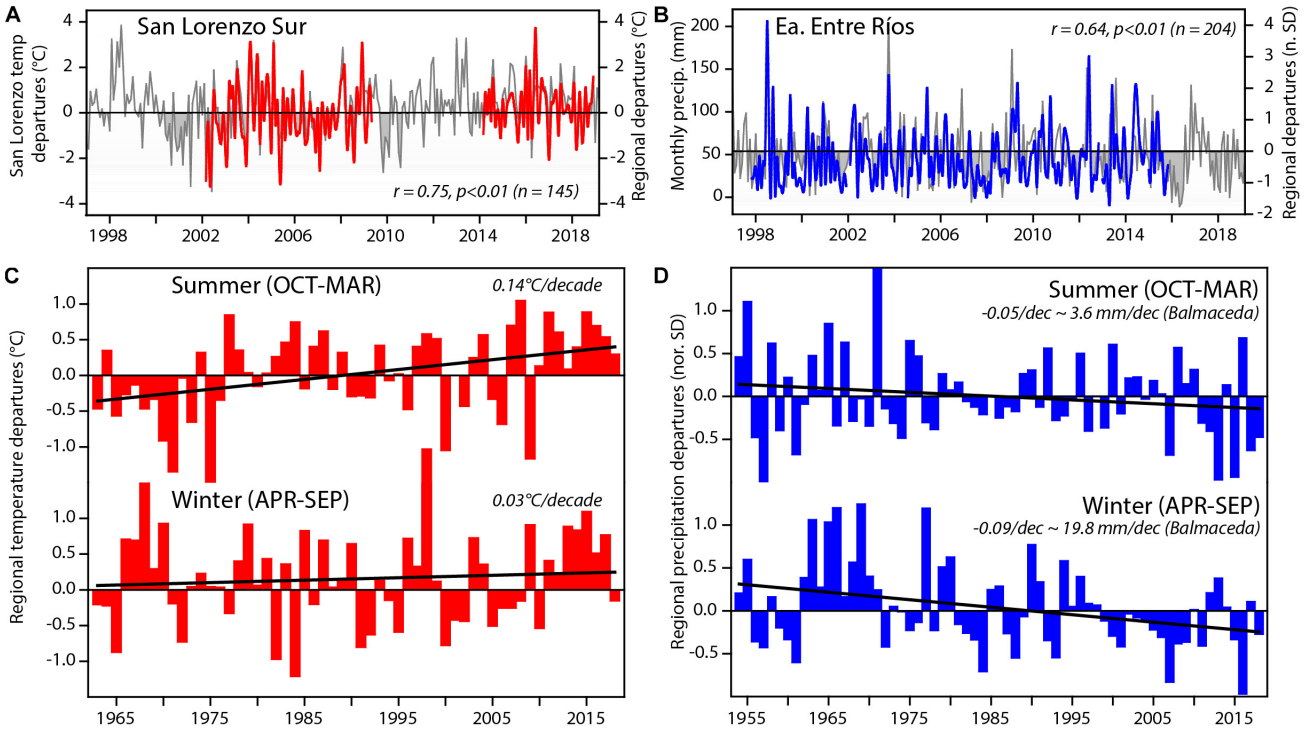

FIGURE 6 | Monthly temperature **(A)** and precipitation **(B)** deviations for San Lorenzo Sur (red) and EER (blue) compared to the regional records based on Balmaceda and Cochrane meterorological stations. **(C,D)** Shows the seasonal (austral summer and winter) monthly temperature (1963–2018) and precipitation (1954–2018) regional departures, respectively. See main text for details.

positive deviations in the years 1976–1977 associated with the phase change in the Pacific Decadal Oscillation (see Villalba et al., 2003; Garreaud, 2018). In contrast to summer temperatures, the most important changes in precipitation have been recorded in winter precipitation (**Figure 6D**). Based on Balmaceda's seasonal precipitation, reduction rates are 3.6 mm and 19.8 mm/decade for summer and winter, respectively (**Figure 6D**), representing an annual reduction of around 25 mm/decade approximately from 1954 to the present.

Climate Variability and Mass Balance

We observed a close relationship between the averaged Río Lácteo and San Lorenzo Sur mass balance and summer temperatures over the 1958–2018 period. The average mass loss per period was used since we noticed a similar mass balance for the Río Lácteo and San Lorenzo Sur glaciers (**Table 2**), whereas for Río Oro glacier we did not observe a clear relationship between the temporal mass balance evolution and the regional climatic variability.

The period with the least negative mass balance (1958–1981), showing a mean mass loss of −1.23 m w.e. a^{-1} (−1.27 and −1.18 m w.e. a^{-1} for Río Lácteo and San Lorenzo Sur), corresponds to negative summer temperature deviations of −0.30°C, relative to the 1963–2019 mean. In contrast, the most negative mass budget of −1.9 m w.e. a^{-1} (−2.09 and −1.71 m w.e. a^{-1} for Río Lácteo and San Lorenzo Sur) found for the 2012–2018 interval, was concurrent with a mean summer temperature departure period of + 0.48°C (**Figure 7A**). It is also worth noting that the reduction in the Río Lácteo-San Lorenzo Sur mass loss rate from −1.98 m w.e. a^{-1} to −1.68 m w.e. a^{-1} in 2000 was accompanied by a reduction in summer temperature anomalies between the 1981–2000 and 2000–2012 periods, from 0.16 to 0.09°C, respectively (**Figure 7A**).

Similarly, the loss of mass of the Río Lácteo and San Lorenzo Sur glaciers coincided with a decrease in regional rainfall from at least the mid-1950s, when the precipitation record in Balmaceda started (**Figure 7B**). Total annual rainfalls in the Balmaceda meteorological station were 636, 547, 530, and 455 mm for the 1958–1980, 1981–1999, 2000–2011, and 2012–2018 intervals, respectively. The reduction of total annual precipitation in Balmaceda has been gradual and did not have a recovery period, totalizing a reduction of more than 180 mm between 1958–1980 and 2012–2018.

The overall decrease in winter precipitation (except for the 2012–2018 period) is only consistent with the 1981–2000 shift in mass budget toward more negative conditions (**Figure 7B**) from −1.23 m w.e. a^{-1} (1958–1981) to −1.98 m w.e. a^{-1} (1981−2000).

Correlation analyses between mass balance and climate variables (**Table 4**) show quite high r values, though they are statistically not significant owed to the small number of observations (just 4 mass balance observation intervals). Summer temperatures (October–March) and annual precipitation show the greatest r values (r = −0.865 and p = 0.135; r = 0.79 and p = 0.20, respectively.

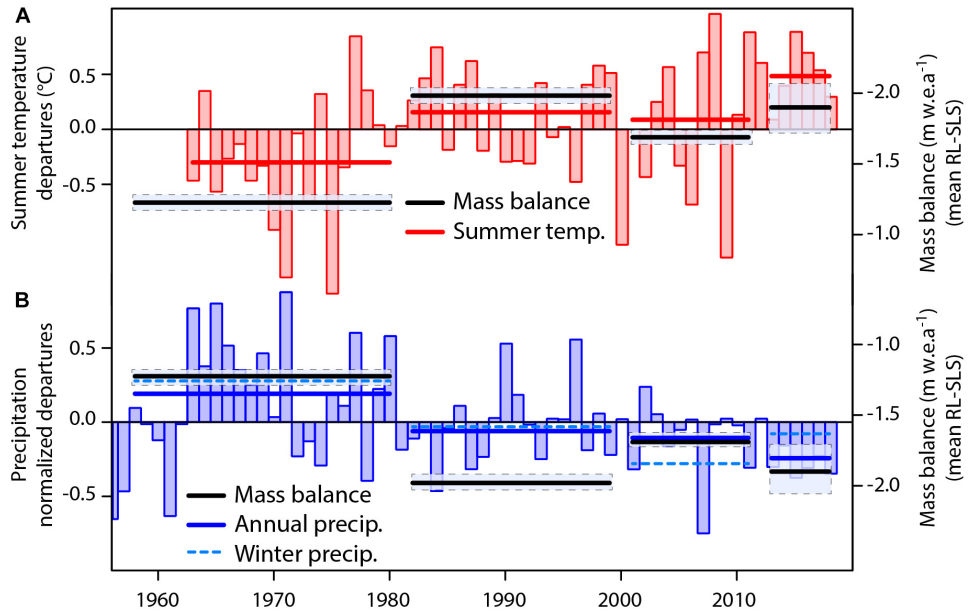

FIGURE 7 | Time-interval variations in glacier mass balance and **(A)** summer (October–March) temperature and **(B)** annual/winter precipitation. In the upper **(A)** panel, the mass balance values on the right axis have been reversed for a better interpretation. Mass balance error bars are shown in the semitransparent boxes.

DISCUSSION

Differences in Mass Balance Among the Investigated Glacier

We have seen that the area and mass losses of glaciers in the Monte San Lorenzo area from 1958 to 2018 are consistent with diminishing precipitations and increasing temperatures in the region (Masiokas et al., 2015). This trend of glacier wastage is in line with glacier changes in Southern Patagonia in general (e.g., Mernild et al., 2015; Dussaillant et al., 2018; Braun et al., 2019). The comparison of our mass budget assessment with that of Dussaillant et al. (2019) for the 2000–2016 period (**Table 3**) shows a relatively good correspondence. At the individual glacier scale, however, some differences arise as a result of (1) different survey time interval (2) local artifacts and data gaps in accumulation regions in the ASTER DEMs (see Dussaillant et al., 2018) or in our own DEMs and particularly (3) the rawness of the Randolph Glacier Inventory outlines used in Dussaillant et al. (2019), which often miss debris covered ice parts and have limitations on the definition of glacier divides, leading to rather different glacier limits. Whilst artifacts and varying ice divides may lead to either positive or negative biases in mass balance (e.g., Tres Lagunas, Cumbre Sur), omitting debris cover ice leads to less negative mass budgets, as debris concentrates in the lowermost parts of glaciers where thinning is usually at the highest. The mass balance of some glaciers (e.g., del dedo Soto, del Tranquilo Este) seems to have changed quite significantly from 2000–2012 to 2012–2018. Consequently, our geodetic mass balance assessment with intermediate points in time (2000-2012-2018) should in principle shed more light on shorter-term variations in comparison with the continuous (2000–2016) survey.

The described pattern of highly negative mass balance conditions at Río Lácteo and San Lorenzo Sur and milder rates at Río Oro and overall of the other 15 mountain glaciers described in Sections "Rio Oro, Río Lácteo, and San Lorenzo Sur 1958–2018 Mass Balance" and "2012–2018 Mass Balance in the Greater San Lorenzo Massif" is consistent throughout the full 1958–2018 period. We interpret these results in view of the different glaciological characteristics such as glacier morphometry, debris cover, ice-calving fronts and supra- and proglacial lakes in particular.

In a regional scale assessment, Falaschi et al. (2017) found significant correlation between mass balance and glacier size (negative) and orientation (positive), implying that on average, the largest, N-NE facing glaciers have the highest thinning rates. Also, we noted a negative correlation between mass balance and slope and no apparent relation between mass balance and median elevation (see also Le Bris and Paul, 2015). These relations emerge from the fact that the larger glaciers in the area (Río Lácteo and San Lorenzo Sur among them) are typically valley

TABLE 4 | Climate and mass balance correlation analyses.

Climate variable	Correlation with Río Lácteo and San Lorenzo Sur averaged mass balance	
	R	p
Summer (October–March) temperature	−0.865	0.135
Summer (December—March) temperature	−0.791	0.208
Annual precipitation	0.793	0.207
Summer (October–March) precipitation	0.577	0.422
Winter (April–September) precipitation	0.669	0.330

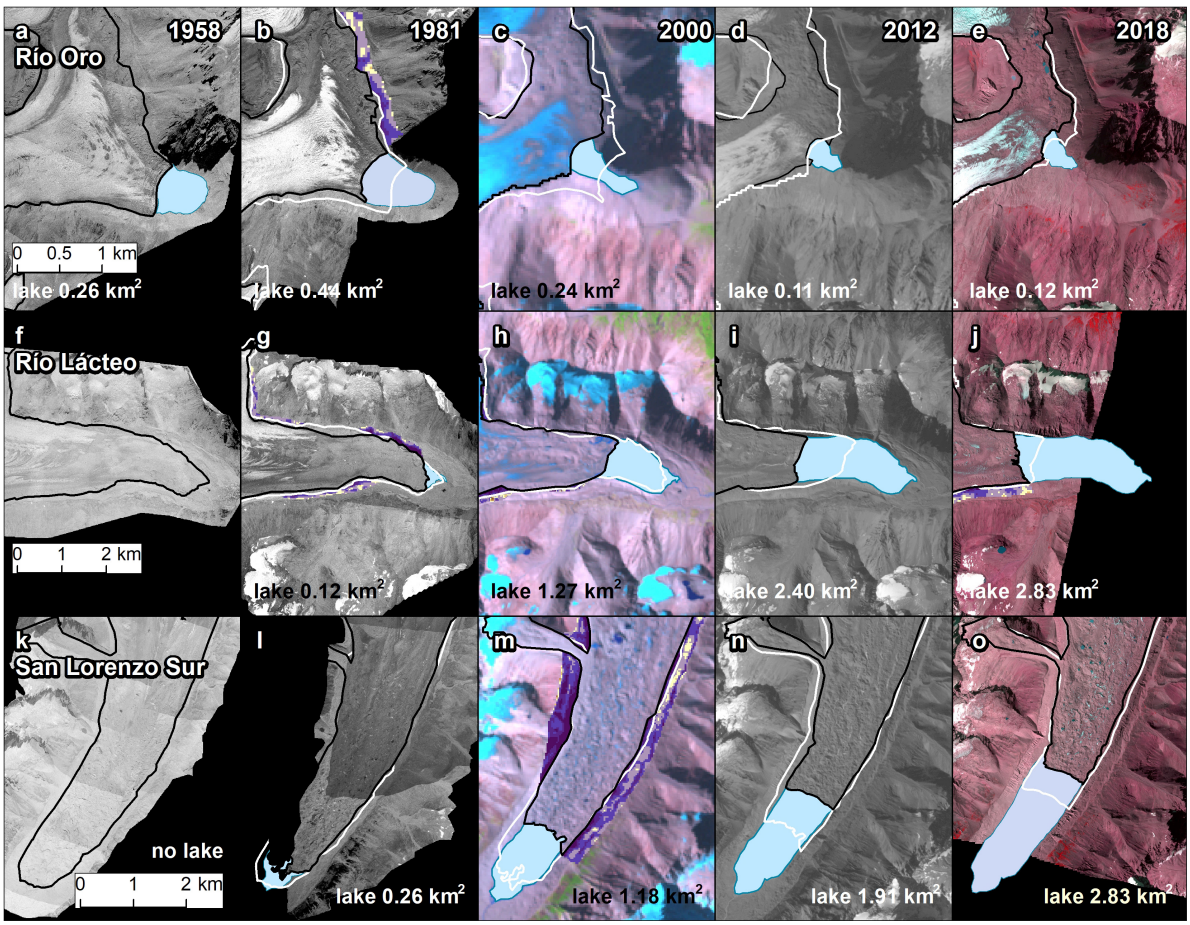

FIGURE 8 | Glacier outline and proglacial lake changes in the Río Oro **(a–e)**, Río Lácteo **(f–j)**, and San Lorenzo Sur **(k–o)** glaciers. Black lines represent glacier outlines from the actual survey year on each panel and white lines correspond to the previous survey year. The bluish areas adjacent to glacier outlines show the degradation of lateral moraines in response to glacier downwasting (the color scheme is the same as in **Figure 3**).

glaciers with flatter termini compared with the smaller and steeper mountain glaciers (the mean slope of the San Lorenzo Sur [∼7°] and Río Lácteo [∼8°] tongues, considerably lower than the Río Oro snout [∼18°]) and flow down into the valley floors, where air temperatures are higher and melt rates increase. On the other hand, and in the Southern Hemisphere, N-NE facing slopes receive the most solar radiation, whereas S-SE orientated slopes receive the least and are in the lee side of the prevailing Westerlies.

The aforementioned variable glacier geometry, that in turn affects glacier climatic response, may be further modified by the presence of debris cover and proglacial lakes. Debris cover can lead to more stable glacier tongues (e.g., Scherler et al., 2011; Basnett et al., 2013 and references therein). Whilst the debris cover of Río Lácteo and San Lorenzo Sur were extensive from early on (**Figures 8f,k**), the lowermost portion of the Río Oro tongue has progressively been covered over time (**Figures 8a–e**), resulting in decreasing thinning rates. The sheltering effect can be nevertheless removed if glacier tongues are associated with lake expansion (Basnett et al., 2013; King et al., 2019). Under such circumstances, enhanced downwasting of glacier tongues can be promoted by (a) glacier calving on proglacial lakes leading to glacier disintegration (b) supraglacial lakes and thermokarst ponds, as they represent low-albedo spots and (c) gentle slopes resulting in low flow rates at the glacier terminus causing glacier stagnation (Lüthje et al., 2006; Quincey et al., 2007; Bolch et al., 2008). San Lorenzo Sur and Río Lácteo calve indeed into steadily expanding proglacial lakes, and pro-and supraglacial lakes are common on their surface (see **Figure 8**), whereas neither Río Oro nor the 15 mountain glaciers have proglacial lakes adjoining glacier terminus (**Figure 1**).

The difference in mass budget, owed to the presence of freshwater calving fronts at Río Lácteo and San Lorenzo Sur and the land-terminating northern snout of Río Oro, was already noted by Falaschi et al. (2017). Using the same dataset from these authors, we conducted a *t*-test and found that in the glacierized area east of the NPI and SPI, the 2000–2012 thinning rate of lake terminating glaciers (-0.88 m a^{-1}) was significantly higher ($p < 10^{-8}$) than that of land terminating glaciers (-0.27 m a^{-1}) at the 95% confidence level. At an even broader scale, also the

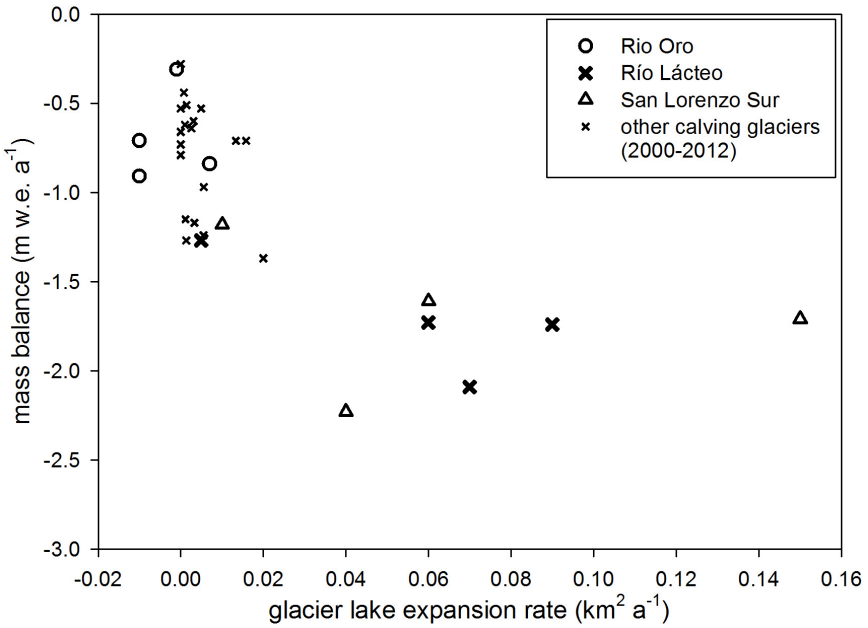

FIGURE 9 | Scatter plot showing the relation between glacier mass balance and proglacial lake expansion rates.

outlet glaciers of the SPI and NPI have shrank alongside the increase in debris covered-ice and glacial lake area, whereas for the smaller, mostly debris-free glaciers, no relation was found between the proportion of debris-covered ice and annual rates of glacier retreat (Loriaux and Casassa, 2013; Glasser et al., 2016). Moreover, the negative 1981–2000 Río Lácteo and San Lorenzo Sur mass budget might be underestimated to some extent, as proglacial lake depth has not been accounted for due to the lack of bathymetry data (Bolch et al., 2011a).

To sum up, the 2000–2012 and 2012–2018 mass budgets of Río Lácteo and San Lorenzo Sur are much more negative when put into a wider regional context where land-terminating glaciers prevail (**Table 2**) whereas the mass budget of Río Oro fits well within the variability of the remaining glaciers in the Monte San Lorenzo (**Table 3**). We thus suggest that, whilst the overall negative mass budget in the Monte San Lorenzo area is congruent with the observed climatic trends of increasing summer temperatures and decreasing precipitation, the enhanced ablation owed to the presence of proglacial lakes is added or superimposed on the climatic signal, leading to much more negative mass balance values for Río Lácteo and San Lorenzo Sur. Research results in the Himalaya, where glacier-lake interactions are common, concluding that lake-terminating glaciers thin and retreat at a higher rate compared to neighboring land-terminating glaciers (Basnett et al., 2013; Thakuri et al., 2016; King et al., 2018, 2019).

Evolution of Proglacial Lakes

We put forward that the variation in mass balance along the study period is linked to the timing of initiation and expansion of proglacial lakes (**Figure 8**). In general terms, it can be argued that higher expansion rates are consistent with more negative mass balances, whilst for low rates of expansion, the mass balance seems to be insensitive (**Figure 9**). **Figure 9** also confirms that the San Lorenzo Sur and Río Lácteo mass balance is considerably more negative compared to other glaciers in the area and expansion of their respective proglacial lakes occurs at a much higher rate. A closer look at the San Lorenzo Sur and Río Lácteo lake area values in **Figure 8** reveals nonetheless that the relation between thinning rates and lake expansion rates is not straightforward. Before 1981, formation of proglacial lakes was merely incipient (**Figures 8b,g,l**) and calving presumably limited, hence minor thinning rates were observed. The greatest thinning rates for San Lorenzo Sur occurred between 1981 and 2000, and comparatively minor rates persisted, though the proglacial lake expanded at increasing rates in the subsequent years (0.06–0.15 km a^{-1}, see **Figures 8n,o** and **Table 5**). On the other hand, the negative mass budget of Río Lácteo peaked only in the most recent years, and yet the lake expansion rate has remained fairly constant (0.06–0.09 km a^{-1}) since 1981. Such contrasting patterns of glacier thinning and lake area increase were also found in the Himalayas (Basnett et al., 2013; Thakuri et al., 2016). In some instances, however, lake growth can be limited due to steep glacier or headwall topography (Zhang et al., 2019). In the case of Río Lácteo and San Lorenzo Sur, proglacial lakes are mostly developing at the expense of relatively flat glacier tongues, and thus are free to expand further and may eventually coalesce in future years. The onset of calving, following proglacial lake formation, accelerating glacier retreat and thinning is not new for Patagonia, as it had been already acknowledged in the large calving glaciers in the Patagonian Icefields by Warren and Aniya (1999). Moreso, proglacial lakes in Southern Patagonia, have been expanding at increasingly higher rates since the 1980s (Wilson et al., 2018).

TABLE 5 | Time-interval proglacial lake growth rates.

Glacier	Glacial lake expansion rate (km^2 a^{-1})			
	1958–1981	1981–2000	2000–2012	2012–2018
Rio Oro	0.007	−0.01	−0.01	−0.001
Río Lácteo	0.005	0.06	0.09	0.07
San Lorenzo Sur	0.01	0.04	0.06	0.15

A proglacial lake has also developed at the southeastern tip of Río Oro glacier but contrary to the proglacial lakes at Río Lácteo (**Figures 10a–c**) and San Lorenzo Sur, shrunk in area over time although this proglacial lake is deeply confined by terminal moraines and no observable surface drainage system is evident (**Figures 8a–d**). We hypothesize that water from this small lake has found its way out to the northern terminus of Río Oro glacier via subglacial conduits, following the northward regional slope. The emptying of the lake has been apparently gradual (**Table 5**), and not sudden as in an ice-dammed lake outburst flood (Glazirin, 2010; Grinsted et al., 2017). This way, the proglacial lake has not expanded further and thinning rates have not increased. In addition to the increasingly larger area covered by debris, we suggest that after an initial period of relatively high thinning and mass loss at lower elevations (**Figures 10d,e**), Río Oro glacier is rapidly adjusting to present-day climate conditions and thinning rates are largely independent from glacier-lake interactions.

On a side note, the evolution of these proglacial lakes and glacier area and volume changes must be closely monitored, and the morphometry of its surrounding moraines and valleys evaluated, as potentially dangerous events such as moraine breaching and glacial lake outburst floods (GLOF) need to be identified (Bolch et al., 2011b; Aggarwal et al., 2017; Iribarren Anacona et al., 2015; Wilson et al., 2018; Allen et al., 2019). Slope failure and moraine instability may be induced by stress release in recently deglaciated areas (Cossart et al., 2008) and in effect, certain periods have been characterized by moraine debuttressing at the valley glaciers of Monte San Lorenzo (**Figure 8**, various panels and **Figures 10d,e**). Some minor infrastructure of the Perito Moreno National Park (trekkers trails and huts) lie on the outwash plain and fluvial terraces within very few kilometers of the proglacial lake of Río Lácteo (Laguna Témpanos). The area may be hence subjected to the sudden release of a flash flood in case that a large volume of morainic material shall abruptly enter the lake. As a matter of fact, known GLOFs have occurred recently in rapidly deglaciating, not too distant areas (Harrison et al., 2006; Dussaillant et al., 2010) and elsewhere in Patagonia (Worni et al., 2012).

Putting the Six-Decade Mass Balance Record of Monte San Lorenzo Into a Wider Regional Context

One of the major limitations in glaciological research carried out so far in the Patagonian Andes (45–55° S, sensu Lliboutry, 1956) resides in the fact that the existing records normally initiate after the year 2000 and involve the great outlet glaciers that flow down the Patagonian Icefields but not the smaller, alpine-type glaciers at their margins (Falaschi et al., 2017). These large sea- and lake-terminating glaciers have an inherent cyclic behavior (Rivera et al., 2012), including periods of fast retreat coupled with impressive thinning rates (e.g., Dussaillant et al., 2018; Foresta et al., 2018), which far exceed the observed rates for smaller mountain glaciers nearby (Falaschi et al., 2017). Indeed, these authors found an overall mass loss of 0.46 ± 0.37 m w.e. a^{-1} for the glaciers located east of the NPI and SPI for the 2000–2012 period, including the Monte San Lorenzo area.

A number of researches concerning Patagonian glaciers whose study period is effectively enclosed in our 1958–2018 time span analysis have been nevertheless carried out at the fresh-water calving Chico (SPI) and Benito (NPI) glaciers. Glaciar Chico thinned at 1.7 ± 0.7 m a^{-1} on average during 1975–2001 (Rivera et al., 2005). In coincidence with our results from Río Lácteo and San Lorenzo Sur glaciers, the thinning rates determined for Benito glacier before the year 2000 (2.9 ± 0.4 m a^{-1}) were higher than for the 2000–2013 period (1.9 ± 0.7 m a^{-1}). Yet, the approximately quadrupled (7.7 ± 3.0 m a^{-1}) thinning rates between 2013 and 2017 from Benito glacier (Ryan et al., 2018) are contrary to the somewhat diminished thinning values observed for 2012–2018 at Monte San Lorenzo. Post-2000 mass loss at

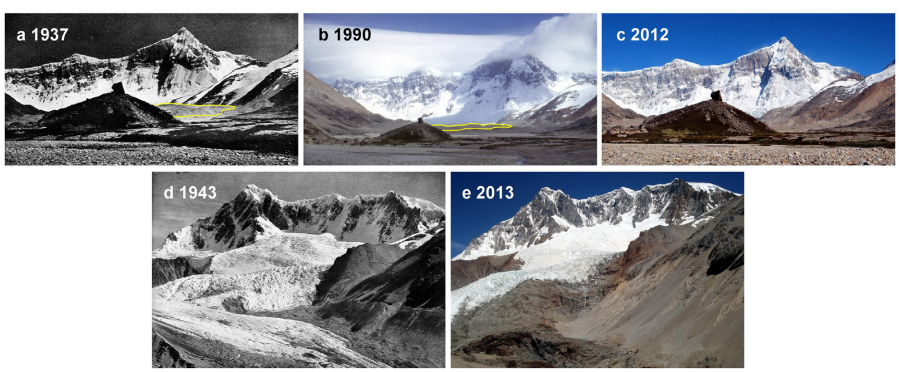

FIGURE 10 | Paired photographs of the Río Lácteo (**a–c**, in yellow line) and Río Oro **(d,e)** glaciers. The 1937 and 1943 shots are taken from De Agostini (1945) and the 1990 photo is courtesy of John Mercer.

Río Lácteo and San Lorenzo Sur is also comparable to the average losses at the Cordillera Darwin (69° S) in Chile -1.5 ± 0.6 m w.e. a^{-1}; Melkonian et al., 2013) but considerably high in the context of small mountain glaciers outside the Patagonian Icefileds (-0.70 ± 0.32 m w.e. a^{-1} [NPI] and -0.54 ± 0.17 m w.e. a^{-1} [SPI]; Braun et al., 2019) and glaciers in Southern Patagonia as a whole (-0.86 ± 0.27 m w.e. a^{-1}; Dussaillant et al., 2019). Regardless of the specific thinning rates, the takeaway message of these contributions in relation to the present study lies in that no periods of positive mass balance conditions have been identified between the year 1973 and 2017, in total agreement with our results from the valley glaciers of Monte San Lorenzo. Also, the mass budget of land-terminating, alpine-type glaciers in the Monte San Lorenzo (-0.31 ± 0.18 and -0.13 ± 0.21 m w.e. a^{-1}) for the 2000–2018 period show analogous values to the early 2000s records available for the Monte Tronador in the northern Patagonian Andes (36–45° S) (-0.17 m w.e. a^{-1}, Ruiz et al., 2017).

CONCLUSION

We have determined glacier elevation changes and derived a geodetic mass balance of three valley glaciers in the San Lorenzo massif in the Patagonian Andes by differencing DEMs from aerial images, SPOT5 and Pleiades satellite images and the SRTM-X band. This six-decade assessment here represents, to our knowledge, the longest mass balance record in the Southern Andes in general and in Patagonia in particular.

For the entire 1958–2018 study period, we found sustained, negative mass balance conditions at the three investigated valley glaciers. This trend is confirmed by the investigation of 15 more glaciers at the San Lorenzo massif during the more recent 2000–2018 period. Thinning and mass loss maxima among the three valley glaciers occurred during the 1981–2000 period (-1.67 ± 0.11 m w.e. a^{-1}), with a peak of -2.23 ± 0.07 m w.e. a^{-1} at San Lorenzo Sur. The observed climatic patterns of temperature increase and precipitation decrease over the study period are well-related to the negative mass balance conditions of glaciers in the area. Therefore, the Rio Oro, Río Lácteo, and San Lorenzo Sur glaciers can serve as reference glaciers for future glaciological research and glacier modeling. Most probably, however, feedback mechanisms between proglacial lakes, calving processes and the lowering of the glacier surface found at the Río Lácteo and San Lorenzo Sur tongues, give explanation to the relatively high mass loss rates found at these two glaciers when compared to the land-terminating Río Oro, or the other, smaller mountain glaciers in the Monte San Lorenzo. As a consequence, and whilst the mass budget of the Río Lácteo and San Lorenzo Sur glaciers in recent years (2012–2018) has remained strongly negative, the wider (massif-scale) signal shows a much lower thinning signal, which seems to be closely linked to the climate trends and largely independent from calving or dynamic phenomena. The negative mass balance trend of the last few years nevertheless points out to continuing glacier shrinkage in the Monte San Lorenzo area in particular but also at a broader, regional scale elsewhere in the Patagonian Andes.

DATA AVAILABILITY STATEMENT

The datasets generated for this study are available on request to the corresponding author.

AUTHOR CONTRIBUTIONS

DF designed the study and wrote the manuscript. ML, RV, TB, and AR contributed to the study design and manuscript writing. DF, ML, RV, and AL analyzed the data. All authors contributed to the final version of the manuscript.

FUNDING

This research was funded by the Agencia Nacional de Promoción Científica y Técnica (Grants PICT 2007-0379 and PICT 2016-1282). RV was partially supported by the Foundation BNP-Paribas through THEMES project. AR acknowledges FONDECYT 1171832 and CECs.

ACKNOWLEDGMENTS

The Pléiades stereo-pair used in this study was provided by the Pléiades Glacier Observatory (PGO) initiative of the French Space Agency (CNES). Pléiades data© CNES 2018, Distribution Airbus D&S. Special thanks go to Dr. Etienne Berthier for kindly facilitating the inclusion of this research under the PGO program and generating the Pleaides orthorectified products used in this study. The authors would also like to thank Sergio Cimbaro (IGN), Martín Matula (AEROMAPA), and Luis Lenzano and Pierre Pitte (IANIGLA) for handling and scanning the photographic negatives, and the Ohio State University at Columbus, United States, for making available the John Mercer personal archive. Finally, the authors thank AH (associate editor) and two reviewers for their support and valuable comments that helped to improve the final manuscript.

REFERENCES

Aggarwal, S. C., Rai, P. K., and Thakur, A. E. (2017). Inventory and recently increasing GLOF susceptibility of glacial lakes in Sikkim, Eastern Himalaya. *Geomorphology* 295, 39–54. doi: 10.1016/j.geomorph.2017.06.014

Allen, S. K., Zhang, G., Wang, W., Yao, T., and Bolch, T. (2019). Potentially dangerous glacial lakes across the Tibetan Plateau revealed using a large-scale automated assessment approach. *Sci. Bull.* 64, 435–445. doi: 10.1016/j.scib.2019.03.011

Aniya, M. (2013). Holocene glaciations of Hielo Patagónico (Patagonia Icefield), South America: a brief review. *Geochem. J.* 47, 97–105. doi: 10.2343/geochemj.1.0171

Bakke, J., and Nesje, A. (2011). ""Equilibrium-line-altitude"," in *Encyclopedia of Snow, Ice and Glaciers*, eds V. Singh, V. P. Singh, and U. Haritashya, (Dordrecht: Springer), 268–277.

Basnett, S., Kulkarni, A. V., and Bolch, T. (2013). The influence of debris cover and glacial lakes on the recession of glaciers in Sikkim Himalaya, India. *J. Glaciol.* 59, 1035–1046. doi: 10.3189/2013JoG12J184

Berthier, E., Arnaud, Y., Kumar, R., Ahmad, S., Wagnon, P., and Chevallier, P. (2007). Remote sensing estimates of glacier mass balances in the Himachal Pradesh (Western Himalaya, India). *Remote Sens. Environ.* 108, 327–338. doi: 10.1016/j.rse.2006.11.017

Berthier, E., Larsen, C., Durkin, W. J., Willis, M. J., and Pritchard, M. E. (2018). Brief communication: unabated wastage of the Juneau and Stikine Icefields (Southeast Alaska) in the Early 21st Century. *Cryosphere* 12, 1523–1530. doi: 10.5194/tc-12-1523-2018

Berthier, E., Vincent, C., Magnússon, E., Gunnlaugsson, Á. Þ., Pitte, P., Le Meur, E., et al. (2014). Glacier topography and elevation changes derived from Pléiades sub-meter stereo images. *Cryosphere* 8, 2275–2291. doi: 10.5194/tc-8-2275-2014

Bertone, M. (1960). *Inventario de los glaciares existentes en la vertiente Argentina entre los paralelos 47° 30' y 51° S*. Buenos Aires: Instituto Nacional del Hielo Continental Patagónico.

Bhambri, R., Bolch, T., Chaujar, R. K., and Kulshreshtha, S. C. (2011). Glacier changes in the Garhwal Himalaya, India, from 1968 to 2006 based on remote sensing. *J. Glaciol.* 57, 543–556. doi: 10.3189/002214311796905604

Bolch, T., Buchroithner, M. F., Peters, J., Baessler, M., and Bajracharya, S. (2008). Identification of glacier motion and potentially dangerous glacial lakes in the Mt. Everest Region/Nepal using spaceborne imagery. *Nat. Hazards Earth Syst. Sci.* 8, 1329–1340. doi: 10.5194/nhess-8-1329-2008

Bolch, T., Pieczonka, T., and Benn, D. I. (2011a). Multi-Decadal mass loss of glaciers in the everest area (Nepal Himalaya) derived from stereo imagery. *Cryosphere* 5, 349–358. doi: 10.5194/tc-5-349-2011

Bolch, T., Peters, J., Yegorov, A., Pradhan, B., Buchroithner, M., and Blagoveshchensky, V. (2011b). Identification of potentially dangerous Glacial Lakes in the Northern Tien Shan. *Nat. Hazards* 59, 1691–1714. doi: 10.1007/s11069-011-9860-2

Bolch, T., Pieczonka, T., Mukherjee, K., and Shea, J. (2017). Brief communication: glaciers in the Hunza Catchment (Karakoram) have been nearly in balance since the 1970s. *Cryosphere* 11, 531–539. doi: 10.5194/tc-11-531-2017

Braun, M. H., Malz, P., Sommer, C., Farías-Barahona, D., Sauter, T., Casassa, G., et al. (2019). Constraining glacier elevation and mass changes in South America. *Nat. Clim. Change* 9, 130–136. doi: 10.1038/s41558-018-0375-7

Brun, F., Wagnon, P., Berthier, E., Jomelli, V., Maharjan, S. B., Shrestha, F., et al. (2019). Heterogeneous influence of glacier morphology on the mass balance variability in high mountain Asia. *J. Geophys. Res. Earth Surf.* 124, 1331–1345. doi: 10.1029/2018JF004838

Buttstädt, M., Möller, M., Iturraspe, R., and Schneider, C. (2009). Mass balance evolution of martial este glacier, Tierra Del Fuego (Argentina) for the period 1960–2099. *Adv. Geosci.* 22, 117–124. doi: 10.5194/adgeo-22-117-2009

Carturan, L., Filippi, R., Seppi, R., Gabrielli, P., Notarnicola, C., Bertoldi, L., et al. (2013). Area and volume loss of the glaciers in the ortles-cevedale group (Eastern Italian Alps): controls and imbalance of the remaining glaciers. *Cryosphere* 7, 1339–1359. doi: 10.5194/tc-7-1339-2013

Cogley, J. G. (2009). Geodetic and direct mass-balance measurements: comparison and joint analysis. *Ann. Glaciol.* 50, 96–100. doi: 10.3189/172756409787769744

Corte, A. E., and Espizúa, L. (1981). *Inventario de Glaciares del la Cuenca del río Mendoza*. Mendoza: IANIGLA-CONICET.

Cossart, E., Braucher, R., Fort, M., Bourlés, D. L., and Carcaillet, J. (2008). Slope instability in relation to glacial debuttressing in alpine areas (Upper Durance catchment, southeastern France): evidence from field data and ^{10}Be cosmic ray exposure ages. *Geomorphology* 95, 3–26. doi: 10.1016/j.geomorph.2006.12.022

Cox, L. H., and March, R. S. (2004). Comparison of geodetic and glaciological mass-balance techniques, Gulkana Glacier, Alaska, U.S.A. *J. Glaciol.* 50, 363–370. doi: 10.3189/172756504781829855

Davies, B. J., and Glasser, N. F. (2012). Accelerating shrinkage of patagonian glaciers from the little ice age (˜AD 1870) to 2011. *J. Glaciol.* 58, 1063–1084. doi: 10.3189/2012JoG12J026

De Agostini, A. M. (1945). *Andes Patagónicos: Viajes de exploración a la cordillera patagónica austral*. Buenos Aires: Talleres Gráficos de Guillermo Kraft.

Dussaillant, A., Benito, G., Buytaert, W., Carling, P., Meier, C., and Espinoza, F. (2010). Repeated glacial-lake outburst floods in Patagonia: an increasing hazard? *Nat. Hazards* 54, 469–481. doi: 10.1007/s11069-009-9479-8

Dussaillant, I., Berthier, E., and Brun, F. (2018). Geodetic mass balance of the Northern Patagonian Icefield from 2000 to 2012 using two independent methods. *Front. Earth Sci.* 6:8. doi: 10.3389/feart.2018.00008

Dussaillant, I., Berthier, E., Brun, F., Masiokas, M., Hugonnet, R., Favier, V., et al. (2019). Two decades of glacier mass loss along the Andes. *Nat. Geosci.* 12, 802–808. doi: 10.1038/s41561-019-0432-5

Espizúa, L. (1983). "Glacier and moraine inventory on the eastern slopes of Cordón del Plata and Cordón del Portillo, Central Andes, Argentina," in *Tills and Related Deposits*, eds E. B. Evenson, J. Rabassa, and Schlüchter, (Avereest: Balkema), 381–395.

Falaschi, D., Bolch, T., Lenzano, M. G., Tadono, T., Lo Vecchio, A., and Lenzano, L. (2018). New evidence of glacier surges in the central andes of Argentina and Chile. *Prog. Phys. Geogr. Earth Environ.* 42, 792–825. doi: 10.1177/0309133318803014

Falaschi, D., Bolch, T., Rastner, P., Lenzano, M. G., Lenzano, L., Lo Vecchio, A., et al. (2017). Mass changes of Alpine Glaciers at the Eastern Margin of the Northern and Southern Patagonian Icefields between 2000 and 2012. *J. Glaciol.* 63, 258–272. doi: 10.1017/jog.2016.136

Falaschi, D., Bravo, C., Masiokas, M., Villalba, R., and Rivera, A. (2013). First Glacier inventory and recent changes in glacier area in the monte San Lorenzo Region (47°S), Southern Patagonian Andes, South America. *Arct. Antarct. Alp. Res.* 45, 19–28. doi: 10.1657/1938-4246-45.1.19

Farías-Barahona, D., Vivero, S., Casassa, G., Schaefer, M., Burger, F., Seehaus, T., et al. (2019). Geodetic mass balances and area changes of Echaurren Norte Glacier (Central Andes, Chile) between 1955 and 2015. *Remote Sens.* 11:260. doi: 10.3390/rs11030260

Fieber, K. D., Mills, J. P., Miller, P. E., Clarke, L., Ireland, L., and Fox, A. J. (2018). Rigorous 3D change determination in Antarctic Peninsula Glaciers from stereo WorldView-2 and Archival Aerial Imagery. *Remote Sens. Environ.* 205, 18–31. doi: 10.1016/j.rse.2017.10.042

Fischer, A. (2011). Comparison of direct and geodetic mass balances on a multi-annual time scale. *Cryosphere* 5, 107–124. doi: 10.5194/tc-5-107-2011

Fischer, M., Huss, M., and Hoelzle, M. (2015). Surface elevation and mass changes of all swiss glaciers 1980–2010. *Cryosphere* 9, 525–540. doi: 10.5194/tc-9-525-2015

Foresta, L., Gourmelen, N., Weissgerber, F., Nienow, P., Williams, J. J., Shepherd, A., et al. (2018). Heterogeneous and rapid ice loss over the patagonian ice fields revealed by Cryosat-2 Swath Radar altimetry. *Remote Sens. Environ.* 211, 441–455. doi: 10.1016/j.rse.2018.03.041

Gardelle, J., Berthier, E., Arnaud, Y., and Kääb, A. (2013). Region-Wide Glacier mass balances over the Pamir-Karakoram-Himalaya during 1999-2011. *Cryosphere* 7, 1263–1286. doi: 10.5194/tc-7-1263-2013

Gardner, A. S., Moholdt, G., Cogley, J. G., Wouters, B., Arendt, A. A., Wahr, J., et al. (2013). A reconciled estimate of glacier contributions to sea level rise: 2003 to 2009. *Science* 340, 852–857. doi: 10.1126/science.1234532

Garibotti, I. A., and Villalba, R. (2017). Colonization of mid- and late-holocene moraines by lichens and trees in the magellanic sub-antarctic province. *Pol. Biol.* 40, 1739–1753. doi: 10.1007/s00300-017-2096-1

Garreaud, R., López, P., Minvielle, M., and Rojas, M. (2013). Large scale control on the Patagonia climate. *J. Clim.* 26, 215–230. doi: 10.1175/JCLI-D-12-001.1

Garreaud, R. D. (2009). The andes climate and weather. *Adv. Geosci.* 22, 3–11. doi: 10.5194/adgeo-22-3-2009

Garreaud, R. D. (2018). Record-breaking climate anomalies lead to severe drought and environmental disruption in Western Patagonia in 2016. *Clim. Res.* 74, 217–229. doi: 10.3354/cr01505

Glasser, N. F., Holt, T. O., Evans, Z. D., Davies, B. J., Pelto, M., and Harrison, S. (2016). Recent spatial and temporal variations in debris cover on Patagonian glaciers. *Geomorphology* 273, 202–216. doi: 10.1016/j.geomorph.2016.07.036

Glasser, N. F., and Jansson, K. N. (2008). The Glacial Map of southern South America. *J. Maps* 4, 175–196. doi: 10.4113/jom.2008.102

Glazirin, G. (2010). A century of investigations on outbursts of the ice-dammed lake Merzbacher (central Tien Shan). *Aust. J. Earth Sci.* 103, 171–179.

Grinsted, A., Hvidberg, C. S., Campos, N., and Dahl-Jensen, D. (2017). Periodic outburst floods from an Ice-Dammed Lake in East Greenland. *Sci. Rep.* 7:9966. doi: 10.1038/s41598-017-07960-9

Hall, D. K., Bayr, K. J., Schöner, W., Bindschadler, R. A., and Chien, J. Y. L. (2003). Consideration of the errors inherent in mapping historical glacier positions

in Austria from the ground and space (1893–2001). *Remote Sens. Environ.* 86, 566–577. doi: 10.1016/S0034-4257(03)00134-2

Harrison, S., Glasser, N., Winchester, V., Haresign, E., Warren, C., and Jansson, K. (2006). A glacial lake outburst flood associated with recent mountain glacier retreat, patagonian andes. *Holocene* 16, 611–620. doi: 10.1191/0959683606hl957rr

Huss, M. (2013). Density assumptions for converting geodetic glacier volume change to mass change. *Cryosphere* 7, 877–887. doi: 10.5194/tc-7-877-2013

Iribarren Anacona, P., Mackintosh, A., and Norton, K. P. (2015). Hazardous processes and events from glacier and permafrost areas: lessons from the Chilean and Argentinean Andes. *Earth Surf. Process. Landf.* 40, 2–21. doi: 10.1002/esp.3524

Kerner, S., Kaufman, I., and Raizman, Y. (2016). "Role of Tie-Points distribution in aerial photography," in *Proccedings of the ISPRS International Archives of the Photogrammetry, Remote Sensing and Spatial Information Sciences XL-3/W4*, Lausanne, 41–44. doi: 10.5194/isprsarchives-XL-3-W4-41-2016

King, O., Bhattacharya, A., Bhambri, R., and Bolch, T. (2019). Glacial lakes exacerbate Himalayan glacier mass loss. *Sci. Rep.* 9:18145. doi: 10.1038/s41598-019-53733-x

King, O., Dehecq, A., Quincey, D., and Carrivick, J. (2018). Contrasting geometric and dynamic evolution of lake and land-terminating Glaciers in the Central Himalaya. *Glob. Planet. Change* 167, 46–60. doi: 10.1016/j.gloplacha.2018.05.006

Koblet, T., Gärtner-Roer, I., Zemp, M., Jansson, P., Thee, P., Haeberli, W., et al. (2010). Reanalysis of multi-temporal aerial images of storglaciären, Sweden (1959-99) Part 1: determination of length, area, and volume changes. *Cryosphere* 4, 333–343. doi: 10.5194/tc-4-333-2010

Korona, J., Berthier, E., Bernard, M., Rémy, F., and Thouvenot, E. (2009). SPIRIT. SPOT 5 stereoscopic survey of Polar Ice: reference images and Topographies during the Fourth International Polar Year (2007–2009). *ISPRS J. Photogramm. Remote Sens.* 64, 204–212. doi: 10.1016/j.isprsjprs.2008.10.005

Le Bris, R., and Paul, F. (2015). Glacier-specific elevation changes in parts of western Alaska. *Ann. Glaciol.* 56, 184–192. doi: 10.3189/2015AoG70A227

Lenzano, M. G. (2013). Assessment of using ASTER-Derived DTM for glaciological applications in the Central Andes, Mt. Aconcagua, Argentina. *Photogramm. Fernerkundung Geoinformation* 3, 197–208. doi: 10.1127/1432-8364/2013/0170

Lliboutry, L. (1956). *Nieves y glaciares de Chile, fundamentos de glaciología. [Snow and glaciers of Chile, foundations of glaciology]*. Santiago de Chile: Universidad de Chile.

Loriaux, T., and Casassa, G. (2013). Evolution of Glacial Lakes from the Northern Patagonia Icefield and Terrestrial Water Storage in a Sea-Level Rise Context. *Glob. Planet. Change* 102, 33–40. doi: 10.1016/j.gloplacha.2012.12.012

Lüthje, M., Pedersen, L. T., Reeh, N., and Greuell, W. (2006). Modelling the evolution of Supraglacial Lakes on the West Greenland Ice-Sheet Margin. *J. Glaciol.* 52, 608–618. doi: 10.3189/172756506781828386

Marzeion, B., Jarosch, A. H., and Hofer, M. (2012). Past and future sea-level change from the surface mass balance of glaciers. *Cryosphere* 6, 1295–1322. doi: 10.5194/tc-6-1295-2012

Masiokas, M. H., Delgado, S., Pitte, P., Berthier, E., Villalba, R., Skvarca, P., et al. (2015). Inventory and recent changes of small glaciers on the Northeast Margin of the Southern Patagonia Icefield, Argentina. *J. Glaciol.* 61, 511–523. doi: 10.3189/2015JoG14J094

Maurer, J. M., Schaefer, J. M., Rupper, S., and Corley, A. (2019). Acceleration of Ice Loss across the Himalayas over the Past 40 Years. *Sci. Adv.* 5:eaav7266. doi: 10.1126/sciadv.aav7266

McNabb, R., Nuth, C., Kääb, A., and Girod, L. (2019). Sensitivity of glacier volume change estimation to DEM void interpolation. *Cryosphere* 13, 895–910. doi: 10.5194/tc-13-895-2019

Melkonian, A. K., Willis, M. J., Pritchard, M. E., Rivera, A., Bown, F., and Bernstein, S. A. (2013). Satellite-derived volume loss rates and glacier speeds for the cordillera darwin icefield, Chile. *Cryosphere* 7, 823–839. doi: 10.5194/tc-7-823-2013

Mercer, J. H. (1968). Variations of some Patagonian glaciers since the Late-Glacial. *Am. J. Sci.* 266, 91–109. doi: 10.2475/ajs.266.2.91

Mernild, S. H., Beckerman, A. P., Yde, J. C., Hanna, E., Malmros, J. K., Wilson, R., et al. (2015). Mass loss and imbalance of glaciers along the andes cordillera to the Sub-Antarctic Islands. *Glob. Planet. Change* 133, 109–119. doi: 10.1016/j.gloplacha.2015.08.009

Metzeltin Buscaini, S. (2005). *El macizo del San Lorenzo*. Belluno: Fondazione Giovanni Angelini.

Mölg, N., and Bolch, T. (2017). Structure-from-Motion using historical aerial images to analyse changes in glacier surface elevation. *Remote Sens.* 9:1021. doi: 10.3390/rs9101021

Mölg, N., Bolch, T., Walter, A., and Vieli, A. (2019). Unravelling the evolution of zmuttgletscher and its debris cover since the end of the little ice age. *Cryosphere* 13, 1889–1909. doi: 10.5194/tc-13-1889-2019

Morano-Büchner, C., and Aravena, J. C. (2013). Lichenometric analysis using genus Rhizocarpon, section Rhizocarpon (Lecanorales: Rhizocarpaceae) at Mount San Lorenzo, southern Chile. *Rev. Chil. Hist. Nat.* 86, 465–473. doi: 10.4067/s0716-078x2013000400008

Nuth, C., and Kääb, A. (2011). Co-Registration and bias corrections of satellite elevation data sets for quantifying glacier thickness change. *Cryosphere* 5, 271–290. doi: 10.5194/tc-5-271-2011

Paul, F., Barrand, N. E., Baumann, S., Berthier, E., Bolch, T., Casey, K., et al. (2013). On the accuracy of glacier outlines derived from remote-sensing data. *Ann. Glaciol.* 54, 171–182. doi: 10.3189/2013AoG63A296

Paul, F., Barry, R. G., Cogley, J. G., Frey, H., Haeberli, W., Ohmura, A., et al. (2009). Recommendations for the compilation of glacier inventory data from digital sources. *Ann. Glaciol.* 50, 119–126. doi: 10.3189/172756410790595778

Paul, F., and Mölg, N. (2014). Hasty retreat of glaciers in northern patagonia from 1985 to 2011. *J. Glaciol.* 60, 1033–1043. doi: 10.3189/2014JoG14J104

Pieczonka, T., and Bolch, T. (2015). Region-Wide glacier mass budgets and area changes for the central tien shan between ˜1975 and 1999 using Hexagon KH-9 imagery. *Glob. Planet. Change* 128, 1–13. doi: 10.1016/j.gloplacha.2014.11.014

Pieczonka, T., Bolch, T., and Buchroithner, M. (2011). Generation and evaluation of multitemporal digital terrain models of the Mt. Everest area from different optical sensors. *ISPRS J. Photogramm. Remote Sens.* 66, 927–940. doi: 10.1016/j.isprsjprs.2011.07.003

Popovnin, V., Tatyana, V., Danilova, A., and Petrakov, D. A. (1999). Pioneer mass balance estimate for a patagonian glacier: glaciar De Los Tres, Argentina. *Glob. Planet. Change* 22, 255–267. doi: 10.1016/S0921-8181(99)00042-9

Quincey, D. J., Richardson, S. D., Luckman, A., Lucas, R. M., Reynolds, J. M., Hambrey, M. J., et al. (2007). Early recognition of glacial lake hazards in the himalaya using remote sensing datasets. *Glob. Planet. Change* 56, 137–152. doi: 10.1016/j.gloplacha.2006.07.013

Racoviteanu, A. E., Yves, A., Williams, M. W., and Manley, W. F. (2015). Spatial patterns in glacier characteristics and area changes from 1962 to 2006 in the Kanchenjunga–Sikkim area, eastern Himalaya. *Cryosphere* 9, 505–523. doi: 10.5194/tc-9-505-2015

Racurs, (2006). *Photomod 4.1 User Manual*. Moscow: Racurs.

Ragettli, S., Bolch, T., and Pellicciotti, F. (2016). Heterogeneous glacier thinning patterns over the last 40 years in LangtangHimal, Nepal. *Cryosphere* 10, 2075–2097. doi: 10.5194/tc-10-2075-2016

Rignot, E., Rivera, A., and Casassa, G. (2003). Contribution of the Patagonia Icefields of South America to Sea Level Rise. *Science* 302, 434–437. doi: 10.1126/science.1087393

Rivera, A., Benham, T., Casassa, G., Bamber, J., and Dowdeswell, J. A. (2007). Ice Elevation and Areal Changes of Glaciers from the Northern Patagonia Icefield, Chile. *Glob. Planet. Change* 59, 126–137. doi: 10.1016/j.gloplacha.2006.11.037

Rivera, A., Casassa, G., Bamber, J., and Kääb, A. (2005). Ice-Elevation changes of glaciar chico, southern patagonia, using ASTER DEMs, aerial photographs and GPS data. *J. Glaciol.* 51, 105–112. doi: 10.3189/172756505781829557

Rivera, A., Corripio, J., Bravo, C., and Cisternas, S. (2012). Glaciar jorge montt (chilean patagonia) dynamics derived from photos obtained by fixed cameras and satellite image feature tracking. *Ann. Glaciol.* 53, 147–155. doi: 10.3189/2012AoG60A152

Rolstad, C., Haug, T., and Denby, B. (2009). Spatially integrated geodetic glacier mass balance and its uncertainty based on geostatistical analysis: application to the western Svartisen ice cap, Norway. *J. Glaciol.* 55, 666–680. doi: 10.3189/002214309789470950

Ruiz, L., Berthier, E., Viale, M., Pitte, P., and Masiokas, M. (2017). Recent geodetic mass balance of monte tronador glaciers, North Patagonian Andes. *Cryosphere* 11, 619–634. doi: 10.5194/tc-11-619-2017

Ryan, J. C., Sessions, M., Wilson, R., Wündrich, O., and Hubbard, A. (2018). Rapid surface lowering of benito glacier, Northern Patagonian Icefield. *Front. Earth Sci.* 6:47. doi: 10.3389/feart.2018.00047

Sagredo, E. A., and Lowell, T. V. (2012). Climatology of Andean glaciers: a framework to understand glacier response to climate change. *Glob. Planet. Change* 8, 101–109. doi: 10.1016/j.gloplacha.2012.02.010

Sagredo, E. A., Lowell, T. V., Kelly, M. A., Rupper, S., Aravena, J. C., Ward, D. J., et al. (2017). Equilibrium line altitudes along the Andes during the Last millennium: paleoclimatic implications. *Holocene* 27, 1019–1033. doi: 10.1177/0959683616678458

Sapiano, J. J., Harrison, W. D., and Echelmeyer, K. A. (1998). Elevation, volume and terminus changes of nine glaciers in North America. *J. Glaciol.* 44, 119–135. doi: 10.3189/S0022143000002410

Scherler, D., Bookhagen, B., and Strecker, M. R. (2011). Spatially variable response of himalayan glaciers to climate change affected by debris cover. *Nat. Geosci.* 4, 156–159. doi: 10.1038/ngeo1068

Schmidt, S., and Nüsser, M. (2017). Changes of high altitude glaciers in the Trans-Himalaya of Ladakh over the Past Five Decades (1969–2016). *Geosciences* 7:27. doi: 10.3390/geosciences7020027

Schwikowski, M., Schläppi, M., Santibañez, P., Rivera, A., and Casassa, G. (2013). Net accumulation rates derived from ice core stable isotope records of Pío XI Glacier, Southern Patagonia Icefield. *Cryosphere* 7, 1635–1644. doi: 10.5194/tc-7-1635-2013

Shean, D. E., Alexandrov, O., Moratto, Z. M., Smith, B. E., Joughin, I. R., Porter, C., et al. (2016). An automated, open-source pipeline for mass production of digital elevation models (DEMs) from very-high-resolution commercial stereo satellite imagery. *ISPRS J. Photogramm. Remote Sens.* 116, 101–117. doi: 10.1016/j.isprsjprs.2016.03.012

Strelin, J. A., and Iturraspe, R. (2007). Recent evolution and mass balance of Cordón Martial glaciers. Cordillera Fueguina Oriental. *Glob. Planet. Change* 59, 17–26. doi: 10.1016/j.gloplacha.2006.11.019

Thakuri, S., Salerno, F., Bolch, T., Guyennon, N., and Tartari, G. (2016). Factors controlling the accelerated expansion of Imja Lake, Mount Everest region, Nepal. *Ann. Glaciol.* 57, 245–257. doi: 10.3189/2016AoG71A063

Vargo, L., Amderson, B., Horgan, H., Mackintosh, A., Lorrey, A., and Thornton, M. (2017). Using structure from motion photogrammetry to measure past glacier changes from historic aerial photographs. *J. Glaciol.* 63, 1105–1118. doi: 10.1017/jog.2017.79

Villalba, R., Lara, A., Boninsegna, J. A., Masiokas, M., Delgado, S., Aravena, J. C., et al. (2003). Large-scale temperature changes across the southern Andes: 20th-century variations in the context of the past 400 years. *Clim. Change* 59, 177–232. doi: 10.1007/978-94-015-1252-7_10

Warren, C., and Aniya, M. (1999). The calving glaciers of southern South America. *Glob. Planet. Change* 22, 59–77. doi: 10.1016/S0921-8181(99)00026-0

Wenzens, G. (2002). The influence of tectonically derived relief and climate on the extent of the last glaciation east of the Patagonian ice fields (Argentina, Chile). *Tectonophysics* 345, 329–344. doi: 10.1016/S0040-1951(01)00219-0

WGMS (2017). "Global glacier change bulletin no. 2 (2014-2015)," in *ICSU(WDS)/IUGG(IACS)/UNEP/UNESCO/WMO*, eds M. Zemp, S. U. Nussbaumer, I. Gärtner-Roer, J. Huber, H. Machguth, F. Paul, et al. (Zürich: World Glacier Monitoring Service). doi: 10.5904/wgms-fog-2017-06

Willis, M. J., Melkonian, A. K., Pritchard, M. E., and Rivera, A. (2012). Ice loss from the Southern Patagonian Ice Field, South America, between 2000 and 2012. *Geophys. Res. Lett.* 39:L17501. doi: 10.1029/2012GL053136

Wilson, R., Glasser, N. F., Reynolds, J. M., Harrison, S., Iribarren Anacona, P., Schaefer, M., et al. (2018). Glacial lakes of the Central and Patagonian Andes. *Glob. Planet. Change* 162, 275–291. doi: 10.1016/j.gloplacha.2018.01.004

Wolff, I. W., Glasser, N., and Hubbard, A. (2013). The reconstruction and climatic implication of an independent palaeo ice cap within the Andean rain shadow east of the former Patagonian ice sheet, Santa Cruz Province, Argentina. *Geomorphology* 185, 1–15. doi: 10.1016/j.geomorph.2012.10.018

Worni, R., Stoffel, M., Huggel, C., Volz, C., Casteller, A., and Luckman, B. (2012). Analysis and dynamic modeling of a moraine failure and glacier lake outburst flood at Ventisquero Negro, Patagonian Andes (Argentina). *J. Hydrol.* 444–445, 134–145. doi: 10.1016/j.jhydrol.2012.04.013

Zemp, M., Huss, M., Thibert, E., Eckert, N., McNabb, R., Huber, J., et al. (2019). Global glacier mass changes and their contributions to sea-level rise from 1961 to 2016. *Nature* 568, 382–386. doi: 10.1038/s41586-019-1071-0

Zhang, G., Bolch, T., Allen, S., Linsbauer, A., Chen, W., and Wang, W. (2019). Glacial lake evolution and glacier-lake interactions in the Poiqu River basin, central Himalaya, 1964–2017. *J. Glaciol.* 65, 347–365. doi: 10.1017/jog.2019.13

Conflict of Interest: The authors declare that the research was conducted in the absence of any commercial or financial relationships that could be construed as a potential conflict of interest.

frontiers in Earth Science

ORIGINAL RESEARCH
published: 21 February 2020
doi: 10.3389/feart.2020.00035

Elevation Changes of West-Central Greenland Glaciers From 1985 to 2012 From Remote Sensing

Jacqueline Huber[1]*, *Robert McNabb*[2,3] *and Michael Zemp*[1]

[1] Department of Geography, University of Zurich, Zurich, Switzerland, [2] Department of Geosciences, University of Oslo, Oslo, Norway, [3] School of Geography and Environmental Sciences, Ulster University, Coleraine, United Kingdom

Greenlandic glaciers distinct from the ice sheet make up 12% of the global glacierized area and store about 10% of the global glacier ice volume (Farinotti et al., 2019). However, knowledge about recent climate change-induced volume changes of these 19,000 individual glaciers is limited. The small number of available glaciological and geodetic mass-balance observations have a limited spatial coverage, and the representativeness of these measurements for the region is largely unknown, factors which make a regional assessment of mass balance challenging. Here we use two recently released digital elevation models (DEMs) to assess glacier-wide elevation changes of 1,526 glaciers covering 3,785 km^2 in west-central Greenland: The historical AeroDEM representing the surface in 1985 and a TanDEM-X composite representing 2010–2014. The results show that on average glacier surfaces lowered by about 14.0 ± 4.6 m from 1985 until 2012 or 0.5 ± 0.2 m yr^{-1}, which is equivalent to a sample mass loss of ∼45.1 ± 14.9 Gt in total or 1.7 ± 0.6 Gt yr^{-1}. Challenges arise from the nature of the DEMs, such as large areas of data voids, fuzzy acquisition dates, and potential radar penetration. We compared several different interpolation methods to assess the best method to fill data voids and constrain unknown survey dates and the associated uncertainties with each method. The potential radar penetration is considered negligible for this assessment in view of the overall glacier changes, the length of the observation period, and the overall uncertainties. A comparison with earlier studies indicates that for glacier change assessments based on ICESat, data selection and averaging methodology strongly influences the results from these spatially limited measurements. This study promotes improved assessments of the contribution of glaciers to sea-level rise and encourages to extend geodetic glacier mass balances to all glaciers on Greenland.

Keywords: glacier, elevation changes, Greenland periphery, TanDEM-X (TDX), remote sensing, mass change, AeroDEM

OPEN ACCESS

Edited by:
Petra Heil,
Australian Antarctic Division, Australia

Reviewed by:
Ellyn Mary Enderlin,
University of Maine, United States
Ninglian Wang,
Chinese Academy of Sciences, China

***Correspondence:**
Jacqueline Huber
jacqueline.huber@geo.uzh.ch

Specialty section:
This article was submitted to Cryospheric Sciences, a section of the journal Frontiers in Earth Science

Received: *20 September 2019*
Accepted: *31 January 2020*
Published: *21 February 2020*

Citation:
Huber J, McNabb R and Zemp M (2020) Elevation Changes of West-Central Greenland Glaciers From 1985 to 2012 From Remote Sensing. Front. Earth Sci. 8:35. doi: 10.3389/feart.2020.00035

INTRODUCTION

Greenland's peripheral glaciers are key indicators of climate change, respond faster to climate change than the Ice Sheet and contribute strongly to sea-level rise (Zemp et al., 2019). The fronts of Greenlandic glaciers have retreated since the beginning of the twentieth century, with intermittent re-advances of some glaciers between 1950 and 1980 (Bjørk et al., 2012; Leclercq et al., 2014) indicating predominantly negative glacier mass balances. However, understanding of the evolution

of their volume and mass is still poor due to observational gaps. *In situ* mass-balance measurements on Greenland's peripheral glaciers exist (e.g., Mittivakkat, Freya and Qasigiannguit glacier, cf. WGMS, 2019) and are important for evaluating models and remote sensing data (Machguth et al., 2016) but are limited to a small number of accessible glaciers. To assess glacier mass changes of larger regions the geodetic method using digital elevation model (DEM) differencing (cf. Cogley et al., 2011) is a well-established approach (e.g., Paul and Haeberli, 2008; Fischer, 2011; Gardelle et al., 2013; Fischer et al., 2015; Brun et al., 2017). So far, geodetic mass-balance assessments of Greenland's peripheral glaciers are either restricted to single glaciers (Marcer et al., 2018) or ice caps (Albedyll et al., 2018). The studies by Bolch et al. (2013) and Gardner et al. (2013) are heretofore the only studies that have estimated volume changes for all glaciers around the Greenland Ice Sheet based on ICESat laser altimetry data from 2003 to 2008 (Bolch et al., 2013) and 2003 to 2009 (Gardner et al., 2013), respectively. ICESat provides precise elevation information at point locations but is challenged in mountainous terrain by non-alignment of repeat tracks, limited coverage, and possible sampling bias with respect to accumulation/ablation distribution of glaciers, which results in high uncertainty ranges.

The study by Albedyll et al. (2018) has shown that recently released high-resolution DEMs covering polar regions, such as the AeroDEM (1978–1987) (Korsgaard et al., 2016), the ArcticDEM (2012–2017) (Porter et al., 2018) and DEMs from the TanDEM-X mission (2010–2014, German Aerospace Center) (Wessel et al., 2016), have the potential to provide geodetic volume change estimates for large glacier samples in polar regions.

Here we use the AeroDEM and a TanDEM-X composite (hereafter TanDEM-X) to assess glacier-wide surface elevation changes for a sample of 1,526 glaciers in west-central Greenland from 1985 to 2012, and calculate the corresponding mass change. Further, a sound error assessment complements this study, considering uncertainties originating from the input data as well as from the methods applied. Subsequently, we focus on the comparison of the elevation and mass change estimates of our study in comparison to results by Bolch et al. (2013) and Gardner et al. (2013).

STUDY SITE AND DATA

West-Central Greenland

Peripheral glaciers in Greenland cover ∼90,000 km^2, considering the glaciers with no or weak connection to the ice sheet (connectivity levels 0 and 1, cf. Rastner et al., 2012). Unfortunately, for many regions around Greenland the quality of the DEMs currently available is too poor, challenging proper elevation change assessments for all peripheral glaciers. Hence, based on a qualitative data evaluation considering (a) good data coverage and (b) high glacier density, west-central Greenland emerged to be an appropriate region for a first regional elevation change assessment. The selected study region extends from ∼69–72.5°N and 50–56°W (**Figure 1A**). For glacier-wide elevation change assessments, glacier outlines are needed to include only glacierized areas and (RGI Consortium, 2017) to exclude the surrounding areas, respectively. For west-central Greenland, the RGI 6.0 (RGI Consortium, 2017) provides glacier outlines from 2001 based on Rastner et al. (2012). For this study, we follow their recommendations and only consider glaciers with connectivity levels 0 (no connection) and 1 (weak connection) with respect to the ice sheet. Based on this, we consider a sample of 2,385 glaciers in west-central Greenland covering an area of 5,566 km^2, with an elevation range from 0 to 2,270 m a.s.l. Further, a wide range of glacier types can be found in this region, including surge-type glaciers and differently-sized valley glaciers. The Fluctuations of Glaciers database (WGMS, 2019) hosted by the World Glacier Monitoring Service (WGMS) provides a variety of observation series for individual glaciers in this region, such as glaciological mass balance measurements, frontal variation observations, and reports of surge events (**Figure 1**).

Digital Elevation Models

The AeroDEM (Korsgaard et al., 2016) represents the surface elevation in west-central Greenland in 1985, made from aerial photos acquired in July and August. It has a 25 m horizontal resolution, an accuracy of 10 m horizontally and 6 m vertically, assessed by co-registration to the ICESat data (Korsgaard et al., 2016). One challenge in using the AeroDEM arises from the use of optical images as source data for the DEM generation. They tend to have low contrast in snow-covered areas, especially in the accumulation areas of glaciers, or areas where no signal is captured from the surface due to clouds or shadows because of the viewing geometry (Korsgaard et al., 2016). Subsequently, they interpolated those areas resulting in partially strong artifacts in the DEM (i.e., rectangular features with improbable step-wise elevation changes of up to 60 m) (**Supplementary Figure 1B**). Following Korsgaard et al. (2016), we used the provided reliability mask to identify and remove those low quality areas resulting in data voids in the DEM. The reliability mask ranges from 0 to 100 differentiating between successful/good measurements (≥40), manually edited values or LIDAR points (22–39), and interpolated values (0–21). For elevation change assessments, Korsgaard et al. (2016) recommend filtering out values <40. After a plausibility check, we decided to also include areas with liability values 22–39 as we expect these areas to be of reasonable quality. These intermediate-valued pixels are distributed over the entire study area and cover ∼200 km^2 of the glacierized area. Hence, areas with values <22 are claimed to be "low data quality" (**Supplementary Figure 1C**) and were therefore set to no data, resulting in data voids. By doing so, the AeroDEM covers ∼53% of the total glacierized area and, hence, the remaining 47% are data voids. Visual inspection confirmed that with our approach, areas with strong artifacts have been removed (see **Supplementary Figure 1C**). We hereafter refer to the masked version of the AeroDEM as the AeroDEM for simplicity.

For this study we further used the recent high resolution TanDEM-X model for Greenland (Wessel et al., 2016) which was provided by the German Aerospace Center (DLR) for scientific studies. It originates from SAR X-band satellite imagery taken between December 2010 and July 2014 resulting in a mostly complete DEM with 12 m resolution. Hence, it represents the

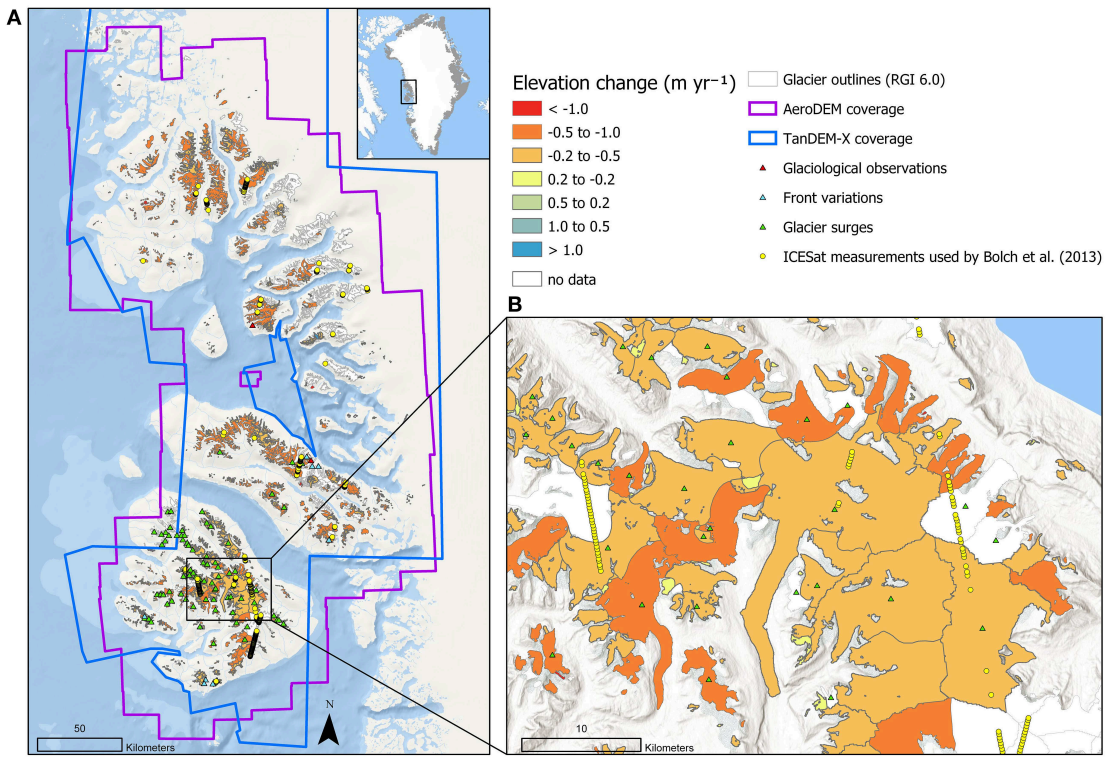

FIGURE 1 | Glacier elevation changes in west-central Greenland. **(A)** The overview map shows the glacierized areas as based on RGI 6.0 together with elevation change rates from AeroDEM (1985) and TanDEM-X (2012) as well as ICESat tracks used by Bolch et al. (2013) and available information in the FoG database of the WGMS. **(B)** The inset map shows a close up of the study region located on Disko Island. This extract is subsequently used for close ups in **Figures 2**, **5** and **Supplementary Figures 1**, **3**. Note that the points representing ICESat measurements (yellow points) are enlarged for visualization purposes and do not represent the actual footprint.

surface of the corresponding period based on weighted height averages of all data contributing to a scene. In our study region, 71 individual acquisitions (representing dates between 2010 and 2014) contributed to the final product. On the glacier basis, 3–15 acquisitions contribute to the surface of an individual glacier. Therefore, and as handled by Albedyll et al. (2018), we dated the TanDEM-X to 2012 ± 2 years and included the unknown difference in survey dates in the uncertainty assessment as described in the methods section. A bias is potentially introduced through the penetration of the X-band into snow and firn depending on the conditions of the surface layers. We discuss the potential influence of penetration biases on our results in the Discussion section Uncertainties and Bias. The comparison with ICESat elevation revealed good correspondence of the TanDEM-X at coastal regions whereas in inner parts the penetration can reach up to 10 m (Wessel et al., 2016). **Supplementary Figure 1A** shows the hillshade of the TanDEM-X of the same extent as for the AeroDEM.

METHODS

The general workflow to calculate, amongst others, elevation and mass changes is shown in **Supplementary Figure 2**. The individual processing steps have been performed within a GIS and/or Python environment. Note that we calculated glacier changes for three different spatial levels: (1) individual glaciers (also called glacier-wide), (2) a glacier sample (consisting of the 1,526 glaciers with geodetic observations), and (3) the entire region of west-central Greenland (including the 1,526 glaciers with as well as the 859 without geodetic observations), as well as for entire Greenland periphery (including the 1,526 glaciers with as well as the 17,780 glaciers without geodetic observations).

Pre-processing

First, we re-projected all input data (AeroDEM, TanDEM-X, glacier outlines) to WGS 1984 UTM zone 22 N. After the removal of artifacts as described above, we re-sampled the TanDEM-X to the lower resolution of the AeroDEM (25 m) using bi-linear interpolation following Nuth and Kääb (2011). Subsequently, we co-registered the AeroDEM and the TanDEM-X following Nuth and Kääb (2011) using the TanDEM-X as the master DEM.

DEM Differencing and Outlier Filtering

By subtracting the AeroDEM from the TanDEM-X we calculated the difference DEM (dDEM) representing the change in surface elevation from 1985 to 2012 ± 2 years.

We next applied a filter to remove outlying elevation change values. However, several surging glaciers in this region locally

produce very large elevation changes that are challenging for outlier statistics. Accordingly, we could not apply one global threshold to remove outliers (e.g., ±200 m) as this might also remove an actual signal. Therefore, we used an elevation-bin specific filter applied on a glacier-by-glacier basis: For each elevation bin, we calculated the mean and standard deviation of the elevation differences. Values that are more than three standard deviations from the mean were set to no data. Subsequently, the mean and standard deviation have been re-calculated, continuing until there were no more points to be filtered out (typically 2–3 iterations were necessary).

Void Filling and Calculation of Glacier-Wide Elevation Change

As we introduced data voids into the AeroDEM, they are obviously also present in the dDEM. The interpolation of voids in DEMs and dDEMs is a common procedure; however, the precise interpolation method is not standard. McNabb et al. (2019) assessed the impact and sensitivity of different void-filling methods on estimates of glacier volume change. Following the recommendations by McNabb et al. (2017), we chose to fill voids in the dDEM rather than in the original DEMs and, hence, selected five approaches to fill the voids in our dDEM. The subdivision "global" and "local" means that the mean/median was either calculated by considering the values of the entire region laying in the same elevation bin (i.e., "global"), or was calculated considering only values of the individual glacier (i.e., "local"). The five methods we have chosen are:

1. Linear interpolation of elevation differences (hereafter called *linear*),
2. mean elevation difference by elevation bin *locally* (hereafter called *local mean*),
3. median elevation difference by elevation bin *locally* (hereafter called *local median*),
4. mean elevation difference by elevation bin *globally* (hereafter called *global mean*), and,
5. median elevation difference by elevation bin *globally* (hereafter called *global median*).

The first method is the only method that used values from off-glacier pixels around the glacier outlines to linearly interpolate the voids inside the glacier outlines. All other methods exclusively considered areas within the glacier outlines. This is because we are assuming that the off-glacier changes are zero. For the *linear* interpolation [implemented using the griddata function provided as part of the SciPy python package (Jones et al., 2001)], it is reasonable to spatially interpolate from zero to the on-glacier value. For methods 2–3, the inclusion of off-ice pixels with (approximately) zero values would most likely depress the mean/median and so we excluded these data from our interpolation.

Methods 2–5 are so-called "hypsometric methods" building upon the assumption "that there is a relationship between elevation change and elevation" (e.g., McNabb et al., 2019). For this, we divided the dDEM in 100 m elevation bins (based on the TanDEM-X) and for each bin, we calculated the mean/median elevation change. Additionally, we applied a 2-fold void threshold for the hypsometric methods. The first threshold considered the fraction of voids per elevation bin: If an elevation bin had <40% coverage, the corresponding bin was rejected. If the entire glacier had <2/3 elevation range covered, the entire glacier was excluded from the sample. For the remaining glacier sample, we applied a second threshold considering the overall data coverage per glacier: If a glacier had <1/3 of its area covered by the dDEM, the glacier was excluded from the sample. For glaciers that were not excluded from the sample, we filled in any no-data bins using a third-order polynomial fit to the valid data.

Finally, based on the void-filled dDEMs and the glacier outlines, we calculated glacier-wide elevation changes as well as sample means for the entire observation period (1985–2012) and annually. So far, no multi-temporal glacier inventory is available for Greenland delineating the glaciers in the years the two DEMs reproduce the surface. Therefore, we used the outlines from RGI 6.0 representing the year 2001, which lays temporally between the DEMs and thus introduces a random error (cf. in the uncertainty assessment).

The specific elevation changes ($\Delta\overline{h}_i$) of the individual glacier in the unit m over the period of record (1985–2012) is simply the average glacier elevation change calculated from the difference between the AeroDEM and the TanDEM-X within the glacier outline. We calculated the sample average elevation change in two different ways:

(1) as the arithmetic mean:

$$\overline{\Delta h}_{sample\ arithmetic} = \frac{\sum \overline{\Delta h}_i}{n} \quad (1)$$

(2) as the area-weighted average:

$$\overline{\Delta h}_{sample\ area-weighted} = \frac{\Delta V_{tot\ area}}{A_{sample}} = \frac{\sum_{i=1}^{n} \overline{\Delta h}_i \cdot A_i}{A_{sample}} \quad (2)$$

where n is the number of glaciers (i.e., 1,526) and A_i is the area of the individual glaciers in 2001.

We calculated the sample mass change ΔM_{tot} (in the unit Gt)

$$\Delta M_{tot} = \Delta V_{tot\ area} \cdot \overline{\rho} \quad (3)$$

where $\overline{\rho}$ is a conversion factor assuming a density of 850 ± 60 kg m^{-3}, following Huss (2013). Hence, the sample mass change is based on the area-weighted average elevation change. We calculated regional mass changes analogously using A_{region} instead of A_{sample}.

For the annual elevation and mass-change rates we divided $\overline{\Delta h}_i$, $\overline{\Delta h}_{sample\ arithmetic}$, $\overline{\Delta h}_{sample\ area-weighted}$ and ΔM_{tot} by the number of years between the two DEMs (i.e., 27 years).

Uncertainty Assessment

For the uncertainty assessment we followed Zemp et al. (2019) and extended their calculations using additional terms to account for the uncertainties introduced by the void-filling approach ($\sigma_{void\ fill}$), and the fuzzy date of TanDEM-X

($\sigma_{TDX\ date}$). We assumed all errors are uncorrelated and random. **Supplementary Figure 2** indicates from which input data or processing step the individual error components originated.

For an Individual Glacier

As the individual errors for the uncertainty of the glacier-wide specific elevation change ($\sigma_{\Delta h}$) are independent, we calculated it based on the following formula:

$$\sigma_{\Delta h} = \sqrt{\sigma_{DEM}{}^2 + \sigma_{void\ fill}{}^2 + \sigma_{TDX\ date}{}^2} \quad (4)$$

For the uncertainty of the mass change ($\sigma_{\Delta M}$), we had to consider the uncertainties of the glacier-wide specific elevation change ($\sigma_{\Delta h}$), the uncertainty in the density assumption (σ_ρ) as well as the error of the glacier area (σ_{area}) and was calculated as follows:

$$\sigma_{\Delta M} = |\Delta M| \cdot \sqrt{\left(\frac{\sigma_{\Delta h}}{\overline{\Delta h}}\right)^2 + \left(\frac{\sigma_{\overline{\rho}}}{\overline{\rho}}\right)^2 + \left(\frac{\sigma_{area}}{\overline{A_{sample}}}\right)^2} \quad (5)$$

Individual Error Components

For each glacier, we estimated the error in the variable σ_{DEM} following McNabb et al. (2019) based on the equation:

$$\sigma_{DEM} = \sqrt{(\sigma_{\Delta z}\, A)^2 + (\sigma_{area}\, \Delta z)^2} \quad (6)$$

where $\sigma_{\Delta z}$ was estimated based on the mean off-glacier difference between the two DEMs after co-registration and the residual differences after co-registration to ICESat (i.e., the triangulation procedure described in Paul et al., 2017), A is the glacier area, σ_{area} is the error in glacier area, here equal to 0.1 in order to conservatively consider the uncertainty for the glacier areas which is 5% (or 0.05) according to Rastner et al. (2012), and Δz is the mean elevation difference of on-glacier pixels.

The uncertainty introduced by the void-filing approach ($\sigma_{void\ fill}$) we estimated for each glacier as 1.96 standard deviations of the elevation changes resulting from the two void-filling methods considered to produce reasonable results (i.e., *local mean* and *local median*, cf. discussion). By doing so, we implicitly consider the fraction of data voids, as the error is potentially larger for glaciers with a larger fraction of voids.

The date uncertainty of the TanDEM-X ($\sigma_{TDX\ date}$) we estimated to be $\pm$ 2 times the annual elevation change rate from 1985 to 2012. Note that it does not consider the influence of seasonal variations, however it is (most likely) minimized as the period of record is more than 20 years.

The uncertainty for the volume-to-mass conversion $\sigma_{\overline{\rho}}$ was set to $\pm$ 60 kg m^{-3} based on Huss (2013).

For the uncertainty in the glacier area (σ_{area}) we again refer to the study of Rastner et al. (2012) that reported a mean area uncertainty of 5% for the glacier outlines used here. Further, the absence of outlines around the time of the DEMs introduced an additional uncertainty due to two compensatory effects: Distinct negative elevation changes right in front of the glacier tongue imply that this area actually was glacierized before 2001 and should be included (e.g., visible for the glacier in the lower left corner in **Supplementary Figure 3**). Hence, the estimated on-glacier averages are too positive, since the areas excluded tend to have more negative elevation changes overall (i.e., estimated elevation change is slightly too positive). This effect is balanced by the fact that the area we are using is too small as the outlines represent the area after the mid-period between 1985 and 2012 (i.e., estimated elevation change is slightly too negative). The latter could be adjusted by the application of an area change rate but this was not required here as those effects matter only for time series. Nevertheless, we applied a conservative uncertainty in the area by doubling the uncertainty given by Rastner et al. (2012) to account for this effect, too.

Composite Sample Errors

These calculations above have been done for individual glacier outlines (i.e., for each of the 1,526 glaciers). To assign uncertainties to the sample average (as in **Table 2**), we calculated the uncertainty of the sample-wide elevation change ($\sigma_{\Delta h\ sample}$, for the arithmetic mean and the area-weighted average) as well as of the sample-wide mass change ($\sigma_{\Delta M\ sample}$) as:

$$\sigma_{\Delta M\ sample} = \sqrt{\sum_{i=1}^{n} \sigma_{\Delta M,\, i}^2} \quad (7)$$

$$\sigma_{\Delta h\ sample\ arithmetic} = \frac{\sqrt{\sum_{i=1}^{n} \sigma_{\Delta h,\, i}{}^2}}{n} \quad (8)$$

$$\sigma_{\Delta h\ sample\ area-weighted} = \frac{\sigma_{\Delta M\ sample}}{\overline{\rho} \cdot A_{sample}} \quad (9)$$

TABLE 1 | Comparison of glacier elevation changes of the 1,526 glaciers in west-central Greenland from 1985 to 2012 based on different void-interpolation method.

Interpolation method	Sample average elevation change [m] (area-weighted)	Glacier-wide elevation change [m]	
		A surging glacier	A non-surging glacier
Local mean	−14.03	−5.68	−10.27
Local median	−13.82	−0.99	−9.28
Global mean	−15.98	−13.24	−13.72
Global median	−15.74	−12.77	−13.13
Linear	−15.47	−13.25	−10.03

*In addition to the sample average elevation changes, we show glacier-wide elevation changes for two selected glaciers: a surging glacier (1) and a non-surging glacier (2). Both glaciers are pinpointed in **Figure 2**. Note that the differences among the methods are negligible for the sample average. However, on a glacier-by-glacier basis, the differences can be significant. The local mean method is the only method that appropriately reproduces the signal of surging glaciers, whereas the linear and global methods highly overestimate the elevation loss.*

TABLE 2 | Elevation and mass changes of the observed glacier sample in west-central Greenland between 1985 and 2012.

Glaciers	Area [km^2]	Specific elevation change				Mass change		
		Total 1985–2012 [m]		Annual change rate [m yr^{-1}]		Total 1985–2012		Annual change rate
		Arithmetic mean	Area-weighted mean	Arithmetic mean	Area-weighted mean	Gt	SLE [mm]	Gt yr^{-1}
1,526	3,784.57	−12.31 ± 0.86	−14.03 ± 4.62	−0.46 ± 0.03	−0.52 ± 0.17	−45.14 ± 14.85	0.13	−1.67 ± 0.55

Average elevation and mass change for the glacier sample, annually and in total, based on the local mean void-filling method. The results from the arithmetic mean are somewhat less negative compared to the area-weighted mean indicating that a few larger glaciers have more negative elevation changes. For the conversion from volume to mass change, a density of 850 kg m^{-3} has been used.

RESULTS

Pre-processing, DEM Differencing, and Void Filling

Before the co-registration the shift on stable terrain between the AeroDEM and TanDEM-X was 6.1/−12.3/−0.9 m in x/y/z directions. After the co-registration, these values have been reduced to 0.7/0.5/−0.1 m with a mean vertical offset of 0.1 m, which is considered in the uncertainty analysis.

Supplementary Figure 3 shows the result of the subtraction of the TanDEM-X from the AeroDEM for glacierized as well as for the surrounding areas. White areas are data voids resulting from the previously generated data voids in the AeroDEM. Several glaciers, for instance the glacier in the middle of the image, clearly show the pattern of surging activity between geodetic survey dates (rising surface at the tongue, surface lowering in the accumulation area).

Figure 2 shows the dDEMs for the glacierized areas resulting from application of the five different void-filling methods. Note that for the four hypsometric methods, some glaciers do not have elevation change information as the data void threshold process described above has filtered them out. Comparing the results, several differences are visible among the approaches which are also described by McNabb et al. (2019):

1. The hypsometric methods (**Figures 2B–E**) smooth the elevation change pattern, whereas the *linear* method preserves the pattern that is already existent in the non-filled dDEM.
2. The *local* hypsometric methods produce discontinuities at the lines dividing neighboring glaciers, as the calculations are glacier-wide. Especially for ice caps, such disruptive changes are not very plausible for neighboring glaciers.
3. The *global* methods do not appropriately reproduce the elevation change pattern of some individual glaciers, as is clearly visible for the surging glaciers.

Table 1 compares the average sample elevation change values for the entire observation period resulting from the different interpolation methods for the entire region as well as for two individual glaciers which have ∼60% data voids in the dDEM: one surging glacier (1) and one non-surging glacier (2). The results summarized in **Table 1** show that for the sample average the different methods produce similar values. However, for glacier-wide calculations, mainly for surging glaciers, the values can vary significantly: the *linear* and *global* methods give very high glacier-wide elevation change values, whereas the *local median* method gives very low values. In general, for regional assessments, the differences among the methods are not significant but for glacier-wide assessments, the method selection appears crucial, as some methods are unable to reproduce the pattern among differently behaving glaciers, such as surging vs. non-surging glaciers.

For this study, we used the *local mean* (per elevation bin) method as our best guess to fill the voids in the dDEM of our study region. This choice is recommended by our results, by the findings in McNabb et al. (2019), by the distribution of voids in the data, and by the characteristics of the glaciers in this region as it better accounts for the characteristics of individual glaciers when compared to the other methods (cf. discussion). However, this remains a best guess, as the true elevation changes across the data gaps are unknown. Nevertheless, the following results are based on the application of the *local mean* method to interpolate missing elevation change values.

Glacier Elevation and Mass Changes

The 2-fold data void threshold applied to the hypsometric methods caused the exclusion of ∼850 glaciers. Accordingly, our approach made it possible to calculate glacier-wide elevation changes for 1,526 glaciers covering approximately two third of the total number and 68% (3,785 km^2) of the total glacierized area of west-central Greenland (**Figure 1A**). **Figure 3A** shows the hypsometry, the corresponding annual elevation change per elevation bin, and the annual volumetric change per elevation bin for the entire glacier sample. **Figures 3B–E** show the same for four subsamples, which are further analyzed in the discussion. The data voids that have been interpolated (red bars) are mainly in the accumulation area and make up ∼37% of the area. The gray bars indicate the hypsometry for all the 2,385 glaciers located in west-central Greenland.

Regarding surges, 63 of the 1,526 glaciers, almost all of them located on Disko Island, show evidence of surging activity: Based on the dataset of Sevestre and Benn (2015), for 52 of these glaciers surging activity is "probable" and for four of these glaciers surging activity has been observed. Based on our dDEM, we flagged seven additional glaciers as surging glaciers (cf. discussion). Three glaciers are labeled as marine terminating glaciers in the RGI. However, based on a visual inspection of RapidEye data, two of

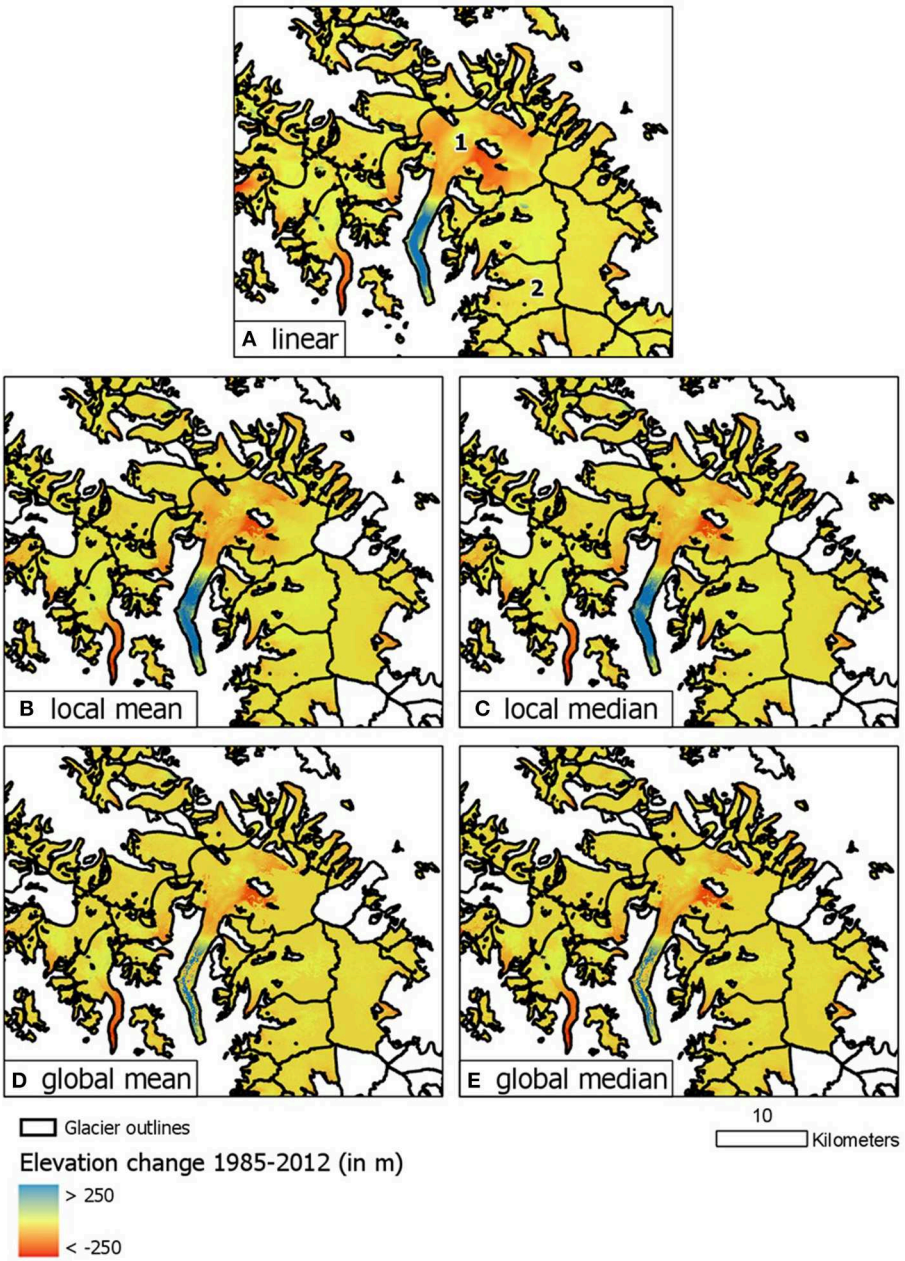

FIGURE 2 | Visual comparison of the DEM differencing resulting from the various void-interpolation methods: **(A)** linear interpolation of elevation differences, **(B)** mean elevation difference by elevation bin locally, **(C)** median elevation difference by elevation bin locally, **(D)** mean elevation difference by elevation bin globally, **(E)** median elevation difference by elevation bin globally. In general, the glaciers show elevation losses with higher losses at the tongues whereas the large surging glacier in the middle shows a reversed pattern (elevation gain at the tongue, elevation loss higher up). Note how the different void-interpolation methods influence the elevation change pattern. For instance, the global methods do no generate appropriate results for the surging glacier. In case a glacier had a large fraction of voids, no elevation changes have been calculated (white glaciers, cf. methods). Glaciers 1 and 2 in **(A)** refer to the results in **Table 1**.

these glaciers do not appear to reach the sea any more, and hence, we do not discuss these glacier-types here.

Additionally, we want to point out the reduced elevation changes in the lowest elevation bin visible in **Figure 3C** and slightly visible in **Figure 3E**. This might be explained through the lack of a second glacier inventory coincident with the TanDEM-X. That is, we include areas that became deglaciated between 2001 and 2012 and hence there is no more potential ice present to cause negative elevation changes. As a result, the mean elevation changes per bin can be less negative. However, this fraction compared to the overall glacier area is small and considered in the uncertainties.

Table 2 summarizes the average elevation and mass change (in m, Gt, and SLE) of our sample for the entire observation period as

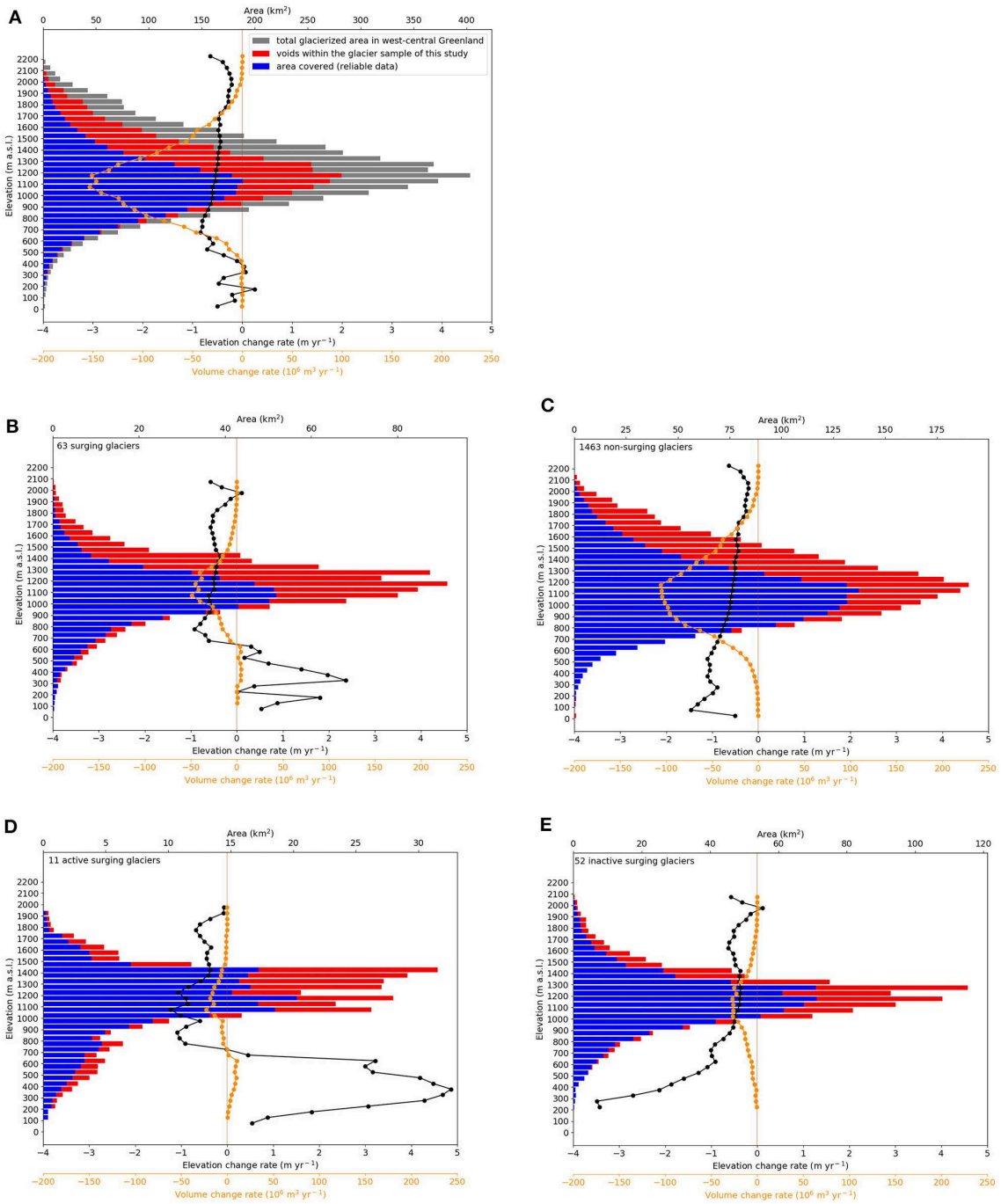

FIGURE 3 | Hypsometric glacier changes in west-central Greenland between 1985 and 2012. **(A)** The plot in the first row shows the glacier distribution with elevation (y-axis) for all glaciers in the region (gray) as well as for the investigated glacier sample with geodetic observations (blue) and original data voids (red). The average elevation and volumetric changes per elevation bin are shown as black and oranges lines, respectively, with corresponding y-axes. The second row shows the same plot but dividing the sample into glaciers with **(B)** and without **(C)** reported surge activities. In the third row, the surge glaciers **(B)** are divided into active **(D)** and inactive **(E)** subsamples based on corresponding indications in the elevation change fields.

well as annually. Regarding the elevation change, there are slight differences between the arithmetic and the area-weighted mean showing that a few large glaciers have more negative elevation changes. We considered the latter to be most appropriate for regional mass-change assessments and was therefore used for further calculations. Hence, the observed glacier sample on west-central Greenland lost $\sim$14.0 $\pm$ 4.6 m of ice thickness from 1985 to 2012 or 0.5 $\pm$ 0.2 m yr^{-1}, respectively. This is equivalent to

a total mass change of -45.1 ± 14.9 Gt (-1.7 ± 0.6 Gt yr^{-1}), or 0.13 mm SLE, assuming an ice density of 850 ± 60 kg m^{-3}. Further, comparing the signal (−14 m) and the bias identified by the co-registration shows the relevance of the latter: without the co-registration there would be a bias of ∼6% of the actual signal.

DISCUSSION

Void-Filling Methods

The handling of data voids for elevation-change assessments is neither straight forward nor does a commonly used and established method yet exist. The different methods described in the literature can have different effects on the resulting estimates (McNabb et al., 2019). The major challenge arises from the ignorance about the true elevation changes across the data gaps. Therefore, McNabb et al. (2019) artificially produced data voids in DEMs over southeast Alaska to identify which method reproduces the reality most accurate. However, the best-performing method in that study (*linear* interpolation of voids in the dDEM) cannot just be transferred to any other region with data voids in the DEMs. Three conditions majorly influence the identification of the appropriate void-filling method: (a) the aim of the study: calculation of region-wide vs. glacier-wide elevation changes, (b) the characteristics of the glaciers in the study area (e.g., surging glaciers), and (c) the distribution of the data voids which is not expected to be the same for each region, or even each DEM. Given the circumstances for this study of glaciers in west-central Greenland [(a) aiming for glacier-wide elevation changes, (b) the presence of surging glaciers, and (c) voids mainly in accumulation area], we chose five methods recommended by McNabb et al. (2019) to identify the influence on the estimates for our study region. Additionally, this multi-method approach allowed an uncertainty assessment of the void-filling method (see Methods). Our results indicate that for these circumstances, the *global* methods are inappropriate for glacier-wide elevation change assessments. Additionally, the *linear* method is not appropriate considering that the resulting dDEM has a frequently noisy dhdt signal. Nevertheless, these methods produce reasonable results for regional assessments.

Hence, for our study we used (a) a local method because surge glaciers are abundant in our region and (b) we used a hypsometric method because of the elevation-dependency of the signal (at least for non-surging glacier, cf. **Figure 3**). Of the remaining methods, it was difficult to identify the one method performing best, as we do not know the true values. However, as in McNabb et al. (2019) the (artificial) voids also prevail in the accumulation area, we followed their recommendations and agreed that the *local mean* method potentially reflects the change of the individual glaciers appropriately as it includes the area-elevation distribution of each individual glacier.

The threshold applied to reject glaciers based on the fraction of data voids can influence the sample size as well as the results. For regional glacier mass balances, such a threshold is usually and justifiably not applied and all the data available is considered for the corresponding study region. For glacier-wide studies, such a threshold is either most often not applied, the fraction of data voids is not declared, or the handling of data voids is not clear. Otherwise, different void thresholds on a glacier-wide basis are applied to exclude glaciers, such as 30% (e.g., Brun et al., 2017) or 20% voids (e.g., Le Bris and Paul, 2015). Hence, there is no consensus as to how much of the area of a glacier should be covered by data in order to be considered. Due to the partly large fraction of data voids in the DEM used here, a void threshold of 30% would have substantially reduced our sample to ∼600 glaciers. Therefore, we used a 2-fold threshold: As it considers the minimal area covered in combination with a minimal fraction of the hypsometry covered, we ensured to get a glacier sample that is optimally covered with data. Nevertheless, based on the aim of the study and the end user, a modification of this threshold might be reasonable. For regional estimates, the thresholds (for exclusion) can be set relatively low to increase the sample size. However, for analyses interested in individual glaciers, these thresholds need to be set in a much more rigorous way. This study tries to combine both: a statistically representative sample (about two third coverage) for regional mass-change estimates with plausible glacier-wide results (for submission to the WGMS).

Uncertainties and Bias

The total error related to the elevation changes of our sample is a composite of three different error sources: DEM, void-filling, and date. The former two errors vary widely among the individual glaciers and account for the largest contribution. The error related to the date uncertainty contributes only minimally due to the long observation period. However, its consideration is important as it contributes more with decreasing observation length and increasing rate of elevation change.

The application of TanDEM-X data introduces a bias caused by the penetration of the radar signal into snow. However, the magnitude of this effect depends strongly on snow and firn conditions and, hence, can vary considerably (Lambrecht et al., 2018).

In the following, we illustrate, using our data, how the results could be corrected to account for the radar penetration in cases where the observation period is shorter and hence the penetration has a significant effect on the results. We can estimate signal penetration similar to previous studies (e.g., Malz et al., 2018; Braun et al., 2019): The radar penetration takes place only in the accumulation area (assumed AAR of 50%) and is between 0 m (at ELA) to 5 m at the summit. On average (over the elevation range of the accumulation zone), this makes 2.5 m with an uncertainty of 2.5 m. Averaged over the entire glacier, then, this is halved again to 1.25 ± 1.25 m (because only the accumulation area, which covers about half of the glacier, will be affected by radar penetration). Obviously, this correction introduces another uncertainty related to whether a glacier is actually affected by the radar penetration. Hence, this has to be considered in the uncertainties by adding the factor $\sigma_{radar\ penetration}$ to the uncertainty assessment, which we propose to be as high as the correction factor itself (1.25 m). Due to the long period of records (27 years), the strong signal (−14 m), the relatively large uncertainty (±4.6 m), and due to the fact that the TanDEM-X is a stacked product using acquisitions over multiple seasons and years making a coherent radar penetration unlikely, the bias and related uncertainty of a potential radar penetration

could be ignored in our study. Hence, we did not correct our results by an estimated correction value also because such a correction might result in a disimprovement. Nevertheless, for shorter observations periods and if the TanDEM-X represents only winter acquisitions which would favor significant radar penetration, a correction is strongly advised.

Influence of Surge Type Glaciers on Elevation Changes

Surging glaciers display a distinct dynamic behavior (e.g., Hewitt, 2007; Gardelle et al., 2013; Rankl et al., 2014; Paul, 2015). Typically during a surge, a large amount of ice in a reservoir further upglacier is transported downwards, where it is then more prone to ablation (Paul, 2015). If this happens between two points in time represented by DEMs, the process becomes apparent when subtracting the two DEMs (i.e., negative elevation changes will be observed in the accumulation area, positive changes in the ablation area; e.g., the large glacier in **Figure 2**). Hence, they show the opposite pattern to glaciers reacting to current climate change (negative elevation changes at the tongues, no/slight positive elevation changes in the accumulation area). In the case of west-central Greenland, 63 glaciers were marked as glaciers with (evidence for) surging activity. However, we identified this switched pattern in our dDEM for only 11 glaciers. Hereafter we name these glaciers "active surging glaciers" for our observation period and the remaining 52 glaciers previously identified as surging glaciers are named "inactive surging glaciers." **Figure 3A** shows the glacier hypsometry, the mean elevation change per bin as well as the volumetric change per bin for the entire glacier sample. **Figures 3B–E** show the same but for the 63 glaciers with evidence for surging activity, the 11 active surging glaciers, the 52 inactive surging glaciers and the 1,463 non-surging glaciers, respectively. In terms of elevation change per elevation bin, the 63 surging glaciers partly show the expected switched pattern which is very pronounced for the 11 active surging glaciers. Interestingly, the strong positive elevation change at the tongues from the 11 active surging glaciers dominates the lowest bins of the 1,526 glaciers, as the pattern is apparent in the elevation changes, too. The 52 inactive surging glaciers show pronounced negative elevation changes at the tongues. However, this pattern is induced by approximately seven glaciers that are in this state of post-surge recovery (i.e., strong ablation at the tongue and pronounced accumulation further up). This is typical for glaciers after a surge as the mass transported further down is now prone to melting (Paul, 2015). The rest of the inactive surging glaciers as well as the non-surging glaciers show the typical negative elevation changes at low elevations that decrease with increasing elevation. All figures, especially **Figures 3A,C**, show that in terms of volumetric balance the mid-elevations with the highest fraction of area majorly contribute to the volume change. Whereas, the contributions from the lowest (i.e., glacier tongues) and highest areas are nearly negligible due to the small area, and hence, so is the influence of surging glaciers on the volume change per bin. Consequently, an exclusion of the 63 glaciers with evidence for surging does not affect the sample average (hypsometry-weighted) elevation change.

Comparison With ICESat Based Studies

Here we focus on the comparison of the elevation changes for our sample with the ones estimated by Bolch et al. (2013) and Gardner et al. (2013). Their studies are pioneering, as they are currently the only studies that have determined the mass change of Greenland's peripheral glaciers including the glaciers in our study region. Hence, the comparison with their work is fundamental.

Bolch et al. (2013) applied ICESat data from October 2003 to March 2008 and also used the glacier inventory from Rastner et al. (2012) but an older version (RGI 2.0). In their study the west-central sector covers 5,045 km^2 (521 km^2 less than the west-central sector in this study) as it spreads about 65 km less toward north. They calculated an average elevation change rate for the west-central sector of $-0.28\ m\ yr^{-1}$ for the period 2003–2008 by simply averaging the elevation change values of 285 ICESat measurements laying on 47 glaciers (CL0-1) in west-central Greenland. Their result is about half of the change rate as calculated for the sample of this study covering the period 1985–2012 ($-0.52\ m\ yr^{-1}$). As the processed ICESat footprints of their study are available for comparison, we further discuss these differences between the elevation changes in the following.

First, it has to be noted that we are comparing different time periods, hence a period of enhanced mass loss before 2003 relative to the time period after would explain our more negative values. However, we found no indication of a more negative mass-balance period before 2003, in fact rather the opposite. The negative glacier length changes on Greenland, in the late twentieth century (Leclercq et al., 2014) reject this hypothesis. In addition, Zemp et al. (2019) combine our dDEM results with the temporal variability from glaciological observations [i.e., from Freya (E-GL), Mittivakkat (E-GL), Qasigiannguit (SW-GL), Storglaciären (SE), Storbreen (NO), White (CA)] indicating that recent mass changes in Polar Regions are at least as negative as since the 1980s.

Regarding the coverage of the applied ICESat measurements, we want to highlight that the 285 footprints of 70 m cover an area of ∼1.1 km^2. Hence, they cover only about 0.03% of the area of west-central Greenland that we cover in this study. Further, the distribution of the ICESat measurements applied by Bolch et al. (2013) on the glaciers in the study region (**Figure 1B**) shows that they are mainly located in the accumulation area. However, the missing representation of the glacier tongues is probably not sufficient to explain the differences, given the large number of surging glaciers observed in the region, which pose a major challenge for elevation change assessments using ICESat data. Therefore, we compare their results with our results in more detail.

The 285 ICESat measurements used by Bolch et al. (2013) cover 47 glaciers in west-central Greenland, of which 27 glaciers representing an area of 604 km^2 (and 136 ICESat measurements covering 0.5 km^2) overlap with the 1,526 glaciers considered in this study. Comparing those 27 glaciers with our 1,526 glaciers regarding the latitudinal distribution and the variety of glacier size, indicates that the sample of Bolch et al. (2013) reasonably well represents our glacier sample. Their sample

slightly underrepresents low- and high-lying glaciers (none of the 27 glaciers has a median elevation below 700 and above 1,600 m a.s.l). Nevertheless, the limited representation of the ICESat measurements due to their small footprint is undisputable as shown in **Figure 4**. It shows the hypsometries of the 1,526 glaciers covered in this study, for the 27 glaciers covered in both studies, and for the 136 ICESat measurements. However, the latter is only visible by considerably zooming in on the former hypsometries due to the very little area coverage by the ICESat measurements (**Figure 4**, inset). Nevertheless, limited coverage does not necessarily mean the result is less correct. It depends on whether the subsample is representative for the population. Bolch et al. (2013) cover the elevations where most of the glacierized areas are located and majorly contribute to the volume changes as seen in **Figure 3**. The question is now, whether these few elevation-change measurements are representative for the full glacier sample. **Figure 4** also shows the elevation changes per elevation bin for the 1,526 glaciers of this study (black), for the 136 ICESat measurements (yellow) and the 136 measurements extracted from our dDEM at the ICESat locations (blue). We extracted the point values from our filled dDEM using cubic interpolation of the dDEM values surrounding the footprint center. **Figure 4** shows a pronounced variation of the ICESat measurements among the elevation bins as well as two outliers with strong positive values for bins where the coverage of the ICESat data is exceptionally low (750 and 1,500 m a.s.l.). This indicates that these measurements are rather accidental and not representative for the corresponding elevation bin. Hence, such values are highly sensitive for the calculation of the average elevation change by simple averaging, especially if the coverage is limited.

The comparison of different averaging methods can identify whether an averaging method that is less prone to outliers leads to more accurate elevation change values (assuming our results with full observational coverage as reference). To do so, we compare the annual elevation change-rates for 136 locations based on (a) the dDEM calculated in this study (hereafter called 136 dDEM measurements) and (b) the ICESat measurements as used in Bolch et al. (2013) (still called 136 ICESat measurements). We averaged the 136 values, either from the dDEM or from the ICESat measurement, by four methods: (1) by the arithmetic mean of all points, (2) by the arithmetic mean of the 27 glacier-wide mean values, (3) by the area-weighted mean of the glacier-wide mean values, and (4) by the hypsometry-weighted mean. For the latter, we averaged the elevation changes for each elevation bin (over all 27 glaciers), multiplied this value with the area of the corresponding bin and divided the sum by the total area of the 27 glaciers. Method (1) was used by Bolch et al. (2013) to calculate the regional elevation change based on their entire sample (285 ICESat points). We averaged the elevation changes for each elevation bin, multiplied this value with the area of the corresponding bin and again divided the sum by the total area of the 27 glaciers. As we applied each of the four methods to the 136 dDEM and 136 ICESat measurements, we end up with eight different results. An additional result is given, referred to as the reference, by calculating the area weighted mean based on the entire dDEM for the 27 glaciers. **Figure 5** illustrates the calculations using the extract on Disko Island and gives the corresponding results for all 27 glaciers and 136 measurements, respectively. The two columns indicate which dataset has been used (our dDEM or the ICESat measurements), (a) gives the reference result (-0.48 m yr^{-1}) referring to the area-weighted mean elevation change-rate for the 27 glaciers based on the entire dDEM of this study. This value is similar to the elevation change calculated for our entire sample of 1,526 glaciers (-0.52 m yr^{-1}) indicating that these 27 glaciers are an appropriate representation of the 1,526 glaciers in terms of elevation change. **Figures 5b–i** show the change rates based on the four different averaging methods, as based on the 136 dDEM for the period 1985–2012 and based on the 136 ICESat data for the period 2003–2009.

From these results, we can deduce two main findings: (1) Applying the four methods to the 136 dDEM measurements (b-e) shows that the ICESat footprint has a negative bias with respect to the reference result. However, this does not help to explain the difference between our result and Bolch et al. (2013). In fact, the difference would increase when applying such a bias-correction. (2) The ICESat column (f–i) shows that the ICESat observations seem to be less equally distributed with respect to glaciers and elevations bins and hence are more sensitive to the averaging method. Thus, the ICESat results seem to have a stronger variability and feature a different elevation change pattern as compared to our dDEM. In conclusion, the ICESat coverage is too small and very sensitive to the averaging method. Therefore, the sample is not representative for estimating the regional glacier changes.

Moreover, we would expect that the results from the arithmetic mean of the 136 ICESat measurements (f) are less negative than of the 136 dDEM measurements (b). Zemp et al. (2019) show that the annual mass change in Greenland increased significantly from the 1980s until 2016. Hence, the ICESat measurements should be more negative than the dDEM values. However, the results show the opposite is true. Besides the limited, non-representative coverage being the cause for this, an additional issue might add to the underestimation of the elevation changes. We assume a regression issue exists in the ICESat data used by Bolch et al. (2013): For the regression procedure to determine the elevation changes, they used ICESat data from October 2003 to March 2008. Hence, their observations start at the end of the ablation season but terminate at about the time of highest (winter) accumulation. This might cause the regression to be less negative, as it would be using data from a low point (late summer) as the end point for the regression. An additional indication for this effect can also be seen in **Figure 4**: for 13 out of 21 elevation bins, the ICESat measurements are less negative than the dDEM values.

Gardner et al. (2013) also determined the average elevation and volume change for, amongst others, west-central Greenland based on ICESat data. They applied methods comparable to the ones from Bolch et al. (2013), however, based on their publication we came across two main differences: First, they used data between October 2003 and October 2009, hence the regression issue does not arise. Second, their selection of ICESat measurement sample is different and larger. This potentially explains why they calculate an elevation change for west-central

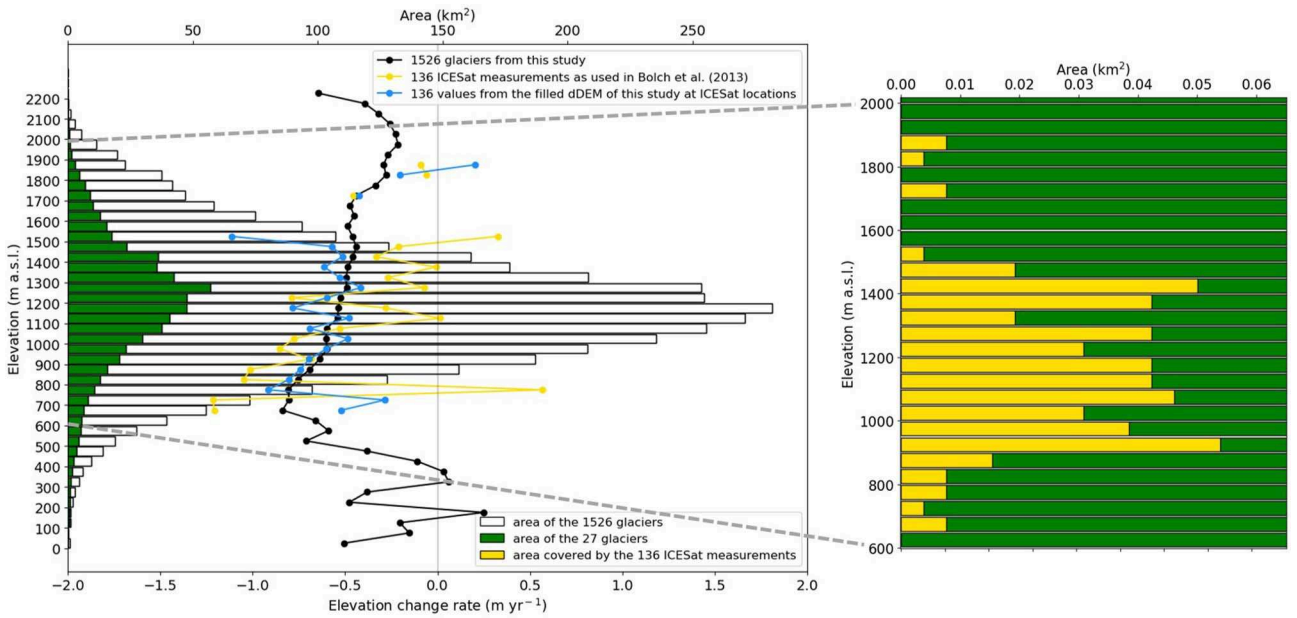

FIGURE 4 | Comparison of hypsometric elevation change rates between the present study and ICESat estimates from Bolch et al. (2013). The average elevation changes per elevation bin from this study, from the 136 ICESat estimates and from the 136 values from our change field at the ICESat locations are shown as black, yellow and blue lines, respectively. The bars represent the glacierized area with elevation covered by the 1,526 glaciers of this study (white), by the 27 glaciers that overlap between this study and the study of Bolch et al. (2013) (green), and by the 136 ICESat measurements (yellow). The latter is only visible when considerably zooming in as shown in the inset on the right (note the different scales for area).

Greenland of -0.51 ± 0.26 (95% CI) m yr^{-1}, which is consistent with our estimates.

Overall, the comparisons above show that a coverage issue in ICESat measurements does not necessarily result in inaccurate results (as shown by the results in Gardner et al., 2013). However, the selection of the ICESat points is crucial: If data are sparse, the result can be much more vulnerable to inappropriate representativeness of the point measurements for the entire glacierized area. Additionally, the selection of the start and end point for regression analysis in short observation periods (<10 years) might be crucial as it potentially influences the annual change rate.

Mass Change and Its Extrapolation to Unmeasured Regions

Based on the average elevation change of the 1,526 glaciers, we calculated the specific mass change for these glaciers by applying a density assumption of 850 ± 60 kg m^{-3} (Huss, 2013). We calculated the total mass change of the region by multiplying the mean specific mass change of our sample by the area of the entire glacierized region (i.e., entire west-central Greenland and entire Greenland periphery). **Table 3** illustrates the resulting mass changes for all 2,385 glaciers in west-central Greenland, for all of west-central Greenland as defined by Bolch et al. (2013), as well as for all peripheral glaciers on Greenland. Additionally, for west-central Greenland and the whole of Greenland periphery the estimates from Bolch et al. (2013) and Gardner et al. (2013) are given for their corresponding time period. The difference in the annual mass change rates estimated here, and the estimates of Bolch et al. (2013), are mainly caused by the strong differences in the elevation change estimates, and to some degree by their lower ice density assumption. Our study suggests annual mass loss rates (-2.23 Gt yr^{-1}) about twice as large for the same extent of west-central Greenland. We point out that the extrapolation of our estimates to entire peripheral Greenland (-40 Gt yr^{-1}) might be associated with large uncertainties, provides only a rough estimate and serves for an order of magnitude comparison with existing studies. In general, the average annual mass loss of west-central Greenland is somewhat lower than the average loss for the rest of Greenland periphery (Bolch et al., 2013). Hence, our extrapolated values might even underestimate the Greenland-wide overall mass change. Accordingly, based on our estimates we determined an annual mass loss for the entire Greenland periphery of 40 Gt yr^{-1} for 1985–2012 which is ∼30% more than estimated by Bolch et al. (2013). However, our values correspond to the estimate provided by Gardner et al. (2013) of an annual mass loss for the whole of peripheral Greenland of 38 ± 7 Gt, even though they applied different density assumptions for the accumulation and ablation area, and not a constant value as we did.

CONCLUSIONS

This study presents for the first time glacier-wide elevation changes for a large sample of Greenland's peripheral glaciers. We assessed geodetic balances for 1,526 glaciers in west-central Greenland from 1985 to 2012 based on the recently released AeroDEM and TanDEM-X. These two DEMs offer great opportunities for geodetic elevation change assessments but also introduce various challenges, such as artifacts or data voids in

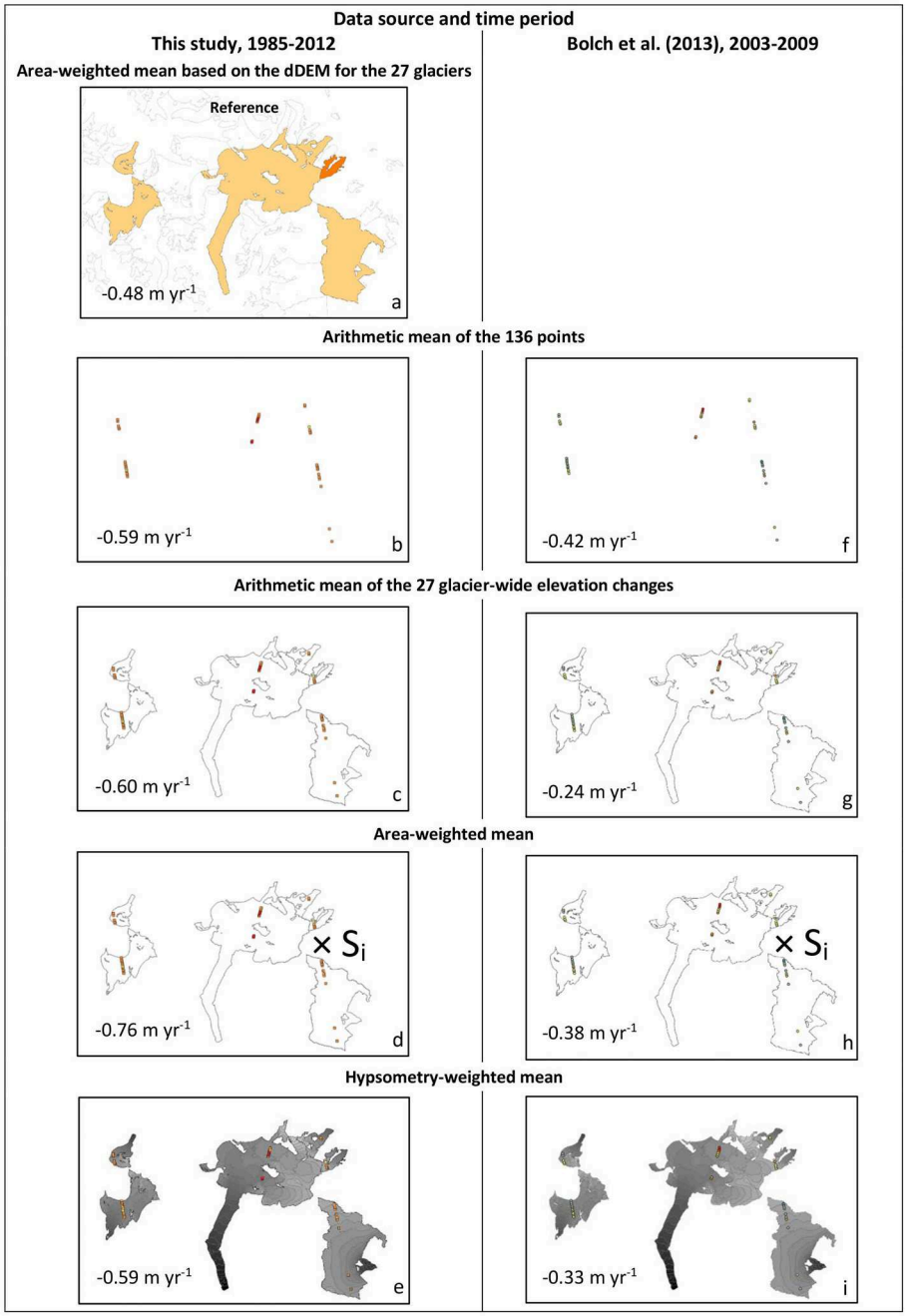

FIGURE 5 | Illustration and corresponding results of the different averaging methods (rows) to calculated the mean elevation change for the 27 glaciers based on **(a–e)** measurements from this study at 136 ICESat locations and **(f–i)** 136 ICESat measurements used by Bolch et al. (2013). See text for calculations. Note that the points and squares representing dhdt measurement locations do not represent the actual area of the 70 m footprints.

the AeroDEM or radar penetration and the imprecise date of the TanDEM-X data. For the handling of artifacts and data voids, various methods exist, each of which have a different effect on the resulting elevation change values. Hence, the selection of an appropriate method is not straightforward and no general procedure can be given, as this strongly depends on the research questions, the distribution of the data voids, and the glacier characteristics of the study area. Given these criteria, we found the *local mean* hypsometric method to be suitable for west-central Greenland where surge-type glaciers are abundant. The uncertainty introduced by the imprecise date of the TanDEM-X is reflected in our uncertainty analysis. We discussed how any potential radar penetration can be taken into account, however we refrained from a corresponding correction in this study as the

TABLE 3 | Regional glacier mass changes for Greenland.

Region	Based on	Time period	Area [km^2]	Total mass change [Gt]	Annual mass change [Gt yr^{-1}]	Total SLE [mm]
West-central Greenland	Extrapolation of the sample average of this study	1985–2012	5,566	−66	−2	0.18
West-central Greenland as defined in Bolch et al. (2013)	Extrapolation of the sample average of this study	1985–2012	5,045	−60	−2	0.17
	Bolch et al. (2013)	2003–2008	5,045	−5	−1	0.01
Entire Greenland periphery	Extrapolation of the sample average of this study	1985–2012	89,717	−1,070	−40	2.96
	Bolch et al. (2013)	2003–2008	89,324	−140	−28	0.39
	Gardner et al. (2013)	2003–2009	89,700	−228	−38	0.63

The table compares the results from the present study with the ICESat estimates by Bolch et al. (2013) and by Gardner et al. (2013).
*Extrapolation of the sample elevation changes as given in **Table 2** to regions not (entirely) covered in this study to estimate regional mass change estimates. The table also shows results from different studies for west-central Greenland as well as for entire Greenland. Note that the total mass change and SLE refer to different observation periods. The studies of Gardner et al. (2013) and Bolch et al. (2013) relied on the RGI 2.0 version whereas this study relies on the 6.0 version.*

potential bias and related uncertainties are negligible in view of the length of the time period, the overall glacier change rates, and the overall uncertainties.

Our results show that the glaciers in west-central Greenland have lost $\sim$14.0 $\pm$ 4.6 m of ice from 1985 to 2012 or -0.5 ± 0.2 m yr^{-1}, respectively. This is equivalent to a total mass change of -45.1 ± 14.9 Gt or 0.13 mm SLE and an annual mass change of -1.7 ± 0.6 Gt yr^{-1}.

The comparison of our results with the two ICESat-based elevation and mass change assessments of Gardner et al. (2013) and Bolch et al. (2013) revealed that our sample results correspond with the former but show higher losses than the latter. We could show that the elevation changes by Bolch et al. (2013) are most likely underestimated indicated by the lack of data in combination with a lack of representativeness of the applied ICESat point measurements. In addition, we suspect that the selection of the observation period (starting in fall 2003 but ending in spring 2008) in combination with the use of a regression approach for the determination of elevation change rates might have introduced a positive bias into the ICESat results reported by Bolch et al. (2013).

This study presents for the first time glacier-wide elevation changes for a large sample of Greenland peripheral glaciers. We encourage the extension of our dataset to all peripheral glaciers in Greenland once improved DEMs are available. Despite the described challenges introduced by the input data, the increasing number of accurate DEMs as well as the improvement of historical data through re-processing opens the opportunity that this can be achieved in the near future.

DATA AVAILABILITY STATEMENT

Glacier-wide elevation changes for 1,526 glaciers including uncertainties are available from the Fluctuations of Glaciers (FoG) databased hosted by the World Glacier Monitoring Service (WGMS, https://doi.org/10.5904/wgms-fog-2019-12). The C3S aims and is in progress to extend the FoG database hosted by the WGMS in space, time and to improve its regional representativeness by the integration of datasets derived from remote sensing platforms (i.e., geodetic glacier elevation change data). The scripts for the DEM co-registration are documented here: https://pybob.readthedocs.io/.

AUTHOR CONTRIBUTIONS

JH coordinated the study and wrote the manuscript, and produced the figures. RM and JH computed the geodetic results. JH, RM, and MZ contributed to the analysis of the data and the revision of the manuscript.

FUNDING

This study was enabled by support from the Copernicus Climate Change Service (C3S) implemented by ECMWF on behalf of the European Commission, the European Space Agency (ESA) project Glaciers_cci (4000109873/14/I-NB) and the European Research Council (ERC) Advance Grant ICEMASS (320816). The TanDEM-X data was kindly provided by Horst Machguth within the DLR project Glaciers and ice thickness changes at the Greenland periphery (DEM-GLAC0606).

ACKNOWLEDGMENTS

We thank Frank Paul, Christopher Nuth, and Nicolas Eckert for fruitful discussions, Andreas Kääb for the scientific research stay of JH in Oslo to work on this study as well as Tobias Bolch and Horst Machguth for providing the ICESat data. The AeroDEM was kindly available from the NOAA National Centers for Environmental Information. Further, we thank the Global Land Ice Measurements from Space (GLIMS) and RGI communities for free and open access to their data sets. We thank the chief

editor, the editor, Petra Heil, and the two reviewers for their constructive comments on our manuscript.

SUPPLEMENTARY MATERIAL

The Supplementary Material for this article can be found online at: https://www.frontiersin.org/articles/10.3389/feart.2020.00035/full#supplementary-material

Supplementary Figure 1 | The extract of Disko Island shows the hillshades of the two DEMs used in this study and glacier outlines (red) representing the glaciers in 2001. **(A)** Hillshade of the TanDEM-X DEM (2010–2014) with 12 m resolution. No artifacts visible. **(B)** AeroDEM (1985) with 25 m resolution. Rectangular features in accumulation area are artifacts. **(C)** Reliability mask indicating areas of low data reliability (light yellow) laying over the AeroDEM. These areas declared as low data quality correspond with the artifacts visible in the DEM and hence are set to no data.

Supplementary Figure 2 | General workflow to assess glacier-wide elevation changes for west-central Greenland 1985–2012 including the sources for the individual components of the uncertainty assessment.

Supplementary Figure 3 | dDEM illustrating the elevation changes from 1985 to 2012 in the corresponding extract. Red and blue represent negative and positive elevation change values, respectively. White areas represent data voids. In black are the glacier outlines representing the state in 2001.

REFERENCES

Albedyll, L., von, Machguth, H., Nussbaumer, S. U., and Zemp, M. (2018). Elevation changes of the Holm Land Ice Cap, northeast Greenland, from 1978 to 2012–2015, derived from high-resolution digital elevation models. *Arct. Antarct. Alp. Res.* 50:e1523638. doi: 10.1080/15230430.2018.1523638

Bjørk, A. A., Kjær, K. H., Korsgaard, N. J., Khan, S. A., Kjeldsen, K. K., Andresen, C. S., et al. (2012). An aerial view of 80 years of climate-related glacier fluctuations in southeast Greenland. *Nat. Geosci.* 5, 427–432. doi: 10.1038/ngeo1481

Bolch, T., Sandberg Sørensen, L., Simonsen, S. B., Mölg, N., Machguth, H., Rastner, P., et al. (2013). Mass loss of Greenland's glaciers and ice caps 2003–2008 revealed from ICESat laser altimetry data. *Geophys. Res. Lett.* 40, 875–881. doi: 10.1002/grl.50270

Braun, M. H., Malz, P., Sommer, C., Farías-Barahona, D., Sauter, T., Casassa, G., et al. (2019). Constraining glacier elevation and mass changes in South America. *Nat. Clim. Change* 9, 130–136. doi: 10.1038/s41558-018-0375-7

Brun, F., Berthier, E., Wagnon, P., Kääb, A., and Treichler, D. (2017). A spatially resolved estimate of High Mountain Asia glacier mass balances from 2000 to 2016. *Nat. Geosci.* 10, 668–673. doi: 10.1038/ngeo2999

Cogley, J. G., Hock, R., Rasmussen, L. A., Arendt, A. A., Bauder, A., Braithwaite, R. J., et al. (2011). *Glossary of Glacier Mass Balance and Related Terms. IHP-VII Technical Documents in Hydrology*. Vol. 86. Paris, UNESCO/IHP: IACS Contribution No. 2.

Farinotti, D., Huss, M., Fürst, J. J., Landmann, J., Machguth, H., Maussion, F., et al. (2019). A consensus estimate for the ice thickness distribution of all glaciers on Earth. *Nat. Geosci.* 12, 168–173. doi: 10.1038/s41561-019-0300-3

Fischer, A. (2011). Comparison of direct and geodetic mass balances on a multi-annual time scale. *Cryosphere* 5, 107–124. doi: 10.5194/tc-5-107-2011

Fischer, M., Huss, M., and Hoelzle, M. (2015). Surface elevation and mass changes of all Swiss glaciers 1980–2010. *Cryosphere* 9, 525–540. doi: 10.5194/tc-9-525-2015

Gardelle, J., Berthier, E., Arnaud, Y., and Kääb, A. (2013). Region-wide glacier mass balances over the Pamir-Karakoram-Himalaya during 1999-2011. *Cryosphere* 7, 1263–1286. doi: 10.5194/tc-7-1263-2013

Gardner, A. S., Moholdt, G., Cogley, J. G., Wouters, B., Arendt, A. A., Wahr, J., et al. (2013). A reconciled estimate of glacier contributions to sea level rise: 2003 to 2009. *Science* 340, 852–857. doi: 10.1126/science.1234532

Hewitt, K. (2007). Tributary glacier surges: an exceptional concentration at Panmah Glacier, Karakoram Himalaya. *J. Glaciol.* 53, 181–188. doi: 10.3189/172756507782202829

Huss, M. (2013). Density assumptions for converting geodetic glacier volume change to mass change. *Cryosphere* 7, 877–887. doi: 10.5194/tc-7-877-2013

Jones, E., Oliphant, E., and Peterson, P. (2001). *Open Source Scientific Tools for Python*. Available online at: http://www.scipy.org/ (accessed July 19, 2019).

Korsgaard, N. J., Nuth, C., Khan, S. A., Kjeldsen, K. K., Bjørk, A. A., Schomacker, A., et al. (2016). Digital elevation model and orthophotographs of Greenland based on aerial photographs from 1978-1987. *Sci. Data* 3:160032. doi: 10.1038/sdata.2016.32

Lambrecht, A., Mayer, C., Wendt, A., Floricioiu, D., and Völksen, C. (2018). Elevation change of Fedchenko Glacier, Pamir Mountains, from GNSS field measurements and TanDEM-X elevation models, with a focus on the upper glacier. *J. Glaciol.* 64, 637–648. doi: 10.1017/jog.2018.52

Le Bris, R., and Paul, F. (2015). Glacier-specific elevation changes in parts of western Alaska. *Ann. Glaciol.* 56, 184–192. doi: 10.3189/2015AoG70A227

Leclercq, P. W., Oerlemans, J., Basagic, H. J., Bushueva, I., Cook, A. J., and Le Bris, R. (2014). A data set of worldwide glacier length fluctuations. *Cryosphere* 8, 659–672. doi: 10.5194/tc-8-659-2014

Machguth, H., Thomsen, H. H., Weidick, A., Ahlstrøm, A. P., Abermann, J., Andersen, M. L., et al. (2016). Greenland surface mass-balance observations from the ice-sheet ablation area and local glaciers. *J. Glaciol.* 62, 861–887. doi: 10.1017/jog.2016.75

Malz, P., Meier, W., Casassa, G., Jaña, R., Skvarca, P., and Braun, M. (2018). Elevation and mass changes of the Southern Patagonia Icefield derived from TanDEM-X and SRTM data. *Remote Sens.* 10:188. doi: 10.3390/rs10020188

Marcer, M., Stentoft, P. A., Bjerre, E., Cimoli, E., Bjørk, A., Stenseng, L., et al. (2018). Three decades of volume change of a small Greenlandic glacier using ground penetrating radar, Structure from Motion, and aerial photogrammetry. *Arct. Antarct. Alp. Res.* 49, 411–425. doi: 10.1657/AAAR0016-049

McNabb, R., Nuth, C., Kääb, A., and Girod, L. (2019). Sensitivity of glacier volume change estimation to DEM void interpolation. *Cryosphere* 13, 895–910. doi: 10.5194/tc-13-895-2019

McNabb, R. W., Nuth, C., and Kääb, A. (2017). Phase 2: option 2, algorithm development: Voids. Technical Report. Glaciers_cci-D1.2_LAR, European Space Agency Glaciers CCI Project.

Nuth, C., and Kääb, A. (2011). Co-registration and bias corrections of satellite elevation data sets for quantifying glacier thickness change. *Cryosphere* 5, 271–290. doi: 10.5194/tc-5-271-2011

Paul, F. (2015). Revealing glacier flow and surge dynamics from animated satellite image sequences: examples from the Karakoram. *Cryosphere* 9, 2201–2214. doi: 10.5194/tc-9-2201-2015

Paul, F., Bolch, T., Briggs, K., Kääb, A., McMillan, M., McNabb, R., et al. (2017). Error sources and guidelines for quality assessment of glacier area, elevation change, and velocity products derived from satellite data in the Glaciers_cci project. *Remote Sens. Environ.* 203, 256–275. doi: 10.1016/j.rse.2017.08.038

Paul, F., and Haeberli, W. (2008). Spatial variability of glacier elevation changes in the Swiss Alps obtained from two digital elevation models. *Geophys. Res. Lett.* 35:202. doi: 10.1029/2008GL034718

Porter, C., Morin, P., Howat, I., Noh, M.-J., Bates, B., Peterman, K., et al. (2018). ArcticDEM. *Harvard Dataverse, V1*. doi: 10.7910/DVN/OHHUKH

Rankl, M., Kienholz, C., and Braun, M. (2014). Glacier changes in the Karakoram region mapped by multimission satellite imagery. *Cryosphere* 8, 977–989. doi: 10.5194/tc-8-977-2014

Rastner, P., Bolch, T., Mölg, N., Machguth, H., Le Bris, R., and Paul, F. (2012). The first complete inventory of the local glaciers and ice caps on Greenland. *Cryosphere* 6, 1483–1495. doi: 10.5194/tc-6-1483-2012

RGI Consortium (2017). *Randolph Glacier Inventory – A Dataset of Global Glacier Outlines: Version 6.0.* Technical Report. RGI Consortium.

Sevestre, H., and Benn, D. I. (2015). Climatic and geometric controls on the global distribution of surge-type glaciers: implications for a unifying model of surging. *J. Glaciol.* 61, 646–662. doi: 10.3189/2015JoG14J136

Wessel, B., Bertram, A., Gruber, A., Bemm, S., and Dech, S. (2016). A new high-resolution elevation model of Greenland derived from TanDEM-X. *ISPRS Ann. Photogramm. Remote Sens. Spatial Inf. Sci.* 3, 9–16. doi: 10.5194/isprs-annals-III-7-9-2016

WGMS (2019). *Fluctuations Of Glaciers Database* (Zurich: World Glacier Monitoring Service). doi: 10.5904/wgms-fog-2019-12

Zemp, M., Huss, M., Thibert, E., Eckert, N., McNabb, R., Huber, J., et al. (2019). Global glacier mass changes and their contributions to sea-level rise from 1961 to 2016. *Nature* 568, 382–386. doi: 10.1038/s41586-019-1071-0

Conflict of Interest: The authors declare that the research was conducted in the absence of any commercial or financial relationships that could be construed as a potential conflict of interest.

frontiers in Earth Science

ORIGINAL RESEARCH
published: 27 May 2020
doi: 10.3389/feart.2020.00156

Reconciling Svalbard Glacier Mass Balance

Thomas V. Schuler[1,2], Jack Kohler[3], Nelly Elagina[4], Jon Ove M. Hagen[1], Andrew J. Hodson[5,6], Jacek A. Jania[7], Andreas M. Kääb[1], Bartłomiej Luks[8], Jakub Małecki[9], Geir Moholdt[3], Veijo A. Pohjola[10], Ireneusz Sobota[11] and Ward J. J. Van Pelt[10]*

[1] Department of Geosciences, University of Oslo, Oslo, Norway, [2] Department of Arctic Geophysics, The University Centre in Svalbard (UNIS), Longyearbyen, Norway, [3] Norwegian Polar Institute, Fram Centre, Tromsø, Norway, [4] Institute of Geography, Russian Academy of Sciences, Moscow, Russia, [5] Department of Arctic Geology, The University Centre in Svalbard (UNIS), Longyearbyen, Norway, [6] Department of Environmental Sciences, Western Norway University of Applied Sciences, Sogndal, Norway, [7] Centre for Polar Studies, Institute of Earth Sciences, University of Silesia, Katowice, Poland, [8] Institute of Geophysics, Polish Academy of Sciences, Warsaw, Poland, [9] Institute of Geoecology and Geoinformation, Adam Mickiewicz University, Poznań, Poland, [10] Department of Earth Sciences, Uppsala University, Uppsala, Sweden, [11] Department of Hydrology and Water Management, Polar Research Center, Nicolaus Copernicus University, Toruń, Poland

OPEN ACCESS

Edited by:
Michael Zemp,
University of Zürich, Switzerland

Reviewed by:
Noel Gourmelen,
The University of Edinburgh, United Kingdom
Ingo Sasgen,
Helmholtz Centre for Polar and Marine Research (AWI), Germany

***Correspondence:**
Thomas V. Schuler
t.v.schuler@geo.uio.no

Specialty section:
This article was submitted to Cryospheric Sciences, a section of the journal Frontiers in Earth Science

Received: *23 January 2020*
Accepted: *27 April 2020*
Published: *27 May 2020*

Citation:
Schuler TV, Kohler J, Elagina N, Hagen JOM, Hodson AJ, Jania JA, Kääb AM, Luks B, Małecki J, Moholdt G, Pohjola VA, Sobota I and Van Pelt WJJ (2020) Reconciling Svalbard Glacier Mass Balance. Front. Earth Sci. 8:156. doi: 10.3389/feart.2020.00156

Since the first estimates of Svalbard-wide glacier mass balance were made in the early 2000s, there has been great progress in remote sensing and modeling of mass balance, existing field records have been extended, field records at new locations have been added, and there has been considerable environmental change. There is a wide spread in the available estimates of both total mass balance and surface or climatic mass balance, but there is overall agreement that the glaciers on Svalbard have been losing mass since the 1960s, with a tendency toward more negative mass balance since 2000. We define criteria to select data that are representative and of high credibility; this subset shows a more coherent evolution and reduced spread. In addition, we combine individual field mass balance records collected by different groups into a single dataset that samples glaciers across Svalbard and a range of different size classes. We find a close relationship between measured specific surface mass balance and size of the glacier, in such a way that smaller glaciers experience more negative surface mass balances. A qualitatively similar relationship between the accumulation area ratio and glacier area is found for all glaciers in the Svalbard, suggesting that the relation derived from glaciological records is not only an artifact caused by the limited number of samples (n = 12). We apply this relation to upscale measured surface mass balance for a new estimate for all glaciers of Svalbard. Our reconciled estimates are -7 ± 4 Gt a^{-1} (2000–2019) for the climatic mass balance, and -8 ± 6 Gt a^{-1} for the total mass balance. The difference between the two represents the sum of frontal ablation and the combined uncertainty, which together amount to ca. -2 ± 7 Gt a^{-1}. While this is consistent with a previous estimate of Svalbard-wide frontal ablation, the uncertainties are large. Furthermore, several large and long-lasting surges have had considerable and multi-year impact on the total mass balance, and in particular on calving rates, emphasizing the need for better-resolved and more frequently updated estimates of frontal ablation.

Keywords: Svalbard, Arctic glaciers, glacier mass balance, mass balance modeling, glaciological mass balance, geodetic mass balance, glacier gravimetry

INTRODUCTION

Ongoing climate change alters the energy and mass balances of glaciers, which in turn have hydrological and ecological implications at the regional scale and which additionally drive global sea-level changes. For instance, the collective volume of water stored in Arctic glaciers has the potential to rise global sea level by ∼0.3 m if melted completely (AMAP, 2017). Although this is a much smaller volume than the sea-level equivalent of the ice sheets on Greenland and Antarctica, the contribution from Arctic glaciers (-213 ± 29 Gt a^{-1}) currently accounts for about one third of the eustatic sea level change (IPCC, 2019) and is projected to be significant throughout the 21st century (Meier et al., 2007; Church et al., 2014; Hock et al., 2019). Meltwater released by the retreat of glaciers controls the hydrology of downstream systems, as well as influences terrestrial and marine ecosystems and fjord circulation. Moreover, glacier retreat leads to significant topographic changes, such as increased fjord length and glacier forefield area (Błaszczyk et al., 2013; Grabiec et al., 2018).

This paper reviews the current state of Svalbard glacier mass balance, and updates the previous assessments by Hagen et al. (2003a, 2003b), who used the data available at that time and different approaches to assess the Svalbard-wide total glacier mass balance. More than 15 years have passed since these previous works, during which measurements have been continued, new series from formerly under-represented areas have been initiated and new techniques have become available.

The surface mass balance (SMB) quantifies the mass fluxes between the atmosphere and the glacier at the surface, as well as within the current period's snow layer. It comprises therefore also refreezing within the annual layer, whereas the climatic mass balance (CMB) additionally accounts for mass changes below the last summer surface. Total glacier mass balance is the sum of CMB, basal mass balance and frontal ablation, which in turn comprises calving and subaqueous melting (Cogley et al., 2011). Here, we assemble a dataset of directly measured SMB that has improved representativeness in terms of location and glacier size to derive a new estimate for Svalbard-wide SMB. Further, we discuss new technologies that have become available in the past 20 years. These include improved capability of satellite remote sensing for mass balance monitoring and meteorologically forced models to simulate climatic mass balance. Both techniques enable issues with temporal gaps and spatial representativeness of glaciological measurements to be overcome and to be linked optimally with adjacent disciplines in an Earth System perspective. Finally, we highlight important knowledge gaps and outline the future research needed to close them.

SVALBARD GLACIERS

Located between 75° and 82°N, at the junction of contrasting atmospheric and oceanic regimes and close to the fluctuating sea-ice edge, Svalbard is currently among the fastest warming regions on Earth (Maturilli et al., 2013; Nordli et al., 2014; Isaksen et al., 2016). Strong gradients characterize the climate of Svalbard, ranging from milder and more humid conditions in the south and west, to the colder and drier conditions in the northeast. These gradients are reflected in the spatial pattern of climatic mass balance, and therefore also in the distribution of glacier-covered area. The largest glaciers are found in the colder northeast, whereas glacier coverage is much less in the milder and drier area of central Spitsbergen, the main island.

About 34,000 km^2, i.e., 57% of the ∼60,000 km^2 land area of Svalbard are covered by glaciers (Nuth et al., 2013), corresponding to ∼10% of the glacier area in the Arctic, outside the Greenland ice sheet. The more than 1,000 individual glaciers larger than 1 km^2 comprise a wide range of glacier types from small cirque glaciers and valley glaciers that mainly terminate on land to large ice fields and ice caps (up to ∼8,000 km^2) each feeding several outlet glaciers. Adopting the methodology proposed by Parkes and Marzeion (2018), the area of uncharted, small glaciers is estimated to be 366 km^2, about 1% of the area accounted for by the inventory (**Supplementary Material S3**). About 15% of all glaciers on Svalbard by number and as much as 60% by area (Błaszczyk et al., 2009) are tidewater glaciers, that terminate into fjord or ocean water. Tidewater glaciers introduce freshwater at depth into the marine waters, both from subglacial channels and submarine melting, as well as icebergs, which calve off of the glacier fronts. Svalbard's total ice volume has been assessed using different methods, with estimates ranging from 4,000 to 9,600 km^3, but most studies (Hagen et al., 1993; Martin-Espanol et al., 2015; Fürst et al., 2018) agree more closely on a value of ca. 6,200 km^3, corresponding to a sea-level equivalent of 1.5 cm. Most Svalbard glaciers are polythermal (Hagen et al., 1993), i.e., they consist of both cold and temperate ice. Temperate ice is at the melting point, thus permitting the presence of liquid water in the glacier body even during the cold winter period.

Glacier Monitoring

Annual glaciological mass balance surveys of Svalbard glaciers have been conducted since 1966 (Hagen and Liestøl, 1990). **Table 1** provides an overview of the glaciers currently being surveyed that have records of 5 years or longer, along with some of their characteristics. Regular measurements have been performed on glaciers in the vicinity of settlements (Ny-Ålesund, Hornsund, Longyearbyen, and Barentsburg, see **Figure 1**), due to their ease of access; even though these sites may not fully represent conditions across Svalbard. In addition, dedicated measurement campaigns have been conducted on the less accessible ice caps in the eastern parts of Svalbard (e.g., Ahlmann, 1933; Schytt, 1964; Pinglot et al., 2001). At some locations, these measurements have been maintained on a regular basis, and now provide invaluable data for assessing the climate-glacier interaction.

MATERIALS AND METHODS

Glaciological Mass Balance

The SMB refers to mass balance measured according to the glaciological method and is obtained from repeated field visits; it comprises end-of-winter snow-depth sounding, density

TABLE 1 | List of currently surveyed glaciers with records of 5 years or longer, and their characteristics. Annual glacier mass balance B_a refers to the temporal average over 2000–2019.

Glacier name	Area (km^2)	Elevation (m a.s.l.)	Surveyed since	Terminus (Land or Sea)	Specific B_a (m w.e. a^{-1})	Dataset DOI
Northwest Spitsbergen						
Austre Brøggerbreen[1]	6	80–680	1966	L	−0.62	10.21334/npolar.2013.ad6c4c5a
Midtre Lovénbreen[1]	5	50–690	1968	L	−0.49	10.21334/npolar.2013.ad6c4c5a
Kongsvegen[1]	107	0–1000	1987	S	−0.15	10.21334/npolar.2013.ad6c4c5a
Kronebreen/Holtedahlfonna[1]	380	0–1400	2003	S	−0.09	10.21334/npolar.2013.ad6c4c5a
Waldemarbreen[2]	3	140–590	1995	L	−0.89	0.1016/j.gloplacha.2016.07.006 10.5904/wgms-fog-2019-12
Irenebreen[2]	4	90–730	2001	L	−0.92	0.1016/j.gloplacha.2016.07.006 10.5904/wgms-fog-2019-12
Central Spitsbergen						
Svenbreen[3]	4	180–700	2011	L	−0.71	10.21334/npolar.2020.b3bb4ee2
Nordenskiöldbreen[4]	206	0–1200	2006	S	−0.07	10.5904/wgms-fog-2019-12
Austre Grønfjordbreen[5]	7	40–450	2014	L	−1.61	10.21334/npolar.2020.0f0526ae
Southern Spitsbergen						
Hansbreen[4]	56	0–695	1989	S	−0.26	10.5904/wgms-fog-2019-12
Werenskioldbreen[4]	27	50–600	1999	L	−0.49	10.5904/wgms-fog-2019-12
Northeast Svalbard						
Etonbreen (Austfonna)[6]	880	0–800	2004	S	−0.03	http://www.mosj.no/en/climate/land/mass-balance-glaciers.html

[1]Kohler, 2013; [2]Sobota et al., 2016; [3]Małecki, 2020; [4]WGMS, 2019; [5]IGRAS, 2020; [6]Norwegian Polar Institute and University of Oslo, 2020.

measurements and repeated height readings of an array of stakes. Balance estimates are typically extrapolated over the entire glacier basin by determining the balance as function of elevation, and averaging them, applying weights determined from the distribution of glacier area as a function of elevation. This method quantifies the SMB, i.e., the mass changes at the surface of the glacier, exposed to the atmosphere, and within near-surface layers, but does not include internal mass changes below the last summer surface, frontal ablation due to calving and submarine melting at the front of tidewater glaciers (Cogley et al., 2011).

Although SMB has been measured at many glaciers, only a few records have been maintained for more than 10 years. Furthermore, many records have been held by the different institutions responsible for the programs, complicating representative assessments of a Svalbard-wide glacier mass balance. This situation has changed in recent years, with the increased focus on open access to the measurements, for instance through the World Glacier Monitoring Service[1], the Svalbard-Jan Mayen Environmental Monitoring database[2] or the SIOS data management system[3].

Previous studies have used an average of available specific balance records and multiplied by the glacier-covered area to obtain estimates of climatic mass balance for all Svalbard glaciers (Hagen et al., 2003a; Dyurgerov and Meier, 2005; Ohmura, 2006; Radic and Hock, 2011). Radic and Hock (2011) used different size classes in their upscaling, while Zemp et al. (2019) used the more complete Randolph Glacier Inventory (Pfeffer et al., 2014). Marzeion et al. (2012, 2015) used glaciological mass balance records to calibrate a global model of climatic mass balance. All these approaches used the glaciological records that were then readily available, which were exclusively from smaller glaciers along the west coast of Svalbard; extrapolating these data to the entire archipelago is questionable. In an alternative approach, Hagen et al. (2003b) used climatic mass balance gradients for 13 different regions, each having a different equilibrium-line altitude, to derive a spatially distributed estimate, accounting for measurements and snowline observations from all parts of Svalbard.

Geodetic Mass Balance

The geodetic mass balance refers to the mass balance determined by geodetic methods. Differencing elevation data over the entire glacier area from two or more different times yields a volume change that is converted into a mass balance accounting for the bulk density of the volume change. Different studies have made different assumptions (e.g., Moholdt et al., 2010; Nuth et al., 2010) about the value of the bulk density, but all agree with the recommended value by Huss (2013) within the uncertainty range.

Elevation data can be from a variety of sources: surface surveys; contours from older maps; digital elevation models made photogrammetrically from aerial photographs or satellite imagery; or satellite altimeters. This balance estimate accounts for frontal ablation, hence represents the total mass balance.

The most striking change since the Hagen et al. (2003a, 2003b) assessments is the more widespread availability of different remote-sensing data. Since the 2000s, the number of sensor types and platforms has grown considerably, and the resolution,

[1]https://wgms.ch/

[2]http://www.mosj.no/en/climate/land/mass-balance-glaciers.html

[3]https://sios-svalbard.org/metadata_search

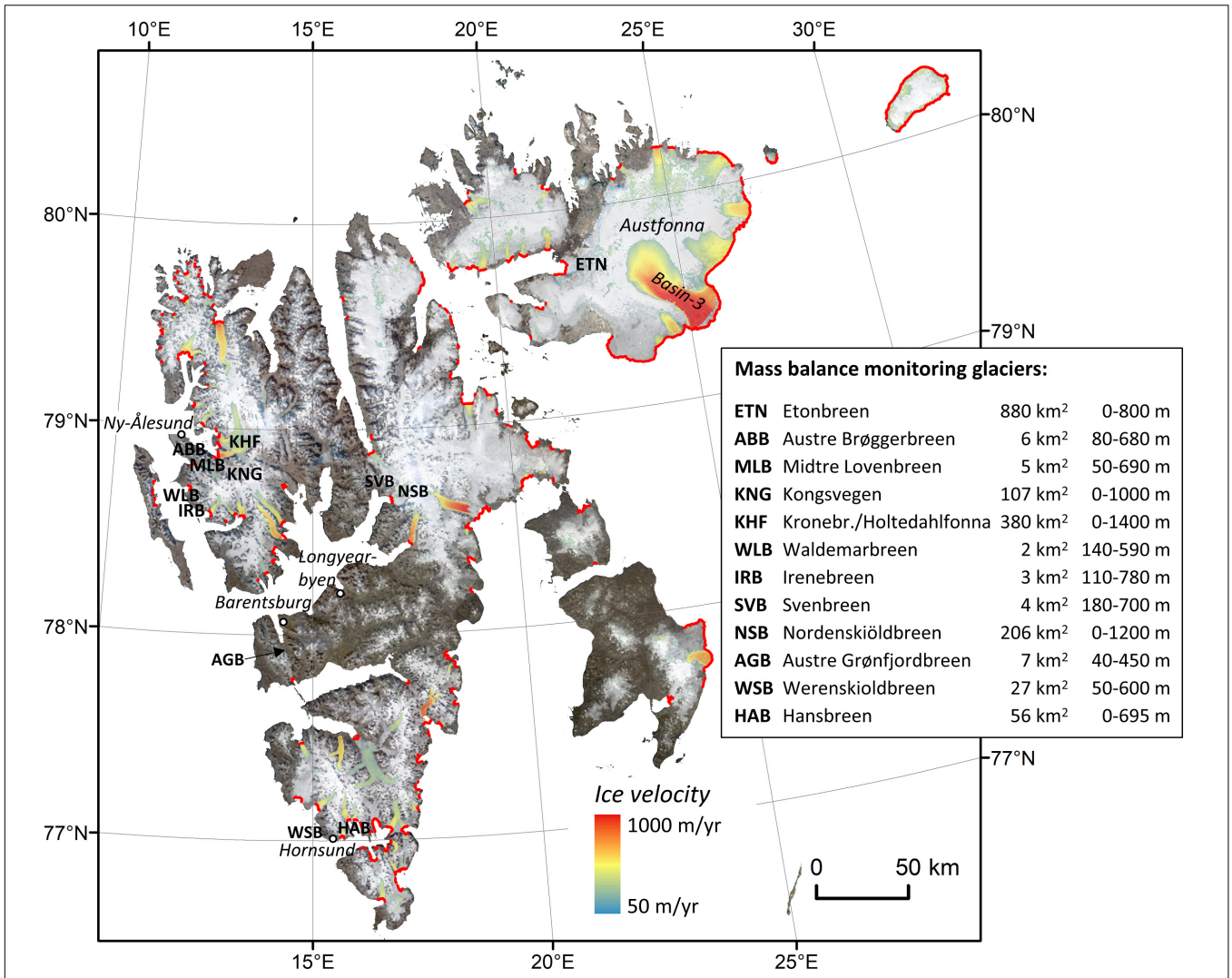

FIGURE 1 | Overview map of Svalbard, showing glacier-covered areas (white) with color-shaded surface velocities for 2018 in cases where glaciers moved faster than 50 m a^{-1}. Surface velocities have been retrieved from the NASA MEaSUREs ITS_LIVE project (Gardner et al., 2019). The red coastal lines show termini of tidewater glaciers from 2018. The background image is a Landsat-mosaic from toposvalbard.npolar.no. Abbreviated labels show the location of present glaciological mass balance monitoring glaciers on Svalbard, along with glacier area and elevation range.

accuracy and frequency of measurements have increased. Access to these data has become easier for a growing number of glacier-relevant measurements, such as surface elevation changes, digital elevation models (DEM) as well as land-surface temperatures, albedo, and glacier facies (e.g., Moholdt et al., 2010; Nuth et al., 2010; Østby et al., 2014; Gray et al., 2015).

Digital elevation models differencing to estimate the glacier volume change of Svalbard glaciers is mainly based on DEMs from older aerial photographs from the 1930s onward (Nuth et al., 2007; Girod et al., 2018), and on various DEMs from satellite data, including both optical stereo and radar interferometry (Nuth et al., 2019). While these DEMs cover large parts of Svalbard, some DEMs are also available locally, such as from optical satellite stereo (Deschamps-Berger et al., 2019), airborne laser scanning, and opportunistic flights (Girod et al., 2017). In general, all these DEMs have improved over time in coverage and spatial resolution, and are currently quickly improving on temporal resolution, providing unprecedented views on regional variability. In contrast to other methods, geodetic mass balance includes frontal ablation by iceberg calving from marine-terminating glaciers. The number of large surges that have occurred since 2003 (e.g., Nathorstbreen, Austfonna Basin-3, Negribreen) underscores the need to capture these dynamic ice losses for volume change estimates, and thus the value of the DEM differencing method to compute Svalbard-wide total mass balance. While DEM differencing is typically performed over several years to decades, the increasing availability of optical and radar satellite imagery allows annual or even sub-seasonal glacier surface velocity fields, contributing to better constraints upon the magnitude and variability of calving

fluxes (Dunse et al., 2015; Schellenberger et al., 2015). Despite the significantly improved possibility to estimate Svalbard's geodetic mass balance, temporally and spatially consistent and unbiased DEMs are still rare. DEM differencing thus requires often advanced analysis to remove effects such as those caused by spatial shifts between DEMs, or to handle data gaps (Nuth and Kääb, 2011; McNabb et al., 2019).

ICES at laser altimetry provided a consistent set of elevations and elevation changes over 2003–2009 (Moholdt et al., 2010; Nuth et al., 2010). The follow-up mission ICES at-2, which was successfully launched in late 2018, is expected to provide improved data. The new instrument will yield elevation data at higher spatial density, coverage and accuracy than its predecessor (Abdalati et al., 2010). Laser altimetry requires clear sky conditions, but offers high elevation accuracy, typically better than 20 cm (Shuman et al., 2006). While ICES at elevation measurements had a relatively large spacing (>150 m along ground track, and >10 km across track), which required special schemes to extrapolate elevation changes to the entire region, ICES at-2 tracks are much denser (<1 m along track, <2 km across track) and will improve regional volume change estimates.

Radar altimetry (CryoSat-2) (McMillan et al., 2014; Gray et al., 2015) is independent of cloud coverage and has high spatial and temporal coverage. Radar backscatter is affected by signal penetration into snow and firn, and some effort is necessary to better understand and quantify this effect. The spatial coverage of radar returns and thus ground elevation measurements is highly variable and depends on topography as it is determined by the point of closest approach (POCA). Interferometric processing (SARin) enables a more complete coverage; known as SWATH processing, the analysis takes into account the entire swath illuminated by the satellite radar beam during one overpass (Gray et al., 2013; Foresta et al., 2016, 2018; Gourmelen et al., 2018).

Gravimetry

A direct method for estimating mass change by gravimetry comes from the GRACE (Gravity Recovery and Climate Experiment) satellites, which mapped the time-varying gravity field of the Earth over the period 2002–2017. Spaceborne gravimetry allows monitoring mass changes, which, if corrected for a range of other gravitational effects, can provide information on regional glacier-related mass changes at monthly resolution (Wouters et al., 2008, 2019; Mémin et al., 2011; Matsuo and Heki, 2013). However, the GRACE footprint is large, typically >100,000 km^2 (Wouters et al., 2019), and so just a few points already cover a region the size of Svalbard. Furthermore, corrections must be made for ongoing and long-term isostatic rebound, as well as for unmixing the sea and land components of the combined gravimetric signal.

Modeling

Mass balance models, forced either by meteorological observations or output from regional climate models, evaluate the surface energy balance to compute the climatic mass balance. The most complete models contain a subsurface routine to account for the impact of water storage and refreezing on the mass and energy budgets. Field data are used to calibrate model parameters and to validate model output.

This approach typically requires two steps: the first is to derive meteorological input at appropriate spatial and temporal resolution and the second is to calculate CMB from this input.

Meteorological Forcing

As part of global glacier change estimates, some studies have either used globally gridded meteorological observations (Marzeion et al., 2012, 2015) or output from global climate models and reanalyses (Radic and Hock, 2011). These global products typically have coarse spatial resolution (0.5–1.0° or more), and therefore may be less representative for surface conditions in Svalbard. CMB processes vary at scales of a few km or less, due to orographic enhancement of precipitation, wind redistribution of snow, or topographically induced temperature variability. Models with global coverage typically do not resolve these scales.

Typically, Svalbard-specific studies have applied some refinement of reanalyses to adequately resolve these fines spatial scales. One way is to dynamically downscale global fields using a high-resolution, regional climate model. This method is computationally expensive and often compromises have to be made to keep the cost low, by limiting either the spatial resolution (Lang et al., 2015) or the modeling period (Aas et al., 2016).

Another approach is statistical downscaling: Möller et al. (2016) and Van Pelt et al. (2019) employed empirical relations to correct for the bias between intermediate-resolution regional climate model variables and corresponding local observations. The application of these methods to areas and periods not covered by observations implicitly assumes that the empirical relations are transferable in both space and time.

Finally, there is hybrid downscaling. Østby et al. (2017) employed simplified dynamical downscaling for some variables, whereas other variables were derived from spatio-temporal interpolation of coarsely resolved reanalysis data to the desired scale of the high-resolution grid used for CMB simulation (Schuler and Østby, 2020).

The performance of downscaling is usually assessed by comparison to meteorological measurements; however, there are only a few meteorological stations in Svalbard, and most of these located at low elevations in the more accessible fjords along the west coast of Spitsbergen. Therefore, the operational records are biased and are not representative for large parts of the mountainous archipelago. The CMB modeling studies make partial use of glaciological data from higher elevations and from eastern regions (Aas et al., 2016; Østby et al., 2017; Möller and Kohler, 2018; Van Pelt et al., 2019), not only to evaluate the performance of the CMB model but also to evaluate the downscaling of meteorological variables. In less rough topography, such as the smooth surface of the Austfonna ice cap, snow distribution on the surface is largely dominated by the spatial pattern of precipitation (Taurisano et al., 2007). Hence, measurements of snow accumulation at the end of the winter represent a little used opportunity to evaluate the performance of precipitation models on a seasonal timescale.

The availability of global atmospheric reanalysis data at improved spatial and temporal resolution, and improved consistency with available observations (e.g.,

Schuler and Østby, 2020), has sparked the application of gap-free meteorologically forced climatic mass balance models that cover the entire archipelago (e.g., Østby et al., 2017; Van Pelt et al., 2019). These models either directly incorporate local measurements or have been optimized to ensure agreement between simulated and observed values, and therefore play an important role in synthesizing the wealth of information that has become available.

Climatic Mass Balance (CMB) Models

A variety of different methods is available to compute CMB from meteorological forcing, ranging from simplified approaches that require extensive calibration, to physically based, coupled models of surface energy balance and snowpack evolution. Correspondingly, the output of physically based models provide a multitude of results that correspond to observable quantities. On the other hand, while the simplest models provide spatially and temporally integrated quantities like glacier-wide, annual climatic mass balance, they are potentially afflicted with considerable uncertainty due to compensating effects and biases.

The potential of using multiple and spatially distributed data sources for evaluating different aspects of model results has only been exploited in a few studies (e.g., Aas et al., 2016). Schuler et al. (2007) suggested that using multiple criteria was helpful in constraining parameter values for a temperature-index based CMB model of Austfonna. Rye et al. (2012) applied a formal procedure in multi-objective calibration of a CMB model of Midtre Lovenbreen, but used only different representations of the same underlying data as different objectives. Möller et al. (2011) directly used satellite-derived albedo and cloud cover in modeling. Østby et al. (2013) applied a Monte-Carlo scheme to determine a set of best-performing parameter combinations that render results within the uncertainties of measured CMB, land-surface temperature, albedo, and subsurface snow temperature distributions. Van Pelt et al. (2019) used a combination of stake and weather station data to calibrate the downscaling of precipitation, as well as energy balance parameters (Małecki, 2013). Małecki (2016) More sophisticated, formal data-assimilation methods, for instance Ensemble Kalman-filtering techniques (Małecki, 2020), have been applied in snow modeling with promising results (e.g., Aalstad et al., 2018), but this approach has not yet been adopted in glacier mass-balance modeling.

Frontal Ablation

Frontal ablation comprises both calving of ice at the glacier front as well as underwater melting. It is usually quantified by determining the mass flux through a gate close to the marine glacier terminus and considering mass changes down-glacier of this gate. This requires knowledge of the ice flow velocity, the cross-sectional area of the gate, as well as the advance or retreat of the glacier front and the CMB down-glacier from the gate. These quantities can be determined using satellite remote sensing, which provides information over large, often inaccessible areas. However, ice thickness along the flux gate is often not well determined, thus contributing to uncertainty in estimating frontal ablation.

Nuth et al. (2012) have determined the long-term mass change due to frontal ablation from the residual between the geodetic mass balance and simulated CMB. Their estimate applies to a single glacier, Kronebreen, but, in principle, this method could be extended to comprise all of Svalbard's tidewater glaciers.

Combined Approaches

Finally, some studies fused Svalbard-wide estimates with glaciological records to obtain annual resolution estimates of geodetic mass balance (Box et al., 2018; Zemp et al., 2019) or to obtain spatial variability based on satellite-elevation differencing (Gardner et al., 2013; Wouters et al., 2019).

RESULTS

Glaciological Mass Balance

Available long-term glaciological mass balance records (**Figure 2**) reveal a complex picture of different glacier evolution, with clear differences between small glaciers (<10 km^2) that are rapidly losing mass (Austre Brøggerbreen, Midtre Lovénbreen, Waldemarbreen, Irenebreen, Svenbreen, and Austre Grønfjordbreen) and larger glaciers (>50 km^2) like Kongsvegen, Kronebreen-Holtedahlfonna, Nordenskiöldbreen, Etonbreen, and Hansbreen, which are typically outlets from larger contiguous ice masses (ice fields and ice caps). The steeper slope of the cumulative mass balances shows that glaciers in southern and central Spitsbergen (Werenskioldbreen, Svenbreen, and Austre Grønfjordbreen) have more negative SMB than those located in NW Svalbard (Austre Brøggerbreen and Midtre Lovénbreen). Similarly, larger glaciers such as Hansbreen are losing mass more rapidly than at Kongsvegen, Kronebreen-Holtedahlfonna, Nordenskiöldbreen, or Etonbreen. The latter is an outlet from Austfonna and shows SMB conditions close to zero with little variability, although with a more negative trend after 2012.

Different slopes of the cumulative SMB in **Figures 2A,B** indicate a relationship between SMB and area of the respective glacier, which we illustrate in **Figure 2C** for four selected area classes. The relationship is such that smaller glaciers lose mass at much higher rates than larger glaciers due to their hypsometric distributions of area with elevation. A qualitatively similar relationship between the accumulation area ratio and glacier area is found for all glaciers in the Svalbard (see **Supplementary Material S1**), suggesting that the area-SMB relation is not only an artifact caused by the limited number of samples ($n = 12$). This area–SMB relation allows for upscaling of the 12 individual glaciological records to the entire glacier-covered area of Svalbard. In contrast to previous studies that have averaged all glaciological mass balance values and multiplied by the glacier area (either for all of Svalbard or sub-regions), we exploit the relationship between CMB and glacier size and apply it to each glacier of the Svalbard glacier database (Nuth et al., 2013; König et al., 2014) (**Figure 2D**). In this way, we obtain a new SMB estimate for Svalbard glaciers of -7 ± 2.1 Gt a^{-1} (2000–2019), the uncertainty of which has been derived from the 25 and 75 percentiles of the SMB distributions in each class (blue boxes in

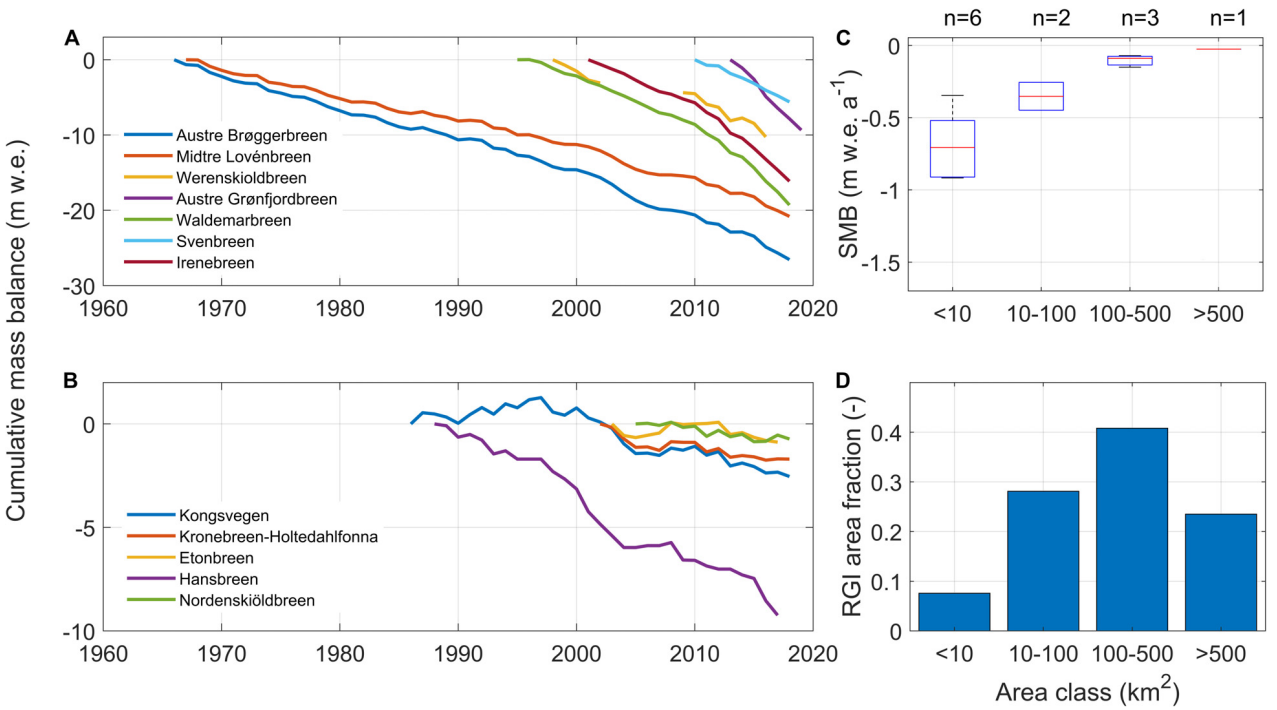

FIGURE 2 | Cumulative specific, glaciological mass balance (excluding frontal ablation) from *in situ* measurements at selected Svalbard glaciers, for glaciers smaller **(A)** and larger **(B)** than 50 km^2. Note the different scaling of the *y*-axes. **(C)** Boxplots of annual specific SMB averaged over the period since 2000 for four different area classes. **(D)** Fractions of glacier area occupied by glaciers in respective area classes, relative to the entire glacier area, for all Svalbard glaciers in the Randolph Glacier Inventory (Pfeffer et al., 2014); n indicates the number of surveyed glaciers in each area class.

Figure 2C). The mass loss of the individual area classes amounts to −2.1, −3.3, −1.4, and −0.2 Gt a^{-1} for the >10, 10–100, 100–500, and <500 km^2 classes, respectively. Interestingly, the number of surveyed glaciers for each area class demonstrates a bias of the monitoring programs toward logistically simpler, small glaciers. About half of the selected records are from glaciers smaller than 10 km^2; glaciers of that size occupy less than 10% of the total glacier-covered area, whereas glaciers in the two largest area classes together comprise 65% of the glacier-covered area but are monitored by only one third of the glaciological mass balance programs. The longest records are from small glaciers, and so the representativeness issue may explain the bias of previous assessments that were based on upscaling measurements from small glaciers only (**Supplementary Materials S1, S2**).

Geodetic Mass Balance

Nuth et al. (2010) compared satellite altimetry data from the ICES at mission for the period 2003–2007 to older topographic maps and digital elevation models for different epochs (1965–1990). Because the ICES at tracks are relatively sparse, they extrapolated along-track changes to the larger regions using glacier hypsometry. Significant thinning was detected at the lower elevations of most glaciers, and either slight thinning or thickening in the accumulation areas, except for glaciers that surged during the observation period; these glaciers showed thickening in the ablation area and thinning in the accumulation areas. However, the overall balance was very negative at −0.36 m w.e. a^{-1}, corresponding to −9.7 Gt a^{-1} (**Table 2**). As with the modeling results, the most negative geodetic balances are found in the south and the least negative balances in the northeast.

Moholdt et al. (2010) determined elevation changes along the ICES at tracks for the period 2003–2008, extrapolating these changes to the remaining glacier area using the same hypsometric approach as Nuth et al. (2010) to yield a Svalbard-wide estimate of −0.12 m w.e. a^{-1}, or −4.3 Gt a^{-1}. They found that most regions experienced low-elevation thinning and high-elevation balance or thickening, and that the largest ice losses occurred in the west and south, while northeastern Spitsbergen and the Austfonna ice cap slightly gained mass. This general pattern, however, does not apply for central Spitsbergen, with its mostly small alpine glaciers. Małecki (2016) demonstrated that glacier thinning here has been occurring at all elevations up to 1,000 m asl, for the period 1990–2011.

Analysis of older maps and modern DEMs (Kohler et al., 2007) shows that mass loss rates at Midtre Lovénbreen and Slakbreen, appear to have accelerated. For Midtre Lovénbreen, thinning rates for 2003–2005, were more than four times larger than the average for the first measurement period 1936–1962. On Slakbreen, thinning rates for the period 1990–2003 were more than four times that of the period 1961–1977. James et al. (2012) and Małecki (2013) found a similar increase in thinning rates for other glaciers around Svalbard, particularly in high-elevation areas. More pronounced thinning has been noted for Hansbreen and Hornbreen for two recent periods

TABLE 2 | Comparison of several Svalbard-wide estimates of annual glacier mass balance B_a using different methods.

Reference	Period	Method	Specific B_a (m w.e. a^{-1})	B_a (Gt a^{-1})	Balance component
Hagen et al., 2003a	∼1970–1999	Upscaling 1	−0.38 ± 0.33	−14 ± 12	Total
			−0.11	−4	Calving
Hagen et al., 2003b	∼1970–1999	Upscaling, 2	−0.12 ± 0.03	−4.5 ± 1	Total
Błaszczyk et al., 2009	1999–2006	Flux		−6.75 ± 1.7	Calving
Dunse et al., 2015	2013 (Basin-3)	Flux		−4.2 ± 1.6	Calving
Nuth et al., 2010	1965/90–2003/7	dh	−0.36 ± 0.02	−9.7 ± 0.55	Total
Moholdt et al., 2010	2003–2008	dh	−0.12 ± 0.04	−4.1 ± 1.4	Total
Lang et al., 2015	1979–2013	Model (10 km)	−0.04	−1.6	CMB
Aas et al., 2016	2003–2013	Model (3 km)	−0.26	−8.7	CMB
Østby et al., 2017	1957–2014	Model (1 km)	0.08	2.7	CMB
Möller and Kohler, 2018	1900–2010	Model (0.25 km)	−0.002	−0.07	CMB
Hanssen-Bauer et al., 2019	2004–2017	Model (2.5 km)	−0.26	−8.7	CMB
Van Pelt et al., 2019	1957–2018	Model (1 km)	0.09	3.0	CMB
Wouters et al., 2008	2003–2008	Gravimetry	−0.26 ± 0.09	−8.8 ± 3	Total
Jacob et al., 2012	2003–2010	Gravimetry	−0.09 ± 0.06	−3 ± 2	Total
Mémin et al., 2011	2003–2009	Gravimetry 1	−0.27 ± 0.03	−9.1 ± 1.0	Total
		Gravimetry 2	−0.46 ± 0.07	−15.5 ± 2.4	Total
Matsuo and Heki, 2013	2004–2012	Gravimetry	−0.11 ± 0.09	−3.7 ± 3.0	Total
Gardner et al., 2013	2003–2009	Gravimetry 1	−0.20 ± 0.06	−6.8 ± 2.0	Total
		Gravimetry 2	−0.13 ± 0.12	−4.4 ± 4.1	
Wouters et al., 2019	2002–2016	Gravimetry 1	−0.21 ± 0.04	−7.2 ± 1.4	Total
		Gravimetry 2	−0.27 ± 0.21	−9.1 ± 4.1	
Möller et al., 2016	2000–2011	Model (10 km)	−0.05 ± 0.4	−1.7 ± 13.6	CMB
Radic and Hock, 2011	1961–2000	Model	−0.04	−1.36	CMB
Dyurgerov and Meier, 2005	1961–2003	Upscaling	−0.17 ± 0.04	−5.78 ± 1.36	SMB
Marzeion et al., 2012, 2015	1901–2009	Model	−1.06 ± 0.15	−35.9 ± 5.3	SMB
Ohmura, 2006	1967–2001	Upscaling	−0.38	−13	SMB
Zemp et al., 2019	2006–2016	dh	−0.47 ± 0.23	−16 ± 8	Total
Box et al., 2018	1971–2017	Gravimetry, mix	−0.32 ± 0.09	−11 ± 3	Total
This study	2000–2019	Upscaling	−0.21 ± 0.06	−7.0 ± 2.1	SMB

The "flux" method refers to a combination of remotely sensed velocity fields and frontal area changes. "dh" refers to differencing elevation measurements by ground-based GPS profiling, air- or spaceborne photogrammetry, and laser or radar altimetry. "Gravimetry" refers to estimates derived from GRACE measurements; some studies use different corrections and obtain two estimates, indicated by numbers. Some estimates refer to different components of the total mass balance: calving, surface mass balance (SMB) and climatic mass balance (CMB) are marked in the table, where Total = CMB + Calving.

(2011–2015 and 2015–2017), based on differencing elevations obtained by photogrammetry using high-resolution satellite images (Błaszczyk et al., 2019). The surge of Basin 3 of Austfonna led to significant mass loss that has been quantified by McMillan et al. (2014) using repeat altimetry. This increasingly negative mass balance trend is consistent with both worldwide glacier trends as well as developments in the Arctic (Kaser et al., 2006).

Gravimetry

While satellite gravimetry provides an absolute measure of the total mass change in the region, the spatial resolution of GRACE is typically in the order of 0.5–1.0° (Wouters et al., 2019) and so determination of glacier mass balance is challenging. A number of studies (Mémin et al., 2011; Jacob et al., 2012; Matsuo and Heki, 2013; Wouters et al., 2019) working with the same dataset but covering slightly different periods, and using different data filtering methods, obtain a range of values for the total mass loss (**Table 1**). However, the main conclusion one can reach from the body of GRACE analyses is that all find a negative total mass balance for the Svalbard archipelago, with values ranging from −0.46 to −0.09 m w.e. a^{-1}, or −15.5 to −3.0 Gt a^{-1} (**Table 2**), even if the error range for some of the estimates extends them into the positive territory. Nevertheless, even though the reported range of absolute mass changes is large, gravimetry may still provide valuable information on the temporal evolution. The most recent regional estimate, covering the entire GRACE mission from 2002 to 2016, indicates an average total mass balance of -7.2 ± 1.4 Gt a^{-1} (Wouters et al., 2019).

Mass Balance Modeling

Compared to the first Svalbard-wide assessments (Hagen et al., 2003a,b), numerical modeling now plays an increasingly prominent role in glacier studies on Svalbard. Stimulated by the growing availability of observational data for model optimization, models have been increasingly used to simulate climatic mass balance (e.g., Lang et al., 2015; Aas et al., 2016; Østby et al., 2017; Möller and Kohler, 2018; Van Pelt et al., 2019) and ice flow (e.g., Dunse et al., 2011; Gladstone et al., 2014; Schäfer et al., 2014;

Vallot et al., 2017; Gong et al., 2018). Modeled CMB is spatially complete and covers the entire glacierized area of Svalbard, providing information at relatively high temporal resolution (sub-daily to hourly), depending on the meteorological forcing. These products can therefore be understood as spatial-temporal interpolators, and have great potential to synthesize a large amount of individual measurements for regional assessments.

Climatic mass balance models have been used both inline, coupled to regional climate models (Lang et al., 2015; Aas et al., 2016), and offline, forced by downscaled meteorological variables. Offline applications have used an entire spectrum of downscaling procedures, ranging from statistical relations (Möller and Kohler, 2018), intermediately complex methods (Østby et al., 2017; Van Pelt et al., 2019), and dynamical downscaling (Hanssen-Bauer et al., 2019). Temporal coverage varies and is either limited by computational cost or by availability of atmospheric reanalysis data. For instance, ERA-interim (Dee et al., 2011) reanalysis data are available since 1979, ERA-40 (Uppala et al., 2005) start in 1957, allowing longer-term simulations (Østby et al., 2017; Van Pelt et al., 2019), and the ERA-20C reanalysis dataset (Poli et al., 2016) pushes the limit even back to 1900 (Möller and Kohler, 2018).

To various degrees, all model studies so far have used an extensive set of measurements from mass balance stakes, AWSs, and firn cores across Svalbard for calibration and validation. **Table 2** provides an overview over the different applications, their temporal coverage as well as spatial resolution. All models reveal a distinctive pattern, ranging from negative CMB in southern Spitsbergen to more positive values in northeast Svalbard. This pattern reflects the gradient of air temperature (Hanssen-Bauer et al., 2019), and is also observed in the remotely sensed geodetic mass balance estimates (e.g., Nuth et al., 2010). Over the long-term (>50 years), all studies indicate a slightly positive CMB, but all show a clearly negative CMB for more recent periods, especially after 2000 (**Figure 3**). Although there is agreement on a tendency toward more negative CMB, trend analysis reveals its significance is largest in southern Svalbard, contributing to a Svalbard-wide trend of −0.06 m w.e. a^{-1} $decade^{-1}$ (Van Pelt et al., 2019). The simulated time series support the view that most of the variability of annual CMB is largely due to variations in summer, whereas winter CMB is more stable. Both Østby et al. (2017) and Van Pelt et al. (2019) find that increased melt and reduced refreezing leads to doubling in glacier runoff over the simulation period. In addition, Østby et al. (2017) find a strong correlation between CMB and summer temperature.

For all of Svalbard glaciers, specific refreezing amounts to about 0.22 m w.e. a^{-1}, i.e., corresponding to about 25% of the annual accumulation (Aas et al., 2016; Østby et al., 2017; Van Pelt et al., 2019). There is general agreement about the magnitude of refreezing in the different studies that quantify it, except for

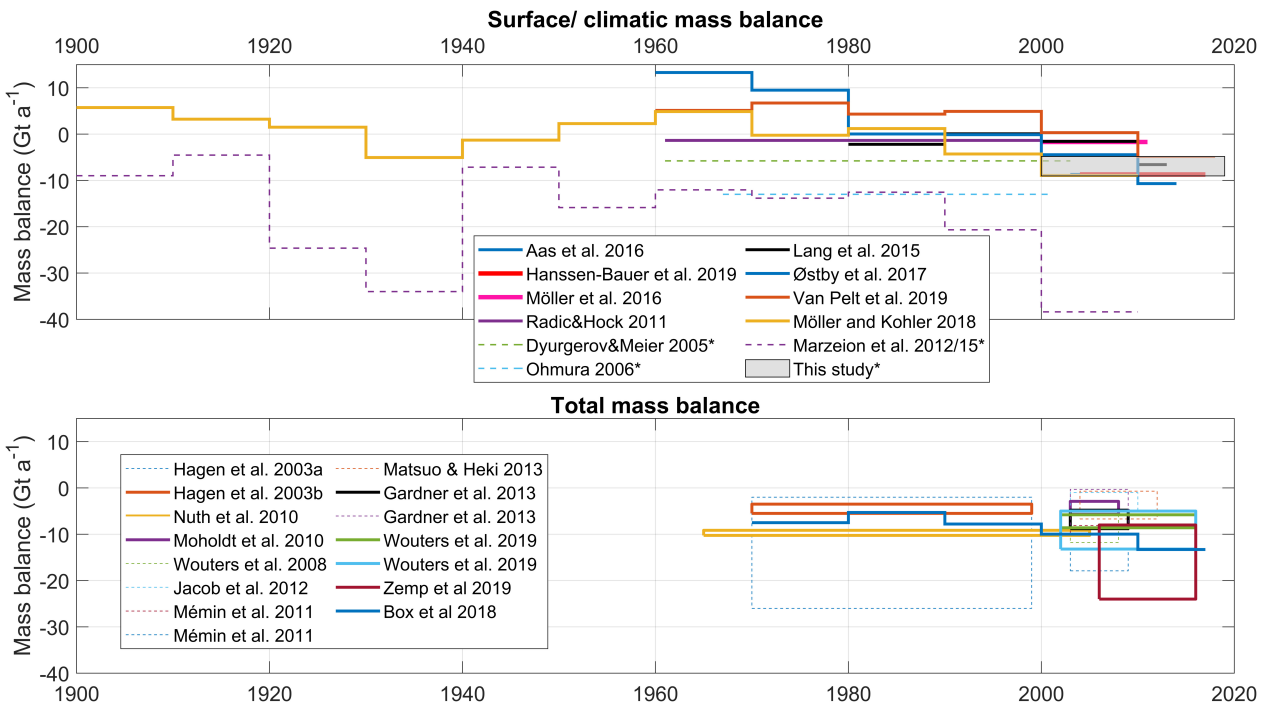

FIGURE 3 | Overview over different estimates of Svalbard glacier mass balance illustrating the period of coverage and related uncertainties of individual studies. The top panel shows estimates of surface mass balance and climatic mass balance, derived from upscaling of available *in situ* records and model simulations, respectively. Our new SMB estimate based on size-specific upscaling of measurements is shown as a gray box. The asterisks in the legend mark those estimates that refer to SMB whereas the others refer to CMB. The bottom panel illustrates estimates of total mass balance, based on geodetic and gravimetric methods. Most GRACE studies published two different estimates based on different processing of the underlying gravimetry data. Line styles indicate agreement with criteria defined in the text (solid = included in reconciliation, dashed = not included).

Lang et al. (2015), who come up with a considerably larger value of approximately 0.35 m w.e. a^{-1}. This presumably compensates for the reduced precipitation due to their lower model resolution (10 km), such that the CMB agrees with other studies. Refreezing generally decreases with time (Østby et al., 2017; Van Pelt et al., 2019) due to general warming and associated decrease in firn volume. However, these latter two studies do not show an obvious tipping point when increased refreezing due to increased meltwater production changes over to reduced refreezing caused by the reduction of the firn volume. Although this presumably has happened on Svalbard glaciers, the transition may have been smoother than that observed at the peripheral glaciers surrounding the Greenland ice sheet (Noel et al., 2017), and in addition, it may be masked by large year-to-year variability.

Frontal Ablation

The Błaszczyk et al. (2009) calving estimate is the only available study quantifying frontal ablation of all Svalbard glaciers. It is based on glacier flow velocities and front position changes extracted from ASTER images acquired from 2000 to 2006. However, due to its close dependence on glacier dynamics and ocean temperature (Luckman et al., 2015), frontal ablation varies over many time scales: seasonal, annual and especially, from irregularly occurring surges. Thus, the Błaszczyk et al. (2009) estimate represents a composite of snapshots over the 7-year period, rather than a temporal mean. The variability imposed by glacier surging can be considerable. For example, Dunse et al. (2015) quantified the sea-level effect of a single surge in Austfonna over the period 2012–2013, and found that the surge contributed 7 Gt a^{-1}, approximately matching the Błaszczyk et al. (2009) estimate, hence doubling the sea-level contribution per year of entire Svalbard during the surge period. When the only available estimate of frontal ablation from Svalbard glaciers (Błaszczyk et al., 2009) of nearly −7 Gt a^{-1} is added to the different CMB results, the overall Svalbard total mass balance becomes clearly negative (**Table 2** and **Figure 3**).

In response to climatically induced mass loss, the flux of ice toward the glacier terminus decreases and marine termini can quickly retreat. Many areas around Svalbard are experiencing rapid ice cliff recessions (tens to hundreds of meters annually), which significantly affects the marine physical environment and ecosystem (Torsvik et al., 2019). A special case is in Hornsund: bed elevations for the Hornbreen – Hambergbreen glacier system are approximately 40 m below sea level, such that a new strait between the Greenland Sea and the Barents Sea is expected within the next two to three decades, once the glacier termini have retreated there (Grabiec et al., 2018).

Synthesis

The spatial coverage of available glaciological mass balance measurements has improved over the past 20 years, especially with the inclusion of data from Austfonna, Nordenskiöldbreen, and Svenbreen, filling gaps both in terms of glacier types and location. Therefore, the presently available data are more representative for Svalbard than the pre-2000 record that was biased toward smaller glaciers in the vicinity of settlements in western Spitsbergen. For a representative picture of Svalbard-wide SMB, it is therefore imperative to have adequate spatial sampling and include records from the logistically more challenging eastern parts of Svalbard. CMB modeling is a valuable tool to link these measurements and to provide a gap-free product with high spatial and temporal resolution.

Glaciologically determined SMB and CMB differ where internal accumulation takes place below the last summer horizon. Locally, this difference may be significant and amount up to one third of total refreezing (Van Pelt and Kohler, 2015; Østby et al., 2017), but very few studies have determined internal accumulation. Internal accumulation is largest in areas of deep firn and on a glacier-wide scale or even regional scale, its effects may be less significant. Østby et al. (2017) are the only to report internal accumulation for all of Svalbard; their estimate for the years after 2000 is about 0.05 m w.e. a^{-1}, about the same magnitude as the uncertainty of our SMB estimate. Therefore, and as illustrated in **Figure 3, SMB** and **CMB** do not significantly differ, and for practical purposes, in the following synthesis, we treat both quantities in a single category (i.e., CMB).

Figure 4 shows some variation between the different estimates due to different periods covered and different methods employed. Nevertheless, the different results are consistent in that the CMB is negative in general and significantly more negative when frontal ablation at tidewater glaciers (**Figure 1**) is accounted for. The latter can cause drastic recession and thinning of marine terminating glaciers and extension of new branches of fjords. Analysis of time series indicates that there is a tendency toward increased mass loss over time.

Our new estimate, which is based on glaciologically measured CMB (**Figure 2**), aligns well with model results (**Figure 3**). The modeled timeseries (Lang et al., 2015; Østby et al., 2017; Möller and Kohler, 2018; Van Pelt et al., 2019) show a similar evolution after 1980, but differ before 1980. These differences in a period of positive CMB are indicative of differences in the way in which the different models distribute precipitation.

Before reconciling the ensembles of climatic and total mass balance estimates, we define criteria to reflect degrees of representativeness and confidence. Specifically, we focus on records that have:

1. Complete coverage of all regions (to avoid spatial bias),
2. Coverage of all glacier size classes (to avoid bias toward small glaciers),
3. High spatial resolution (10 km or better for model more representative model forcing).

Application of these criteria effectively removed records that are based on simple upscaling of a few datasets with location and size biases, as well as those gravimetry records that do not fuse with other techniques to achieve higher spatial resolution. The estimates selected for reconciling are indicated by thick lines in **Figure 4**.

Furthermore, the temporal resolution of geodetic estimates allows tracking the evolution of total mass balance for three epochs: 1970–1999, 2000–2009, and 2010–2019. For each of these epochs, we simply average the available ensemble members, as

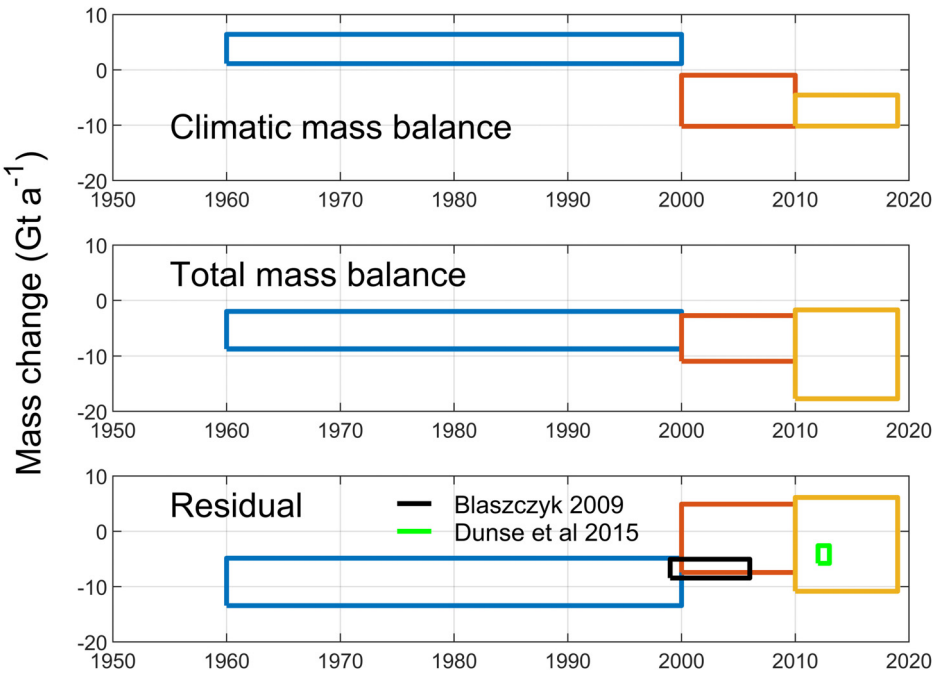

FIGURE 4 | Reconciled estimates for climatic mass balance, total mass balance and residuals for the three epochs. The residual comprises frontal ablation and the related uncertainty. The estimates are represented by colored boxes, their width representing the period for which the estimate has been derived and the height representing the uncertainty of the mass change.

well as derive a conservative error estimate, based on the spread of the ensemble. **Figure 4** illustrates the obtained reconciled estimates for CMB and total mass balance, together with the residuals. We consider the estimates for climatic and total mass balance as statistically independent and use the root sum of squares (RSS) to represent the combined uncertainty. According to Nuth et al. (2012), this residual represents the frontal ablation plus all errors. The boxes indicate that long-term frontal ablation is somewhere between −5 and −10 Gt a^{-1}, with considerable uncertainty. This estimate is supported by the independent Błaszczyk et al. (2009) estimate, which has some overlap with ours. The Dunse et al. (2015) value is only for Basin-3 of Austfonna, and demonstrates that surges can have a significant effect on the frontal ablation and add to variability over several years.

CONCLUDING DISCUSSION

In this study, we provide an overview over the different estimates of Svalbard-wide CMB and total mass balance, we describe the different methods that have been used and outline their fundamental differences and potentially associated problems. Several of the described techniques are new and have not been available for previous estimates (Hagen et al., 2003a,b). We further discuss new challenges for determining mass balance and highlight existing research gaps.

Increased activity, especially during the International Polar Year (Krupnik et al., 2011) paved the road to improving accuracy, spatial and temporal resolution and coverage as well as overall reliability of all the presented methods. Modeled values are the outcome of a chain of different process descriptions and should be evaluated at different stages along this chain.

New Challenges

As climate warms, glaciers experience more surface melting. However, because most Svalbard glaciers are polythermal, they have a considerable retention capacity, and large amounts of meltwater can refreeze in the porous snow and firn. Model estimates described above account for this process (in simplified ways), and all agree that this retention capacity has considerably decreased due to general warming and a reduction in firn areas (Østby et al., 2017; Van Pelt et al., 2019). Consequently, firn refreezing capacity has been reduced, and more surface meltwater will exit the glacier as runoff, although some of this water may be temporarily stored in surficial lakes or within perennial firn aquifers (Christianson et al., 2015). Due to their potential for releasing large amounts of water, for instance when intercepted by a crevasse, firn aquifers are of considerable interest for glacier dynamics and hydrology. Furthermore, these aquifers may promote microbial production (e.g., Anesio et al., 2017), and are the focus of ongoing research on glacier ecology (Hodson et al., 2015). In general, more sophisticated drainage system models have to be developed, to account for differences in spatially distributed or localized recharge (Gulley et al., 2012; Decaux et al., 2019). However, our understanding of processes that control the vertical percolation of surface meltwater and associated firn warming

needs to be refined, and studies of horizontal water motion are largely absent.

Changes in the size and volume of temperate ice bodies in polythermal glaciers are important for understanding their hydrothermal regime, their potential dynamic instability, and therefore, their response to climate change. Analysis of ground-based radio-echo sounding data of 16 glaciers at Nordenskiöld Land in Spitsbergen shows that 11 of them are polythermal (Macheret et al., 2019), with temperate ice volume fractions varying from 1 to 74%. Repeated radar surveys on selected polythermal glaciers along the same tracks serve as a useful tool in long-term glacier observation projects.

As mentioned above, several major surges have been observed since 2000 (Sund et al., 2009, 2014; Dunse et al., 2015; Sevestre et al., 2018; Nuth et al., 2019), despite an earlier prognosis that there might be a decline with ongoing warming (Dowdeswell et al., 1995). Instead, there has been an apparent increase in the number of surges, although it is still unclear whether this is due to more frequent surging or to improved observation capabilities (cf. Farnsworth et al., 2016). A related issue is the seasonal dynamical adjustment of ice speed during the start of the ablation period, due to the decrease of basal friction. The use of continuous GPS on Svalbard glaciers (Vieli et al., 2004; Dunse et al., 2012; Vallot et al., 2017; Van Pelt et al., 2018) has confirmed the relation between water supply and ice speed-ups observed elsewhere (Iken et al., 1983; Iken and Bindschadler, 1986).

Measurements of surging glaciers on Svalbard (e.g., Nuth et al., 2019) have led to recent theoretical progress in understanding the mechanics of destabilization and surge propagation (Sevestre et al., 2018; Thøgersen et al., 2019) and climatic controls on the global distribution of surging glaciers (Sevestre and Benn, 2015; Benn et al., 2019). While frequent surging in Svalbard imposes a challenge in determining the mass flux to the ocean, it also represents an opportunity for improving our understanding of dynamic instabilities and potential links to climate change. Svalbard is an ideal field laboratory for advancing our understanding of these processes, given the relative ease of access and an already existing knowledge and research infrastructure. Better understanding of glacier flow instabilities may provide important insights into the stability of the larger ice sheets of Greenland and Antarctica in a warming climate. The underlying processes could be studied on Svalbard not only with considerably lower logistical effort but also under a strong ongoing warming trend that anticipates the conditions which the ice-sheets are expected to face.

The total mass balance of Svalbard glaciers consists of two main parts, the climatic mass balance and the frontal ablation (calving and submarine melting). The only available estimate of current frontal ablation from Svalbard glaciers (Błaszczyk et al., 2009) is a composite of snapshots in the period 2000–2006 and amounts to 5.0–8.4 Gt a^{-1} (mean 6.75 Gt a^{-1}), hence, frontal ablation is roughly equivalent to the mass loss by climatic mass balance in the same period.

This work urgently needs to be updated, especially in light of several large glacier surges that discharged large volumes of ice into the ocean over short periods. In addition, surges transfer huge amounts of ice from the accumulation area to the lower receiving area, where it is exposed to intensified melting. There are some suggestions that increased melt hastens the triggering effect on surges (Dunse et al., 2015) and a number of other large-scale surges have been reported in Svalbard (Sund et al., 2014) as well as other Arctic regions (e.g., Willis et al., 2018). Surges affect frontal ablation and have the potential to considerably increase the sea-level contribution from land ice over short time periods.

Knowledge Gaps

We summarize the key questions that future research should address:

1. How large is the frontal ablation component? How much does it vary on different time scales (seasonal, interannual, and decadal)? How large are the relative contributions of calving and submarine melting? What are the governing processes?
2. What is the importance of surges for the total mass balance? What are the mechanisms that trigger instability and how does it propagate? Does climate change have an influence on surging?
3. How large is the retention capacity of Svalbard glaciers? How does it change and what is the partitioning between refreezing and liquid water storage? What are the implications of firn aquifers and supraglacial lakes for biogeochemistry and glacier dynamics?

Process understanding and quantification of these components is imperative for reliably assessing the future evolution:

1. How will glacier melt, refreezing and runoff evolve in the future?
2. How do dynamics and geometry of Svalbard glaciers respond to climate change?
3. What are the impacts on calving, surging and frontal ablation?

To adequately address the questions outlined above, the following research is needed:

1. Process studies of unstable glacier flow and its potential relationship to surface water meltwater.
2. Development of a coupled glacier mass balance-glacier dynamics model that can be applied to investigate the effects of different climate scenarios.
3. Detailed measurements (for instance of frontal ice thickness, subaqueous melt rates, meltwater plume dynamics) to quantify and understand frontal ablation and its drivers and to separate its components submarine melting and calving and their relative importance related to the climatic mass balance.
4. Geophysical characterization of firn aquifers and changes thereof, along with multi-disciplinary efforts to understand their implications for biogeochemistry.

DATA AVAILABILITY STATEMENT

Glaciological and glacier-related data from Svalbard are available from different repositories and meta-data bases. The most important examples are:

1. A digital elevation model at https://doi.org/10.21334/npolar.2014.dce53a47.
2. Glacier outlines at https://doi.org/10.21334/npolar.2013.89f430f8 (König et al., 2014). These data are also included in the Randolph Glacier Inventory (Pfeffer et al., 2014).
3. Glacier-wide glaciological mass balances in the database of the World Glacier Monitoring Service (WGMS; https://wgms.ch/), at the Norwegian Polar Data Centre https://data.npolar.no/home/ and Environmental monitoring of Svalbard and Jan Mayen (MOSJ): http://www.mosj.no/en/climate/land/mass-balance-glaciers.html.
4. The Centre for Polar Studies, University of Silesia in Katowice provides glacier relevant data and metadata at http://ppdb.us.edu.pl/geonetwork/srv/eng/catalog.search#/home.
5. Unrestricted access to the point stake mass balance, and the remaining AWS time series is provided upon request by contacting the institutes that collected the data.
6. Meteorological records for Ny-Ålesund, Hornsund, and Longyearbyen are accessible through https://seklima.met.no/observations/; and Kongsvegen AWS data at https://doi.org/10.21334/npolar.2017.5dc31930.
7. Surface velocities shown in **Figure 1** have been generated using auto-RIFT (Gardner et al., 2018) and provided by the NASA MEaSUREs ITS_LIVE project (Gardner et al., 2019).

AUTHOR CONTRIBUTIONS

This study is a collaborative effort where all authors have contributed data, discussed the design of the analysis as well as contributed to the writing and reviewing of the manuscript. TS coordinated the work of the consortium and writing of the manuscript. JK and AH edited English language of the manuscript.

FUNDING

This work was supported by the Research Council of Norway, project number 251658, Svalbard Integrated Arctic Earth Observing System – Knowledge Centre (SIOS-KC).

ACKNOWLEDGMENTS

We appreciate comments and contribution of data by B. Barzycka, M. Grabiec, and D. Ignatiuk (Centre for Polar Studies, University of Silesia in Katowice). Comments and suggestions of the Editor MZ and two reviewers helped to improve the quality of the manuscript and are highly appreciated.

SUPPLEMENTARY MATERIAL

The Supplementary Material for this article can be found online at: https://www.frontiersin.org/articles/10.3389/feart.2020.00156/full#supplementary-material

REFERENCES

Aalstad, K., Westermann, S., Schuler, T. V., Boike, J., and Bertino, L. (2018). Ensemble-based assimilation of fractional snow-covered area satellite retrievals to estimate the snow distribution at Arctic sites. *Cryosphere* 12, 247–270. doi: 10.5194/tc-12-247-2018

Aas, K. S., Dunse, T., Collier, E., Schuler, T. V., Berntsen, T. K., Kohler, J., et al. (2016). The climatic mass balance of Svalbard glaciers. *Cryosphere* 10, 1089–1104. doi: 10.5194/tc-10-1089-2016

Abdalati, W., Zwally, H. J., Bindschadler, R., Csatho, B., Farrell, S. L., Fricker, H. A., et al. (2010). The ICES at-2 laser altimetry mission. *Proc. IEEE* 98, 735–751. doi: 10.1109/JPROC.2009.2034765

Ahlmann, H. W. S. (1933). Scientific results of the swedish-norwegian arctic expedition in the summer of 1931. Part VIII. Glaciology. *Geogr. Ann.* 15, 161–216. doi: 10.1080/20014422.1933.11880566

AMAP (2017). *Snow, Water, Ice and Permafrost in the Arctic (SWIPA) 2017*. Oslo: Arctic Monitoring and Assessment Programme (AMAP).

Anesio, A. M., Lutz, S., Chrismas, N. A. M., and Benning, L. G. (2017). The microbiome of glaciers and ice sheets. *NPJ Biofilms Microb.* 3:10. doi: 10.1038/s41522-017-0019-0

Benn, D. I., Fowler, A. C., Hewitt, I., and Sevestre, H. (2019). A general theory of glacier surges. *J. Glaciol.* 65, 701–716. doi: 10.1017/jog.2019.62

Błaszczyk, M., Ignatiuk, D., Grabiec, M., Kolondra, L., Laska, M., Decaux, L., et al. (2019). Quality assessment and glaciological applications of digital elevation models derived from space-borne and aerial images over two tidewater glaciers of southern spitsbergen. *Remote Sens.* 11:1121. doi: 10.3390/rs11091121

Błaszczyk, M., Jania, J. A., and Hagen, J. O. (2009). Tidewater glaciers of Svalbard: recent changes and estimates of calving fluxes. *Pol. Polar Res.* 30:85.

Błaszczyk, M., Jania, J. A., and Kolondra, L. (2013). Fluctuations of tidewater glaciers in Hornsund Fjord (Southern Svalbard) since the beginning of the 20th century. *Pol. Polar Res.* 34, 327–352.

Box, J. E., Colgan, W. T., Wouters, B., Burgess, D. O., O'Neel, S., Thomson, L. I., et al. (2018). Global sea-level contribution from Arctic land ice: 1971–2017. *Environ. Res. Lett.* 13:125012. doi: 10.1088/1748-9326/aaf2ed

Christianson, K., Kohler, J., Alley, R. B., Nuth, C., and van Pelt, W. J. J. (2015). Dynamic perennial firn aquifer on an Arctic glacier. *Geophys. Res. Lett.* 42, 1418–1426. doi: 10.1002/2014gl062806

Church, J. A., Clark, P. U., Cazenave, A., Gregory, J. M., Jevrejeva, S., Levermann, A., et al. (2014). "Sea Level Change," in *Climate Change 2013 – The Physical Science Basis: Working Group I Contribution to the Fifth Assessment Report of the Intergovernmental Panel on Climate Change*, ed. Intergovernmental Panel on Climate (Cambridge: Cambridge University Press), 1137–1216.

Cogley, J. G., Hock, R., Rasmussen, L. A., Arendt, A. A., Bauder, A., Braithwaite, R. J., et al. (2011). "Glossary of Glacier mass balance and related terms," in *IHP-VII Technical Documents in Hydrology*, ed. IACS (Paris: UNESCO-IHP).

Decaux, L., Grabiec, M., Ignatiuk, D., and Jania, J. (2019). Role of discrete water recharge from supraglacial drainage systems in modeling patterns of subglacial conduits in Svalbard glaciers. *Cryosphere* 13, 735–752. doi: 10.5194/tc-13-735-2019

Dee, D. P., Uppala, S. M., Simmons, A. J., Berrisford, P., Poli, P., Kobayashi, S., et al. (2011). The ERA-Interim reanalysis: configuration and performance of the data assimilation system. *Q. J. R. Meteorol. Soc.* 137, 553–597. doi: 10.1002/qj.828

Deschamps-Berger, C., Nuth, C., Van Pelt, W., Berthier, E., Kohler, J., and Altena, B. A. S. (2019). Closing the mass budget of a tidewater glacier: the example of Kronebreen. Svalbard. *J. Glaciol.* 65, 136–148. doi: 10.1017/jog.2018.98

Dowdeswell, J. A., Hodgkins, R., Nuttall, A.-M., Hagen, J. O., and Hamilton, G. S. (1995). Mass balance change as a control on the frequency and occurrence of glacier surges in Svalbard. Norwegian High Arctic. *Geophys. Res. Lett.* 22, 2909–2912. doi: 10.1029/95gl02821

Dunse, T., Greve, R., Schuler, T. V., and Hagen, J. O. (2011). Permanent fast flow versus cyclic surge behaviour: numerical simulations of the Austfonna ice cap and Svalbard. *J. Glaciol.* 57, 247–259.

Dunse, T., Schellenberger, T., Hagen, J. O., Kääb, A., Schuler, T. V., and Reijmer, C. H. (2015). Surge mechanisms by hydro-thermodynamic feedback. *Cryosphere* 9, 197–215. doi: 10.5194/tc-9-197-2015

Dunse, T., Schuler, T. V., Hagen, J. O., and Reijmer, C. H. (2012). Seasonal speed-up of two outlet glaciers of Austfonna. Svalbard, inferred from continuous GPS measurements. *Cryosphere* 6, 453–466. doi: 10.5194/tc-6-453-2012

Dyurgerov, M., and Meier, M. F. (2005). "Glaciers and the changing earth system: a 2004 snapshot," in *Occasional paper 58*, (Boulder, CO: Institute of Arctic and Alpine Research).

Farnsworth, W. R., Ingólfsson, Ó, Retelle, M., and Schomacker, A. (2016). Over 400 previously undocumented Svalbard surge-type glaciers identified. *Geomorphology* 264, 52–60. doi: 10.1016/j.geomorph.2016.03.025

Foresta, L., Gourmelen, N., Pálsson, F., Nienow, P., Björnsson, H., and Shepherd, A. (2016). Surface elevation change and mass balance of Icelandic ice caps derived from swath mode CryoSat-2 altimetry. *Geophys. Re. Lett.* 43, 12,138–12,145. doi: 10.1002/2016GL071485

Foresta, L., Gourmelen, N., Weissgerber, F., Nienow, P., Williams, J. J., Shepherd, A., et al. (2018). Heterogeneous and rapid ice loss over the patagonian ice fields revealed by CryoSat-2 swath radar altimetry. *Remote Sens. Environ.* 211, 441–455. doi: 10.1016/j.rse.2018.03.041

Fürst, J. J., Navarro, F., Gillet-Chaulet, F., Huss, M., Moholdt, G., Fettweis, X., et al. (2018). The Ice-Free Topography of Svalbard. *Geophys. Res. Lett.* 45, 11760–11769. doi: 10.1029/2018gl079734

Gardner, A. S., Moholdt, G., Scambos, T., Fahnstock, M., Ligtenberg, S., and van den Broeke, M., et al. (2018). Increased West Antarctic and unchanged East Antarctic ice discharge over the last 7 years. *Cryosphere*. 12, 521–547. doi: 10.5194/tc-12-521-2018

Gardner, A. S., Fahnestock, M. A., and Scambos, T. A. (2019). *ITS_LIVE Regional Glacier and Ice Sheet Surface Velocities*. Boulder, CO: National Snow and Ice Data Center.

Gardner, A. S., Moholdt, G., Cogley, J. G., Wouters, B., Arendt, A. A., Wahr, J., et al. (2013). A reconciled estimate of glacier contributions to sea level rise: 2003 to 2009. *Science* 340, 852–857. doi: 10.1126/science.1234532

Girod, L., Nielsen, N. I., Couderette, F., Nuth, C., and Kääb, A. (2018). Precise DEM extraction from Svalbard using 1936 high oblique imagery. *Geosci. Instrum. Method. Data Syst.* 7, 277–288. doi: 10.5194/gi-7-277-2018

Girod, L., Nuth, C., Kääb, A., Etzelmüller, B., and Kohler, J. (2017). Terrain changes from images acquired on opportunistic flights by SfM photogrammetry. *Cryosphere* 11, 827–840. doi: 10.5194/tc-11-827-2017

Gladstone, R., Schäfer, M., Zwinger, T., Gong, Y., Strozzi, T., Mottram, R., et al. (2014). Importance of basal processes in simulations of a surging Svalbard outlet glacier. *Cryosphere* 8, 1393–1405. doi: 10.5194/tc-8-1393-2014

Gong, Y., Zwinger, T., Åström, J., Altena, B., Schellenberger, T., Gladstone, R., et al. (2018). Simulating the roles of crevasse routing of surface water and basal friction on the surge evolution of Basin 3. Austfonna ice cap. *Cryosphere* 12, 1563–1577. doi: 10.5194/tc-12-1563-2018

Gourmelen, N., Escorihuela, M. J., Shepherd, A., Foresta, L., Muir, A., Garcia-Mondéjar, A., et al. (2018). CryoSat-2 swath interferometric altimetry for mapping ice elevation and elevation change. *Adv. Space Res.* 62, 1226–1242. doi: 10.1016/j.asr.2017.11.014

Grabiec, M., Ignatiuk, D., Jania, J. A., Moskalik, M., Głowacki, P., Błaszczyk, M., et al. (2018). Coast formation in an Arctic area due to glacier surge and retreat: the Hornbreen–Hambergbreen case from Spistbergen. *Earth Surf. Proc. Landforms* 43, 387–400. doi: 10.1002/esp.4251

Gray, L., Burgess, D., Copland, L., Cullen, R., Galin, N., Hawley, R., et al. (2013). Interferometric swath processing of Cryosat data for glacial ice topography. *Cryosphere* 7, 1857–1867. doi: 10.5194/tc-7-1857-2013

Gray, L., Burgess, D., Copland, L., Demuth, M. N., Dunse, T., Langley, K., et al. (2015). CryoSat-2 delivers monthly and inter-annual surface elevation change for Arctic ice caps. *Cryosphere* 9, 1895–1913. doi: 10.5194/tc-9-1895-2015

Gulley, J. D., Grabiec, M., Martin, J. B., Jania, J., Catania, G., and Glowacki, P. (2012). The effect of discrete recharge by moulins and heterogeneity in flow-path efficiency at glacier beds on subglacial hydrology. *J. Glaciol.* 58, 926–940. doi: 10.3189/2012JoG11J189

Hagen, J. O., Kohler, J., Melvold, K., and Winther, J.-G. (2003a). Glaciers in Svalbard: mass balance, runoff and freshwater flux. *Polar Res.* 22, 145–159. doi: 10.1111/j.1751-8369.2003.tb00104.x

Hagen, J. O., Melvold, K., Pinglot, F., and Dowdeswell, J. A. (2003b). On the net mass balance of the glaciers and ice caps in Svalbard, Norwegian Arctic. *Arctic Antarctic Alp. Res.* 35, 264–270. doi: 10.1657/1523-0430

Hagen, J. O., and Liestøl, O. (1990). Long-term glacier mass-balance investigations in svalbard, 1950–88. *Ann. Glaciol.* 14, 102–106. doi: 10.3189/S0260305500008351

Hagen, J. O., Liestøl, O., Roland, E., and Jørgensen, T. (1993). *Glacier Atlas of Svalbard and Jan Mayen*. Oslo: Norwegian Polar Institute.

Hanssen-Bauer, I., Førland, E., Hisdal, H., Mayer, S., Sandø, A., Sorteberg, A., et al. (2019). "Climate in Svalbard 2100 - a knowledge base for climate adaptation," in *Norwegian Environment Agency (Miljødirektoratet)*. Oslo: Norwegian Centre for Climate Services).

Hock, R., Bliss, A., Marzeion, B. E. N., Giesen, R. H., Hirabayashi, Y., Huss, M., et al. (2019). GlacierMIP – A model intercomparison of global-scale glacier mass-balance models and projections. *J. Glaciol.* 65, 453–467. doi: 10.1017/jog.2019.22

Hodson, A., Brock, B., Pearce, D., Laybourn-Parry, J., and Tranter, M. (2015). Cryospheric ecosystems: a synthesis of snowpack and glacial research. *Environ. Res. Lett.* 10:110201. doi: 10.1088/1748-9326/10/11/110201

Huss, M. (2013). Density assumptions for converting geodetic glacier volume change to mass change. *Cryosphere* 7, 877–887. doi: 10.5194/tc-7-877-2013

IGRAS (2020). *Mass Balance of Austre Grønfjordbreen*. Moscow: Institute of Geography, Russian Academy of Sciences .

Iken, A., and Bindschadler, R. A. (1986). Combined measurements of subglacial water pressure and surface velocity of Findelengletscher, Switzerland: conclusions about drainage system and sliding mechanism. *J. Glaciol.* 32, 101–119. doi: 10.3189/S0022143000006936

Iken, A., Röthlisberger, H., Flotron, A., and Haeberli, W. (1983). The uplift of unteraargletscher at the beginning of the melt season—A Consequence of Water Storage at the Bed? *J. Glaciol.* 29, 28–47. doi: 10.3189/S0022143000005128

IPCC (2019). in *IPCC Special Report on the Ocean and Cryosphere in a Changing Climate*, eds H.-O. Pörtner, P. Masson-Delmotte, M. Zhai, E. Tignor, K. Poloczanska, A. Mintenbeck, et al. (Geneva: IPCC).

Isaksen, K., Nordli, Ø, Førland, E. J., Łupikasza, E., Eastwood, S., and Niedźwiedź, T. (2016). Recent warming on Spitsbergen—Influence of atmospheric circulation and sea ice cover. *J. Geophys. Res. Atmosph.* 121, 913–911. doi: 10.1002/2016JD025606

Jacob, T., Wahr, J., Pfeffer, W. T., and Swenson, S. (2012). Recent contributions of glaciers and ice caps to sea level rise. *Nature* 482, 514–518. doi: 10.1038/nature10847

James, T. D., Murray, T., Barrand, N. E., Sykes, H. J., Fox, A. J., and King, M. A. (2012). Observations of enhanced thinning in the upper reaches of Svalbard glaciers. *Cryosphere* 6, 1369–1381. doi: 10.5194/tc-6-1369-2012

Kaser, G., Cogley, J. G., Dyurgerov, M. B., Meier, M. F., and Ohmura, A. (2006). Mass balance of glaciers and ice caps: consensus estimates for 1961–2004. *Geophys. Res. Lett.* 33:L19501. doi: 10.1029/2006GL027511

Kohler, J. (2013). *Mass Balance for Glaciers Near Ny-Ålesund*. Tromsø: Norwegian Polar Institute., doi: 10.21334/npolar.2013.ad6c4c5a

Kohler, J., James, T. D., Murray, T., Nuth, C., Brandt, O., Barrand, N. E., et al. (2007). Acceleration in thinning rate on western Svalbard glaciers. *Geophys. Res. Lett.* 34:L18502. doi: 10.1029/2007GL030681

König, M., Nuth, C., Kohler, J., Moholdt, G., and Pettersen, R. (2014). "A digital glacier database for svalbard," in *Global Land Ice Measurements from Space*, eds J. S. Kargel, G. J. Leonard, M. P. Bishop, A. Kääb, and B. H. Raup (Berlin: Springer Berlin Heidelberg), 229–239.

Krupnik, I., Allison, I., Bell, R., Cutler, P., Hik, D., López-Martínez, J., et al. (2011). *Understanding Earth's Polar Challenges:International Polar Year 2007-2008. Summary by the IPY Joint Committee*. Rovaniemi: University of the Arctic.

Lang, C., Fettweis, X., and Erpicum, M. (2015). Stable climate and surface mass balance in Svalbard over 1979-2013 despite the Arctic warming. *Cryosphere* 9, 83–101. doi: 10.5194/tc-9-83-2015

Luckman, A., Benn, D. I., Cottier, F., Bevan, S., Nilsen, F., and Inall, M. (2015). Calving rates at tidewater glaciers vary strongly with ocean temperature. *Nat. Commun.* 6:8566. doi: 10.1038/ncomms9566

Macheret, Y., Glazovsky, A., Lavrentiev, I., and Marchuk, I. (2019). Distribution of cold and temperate ice in glaciers on the Nordenskiöld Land, Spitsbergen, from ground-based radio-echo sounding. *Ice and Snow* 59, 149–166. doi: 10.15356/20766734-2019-2-430

Małecki, J. (2013). Elevation and volume changes of seven Dickson Land glaciers. Svalbard, 1960-1990-2009. *Polar Res.* 32:18400. doi: 10.3402/polar.v32i0.18400

Małecki, J. (2016). Accelerating retreat and high-elevation thinning of glaciers in central Spitsbergen. *Cryosphere* 10, 1317–1329. doi: 10.5194/tc-10-1317-2016

Małecki, J. (2020). *Annual Mass Balance of Svenbreen*. Poznań: Adam Mickiewicz University.

Martin-Espanol, A., Navarro, F. J., Otero, J., Lapazaran, J. J., and Błaszczyk, M. (2015). Estimate of the total volume of Svalbard glaciers, and their potential contribution to sea-level rise, using new regionally based scaling relationships. *J. Glaciol.* 61, 29–41. doi: 10.3189/2015JoG14J159

Marzeion, B., Jarosch, A. H., and Hofer, M. (2012). Past and future sea-level change from the surface mass balance of glaciers. *Cryosphere* 6, 1295–1322. doi: 10.5194/tc-6-1295-2012

Marzeion, B., Leclercq, P. W., Cogley, J. G., and Jarosch, A. H. (2015). Brief Communication: Global reconstructions of glacier mass change during the 20th century are consistent. *Cryosphere* 9, 2399–2404. doi: 10.5194/tc-9-2399-2015

Matsuo, K., and Heki, K. (2013). Current ice loss in small glacier systems of the Arctic Islands (Iceland, Svalbard, and the Russian High Arctic) from satellite gravimetry. *Terr. Atmos. Oceanic Sci.* 24, 657–670. doi: 10.3319/TAO.2013.02.22.01(TibXS)

Maturilli, M., Herber, A., and König-Langlo, G. (2013). Climatology and time series of surface meteorology in Ny-Ålesund, Svalbard. *Earth Syst. Sci. Data* 5, 155–163.

McMillan, M., Shepherd, A., Gourmelen, N., Dehecq, A., Leeson, A., Ridout, A., et al. (2014). Rapid dynamic activation of a marine-based Arctic ice cap. *Geophys. Res. Lett.* 41, 8902–8909. doi: 10.1002/2014GL062255

McNabb, R., Nuth, C., Kääb, A., and Girod, L. (2019). Sensitivity of glacier volume change estimation to DEM void interpolation. *Cryosphere* 13, 895–910. doi: 10.5194/tc-13-895-2019

Meier, M. F., Dyurgerov, M. B., Rick, U. K., Neel, S., Pfeffer, W. T., Anderson, R. S., et al. (2007). Glaciers dominate eustatic sea-level rise in the 21st century. *Science* 317:1064. doi: 10.1126/science.1143906

Mémin, A., Rogister, Y., Hinderer, J., Omang, O. C., and Luck, B. (2011). Secular gravity variation at Svalbard (Norway) from ground observations and GRACE satellite data. *Geophys. J. Int.* 184, 1119–1130. doi: 10.1111/j.1365-246X.2010.04922.x

Moholdt, G., Nuth, C., Hagen, J. O., and Kohler, J. (2010). Recent elevation changes of Svalbard glaciers derived from ICES at laser altimetry. *Remote Sens. Environ.* 114, 2756–2767. doi: 10.1016/j.rse.2010.06.008

Möller, M., Finkelnburg, R., Braun, M., Hock, R., Jonsell, U., Pohjola, V. A., et al. (2011). Climatic mass balance of the ice cap vestfonna, svalbard: a spatially distributed assessment using ERA-Interim and MODIS data. *J. Geophys.Res. : Earth Surf.* 116:F03009. doi: 10.1029/2010JF001905

Möller, M., and Kohler, J. (2018). Differing climatic mass balance evolution across svalbard glacier regions over 1900-2010. *Front. Earth Sci.* 6:128. doi: 10.3389/feart.2018.00128

Möller, M., Navarro, F., and Martín-Español, A. (2016). Monte Carlo modelling projects the loss of most land-terminating glaciers on Svalbard in the 21st century under RCP 8.5 forcing. *Environ. Re. Lett.* 11:94006. doi: 10.1088/1748-9326

Noel, B., van de Berg, W. J., Lhermitte, S., Wouters, B., Machguth, H., Howat, I., et al. (2017). A tipping point in refreezing accelerates mass loss of Greenland's glaciers and ice caps. *Nat. Commun.* 8:14730. doi: 10.1038/ncomms14730

Nordli, O., Przybylak, R., Ogilvie, A. E. J., and Isaksen, K. (2014). Long-term temperature trends and variability on Spitsbergen: the extended Svalbard Airport temperature series, 1898-2012. *Polar Res.* 33:21349. doi: 10.3402/polar.v33.21349

Norwegian Polar Institute, and University of Oslo (2020). "Cumulative mass balance for glaciers in Svalbard," in *Environmental monitoring of Svalbard and Jan Mayen*. New Delhi: MOS

Nuth, C., Gilbert, A., Köhler, A., McNabb, R., Schellenberger, T., Sevestre, H., et al. (2019). Dynamic vulnerability of an Arctic tidewater glacier. *Sci. Rep.* 9:5541. doi: 10.1038/s41598-019-41117-0

Nuth, C., and Kääb, A. (2011). Co-registration and bias corrections of satellite elevation data sets for quantifying glacier thickness change. *Cryosphere* 5, 271–290. doi: 10.5194/tc-5-271-2011

Nuth, C., Kohler, J., Aas, H. F., Brandt, O., and Hagen, J. O. (2007). Glacier geometry and elevation changes on Svalbard (1936-90): a baseline dataset. *Ann. Glaciol.* 46, 106–116. doi: 10.3189/172756407782871440

Nuth, C., Kohler, J., Konig, M., von Deschwanden, A., Hagen, J. O., Kaab, A., et al. (2013). Decadal changes from a multi-temporal glacier inventory of Svalbard. *Cryosphere* 7, 1603–1621. doi: 10.5194/tc-7-1603-2013

Nuth, C., Moholdt, G., Kohler, J., Hagen, J. O., and Kaab, A. (2010). Svalbard glacier elevation changes and contribution to sea level rise. *J. Geophys. Res. -Earth Surf.* 115, F01008. doi: 10.1029/2008jf001223

Nuth, C., Schuler, T. V., Kohler, J., Altena, B., and Hagen, J. O. (2012). Estimating the long-term calving flux of Kronebreen, Svalbard, from geodetic elevation changes and mass-balance modelling. *J. of Glaciol* 58, 119–133.

Ohmura, A. (2006). Changes in mountain glaciers and ice caps during the 20th century. *Ann. Glaciol.* 43, 361–368. doi: 10.3189/172756406781812212

Østby, T. I., Schuler, T. V., Hagen, J. O., Hock, R., Kohler, J., and Reijmer, C. H. (2017). Diagnosing mass balance of glaciers in Svalbard. *Cryosphere* 11, 191–215. doi: 10.5194/tc-11-191-2017

Østby, T. I., Schuler, T. V., Hagen, J. O., Hock, R., and Reijmer, L. H. (2013). Parameter uncertainty, refreezing and surface energy balance modelling at Austfonna ice cap, Svalbard, 2004-08. *Ann. Glaciol.* 54, 229–240. doi: 10.3189/2013AoG63A280

Østby, T. I., Schuler, T. V., and Westermann, S. (2014). Severe cloud contamination of MODIS Land Surface Temperatures over an Arctic ice cap. Svalbard. *Remote Sens. Environ.* 142, 95–102. doi: 10.1016/j.rse.2013.11.005

Parkes, D., and Marzeion, B. (2018). Twentieth-century contribution to sea-level rise from uncharted glaciers. *Nature* 563, 551–554. doi: 10.1038/s41586-018-0687-9

Pfeffer, W. T., Arendt, A. A., Bliss, A., Bolch, T., Cogley, J. G., Gardner, A. S., et al. (2014). The randolph glacier inventory: a globally complete inventory of glaciers. *J. Glaciol.* 60, 537–552. doi: 10.3189/2014JoG13J176

Pinglot, J. F., Hagen, J. O., Melvold, K., Eiken, T., and Vincent, C. (2001). A mean net accumulation pattern derived from radioactive layers and radar soundings on Austfonna. Nordaustlandet, Svalbard. *J. Glaciol.* 47, 555–566. doi: 10.3189/172756501781831800

Poli, P., Hersbach, H., Dee, D. P., Berrisford, P., Simmons, A. J., Vitart, F., et al. (2016). ERA-20C: an atmospheric reanalysis of the Twentieth Century. *J. Clim.* 29, 4083–4097. doi: 10.1175/Jcli-D-15-0556.1

Radic, V., and Hock, R. (2011). Regionally differentiated contribution of mountain glaciers and ice caps to future sea-level rise. *Nat. Geosci.* 4, 91–94. doi: 10.1038/Ngeo1052

Rye, C. J., Willis, I. C., Arnold, N. S., and Kohler, J. (2012). On the need for automated multiobjective optimization and uncertainty estimation of glacier mass balance models. *J. Geophys. Res. Earth Surf.* 117:F02005. doi: 10.1029/2011JF002184

Schäfer, M., Gillet-Chaulet, F., Gladstone, R., Pettersson, R., Pohjola, V. A., Strozzi, T., et al. (2014). Assessment of heat sources on the control of fast flow of Vestfonna ice cap. Svalbard. *Cryosphere* 8, 1951–1973. doi: 10.5194/tc-8-1951-2014

Schellenberger, T., Dunse, T., Kääb, A., Kohler, J., and Reijmer, C. H. (2015). Surface speed and frontal ablation of Kronebreen and Kongsbreen. NW Svalbard, from SAR offset tracking. *Cryosphere* 9, 2339–2355. doi: 10.5194/tc-9-2339-2015

Schuler, T. V., Loe, E., Taurisano, A., Eiken, T., Hagen, J. O., and Kohler, J. (2007). Calibrating a surface mass-balance model for Austfonna ice cap. Svalbard. *Ann. Glaciol.* 46, 241–248. doi: 10.3189/172756407782871783

Schuler, T. V., and Østby, T. I. (2020). Sval_Imp: a gridded forcing dataset for climate change impact research on Svalbard. *Earth Syst. Sci. Data* 12, 875–885. doi: 10.5194/essd-12-875-2020

Schytt, V. (1964). Scientific results of the swedish glaciological expedition to Nordaustlandet, Spitsbergen, 1957 and 1958. *Geogr. Ann.* 46, 242–281. doi: 10.2307/520382

Sevestre, H., and Benn, D. I. (2015). Controls on the global distribution of surge-type glaciers. *J. Glaciol.* 228, 646–662. doi: 10.3189/2015JoG14J136

Sevestre, H., Benn, D. I., Luckman, A., Nuth, C., Kohler, J., Lindback, K., et al. (2018). Tidewater glacier surges initiated at the terminus. *J. Geophys. Res. Earth Surf.* 123, 1035–1051. doi: 10.1029/2017jf004358

Shuman, C. A., Zwally, H. J., Schutz, B. E., Brenner, A. C., DiMarzio, J. P., Suchdeo, V. P., et al. (2006). ICES at antarctic elevation data: preliminary precision and accuracy assessment. *Geophys. Res. Lett.* 33:L07501. doi: 10.1029/2005GL025227

Sobota, I., Nowak, M., and Weckwerth, P. (2016). Long-term changes of glaciers in north-western Spitsbergen. *Global Planet. Change* 144, 182–197. doi: 10.1016/j.gloplacha.2016.07.006

Sund, M., Eiken, T., Hagen, J. O., and Kaab, A. (2009). Svalbard surge dynamics derived from geometric changes. *Ann. Glaciol.* 50, 50–60. doi: 10.3189/172756409789624265

Sund, M., Lauknes, T. R., and Eiken, T. (2014). Surge dynamics in the Nathorstbreen glacier system. Svalbard. *Cryosphere* 8, 623–638. doi: 10.5194/tc-8-623-2014

Taurisano, A., Schuler, T. V., Hagen, J. O., Eiken, T., Loe, E., Melvold, K., et al. (2007). The distribution of snow accumulation across the Austfonna ice cap. Svalbard: direct measurements and modelling. *Polar Res.* 26, 7–13.

Thøgersen, K., Gilbert, A., Schuler, T. V., and Malthe-Sorenssen, A. (2019). Rate-and-state friction explains glacier surge propagation. *Nat. Commun.* 10:2823. doi: 10.1038/s41467-019-10506-4

Torsvik, T., Albretsen, J., Sundfjord, A., Kohler, J., Sandvik, A. D., Skarðhamar, J., et al. (2019). Impact of tidewater glacier retreat on the fjord system: modeling present and future circulation in Kongsfjorden. Svalbard. *Estuar. Coast. Shelf Sci.* 220, 152–165. doi: 10.1016/j.ecss.2019.02.005

Uppala, S. M., Kallberg, P. W., Simmons, A. J., Andrae, U., Bechtold, V. D., Fiorino, M., et al. (2005). The ERA-40 re-analysis. *Q. J. R. Meteorol. Soc.* 131, 2961–3012. doi: 10.1256/qj.04.176

Vallot, D., Pettersson, R., Luckman, A., Benn, D. I., Zwinger, T., Van Pelt, W. J. J., et al. (2017). Basal dynamics of Kronebreen, a fast-flowing tidewater glacier in Svalbard: non-local spatio-temporal response to water input. *J. Glaciol.* 63, 1012–1024. doi: 10.1017/jog.2017.69

Van Pelt, W., and Kohler, J. (2015). Modelling the long-term mass balance and firn evolution of glaciers around Kongsfjorden. Svalbard. *J. Glaciol.* 61, 731–744. doi: 10.3189/2015JoG14J223

Van Pelt, W. J. J., Pohjola, V., Pettersson, R., Marchenko, S., Kohler, J., Luks, B., et al. (2019). A long-term dataset of climatic mass balance, snow conditions, and runoff in Svalbard (1957-2018). *Cryosphere* 13, 2259–2280. doi: 10.5194/tc-13-2259-2019

Van Pelt, W. J. J., Pohjola, V. A., Pettersson, R., Ehwald, L. E., Reijmer, C. H., Boot, W., et al. (2018). Dynamic response of a high arctic glacier to melt and runoff variations. *Geophys. Res. Lett.* 45, 4917–4926. doi: 10.1029/2018gl077252

Vieli, A., Jania, J., Blatter, H., and Funk, M. (2004). Short-term velocity variations on Hansbreen, a tidewater glacier in Spitsbergen. *J. Glaciol.* 50, 389–398. doi: 10.3189/172756504781829963

WGMS. (2019). *Fluctuations of Glaciers Database*. Zurich: World Glacier Monitoring Service.

Willis, M. J., Zheng, W., Durkin, W. J., Pritchard, M. E., Ramage, J. M., Dowdeswell, J. A., et al. (2018). Massive destabilization of an Arctic ice cap. *Earth Planet. Sci. Lett.* 502, 146–155. doi: 10.1016/j.epsl.2018.08.049

Wouters, B., Chambers, D., and Schrama, E. J. O. (2008). GRACE observes small-scale mass loss in Greenland. *Geophys. Res. Lett.* 35:L20501. doi: 10.1029/2008gl034816

Wouters, B., Gardner, A. S., and Moholdt, G. (2019). Global glacier mass loss during the GRACE satellite Mission (2002-2016). *Front. Earth Sci.* 7:96. doi: 10.3389/feart.2019.00096

Zemp, M., Huss, M., Thibert, E., Eckert, N., McNabb, R., Huber, J., et al. (2019). Global glacier mass changes and their contributions to sea-level rise from 1961 to 2016. *Nature* 568, 382–386. doi: 10.1038/s41586-019-1071-0

Conflict of Interest: The authors declare that the research was conducted in the absence of any commercial or financial relationships that could be construed as a potential conflict of interest.

The handling Editor declared a past co-authorship with one of the authors JH.

frontiers in Earth Science

ORIGINAL RESEARCH
published: 28 May 2020
doi: 10.3389/feart.2020.00149

Region-Wide Annual Glacier Surface Mass Balance for the European Alps From 2000 to 2016

Lucas Davaze[1], Antoine Rabatel[1]*, Ambroise Dufour[1,2], Romain Hugonnet[3,4,5] and Yves Arnaud[1]*

[1] Univ. Grenoble Alpes, CNRS, IRD, Grenoble INP, Institut des Géosciences de l'Environnement (IGE, UMR 5001), Grenoble, France, [2] P.P. Shirshov Institute of Oceanology, Russian Academy of Sciences, Moscow, Russia, [3] LEGOS, Université de Toulouse, CNES, CNRS, IRD, UPS, Toulouse, France, [4] Laboratory of Hydraulics, Hydrology and Glaciology (VAW), ETH Zürich, Zurich, Switzerland, [5] Swiss Federal Institute for Forest, Snow and Landscape Research (WSL), Birmensdorf, Switzerland

Studying glacier mass changes at regional scale provides critical insights into the impact of climate change on glacierized regions, but is impractical using *in situ* estimates alone due to logistical and human constraints. We present annual mass-balance time series for 239 glaciers in the European Alps, using optical satellite images for the period of 2000 to 2016. Our approach, called the SLA-method, is based on the estimation of the glacier snowline altitude (SLA) for each year combined with the geodetic mass balance over the study period to derive the annual mass balance. *In situ* annual mass-balances from 23 glaciers were used to validate our approach and underline its robustness to generate annual mass-balance time series. Such temporally-resolved observations provide a unique potential to investigate the behavior of glaciers in regions where few or no data are available. At the European Alps scale, our geodetic estimate was performed for 361 glaciers (75% of the glacierized area) and indicates a mean annual mass loss of -0.74 ± 0.20 m w.e. yr^{-1} from 2000 to 2016. The spatial variability in the average glacier mass loss is significantly correlated to three morpho-topographic variables (mean glacier slope, median, and maximum altitudes), altogether explaining 36% of the observed variance. Comparing the mass losses from *in situ* and SLA-method estimates and taking into account the glacier slope and maximum elevation, we show that steeper glaciers and glaciers with higher maximum elevation experienced less mass loss. Because steeper glaciers ($>20°$) are poorly represented by *in situ* estimates, we suggest that region-wide extrapolation of field measurements could be improved by including a morpho-topographic dependency. The analysis of the annual mass changes with regard to a global atmospheric dataset (ERA5) showed that: (i) extreme climate events are registered by all glaciers across the European Alps, and we identified opposite weather regimes favorable or detrimental to the mass change; (ii) the interannual variability of glacier mass balances in the "central European Alps" is lower; and (iii) current strong imbalance of glaciers in the European Alps is likely mainly the consequence of the multi-decadal increasing trend in atmospheric temperature, clearly documented from ERA5 data.

Keywords: glacier, optical remote-sensing, mass-balance, climate, geomorphology

OPEN ACCESS

Edited by:
Michael Zemp,
University of Zurich, Switzerland

Reviewed by:
Martina Barandun,
Université de Fribourg, Switzerland
Roger James Braithwaite,
University of Manchester,
United Kingdom

****Correspondence:***
Lucas Davaze
lucas.davaze@gmail.com
Antoine Rabatel
antoine.rabatel@univ-grenoble-alpes.fr

Specialty section:
This article was submitted to Cryospheric Sciences, a section of the journal Frontiers in Earth Science

Received: *17 December 2019*
Accepted: *21 April 2020*
Published: *28 May 2020*

Citation:
Davaze L, Rabatel A, Dufour A, Hugonnet R and Arnaud Y (2020) Region-Wide Annual Glacier Surface Mass Balance for the European Alps From 2000 to 2016. Front. Earth Sci. 8:149. doi: 10.3389/feart.2020.00149

INTRODUCTION

Beyond their role as an iconic symbol of climate change (Mackintosh et al., 2017), mountain glaciers are considered as a natural "climate-meter" (Vaughan et al., 2013) because of their high sensitivity to climate change. Glaciers can be found in ∼26% of the main hydrological basins outside Greenland and Antarctica (Huss and Hock, 2018) and about one-third of Earth's inhabitants directly or indirectly rely on glacier meltwater (Beniston, 2003). Because of the rapid atmospheric warming, which is amplified in mountainous regions (Pepin et al., 2015), mountain glaciers are losing mass worldwide (Zemp et al., 2019), thereby contributing to a third of the observed sea-level rise (IPCC, 2019), with ice mass loss expected to peak from 2040 to 2100 depending on the considered climate scenario (Hock et al., 2019). The glacier-wide annual mass balance is considered as the most comprehensive metric to assess changes in both glacier mass and dynamics, and the interactions with climate. Quantifying the annual mass balance of individual glaciers at regional scale remains challenging today, especially using the "logistically expensive" glaciological method from *in situ* data. Recent remote sensing-based methods have taken advantage of the variety of sensors, leading to regional estimates of glacier mass balance on multi-decadal time scales using gravimetry (e.g., Jacob et al., 2012; Wouters et al., 2019), multi-temporal digital elevation models analysis (DEM, e.g., Willis et al., 2012; Pieczonka and Bolch, 2015; Dussaillant et al., 2019; Menounos et al., 2019; Seehaus et al., 2020; Shean et al., 2020), altimetry (e.g., Bolch et al., 2013; Gardner et al., 2013), or glacier length change (Hoelzle et al., 2003; Leclercq et al., 2014). However, these methods fail to estimate the inter-annual variability of the mass balance. Increasing the availability of annual mass balance time series is therefore timely and highly relevant to gain insights into the impact of climate variability at a regional scale, better document the glacier contribution to the hydrological functioning of glacierized watersheds, and constrain glacio-hydrological models.

In this study, we propose an automation and a regional application of the SLA-method based on the estimation of the end-of-summer snowline altitude (SLA), a known proxy of the equilibrium-line altitude (ELA) for glacier where superimposed ice is negligible (Lliboutry, 1965), and whose position is a predictor of annual mass change (e.g., Braithwaite, 1984; Rabatel et al., 2005, 2017; Pelto, 2011; Chandrasekharan et al., 2018). Regional application was so far limited due to the absence of both automatic SLA delineation and multi-decadal geodetic mass balance estimates (Rabatel et al., 2017). The recent development of algorithms to automate the processing of satellite images (e.g., Sirguey, 2009; Noh and Howat, 2015; Shean et al., 2016; Beyer et al., 2018), the increasing storage and computing capacities, and the amount of free optical satellite data (e.g., Landsat, Sentinel-2, ASTER) suitable to monitor glacier surface elevation changes or snowline altitude have encouraged the development of automatic methods enabling to overcome the above mentioned limitations (e.g., Brun et al., 2017; Racoviteanu et al., 2019; Rastner et al., 2019).

Despite their minor potential impact on the future expected sea-level rise (Farinotti et al., 2019) and the relatively low ice extent (2,092 km^2, Randolph Glacier Inventory RGI 6.0, RGI Consortium, 2017), we applied the SLA-method on the European Alps for the period 2000–2016 because of the availability of a high number of *in situ* monitored glaciers with annual mass balance data (23 in this study), among which nine are considered as reference glaciers by the World Glacier Monitoring Service (WGMS, 2019, see **Supplementary Table S3** for detailed list), and manually delineated snowlines from 34 glaciers in our dataset (Rabatel et al., 2013, 2016) suitable to validate our estimates.

Besides providing a new estimate of the mean European Alps mass balance for the period from 2000 to 2016, we used these data to: (i) propose and assess a new methodological framework to derive the annual mass balance times series for individual glaciers at regional scale from optical satellite data; (ii) investigate the spatial and temporal patterns of annual mass changes across the European Alps; (iii) assess the possible climatic and morpho-topographic drivers affecting the mass balance variability at sub-regional scale; and (iv) determine the representativeness of the glaciological annual mass balance data gathered by the WGMS.

STUDY AREA

We define the European Alps as the region located between the coordinates 44° to 48°N and 5° to 14°E. The European Alps are the second most glacierized region of Europe after Scandinavia (2,092 km^2 vs. 2,949 km^2 according to the RGI 6.0). **Table 1** shows the number of glaciers within the European Alps that have been used in the current study. We selected 361 glaciers considering the following criteria: (i) larger than 0.5 km^2 for the geodetic mass balance quantification using the ASTER images archive according to Menounos et al. (2019); (ii) a maximum elevation higher than 3100 m a.s.l. and a suitable surface topography (e.g., excluding glaciers highly crevassed or permanently shaded) to allow the detection of the snowline for each year in order to quantify the annual mass balance computation using the SLA-method. Among the 361 selected glaciers, 239 glaciers were ultimately kept for the annual glacier wide mass balance quantification using the SLA-method. The other 122 were filtered out by our semi-automatic method to derive the SLA (see section Reconstructing Annual Surface Mass Balance Time Series From Optical Satellite Images). Glaciers for which the annual mass-balance time series have been computed are distributed over 10 sub-regions following a 1 × 1 degree regular grid. Although arbitrary, this choice has been made for

TABLE 1 | Glacier datasets used in the present study, together with their respective cumulative area and the corresponding fraction of the RGI 6.0.

Glacier dataset	Glacier count (Nb)	Area (km^2)	Fraction of the RGI 6.0 (%)
RGI 6.0	3,927	2,092	100
Geodetic	361	1,563	75
SLA-method	239	1,215	58

practical reasons to be compatible with the climatic data used for data interpretation.

DATA AND METHODS

In order to assess the glacier mass change over the 17 years of the study period, we computed for every selected glacier both the geodetic mass balance corresponding to a multi-decadal average and the annual mass-balance time series from the SLA-method.

Reconstructing Multi-Decadal Mass Balance From Digital Elevation Models

Over our study area, 7306 ASTER DEMs were generated using the Ames Stereo Pipeline (Shean et al., 2016; Beyer et al., 2018). DEMs are co-registered over stable terrain (excluding ice and lakes) following the Nuth and Kääb (2011) approach and using the Global DEM (GDEMv2, Tachikawa et al., 2011) as a reference. Following Berthier et al. (2016), for each 30 m pixel, a two-step linear regression is fitted to the ASTER-derived DEMs to estimate the temporal trend in elevation change (dh/dt). The overall dh/dt for each considered individual glacier is derived using the RGI 6.0 outlines (RGI Consortium, 2017). These outlines are also used to separate glacierized and ice-free terrain and to average dh/dt for individual glaciers. Data gaps are filled using the local hypsometric approach (McNabb et al., 2019).

In order to estimate the decadal glacier-wide mass balance, surface elevation changes are converted into mass changes by applying the volume-to-mass conversion of 850 $\pm$ 60 kg.m^{-3} (Huss, 2013).

Although the ASTER geodetic mass balance method has its limitations (mostly related to the spatial resolution of the DEMs), it also has the prominent advantage to make possible regional applications, as demonstrated by several recent studies (e.g., Brun et al., 2017; Menounos et al., 2019; Dussaillant et al., 2019; Shean et al., 2020). Far less glaciers are covered by existing high resolution DEMs in the European Alps, and those are restricted to specific time periods. Quality assessment of the ASTER method in comparison with high resolution DEM-differencing has been performed over the Mont-Blanc range by Berthier et al. (2016) using SPOT5 and Pléiades DEMs, or for glaciers in British Columbia by Menounos et al. (2019) using LiDAR DEMs. Both studies concluded that there was an absence of bias using ASTER and a very good agreement between the geodetic mass balances quantified for individual glaciers down to 0.5 km^2 in area.

Reconstructing Annual Surface Mass Balance Time Series From Optical Satellite Images

The geodetic approach provides spatially-resolved mass balance estimation over decadal time spans, but is currently unable to resolve the annual fluctuations for mountain glaciers. To derive the annual surface mass balance using the SLA-method, the first step consists of estimating the SLA. Because of the large number of glaciers considered in this study, we semi-automatically identified the transient snowline altitude using the algorithm detailed in **Supplementary Material**. We used images of decametric resolution from optical satellite sensors (i.e., LANDSAT 5, 7, 8, Sentinel-2, ASTER) and identified the transient SLA using a band ratio NIR^2/SWIR to enhance the snow/ice contrast. The ASTER GDEM v2 was used to compute the snowline altitude. To avoid side effects on the glacier (e.g., shadows from the surrounding rock faces, avalanche deposits), transient SLAs were derived on a central part of the glacier. For each image, the algorithm allows detection of the glacier's transient SLA as the steepest gradient in the surface band ratio signature, corresponding to the local transition between ice and snow. For each glacier and each year, we then considered the highest transient SLA to be representative of the glacier's annual SLA. For a given glacier, when the time series of annual SLAs contained gaps, for example those due to cloud cover or image unavailability, we used the statistical linear approach of Lliboutry (1974) for gap-filling. This approach takes into account inter-annual (regional effect, according to neighboring glaciers from the surrounding region) and spatial (site effect, according to the average of each individual glacier) variability to reconstruct missing annual SLAs values in the time series. Glaciers for which the time series of annual SLAs contains more than 68.2% (1σ) of missing data were discarded leading to the number of 239 glaciers monitored. To define the neighboring glaciers used in the gap-filling approach, we followed the conclusion by Vincent et al. (2017) and Pelto (2018) that showed that glaciers 100 km apart have a significant common variance (75% in the European Alps for surface mass balance data, Vincent et al., 2017). As the SLA is a good proxy of the mass balance, we assumed that the same relationship applies, with neighboring glaciers (100 km apart) having coherent migration of the SLA from one year to another.

Using the SLA-method presented in Rabatel et al. (2005, 2008, 2016, 2017), the glacier-wide annual mass balance has been reconstructed for the period from 2000 to 2016. In summary, with this method, the cumulative mass loss of the glacier over the study period (the average annual mass balance rate, $\dot{M}$, in m w.e. yr^{-1}) is given by the geodetic method. On the other hand, the annual glacier-wide mass change (M_i, in m w.e.) for every year i of the study period results from the difference between altitude of the snowline at the end of the ablation season (SLA_i, in m a.s.l.) and the theoretical altitude of the equilibrium line if the glacier had a balanced budget (glacier wide mass balance = 0) over the study period (ELA_{eq}, in m a.s.l.), multiplied by the mass-balance gradient (∂b/∂z) in the vicinity of the ELA.

Therefore, assuming that SLAs are approximations of ELAs, ELA_{eq} is computed as:

$$ELA_{eq} = \frac{1}{n}\sum_{1}^{n}(SLA_i) + \frac{\dot{M}}{\partial b/\partial z} (1),$$

and M_i is computed as:

$$M_i = (\mathrm{ELA}_{eq} - SLA_i) \times \frac{\partial b}{\partial z} (2).$$

Regarding ∂b/∂z, it may vary from one glacier to another due to local influences on the meteorological conditions that govern accumulation and ablation patterns, and also from one year

to another considering any single glacier (e.g., Kuhn, 1984; Mayo, 1984; Benn and Lehmkuhl, 2000; Rabatel et al., 2005). For instance, on the basis of the three glaciers in the French Alps, Rabatel et al. (2005) quantified a coefficient of variation of the mass balance gradient of 30%. However, several studies demonstrated that choosing a regional $\partial b/\partial z$ does not depreciate the results and leads to similar results that individual glacier $\partial b/\partial z$ estimates (Rabatel et al., 2005, 2016; Chandrasekharan et al., 2018). This underlines the low sensitivity of the SLA-method to the $\partial b/\partial z$ value, which allows using the SLA-method on unmonitored glaciers and avoiding calibration. It is noteworthy that Braithwaite (1984) already mentioned that the value of what he called the "effective balance gradient" was not the main source of error, but rather the value of the "balanced-budget ELA" (called ELA_{eq} in our case). We therefore selected a mass-balance gradient of 0.0078 m w.e. m^{-1} according to Rabatel et al. (2005) and assumed its validity at the scale of the European Alps, considering an uncertainty of $\pm$ 30% to take into account its spatio-temporal variability.

Uncertainty in the Annual and Decadal Retrieved Glacier-Wide Mass Balance

The uncertainty in multi-decadal geodetic mass balance of individual glaciers is related to three independent sources: the uncertainty in the glacier area, the uncertainty in dh/dt, and the uncertainty in the volume-to-mass conversion factor. The uncertainty in the rate of elevation change integrated over the area of each glacier is estimated following Rolstad et al. (2009) with a 500 m range spherical variogram (Menounos et al., 2019). The standard deviation of dh/dt over stable terrain is computed in 1 × 1 degree tiles and applied to glaciers in the corresponding tile, with an average value of 0.5 m yr^{-1}. The uncertainty in the glacier surface area is conservatively defined as 5% for clean-ice glaciers (Paul et al., 2013), and the uncertainty in the volume-to-mass conversion factor is estimated as $\pm$ 60 kg m^{-3} (Huss, 2013). We considered these uncertainties to be applicable on the very few glaciers that have a covered glacier tongue in our sample. The geodetic mass balance uncertainty is estimated for each glacier, with a mean value of $\pm$ 0.16 m w.e. yr^{-1}, ranging from $\pm$ 0.06 to $\pm$ 0.83 m w.e. yr^{-1} for the 361 glaciers monitored with the geodetic method.

The overall uncertainty in the retrieved annual mass change is due to the propagation of the uncertainty of each variable used in the calculation (Equations 1 and 2). It therefore corresponds to the quadratic sum of:

- The uncertainty in the semi-automatically retrieved SLA, equal to $\pm$ 123 m. It takes into account: (i) the DEM resolution and uncertainty; (ii) the pixel size and resampling of the satellite images used for the detection; (iii) uncertainties related to the detection method and potential false detections caused by the presence of a firn line, the presence of crevasses, undetected clouds or changes of slope not mitigated by the algorithm; and (iv) uncertainties related to the gap-filling approach. A full description is presented in **Supplementary Material**.
- The uncertainty related to $\partial b/\partial z$ in the vicinity of the ELA, considered as $\pm$ 30% of $\partial b/\partial z$ as suggested by Rabatel et al. (2005).
- The uncertainty in the computed geodetic mass balance presented above.
- The time difference between the image acquisition used to estimate SLA, and the last day of the hydrological year. Rabatel et al. (2016) estimated this uncertainty at $\pm$ 0.09 m w.e. yr^{-1} in average on 30 glaciers in the French Alps for a 30 years study period. This estimate made for glaciers in the French Alps is assumed to be valid at the scale of the European Alps.

The uncertainty in the computed annual mass balance of the 239 glaciers monitored with the SLA-method equals $\pm$ 0.52 m w.e. on average, ranging from $\pm$ 0.49 to $\pm$ 0.60 m w.e. depending on the year and the glacier. It should be noted that the uncertainty in the annual mass balance can be assumed to be higher for small glaciers (because of a higher signal/noise ratio in the dh/dt maps used for the geodetic mass balance) or for steep glaciers (because of a higher uncertainty in the SLA estimate) or for years with fewer images. If the first two sources are considered in our uncertainty estimate, it is much more difficult for the third point as it depends on the year considered and the meteorological conditions during the summer seasons. Indeed, for a given year, one single image might be available, but if recorded at the good moment of the summer season, the SLA estimate will be accurate. On the contrary, the retrieved SLA will likely be considered as an outlier and be removed by the post-processing steps of the workflow (see section 1.2.2.10 in **Supplementary Material**).

Finally, one must keep in mind that a good way to validate the method is the comparison between the retrieved annual mass balance time series with the ones quantified from field measurements where such data are available (see below, section Remotely-Sensed SLA and Annual Mass Balance Validation).

Climatological Data

In order to evaluate the role of climate forcing on the observed glacier mass changes, we analyzed the climatic conditions during the period from 1984 to 2016 using data from the ERA5 reanalysis (Copernicus Climate Change Service [C3S], 2017). The reason for doubling the time window is to study the climatic trends over a sufficient time span (conform to the standard of 30 years). Direct links with the computed annual mass balance were performed on the same period (2000–2016). We used ERA5, a global atmospheric reanalysis produced by the European Centre for Medium-Range Weather Forecasts (ECMWF), at a horizontal resolution of 30 km and on 137 vertical levels, currently starting in 1979. Atmospheric reanalyses accommodate conventional and satellite observations within the physically consistent framework of a numerical prediction model. ERA5 is the state-of-the-art global reanalysis. In this study we analyzed glacier-relevant variables from ERA5 such as 2 m air temperature, precipitation, sea-level pressure, wind speed at 700 hPa, precipitable water, moisture, and heat transport. To analyze predominant climatic factors on the computed annual mass

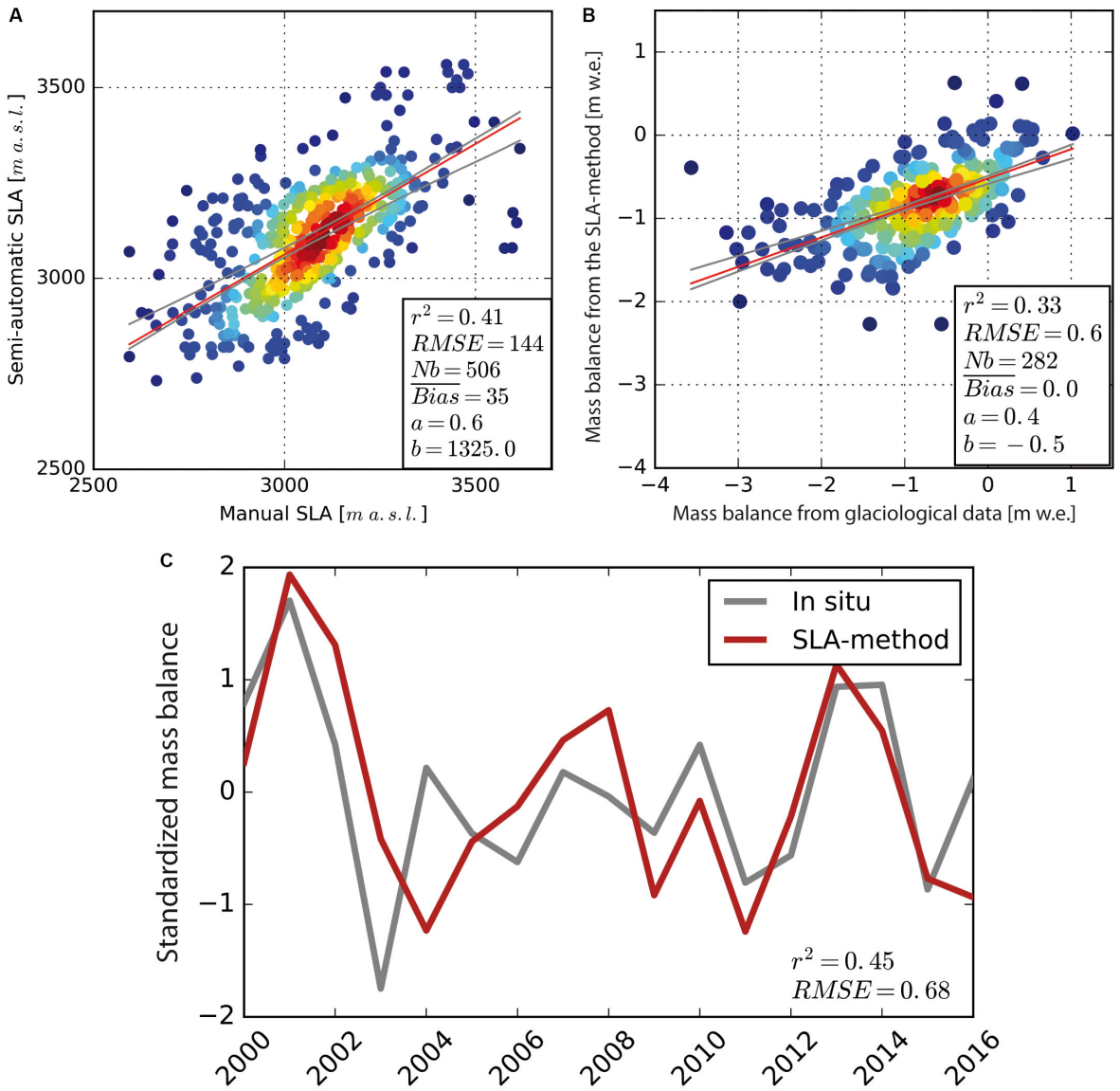

FIGURE 1 | (A) Illustrates the comparison for filtered and gap-filled SLA on 34 glaciers in the western Alps (506 compared SLA). **(B)** Illustrates the comparison between mass balances computed with the SLA-method vs. annual mass balances from the glaciological method on 23 glaciers (282 compared annual values). Error bars are not shown in **(A,B)** for better readability; refer to the text for their ranges. In **(C)**, the mean standardized interannual variability is represented for *in situ* and SLA-method estimates for the 23 glaciers monitored *in situ* and detailed in **Supplementary Table S3**. For **(A,B)**, the red line indicates a robust linear regression with support for the M-estimators (Susanti et al., 2014), together with the 95% confidence interval, materialized by the gray lines. Heat-map style colors are an indicator of the point density with one point representing one glacier and one year. For **(A–C)**, statistics are displayed to assess the correlation between both datasets; *a* represents the slope of the linear regression and *b* the intercept.

balance, we performed principal component analysis (Wilks, 2011) on these variables.

RESULTS

Remotely-Sensed SLA and Annual Mass Balance Validation

Taking advantage of manually derived SLA for 34 glaciers in the western Alps (Rabatel et al., 2013, 2016), we were able to validate our semi-automatic estimates of SLA (displayed **Figure 1A**, further assessments in **Supplementary Material**). Overall, our estimates are largely able to reproduce manual estimations of the annual glacier SLA (r^2 = 0.41 for 506 compared SLA, significant at the 1% risk level), with a mean observed bias of + 35 m. Despite the filtering and gap-filling post-treatment, discrepancies persist (RMSE = 144 m). Those discrepancies can arise from the date differences between both estimates, the different SLA detection zone (central part of the glacier vs. full glacier width for the manual estimates), or errors inherent to the SLA detection.

Our estimated uncertainty in the semi-automatically derived SLA (± 123 m), although slightly smaller than the computed RMSE, accounts for these sources of errors when estimating the annual SLA and the associated annual mass balance.

Using the SLA-method, we reconstructed glacier-wide annual mass balance time series for the period from 2000 to 2016. The European Alps being one of the most monitored glacierized regions worldwide, we were able to validate our estimates by comparing to 23 glacier-wide annual mass balance time series estimated with the glaciological method (full list and time series length are presented in **Supplementary Table S3**). As displayed in **Figure 1B**, annual mass balance from the SLA-method and from *in situ* data are in general agreement, with 33% of common variance, no observed mean bias, and a RMSE (0.6 m w.e. yr^{-1}) slightly larger than the uncertainty for SLA-method mass balances (± 0.52 m w.e. yr^{-1} in average). There is an underestimation for highly negative annual mass balances (and to a lesser extent for very positive ones), resulting in the slope of the linear regression being equal to 0.4 rather than 1. In **Figure 1C**, we compare the standardized glacier-wide annual mass-balance time series (average of the 23 glaciers monitored *in situ*) quantified from *in situ* and SLA-method estimates. Standardized values are calculated as described by Equation S4 in **Supplementary Material** replacing SLA by mass balance. One can note the overall good agreement between the two-time series in terms of interannual variability (r^2 = 0.45), except between 2004 and 2008. There are several possible explanations for the remaining discrepancies:

- Errors in SLA estimation,
- Lack of representativeness of the computed glacier-wide mass-balances from sparse *in situ* data,
- Difference of glacier extent used to compute the glacier-wide mass balance in the two methods,
- Errors and/or difference between geodetic estimates used to constrain glacier-wide annual mass balance.

Indeed, when comparing manually delineated and semi-automatically derived SLA (**Figure 1A** and section 1.3.1 and 1.3.2 in **Supplementary Material**), the algorithm fails to reproduce extremely high or sometimes very low SLA due to the position of the SLA itself, either too close to the glacier head or snout. Therefore, retrieved mass balances from the SLA method do not capture extreme years (mainly the most negative ones) as well as others, explaining part of the observed discrepancy. Furthermore, most of the SLA estimates between 2003 and 2008 were based on Landsat 7 images, for which the Scan Line Corrector (SLC) failed in May 2003, resulting in stripped images and thus reducing drastically the number of usable images to detect the SLA. On the other hand, glacier-wide estimates from *in situ* data using the glaciological method are dependent on the point measurements distribution on the glacier (often biased toward the ablation area due to access facilities), on the interpolation method, and on glacier area changes during the monitored period (e.g., Thibert et al., 2008). Geodetic calibrations can reduce the related errors when photogrammetry acquisitions are performed (Zemp et al., 2013). In addition, *in situ* glacier wide mass balances can show surprising values, such as exhibited by the north-facing Corbassière Glacier in 2006, with a measured annual surface mass balance of −3.56 m w.e. and a corresponding ELA at 3,875 m a.s.l., which is more than 450 m above the uppermost manually delineated SLA from neighboring French glaciers for the period 1984–2010 (Rabatel et al., 2013). Such negative surface mass balance values from *in situ* measurements are questionable and can be a potential source of discrepancy with the SLA-method estimates. Finally, the dissimilar glacier surface areas considered in the two methods could explain part of the differences. Indeed, glacier surface areas used for the SLA and geodetic methods correspond mostly to glacier outlines delineated around 2003 in the European Alps (RGI Consortium, 2017), while the year of delineation used in the glaciological method varies from glacier to glacier and can depend on local inventories. Applying the same methodology than we used to derive geodetic mass balance for the Andean glaciers over a similar time period, Dussaillant et al. (2019) estimated that considering a single or multiple inventories could lead to a difference of mass balance rate up to 10% for individual fast retreating glaciers, but of only a few% for glacier larger than 3 km^2 (see section 7 of **Supplementary Information** of their paper).

Despite the observed discrepancies, the annual mass balances computed from the SLA-method are able to reproduce the monitored surface mass balance from *in situ* measurements together with the interannual variability (**Figures 1B,C**). Therefore, this justifies the application of the SLA-method at a regional scale, and underlines the ability of the method to: (i) reconstruct the annual mass-balance time series; (ii) investigate the behavior of the glaciers for the different regions; and (iii) observe the annual variability for inaccessible glaciers.

Regional Mass Balance Over the European Alps

Multi-decadal mass balances and annual mass-balance time series averaged by sub-regions are presented in **Figures 2**, **3**, respectively. According to **Figure 2**, the sub-region #4 (Eastern Berner and Urner ranges) experienced the strongest mass loss between 2000 and 2016, with an average of −0.90 ± 0.20 m w.e. yr^{-1}. On the other hand, the sub-region #1 (North of Ötztaler, Stubai, and Zillertal ranges) experienced the least negative mass balance, with −0.54 ± 0.28 m w.e. yr^{-1} on average. The length of the ASTER images archive gives the opportunity to divide the study period (2000–2016) into two sub-periods (2000–2009 and 2009–2016), as was done in the study by Menounos et al. (2019) and Dussaillant et al. (2019), although no contrasted pattern was observed between the two. The multi-decadal mass balance for the European Alps over the period from 2000 to 2016 is −0.74 ± 0.20 m w.e. yr^{-1}, corresponding to an average annual loss of −1.54 ± 0.38 Gt. Over the same period, Zemp et al. (2019) computed a region-wide mass balance of −0.83 ± 0.07 m w.e. yr^{-1} for glaciers of the European Alps. Our estimate is lower even if the values are not statistically different considering the uncertainties. Because Zemp et al. (2019) computed their region-wide mass balance by combining the temporal variability from *in situ* measurements with geodetic estimates different from ours,

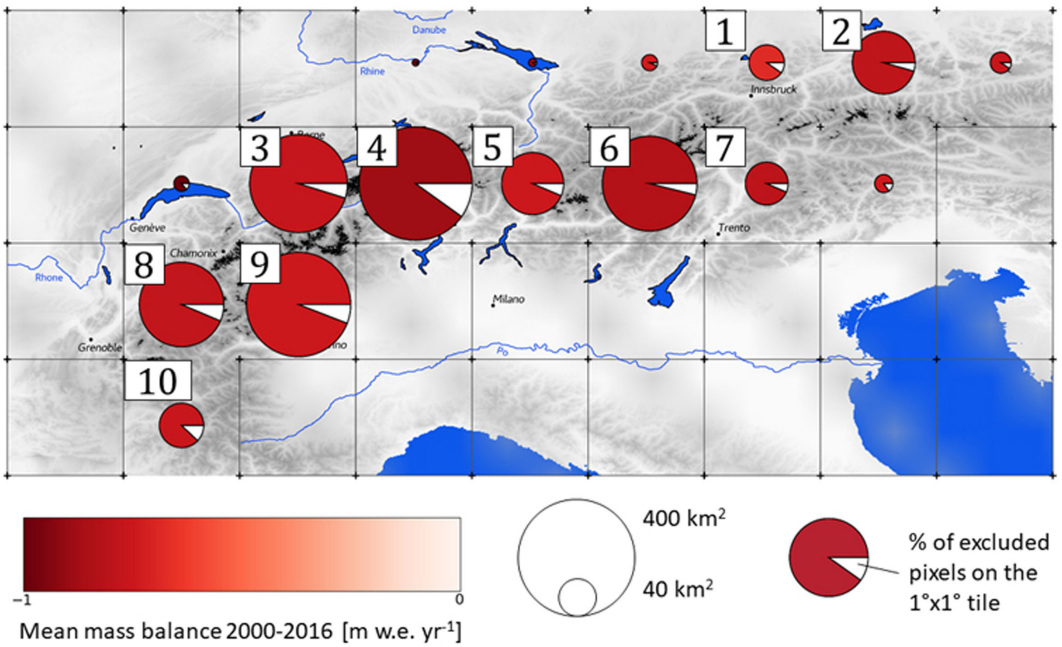

FIGURE 2 | Map of the European Alps illustrating the glacierized and the ice-free (thin black frames) 1 × 1 degree grid cells. For each glacierized cell, the pie charts illustrate the mean mass balance from 2000 to 2016 computed with the geodetic method, with white slices corresponding to the percentage of outliers removed during the filtering of the dh/dt maps within each tiles. Numbers (1–10) denominate regions where annual mass balance time series have been computed using the SLA-method.

the discrepancy with our region-wide mass balance is therefore also related to the used methods and data.

Regarding the interannual variability of the annual mass-balance time series, contrasted patterns can be observed from one region to another, as displayed in **Figure 3**. The easternmost and westernmost sub-regions (respectively, sub-regions #2 and #3, #8, #9, #10) show a high temporal variability from one year to another. For the central part of the European Alps (sub-regions #1, #4, #5, #6 and #7), the interannual variability in the computed mass balance is less pronounced from 2003 to 2012, experiencing almost constant mass balance (between −0.5 and −1 m w.e. yr^{-1}, function of the sub-region). Peculiar events can be observed across the entire range, during 2001–2002 and 2013–2014 for low losses and 2003 and 2004 for high losses years. These results are discussed in relation to the variability of climatic variables in section Analysis of Climatic Drivers below.

Glacier Morpho-Topographic Features, One of the Multi-Decadal Mass Balance Drivers?

Previous studies showed that multi-decadal mass balances of individual glaciers can be related to glacier morpho-topography (e.g., Paul and Haeberli, 2008; Rabatel et al., 2013, 2016; Fischer et al., 2015; Brun et al., 2019). In addition, according to Vincent (2002); Abermann et al. (2011), or Huss (2012), differences in specific mass balance between neighboring glaciers can often be controlled more by glacier morpho-topography than by climate variability, and observed mass balance response to similar climate forcing can largely differ from one glacier to another (e.g., factor of four in terms of cumulative mass losses between Silvretta and Sarennes glacier, Vincent et al., 2017). However, assessing the impact of glacier morpho-topography on the average glacier mass balance is challenging due to the limited number of *in situ* measurements, which are not necessarily representative of the diversity of glaciers within the same region (Gardner et al., 2013). Therefore, geodetic estimates of multi-decadal mass changes for individual glaciers at regional scale provide a lever to investigate the impact of glacier geometry on the decadal mass balance variability from one glacier to another. We tested the relationship between the geodetic multi-decadal mass balance for 361 glaciers for the period from 2000 to 2016, and several glacier morpho-topographic features (i.e., mean glacier slope, minimum, median and maximum altitude, aspect, and area, displayed in **Figure 4**).

We computed the mean glacier slope on purpose rather than the largely used glacier tongue slope to also take into account accumulation basin geometries. Out of the six features studied, three can be significantly correlated to the multi-decadal mass balance (with a statistical confidence level > 95% according to a Student's *t*-test): the median altitude (r^2 = 0.24), the mean glacier slope (r^2 = 0.19), and the maximum altitude (r^2 = 0.12). Using a least absolute shrinkage and selection operator (LASSO) regression analysis, the slope and the median altitude, being the dominant terms, explain 36% of the variance of the observed geodetic multi-decadal mass balance. Adding other variables (area, maximum and minimum altitude, and mean aspect) only raises the explained variance to 39%, which shows their

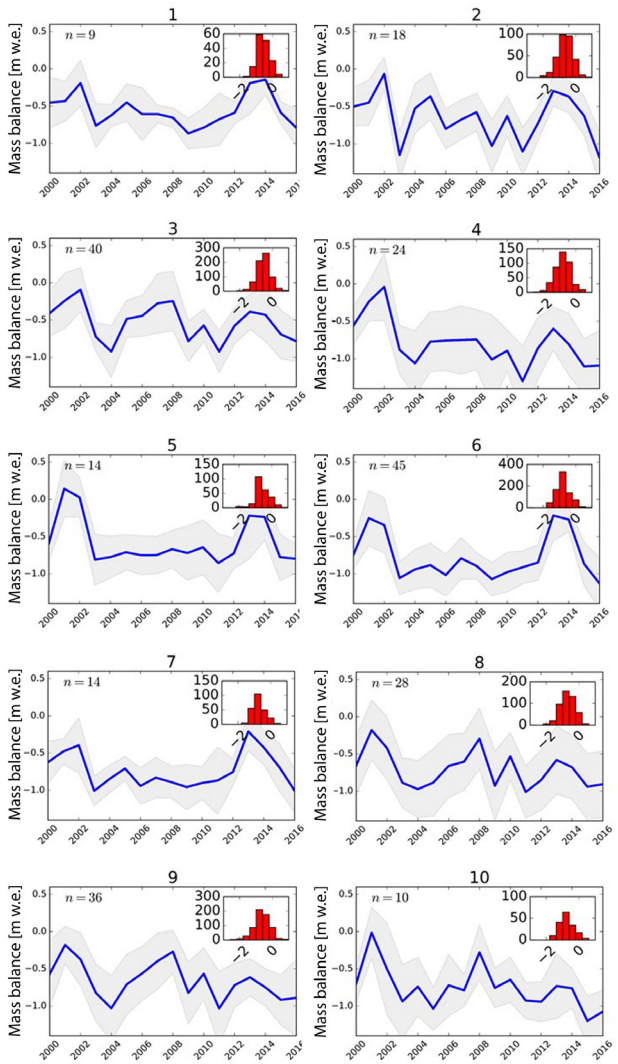

FIGURE 3 | Mean annual mass balance time series (in m w.e.) for each of the ten studied sub-regions (defined in **Figure 2**). The gray shade illustrates the annual dispersion of the mass balance estimates for individual glaciers in the sub-region, computed using the standard deviation at 1σ. The number of glaciers (n) is given on the top-left corner of each subplot. The red histograms present the statistical distribution of annual mass balances as a function of its value, in m w.e.

relatively low control on the multi-decadal mass balance at regional scale. This result strengthens previous analyses made in the European Alps (e.g., Huss, 2012; Fischer et al., 2015; Rabatel et al., 2016) and in other mountain regions (e.g., Brun et al., 2019), even if we did not find a significant statistical correlation between the glacier area and the multi-decadal mass balance as in previous work (Paul and Haeberli, 2008; Huss, 2012). This difference could rest on the absence of small glaciers (<0.5 km^2) in our dataset.

It is finally worth noting that correlations are positive for the three significantly correlated morpho-topographic variables, suggesting that steep and high glaciers with a high accumulation basin experience the least negative multi-decadal mass balances.

DISCUSSION

Analysis of Climatic Drivers

Spatio-Temporal Variability of the Annual Glacier-Wide Mass Balance Time Series

Rabatel et al. (2013) analyzed the spatio-temporal variability of the ELA in the western Alps using a 25 years time series for 43 glaciers and concluded that the temporal variability of the reconstructed time series is mainly related to the climatic drivers, and the morpho-topographic factors mostly control the average ELA over the study period. Following these statements and assuming they apply to the annual glacier-wide mass balance, we analyzed the spatio-temporal variability of the reconstructed annual mass-balance time series considering different climatic variables commonly used in multiple regression studies on glacier mass balance (e.g., Hoinkes, 1968; Martin, 1974; Braithwaite and Zhang, 2000; Bolibar et al., 2020). As such, for each sub-region (1 × 1 degree grid cell), we computed from ERA5 data: the summer average of the 2 m air temperature (T2ms) and sea-level pressure (SLPs), the zonal and meridian temperature advection (Tus and Tvs), the winter average of precipitation (Pw) and sea level pressure (SLPw), the precipitable water over the entire atmospheric column (Pwatw), and the zonal and meridional humidity advection (Quw and Qvw). We then performed, for each sub-region, a LASSO regression analysis between these climatic variables and the median annual mass-balance time series over the 2000 to 2016 period. For each sub-region, a maximum of three variables explaining most of the observed variance are identified and reported in **Table 2**. It is worth noting that this statistical analysis is conducted over a 17 years time period, which is rather short from a climate point of view. Therefore, the interpretation of the results has to be considered with caution and as a preliminary study of the relationship between the mass balance and climate inter-annual variability at the European Alps scale.

Interestingly, from the LASSO analysis, the two groups of sub-regions identified from the annual mass-balance time series also emerge. For the sub-regions #1, #5, #6, and #7, the only climatic variable statistically significant and explaining more than 30% of the observed inter-annual mass balance variance is the precipitable water during winter, which is largely impacted by the winter air temperature (maximum water content in humid air depending on temperature). This is in agreement with observations made for glaciers in these regions (i.e., Austrian Alps, Abermann et al., 2011) suggesting that glaciers in this area could be maintained because of "above-average accumulation."

Sub-regions #3, #4, #9, and #10 have the same first explicative variable (Quw, except for #3 and #8 where it is second), corresponding to eastward advection of humidity and seems also highly impacted by summer air temperature and summer meteorological conditions (Tvs, SLPs, and T2ms), mainly dominated by southward fluxes. These sub-regions are all in the western European Alps and could therefore

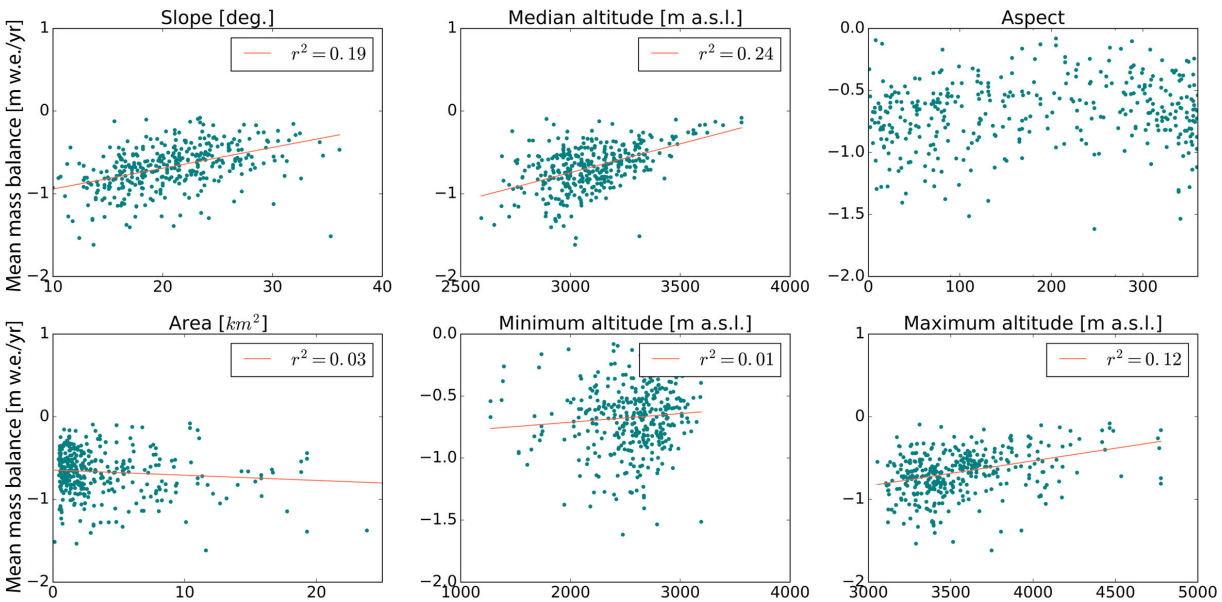

FIGURE 4 | Geodetic multi-decadal average mass balance for the period from 2000 to 2016 as a function of six morpho-topographic variables. A correlation coefficient is provided for each of the variables. A regression has been computed following a robust linear model with support for the M-estimators (Susanti et al., 2014), and is represented by a red line, excepted for the glacier aspect, for which a linear regression was not relevant.

TABLE 2 | Results from multi-linear LASSO regression analysis in between the median annual mass balance and nine climatic variables from ERA5 for each sub-region of the study area.

Region	r^2_{b3}	r^2_b	$T2m_s$	P_w	SLP_s	SLP_w	$Pwat_w$	Tu_s	Tv_s	Qu_w	Qv_w
#1	0.36	–									
#2	0.41	0.38									
#3	0.45	0.33									
#4	0.53	0.44									
#5	0.37	–									
#6	0.37	–									
#7	0.31	–									
#8	0.68	0.41									
#9	0.52	0.33									
#10	0.52	0.38									

r^2_{b3} displays the correlation coefficient with the computed inter-annual mass balance considering the most explanatory climatic variables (three as a maximum), and r^2_b, the correlation coefficient of the most explanatory variable. Scores displayed are significant (error risk < 5%) according to a Student's t-test. The explanatory variables are colored according to their significance, with red the most significant, salmon the second, and blue the third.

experience similar meteorological forcing during zonal or meridian meteorological events.

Sub-region #2 seems to be highly impacted by summer meteorological conditions and could not be assimilated to any other sub-region. Contrary to sub-region #3, #2 does not seem impacted by temperature or humidity advection and is too distant from #3 to be grouped with, despite their common high dependence to summer air temperature. Finally, the sub-region #8 is dominated by summer meteorological conditions, winter eastward humidity advection, and precipitable water. The predominating drivers and observed inter-annual mass balances are not identical from the surrounding regions despite their close geographical distances, and our analysis does not allow concluding on the reasons for this peculiar behavior.

Surprisingly, winter precipitation is not identified as an explanatory variable for any of the monitored regions. One hypothesis could rest on the poor capacity of ERA5 to spatialize precipitation regarding the relatively low resolution of the used DEM (i.e., 30 km), particularly important in mountainous terrain. Precipitable water is often considered as a more accurate variable as it does not provide a spatial estimation of precipitation but rather a budget of precipitable water.

Climatic Patterns for Extreme Years

Our results also allow analyzing peculiar years such as the most/least negative one (**Figure 5A**) and relate them to climate forcings. On a year to year basis, the regional mass-balance variability during high loss years is dominated by a pattern

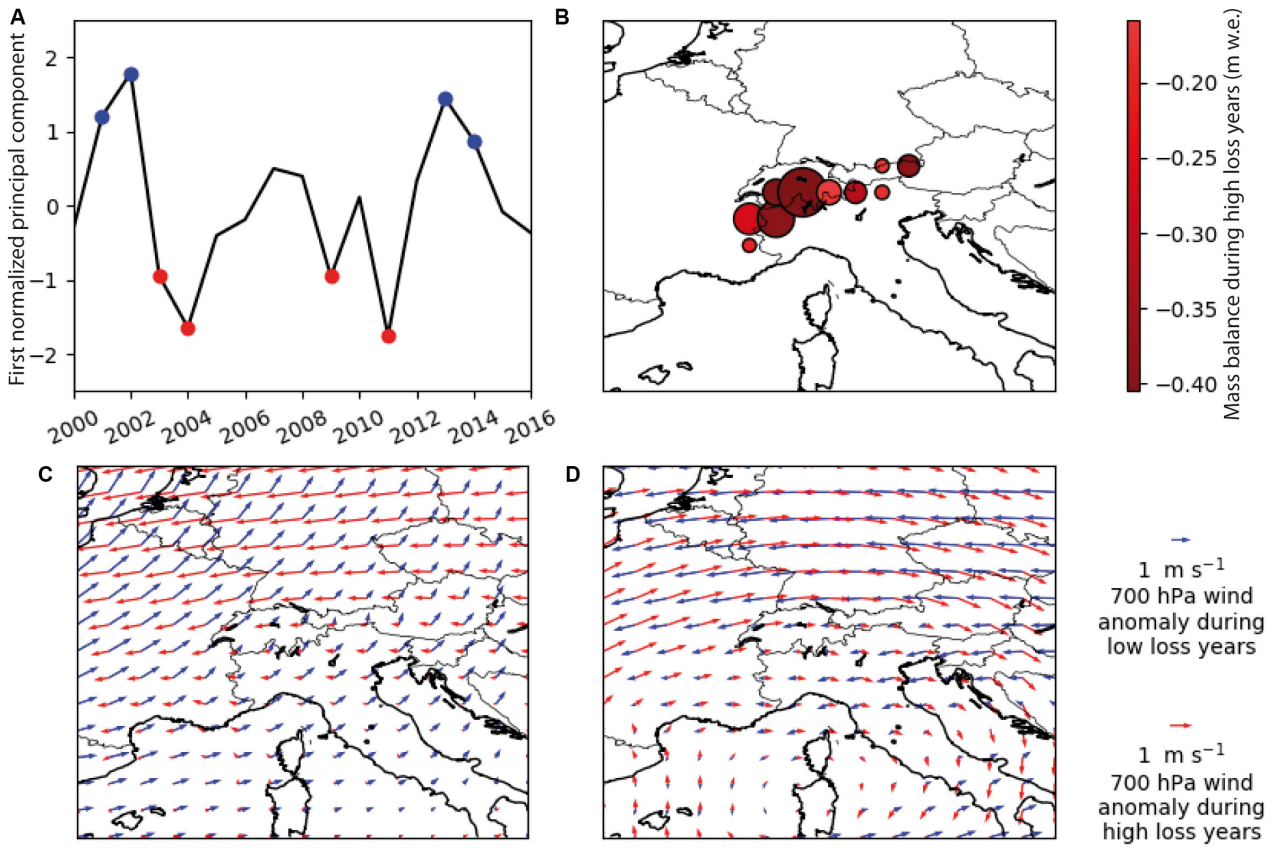

FIGURE 5 | Time series of the normalized first principal component of annual regional mass balances **(A)**, composite of annual regional mass balances during high loss years **(B)**, 700 hPa composites during high and low loss years (red and blue arrows) in winter **(C)** and summer **(D)**.

which is common to the entire Alpine range (80% of variance explained, **Figure 5B**). This uniformity was already observed when comparing annual mass balance between each of the ten sub-regions for certain years (**Figure 3**, section Regional Mass Balance Over the European Alps). We used a principal component analysis to define years of high loss (PC1 $< \sigma/2$: 2003, 2004, 2009, 2011) and years of low loss (i.e., positive anomalies, PC1 $> \sigma/2$: 2001, 2002, 2013, 2014). The composites of the 700 hPa wind anomalies yield approximately opposite in either case and between winter and summer. During low loss years, the main atmospheric flow is westerly in winter, advecting moist air from the Atlantic (blue arrows, **Figure 5C**). Conversely, the easterly flow during high loss years is less favorable to precipitation with potentially colder and drier climate conditions. The composites of 500 hPa geopotential height for low and high mass loss years correspond to the positive and negative phases of the North Atlantic Oscillation in the winter weather regime classification of Cassou et al. (2004). In summer, the wind is easterly during low mass loss years and westerly during high mass loss years (blue arrows in **Figure 5D**). The associated 500 hPa fields match the "Blocking" and "Atlantic low" patterns, respectively (Cassou et al., 2005).

The second principal component opposes East to West in terms of interannual mass-balance patterns, with the boundary falling between regions #3 and #4. This pattern could also be observed visually on **Figure 3**, with regions #1, #5, #6, and #7 experiencing sustained mass losses from 2003 to 2012, while Western regions experience more interannual variability. However, the second principal component accounts for only 7% of the variance and could not be related to a straightforward atmospheric mechanism.

Attribution of Today's Glaciers' Mass Loss in the European Alps

According to the ERA5 reanalysis, summer temperature shows an overall increase over the entire region, ranging from + 0.4 to + 0.8K from 1984 to 2016 (significant at the 5% level). For winter precipitation, changes are not statistically significant. Interestingly, the 2000–2016 period we studied here is characterized by important glacier mass losses in the European Alps (-0.74 ± 0.20 m w.e. yr^{-1} in average from our findings) which can be mainly attributed to high melting compared with the period from 1960 to 1990, when glaciers experienced very limited mass losses (e.g., Beniston et al., 2018; Zemp et al., 2019). Considering Braithwaite and Zhang's (2000) findings that showed a sensitivity of glacier wide mass balance of −0.77 m w.e. $a^{-1}{}^{\circ}C^{-1}$ for five glaciers in the Swiss Alps, we can state that the strong glacier imbalance currently experienced by glaciers in

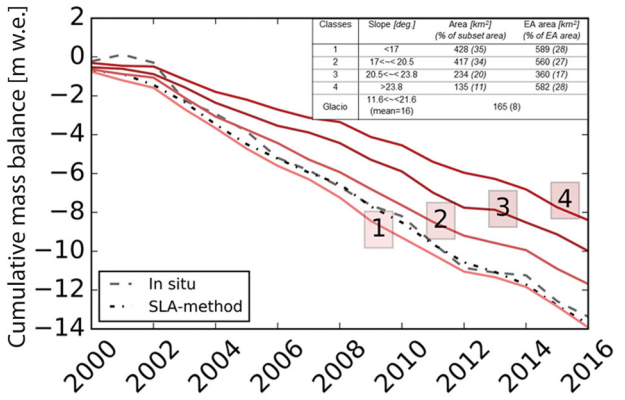

FIGURE 6 | Cumulative mass balance of glaciers from the European Alps vs. their mean slopes. The dashed lines represent the median cumulative mass balance of 23 glaciers obtained from *in situ* data (gray) and with SLA-method (black). The curves 1, 2, 3, and 4 correspond to the cumulative mass balance of glaciers sorted into quartiles on the basis of their mean slope. Each class has the same number of glaciers but corresponds to a peculiar total glacier area. The classes' glacier area of our subset and the corresponding glacier area for the entire European Alps (EA) are displayed in the inset table.

the European Alps is likely mainly the result of the atmospheric temperature increase that can be observed in the ERA5 data.

Representativeness of *in situ* Monitored Mass Change

Historically, glacier-wide mass change was monitored *in situ* and glaciers have often been chosen because of their access, their morpho-topographic features enabling their instrumentation, or for political and historical reasons (Kaser et al., 2003). The "ideal" glacier for mass balance investigation does not represent the global glacier diversity, which may lead to biases if such a glacier is considered as representative of the regional scale glacier behavior. Indeed, negative biases have already been observed when comparing region-wide mass balance estimations using laser altimetry to interpolations of sparse glaciological measurements (Gardner et al., 2013). Recently developed geodetic methods help overcoming this issue of representativeness due to higher temporal and spatial resolutions of the computed mass balances (e.g., Menounos et al., 2019; Zemp et al., 2019).

To see whether the *in situ* monitored glaciers in the European Alps are representative of the regional behavior, we analyzed the cumulative mass balance of the 239 glaciers in the European Alps for which annual mass-balance time series have been computed, as a function of the glacier morpho-topographic features, such as mean glacier slope, median and maximum altitude (significantly correlated to the average glacier wide mass balance, see section Glacier Morpho-Topographic Features, one of the Multi-Decadal Mass Balance Drivers?). **Figure 6** illustrates the cumulative mass balance from 239 glaciers computed from the SLA-method divided into glacier slope quartiles, and the average of the 23 mass balance time series obtained with the *in situ* glaciological method.

As described in section Remotely-Sensed SLA and Annual Mass Balance Validation, annual mass changes computed with the SLA-method slightly underestimates extremely high and low mass balance values (e.g., a year with positive mass balance in the studied period and 2003, a very low mass balance year in the European Alps). As illustrated in **Figure 6**, our study period has both positive and negative extremes in the first four years, and the cumulative mass balance quantified from *in situ* measurements is poorly reproduced by SLA-method for those years. For the rest of the time period, the cumulative mass balance of the SLA-method is able to match the *in situ* monitored cumulative mass balance. The mean slope of the *in situ* monitored glaciers (16° ranging from 11.6 to 21.6°) falls into classes 1 and 2 (slopes gentler than 20.5°), and **Figure 6** (+ the inset Table herein) shows that the median of the 23 *in situ* mass balance time series is in agreement with the SLA-method mass balance for glaciers having a similar mean slope. As shown in **Figure 4**, the gentler the glacier slope, the higher the overall mass loss. This relationship has already been observed, either sporadically on small sets of glaciers (e.g., Huss, 2012; Rabatel et al., 2016), or at a larger scale (e.g., Fischer et al., 2015; Brun et al., 2019). From **Figure 6**, we can also note that the *in situ* mass-balance time series fails to represent glaciers from classes 3 and 4 (slope greater than 20.5°), yet these classes account for 45% of the glacierized area of the European Alps. We therefore suggest that *in situ* mass-balance time series may convey a negatively biased picture of the regional behavior because they under-sample steep glaciers, representing almost half of the glacier coverage in the European Alps.

A similar analysis has been conducted using the glacier median altitude (instead of classes of glacier slope), but the only noteworthy class (with a median altitude greater than 3,207 m a.s.l. vs. 3,103 m a.s.l. in average for *in situ* monitored glaciers, **Supplementary Figure S9**) concerns about 20% of the total European Alps' glacierized area, and glaciers from the glaciological sample are spanning over the four defined classes, not permitting to conclude on significant relationships or mis-representativeness of the glaciological sample. When dividing our glacier sample into classes of maximum altitude, glaciers with higher maximum elevations seem to experience less negative mass balances (see **Supplementary Figure S10**). It is important to highlight that SLAs are rarely observable at the end of the melt season during high loss years for glaciers with low maximum elevations (<3,100 m a.s.l.). These glaciers were therefore discarded in our study, and our subset is not representative of the total European Alps population (12% in our subset vs. 46% for the entire European Alps, in terms of corresponding area for glaciers with maximum altitude < 3,471 m a.s.l.).

From these analyses and in line with the results presented in section Glacier Morpho-Topographic Features, One of the Multi-Decadal Mass Balance Drivers?, we can mention that glaciers with steep slopes and high maximum elevation experienced lower mass loss over the study period. Possible interpretations are that the mean slope and the mass transfer are related, with steeper glaciers having faster dynamics and, that glaciers with higher accumulation areas (i.e., still having a wide accumulation zone) have lower

mass balance sensitivity. This hypothesis would imply that steeper glaciers with wide accumulation area faster reach a balanced-state with less negative mass balances while glaciers with low slope remain imbalanced for a longer time, experiencing more negative mass balances to adapt to changing climatic conditions (corroborated by e.g., Brun et al., 2019; Zekollari et al., 2020).

CONCLUSION

We quantified a spatially resolved estimate of individual annual mass-balance time series for 239 glaciers in the European Alps, using both geodetic and snowline altitude estimates for the period from 2000 to 2016. Benefiting from *in situ* mass changes data from 23 glaciers, we were able to validate our approach, which is based on the SLA-method to quantify the annual mass balance of individual glaciers at regional scale. The observed discrepancies with *in situ* estimates are attributable to both the uncertainties and limitations in the semi-automatic SLA algorithm (e.g., underestimation of very negative mass balance years) and to glacier-wide estimates from *in situ* surface mass balance.

Geodetic estimates of long-term mass changes were used to analyze the impact of glacier morpho-topographic features on the mass changes. Three morpho-topographic variables – mean glacier slope, median, and maximum altitude – appear to explain 19, 24, and 12%, respectively, of the observed variance of the long-term mass changes. An analysis of the cumulative mass balance from *in situ* and SLA-method estimates suggests that steeper and higher glaciers experienced reduced mass losses. Our analysis suggests that the mass balance time series from glaciers with *in situ* measurements are not fully representative of the regional behavior of glaciers in the European Alps. Indeed, these glaciers belong to the "gentle slope glaciers" ($<20°$), and half of the glaciers in the European Alps with higher slope experienced a lower cumulative mass loss. Nonetheless, *in situ* measurements still provide essential data (particularly point measurements) for the comprehension and modeling of surface processes and glacier response to climate forcing at fine spatial and temporal scales. They are also essential to validate mass change estimates from different remote-sensing methods.

The broad coverage of the Alpine region allowed our mass change estimates to be analyzed in relation with a global atmospheric dataset, namely the ERA5 reanalysis. The yearly resolution of the mass balance time series allowed the identification of two opposite weather regimes favorable or detrimental to the mass balance depending on the time of the year.

Finally, this study proposes a new methodological framework to quantify the long-term trends and the annual mass-balance time series of individual glaciers at regional scale from optical satellite remote sensing only. It also shows an example of data combination to assess climatic causes of observed regional mass changes. The satisfactory results we obtained should encourage applying this framework to other glacierized regions, for example, on hardly accessible glaciers and in regions with few or no available annual mass-balance time series.

DATA AVAILABILITY STATEMENT

Geodetic mass balance and annual surface mass balance data are provided as **Supplementary Material** (in CSV format). Additionally, annual ELA are available to the international community through a French data portal THEIA: https://www.theia-land.fr/product/altitude-de-ligne-dequilibre-glaciaire-annuelle/. The ERA 5 reanalysis can be found at https://climate.copernicus.eu/climate-reanalysis.

AUTHOR CONTRIBUTIONS

LD, AR, and YA developed the method to automatize the detection of the SLA. AR computed and provided the reference dataset of manually derived SLA. LD and AD performed the analysis between glacier mass changes and climate. RH computed the geodetic mass balances for the entire European Alps and for the period from 2000 to 2016. LD and AR led the writing of the manuscript. All co-authors contributed to the manuscript.

FUNDING

This study was conducted in the context of the French glacier observatory GLACIOCLIM (https://glacioclim.osug.fr) and the Labex OSUG@2020 (*Investissements d'Avenir* – ANR10 LABX56). We acknowledge the Helmholtz-RSF project grant #18-47-06202. This was IORAS contribution to the St. Arg. #0149-2019-0002.

ACKNOWLEDGMENTS

We are grateful to the satellite data providers: Copernicus/EU/ESA for Sentinel-2, USGS for Landsat, and JPL/NASA and METI for ASTER. The ERA 5 reanalysis was made available by courtesy of ECMWF/Copernicus. We are also grateful to Etienne Berthier for numerous fruitful discussions, advice, and comments on the present manuscript. We thank Pascal Sirguey for helping the development of the detection algorithm and for developing part of the images' corrections. We also acknowledge Fabien Maussion for processing the glacier central flow lines, Delphine Six for fruitful discussions on the method and the manuscript, Juliette Blanchet for advice on the statistical approach developed for the snowline detection algorithm, Maxim Lamare for discussions on topographic correction models, Fanny Brun for glaciological discussions, and Jean Pierre Dedieu for his involvement in the development of the SLA-method. Finally, we are grateful to the scientific editor, MZ, and the two reviewers for their careful review of the manuscript and comments used to improve the study.

SUPPLEMENTARY MATERIAL

The Supplementary Material for this article can be found online at: https://www.frontiersin.org/articles/10.3389/feart.2020.00149/full#supplementary-material

REFERENCES

Abermann, J., Kuhn, M., and Fischer, A. (2011). Climatic controls of glacier distribution and glacier changes in Austria. *Ann. Glaciol.* 52, 83–90. doi: 10.3189/172756411799096222

Beniston, M. (2003). Climatic change in mountain regions: a review of possible impacts. *Clim. Change* 59, 5–31. doi: 10.1023/A:1024458411589

Beniston, M., Farinotti, D., Stoffel, M., Andreassen, L. M., Coppola, E., Eckert, N., et al. (2018). The European mountain cryosphere: a review of past, current and future issues. *Cryosphere* 12, 759–794. doi: 10.5194/tc-12-759-2018

Benn, D. I., and Lehmkuhl, F. (2000). Mass balance and equilibrium-line altitudes of glaciers in high-mountain environments. *Quat. Int.* 6, 15–29. doi: 10.1016/S1040-6182(99)00034-8

Berthier, E., Cabot, V., Vincent, C., and Six, D. (2016). Decadal region-wide and glacier-wide mass balances derived from multi-temporal ASTER satellite digital elevation models. Validation over the Mont-Blanc area. *Front. Earth Sci.* 4:63. doi: 10.3389/feart.2016.00063

Beyer, R. A., Alexandrov, O., and McMichael, S. (2018). The Ames Stereo Pipeline: NASA's open source software for deriving and processing terrain data. *Earth Space Sci.* 5, 537–548. doi: 10.1029/2018EA000409

Bolch, T., Sørensen, L. S., Simonsen, S. B., Mölg, N., Machguth, H., Rastner, P., et al. (2013). Mass loss of Greenland's glaciers and ice caps 2003–2008 revealed from ICESat laser altimetry data. *Geophys. Res. Lett.* 40, 875–881. doi: 10.1002/grl.50270

Bolibar, J., Rabatel, A., Gouttevin, I., Galiez, C., Condom, T., and Sauquet, E. (2020). Deep learning applied to glacier evolution modelling. *Cryosphere* 14, 565–584. doi: 10.5194/tc-14-565-2020

Braithwaite, R. J. (1984). Can the mass balance of a glacier be estimated from its equilibrium-line altitude? *J. Glaciol.* 30, 364–368. doi: 10.1017/S0022143000006237

Braithwaite, R. J., and Zhang, Y. (2000). Sensitivity of mass balance of five Swiss glaciers to temperature changes assessed by tuning a degree-day model. *J. Glaciol.* 46, 7–14. doi: 10.3189/172756500781833511

Brun, F., Berthier, E., Wagnon, P., Kääb, A., and Treichler, D. (2017). A spatially resolved estimate of High Mountain Asia glacier mass balances, 2000-2016. *Nat. Geosci.* 10, 668–673. doi: 10.1038/NGEO2999

Brun, F., Wagnon, P., Berthier, E., Jomelli, V., Maharjan, S. B., Shrestha, F., et al. (2019). Heterogeneous influence of glacier morphology on the mass balance variability in High Mountain Asia. *J. Geophys. Res. Earth Surf.* 124, 1331–1345. doi: 10.1029/2018JF004838

Cassou, C., Terray, L., Hurrell, J. W., and Deser, C. (2004). North Atlantic winter climate regimes: spatial asymmetry, stationarity with time, and oceanic forcing. *J. Clim.* 17, 1055–1068.

Cassou, C., Terray, L., and Phillips, A. S. (2005). Tropical Atlantic influence on European heat waves. *J. Clim.* 18, 2805–2811. doi: 10.1175/JCLI3506.1

Chandrasekharan, A., Ramsankaran, R., Pandit, A., and Rabatel, A. (2018). Quantification of annual glacier surface mass balance for the Chhota Shigri Glacier, Western Himalayas, India using an Equilibrium-Line Altitude (ELA) based approach. *Int. J. Remote Sens.* 39, 9092–9112. doi: 10.1080/01431161.2018.1506182

Copernicus Climate Change Service [C3S] (2017). ERA5: Fifth Generation of ECMWF Atmospheric Reanalyses of the Global Climate. Copernicus Climate Change Service Climate Data Store (CDS). Available online at: https://cds.climate.copernicus.eu/cdsapp#!/home (accessed October–November, 2019).

Dussaillant, I., Berthier, E., Brun, F., Masiokas, M., Hugonnet, R., Favier, V., et al. (2019). Two decades of glacier mass loss along the Andes. *Nat. Geosci.* 12, 802–808. doi: 10.1038/s41561-019-0432-5

Farinotti, D., Huss, M., Fürst, J. J., Landmann, J., Machguth, H., Maussion, F., et al. (2019). A consensus estimate for the ice thickness distribution of all glaciers on Earth. *Nat. Geosci.* 12, 168–173. doi: 10.1038/s41561-019-0300-3

Fischer, M., Huss, M., and Hoelzle, M. (2015). Surface elevation and mass changes of all Swiss glaciers 1980–2010. *Cryosphere* 9, 525–540. doi: 10.5194/tc-9-525-2015

Gardner, A. S., Moholdt, G., Cogley, J. G., Wouters, B., Arendt, A. A., Wahr, J., et al. (2013). A reconciled estimate of glacier contributions to sea level rise: 2003 to 2009. *Science* 340, 852–857. doi: 10.1126/science.1234532

Hock, R., Bliss, A., Marzeion, B., Giesen, R. H., Hirabayashi, Y., Huss, M., et al. (2019). GlacierMIP – A model intercomparison of global-scale glacier mass-balance models and projections. *J. Glaciol.* 65, 453–467. doi: 10.1017/jog.2019.22

Hoelzle, M., Haeberli, W., Dischl, M., and Peschke, W. (2003). Secular glacier mass balances derived from cumulative glacier length changes. *Glob. Planet. Change* 36, 295–306. doi: 10.1016/S0921-8181(02)00223-220

Hoinkes, H. C. (1968). Glacier variation and weather. *J. Glaciol.* 7, 3–18. doi: 10.3189/S0022143000020384

Huss, M. (2012). Extrapolating glacier mass balance to the mountain-range scale: the European Alps 1900–2100. *Cryosphere* 6, 713–727.

Huss, M. (2013). Density assumptions for converting geodetic glacier volume change to mass change. *Cryosphere* 7, 877–887. doi: 10.5194/tc-7-877-2013

Huss, M., and Hock, R. (2018). Global-scale hydrological response to future glacier mass loss. *Nat. Clim. Change* 8, 135–140. doi: 10.1038/s41558-017-0049-x

IPCC (2019). "Summary for Policymakers," in *IPCC Special Report on the Ocean and Cryosphere in a Changing Climate*, eds H.-O. Pörtner, D. C. Roberts, V. Masson-Delmotte, P. Zhai, E. Poloczanska, et al. (Geneva: IPCC).

Jacob, T., Wahr, J., Pfeffer, W. T., and Swenson, S. (2012). Recent contributions of glaciers and ice caps to sea level rise. *Nature* 482, 514–518. doi: 10.1038/nature10847

Kaser, G., Fountain, A., and Jansson, P. (2003). *A Manual for Monitoring the Mass Balance of Mountain Glaciers*. Paris: UNESCO.

Kuhn, M. (1984). Mass budget imbalances as criterion for a climatic classification of glaciers. *Geogr. Ann. Ser. Phys. Geogr.* 66, 229–238. doi: 10.1080/04353676.1984.11880111

Leclercq, P. W., Oerlemans, J., Basagic, H. J., Bushueva, I., Cook, A. J., and Le Bris, R. (2014). A data set of worldwide glacier length fluctuations. *Cryosphere* 8, 659–672. doi: 10.5194/tc-8-659-2014

Lliboutry, L. (1965). *Traité de Glaciologie: Glaciers, Variations du Climat, sols Gelés*. Paris: Masson et Cie.

Lliboutry, L. (1974). Multivariate statistical analysis of glacier annual balances. *J. Glaciol.* 13, 371–392. doi: 10.1017/S0022143000023169

Mackintosh, A. N., Anderson, B. M., and Pierrehumbert, R. T. (2017). Reconstructing climate from glaciers. *Annu. Rev. Earth Planet. Sci.* 45, doi: 10.1146/annurev-earth-063016-020643

Martin, S. (1974). Correlation bilans de masse annuels-facteurs météorologiques dans les Grandes Rousses. *Z. Gletscherkde Glazialgeol.* 10, 89–100.

Mayo, L. R. (1984). Glacier mass balance and runoff research in the U.S.A. *Geogr. Ann. Ser. Phys. Geogr.* 66, 215–227. doi: 10.2307/520695

McNabb, R., Nuth, C., Kääb, A., and Girod, L. (2019). Sensitivity of glacier volume change estimation to DEM void interpolation. *Cryosphere* 13, 895–910. doi: 10.5194/tc-13-895-2019

Menounos, B., Hugonnet, R., Shean, D., Gardner, A., Howat, I., Berthier, E., et al. (2019). Heterogeneous changes in Western North American glaciers linked to decadal variability in zonal wind strength. *Geophys. Res. Lett.* 46, 200–209. doi: 10.1029/2018GL080942

Noh, M.-J., and Howat, I. M. (2015). Automated stereo-photogrammetric DEM generation at high latitudes: surface Extraction with TIN-based Search-space Minimization (SETSM) validation and demonstration over glaciated regions. *GISci. Remote Sens.* 52, 198–217. doi: 10.1080/15481603.2015.1008621

Nuth, C., and Kääb, A. (2011). Co-registration and bias corrections of satellite elevation data sets for quantifying glacier thickness change. *Cryosphere* 5, 271–290. doi: 10.5194/tc-5-271-2011

Paul, F., Barrand, N. E., Baumann, S., Berthier, E., Bolch, T., Casey, K., et al. (2013). On the accuracy of glacier outlines derived from remote-sensing data. *Ann. Glaciol.* 54, 171–182.

Paul, F., and Haeberli, W. (2008). Spatial variability of glacier elevation changes in the Swiss Alps obtained from two digital elevation models. *Geophys. Res. Lett.* 35:L21502. doi: 10.1029/2008GL034718

Pelto, M. (2011). Utility of late summer transient snowline migration rate on Taku Glacier, Alaska. *Cryosphere* 5, 1127–1133. doi: 10.5194/tc-5-1127-2011

Pelto, M. S. (2018). How unusual was 2015 in the 1984–2015 period of the north cascade glacier annual mass balance? *Water* 10:543. doi: 10.3390/w10050543

Pepin, N., Bradley, R. S., Diaz, H. F., Baraer, M., Caceres, E. B., Forsythe, N., et al. (2015). Elevation-dependent warming in mountain regions of the world. *Nat. Clim. Change* 5, 424–430. doi: 10.1038/nclimate2563

Pieczonka, T., and Bolch, T. (2015). Region-wide glacier mass budgets and area changes for the Central Tien Shan between ˜1975 and 1999 using Hexagon KH-9 imagery. *Glob. Planet. Change* 128, 1–13. doi: 10.1016/j.gloplacha.2014.11.014

Rabatel, A., Dedieu, J.-P., Thibert, E., Letreguilly, A., and Vincent, C. (2008). Twenty-five years of equilibrium-line altitude and mass balance reconstruction on the Glacier Blanc, French Alps (1981-2005), using remote-sensing method and meteorological data. *J. Glaciol.* 54, 307–314. doi: 10.3189/002214308784886063

Rabatel, A., Dedieu, J.-P., and Vincent, C. (2005). Using remote-sensing data to determine equilibrium-line altitude and mass-balance time series: validation on three French glaciers, 1994–2002. *J. Glaciol.* 51, 539–546. doi: 10.3189/172756505781829106

Rabatel, A., Dedieu, J. P., and Vincent, C. (2016). Spatio-temporal changes in glacier-wide mass balance quantified by optical remote sensing on 30 glaciers in the French Alps for the period 1983–2014. *J. Glaciol.* 62, 1153–1166. doi: 10.1017/jog.2016.113

Rabatel, A., Letréguilly, A., Dedieu, J.-P., and Eckert, N. (2013). Changes in glacier equilibrium-line altitude in the western Alps from 1984 to 2010: evaluation by remote sensing and modeling of the morpho-topographic and climate controls. *Cryosphere* 7, 1455–1471. doi: 10.5194/tc-7-1455-2013

Rabatel, A., Sirguey, P., Drolon, V., Maisongrande, P., Arnaud, Y., Berthier, E., et al. (2017). Annual and seasonal glacier-wide surface mass balance quantified from changes in glacier surface state: a review on existing methods using optical satellite imagery. *Remote Sens.* 9:507. doi: 10.3390/rs9050507

Racoviteanu, A. E., Rittger, K., and Armstrong, R. (2019). An automated approach for estimating snowline altitudes in the Karakoram and Eastern Himalaya from remote sensing. *Front. Earth Sci.* 7:220. doi: 10.3389/feart.2019.00220

Rastner, P., Prinz, R., Notarnicola, C., Nicholson, L., Sailer, R., Schwaizer, G., et al. (2019). On the automated mapping of snow cover on glaciers and calculation of snow line altitudes from multi-temporal Landsat data. *Remote Sens.* 11:1410. doi: 10.3390/rs11121410

RGI Consortium (2017). *Randolph Glacier Inventory (RGI) – A Dataset of Global Glacier Outlines: Version 6.0. Technical Report, Global Land Ice Measurements from Space*. Boulder, CO: Digital Media. doi: 10.7265/N5-RGI-60

Rolstad, C., Haug, T., and Denby, B. (2009). Spatially integrated geodetic glacier mass balance and its uncertainty based on geostatistical analysis: application to the western Svartisen ice cap, Norway. *J. Glaciol.* 55, 666–680. doi: 10.3189/002214309789470950

Seehaus, T., Malz, P., Sommer, C., Soruco, A., Rabatel, A., and Braun, M. (2020). Mass balance and area changes of glaciers in the Cordillera Real and Tres Cruces, Bolivia, between 2000 and 2016. *J. Glaciol.* 66, 124–136. doi: 10.1017/jog.2019.94

Shean, D. E., Alexandrov, O., Moratto, Z. M., Smith, B. E., Joughin, I. R., Porter, C., et al. (2016). An automated, open-source pipeline for mass production of digital elevation models (DEMs) from very-high-resolution commercial stereo satellite imagery. *ISPRS J. Photogramm. Remote Sens.* 116, 101–117. doi: 10.1016/j.isprsjprs.2016.03.012

Shean, D. E., Bhushan, S., Montesano, P., Rounce, D. R., Arendt, A., and Osmanoglu, B. (2020). A systematic, regional assessment of High Mountain Asia glacier mass balance. *Front. Earth Sci.* 7:363. doi: 10.3389/feart.2019.0036

Sirguey, P. (2009). Simple correction of multiple reflection effects in rugged terrain. *Int. J. Remote Sens.* 30, 1075–1081. doi: 10.1080/01431160802348101

Susanti, Y., Pratiwi, H., Sri Sulistijowati, H., and Liana, T. (2014). M estimation, S estimation, and MM estimation in robust regression. *Int. J. Pure Appl. Math.* 91, 349–360. doi: 10.3390/s19245402

Tachikawa, T., Hato, M., Kaku, M., and Iwasaki, A. (2011). "Characteristics of ASTER GDEM version 2," in *Proceedings of the 2011 IEEE International Geoscience and Remote Sensing Symposium*, Vancouver, 3657–3660. doi: 10.1109/IGARSS.2011.6050017

Thibert, E., Blanc, R., Vincent, C., and Eckert, N. (2008). Glaciological and volumetric mass-balance measurements: error analysis over 51 years for Glacier de Sarennes. *French Alps. J. Glaciol.* 54, 522–532. doi: 10.3189/002214308785837093

Vaughan, D. G., Comiso, J. C., Allison, I., Carrasco, J., Kaser, G., Kwok, R., et al. (2013). *Observations: Cryosphere*. Available online at: http://www.cambridge.org/au/academic/subjects/earth-and-environmental-science/climatology-and-climate-change/climate-change-2013-physical-science-basis-working-group-i-contribution-fifth-assessment-report-intergovernmental-panel-climate-change (accessed July 24, 2017).

Vincent, C. (2002). Influence of climate change over the 20th Century on four French glacier mass balances. *J. Geophys. Res. Atmos.* 107:4375. doi: 10.1029/2001JD000832

Vincent, C., Fischer, A., Mayer, C., Bauder, A., Galos, S. P., Funk, M., et al. (2017). Common climatic signal from glaciers in the European Alps over the last 50 years. *Geophys. Res. Lett.* 44, 1376–1383. doi: 10.1002/2016GL072094

WGMS (2019). *Fluctuations of Glaciers Database*. Zurich: World Glacier Monitoring Service. doi: 10.5904/wgms-fog-2019-12

Wilks, D. S. (2011). *Statistical Methods in the Atmospheric Sciences*, 3rd Edn. Oxford: Academic press.

Willis, M. J., Melkonian, A. K., Pritchard, M. E., and Rivera, A. (2012). Ice loss from the Southern Patagonian Ice Field, South America, between 2000 and 2012. *Geophys. Res. Lett.* 39:L17501. doi: 10.1029/2012GL053136

Wouters, B., Gardner, A. S., and Moholdt, G. (2019). Status of the global glaciers from GRACE (2002-2016). *Front. Earth Sci.* 7:75. doi: 10.3389/feart.2019.00096

Zekollari, H., Huss, M., and Farinotti, D. (2020). On the imbalance and response time of glaciers in the European Alps. *Geophys. Res. Lett.* 47:e2019GL085578. doi: 10.1029/2019GL085578

Zemp, M., Huss, M., Thibert, E., Eckert, N., McNabb, R., Huber, J., et al. (2019). Global glacier mass changes and their contributions to sea-level rise from 1961 to 2016. *Nature* 568, 382–386. doi: 10.1038/s41586-019-1071-0

Zemp, M., Thibert, E., Huss, M., Stumm, D., Rolstad Denby, C., Nuth, C., et al. (2013). Reanalysing glacier mass balance measurement series. *Cryosphere* 7, 1227–1245. doi: 10.5194/tc-7-1227-2013

Conflict of Interest: The authors declare that the research was conducted in the absence of any commercial or financial relationships that could be construed as a potential conflict of interest.

frontiers in Earth Science

ORIGINAL RESEARCH
published: 03 June 2020
doi: 10.3389/feart.2020.00163

Mass Balance of 14 Icelandic Glaciers, 1945–2017: Spatial Variations and Links With Climate

Joaquín M. C. Belart[1,2,3]*, *Eyjólfur Magnússon*[1], *Etienne Berthier*[2], *Ágúst Þ. Gunnlaugsson*[1,4], *Finnur Pálsson*[1], *Guðfinna Aðalgeirsdóttir*[1], *Tómas Jóhannesson*[4], *Thorsteinn Thorsteinsson*[4] *and Helgi Björnsson*[1]

[1] *Institute of Earth Sciences, University of Iceland, Reykjavík, Iceland* , [2] *Laboratoire d'Etudes en Géophysique et Océanographie Spatiales, Université de Toulouse, CNES, Toulouse, France,* [3] *National Land Survey of Iceland, Akranes, Iceland,* [4] *Icelandic Meteorological Office (IMO), Reykjavík, Iceland*

To date, most mass balance studies in Iceland have concentrated on the three largest ice caps. This study turns the focus toward smaller Icelandic glaciers, presenting geodetic mass-balance estimates for 14 of them (total area 1,005 km^2 in 2017) from 1945 to 2017, in decadal time spans. These glaciers, distributed over the country, are subject to different climatic forcing. The mass balance, derived from airborne and spaceborne stereo imagery and airborne lidar, is correlated with precipitation and air temperature by a first-order equation including a reference-surface correction term. This permits statistical modeling of annual mass balance, used to temporally homogenize the mass balance for a region-wide mass balance assessment for the periods 1945–1960, 1960–1980, 1980–1994, 1994–2004, 2004–2010, and 2010–2017. The 14 glaciers were close to equilibrium during 1960–1994, with an area-weighted mass balance of 0.07 ± 0.07 m w.e. a^{-1}. The most negative mass balance occurred in 1994–2010, accounting for −1.20 ± 0.09 m w.e. a^{-1}, or 21.4 ± 1.6 Gt (1.3 ± 0.1 Gt a^{-1}) of mass loss. Glaciers located along the south and west coasts show higher decadal mass-balance variability and static mass-balance sensitivities to summer temperature and winter precipitation, −2.21 ± 0.25 m w.e. a^{-1} K^{-1} and 0.22 ± 0.11 m w.e. a^{-1}(10%)$^{-1}$, respectively, while glaciers located inland, north and northwest, have corresponding mass-balance sensitivities of −0.72 ± 0.10 m w.e. a^{-1} K^{-1} and 0.13 ± 0.07 m w.e. a^{-1}(10%)$^{-1}$. These patterns are likely due to the proximity to warm (south and west) vs. cold (northwest) oceanic currents.

Keywords: region-wide mass balance, glacier–climate relationship, mass-balance sensitivity, Iceland, remote sensing, historical aerial photographs

OPEN ACCESS

Edited by:
Michael Zemp,
University of Zurich, Switzerland

Reviewed by:
Thomas Vikhamar Schuler,
University of Oslo, Norway
Matthias Huss,
ETH Zürich, Switzerland

***Correspondence:**
Joaquín M. C. Belart
joaquin@lmi.is

Specialty section:
This article was submitted to Cryospheric Sciences, a section of the journal Frontiers in Earth Science

Received: *22 December 2019*
Accepted: *29 April 2020*
Published: *03 June 2020*

Citation:
Belart JMC, Magnússon E, Berthier E, Gunnlaugsson ÁÞ, Pálsson F, Aðalgeirsdóttir G, Jóhannesson T, Thorsteinsson T and Björnsson H (2020) Mass Balance of 14 Icelandic Glaciers, 1945–2017: Spatial Variations and Links With Climate. Front. Earth Sci. 8:163. doi: 10.3389/feart.2020.00163

1. INTRODUCTION

Glacier mass balance is a robust proxy closely linked to climate variations (Ahlmann, 1940; Ohmura, 2011; Vaughan et al., 2013; Bojinski et al., 2014). At high latitudes, mass balance is related to winter precipitation (winter snow) and summer temperature (a proxy for available energy to melt snow and ice). Glaciers have variable response times to changing climate, ranging from a few years to several decades depending on their thickness, slope and mass turnover (Jóhannesson et al., 1989; Lüthi and Bauder, 2010; Harrison, 2013; Roe et al., 2017). They filter out the high frequency seasonal and shorter-term climate variability, resulting in length or volume changes that represent

integrated response to longer-term climate variability (Elsberg et al., 2001; Marzeion et al., 2012; Christian et al., 2018).

Glaciological mass-balance observations are sparse and costly, whereas mass balance inferred from remote-sensing observations, e.g., geodetic mass balance (Cogley et al., 2011), has become the most common method to measure glacier-mass changes in glacierized regions without demanding field logistics (Zemp et al., 2019). The remote sensing era started during the early 1900s, and the mapping cameras developed rapidly in the 1930s, leading to numerous airborne and spaceborne photogrammetric and photoreconnaissance surveys worldwide (Livingston, 1963; Spriggs, 1966; Bindschadler and Vornberger, 1998). These surveys provide valuable sources to create Digital Elevation Models (DEMs) with the potential for geodetic mass-balance measurements (e.g., Finsterwalder, 1954; Bolch et al., 2011; Magnússon et al., 2016a; Fieber et al., 2018).

Despite the vast amount of historical archives of stereo images, the geodetic records of the first half of the twentieth century are still scarce and mostly based on contour maps (e.g., Bauder et al., 2007). Observations became fairly common after 1980 (e.g., Fischer et al., 2015) and have been very frequent since 2000 (e.g., Zemp et al., 2019) due to the rapid development and availability of sensors with capabilities to measure the glacier surface geometry (e.g., optical stereoscopic imagery, radar, and lidar).

Spatially distributed geodetic mass balance is available for several glacierized regions, e.g., the Alps (Fischer et al., 2015; Huss et al., 2015; Berthier et al., 2016), Andes (Soruco et al., 2009; Braun et al., 2019; Dussaillant et al., 2019), Greenland (Gardner et al., 2013; Huber et al., 2020), Norway (Andreassen et al., 2020), and High Mountain Asia (Kääb et al., 2012; Brun et al., 2017; Shean et al., 2020). These studies advance the understanding of the relationship between glacier variations and climate, are useful to calibrate regional and global climate models and constrain regional glacier-mass loss and sea-level rise (e.g., Marzeion et al., 2014; Huss et al., 2015).

In Iceland, mass-balance observations have mostly focused on the three largest ice caps: Vatnajökull, Langjökull, and Hofsjökull (7,676, 844, and 813 km^2 in 2017, respectively; Hannesdóttir et al., submitted), with a 30-year record of glaciological mass balance (Björnsson and Pálsson, 2008; Pálsson et al., 2012; Björnsson et al., 2013; Thorsteinsson et al., 2017, Aðalgeirsdóttir et al., submitted). These account for about 90% of the total glacierized area, and their mass-balance records have been used to estimate the Icelandic glacier-mass loss and sea-level rise contribution (Björnsson et al., 2013). Other glaciers and ice caps are less significant for the total Icelandic mass loss, but they are spatially distributed across all parts of Iceland and have the potential to provide insights into regional climate variations.

The aim of this study is to produce a catalog of maps of elevation difference and a 70-year record of geodetic mass balance of spatially distributed glaciers in Iceland. The mass balance is statistically correlated to records of temperature and precipitation to infer its static sensitivity to climate fluctuations, and the mass balance is temporally homogenized for a region-wide multi-temporal mass-balance study. The results are discussed in the context of climate-driven changes of the 14 glaciers.

2. STUDY AREAS

For the current study, 14 glaciers and ice caps were selected, distributed across all parts of Iceland (**Figure 1**). They are located in different climatic regimes: the climate near the southern coast is influenced by the warm Irminger oceanic current, whereas the climate at the northern coast is affected by the cold East Greenland oceanic current (e.g., Björnsson and Pálsson, 2008; Björnsson et al., 2013). Geodetic mass-balance estimates have recently been obtained for three of the glaciers: Drangajökull (Magnússon et al., 2016a), Tungnafellsjökull (Gunnlaugsson, 2016), and Eyjafjallajökull (Belart et al., 2019). Glaciological mass-balance observations have been carried out at a few locations on Mýrdalsjökull since 2001 (Ágústsson et al., 2013) and on Drangajökull during 2005–2015 (e.g., Belart et al., 2017; Anderson et al., 2018). Previous studies have also calculated geodetic mass balance over one to two decades on Snæfellsjökull (Jóhannesson et al., 2011), Eyjafjallajökull, Tindfjallajökull, and Torfajökull (Guðmundsson et al., 2011). The rest of the glaciers have very limited, or no, previous mass-balance observations.

The size of the glaciers varies from 3 km^2 for Hofsjökull Eystri to 517 km^2 for Mýrdalsjökull, and their total area is 1,005 km^2, or 9.8% of the total of Icelandic glaciers in 2017; Hannesdóttir et al., submitted. Their elevation span ranges from ∼200 m (Hofsjökull Eystri) to ∼2,000 m (Öræfajökull). Further characteristics of the studied glaciers are shown in **Table 1**.

The three largest ice caps, Vatnajökull, Langjökull, and Hofsjökull, were excluded from this study with the exception of Öræfajökull, which is a part of Vatnajökull (**Figure 1**). This was due to the complexity of the required processing for those large glaciers: the relatively small footprint of the historical aerial photographs in comparison with the glacier area would limit the availability of bare ground areas needed for reference (i.e., in the vicinity of the ice cap and nunataks) for a large amounts of aerial photographs, causing large distortions in the resulting DEMs. The aerial surveys of these ice caps were also carried out over multiple dates (months to years), complicating the mosaicking and interpretation of the results.

3. DATA

The data used in this study are described by Belart et al. (2019), and consists of a large collection of stereoscopic imagery available in Iceland from 1945 to 2017, from airborne and spaceborne, frame camera and pushbroom sensors, together with airborne lidar data (**Figure 2**).

A total of 836 aerial photographs acquired during 1945–1995 were collected from the National Land Survey of Iceland. The interval between surveys for each glacier was ∼10–20 years (e.g., Magnússon et al., 2016a; Pedersen et al., 2018; Belart et al., 2019). An additional series of photographs of Mýrdalsjökull and Torfajökull (acquired in 1999) were obtained from the private company Loftmyndir.

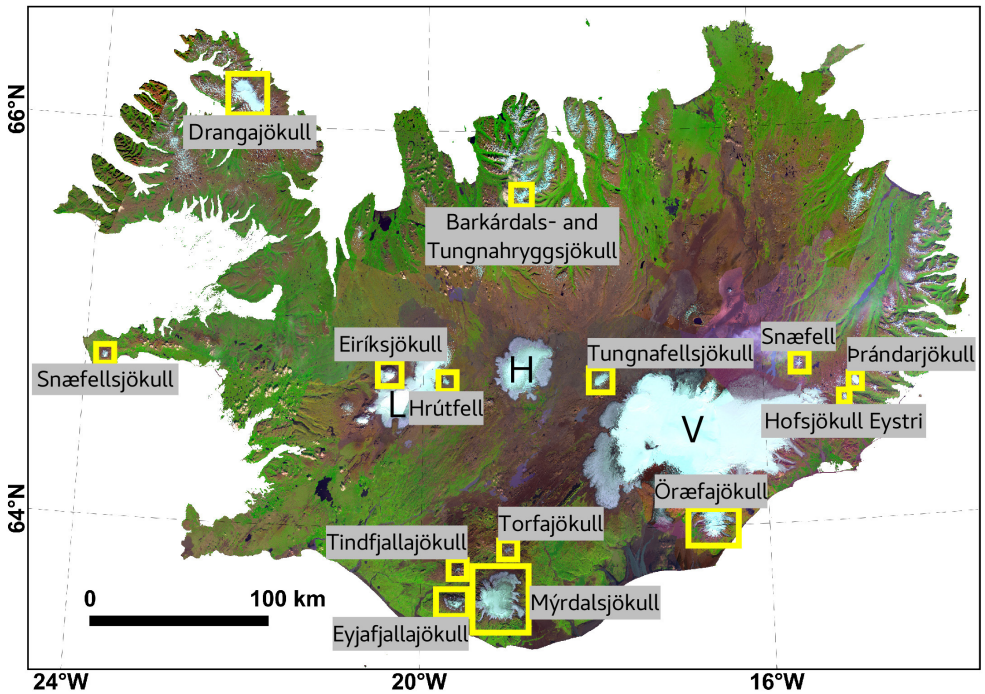

FIGURE 1 | Map of Iceland showing the 14 glaciers of this study (yellow boxes), as well as the three largest ice caps: Langjökull (L), Hofsjökull (H), and Vatnajökull (V). Background: composite mosaic from Landsat 8 (www.usgs.gov), created by the National Land Survey of Iceland (www.lmi.is).

TABLE 1 | Overview of 14 glaciers and ice caps.

	Area (km^2)	Elevation (m a.s.l.)	Mean thickness
Barkárdals- and Tungnahryggsjökull	17.7	762–1,362	N/A
Drangajökull	137.6	60–910	∼100 m (Magnússon et al., 2016b)
Eiríksjökull	18.6	570–1,670	N/A
Eyjafjallajökull	65.5	200–1,630	N/A
Hofsjökull Eystri	3.0	890–1,130	N/A
Hrútfell	4.2	690–1,370	N/A
Mýrdalsjökull	517.0	170–1,490	∼230 m (Björnsson et al., 2000)
Öræfajökull	163.2	0–2,110	∼120 m (Magnússon et al., 2012)
Snæfell	4.3	910–1,830	N/A
Snæfellsjökull	8.3	700–1,490	∼50 m (Björnsson, 2017)
Tindfjallajökull	10.8	670–1,440	N/A
Torfajökull	8.1	760–1,170	N/A
Tungnafellsjökull	32.5	900–1,520	∼60 m (Gunnlaugsson, 2016)
Þrándarjökull	14.0	900–1,220	N/A

The areas are referred to 2017 Hannesdóttir et al., submitted.

This study also used a DEM and orthoimage based on six images from Hexagon KH9 satellite acquired in August 1980, originally processed in Belart et al. (2019). They covered eight of the 14 glaciers, (from south to north) Eyjafjallajökull, Mýrdalsjökull, Tindfjallajökull, Torfajökull, Hrútfell, Tungnafellsjökull, Barkárdals-, and Tungnahryggsjökull.

In 2002–2015, SPOT 5 acquired numerous satellite stereo images of glacierized areas, particularly through the SPOT 5 Stereoscopic Survey of Polar Ice: Reference Images and Topographies (SPIRIT) project (Korona et al., 2009). This provided datapoints through the 2000s for Eyjafjallajökull, Mýrdalsjökull, Tindfjallajökull, Eiríksjökull, Hrútfell, Öræfajökull, and Tungnafellsjökull. The two last-mentioned glaciers include two acquisitions, in 2003/2004 and 2010.

Advanced Spaceborne Thermal Emission and Reflection Radiometer (ASTER) satellite stereo images, with modified gain setup specifically for surveying glaciers through the Global Land Ice Measurements from Space (GLIMS) project (Raup et al., 2007), were used for Barkárdals- and Tungnahryggsjökull, Torfajökull, Þrándarjökull, and Hofsjökull Eystri in 2004, and for Hrútfell in 2013.

The lidar datasets were collected between 2008 and 2012, starting with Snæfellsjökull and Eiríksjökull and finishing with Snæfell and Þrándarjökull (**Figure 2**; Jóhannesson et al., 2013). Pléiades satellite stereo images (Berthier et al., 2014) were acquired over the summers 2016 (Barkárdals- and Tungnahryggsjökull) and 2017 (Öræfajökull). Both of them were surveyed in two satellite acquisitions over the course of two weeks. Data from the ArcticDEM (Porter et al., 2018) from 2013 to 2018 were also used.

The large majority of the surveys (∼80%) were carried out in August, September, or October. ∼15% were carried out in July, one in June and one in November. Most of the surveys from 1945/1946 were done in late September or early October.

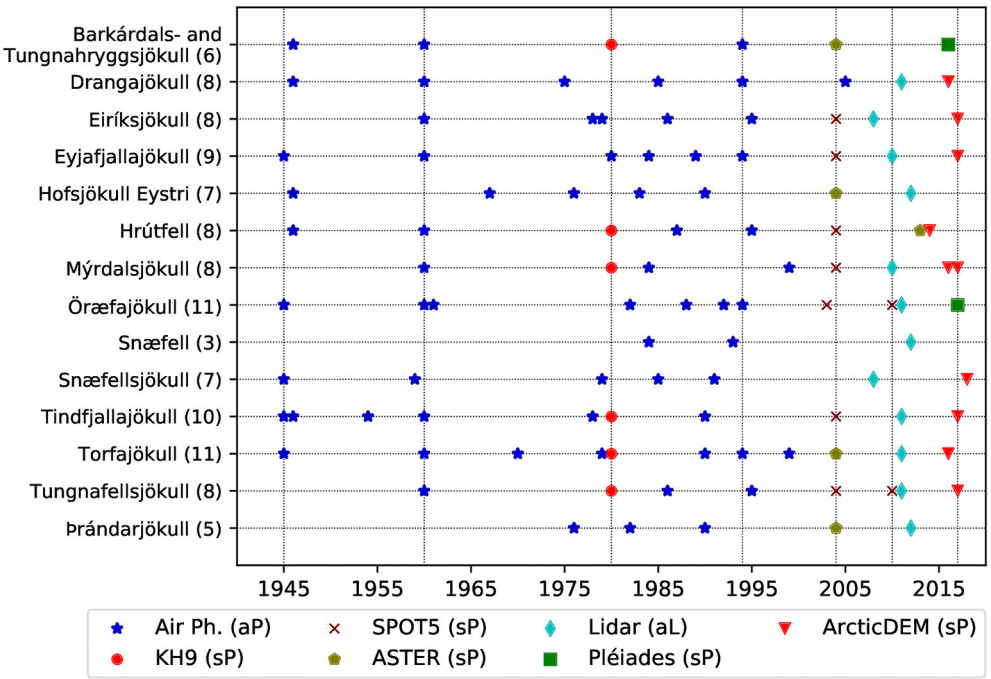

FIGURE 2 | Temporal distribution of the datasets for each glacier. The numbers in parentheses indicate the amount of surveys carried out on each glacier. Vertical lines are emplaced at the most repeated survey times, based on airborne photogrammetry (aP, 1945, 1960, 1994) and spaceborne photogrammetry (sP, 1980). 2004 contained abundant measurements from SPOT 5 (Korona et al., 2009) and ASTER (Raup et al., 2007). The airborne lidar (aL) surveys are spread over five years and adjusted to year 2010 (Jóhannesson et al., 2013). Recent satellite sub-meter stereo images from Pléiades (Berthier et al., 2014) and the ArcticDEMs (Porter et al., 2018) were acquired during 2016–2018 and adjusted to 2017.

Daily gridded climatic records were used: linearly modeled precipitation from 1958 to 2007 (LT, 1 × 1 km; Crochet et al., 2007), numerically downscaled modeled precipitation from 1980–2019 (HARMONIE, 2.5 × 2.5 km; Nawri et al., 2017) and interpolated temperature from 1948 to 2019 based on meteorological stations (1 × 1 km; Crochet and Jóhannesson, 2011). The gridded precipitation and temperature were measured in millimeters and Celsius degrees, respectively. Remarks on the data quality and associated uncertainties of the climatic records can be found in the mentioned studies and in Belart et al. (2019).

The glacier margins of Icelandic glaciers in ∼2000 were extracted from the GLIMS inventory (Raup et al., 2007), as a first approximation of the glacier outlines of the 14 glaciers.

4. METHODS

For each of the glaciers, the processing steps described by Belart et al. (2019) were followed, and we refer the readers to that article for further technical details. In summary, these consist of: (1) processing of stereo imagery and DEMs for creation of co-registered orthoimages, DEMs and difference of DEMs (dDEM); (2) glacier outline delineating for the two analyzed dates; (3) bias correction and uncertainty estimation in the volume changes using Sequential Gaussian Simulation (SGSim; Magnússon et al., 2016a); (4) filtering of outliers, gap filling and calculation of volume changes; (5) applying a seasonal correction to account for the volume change between the date of each survey and 1 October of the respective year; (6) geodetic mass-balance estimation, using a conversion factor of 850 ± 60 kg m^{-3} between volume and mass change (Huss, 2013). This workflow resulted in two values of geodetic mass balance, $\dot{B}$, one relative to the survey dates (floating-date system) and one fixed to the hydrological year, 1 October to 30 September (fixed-date system).

The photogrammetric processing of the aerial photographs (step 1) was done with MicMac software (Pierrot Deseilligny and Clery, 2011; Rupnik et al., 2017) using Ground Control Points (GCPs) extracted from a reference, in most cases from a lidar DEM, except for Barkárdals- and Tungnahryggsjökull (Pléiades DEM and orthoimage, Papasodoro et al., 2015), and Hrútfell (ArcticDEM). The pushbroom stereo images, i.e., Pléiades, ASTER, and SPOT 5 data, were processed using Ames StereoPipeline (ASP) software (Shean et al., 2016, 2020). The resulting DEMs and orthoimages, as well as the ArcticDEMs, were co-registered to the aforementioned reference using the Iterative Closest Point method in ASP (Shean et al., 2016).

The glacier outlines obtained from GLIMS were updated using the orthoimages (shaded relief images of the DEMs when no orthoimages were available). We modified the definition of the margins of N-Eiríksjökull, where we included the debris-covered ice in the low areas (**Figure S3**). When gaps in the orthoimages were present at particular locations of the margins, due to clouds or bad stereo coverage, the outline was completed using aerial

photographs, Landsat, or ASTER data with dates differing up to 2 years from the year-of-interest.

The SGSim method (Magnússon et al., 2016a), used for retrieving uncertainties and bias correction in the volume changes, required as input the ice-free areas of the dDEMs, manually masked from outliers. Semivariograms were created from the dDEMs on ice-free areas and manually fitted into semivariogram models. A total of 1,000 SGSims were run on each glacier, obtaining a map of errors propagated onto the respective glacier. These maps of errors were then subtracted from the dDEMs to locally remove systematic errors in elevation, and a histogram retrieved from the SGSim was used to extract the uncertainty of the volume change obtained from the dDEMs (95% confidence level).

The seasonal correction applied is based on a degree-day melt model combined with a late-summer snow accumulation model, using the daily gridded climate records. The setup parameters and uncertainties of the model are described in Belart et al. (2019). This seasonal correction model was run using bootstrapping, and from the 1,000 realizations of the runs we obtained a volume change from the date of survey to the 1 Oct, as well as the associated uncertainty (95% confidence level).

In some cases, we combined DEMs from surveys carried out up to two years apart, in order to fill gaps in the maps of elevation difference. This was done for Tindfjallajökull (70% in Sep 1945 and 30% in Sep 1946), Öræfajökull (60% in Aug 1960 and 40% in Jul 1960, and 50% in Aug 1992 and 50% in Aug 1994), Eiríksjökull (80% in Aug 1978 and 20% in Aug 1979), and Mýrdalsjökull (90% in 2016 and 10% in 2017). Each of the surveys covered the majority of the elevation span of the respective ice cap. In these cases the dDEM with smaller coverage was shifted to the main dDEM by the mean difference of the overlapping areas of the mosaic.

Remaining gaps in the maps of elevation difference (due to incomplete surveys, cloud presence, and lack of texture in the images) were interpolated as a function of elevation, using the local hypsometric method (e.g., Brun et al., 2017; McNabb et al., 2019). The uncertainty of these areas was increased based on the number of datapoints and variations in elevation difference for each elevation band (**Supplement S1**). The uncertainty of each geodetic mass balance was calculated as the square root of the sum of squares of the derivative of the mass balance with respect to each of the variables involved (Belart et al., 2019). The resulting uncertainty was subsequently combined with the uncertainty due to data gaps as the root sum of their squares.

Annual mass balance and static mass-balance sensitivities were calculated by correlating the fixed-date geodetic mass balance to the climatic records, using the following equation (Belart et al., 2019)

$$\dot{B} = \phi T_s + \omega P_w + \gamma \Delta\overline{A} + k, \quad (1)$$

where T_s and P_w are mean summer temperature and winter precipitation at the equilibrium line altitude (ELA), respectively. The summer is defined from 21 May to 30 September, the approximate period when the temperature is typically positive at the ELA and the aimed dates for the glaciological mass balance campaigns in Iceland (e.g., Belart et al., 2017, 2019). The winter precipitation is normalized, i.e., divided by the average winter precipitation of the available records (Oerlemans and Reichert, 2000). The ELA is assumed to be the snowline in ∼2004, and unchanged over the period of study for simplicity. The term $\Delta\overline{A}$ is the difference between a reference area, e.g., 1960, and the average area between each two years of survey. Together with γ and k, this serves as a correction to relate conventional and reference-surface mass balance (Elsberg et al., 2001; Harrison et al., 2001), and gives a better correlation of mass balance with climate (Cogley et al., 2011; Huss et al., 2012). The reference-surface term is simplified by assuming that relative changes in glacier area and ice volume are linearly related for the analyzed time period (Pálsson et al., 2012; Belart et al., 2019).

Equation (1) was solved with a least-squares fit, weighted with mass-balance uncertainties (Belart et al., 2019). The coefficients ϕ and ω are equivalent to the static mass-balance sensitivity of mass balance to summer temperature ($\delta\dot{B}/\delta T_s$, m w.e. a^{-1} K^{-1}) and winter precipitation ($\delta\dot{B}/\delta P_w$, m w.e. a^{-1} $(10\%)^{-1}$), respectively. We solved the least-squares fit for individual glaciers, obtaining a set of ϕ, ω, γ and k for each glacier. This, however, led to unrealistically high and low sensitivity to summer temperature for Snæfellsjökull and Þrándarjökull, respectively, likely due to a limited number of observations available for these glaciers. We then grouped the glaciers in two sets, using a threshold of 1.4 m w.e. $a^{-1}K^{-1}$ from the initial sensitivities. This criteria fitted with the regional characteristics of the grouped glaciers: glaciers located at the southern and western coasts (Eyjafjallajökull, Mýrdalsjökull, Öræfajökull, Snæfellsjökull, Tindfjallajökull, and Torfajökull) and glaciers in central, northern, and eastern Iceland (Drangajökull, Eiríksjökull, Hrútfell, Tungnafellsjökull, Barkárdals- and Tungnahryggsjökull, Hofsjökull Eystri, and Þrándarjökull).

We performed the least-squares fit for each group of glaciers, calculating one single coefficient ϕ and ω per group, while the coefficients γ and k were determined for each individual glacier within the group. The least-squares fit did not include Snæfell, for which only two geodetic mass balances are available (**Figure 2**).

For a decadal, region-wide comparison, we selected the years 1945, 1960, 1980, 1994, 2004, 2010, and 2017 as the most common survey years (**Figure 2**). The geodetic mass balance of each glacier was temporally homogenized (e.g., Lambrecht and Kuhn, 2007; Fischer et al., 2015) to these years when needed, by using the modeled annual mass balance from Equation (1). An uncertainty of ±0.5 m w.e. a^{-1} was assumed for each year of modeled annual mass balance when calculating the temporally-homogenized mass balance. The annual correction was not applied to datasets acquired in 1946 due to lack of climate data.

We also estimated the geodetic mass balance for two additional, longer, time periods: 1960–1994 (relatively cold period and close to zero balance) and 1994–2010 (warmer period and the largest ice wastage). These additional geodetic mass balances were estimated using the DEMs closest in time to 1960, 1994, and 2010. They were corrected to the hydrological year, and temporally homogenized when needed, using the modeled annual mass balances.

5. RESULTS

Over 100 DEMs of the 14 glaciers, between 1945 and 2018, were utilized in this study. This included the creation of 63 DEMs from historical aerial photographs. The gaps on the glaciers were on average 15% of the total glacier area; seven DEMs contained gaps that were >30% of the glacier area, with a maximum of 40% on Snæfellsjökull in 1945 and 1959. A time series of elevation changes for each of the glaciers is shown in **Supplement S2**.

A total of 96 geodetic mass balances were computed, a number increasing to 111 after including the results from Magnússon et al. (2016a) and Belart et al. (2019), i.e., eight time periods on average for each of the 14 glaciers, and nine of them starting in 1945 (**Figure 3**). Tabulated observations of floating-date and fixed-date geodetic mass balance are provided in **Supplement S3**. These observations are also available at the World Glacier Monitoring Service (WGMS, www.wgms.ch).

Uncertainties in the geodetic estimates were typically <0.1 m w.e. a^{-1} (95% confidence level) for periods longer than 10 years, but they increased for the shorter time periods (e.g., Huss, 2013) or if the DEMs contained significant gaps. The maximum and minimum fixed-date geodetic mass balances were, respectively, 0.84 ± 0.21 m w.e. a^{-1} on Snæfellsjökull in 1985–1991 and -2.40 ± 0.25 m w.e. a^{-1} on Mýrdalsjökull in 1999–2004. The seasonal correction was generally small (<0.1 m w.e. a^{-1}) over ∼10-year periods, but was significantly larger for the shorter time periods (e.g., Belart et al., 2019).

The obtained mass-balance sensitivity to summer temperature was -2.21 ± 0.25 m w.e. a^{-1} K^{-1} for the group of high-sensitivity glaciers, and -0.72 ± 0.10 m w.e. a^{-1} K^{-1} for the group of low-sensitivity glaciers. The sensitivities to winter precipitation are 0.22 ± 0.11 m w.e. a^{-1} $(10\%)^{-1}$ for the high-sensitivity glaciers, and 0.13 ± 0.07 m w.e. a^{-1} $(10\%)^{-1}$ for the low-sensitivity glaciers.

The fit between mass balance and climatic variables (Equation 1) yielded a high correlation between observed and statistically derived mass balance, with a coefficient of determination $R^2 = 0.71$ for the group of high-sensitivity glaciers and $R^2 = 0.77$ for the group of low-sensitivity glaciers (**Table 2**). This correlation was substantially lower in a combined least-squares fit using all glaciers in one single group ($R^2 = 0.59$) or assuming $\gamma = 0$, i.e., without adding the reference-surface correction term (**Table 2**).

The mean (standard deviation in parenthesis) mass balance, calculated without area-weights, of the 14 glaciers was −0.42 (0.17) m w.e. a^{-1} in 1945–1960, 0.00 (0.21) m w.e. a^{-1} in 1960–1980, 0.12 (0.21) m w.e. a^{-1} in 1980–1994, −1.01 (0.45) m w.e. a^{-1} in 1994–2004, −1.22 (0.63) m w.e. a^{-1} in 2004–2010, and −0.18 (0.22) m w.e. a^{-1} in 2010–2017. The area-weighted mean (standard deviation in parenthesis) was 0.04 (0.12) m w.e. a^{-1} in 1960–1980, 0.10 (0.14) m w.e. a^{-1} in 1980–1994, −1.27 (0.53) m w.e. a^{-1} in 1994–2004, −1.32 (0.51) m w.e. a^{-1} in 2004–2010, and −0.18 (0.22) m w.e. a^{-1} in 2010–2017. No area-weighted value was calculated for 1945–1960 due to the lack of observations for Mýrdalsjökull (by far the largest glacier among the 14) in this time period. Tabulated results of the temporally homogenized geodetic mass balance and associated uncertainties (95% confidence level) are shown in **Supplement S4**.

The overall results from 1960 to 1994 indicate a near-zero balance for the 14 glaciers. Most of the mass loss occurred in 1994–2010: 21.4 ± 1.6 Gt (1.3 ± 0.1 Gt a^{-1}), or 0.059 ± 0.005 mm Sea Level Equivalent (SLE). In this time period, Mýrdalsjökull accounted for about 70% of the mass loss. The group of glaciers <100 km^2 contributed significantly more to the mass loss than some larger (>100 km^2) ice caps such as Öræfajökull, and more than twice as much as Drangajökull for the same period (**Table 3**).

6. DISCUSSION

6.1. Spatio-Temporal Mass Balance and Climate Distribution

The long (>100-year) temperature record from Stykkishólmur (W-Iceland) indicates a maximum in the 1930s followed by gradual cooling until the 1960s, and then warming again in the 1990s. During 1945–1960, the glaciers experienced mass losses (**Figure 4A**). During 1960–1980 most of the glaciers had a close to zero mass balance, with the exception of Torfajökull and Mýrdalsjökull, which had slightly negative mass balance. Most glaciers gained mass or were close to equilibrium in 1980–1994, with the highest mass gain on Snæfellsjökull (W) and Eyjafjallajökull (S) (**Figures 3**, **4B,C**, **5**). These observations of mass balance during 1945–1990 agree with previous studies on several Icelandic glaciers (Pálsson et al., 2012; Björnsson et al., 2013; Hannesdóttir et al., 2015).

A substantial mass loss was experienced by the 14 glaciers in 1994–2010 (**Figures 4D,E**). The highest mass loss is found at coastal glaciers in the south and west and glaciers located at lower elevations (lower than ca. 1,200 m a.s.l., **Table 1**). The area-weighted mass balance of the 14 glaciers was -1.27 ± 0.09 m w.e. a^{-1} in this period (**Table 3**), similar to the glaciological mass balance measured at Hofsjökull and Langjökull (−1.3 m w.e. a^{-1}), but more negative than for Vatnajökull (−0.8 m w.e. a^{-1}) (Pálsson et al., 2012; Björnsson et al., 2013; Thorsteinsson et al., 2017) during the same period. The presented results for the periods 1994–2010 and 2004–2010 also encompass the effects of the increased summer melt of 2010 as a consequence of the Eyjafjallajökull eruption in 2010 (e.g., Björnsson et al., 2013).

There was less mass loss in 2010–2017 than in the previous two decades (**Figure 4F**), as has been also observed in Greenland (Shepherd et al., 2020), in mainland Norway (Andreassen et al., 2020), and also in Iceland by gravimetric methods (Wouters et al., 2019) and by glaciological observations (Aðalgeirsdóttir et al., submitted). Öræfajökull gained mass during this period (0.43 ± 0.08 m w.e. a^{-1}) and some of its outlets have shown significant advances (**Figure S9**). It covers the largest elevation range (0–2,100 m a.s.l.), collects the highest amount of precipitation in Iceland (Crochet et al., 2007) with likely summer snowfalls and has steep outlets leading to rapid mass transport. The modeled precipitation used in our study (Nawri et al., 2017) indicates increased winter precipitation in recent years on Öræfajökull.

The decadal variability of mass balance is strongly related to the proximity of the glaciers to the coasts (**Figure 6**). Glaciers located at the south and west coast are classified as maritime (e.g., De Woul and Hock, 2005) and show large mass-balance

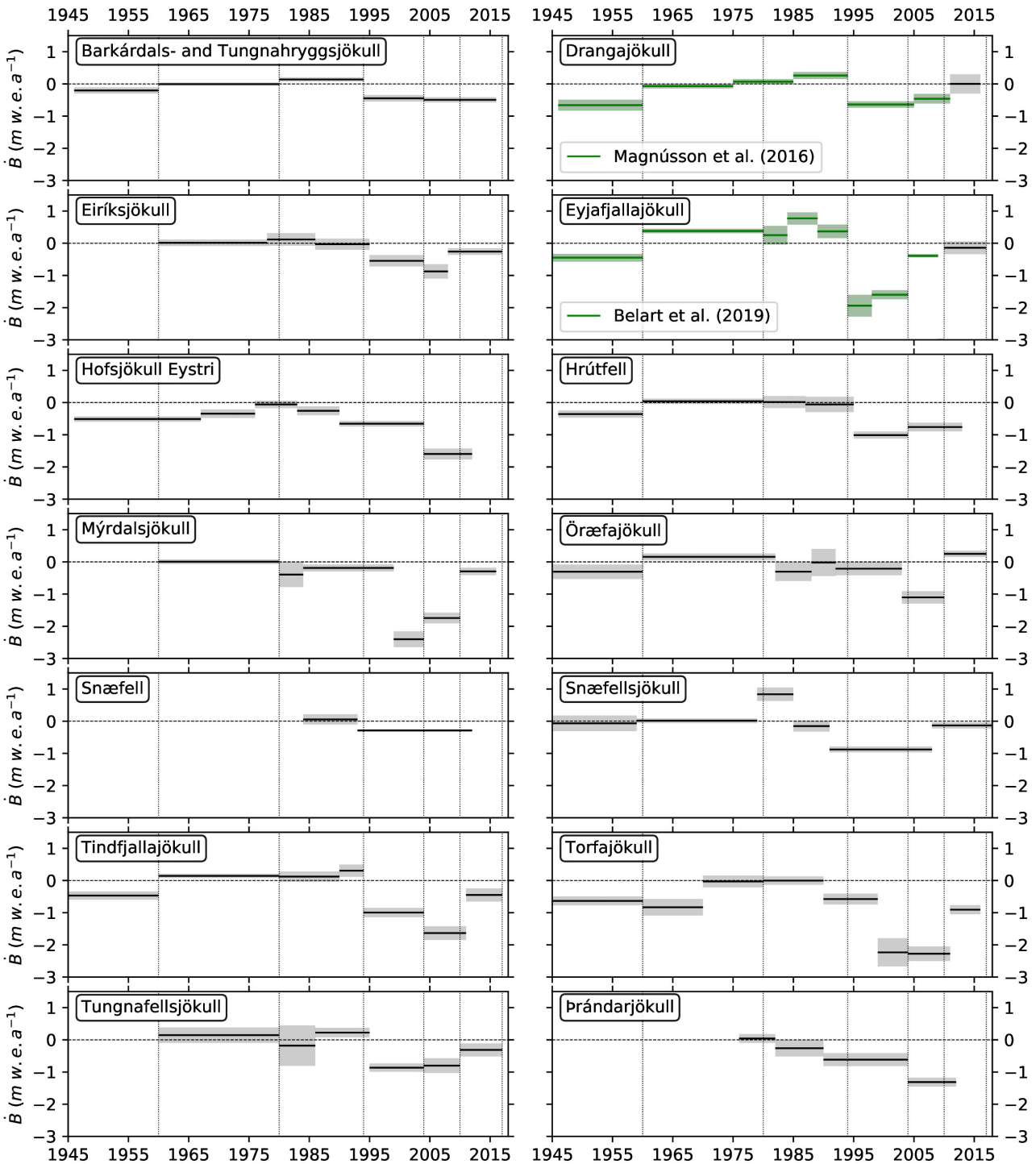

FIGURE 3 | Glacier-wide geodetic mass balance of the 14 glaciers. The mass balance is estimated from 1 October to 30 September (fixed-date system), based on seasonal corrections. Gray bands indicate uncertainty at 95% confidence level (Magnússon et al., 2016a). Dashed vertical lines show the years selected for a region-wide, temporally homogenized mass-balance comparison. Additional mass balances can be found in **Table S1**, relative to longer time periods and for Torfajökull (1970–1979 and 1979–1990) and Tindfjallajökull (1960–1978 and 1978–1980), which are further analyzed in the discussion.

variations and high static sensitivities to summer temperature and winter precipitation. The inland glaciers are subject to rain shadows and experience less variable precipitation. Their temporal variability in mass balance may be explained by differences in elevation. Torfajökull and Tindfjallajökull have a narrower elevation span, larger decadal mass-balance variability

TABLE 2 | Mass-balance sensitivities of the glaciers to a 1°C rise in temperature and to a 10% increase in precipitation.

	$\delta\dot{B}/\delta T_s$ (m w.e. $a^{-1}K^{-1}$)	$\delta\dot{B}/\delta P_w$ (m w.e. $a^{-1}(10\%)^{-1}$)	R^2	R^2 ($\gamma = 0$)
All glaciers	–1.10 ± 0.14	0.17 ± 0.08	0.59	0.53
High-sensitivity glaciers (South and West)	–2.21 ± 0.25	0.22 ± 0.11	0.71	0.67
Low-sensitivity glaciers (North, inland and East)	–0.72 ± 0.10	0.13 ± 0.07	0.79	0.57

Uncertainties (1σ) were extracted from the variance matrix as result of the least-squares fit. The high-sensitivity glaciers comprise Eyjafjallajökull, Mýrdalsjökull, Öræfajökull, Snæfellsjökull, Tindfjallajökull, and Torfajökull. The low-sensitivity glaciers comprise Barkárdals- and Tungnahryggsjökull, Drangajökull, Eiríksjökull, Hofsjökull Eystri, Hrútfell, Tungnafellsjökull, and Þrándarjökull.

TABLE 3 | Mass changes of 14 Icelandic glaciers from 1945–1960 to 1994–2010.

	Area (2017)	$\dot{B}^{1960}_{1945}$ (m w.e. a^{-1})	$\dot{B}^{1994}_{1960}$ (m w.e. a^{-1})	$\dot{B}^{2010}_{1994}$ (m w.e. a^{-1})
	(km^2)	[Gt]*	[Gt]	[Gt]
Drangajökull	137.6	–0.66 ± 0.17	0.13 ± 0.04	–0.62 ± 0.09
		[–1.5 ± 0.4]	[0.7 ± 0.2]	[–1.4 ± 0.2]
Mýrdalsjökull	517.0	N/A	0.02 ± 0.05	–1.48 ± 0.17
		[N/A]	[0.4 ± 1.0]	[–13.9 ± 1.6]
Öræfajökull	163.2	–0.31 ± 0.23	0.09 ± 0.07	–1.01 ± 0.1
		[–0.8 ± 0.6]	[0.6 ± 0.5]	[–2.8 ± 0.3]
Others**	187.0	–0.42 ± 0.07	0.16 ± 0.02	–0.99 ± 0.05
		[–1.0 ± 0.2]	[1.3 ± 0.1]	[–3.4 ± 0.2]
Total	1,004.8	N/A	0.07 ± 0.03	–1.20 ± 0.09
		[N/A]	[2.9 ± 1.1]	[–21.4 ± 1.6]

*The table shows area (km^2, Hannesdóttir et al., submitted), specific (m w.e. a^{-1}) and total (Gt, in brackets) mass change rates for the three largest glaciers and for the sum of the other glaciers (glaciers <100 km^2) as investigated in this study. The values correspond to the fixed-date geodetic mass balance, after temporal homogenization when needed. Mass balance and mass loss involving multiple glaciers is calculated using area-weights. *Values used for Mýrdalsjökull, Eiríksjökull, and Tungnafellsjökull reach only back to 1960. **Þrándarjökull and Snæfell are excluded in this analysis, due to limited data coverage.*

and are more sensitive to temperature changes than other inland glaciers, hence they were included in the coastal glaciers group. Glaciers farther north, like Drangajökull and the glaciers on Tröllaskagi, have significantly lower mass-balance decadal variability and sensitivities and are situated close to the cold East Greenland oceanic current (Björnsson et al., 2013). Þrándarjökull and Hofsjökull Eystri, despite being located near the SE coast, show lower sensitivity to summer temperature and were grouped with the central and northern glaciers.

The regional pattern of high decadal mass-balance variability and sensitivities also fits the regional pattern of average melt-season albedo during 2000–2019 estimated for most Icelandic glaciers by Gunnarsson et al. (2020). The southern glaciers have significantly lower average melt-season albedo than the glaciers located in central or northern Iceland. This can be partly explained by the two aforementioned climatic regimes: higher summer temperatures in the southern glaciers lead to stronger melt and an early appearance of the firn and ice layer, and the opposite effect would occur in the central and northern glaciers. However, this is also partly explained by the presence of more dust and tephra on the southern glaciers, which can also significantly lower the albedo (e.g., Möller et al., 2014, 2019; Gunnarsson et al., 2020).

We observed high intraregional variability of mass balance, particularly prominent for Tindfjallajökull, Torfajökull, Eyjafjallajökull, and Mýrdalsjökull (S-Iceland, within 40 km of each other). Analogously, different catchments of some of the glaciers can exhibit substantial differences in mass balance: (1) Drangajökull shows strong differences in mass balance between the eastern and western catchments, probably associated with the effects of precipitation and snow drift (Magnússon et al., 2016a,b; Belart et al., 2017). (2) On Mýrdalsjökull, the northern (inland) outlets show an almost continuous lowering during all observed time periods, as opposed to the southern (coastal) outlets, which show fluctuations between lowering and thickening through the past decades (**Figure S8**). The same pattern is observed on Vatnajökull (Björnsson et al., 2013) and can be explained by the maritime regime of the southern outlets, with most precipitation falling at these locations, while the northern outlets are located in a rain shadow (Crochet et al., 2007; Ágústsson et al., 2013). (3) One of the outlets of Öræfajökull is affected by significant calving at its terminus (Magnússon et al., 2012), causing more negative mass balance than the rest of the ice cap (**Figure S9**).

Mýrdalsjökull contributed 70% of the mass loss of the studied glaciers in 1994–2010, although it accounts for only about 50% of the area encompassed by the 14 glaciers (**Table 3**). This shows that extrapolation of mass balance from a few glaciers to an entire region (e.g., Björnsson et al., 2013) can lead to erroneous estimates of mass loss from small glaciers. In this context, Mýrdalsjökull and the southern small glaciers contribute more to sea-level rise than the northern glaciers, like Drangajökull or the cluster of glaciers in Tröllaskagi. Nevertheless, the small glaciers cover 10% of the total glacierized area of Iceland, and their mass loss is close to one order of magnitude smaller than for the entire country (9.5 Gt a^{-1}, Björnsson et al., 2013, vs. 1.3 Gt a^{-1}).

In comparison with to long-term (>50-year) mass-balance observations in other glacierized regions, the evolution of Icelandic glaciers has followed similar patterns during the study period to those observed in the Alps (Huss et al., 2010), Pyrenees (Marti et al., 2015), or in tropical glaciers as in Cordillera Real (Soruco et al., 2009). The intraregional variability observed in Iceland during 1994–2004 (SD = 0.44 m w.e. a^{-1}, $N = 13$) and 2004–2010 (SD = 0.57 m w.e. a^{-1}, $N = 13$) appears to be similar to that in the Himalayas in 2000–2016 (Brun et al., 2017). Some other glacierized regions such as the Alps have, however, experienced more homogeneous mass loss during the last few decades (Fischer et al., 2015).

6.2. Statistical Estimation of Mass Balance From Precipitation and Temperature Records

A first-order equation (Equation 1) can be used to estimate the annual mass balance as a function of summer temperature,

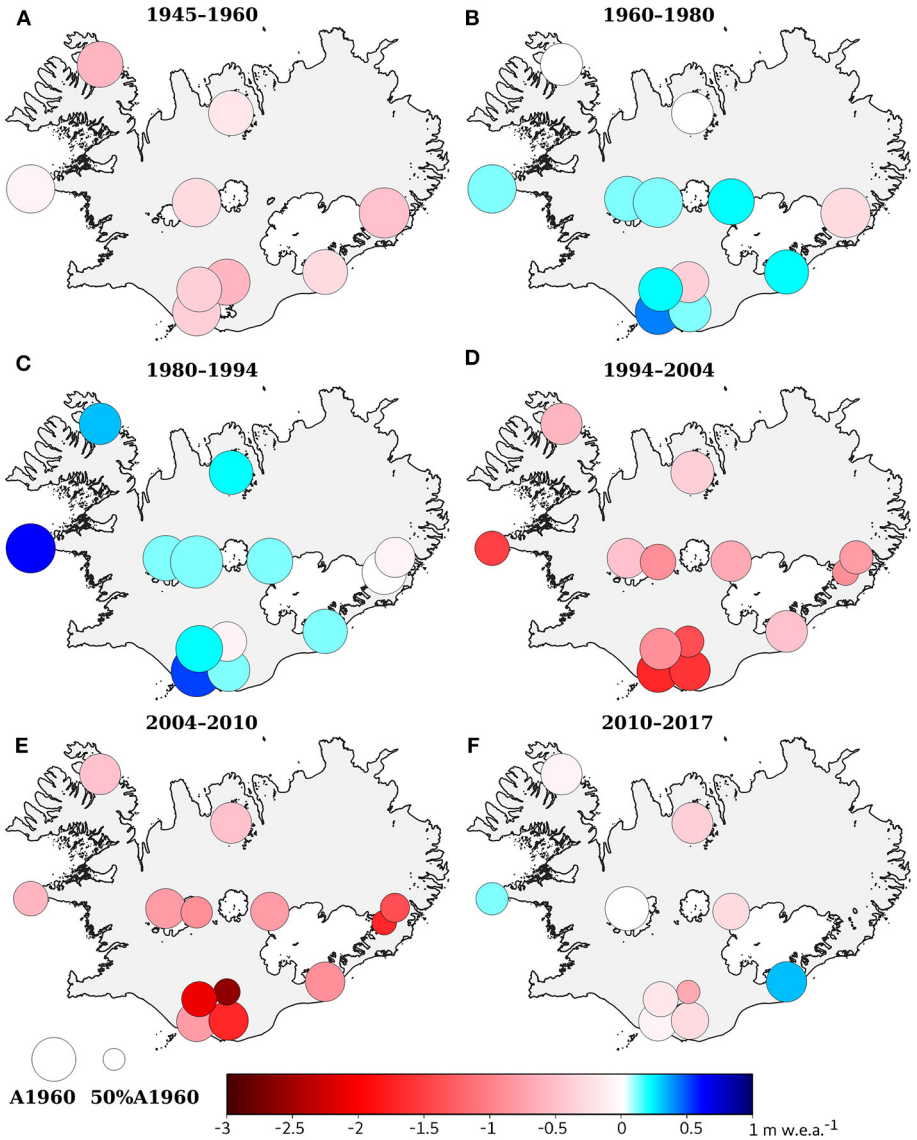

FIGURE 4 | Glacier-wide geodetic mass balance for six time periods between 1945 and 2017. **(A)** 1945–1960. **(B)** 1960–1980. **(C)** 1980–1994. **(D)** 1994–2004. **(E)** 2004–2010. **(F)** 2010–2017. Red and blue colors indicate negative and positive mass balance, respectively. The size of each circle shows the ratio of area changes relative to 1960. Tabulated values of temporally homogenized mass balance and associated uncertainties (95% confidence level) are shown in **Table S2**.

winter precipitation and area, permitting a practical temporal homogenization of geodetic mass balance (e.g., Lambrecht and Kuhn, 2007; Fischer et al., 2015). The mass balance correlates well with climatic variables (Cogley et al., 2011; Huss et al., 2012). In other words, a large fraction of the mass-balance variability can be explained by variations in summer temperature and winter precipitation, in addition to feedback effects due to changes in the geometry of the glacier. The reference-surface correction term improves the fit (R^2, **Table 2**) by up to 20% for the group of central and northern glaciers.

The initial results when the Equation (1) was solved for individual glaciers (as opposed to groups of glaciers) led to unrealistically high and low mass-balance sensitivities for Snæfellsjökull and Þrándarjökull, respectively. This can be attributed to the limited observations used for these two glaciers, but also by other factors mentioned in the following discussion. Grouping the glaciers in two regions added robustness to the statistical analysis. The obtained sensitivities agree with the range of sensitivities calculated by De Woul and Hock (2005) for specific outlet glaciers of Vatnajökull [ranging -1.5 to -2 m w.e. a^{-1} K^{-1} and 0.2 to 0.3 m w.e. a^{-1} $(10\%)^{-1}$], similar to our estimates for the southern glaciers, and for specific outlet glaciers of Hofsjökull [ranging -0.7 to -1.3 m w.e. a^{-1} K^{-1} and 0.1 m w.e. a^{-1} $(10\%)^{-1}$], similar to our estimates for the central and northern glaciers. Based on the joint analysis of mass balance and climate, we find that, for the

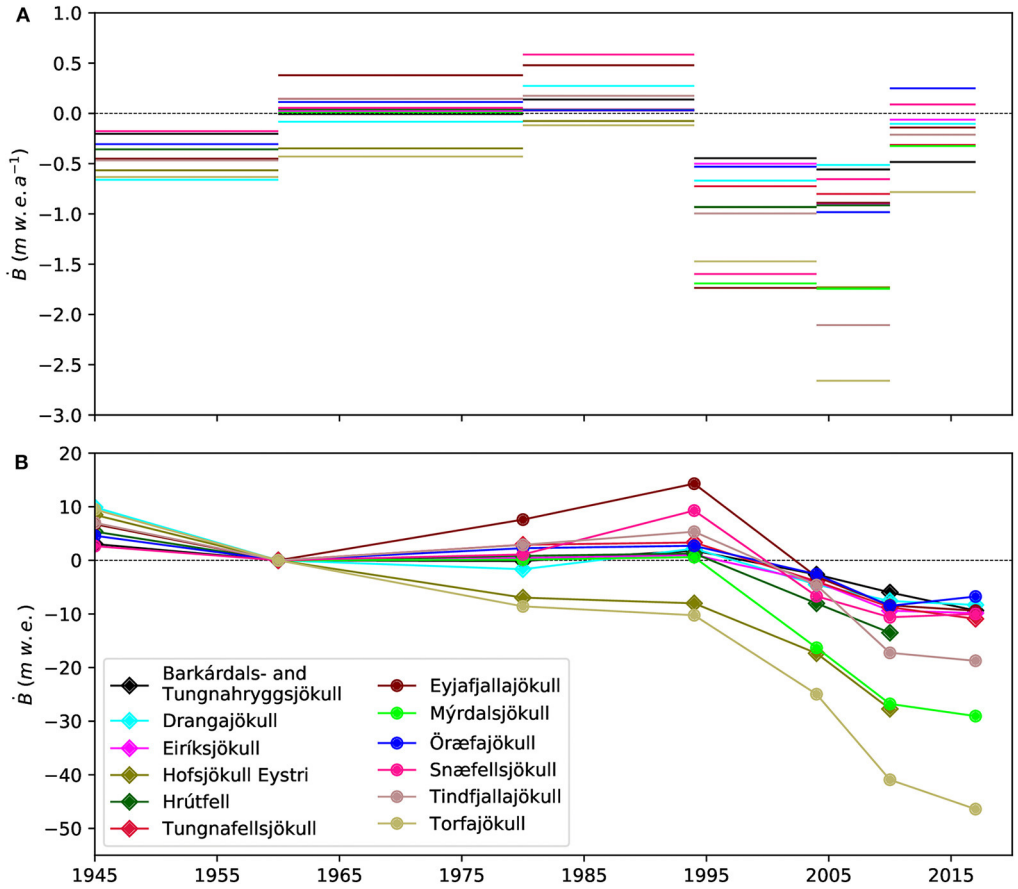

FIGURE 5 | (A) Average mass balance after temporal homogenization during the six time periods. **(B)** Cumulative mass balance centered on 1960 (common year for the selected glaciers). Diamonds indicate glaciers located in the interior, North and East of Iceland and circles glaciers on South and West Iceland.

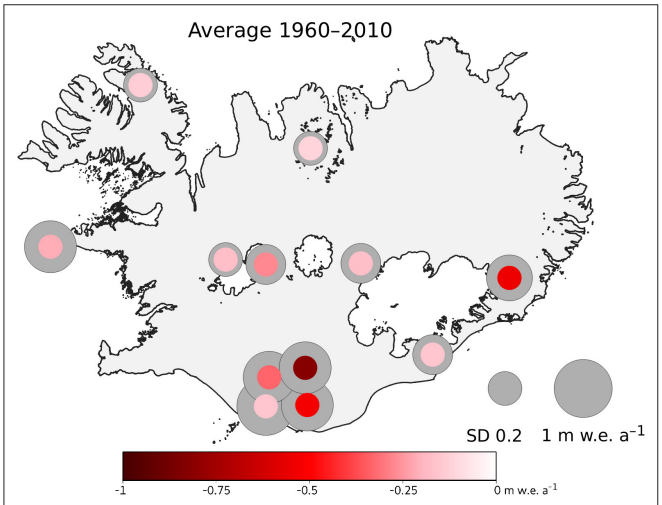

FIGURE 6 | Mass-balance average over the period 1960–2010. The size of the gray circles shows the temporal variability, estimated for each glacier as the standard deviation of the temporally homogenized mass balance, using a weight based on the length of each time period.

group of southern and western glaciers, the mass loss during 1994–2010 was entirely attributed to an increase in summer temperature relative to 1960–1994, while the winter precipitation remained approximately constant on average during these two time periods.

Torfajökull, with DEMs acquired in 1979 and 1980, and Tindfjallajökull, with DEMs acquired in 1978 and 1980, served as a test of the temporal homogenization. For these two glaciers, applying temporal homogenization using the 1978 and 1979 DEMs (i.e., 1 and 2 years apart from 1980) had similar results to using the 1980 DEM, with differences lower than 0.1 m w.e. a^{-1} between observed and temporally homogenized mass balances, which is within the uncertainty of the geodetic estimates. Additionally, area-weighted averages of the annual mass balance obtained from Equation (1) were computed for the two sub-regions. These results are presented in (**Figure 7**), and compared with annual glaciological mass-balance observations for Vatnajökull, Langjökull and Hofsjökull (Thorsteinsson et al., 2017; WGMS, 2019; Hannesdóttir et al., submitted). The annual mass balance obtained for group of southern and western glaciers shows good correlation with the glaciological mass balance of

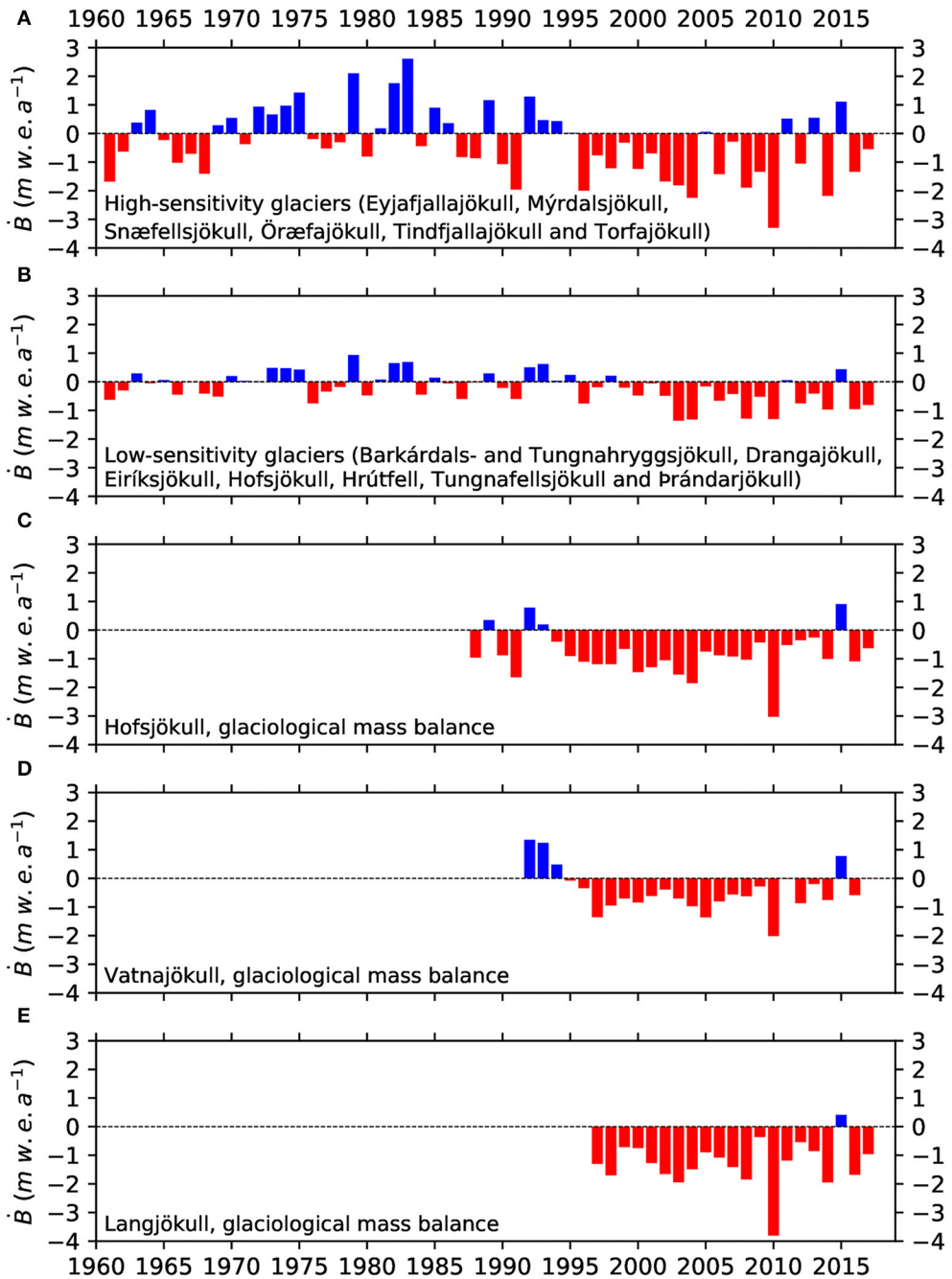

FIGURE 7 | (A,B) Area-weighted average annual mass balance of the two sub-regions, obtained from Equation (1) over the period 1960–2017. **(C–E)** Glaciological mass balance measured on Hofsjökull, Vatnajökull, and Langjökull (Thorsteinsson et al., 2017; WGMS, 2019; Aðalgeirsdóttir et al., submitted).

Vatnajökull ($R^2 = 0.52$), Langjökull ($R^2 = 0.57$), and especially with Hofsjökull ($R^2 = 0.73$).

The annual mass balance should, however, be interpreted with caution, particularly for individual glaciers and for time periods where there is a mismatch between modeled and observed mass balance (**Supplement S5**). The mismatches can be attributed to either an incomplete climate model or to an over-simplified linear fit between climate and mass balance. Measuring and modeling winter precipitation is challenging (e.g., Jarosch et al., 2012). In Öræfajökull, the precipitation is overestimated by the model used (Schmidt et al., 2017). Moreover, the mass balance is controlled by other variables neglected in our simple model. Full energy-balance models can better reproduce the response of glaciers to climate variations (e.g., Arnold et al., 1996; Hock and Holmgren, 2005), accounting, for example, for albedo changes, which can intensify melting if dust (e.g., Arnalds et al., 2016; Wittmann

et al., 2017) or thin tephra (e.g., Möller et al., 2014; Gascoin et al., 2017) is deposited on the glacier, or can decrease the melt if snow fall occurs during summer.

The mass balance of Icelandic glaciers has additional forcing besides temperature and precipitation, such as: (1) Wind-drifted snow can contribute to winter accumulation in individual catchments, as observed for Drangajökull (Magnússon et al., 2016a,b; Belart et al., 2017). (2) Debris (either rock or tephra), present on Icelandic glaciers like Eiríksjökull, enhances or reduces the melt rate depending on the thickness (e.g., Östrem, 1959). (3) Volcanic forcing can affect the mass balance, typically for one hydrological year (Björnsson et al., 2013), and possibly over longer periods (Möller et al., 2019). (4) Local changes in geothermal heat flux underneath the glacier, as observed on Mýrdalsjökull (Guðmundsson et al., 2007), can also affect the mass balance (Björnsson, 2003).

The reference-surface correction term in the mass-balance model (Equation 1) was generalized by Elsberg et al. (2001) and Harrison et al. (2001), and further in Belart et al. (2019) by assuming a linear relationship between the volume changes and area changes of the glacier. This correlation is generally found applicable in the 14 glaciers, with a typical fit R^2>0.8 between volume changes and area changes (e.g., Pálsson et al., 2012; Belart et al., 2019), but it does not apply for three surge-type catchments in Drangajökull and two in Mýrdalsjökull (Björnsson et al., 2003). Several outlet glaciers of Mýrdalsjökull and Öræfajökull, not identified as surge-type glaciers, present a series of noteworthy elevation changes during the 1960s to 1990s: their accumulation area lowered while the ablation area was gained elevation and their margins were advanced, which suggests acceleration in their ice motion. This led to a rapid area increase, while the overall volume remained unchanged (**Figures S8, S9**).

The suggested acceleration in the ice motion during the colder time periods, particularly as observed on Mýrdalsjökull and Öræfajökull is worth further study. This is also a key for fully describing the mass-balance–climate relationship. Due to the availability of bedrock maps of Mýrdalsjökull and Öræfajökull (Björnsson et al., 2000; Magnússon et al., 2012), further studies may include the development of fully coupled mass balance-ice dynamic models which could reproduce the series of dDEMs obtained for these glaciers in this study.

7. CONCLUSIONS

This study presents a 70-year record of elevation changes and geodetic mass balance of glaciers distributed across all parts of Iceland (excluding the three largest ice caps), most of them previously lacking mass-balance measurements. The glaciers were close to equilibrium during the period 1960–1994, with an area-weighted mass balance of 0.07 ± 0.07 m w.e. a^{-1}. This was followed by a rapid decline of the glaciers: −1.20 ± 0.09 m w.e. a^{-1} and a mass loss of 21.4 ± 1.6 Gt (1.3 ± 0.1 Gt a^{-1}), or 0.059 ± 0.005 mm SLE, during the period 1994–2010.

The region-wide, multitemporal intercomparison of mass balance revealed spatial patterns across Iceland: glaciers located close to the south and west coast experience larger decadal oscillations in mass balance, a consequence of larger static mass-balance sensitivities to summer temperature and winter precipitation, than the interior, northern and eastern glaciers. This pattern can likely be explained by different local climate, related to oceanic currents surrounding Iceland, rain shadows, and elevation of the glaciers. Due to a large intraregional variability, particular care should be taken when extrapolating mass balance from one glacier to another, even at close distances.

A linear model relating mass balance, summer temperature and winter precipitation explained more than 70% of the observed mass-balance variability. Yet we acknowledge some limitations of this model, such as other mass balance forcing or the assumption of linearity between area and volume changes. The latter assumption was not satisfied at specific time periods, with lowering in the accumulation area while the glacier fronts were advancing. This was attributed to changes in ice flux toward the ablation area, suggesting additional complexity due to the dynamical response to mass-balance fluctuations. This encourages further studies aiming at coupling mass balance to ice dynamics, especially focused at reproducing events of increased ice flux toward the ablation area.

DATA AVAILABILITY STATEMENT

The mass-balance records calculated in this study are presented in **Supplementary Material**, and have been submitted to WGMS (www.wgms.ch). The glacier outlines will be uploaded to GLIMS [www.glims.org], Hannesdóttir et al., submitted. The DEMs and orthoimages created from aerial photographs, Hexagon KH9 photographs, SPOT 5 and ASTER, as well as the lidar DEMs, are available upon request. Maps of elevation difference using Pléiades data are available upon request.

AUTHOR CONTRIBUTIONS

JB, EM, and EB designed the research study and methods. JB performed the data processing and calculations. ÁG contributed in processing data for Mýrdalsjökull and Tungnafellsjökull. TJ prepared meteorological data for the statistical analysis of mass balance. FP and HB provided the glaciological mass balance of Vatnajökull and Langjökull. TT provided the glaciological mass balance of Hofsjökull. All coauthors interpreted the results and helped writing the manuscript.

FUNDING

This study was funded by the University of Iceland (UI) Research Fund and the Icelandic research council (Rannís) through the project Katla Kalda (number 163391-053), the Jules Vernes research fund, and Landsvirkjun. EB acknowledges support from the French Space Agency (CNES).

ACKNOWLEDGMENTS

Karsten Kristinsson is acknowledged for scanning the aerial photographs stored at the National Land Survey of Iceland. Loftmyndir efh. is acknowledged for contributing aerial photographs from 1999. Pléiades images were acquired at research price thanks to the CNES ISIS programme (http://www.isis-cnes.fr). The ArcticDEM project is acknowledged for numerous DEMs used from 2013 to 2018. This study uses the lidar mapping of the glaciers in Iceland, funded by the Icelandic Research Fund, the Landsvirkjun research fund, the Icelandic Road Administration, the Reykjavík Energy Environmental and Energy Research Fund, the Klima- og Luftgruppen research fund of the Nordic Council of Ministers, the Vatnajökull National Park, the organization Friends of Vatnajökull, LMÍ, IMO, and the UI research fund. This study uses the GLIMS database of the outlines of Icelandic glaciers. Bolli Pálmason is acknowledged for providing downscaled precipitation data from regular forecast runs of the IMO for 2016–2019. Ken Moxham is acknowledged for the English-language editing of the manuscript. Michelle Koutnik is thanked for fruitful discussions about potential applications from the datasets. MZ, TS, and MH are acknowledged for their valuable comments during the revision of the manuscript. This study is based on the last chapter of the PhD dissertation of Belart (2018).

SUPPLEMENTARY MATERIAL

The Supplementary Material for this article can be found online at: https://www.frontiersin.org/articles/10.3389/feart.2020.00163/full#supplementary-material

REFERENCES

Ágústsson, H., Hannesdóttir, H., Thorsteinsson, Þ., Pálsson, F., and Oddsson, B. (2013). Mass balance of Mýrdalsjökull ice cap accumulation area and comparison of observed winter balance with simulated precipitation. *Jökull* 63, 91–104.

Ahlmann, H. (1940). The relative influence of precipitation and temperature on glacier regime. *Geogr. Ann.* 22, 188–205. doi: 10.1080/20014422.1940.11880689

Anderson, L. S., Flowers, G. E., Jarosch, A. H., Aðalgeirsdóttir, G., Áslaug, G., Miller, G. H., et al. (2018). Holocene glacier and climate variations in Vestfirðir, Iceland, from the modeling of Drangajökull ice cap. *Quarter. Sci. Rev.* 190, 39–56. doi: 10.1016/j.quascirev.2018.04.024

Andreassen, L. M., Elvehøy, H., Kjøllmoen, B., and Belart, J. M. C. (2020). Glacier change in Norway since the 1960s - an overview of mass balance, area, length and surface elevation changes. *J. Glaciol.* 66, 313–328. doi: 10.1017/jog.2020.10

Arnalds, O., Dagsson-Waldhauserova, P., and Ólafsson, H. (2016). The Icelandic volcanic aeolian environment: processes and impacts – A review. *Aeolian Res.* 20, 176–195. doi: 10.1016/j.aeolia.2016.01.004

Arnold, N. S., Willis, I. C., Sharp, M. J., Richards, K. S., and Lawson, W. J. (1996). A distributed surface energy-balance model for a small valley glacier. I. Development and testing for Haut Glacier d' Arolla, Valais, Switzerland. *J. Glaciol.* 42, 77–89. doi: 10.1017/S0022143000030549

Bauder, A., Funk, M., and Huss, M. (2007). Ice-volume changes of selected glaciers in the Swiss Alps since the end of the 19th century. *Ann. Glaciol.* 46, 145–149. doi: 10.3189/172756407782871701

Belart, J. M. C. (2018). *Mass balance of Icelandic glaciers in variable climate* (Ph.D. thesis). University of Iceland; University of Toulouse III, Paul Sabatier.

Belart, J. M. C., Berthier, E., Magnússon, E., Anderson, L. S., Pálsson, F., Thorsteinsson, Þ., et al. (2017). Winter mass balance of Drangajökull ice cap (NW Iceland) derived from satellite sub-meter stereo images. *Cryosphere* 11, 1501–1517. doi: 10.5194/tc-11-1501-2017

Belart, J. M. C., Magnússon, E., Berthier, E., Pálsson, F., Aðalgeirsdóttir, G., and Jóhannesson, T. (2019). The geodetic mass balance of Eyjafjallajökull ice cap for 1945-2014: processing guidelines and relation to climate. *J. Glaciol.* 65, 395–409. doi: 10.1017/jog.2019.16

Berthier, E., Cabot, V., Vincent, C., and Six, D. (2016). Decadal region-wide and glacier-wide mass balances derived from multi-temporal ASTER satellite digital elevation models. Validation over the Mont-Blanc area. *Front. Earth Sci.* 4:63. doi: 10.3389/feart.2016.00063

Berthier, E., Vincent, C., Magnússon, E., Gunnlaugsson, Á. Þ., Pitte, P., Le Meur, E., et al. (2014). Glacier topography and elevation changes derived from Pléiades sub-meter stereo images. *Cryosphere* 8, 2275–2291. doi: 10.5194/tc-8-2275-2014

Bindschadler, R., and Vornberger, P. (1998). Changes in the West Antarctic ice sheet since 1963 from declassified satellite photography. *Science* 279, 689–692. doi: 10.1126/science.279.5351.689

Björnsson, H. (2003). Subglacial lakes and jökulhlaups in Iceland. *Glob. Planet. Change* 35, 255–271. doi: 10.1016/S0921-8181(02)00130-3

Björnsson, H. (2017). The glaciers of Iceland. *Atlant. Press* 2:613. doi: 10.2991/978-94-6239-207-6

Björnsson, H., and Pálsson, F. (2008). Icelandic glaciers. *Jökull* 58, 365–386.

Björnsson, H., Pálsson, F., and Guðmundsson, M. (2000). Surface and bedrock topography of the Mýrdalsjökull ice cap, Iceland. *Jökull* 49, 29–46.

Björnsson, H., Pálsson, F., Guðmundsson, S., Magnússon, E., Aðalgeirsdóttir, G., Jóhannesson, T., et al. (2013). Contribution of Icelandic ice caps to sea level rise: trends and variability since the Little Ice Age. *Geophys. Res. Lett.* 40, 1–5. doi: 10.1002/grl.50278

Björnsson, H., Pálsson, F., Sigurðsson, O., and Flowers, G. E. (2003). Surges of glaciers in Iceland. *Ann. Glaciol.* 36, 82–90. doi: 10.3189/172756403781816365

Bojinski, S., Verstraete, M., Peterson, T. C., Richter, C., Simmons, A., and Zemp, M. (2014). The concept of essential climate variables in support of climate research, applications, and policy. *Bull. Am. Meteorol. Soc.* 95, 1431–1443. doi: 10.1175/BAMS-D-13-00047.1

Bolch, T., Pieczonka, T., and Benn, D. I. (2011). Multi-decadal mass loss of glaciers in the Everest area (Nepal Himalaya) derived from stereo imagery. *Cryosphere* 5, 349–358. doi: 10.5194/tc-5-349-2011

Braun, M. H., Malz, P., Sommer, C., Farías-Barahona, D., Sauter, T., Casassa, G., et al. (2019). Constraining glacier elevation and mass changes in South America. *Nat. Clim. Change* 9, 130–136. doi: 10.1038/s41558-018-0375-7

Brun, F., Berthier, E., Wagnon, P., Kääb, A., and Treichler, D. (2017). A spatially resolved estimate of High Mountain Asia glacier mass balances from 2000 to 2016. *Nat. Geosci.* 10:668. doi: 10.1038/ngeo2999

Christian, J. E., Koutnik, M., and Roe, G. (2018). Committed retreat: controls on glacier disequilibrium in a warming climate. *J. Glaciol.* 64, 675–688. doi: 10.1017/jog.2018.57

Cogley, J. G., Hock, R., Rasmussen, L. A., Arendt, A. A., Bauder, A., Braithwaite, R. J., et al. (2011). *Glossary of glacier mass balance and related terms, IHP-VII Technical Documents in Hydrology No. 86, IACS Contribution No. 2.* Paris: UNESCO-IHP.

Crochet, P., and Jóhannesson, T. (2011). A dataset of daily temperature in Iceland for the period 1949-2010. *Jökull* 61, 1–17.

Crochet, P., Jóhannesson, T., Jónsson, T., Sigurðsson, O., Björnsson, H., Pálsson, F., et al. (2007). Estimating the spatial distribution of precipitation in Iceland using a linear model of orographic precipitation. *J. Hydrometeorol.* 8, 1285–1306. doi: 10.1175/2007JHM795.1

De Woul, M., and Hock, R. (2005). Static mass-balance sensitivity of Arctic glaciers and ice caps using a degree-day approach. *Ann. Glaciol.* 42, 217–224. doi: 10.3189/172756405781813096

Dussaillant, I., Berthier, E., Brun, F., Masiokas, M., Hugonnet, R., Favier, V., et al. (2019). Two decades of glacier mass loss along the andes. *Nat. Geosci.* 12, 802–808. doi: 10.1038/s41561-019-0432-5

Elsberg, D. H., Harrison, W. D., Echelmeyer, K. A., and Krimmel, R. M. (2001). Quantifying the effects of climate and surface change on glacier mass balance. *J. Glaciol.* 47, 649–658. doi: 10.3189/172756501781831783

Fieber, K. D., Mills, J. P., Miller, P. E., Clarke, L., Ireland, L., and Fox, A. J. (2018). Rigorous 3D change determination in Antarctic Peninsula glaciers from stereo WorldView-2 and archival aerial imagery. *Remote Sens. Environ.* 205(Suppl. C), 18–31. doi: 10.1016/j.rse.2017.10.042

Finsterwalder, R. (1954). Photogrammetry and glacier research with special reference to glacier retreat in the eastern Alps. *J. Glaciol.* 2, 306–315. doi: 10.3189/S0022143000025119

Fischer, M., Huss, M., and Hoelzle, M. (2015). Surface elevation and mass changes of all Swiss glaciers 1980-2010. *Cryosphere* 9, 525–540. doi: 10.5194/tc-9-525-2015

Gardner, A. S., Moholdt, G., Cogley, J. G., Wouters, B., Arendt, A. A., Wahr, J., et al. (2013). A reconciled estimate of glacier contributions to sea level rise: 2003 to 2009. *Science* 340, 852–857. doi: 10.1126/science.1234532

Gascoin, S., Guðmundsson, S., Aðalgeirsdóttir, G., Pálsson, F., Schmidt, L., Berthier, E., et al. (2017). Evaluation of MODIS Albedo product over ice caps in Iceland and impact of volcanic eruptions on their Albedo. *Remote Sens.* 9:399. doi: 10.3390/rs9050399

Guðmundsson, M. T., Högnadóttir, H., Kristinsson, A. B., and Guðbjörnsson, S. (2007). Geothermal activity in the subglacial Katla caldera, Iceland, 1999-2005, studied with radar altimetry. *Ann. Glaciol.* 45, 66–72. doi: 10.3189/172756407782282444

Guðmundsson, S., Björnsson, H., Magnússon, E., Berthier, E., Pálsson, F., Guðmundsson, M. T., et al. (2011). Response of Eyjafjallajökull, Torfajökull and Tindfjallajökull ice caps in iceland to regional warming, deduced by remote sensing. *Polar Res.* 30:7282. doi: 10.3402/polar.v30i0.7282

Gunnarsson, A., Gardarsson, S. M., Pálsson, F., Jóhannesson, T., and Sveinsson, O. G. B. (2020). Annual and interannual variability and trends of albedo for icelandic glaciers. *Cryosphere Discuss.* 2020, 1–32. doi: 10.5194/tc-2019-328

Gunnlaugsson, Á. Þ. (2016). *The geodetic mass balance and ice thickness of Tungnafellsjökull ice cap* (M.Sc. Thesis). University of Iceland, Reykjavik, Iceland.

Hannesdóttir, H., Björnsson, H., Pálsson, F., Aðalgeirsdóttir, G., and Guðmundsson, S. (2015). Changes in the southeast Vatnajökull ice cap, Iceland, between ∼1890 and 2010. *The Cryosphere 9*, 565–585, doi: 10.5194/tc-9-565-2015

Harrison, W. (2013). How do glaciers respond to climate? Perspectives from the simplest models. *J. Glaciol.* 59, 949–960. doi: 10.3189/2013JoG13J048

Harrison, W. D., Elsberg, D. H., Echelmeyer, K. A., and Krimmel, R. M. (2001). On the characterization of glacier response by a single time-scale. *J. Glaciol.* 47, 659–664. doi: 10.3189/172756501781831837

Hock, R., and Holmgren, B. (2005). A distributed surface energy-balance model for complex topography and its application to Storglaciaren, Sweden. *J. Glaciol.* 51, 25–36. doi: 10.3189/172756505781829566

Huber, J., McNabb, R., and Zemp, M. (2020). Elevation changes of west-central Greenland glaciers from 1985 to 2012 from remote sensing. *Front. Earth Sci.* 8:35. doi: 10.3389/feart.2020.00035

Huss, M. (2013). Density assumptions for converting geodetic glacier volume change to mass change. *Cryosphere* 7, 877–887. doi: 10.5194/tc-7-877-2013

Huss, M., Dhulst, L., and Bauder, A. (2015). New long-term mass-balance series for the Swiss Alps. *J. Glaciol.* 61, 551–562. doi: 10.3189/2015JoG15J015

Huss, M., Hock, R., Bauder, A., and Funk, M. (2010). 100-year mass changes in the Swiss Alps linked to the Atlantic Multidecadal Oscillation. *Geophys. Res. Lett.* 37:L10501. doi: 10.1029/2010GL042616

Huss, M., Hock, R., Bauder, A., and Funk, M. (2012). Conventional versus reference-surface mass balance. *J. Glaciol.* 58, 278–286. doi: 10.3189/2012JoG11J216

Jarosch, A. H., Anslow, F. S., and Clarke, G. K. C. (2012). High-resolution precipitation and temperature downscaling for glacier models. *Clim. Dyn.* 38, 391–409. doi: 10.1007/s00382-010-0949-1

Jóhannesson, T., Björnsson, H., Magnússon, E., Guðmundsson, S., Pálsson, F., Sigurðsson, O., et al. (2013). Ice-volume changes, bias estimation of mass-balance measurements and changes in subglacial lakes derived by lidar mapping of the surface of Icelandic glaciers. *Ann. Glaciol.* 54, 63–74. doi: 10.3189/2013AoG63A422

Jóhannesson, T., Björnsson, H., Pálsson, F., Sigurðsson, O., and Thorsteinsson, Þ. (2011). LiDAR mapping of the Snæfellsjökull ice cap, western Iceland. *Jökull* 61, 19–32.

Jóhannesson, T., Raymond, C., and Waddington, E. D. (1989). Time-scale for adjustment of glaciers to changes in mass balance. *J. Glaciol.* 35, 355–369.

Kääb, A., Berthier, E., Nuth, C., Gardelle, J., and Arnaud, Y. (2012). Contrasting patterns of early twenty-first-century glacier mass change in the Himalaya. *Nature* 488, 495–498. doi: 10.1038/nature11324

Korona, J., Berthier, E., Bernard, M., Remy, F., and Thouvenot, E. (2009). SPIRIT. SPOT 5 stereoscopic survey of Polar Ice: Reference Images and Topographies during the fourth International Polar Year (2007-2009). *ISPRS J. Photogr. Remote Sens.* 64, 204–212. doi: 10.1016/j.isprsjprs.2008.10.005

Lambrecht, A., and Kuhn, M. (2007). Glacier changes in the Austrian Alps during the last three decades, derived from the new Austrian glacier inventory. *Ann. Glaciol.* 46, 177–184. doi: 10.3189/172756407782871341

Livingston, R. (1963). *A History of Military Mapping Camera Development.* USAF Liaison Office, U.S. Army Engineer, Geodesy, Intelligence and Mapping R. & D. Agency, 79–110.

Lüthi, M. P., and Bauder, A. (2010). Analysis of alpine glacier length change records with a macroscopic glacier model. *Geogr. Helvetica* 65, 92–102. doi: 10.5194/gh-65-92-2010

Magnússon, E., Belart, J., Pálsson, F., Ágústsson, H., and Crochet, P. (2016a). Geodetic mass balance record with rigorous uncertainty estimates deduced from aerial photographs and lidar data - Case study from Drangajökull ice cap, NW Iceland. *Cryosphere* 10, 159–177. doi: 10.5194/tc-10-159-2016

Magnússon, E., Belart, J. M. C., Pálsson, F., Anderson, L., Gunnlaugsson, A. Þ., Berthier, E., et al. (2016b). The subglacial topography of Drangajökull ice cap, NW-Iceland, deduced from dense RES-profiling. *Jökull* 66, 1–26.

Magnússon, E., Pálsson, F., Björnsson, H., and Guðmundsson, S. (2012). Removing the ice cap of Öræfajökull central volcano, SE-Iceland: mapping and interpretation of bedrock topography, ice volumes, subglacial troughs and implications for hazards assessments. *Jökull* 62, 131–150.

Marti, R., Gascoin, S., Houet, T., Ribière, O., Laffly, D., Condom, T., et al. (2015). Evolution of ossoue glacier (French Pyrenees) since the end of the Little ice age. *Cryosphere* 9, 1773–1795. doi: 10.5194/tc-9-1773-2015

Marzeion, B., Cogley, J. G., Richter, K., and Parkes, D. (2014). Attribution of global glacier mass loss to anthropogenic and natural causes. *Science* 345, 919–921. doi: 10.1126/science.1254702

Marzeion, B., Hofer, M., Jarosch, A. H., Kaser, G., and Mölg, T. (2012). A minimal model for reconstructing interannual mass balance variability of glaciers in the European Alps. *Cryosphere* 6, 71–84. doi: 10.5194/tc-6-71-2012

McNabb, R., Nuth, C., Kääb, A., and Girod, L. (2019). Sensitivity of glacier volume change estimation to dem void interpolation. *Cryosphere* 13, 895–910. doi: 10.5194/tc-13-895-2019

Möller, R., Dagsson-Waldhauserova, P., Möller, M., Kukla, P. A., Schneider, C., and Gudmundsson, M. T. (2019). Persistent albedo reduction on southern Icelandic glaciers due to ashfall from the 2010 Eyjafjallajökull eruption. *Remote Sens. Environ.* 233:111396. doi: 10.1016/j.rse.2019.111396

Möller, R., Möller, M., Björnsson, H., Guðmundsson, S., Pálsson, F., Oddsson, B., et al. (2014). MODIS-derived albedo changes of Vatnajökull (Iceland) due to tephra deposition from the 2004 Grímsvötn eruption. *Int. J. Appl. Earth Observ. Geoinform.* 26, 256–269. doi: 10.1016/j.jag.2013.08.005

Nawri, N., Pálmason, B., Petersen, G. N., Björnsson, H., and Þorsteinsson, A. Þ. (2017). *The ICRA Atmospheric Reanalysis Project for Iceland.* Icelandic Meteorological Office, VÍ 2017-005.

Oerlemans, J., and Reichert, B. K. (2000). Relating glacier mass balance to meteorological data by using a seasonal sensitivity characteristic. *J. Glaciol.* 46, 1–6. doi: 10.3189/172756500781833269

Ohmura, A. (2011). Observed mass balance of mountain glaciers and Greenland Ice Sheet in the 20th Century and the present Trends. *Surveys Geophys.* 32, 537–554. doi: 10.1007/s10712-011-9124-4

Östrem, G. (1959). Ice melting under a thin layer of moraine, and the existence of ice cores in moraine ridges. *Geogr. Ann.* 41, 228–230. doi: 10.1080/20014422.1959.11907953

Pálsson, F., Guðmundsson, S., Björnsson, H., Berthier, E., Magnússon, E., Guðmundsson, S., et al. (2012). Mass and volume changes of Langjökull ice cap, Iceland, ~1890 to 2009, deduced from old maps, satellite images and in situ mass balance measurements. *Jökull* 62, 81–96.

Papasodoro, C., Berthier, E., Royer, A., Zdanowicz, C., and Langlois, A. (2015). Area, elevation and mass changes of the two southernmost ice caps of the Canadian Arctic Archipelago between 1952 and 2014. *Cryosphere* 9, 1535–1550. doi: 10.5194/tc-9-1535-2015

Pedersen, G. B. M., Belart, J. M. C., Magnússon, E., Vilmundardóttir, O. K., Kizel, F., Sigurmundsson, F. S., et al. (2018). Hekla volcano, Iceland, in the 20th century: Lava volumes, production rates and effusion rates. *Geophys. Res. Lett.* 45, 1805–1813. doi: 10.1002/2017GL076887

Pierrot Deseilligny, M., and Clery, I. (2011). Apero, an open source bundle adjusment software for automatic calibration and orientation of set of images. *Int. Arch. Photogr. Remote Sens. Spat. Inform. Sci.* 3816, 269–276. doi: 10.5194/isprsarchives-XXXVIII-5-W16-269-2011

Porter, C., Morin, P., Howat, I., Noh, M.-J., Bates, B., Peterman, K., et al. (2018). *ArcticDEM*. Harvard Dataverse, V1. Polar Geospatial Center, University of Minnesota. doi: 10.7910/DVN/OHHUKH

Raup, B., Racoviteanu, A., Khalsa, S. J. S., Helm, C., Armstrong, R., and Arnaud, Y. (2007). The GLIMS geospatial glacier database: a new tool for studying glacier change. *Glob. Planet. Change* 56, 101–110. doi: 10.1016/j.gloplacha.2006.07.018

Roe, G. H., Baker, M. B., and Herla, F. (2017). Centennial glacier retreat as categorical evidence of regional climate change. *Nat. Geosci.* 10, 95–99. doi: 10.1038/ngeo2863

Rupnik, E., Daakir, M., and Pierrot Deseilligny, M. (2017). MicMac - a free, open-source solution for photogrammetry. *Open Geospatial Data Softw. Stand.* 2:14. doi: 10.1186/s40965-017-0027-2

Schmidt, L. S., Aðalgeirsdóttir, G., Guðmundsson, S., Langen, P. L., Pálsson, F., Mottram, R., et al. (2017). The importance of accurate glacier albedo for estimates of surface mass balance on Vatnajökull: evaluating the surface energy budget in a regional climate model with automatic weather station observations. *Cryosphere* 11, 1665–1684. doi: 10.5194/tc-11-1665-2017

Shean, D. E., Alexandrov, O., Moratto, Z. M., Smith, B. E., Joughin, I. R., Porter, C., et al. (2016). An automated, open-source pipeline for mass production of digital elevation models (DEMs) from very-high-resolution commercial stereo satellite imagery. *ISPRS J. Photogr. Remote Sens.* 116, 101–117. doi: 10.1016/j.isprsjprs.2016.03.012

Shean, D. E., Bhushan, S., Montesano, P., Rounce, D. R., Arendt, A., and Osmanoglu, B. (2020). A systematic, regional assessment of high mountain asia glacier mass balance. *Front. Earth Sci.* 7:363. doi: 10.3389/feart.2019.00363

Shepherd, A., Ivins, E., Rignot, E., Smith, B., van den Broeke, M., Velicogna, I., et al. (2020). Mass balance of the Greenland ice sheet from 1992 to 2018. *Nature* 579, 233–239. doi: 10.1038/s41586-019-1855-2

Soruco, A., Vincent, C., Francou, B., Ribstein, P., Berger, T., Sicart, J. E., et al. (2009). Mass balance of Glaciar Zongo, Bolivia, between 1956 and 2006, using glaciological, hydrological and geodetic methods. *Ann. Glaciol.* 50, 1–8. doi: 10.3189/172756409787769799

Spriggs, R. M. (1966). *The Calibration of Military Cartographic Cameras, Technical Note.* Wright-Patterson Air Force Base.

Thorsteinsson, Þ., Jóhannesson, T., Sigurðsson, O., and Einarsson, B. (2017). *Afkomumælingar á Hofsjökli 1988–2017 (Mass balance of Hofsjökull 1988–2017)*. Icelandic Meteorological Office Report 2017-016, 1–82.

Vaughan, D. G., Comiso, J. C., Allison, J., Carrasco, J., Kaser, R., Kwok, R., et al. (2013). "Observations: Cryosphere," in *Climate Change 2013: The Physical Science Basis. Contribution of Working Group I to the Fifth Assessment Report of the Intergovernmental Panel on Climate Change*. Cambridge, UK; New York, NY: Cambridge University Press.

WGMS (2019). *Fluctuations of Glaciers Database.*

Wittmann, M., Groot Zwaaftink, C. D., Steffensen Schmidt, L., Guðmundsson, S., Pálsson, F., Arnalds, O., et al. (2017). Impact of dust deposition on the albedo of Vatnajökull ice cap, Iceland. *Cryosphere* 11, 741–754. doi: 10.5194/tc-11-741-2017

Wouters, B., Gardner, A. S., and Moholdt, G. (2019). Global glacier mass loss during the GRACE satellite mission (2002-2016). *Front. Earth Sci.* 7:96. doi: 10.3389/feart.2019.00096

Zemp, M., Huss, M., Thibert, E., Eckert, N., McNabb, R., Huber, J., et al. (2019). Global glacier mass changes and their contributions to sea-level rise from 1961 to 2016. *Nature* 568, 382–386. doi: 10.1038/s41586-019-1071-0

Conflict of Interest: The authors declare that the research was conducted in the absence of any commercial or financial relationships that could be construed as a potential conflict of interest.

frontiers in Earth Science

DATA REPORT
published: 14 July 2020
doi: 10.3389/feart.2020.00251

Annual Surface Mass Balance Records (2009–2019) From an Automatic Weather Station on Mittivakkat Glacier, SE Greenland

Robert S. Fausto[1]*, *Jakob Abermann*[2] and *Andreas P. Ahlstrøm*[1]

[1] Geological Survey of Denmark and Greenland (GEUS), Copenhagen, Denmark, [2] Department of Geography and Regional Science, University of Graz, Graz, Austria

Keywords: Greenland, automatic weather station (AWS), surface mass balance, ablation, mittivakkat glacier

OPEN ACCESS

Edited by:
Fanny Brun,
Université Grenoble Alpes, France

Reviewed by:
Ellyn Mary Enderlin,
University of Maine, United States
David F. Porter,
Columbia University, United States

***Correspondence:**
Robert S. Fausto
rsf@geus.dk

Specialty section:
This article was submitted to Cryospheric Sciences, a section of the journal Frontiers in Earth Science

Received: *19 December 2019*
Accepted: *08 June 2020*
Published: *14 July 2020*

Citation:
Fausto RS, Abermann J and Ahlstrøm AP (2020) Annual Surface Mass Balance Records (2009–2019) From an Automatic Weather Station on Mittivakkat Glacier, SE Greenland. Front. Earth Sci. 8:251. doi: 10.3389/feart.2020.00251

INTRODUCTION

Quantifying area and volume loss of the world's glaciers outside the large ice sheets has caught the attention of policy makers and the public due to the potential impact on sea-level rise (e.g., AMAP, 2019; IPCC, 2019; Wouters et al., 2019; Zemp et al., 2019). Recent *in-situ* measurements from the Greenland Ice Sheet and its peripheral glaciers show that they are on average losing mass due to climate change (e.g., AMAP, 2019).

The robustness of sea-level rise predictions rely heavily on observational data from glaciers in the world, which is why reliable mass balance measurements are in high demand (AMAP, 2019; IPCC, 2019). The Programme for Monitoring of the Greenland ice sheet (PROMICE) initiated in 2007, is delivering such *in situ* data from a network of automatic weather stations (AWSs) covering eight different regions of the Greenland ice sheet and one location on the peripheral glacier Mittivakkat in south-east Greenland (**Figure 1**, Van As et al., 2011). The PROMICE *in situ* data is also valuable for calibrating and validating melt and energy balance estimates from remote sensing or surface mass balance models (AMAP, 2019; IPCC, 2019). A database accessible through the PROMICE data portal (https://www.promice.org/PromiceDataPortal) provides a Greenland wide mass balance data collection with associated background information (Machguth et al., 2016). In this data report, we focus on the AWS location on the peripheral glacier Mittivakkat (MIT) in south-east Greenland and present its annual surface mass balance for the period 2009–2019 derived from the daily automatic weather station data product found on the PROMICE data portal (https://doi.org/10.22008/promice/data/aws).

METHODS

Mittivakkat Automatic Weather Station

The Mittivakkat (MIT) automatic weather station (AWS) is part of the PROMICE network in Greenland, which currently consists of eight regions with two (or three) AWSs all located at different elevations (see **Figure 1** for details) (Ahlstrøm et al., 2008). In PROMICE, the MIT location is currently the only station on a glacier in Greenland outside the main ice sheet. Mittivakkat glacier is located in SE Greenland on the island of Ammassalik (**Figure 1**, MIT). Mittivakkat glacier covers an area of ca. 32 km^2 (e.g., Mernild et al., 2015) and the AWS is located below the long-term equilibrium altitude (ELA), resulting on average in a negative surface mass balance at the AWS site. The AWS location is 65.69 N 37.83 W 440 m a.s.l and it was established on 3 May 2009 at the start of the melt season on top of winter snowpack. During the establishment, we also made a snowpit with a snowheight of 2.7 m and a mean bulk density of 425 kg m^{-3}.

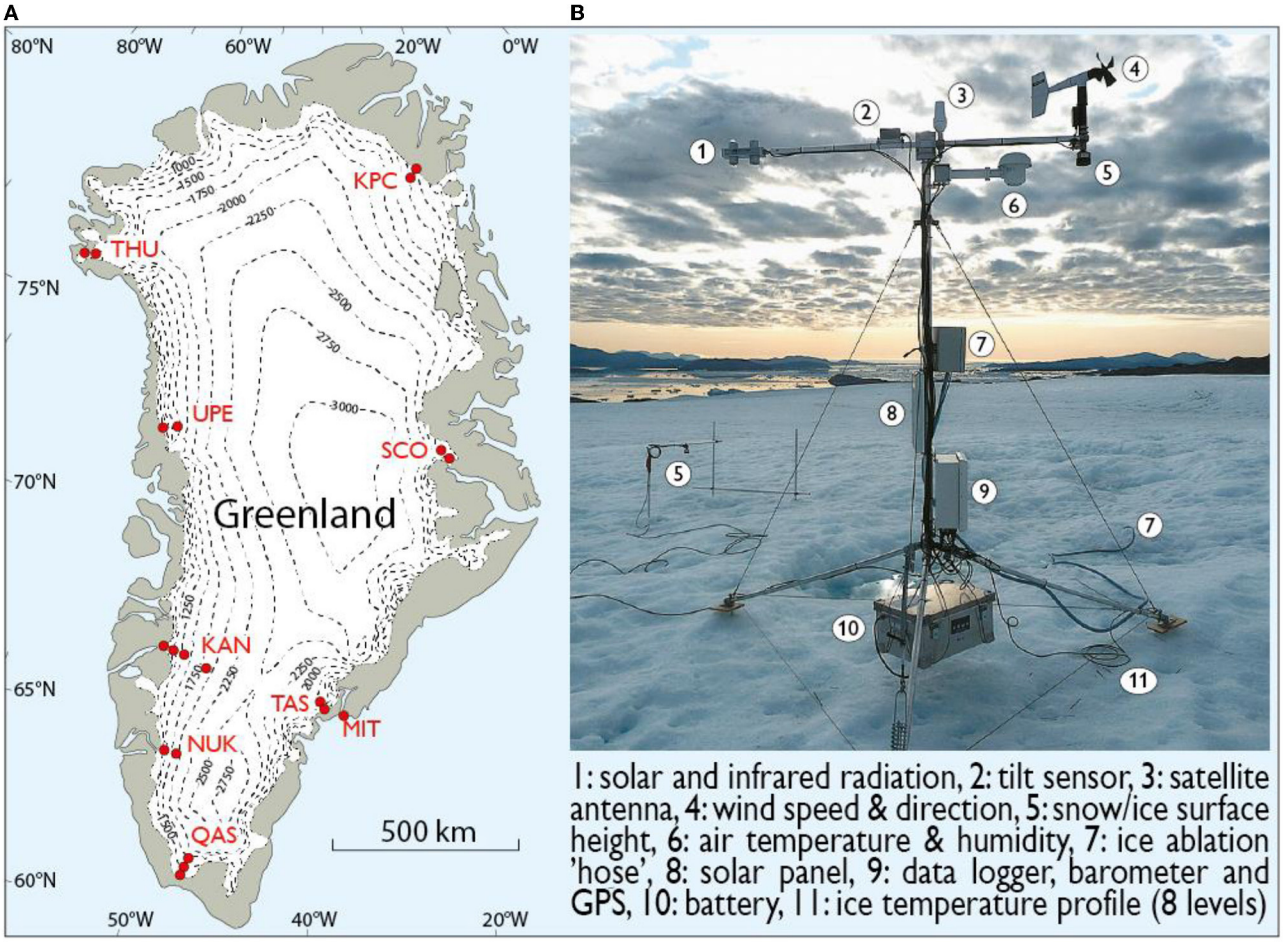

FIGURE 1 | (A) Map of Greenland with the locations of the PROMICE automatic weather stations. Dotted lines: elevation contours. **(B)** Photograph of a standard PROMICE AWS.

In general, the PROMICE AWSs measure the following meteorological variables: air temperature, pressure, humidity, wind speed, and the downward and upward components of shortwave and longwave radiation, originating from the sun and earth system, respectively. The AWSs also record temperature profiles in the upper 10 m of ice, GPS-derived location and diagnostic parameters such as station tilt, which is crucial for correcting solar radiation measurements. A GEUS-developed pressure transducer and two sonic ranging devices measure snow and ice surface height change due to ablation and accumulation (Fausto et al., 2012a). The AWSs record instantaneous values of all parameters at a 10-min time interval, apart from wind speed, which is recorded as an average based on the number of propeller rotations. All data is stored locally awaiting collection during maintenance visits. On top of the 10-min data stored locally, the AWS also transmits hourly averages of the most transient variables (**Figure 1**, instruments: 1, 4, and 6) via the Iridium satellite between days 100 and 300 of each year, while the remaining variables are transmitted at 6-h intervals. In the wintertime, transmissions have a daily frequency to save battery power. All data and metadata specifications for all sensors is stored in the PROMICE database and is freely available for download at www.promice.dk (Fausto and Van As, 2019).

Instrumentation and Accuracy

The PROMICE AWSs are equipped with an Ørum & Jensen NT1400/NT1700 pressure transducer assembly (PTA) and two Campbell Scientific SR50A sonic ranging devices that allow us to monitor surface height change due to accumulation and ablation. The pressure transducer assembly is made of a sealed (non-freezing) liquid-filled hose with a pressure transducer located at the bottom/end (**Figure 1**, instrument 7). The hose is drilled into the ice and a pressure signal is then monitored by the transducer, which is exerted by the vertical liquid column over the sensor (see Fausto et al., 2012a for more detail on the setup). The depth of the pressure transducer inside the hose can be scaled to depth using the density of the antifreeze liquid and atmospheric pressure variation. The free-floating tripod of the AWS moves downward with a melting ice surface, while the hose melts out of the ice, effectively reducing the overburden pressure of the liquid column over the pressure transducer at the bottom of the hose. The reduction in pressure thus returns ice ablation estimates.

Bøggild et al. (2004) constructed and deployed the first assembly in 2001 and during its first successful tests, the system was developed further resulting in a significantly improved pressure transducer assembly with an associated improvement in data quality (Fausto et al., 2012a).

Fausto et al. (2012a,b) also demonstrates that the PROMICE ice ablation measurements by pressure transducers are well-suited in remote regions outperforming other established methods. The pressure transducer assembly is especially suitable for high melt areas due to the independency of stakes drilled into the ice. For instance, at every AWS maintenance visit, we perform stake readings, which offer information on changes in the surface height. However, stake readings only produce a low-frequency record because measurements can only be achieved when stakes are visited. The PROMICE AWSs also have two SR50A sonic ranging devices, with one mounted on the tripod sensor boom, while the other is mounted on a separate stake assembly (**Figure 1**, Instrument 5). The manufacturer (Campbell Scientific) of the SR50A gives an accuracy of ± 1 cm or ± 0.4% of the height measured with temperature correction. Fausto et al.

TABLE 1 | Mean annual and June, July, August (JJA) air temperatures.

Year	Mean annual air temperature (°C)	Mean JJA air temperature (°C)	End of winter snowpack height (m)	Surface mass balance (m ice eq.)
2009	-	4.0	2.7 ± 0.1	−1.7 ± 0.1
2010	−2.2	5.2	2.1 ± 0.1	−3.7 ± 0.1
2011	−3.7	3.7	2.0 ± 0.1	−1.5 ± 0.1
2012	−2.4	4.6	2.3 ± 0.1	−2.8 ± 0.1
2013	−3.2	3.7	>2.6*	−0.4 ± 0.1
2014	−1.9	4.6	2.5 ± 0.1	−2.9 ± 0.1
2015	−3.5	3.4	>2.6*	0.0 ± 0.1
2016	−1.8	4.1	2.0 ± 0.1	−3.9 ± 0.1
2017	−2.9	3.1	2.1 ± 0.1	−2.8 ± 0.1
2018	−3.3	2.3	2.2 ± 0.1	−0.6 ± 0.1
2019	−2.9	3.6	2.1 ± 0.1	−3.0 ± 0.1

End of winter snow pack height, as the difference between the surface height at the start of the melt season and the end of the melt season the year before. Annual surface mass balance for MIT, as the difference between the surface height at end of the melt season and that of the year before, in meters ice eq. per year.
**The height of the winter snowpack was covering the sonic ranger, so an accurate estimate could not be made.*

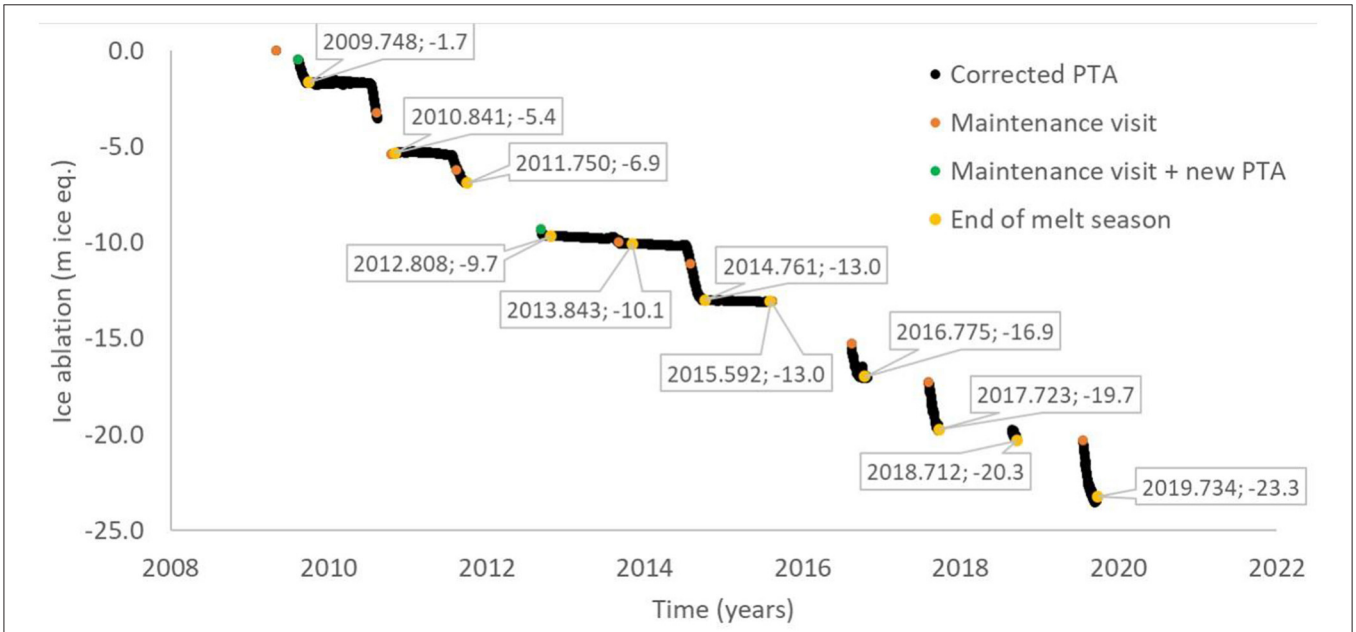

FIGURE 2 | Corrected pressure transducer assembly (PTA) readings following Fausto et al. (2012a). PTA readings were vertically shifted for new PTAs drilled into the ice in order to align the data into a continuous cumulative ice ablation record.

(2012a) tested this accuracy for periods with zero surface mass balance and found standard deviations of 1.7 cm and 0.6 cm (after spike removal) or 0.7 and 0.6% of the measured distance by the two SR50As, respectively. Precision of the readings may in general reduce over time due to sensor degradation. The challenge with surface mass balance studies using sonic ranging devices mounted on stake assemblies drilled into the ice is that the assemblies often become unstable when they melt out more than 3 m. Unstable stake assemblies often move with the wind or could even collapse during strong wind events, making the readings from the sonic ranging device unreliable. In comparison, the PTA continues to stay operational until it has melted out, reducing the need for annual station visits, in turn lowering the expense associated with logistics in Greenland considerably. The manufacturer states that the measurement uncertainty of the pressure transducer sensor is 2.5 cm, while a mean standard deviation outside of the melt season is found to be 1 cm (Fausto et al., 2012a). The relatively small standard deviation indicates a small random error, which is comparable to the sonic ranging device. Fausto et al. (2012a) also investigated the precision of the pressure transducer readings over time and found that it is reduced over time due to a degradation of the sensor because of a continuous pressure. Calibration tests of the pressure transducer show that sensor sensitivity drift amounts to 1.6% on average for a 4-years measuring period, which suggests that drift is not a large source of error. Using the combined information of measurement uncertainty of the pressure transducer and the sensor sensitivity drift, we arrive at an uncertainty on annual surface mass balance estimates of ∼0.1 m ice eq.

Mittivakkat Annual Surface Mass Balance Records for 2009–2019

We present the MIT annual surface mass balance record in **Table 1**. The surface mass balance record is based on the corrected measurements of the PTA from the PROMICE AWS dataset product (Fausto and Van As, 2019). When the PTA fails, we supplement the annual surface mass balance estimate with sonic ranger readings and with manual stake readings obtained during maintenance visits. We calculate the annual surface mass balance as the difference in height between the end-of-melt-season minimum surface level in the given year and the previous year (**Figure 2**).

Table 1 and **Figure 2** shows that 2016 was the largest mass loss year followed by 2010 and 2019 for the 10-years PROMICE dataset. For instance, the record-warm summer of 2012 (in most regions of Greenland) is only ranked the sixth largest mass loss due to a large amount of winter/spring snow at the MIT location that had to melt before negative surface mass balance can occur (**Table 1**). All years showed net mass loss except for 2015, which ended with a zero surface mass balance (**Table 1**). Since snow was present at the surface during maintenance in 2015, we used both sonic rangers on the AWS to confirm that all snow at the surface melted, while no ice under the snowpack was lost before the melt season ended (**Figure 2** and **Table 1**). The years 2010 and 2016 were both characterized by below average winter accumulation with a long period of positive air temperatures during the year, which are both important for net mass loss (Tedesco et al., 2011; Van As et al., 2011). It is the combination of low winter accumulation and relatively high temperatures, which causes low albedo on the glacier in 2010, 2014, and 2016, that resulted in large annual surface mass balance estimates. The inter-annual surface mass balance for the MIT station were successfully obtained every year yielding a 100% success rate with an overall total mass loss of 23.3 m ice equivalent for the whole period at this location.

CONCLUSIONS

The annual surface mass balance were estimated using the PROMICE data product (Fausto and Van As, 2019) and the fieldwork maintenance reports. PROMICE remains committed to maintaining a well-documented database for storing and disseminating Greenland glaciological and meteorological data freely available on https://www.promice.org/PromiceDataPortal.

DATA AVAILABILITY STATEMENT

All datasets generated for this study are included in the article/supplementary material.

AUTHOR CONTRIBUTIONS

RF derived the annual ablation totals and wrote the data report with help from JA and AA. All authors contributed to the article and approved the submitted version.

ACKNOWLEDGMENTS

The Programme for Monitoring of the Greenland Ice Sheet (PROMICE) was funded by the Geological Survey of Denmark and Greenland (GEUS) and the Danish Ministry of Climate, Energy and Utilities under the Danish Cooperation for Environment in the Arctic (DANCEA), and is conducted in collaboration with the National Space Institute (DTU Space) and Asiaq (Greenland Survey).

REFERENCES

Ahlstrøm, A. P., Gravesen, P., Andersen, S. B., Van As, D., Citterio, M., Fausto, R. S., et al. (2008). A new programme for monitoring the mass loss of the Greenland ice sheet. *Geol. Surv. Denmark Greenland Bull.* 15, 61–64. doi: 10.34194/geusb.v15.5045

AMAP (2019). *AMAP Climate Change Update 2019: An Update to Key Findings of Snow, Water, Ice and Permafrost in the Arctic (SWIPA) 2017*. Oslo, Arctic Monitoring and Assessment Programme (AMAP), 12pp.

Bøggild, C. E., Olesen, O. B., Ahlstrøm, A. P., and Jørgensen, P. (2004). Automatic glacier ablation measurements using pressure transducers. *J. Glaciol.* 50, 303–304. doi: 10.3189/172756504781830097

Fausto, R. S., and Van As, D. (2019). Programme for monitoring of the Greenland ice sheet (PROMICE): automatic weather station data. *GEUS*. doi: 10.22008/PROMICE/DATA/AWS

Fausto, R. S., Van As, D., Ahlstrøm, A. P., Andersen, S. B., Andersen, M. L., Citterio, M., et al. (2012b). Ablation observations for 2008-2011 from the Programme for Monitoring of the Greenland Ice Sheet (PROMICE). *Geol. Sur. Denmark Greenland Bull.* 26, 73–76. doi: 10.34194/geusb.v26.4765

Fausto, R. S., Van As, D., Ahlstrøm, A. P., and Citterio, M. (2012a). Assessing the accuracy of Greenland ice sheet ice ablation measurements by pressure transducer. *J. Glaciol.* 58, 1144–1150. doi: 10.3189/2012JoG12J075

IPCC (2019). "IPCC special report on the ocean and cryosphere in a changing climate," in D. C. Pörtner, V. Roberts, P. Masson-Delmotte eds.

Machguth, H., Thomsen, H. H., Weidick, A., Abermann, J., Ahlstrøm, A. P., Andersen, M. L., et al. (2016). Greenland surface mass balance observations from the ice sheet ablation area and local glaciers. *J. Glaciol.* 62, 861–887. doi: 10.1017/jog.2016.75

Mernild, S. H., Malmros, J. K., Yde, J. C., Wilson, R., Knudsen, N. T., Hanna, E., et al. (2015). Albedo decline on Greenland's Mittivakkat Gletscher in a warming climate. *Int. J. Climatol.* 35, 2294–2307. doi: 10.1002/joc.4128

Tedesco, M., Fettweis, X., Van den Broeke, M. R., Van de Wal, R. S. W., Smeets, C. J. P. P., Van de Berg, W. J., et al. (2011). The role of albedo and accumulation in the 2010 melting record in Greenland. *Environ. Res. Lett.* 6:014005. doi: 10.1088/1748-9326/6/1/014005

Van As, D., Fausto, R. S., Ahlstrøm, A. P., Andersen, S. B., Andersen, M. L., Citterio, M., et al. (2011). Programme for Monitoring of the Greenland Ice Sheet (PROMICE): first temperature and ablation records. *Geol. Surv. Denmark Greenland Bull.* 23, 73–76. doi: 10.34194/geusb.v23.4876

Wouters, B., Gardner, A. S., and Moholdt, G. (2019). Global glacier mass loss during the GRACE satellite mission (2002–2016). *Front. Earth Sci.* 7:96. doi: 10.3389/feart.2019.00096

Zemp, M., Huss, M., Thibert, E., Eckert, N., McNabb, R., Huber, J., et al. (2019). Global glacier mass changes and their contributions to sea-level rise from 1961 to 2016. *Nature* 568, 382–386. doi: 10.1038/s41586-019-1071-0

Conflict of Interest: The authors declare that the research was conducted in the absence of any commercial or financial relationships that could be construed as a potential conflict of interest.

frontiers in Earth Science

ORIGINAL RESEARCH
published: 28 July 2020
doi: 10.3389/feart.2020.00259

Assessment of Changes in Mass Balance of the Tuyuksu Group of Glaciers, Northern Tien Shan, Between 1958 and 2016 Using Ground-Based Observations and Pléiades Satellite Imagery

Vassiliy Kapitsa[1], Maria Shahgedanova[2], Igor Severskiy[1], Nikolay Kasatkin[1], Kevin White[2] and Zamira Usmanova[1,3]*

[1] Institute of Geography and Water Safety, Almaty, Kazakhstan, [2] Department of Geography and Environmental Science, University of Reading, Reading, United Kingdom, [3] Faculty of Geography and Environmental Management, Al-Farabi Kazakh National University, Almaty, Kazakhstan

OPEN ACCESS

Edited by:
Fanny Brun,
Université Grenoble Alpes, France

Reviewed by:
Gennady Andreevich Nosenko,
Institute of Geography (RAS), Russia
Ninglian Wang,
Chinese Academy of Sciences (CAS), China

***Correspondence:**
Maria Shahgedanova
m.shahgedanova@reading.ac.uk

Specialty section:
This article was submitted to Cryospheric Sciences, a section of the journal Frontiers in Earth Science

Received: *18 February 2020*
Accepted: *10 June 2020*
Published: *28 July 2020*

Citation:
Kapitsa V, Shahgedanova M, Severskiy I, Kasatkin N, White K and Usmanova Z (2020) Assessment of Changes in Mass Balance of the Tuyuksu Group of Glaciers, Northern Tien Shan, Between 1958 and 2016 Using Ground-Based Observations and Pléiades Satellite Imagery. Front. Earth Sci. 8:259. doi: 10.3389/feart.2020.00259

Continuous measurements of glaciological mass balance have been conducted at the Central Tuyuksu glacier, Tuyuksu group of glaciers, Ile Alatau, northern Tien Shan since 1957, showing that cumulative mass balance was negative since the 1970s. Geodetic mass balance was calculated for the 1958–1998 and 1998–2016 periods using multi-temporal digital elevation models derived from the historic photogrammetric surveys from 1958 and 1998 and the high-resolution Pléiades satellite stereo imagery from 2016. The geodetic measurements revealed a mean surface lowering of 23.2 ± 2.2 m (0.40 ± 0.04 m a^{-1}) and a reduction in volume of (67.7 ± 6.7) × 10^6 m^3 in 1958–2016 at the Central Tuyuksu glacier, yielding a geodetic mass balance of −21.8 ± 2.6 m w.e. Similar trends were observed at other glaciers of the Tuyuksu group, which lost in total 83.4 × 10^6 m^3 of ice. The mass balance annual rates have not changed significantly from 1958–1998 (−0.39 ± 0.05 m w.e. a^{-1}) to 1998–2016 (−0.35 ± 0.18 m w.e. a^{-1}) at the Central Tuyuksu and at other glaciers of the Tuyuksu group whose maximum elevations exceed 4,000 m a.s.l. While glacier thinning intensified in the ablation zone and affected a larger area in 1998–2016, extending to 3,600–3,700 m a.s.l., the accumulation increased at higher elevations in 1998–2016. Geodetic mass balance was more negative in 1998–2016 than in 1958–1998 at the smaller glaciers with lower maximum elevations. At the Central Tuyuksu, the geodetic mass balance was in close agreement with the glaciological mass balance, particularly in 1958–1998 when the difference between the geodetic and the cumulative glaciological mass balance values did not exceed 5%. During 1998–2016, this difference increased to 14%, with the glaciological method producing a more negative mass balance. This discrepancy

was attributed to a systematic bias introduced by the lack of stakes in the accumulation zone of Central Tuyuksu whose contribution to uncertainty increased in 1998–2016 in line with an increase in accumulation. The negative mass balance of the Tuyuksu group of glaciers was attributed to a continuing increase in summer temperatures and a low accumulation observed in the 1970–1980s and at the turn of the century.

Keywords: glacier, mass balance, Pléiades, climate change, Tien Shan, Central Asia

INTRODUCTION

There is ample evidence for glacier wastage in Tien Shan, Central Asia (Unger-Shayesteh et al., 2013). In the last two decades, research focused mainly on documenting changes in the glacier area (Kutuzov and Shahgedanova, 2009; Narama et al., 2010; Severskiy et al., 2016) as repeated satellite imagery has become widely available. However, from the perspective of changes in global sea level (Zemp et al., 2019) and in regional water resources (Huss and Hock, 2018; Shahgedanova et al., 2018, 2020), the changes in glacier volume and in mass are most important.

These changes have been assessed using geodetic mass balance method applied on a regional scale and measurements of the mass balance of individual glaciers using the glaciological (stake) method. Estimations of geodetic mass balance in Central Asia focused on comparisons of the Shuttle Radar Topography Mission (SRTM) digital elevation model (DEM) obtained in 2000 with earlier DEM built from the declassified Corona and Hexagon imagery from the 1970s (e.g., Pieczonka and Bolch, 2015). While an advantage of this method is the wide regional coverage and a relatively long time span, the uncertainties of mass balance measurements are high. In many regions of Tien Shan, they are comparable with the estimated values of mass balance. Distributed geodetic mass balance was derived for the wider region of High Asia by Brun et al. (2017) using SRTM and DEM derived from ASTER stereo imagery for a single time step of 2000–2016. Geodetic mass balance was calculated for several glaciers in Kyrgyzstan using differencing of multiple DEMs produced from high-resolution stereo imagery (Barandun et al., 2018).

Measurements of glacier mass balance using glaciological (stake) method have been conducted on several benchmark glaciers in Tien Shan since the first International Geophysical Year of 1957–1958 (Zemp et al., 2009). However, on most glaciers, the measurements were interrupted in the 1990s, resulting in more than 20 years of gap in data. On several glaciers in Uzbekistan and Kyrgyzstan, mass balance monitoring programs were renewed in the 2010s (Hoelzle et al., 2017). The gaps in the long-term mass balance records of several glaciers were filled using a combination of mass balance modeling and analysis of satellite data (Barandun et al., 2018).

Uninterrupted measurements continued on two benchmark glaciers, the Central Tuyuksu (often referred to as Tuyuksu) in the Ile Alatau, Kazakhstan, and the Urumqi Glacier No. 1 in China. The Tuyuksu mass balance monitoring program, which started in 1957, involves regular measurements of ablation during the melt season and surveys of snow depth at the end of the accumulation season using a network of over 100 stakes. Annual values of accumulation, ablation, and the resulting mass balance are reported to the World Glacier Monitoring Service (WGMS). Geodetic surveys are a part of the monitoring program and the glacier area has been mapped annually since 2006. There are two high-resolution DEM of the Tuyuksu and the surrounding glaciers from 1958 and 1998 (Severskiy et al., 2006). These DEMs were used to assess changes in glacier surface elevation, revealing strong glacier thinning that reached 50 m on the glacier tongue (Severskiy et al., 2006), and to verify the continuing glaciological measurements (Hagg et al., 2004). The latest verification using the 1958 and the 1998 DEMs and conducted for the Central Tuyuksu glacier showed a discrepancy between the geodetic mass balance of –12.6 m w.e. and the cumulative glaciological mass balance of –16.8 m w.e. and attributed it to the uncertainties of the glaciological method amplified in the cumulative record (Hagg et al., 2004).

More recently, however, there were no assessments of geodetic mass balance of the Tuyuksu glacier and the surrounding glaciers using contemporary high-resolution DEM. Such an assessment is needed in order to (i) assess temporal changes in the rates of glacier wastage and (ii) continue the validation of mass balance measured *in situ* under the conditions of rapid climatic warming. The stereo imagery from the Pléiades satellites was recently used to derive high-resolution DEM of glaciers and assess changes in elevation of glacier surface with an accuracy of ±1 m or better at multiple sites in the Andes, European Alps, Himalayas, and Iceland by Berthier et al. (2014), in Central Tien Shan by Barandun et al. (2018), and in Caucasus by Kutuzov et al. (2019). Pléiades is a constellation of satellites launched by the French Space Agency (CNES) in December 2011. It is envisaged that its application, coordinated by the Pléiades Glacier Observatory project[1], will complement *in situ* observations of glacier mass balance conducted at the WGMS reference glaciers. This study is the first attempt of deriving and using Pléiades DEM of the Tuyuksu group of glaciers.

This paper presents three high-resolution DEMs derived for the Tuyuksu group of glaciers from the photogrammetric surveys of 1958 and 1998 and from the Pléiades stereo imagery for 2016. Changes in surface elevation and geodetic mass balance are calculated for three time periods from these DEMs. Geodetic mass balance is compared with cumulative mass balance derived from stake measurements. The observed glacier change is discussed in the context of continuing climatic warming and its impact on the glaciers of the region.

[1]https://wgms.ch/boost-remote-sensing-data/

STUDY AREA

The Tuyuksu group of glaciers is located in the headwaters of the Kishi Almaty River on the northern slope of the Ile (Zailiiskiy) Alatau (**Figure 1**) approximately at 43°N and 77°06' E and between 3,500 and 4,300 m a.s.l. The region is characterized by strong seasonal variations in temperature and precipitation. The westerly flow dominates in autumn and in spring, resulting in the precipitation maxima in April–May on the plains shifting toward June–July in the middle and high mountains, where snow accumulation peaks in spring and in early summer. The snow and glacier melt period is limited to June–July–August, extending to September in individual years.

At the beginning of the monitoring program, the Tuyuksu group included nine glaciers with a combined area of 7.6 km^2 in 1958. Central Tuyuksu is the largest glacier of the mountain–valley type, with an area of 2.99 km^2 in 1958 and declining to 2.28 km^2 in 2016. Between 1958 and 2016, the accumulation–area ratio (AAR) averaged 41%. The equilibrium line altitude (ELA) was positioned on average at 3,830 m, with a standard deviation of ±110 m. Two other glaciers had areas in excess of 1 km^2.

Between 1990 and 2008, the glaciers of the Ile Alatau were losing their area at an average rate of 0.9% a^{-1}, although the rates vary between the catchments depending on their elevation and the size of the glaciers (Narama et al., 2010; Severskiy et al., 2016). These changes have been attributed largely to increasing air temperatures and also to a negative anomaly in precipitation observed in the 1970–1980s (Severskiy et al., 2006, 2016; Shahgedanova et al., 2018), which was forced by changes in the atmospheric circulation and affected most of Tien Shan (Cao, 1998).

The changes in area of the glaciers of the Tuyuksu group correlated well with the changes of the total glacier area in the Ile and Kungey Alatau system (Severskiy et al., 2016). The cumulative mass balance of the Central Tuyuksu remained negative and the annual mass balance was mostly negative, with the exception of 15 years, mostly in the 1960s and in the 21st century (Severskiy et al., 2016).

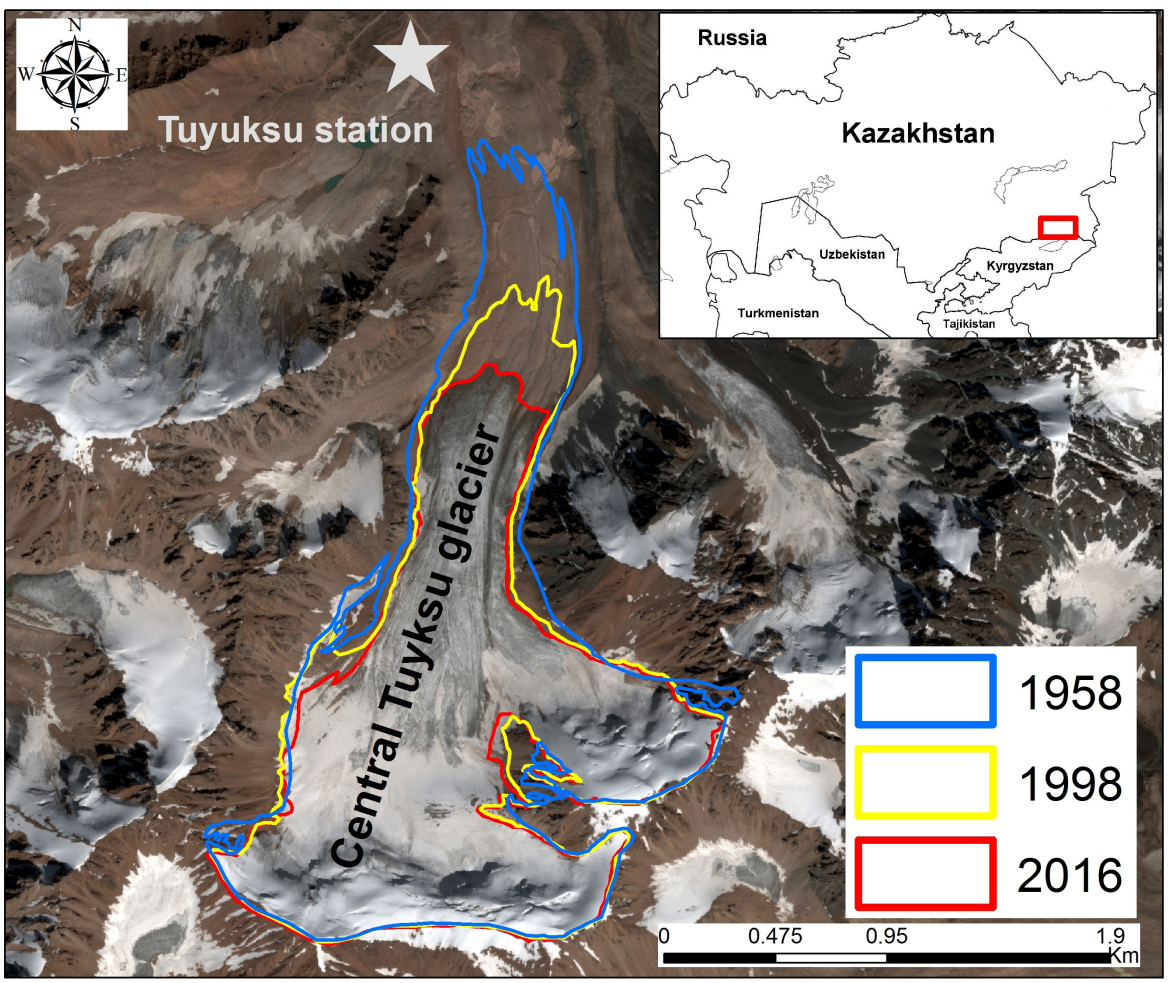

FIGURE 1 | Study area. Outlines of the Central Tuyuksu glacier are shown for 1958, 1998, and 2016. Pléiades image is used as background.

TABLE 1 | Accuracy of digital elevation model (DEM) before bias removal relative to the ground-control points (GCP) network (GCP minus DEM).

Source of DEM	Date	Horizontal resolution (m)	Δ*h* off ice (m)			
			Mean	Maximum	Minimum	Standard deviation
Photogrammetric survey	August 1958	10	2.9	7.0	−1.4	±2.0
Photogrammetric survey	August 1998	10	−0.1	6.1	−9.2	±3.4
Pléiades	27 August 2016	2.5	−0.2	2.3	−4.0	±1.5
Pléiades (re-sampled)	27 August 2016	10	0.1	3.4	−2.7	±1.6

DATA AND METHODS

DEM Generated From Photogrammetric Data From 1958 and 1998

A ground-based photogrammetric survey was conducted in the headwaters of Kishi Almaty River in August 1958 by the Institute of Cartography, Technical University of Dresden, Germany, and Institute of Geography, Kazakhstan. The photogrammetric survey was repeated in the same area in August 1998 by the Institute of Photogrammetry and Cartography, Munich Technical University, and the Commission for Glaciology of the Bavarian Academy of Sciences. Both surveys used the same local coordinate system and the same five ground control points (GCP) established in 1958. Two 1:10,000 maps with 10-m equidistant contours were produced from the surveys' data (Simon et al., 1961; Eder et al., 2002, 2005). The maps covered nine glaciers, including the Central Tuyuksu itself.

Both maps were scanned with a pixel resolution of 1,200 dpi and automatically digitized using ArcScan module of Arc GIS. The centerline method of automatic vectorization was used. Following vectorization, both maps were re-projected to WGS 84, zone 43 N projection. Two DEMs were developed from the digitized and the georeferenced maps using ArcGIS 10.5 software. The elevations were interpolated on regular grids with a resolution of 10 m using the kriging method.

A network of 36 GCP (including five GCP established in 1958) obtained in August 2018 and September 2019 using Topcon and Leica DGPS, respectively, was used for co-registration and correction of DEMs. All GCP were located on the firm terrain, which did not experience a change in elevation due to ice melt or ground movement. Planimetric correction was not required. The elevation differences between the DEMs and the GCP are shown in **Table 1** and these are assumed to be due to errors in DEMs. On average, GCP elevation was 2.9 m higher than the elevation of the corresponding pixels in the 1958 DEM, while the 1998 DEM showed a very close match.

Vertical displacement is a function of aspect and terrain slope (Nuth and Kääb, 2011) and it is desirable to assess and, if required, remove spatially varying elevation errors. In this study, the DEMs covered a relatively small area located on the northern slope of Ile Alatau. Most glaciers have northerly and westerly aspects. A small number of GCP from higher elevations did not allow us to produce a comprehensive assessment of errors due to slope steepness relative to GCP. Therefore, vertical bias was removed from both DEMs by subtracting the mean values of vertical shift registered off ice from all DEM pixels (**Table 1**).

Pléiades DEM From 2016

The Pléiades 1A and 1B twin satellites, launched in 2011 and 2012, respectively, generate stereo images with a pixel size of 0.5 m for the panchromatic channel and 2.5 m for the multi-spectral blue, green, red, and near-infrared channels[2]. For DEM generation, the multispectral data are preferred due to better point matching afforded by multi-channel images (Gim and Shin, 2015). A pair of multispectral images, obtained at the end of the ablation season on 27 August 2016, was used in this study (**Figures 1**, **2A**).

The Pléiades DEM was generated using Leica Photogrammetry Suite software using the Automatic Terrain Extraction processing engine, with the rational polynomial coefficients distributed as metadata with the imagery. These data describe the geometric analytic model between image space and ground space and are based on the direct scene orientation derived from a combination of GNSS, star sensors, and giros (Jacobsen and Topan, 2015). We refined this model using 36 GCP distributed across the image area. A 2.5-m-resolution DEM was derived from the point cloud data derived from automatic image matching. The obtained DEM was co-registered to 36 GCPs, and statistics characterizing the uncertainties of the DEM on stable terrain were calculated following the co-registration (**Table 1**).

The Pléiades DEM was resampled from 2.5 m to a coarser resolution of 10 m using bilinear interpolation method in order to match the spatial resolution of the earlier DEM.

Co-registration of DEM and Accuracy Assessment

Changes in surface elevation were calculated for three time periods as defined by the DEM acquisition dates. Three pairs of co-registered DEM were produced using the re-sampled Pléiades DEMs (1958–1998, 1998–2016, and 1958–2016) to calculate changes in elevation of the terrain by subtracting a later DEM from an earlier DEM for each pair.

At this step, DEMs that was adjusted for bias following the co-registration with GCP were used. There were no planimetric shifts between the DEMs relative to each other. The accuracy of vertical fit between DEMs in each pair was evaluated by computing the pixel-by-pixel difference in elevation (bias) for the ice-free areas where no elevation change was expected (Berthier et al., 2007; Agarwal et al., 2017). As errors in DEM increase with increasing slope, the accuracy assessments are often restricted to the areas with slope less than 30° (e.g., Pieczonka et al., 2011).

[2]http://smsc.cnes.fr/PLEIADES/

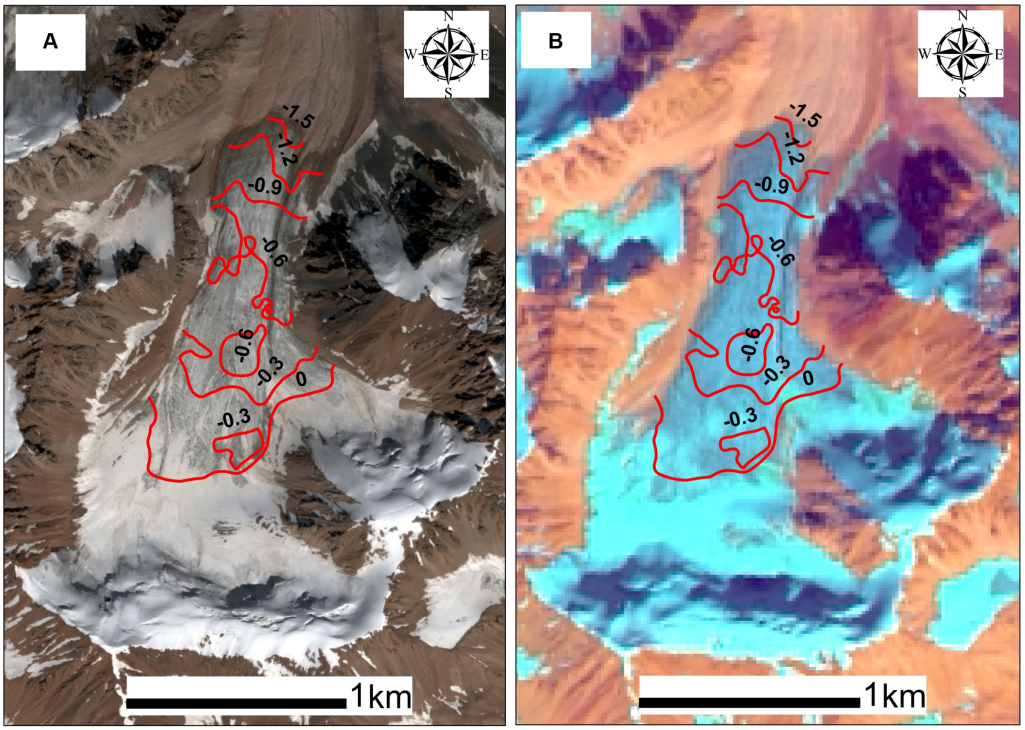

FIGURE 2 | Extent of snow cover on the **(A)** Pléiades image of 27 August 2016 and **(B)** Landsat 8 image of 22 September 2016. Isolines show ice ablation (m w.e.) as measured by the stake method on 24 September 2016. Note that the position of the snow line has not changed significantly between 27 August and the end of the mass balance year in September.

An analysis of error distribution with elevation in the study area confirmed this assumption and 30° slope value was used as a cutoff point for selecting pixels for accuracy assessment.

The error statistics for stable, ice-free terrain are shown in **Table 2**. Despite the initial correction for elevation bias using GCP, large elevation differences were still present in each pair of DEMs. Following Gardelle et al. (2013), we considered the elevation differences outside the range of mean ± three standard deviations as outliers. The outliers were removed and the relative vertical error statistics were recalculated, showing some improvement in standard deviations (**Table 2**).

The difference between the DEMs within stable terrain following the removal of outliers was used to quantify uncertainty in elevation change. We used median absolute deviation (MAD), calculated using Eq. (1), to quantify uncertainty in elevation change. The MAD values, shown in **Table 2**, were applied to the entire footprints of each pair of DEMs.

$$\mathrm{MAD} = \mathrm{median}\ \left|(X_i - \mathrm{median}\ X_n)\right| \qquad (1)$$

where X_n is a sample of differences in elevation between two DEMs used in the accuracy assessment.

To identify outliers within the glacierized area, statistics of elevation change were calculated for 50-m altitudinal belts (Gardelle et al., 2013). Pixels, in which elevation change exceeded mean ± three standard deviations as calculated for a given altitudinal belt, were removed. While few outliers were identified in the ablation zone (particularly at the Central Tuyuksu which has a gentle slope), unrealistic elevation differences were present in areas of steep terrain and deep shadow in the 1998–2016 and 1958–2016 pairs of DEMs built from the optical Pléiades imagery.

Assessment of Elevation Change and Calculation of Geodetic Mass Balance

Elevation changes were calculated for the glacierized areas (open parts of glaciers) including the Central Tuyuksu (**Table 3**) and eight other glaciers of the Tuyuksu group (**Table 4**). The supra-glacier debris cover is almost absent in the region. We note that the 2015–2016 mass balance year was characterized by high accumulation, resulting primarily from precipitation in April–June, and snow was present on the glaciers at the time of the Pléiades imagery acquisition on 27 August 2016. This could potentially introduce additional uncertainty to the calculation of changes in glacier surface elevation and geodetic mass balance. In order to establish whether snow cover melted between the acquisition date and the end of the mass balance year (and therefore the DEM required adjustment) or persisted into the next mass balance year (the DEM does not require adjustment), the position of the snow line on the Pléiades images was compared with the results of the glaciological measurements conducted on 31 August and 24 September 2016 and the Landsat 8 image of 22 September 2016 (**Figure 2**). No further melt was registered on the Central Tuyuksu after the 24 September survey,

TABLE 2 | Digital elevation model (DEM) bias statistics (m) calculated for the areas of stable, ice-free terrain and slope less than 30° following an adjustment between DEM and ground-control points.

Period	Mean	Median	Standard deviation	Maximum	Minimum	MAD
Before the removal of outliers						
1958–1998	+0.6	−0.6	±6.2	+34.1	−17.8	
1998–2016	+2.2	+2.5	±5.3	+25.9	−51.3	
1958–2016	+2.8	+1.2	±6.5	+37.7	−20.4	
After the removal of outliers						
1958–1998	0.0	−0.7	±5.0	+18.3	−15.8	±2.0
1998–2016	+2.4	+2.6	±4.4	+16.8	−11.5	±3.1
1958–2016	+2.5	+1.5	±5.3	+21.2	−14.3	±2.2

MAD is median absolute deviation.

TABLE 3 | Area, volume, and mass balance of the Central Tuyuksu glacier.

Parameter/time period	1958–1998		1998–2016		1958–2016	
Area of open ice (km^2)	2.99 ± 0.09 (1958)		2.53 ± 0.06 (1998)		2.28 ± 0.06 (2016)	
Area reduction (% and % a^{-1})	15.4 ± 3.0	0.39	9.5 ± 2.4	0.53	23.4 ± 2.6	0.40
Mean surface lowering (m and m a^{-1})	17.6 ± 2.0	0.44 ± 0.05	6.2 ± 3.1	0.35 ± 0.17	23.2 ± 2.2	0.4 ± 0.04
Reduction of glacier volume (10^6 m^3 and m^3 a^{-1})	51.1 ± 6.0	1.28 ± 0.15	17.9 ± 8.9	0.99 ± 0.50	67.7 ± 6.7	1.17 ± 0.11
Geodetic mass balance (m w.e. and m w.e.a^{-1})	−15.7 ± 2.1	−0.39 ± 0.05	−6.3 ± 3.2	−0.35 ± 0.18	−21.8 ± 2.6	−0.38 ± 0.05
Glaciological mass balance (m w.e. and m w.e.a^{-1})	−16.6	−0.40	−7.3	−0.38	−23.6	−0.40

For each time period, the first and the second columns show an overall change and the rate per year.

indicating the end of the 2015–2016 mass balance year. **Figure 2** shows that there were no significant changes in the position of the snow line between the two images, while the snow depth measured *in situ* on 31 August and 24 September 2016 did not change significantly either. Therefore, no adjustments were made to the Pléiades DEM.

The area-averaged specific geodetic mass balance was calculated using Eq. (2). The mean density of 850 ± 60 kg m^{-3} was used for volume-to-mass conversion for the calculation of geodetic mass balance according to the recommendations by Huss (2013) and the calculation of the geodetic mass balance of other glaciers in Tien Shan (Barandun et al., 2018).

$$\Delta M_{\text{geod}} = \frac{\Delta V \cdot \rho}{\bar{A}} \quad (2)$$

where ΔV is change in volume (m^3), $\bar{A}$ is the mean of glacier area at the start and at the end of a time interval (m^2), and ρ is density (kg m^{-3}). To calculate the mass balance rate (m w.e.a^{-1}), this value was divided by the number of years between the two DEMs in each pair.

The uncertainty in the calculation of glacier volume change included two terms: relative vertical error and uncertainty of glacier area measurement. The former was quantified using MAD (**Table 2**). The uncertainty in glacier area measurements was quantified using the buffer method, whereby an area of a buffer with a width of 5 m (map accuracy and half of the DEM pixel size), drawn around the glacier shapefile, was normalized by the glacier area.

The uncertainty in geodetic mass balance calculations included the vertical and the area uncertainty terms and the uncertainty due to density assumptions (Huss, 2013). The overall uncertainties in volume and mass balance were calculated according to the standard rule of error propagation as the square root of the sum of the squares of the individual uncertainty terms.

Glaciological Mass Balance

Glaciological mass balance has been measured at the Central Tuyuksu since 1957. Currently, a network of over 100 stakes is used. The maximum snow accumulation is measured at the end of the cold season (winter mass balance) and the mass decrease is measured from maximum snow accumulation until the end of the ablation season (summer mass balance). The sum of winter and summer mass balance is reported as annual mass balance. Snow density is measured on a regular basis at several snow pits located at different elevations.

Although the mass balance program has been run without interruptions, a reduced number of stakes and less frequent surveys took place in 1991–1993 and in 2002–2005. During these periods, the number of stakes declined from 140–150 used before 1991 to approximately 60 and increasing to 100–120 between these periods and after 2005. Importantly, despite a dense network of stakes, there is paucity of measurements in the accumulation zone of the glacier due to accessibility problems.

The uncertainty in glaciological mass balance measurements originates from (i) height determination, (ii) density measurement errors, (iii) presence of superimposed ice, (iv) changing location and density of stakes, (v) spatial averaging and interpolation, (vi) under-sampling in the inaccessible areas, and (vii) using a constant glacier area (Zemp et al., 2013). A large number of stakes, regular density measurements at different

TABLE 4 | Changes in area, surface elevation, volume, and geodetic mass balance of the glaciers of the Tuyuksu group.

Glacier	1958–1998						1998–2016						1958–2016						Geodetic mass balance					
	$A_{1958}/\Delta A$		Δh		$\Delta V * 10^6$		$A_{1998}/\Delta A$		Δh		$\Delta V * 10^6$		$A_{2016}/\Delta A$		Δh		$\Delta V * 10^6$		1958 - 1998		1998 - 2016		1958 - 2016	
	km²	%	m	m a^{-1}	m³	m³ a^{-1}	m²	%	m	m a^{-1}	m³	m³ a^{-1}	km²	%	m	m a^{-1}	m³	m³ a^{-1}	m w.e.	m w.e. a^{-1}	m w.e.	m w.e. a^{-1}	m w.e.	m w.e. a^{-1}
Molodezhniy	1.38 ± 0.03	17 ± 2	19.1 ± 2	0.48 ± 0.05	25.9 ± 2.8	0.65 ± 0.07	1.14 ± 0.03	25 ± 3	8.3 ± 3.1	0.46 ± 0.17	9.9 ± 3.71	0.55 ± 0.20	0.85 ± 0.03	38 ± 2.2	21.1 ± 2.2	0.36 ± 0.04	29.6 ± 3.15	0.51 ± 0.05	17.5 ± 2.20	0.44 ± 0.05	8.5 ± 2.84	0.47 ± 0.16	22.6 ± 2.42	0.39 ± 0.04
Igly Tuyuksu	1.76 ± 0.08	32 ± 5	15.0 ± 2	0.38 ± 0.05	27.0 ± 3.8	0.67 ± 0.10	1.20 ± 0.06	33 ± 5	7.2 ± 3.1	0.40 ± 0.17	7.8 ± 3.38	0.43 ± 0.19	0.80 ± 0.04	55 ± 2.3	18.2 ± 2.2	0.31 ± 0.04	32.1 ± 3.95	0.55 ± 0.07	15.5 ± 2.12	0.39 ± 0.05	6.6 ± 2.84	0.37 ± 0.16	21.3 ± 2.32	0.37 ± 0.04
Kosmodemjanskaya	0.34 ± 0.02	26 ± 6	14.0 ± 2	0.35 ± 0.05	4.9 ± 0.76	0.12 ± 0.02	0.25 ± 0.02	12 ± 8	6.6 ± 3.1	0.37 ± 0.17	1.7 ± 0.81	0.09 ± 0.04	0.22 ± 0.02	35 ± 5.9	15.9 ± 2.2	0.27 ± 0.04	5.7 ± 0.86	0.10 ± 0.01	14.1 ± 2.14	0.35 ± 0.05	6.1 ± 2.86	0.34 ± 0.16	17.3 ± 2.37	0.30 ± 0.04
Ordzhonikidze	0.29 ± 0.02	14 ± 10	12.3 ± 2	0.31 ± 0.05	3.4 ± 0.60	0.09 ± 0.02	0.25 ± 0.01	20 ± 4	8.8 ± 3.1	0.49 ± 0.17	1.9 ± 0.67	0.11 ± 0.04	0.20 ± 0.01	31 ± 3.4	14.6 ± 2.2	0.25 ± 0.04	4.1 ± 0.63	0.07 ± 0.01	10.7 ± 2.10	0.27 ± 0.05	7.2 ± 2.86	0.4 ± 0.16	14.2 ± 2.23	0.25 ± 0.04
Mayakovskiy	0.18 ± 0.02	33 ± 11	8.5 ± 2	0.21 ± 0.05	1.3 ± 0.34	0.03 ± 0.01	0.12 ± 0.01	58 ± 8	6.2 ± 3.1	0.34 ± 0.17	0.8 ± 0.41	0.04 ± 0.02	0.05 ± 0.01	72 ± 5.6	15.1 ± 2.2	0.26 ± 0.04	2.3 ± 0.36	0.04 ± 0.01	7.4 ± 2.06	0.18 ± 0.05	8.0 ± 2.86	0.44 ± 0.16	17.0 ± 2.32	0.29 ± 0.04
Mametova	0.35 ± 0.02	11 ± 6	12.6 ± 2	0.32 ± 0.05	4.1 ± 0.69	0.10 ± 0.02	0.31 ± 0.02	19 ± 7	9.6 ± 3.1	0.53 ± 0.17	3.5 ± 1.15	0.19 ± 0.06	0.25 ± 0.01	29 ± 2.8	22.2 ± 2.2	0.38 ± 0.04	7.3 ± 0.75	0.13 ± 0.01	10.6 ± 2.07	0.26 ± 0.05	10.6 ± 2.91	0.59 ± 0.16	20.7 ± 2.49	0.36 ± 0.04
No. 1	0.13 ± 0.01	31 ± 7	12.0 ± 2	0.30 ± 0.05	1.5 ± 0.34	0.04 ± 0.01	0.09 ± 0.06	77 ± 11	6.1 ± 3.1	0.34 ± 0.17	0.9 ± 0.47	0.05 ± 0.02	0.02 ± 0.01	84 ± 3.8	17.6 ± 2.2	0.30 ± 0.04	2.3 ± 0.30	0.04 ± 0.01	11.59 ± 2.56	0.29 ± 0.06	13.9 ± 2.88	0.77 ± 0.16	25.9 ± 2.35	0.42 ± 0.04
No. 2	0.17 ± 0.01	100 ± 6	11.3 ± 2	0.28 ± 0.05	1.9 ± 0.40	0.05 ± 0.01	0							100 ± 11.8	11.1 ± 2.2		1.9 ± 0.43		19.0 ± 2.27	0.48 ± 0.06				
Total/mean	4.6	27	13.1	0.33	70	0.22	3.36	28.9	7.5	0.42	26.5	0.21	2.39	48	17.8 ± 2.2	0.30 ± 0.04	83.4	0.21	14.9 ± 2.10	0.37 ± 0.05	7.7 ± 2.86	0.43 ± 0.16	20.28 ± 2.32	0.35 ± 0.04

All changes and mass balance values are negative. The total geodetic mass balance and mean annual rate of geodetic mass balance of all glaciers are calculated from the total changes in area and volume.

elevations, and annual area measurements minimize all sources of uncertainty except (iv) and (vi). Vilesov and Uvarov (2001) estimated that the absolute error of the glaciological method varied in different years between ±0.04 m w.e. and ±0.06 m w.e. in the region of direct measurements. This assessment included error sources (i)–(iii) but did not take into account the reduced number of stakes. To test the sensitivity of glaciological mass balance to a changing number of stakes, we re-calculated the annual mass balance for the whole glacier in the period 2007–2016 using those stakes which were retained in 1991–1993 and in 2002–2005. The root mean square error for annual mass balance was ±0.02 m w.e. This value represents 5% of the mean annual mass balance averaged over the whole record of glaciological measurements (−0.40 m w.e.a^{-1}). The impact of under-sampling in the accumulation zone is more difficult to evaluate. Currently, the mass balance above 3,800 m a.s.l. is calculated using regression equations based on 20 years of direct measurements which link mass balance in the 100-m elevation bands to mass balance measured in the 3,700–3,800-m band (Makarevich, 2007).

RESULTS

Changes in Surface Elevation, Volume, and Mass Balance of the Central Tuyuksu

The changes in elevation of the Central Tuyuksu glacier surface are presented in **Figures 3**, **4** and the mean statistics are summarized in **Table 3**. Between 1958 and 2016, the glacier surface lowered on average by 23.2 ± 2.2 m. The altitudinal distribution of elevation changes confirms the expected pattern with glacier downwasting in the ablation zone and thickening in the accumulation zone. In the glacier terminus area, downwasting exceeded 60 m. On average, the annual rates of area loss increased slightly in 1998–2016 in comparison with those in 1958–1998 (**Table 3**). The mean rate of glacier surface lowering decreased, but the change in the annual rates was close to the uncertainty of measurements. The altitudinal distribution of changes in the elevation of glacier surface shows that high rates of glacier downwasting (reaching 2–2.5 m a^{-1}) affected a much larger area of the glacier in the period 1998–2016, extending to 3,600–3,700 m a.s.l. (**Figures 3**, **4**). At the same time, glacier thickening increased in the accumulation zone in the period 1998–2016 (**Figures 3–5**). Overall, $(67.7 \pm 6.7) \times 10^6$ m^3 of ice was lost from the Central Tuyuksu between 1958 and 2016, giving a negative geodetic mass balance of −21.8 ± 2.6 m w.e. The differences between the annual mass balance rates in 1958–1998 and in 1998–2016 were within the accuracy of the measurements (**Table 3**).

Changes in Surface Elevation, Volume, and Geodetic Mass Balance of the Glaciers of the Tuyuksu Group

The trends in loss of area and surface lowering of the other glaciers of the Tuyuksu group were similar to those of the Central Tuyuksu (**Figures 6**, **7** and **Table 4**). As these glaciers are smaller than the Central Tuyuksu, the mean area loss was higher, averaging 48% between 1958 and 2016 (Glacier No. 2 melted completely) against 23.4% lost by the Central Tuyuksu. The mean lowering of glacier surface was 17.8 ± 2.2 m against 23.2 ± 2.2 m (**Tables 3**, **4**). Similarly to the Central Tuyuksu, the annual rates of surface lowering increased at lower elevations in the second assessment period (**Figure 7**). Glacier thickening was observed in the accumulation zone in the second assessment period, while it was close to zero in the first assessment period.

The uncertainty of measurements was higher at three glaciers—Molodezhniy, Kosmodemjanskaya, and Ordzhonikidze—in comparison with the Central Tuyuksu. While at the Central Tuyuksu the changes observed during the period 1958–2016 were very close to the sum of changes measured in 1958–1998 and in 1998–2016, at these three glaciers, there were discrepancies between the changes in surface elevation and volume as measured using the 1958 and 2016 pair of DEMs and a sum of changes in the two assessment periods (**Table 4**). At the other glaciers (Igly Tuyuksu, Mayakovskiy, Mametova, and Glacier No. 1), the changes measured in 1958–2016 were in good agreement with the combined changes in 1958–1998 and in 1998–2016. The quality of the DEMs is the most likely explanation for the observed discrepancies as most GCP were located in proximity to the Central Tuyuksu, which was the primary focus of this study. Both Molodezhniy and Ordzhonikidze are hanging glaciers positioned on steep slopes, where errors in DEM are higher (Pieczonka et al., 2011).

Comparison Between Geodetic and Glaciological Mass Balance of the Central Tuyuksu

The differences between the geodetic mass balance for the periods 1958–1998 and 1958–2016 and the cumulative glaciological mass balance are compared in **Table 3** and **Figure 8**. The two methods were in good agreement in both assessment periods. Overall, the geodetic mass balance was less negative than the glaciological mass balance, but the observed differences were within the uncertainty of measurements. Hagg et al. (2004) and Zemp et al. (2013) provided a comparison of geodetic and glaciological measurements at the glaciers with the well-established mass balance monitoring program, showing that the differences in annual mass balance values were within the 0.01–0.4 m w.e. a^{-1} range. In the case of the Central Tuyuksu, the annual values of geodetic mass balance were −0.39 ± 0.05 and −0.35 ± 0.18 m w.e.a^{-1} in the two assessment periods *versus* the glaciological mass balance of −0.40 m w.e.a^{-1} in both periods, which is within the range of differences obtained in other studies.

Hagg et al. (2004) used the same geodetic surveys of 1958 and 1998 to develop DEMs with a resolution of 20 m and to derive the geodetic mass balance of the Central Tuyuksu. Their value of −12.6 m w.e. showed a 33% difference with the cumulative mass balance, which was attributed to the uncertainties of the glaciological method. In our study, the geodetic mass balance of the Central Tuyuksu was calculated as −15.7 ± 2.1 m w.e. Our comparison showed 5 and 14% difference between the two methods in the 1958–1998

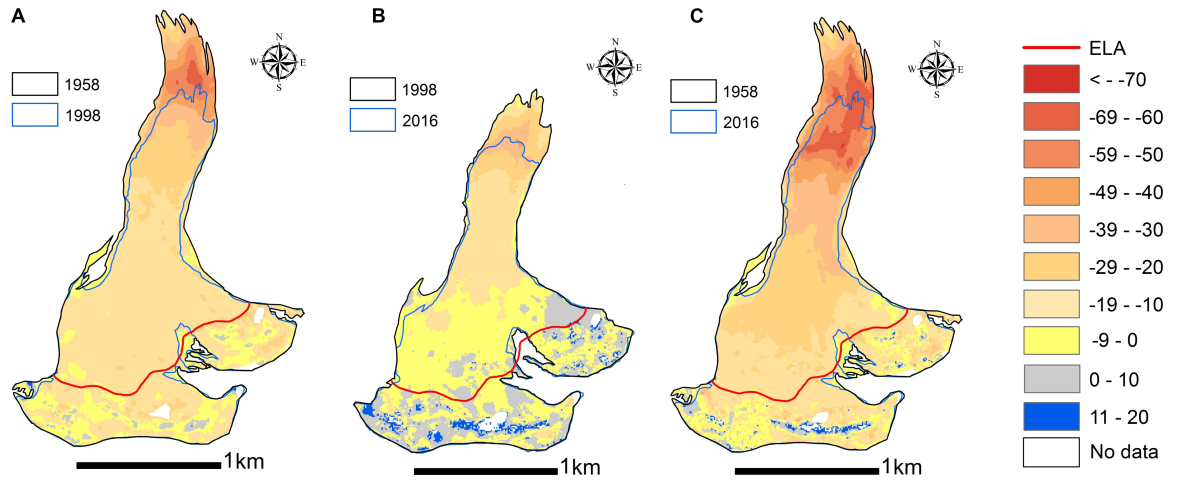

FIGURE 3 | Changes in surface elevation of the Central Tuyuksu glacier (m): **(A)** 1958–1998; **(B)** 1998–2016; **(C)** 1958–2016. The solid line shows the glacier area at the beginning and at the end of each assessment period.

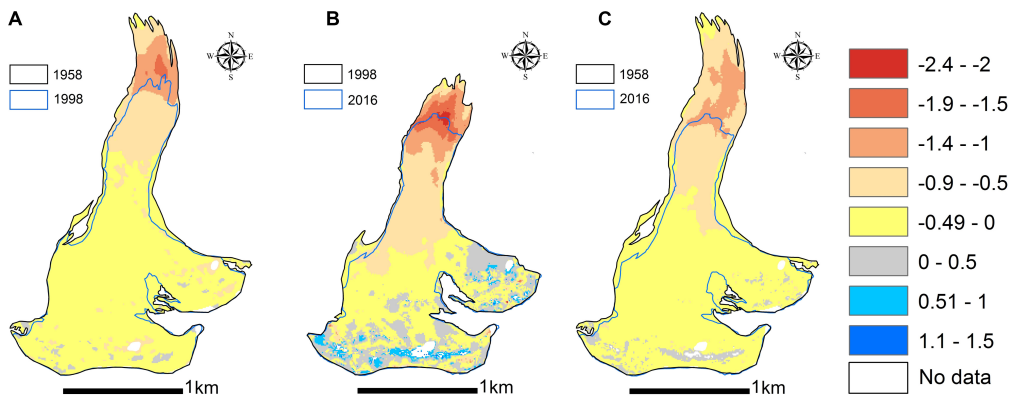

FIGURE 4 | Annual rates of change in the surface elevation of the Central Tuyuksu glacier (m a^{-1}): **(A)** 1958–1998; **(B)** 1998–2016; **(C)** 1958–2016. The solid line shows the glacier area at the beginning and at the end of each assessment period.

and the 1998–2016 assessment periods, respectively, and 8% difference overall. We attribute this improvement to the co-registration of DEMs with a network of GCP established by DGPS surveys and the subsequent correction of DEMs (**Table 2**). These facilities were not available previously, and Hagg et al. (2004) assumed no off-ice difference between the 1958 and the 1998 DEMs, in contrast to this study (**Table 2**). We note a slightly higher discrepancy between the glaciological and the geodetic mass balances in the period 1998–2016, which may be due to the lack of direct measurements in the accumulation zone and thus not capturing an increase in accumulation (**Figures 3**, **4**).

DISCUSSION

The record of the Central Tuyuksu glaciological mass balance is the longest continuous record in Central Asia, providing valuable data for the assessment of the impacts of climate change on glaciers and water resources in the region, which depends on glacier melt for water provision more than any other part of the world (Kaser et al., 2010; Pritchard, 2019). However, as with any long-term observations, the record of the glaciological mass balance from the Central Tuyuksu requires verification, and the best way to achieve it is through the estimation of the geodetic mass balance at regular intervals (Cogley, 2009; Hoelzle et al., 2017). The estimation of geodetic mass balance relies on the availability of high-resolution DEM. Currently, various DEMs are available, e.g., the widely used SPOT and ALOS, a more recent High Mountain Asia 8-m DEM derived from cross-track and along-track optical imagery (Shean, 2017), and Pléiades stereo imagery (Berthier et al., 2014), available through the WGMS Pléiades Glacier Observatory. For the Central Tuyuksu, two geodetic surveys, conducted in 1958 and in 1998, provided two historical DEMs which, together with the DEM derived from the 2016 Pléiades stereo imagery, enabled the calculation of geodetic mass balance for three time intervals.

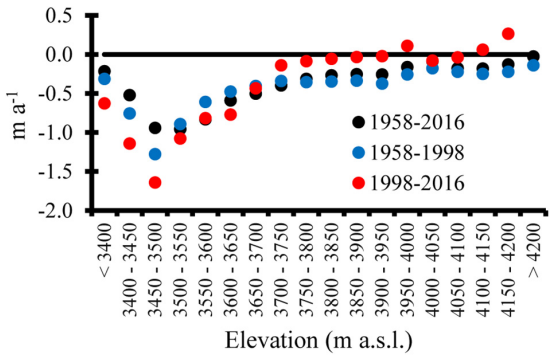

FIGURE 5 | Annual rates of glacier surface elevation change (m a^{-1}) for the Central Tuyuksu as a function of elevation in three assessment periods.

The co-registration of all three DEMs with a network of GCP showed the absence of planimetric shifts and helped to reduce vertical bias. Following co-registration and bias correction, the MAD values, which were used to quantify vertical shifts between two DEMs in each pair, were reduced to ±2–3 m on ice-free, stable, exposed terrain with slope less than 30° (**Table 3**). Few outliers were registered in the ablation zones of the Central Tuyuksu and the other glaciers in all three DEMs. The Pléiades DEM had data voids and unrealistic values of elevation change in the 1998–2016 and the 1958–2016 time periods in the accumulation zones of the Central Tuyuksu and the other glaciers in the areas with steep slope and shading. However, the number of affected pixels was small (**Figures 3**, **4**, **6**, **7**). Overall, all three DEMs showed good performance over the Central Tuyuksu, whereby the sum of changes registered in the periods 1958–1998 (two historic DEMs from photogrammetric surveys) and 1998–2016 (DEMs from 1998 photogrammetric survey and Pléiades) amounted to changes in the period 1958–2016 using DEMs from the 1958 photogrammetric survey and Pléiades (**Table 3**).

At three out of the other seven glaciers of the Tuyuksu group (Molodezhniy, Kosmodemjanskaya, and Ordzhonikidze), larger errors were observed (**Table 4**). There is a discrepancy between the mass balance values calculated for the period 1958–2016 and the two sub-periods, whereby the mass balance of all seven glaciers, calculated from 1958 and 2016 DEMs, is −20.28 ± 2.32 m w.e. and the sum of the mass balances calculated for the two sub-periods is −22.6 ± 2.50 m w.e. (**Table 4**). The difference is within the uncertainty margin, and we attribute it to deficiencies in co-registration due to the very steep slopes

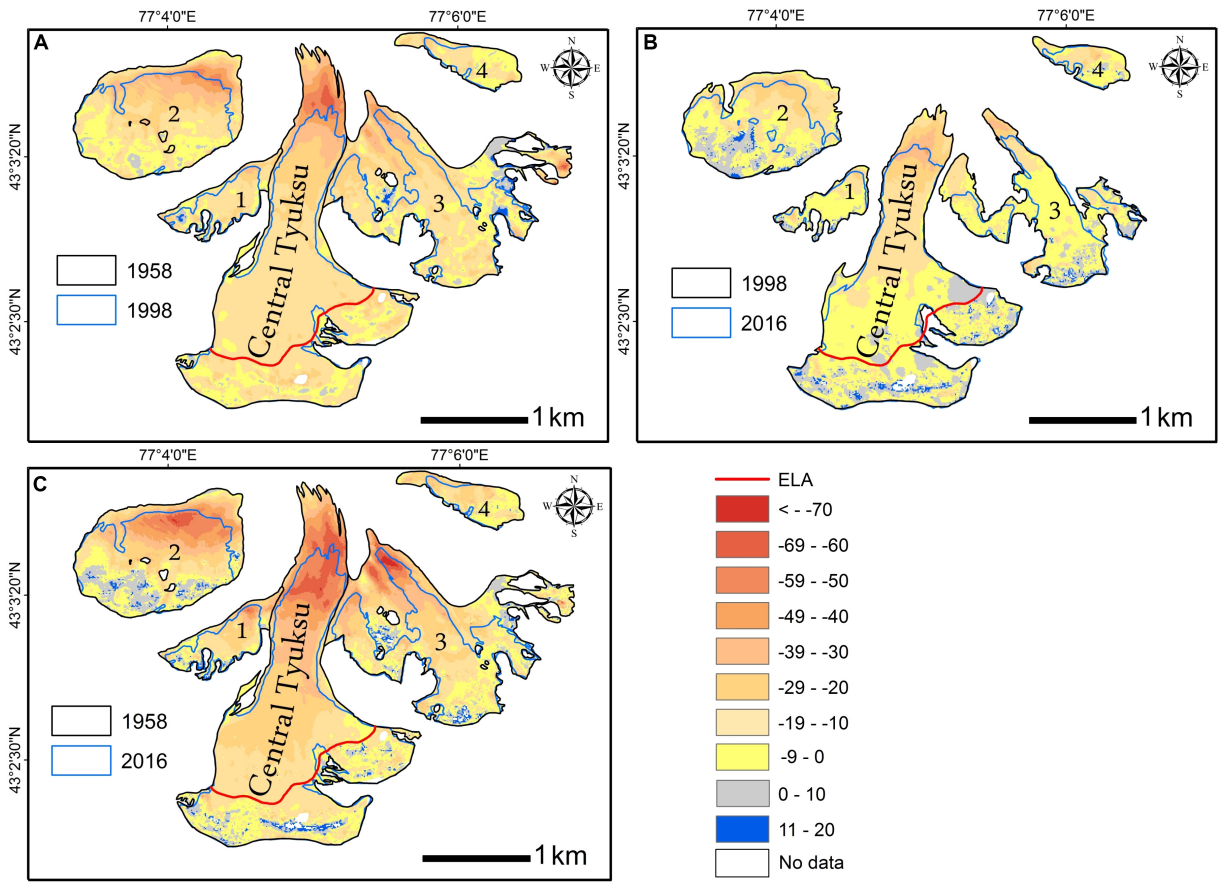

FIGURE 6 | Changes in the surface elevation of glaciers of the Tuyuksu group (m): **(A)** 1958–1998; **(B)** 1998–2016; **(C)** 1958–2016. (1) Kosmodemjanskaya; (2) Molodezhniy; (3) Igly Tuyuksu; and (4) Ordzhonikidze.

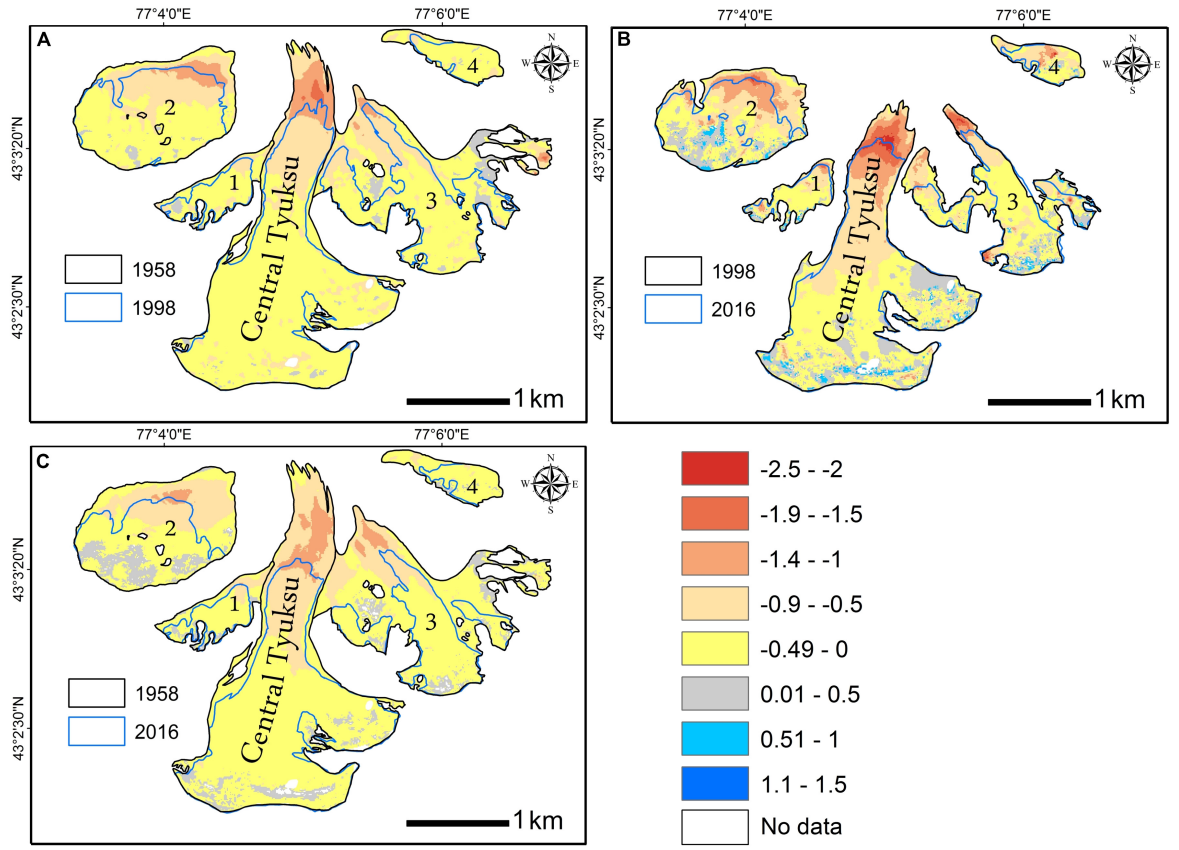

FIGURE 7 | Annual rates of change in the surface elevation of glaciers of the Tuyuksu group (m a^{-1}): **(A)** 1958–1998; **(B)** 1998–2016; **(C)** 1958–2016. The numbers are the same as in **Figure 6**.

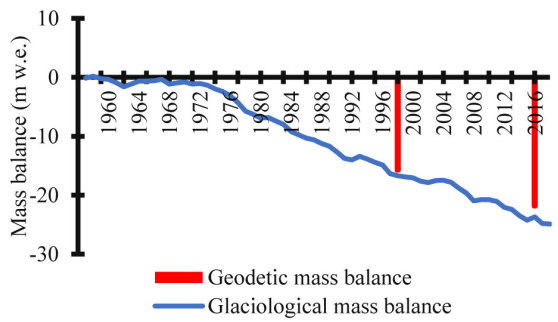

FIGURE 8 | Cumulative glaciological and geodetic mass balances of the Central Tuyuksu glacier.

characterizing these glaciers. We will aim to resolve this problem by establishing a more even distribution of GCP, most of which are currently located in proximity to the Central Tuyuksu because it was the focus of this study.

The derived negative values of geodetic mass balance indicated a strong downwasting of all the glaciers of the Tuyuksu group (**Figures 6**, **7**), confirming the results of the *in situ* measurements (**Figure 8**). While the mean rates of glacier surface lowering, volume loss, and annual rates of geodetic mass balance changed a little from the first to the second assessment period at the Central Tuyuksu, their altitudinal distribution and mass balance gradients did. The period 1998–2016 was characterized by stronger downwasting in the ablation zone and also by a likely increase in accumulation (**Figures 4**, **5**), potentially indicating that mass turnover and water cycle intensified at the Central Tuyuksu in the 21st century. Similarly, for two other larger glaciers, Molodezhniy and Igly Tuyuksu, the rate of geodetic mass balance did not change, but for the smaller glaciers, whose elevations do not exceed 4,000 m a.s.l., therefore limiting accumulation (e.g., Mametova, Glacier No. 1), the annual rates of geodetic mass balance doubled in 1998–2016 due to a rapid loss of glacier area (**Figure 7** and **Table 4**).

The registered increase in accumulation can be a result of the observed decadal variability in precipitation or a result of using DEM for 2016 when high annual precipitation was observed in Ile Alatau (**Figure 9A**). While seasonal snow had melted by late August of 2016 when the Pléiades imagery was obtained and did not contribute to the uncertainty of the DEM (**Figure 2**), the annual glaciological mass balance in 2015–2016 (0.56 m w.e.) was the second highest positive mass balance on record after 1992–1993 as a result of high accumulation (**Figure 10A**).

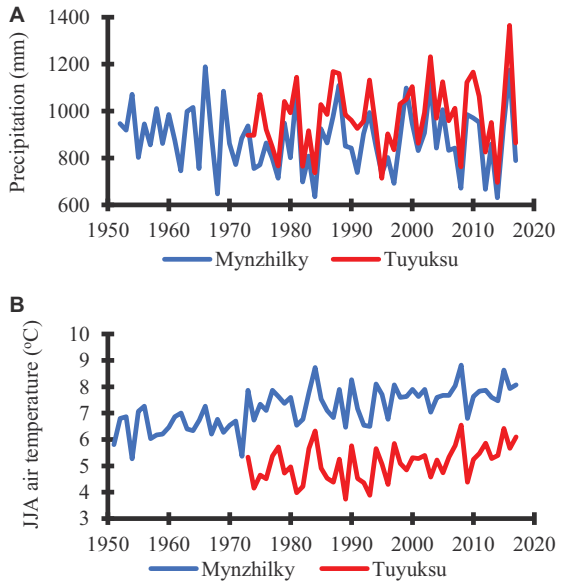

FIGURE 9 | (A) Annual precipitation calculated for mass balance year (October–September) and **(B)** June–July–August temperature at the Mynzhilky (3,100 m a.s.l.) and Tuyuksu (3,438 m a.s.l.) stations.

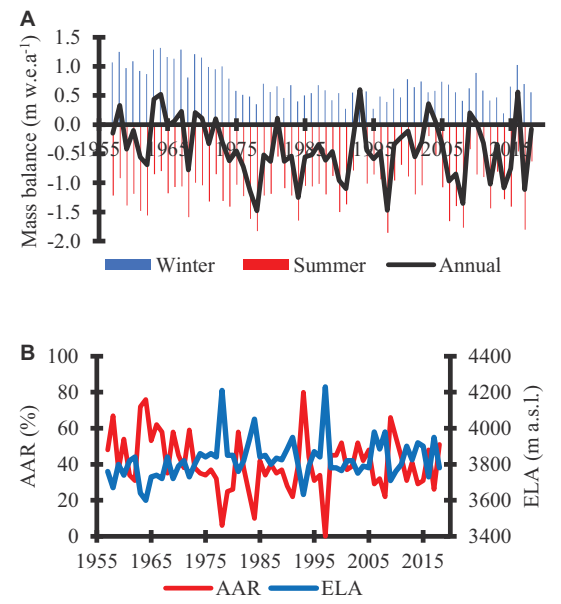

FIGURE 10 | Time series of the **(A)** components of glaciological mass balance and **(B)** equilibrium line altitude and accumulation–area ratio for the Central Tuyuksu glacier.

The time stamp of DEM used for the calculation of geodetic mass balance is key to the interpretation of a derived elevation change (Marzeion et al., 2017). In this study, multi-decadal time periods were used, which helped to reduce the influence of the short-term climatic anomalies and reflect low-frequency climatic fluctuations. While no long-term linear trends have been detected in seasonal or in annual precipitation in northern Tien Shan (Unger-Shayesteh et al., 2013; Shahgedanova et al., 2018), a negative anomaly in regional precipitation, which was observed in the 1970–1990s (Severskiy et al., 2016; Shahgedanova et al., 2018), affected the glacier mass balance across Tien Shan (Farinotti et al., 2015). Dyurgerov (2010) assessed the mass balance for the entire Tien Shan and found that the strongest negative mass balance was observed in the 1970s (−0.61 m w.e. a^{-1} in 1974–1980) and in the mid-1990s (−0.65 m w.e. a^{-1} in 1994–1997).

A step change in precipitation in the early 1970s (Cao, 1998) was evident from the observations at the Mynzhilky meteorological station located in Kishi Almaty valley at 3,010 m a.s.l. (**Figure 9A**). Annual precipitation declined from an annual mean of 920 mm in 1958–1970 to 845 mm in 1971–1998 and increased to 892 mm in 1998–2016. This variability in precipitation has been accompanied by an increase in summer temperature at a rate of 0.03°C a^{-1}, with a linear trend explaining 42% in temperature variance between 1957 and 2016 (**Figure 9B**). While in 1958–1970 the mean ELA and AAR values were 3,742 m a.s.l. and 52%, respectively, during the period 1971–1998, these values were 3,860 m a.s.l. and 35%, reverting to 3,825 m a.s.l. and 41% in 1998–2016 (**Figure 10B**), which is equal to the all-record means (section "Study Area"). In the latter period, the mass balance was positive in five mass balance years at the Central Tuyuksu (**Figure 10A**). This includes the 2015–2016 year when the mass balance was positive both at the Central Tuyuksu and at the Abramov and Golubin glaciers in central Tien Shan (Barandun et al., 2018). Therefore, while the impact of the positive precipitation anomaly of 2016 cannot be excluded, the observed increase in precipitation in the 21st century in comparison with the late 20th century may account for the detected increase in accumulation at higher altitudes (**Figures 3**, **4**, **6**, **7**). The variability in annual precipitation (**Figure 9A**) explains 55% of the total variance in annual mass balance of the Central Tuyuksu, while the variability in air temperature (**Figure 9B**) explains 35%.

The values of geodetic glacier mass balance obtained in this study were in agreement with those obtained for the neighboring regions of Tien Shan. Thus, Barandun et al. (2018) reported annual values of geodetic mass balance, derived from the Pléiades and SPOT imagery, for the Golubina, Abramov, and No. 354 glaciers as ranging between −0.30 and −0.42 m w.e. a^{-1} over the period 2003–2015. Brun et al. (2017) reported annual mass balance values of −0.20 ± 0.08 and −0.40 ± 0.20 m w.e. a^{-1}, as derived from ASTER DEM, for western and eastern Tien Shan, respectively, for the period 2000–2016. Bolch (2015) reported a geodetic mass balance of −0.42 ± 0.66 m w.e. a^{-1} derived from multiple imagery, ASTER, and SRTM DEM for the glaciers of the Ala-Archa basin in central Tien Shan. These assessments, except perhaps the less negative mass balance derived by Brun et al. (2017) for western Tien Shan, are close to the rates of change reported for the Central Tuyuksu (−0.35 ± 0.18 m w.e. a^{-1}) and for the rest of the Tuyuksu group (−0.43 ± 0.16 m w.e. a^{-1}) for 1998–2016, except the very small glaciers positioned at lower elevation (e.g., Mametova and Glacier No. 1) and whose annual

geodetic mass balance was more negative at -0.59 ± 0.16 and -0.77 ± 0.16 m w.e.a^{-1} (**Table 4**).

Importantly, the estimations of geodetic mass balance derived from the stereo Hexagon KH9 imagery for the longer assessment periods are also in broad agreement with the geodetic mass balance derived for the Tuyuksu group. Bolch (2015) reported a geodetic mass balance of -0.45 ± 0.27 m w.e. a^{-1} for the Ala-Archa region in 1964–2010. Pieczonka and Bolch (2015) reported an annual mass loss ranging between -0.70 ± 0.24 and -0.36 ± 0.28 m w.e. a^{-1} for northeastern Tien Shan for 1973–1998. Given the uncertainty ranges, these rates overlap with those derived for the Tuyuksu group where the glaciers were losing mass at a rate of -0.29 ± 0.04 and -0.45 ± 0.04 m w.e. a^{-1} between 1958 and 2016 (**Tables 3**, **4**). The central values of mass balance estimates (i.e., -0.68 ± 0.40 and -0.70 ± 0.24 m w.e.a^{-1}) reported by Pieczonka and Bolch (2015) for eastern Terskey-Alatoo, the region closest to the Tuyuksu group, were more negative than the values derived for the Tuyuksu group possibly because Pieczonka and Bolch (2015) focused on the period with the strongest negative anomalies in precipitation (**Figure 9A**), resulting in a strongly negative mass balance across Tien Shan (Dyurgerov, 2010).

CONCLUSION

The geodetic mass balance of the glaciers of the Tuyuksu group was calculated for two time steps using two historical DEMs and a high-resolution DEM derived from Pléiades stereo imagery. The results confirmed a continuing mass loss at the Central Tuyuksu, where the long-term glaciological mass balance data were available, and at other the glaciers of the group where there were no direct mass balance measurements. Overall, there was a good agreement between the glaciological and the geodetic mass balance values, and the difference between the two methods was within the uncertainty margin for the Central Tuyuksu. The geodetic mass balance values of -0.35 ± 0.18 and -0.43 ± 0.16 m w.e.a^{-1} measured at the Central Tuyuksu and the other glaciers of the group in 1998–2016, respectively, were in agreement with those of other studies conducted in Tien Shan. An increase in accumulation in 1998–2016 in comparison with that in 1958-1998 was registered in the accumulation zone of the Central Tuyuksu, where the direct stake measurements are limited and attributed to an increase in precipitation observed in the 21st century in comparison with the last three decades of the 20th century. As a result of increasing accumulation, the mean annual geodetic mass balance rates of the Central Tuyuksu and the other glaciers extending over 4,000 m a.s.l. did not change between 1958–1998 and 1998–2016, but they became more negative at the smaller glaciers with a smaller elevation span. Following this application of the Pléiades DEM, subsequent Pléiades imagery and other high-resolution DEMs will be used in the future at regular intervals to assess the regional mass balance and, potentially, the trends in precipitation using glaciers as high-elevation gauges.

DATA AVAILABILITY STATEMENT

The datasets generated for this study are available on request to the corresponding author.

AUTHOR CONTRIBUTIONS

VK led the data collection and analysis, assisted by NK and ZU. MS and IS designed the study. MS contributed to the data collection and analysis and produced the initial draft of the manuscript. KW assisted with the production of the digital elevation models and data analysis. All the authors contributed to the discussion of the results and the final draft of the manuscript.

FUNDING

This work was funded by the UK–Kazakhstan Newton–al Farabi Fund (Grant No. 172722855, "Climate Change, Water Resources and Food Security in Kazakhstan"), the UK Global Challenges Research Fund (GCRF) research network Grant, the Central Asia Research and Adaptation Water Network (CARAWAN), and the Ministry of Science and Education of the Republic of Kazakhstan (Grant No. AP05133077).

ACKNOWLEDGMENTS

The Pléiades stereo-pair used in this study was provided to the Pléiades Glacier Observatory project *via* the French Space Agency's (CNES) ISIS program. We are grateful to Dr. Etienne Berthier (LEGOS) for his assistance in obtaining the imagery. We are grateful to the reviewers for their constructive and helpful comments.

REFERENCES

Agarwal, V., Bolch, T., Syed, T. H., Pieczonka, T., Strozzi, T., and Nagaich, R. (2017). Area and mass changes of siachen glacier (East Karakoram). *J. Glaciol.* 63, 148–163. doi: 10.1017/jog.2016.127

Barandun, M., Huss, M., Usubaliev, R., Azisov, E., Berthier, E., Kääb, A., et al. (2018). Multi-decadal mass balance series of three Kyrgyz glaciers inferred from modelling constrained with repeated snow line observations. *Cryosphere* 12, 1899–1919. doi: 10.5194/tc-12-1899-2018

Berthier, E., Arnaud, Y., Kumar, R., Ahmad, S., Wagnon, P., and Chevallier, P. (2007). Remote sensing estimates of glacier mass balances in the Himachal Pradesh (Western Himalaya, India). *Remote Sens. Environ.* 108, 327–338. doi: 10.1016/j.rse.2006.11.017

Berthier, E., Vincent, C., Magnússon, E., Gunnlaugsson, P., Pitte, P., Le Meur, E., et al. (2014). Glacier topography and elevation changes derived from Pléiades sub-meter stereo images. *Cryosphere* 8, 2275–2291. doi: 10.5194/tc-8-2275-2014

Bolch, T. (2015). Glacier area and mass changes since 1964 in the Ala Archa Valley, Kyrgyz Ala-Too, northern Tien Shan. *Ice Snow* 55, 28–39. doi: 10.15356/2076-6734-2015-1-28-39

Brun, F., Berthier, E., Wagnon, P., Kääb, A., and Treichler, D. (2017). A spatially resolved estimate of High Mountain Asia glacier mass balances, 2000-2016. *Nat. Geosci.* 10, 668–673. doi: 10.1038/NGEO2999.A

Cao, M. S. (1998). Detection of abrupt changes in glacier mass balance in the Tien Shan Mountains. *J. Glaciol.* 44, 352–358. doi: 10.1017/s0022143000002677

Cogley, J. G. (2009). Geodetic and direct mass-balance measurements: comparison and joint analysis. *Ann. Glaciol.* 50, 96–100. doi: 10.3189/172756409787769744

Dyurgerov, M. B. (2010). Reanalysis of glacier changes: from the IGY to the IPY, 1960–2008. *Data Glaciol. Stud.* 108, 1–116.

Eder, K., Geiss, T., Rentsch, H., Kokarev, A., and Uvarov, V. (2005). "Surveying and mapping of the Tuyuksu Glacier Region, Kazakhstan, 1:10,000," in *Fluctuations of Glaciers 1995-2000*, eds W. Haeberli, J. Noetzli, M. Zemp, S. Baumann, and R. Frauenfelder (Zurich: World Glacier Monitoring Service), 72–73.

Eder, K., Geiß, T., Hornik, H., Rentsch, H., and Tremel, H. (2002). Neukartierung und DGM aufbau für das Tujuksu Gletschergebiet im Tian Shan. *Z. Gletscherkd. Glazialgeol.* 38, 129–138.

Farinotti, D., Longuevergne, L., Moholdt, G., Duethmann, D., Mölg, T., Bolch, T., et al. (2015). Substantial glacier mass loss in the Tien Shan over the past 50 years. *Nat. Geosci.* 8, 716–722. doi: 10.1038/ngeo2513

Gardelle, J., Berthier, E., Arnaud, Y., and Kääb, A. (2013). Region-wide glacier mass balances over the Pamir-Karakoram-Himalaya during 1999-2011. *Cryosphere* 7, 1263–1286. doi: 10.5194/tc-7-1263-2013

Gim, J. H., and Shin, S. H. (2015). Evaluating positional accuracy of Pléiades 1A satellite imagery in exploiting foreign natural resources. *Spat. Inf. Res.* 24, 85–92. doi: 10.1007/s41324-016-0009-y

Hagg, W., Braun, L. N., Uvarov, V. N., and Makarevich, K. G. (2004). A comparison of three methods of mass-balance determination in the Tuyuksu glacier region, Tien Shan, Central Asia. *J. Glaciol.* 50, 505–510. doi: 10.3189/172756504781829783

Hoelzle, M., Azisov, E., Barandun, M., Huss, M., Farinotti, D., Gafurov, A., et al. (2017). Re-establishing glacier monitoring in Kyrgyzstan and Uzbekistan, Central Asia. *Geosci. Instrument. Methods Data Syst. Discuss.* 6, 397–418. doi: 10.5194/gi-2017-31

Huss, M. (2013). Density assumptions for converting geodetic glacier volume change to mass change. *Cryosphere* 7, 877–887. doi: 10.5194/tc-7-877-2013

Huss, M., and Hock, R. (2018). Global-scale hydrological response to future glacier mass loss. *Nat. Clim. Chang.* 8, 135–140. doi: 10.1038/s41558-017-0049-x

Jacobsen, K., and Topan, H. (2015). DEM generation with short base length Pléiades triplet. *Int. Arch. Photogramm. Remote Sens. Spat. Inf. Sci. ISPRS Arch.* 40, 81–86. doi: 10.5194/isprsarchives-XL-3-W2-81-2015

Kaser, G., Großhauser, M., Marzeion, B., and Barry, R. G. (2010). Contribution potential of glaciers to water availability in different climate regimes. *Proc. Natl. Acad. Sci. U.S.A.* 107, 21300–21305.

Kutuzov, S., Lavrentiev, I., Smirnov, A., and Nosenko, G. (2019). Volume changes of elbrus glaciers from 1997 to 2017. *Front. Earth Sci.* 7:153. doi: 10.3389/feart.2019.00153

Kutuzov, S., and Shahgedanova, M. (2009). Glacier retreat and climatic variability in the eastern Terskey – Alatoo, inner Tien Shan between the middle of the 19th century and beginning of the 21st century. *Glob. Planet. Change* 69, 59–70. doi: 10.1016/j.gloplacha.2009.07.001

Makarevich, K. G. (2007). *Methodological Aspects of Research in Mass Balance and Fluctuations of Mountain Glaciers (Metodiheskie Aspekty Issledovanii Balansa Massy i Kolebanij Gornyh Lednikov)*. Almaty: Kazakhstan Institute of Geography.

Marzeion, B., Champollion, N., Haeberli, W., Langley, K., Leclercq, P., and Paul, F. (2017). Observation-based estimates of global glacier mass change and its contribution to sea-level change. *Surv. Geophys.* 38, 105–130. doi: 10.1007/s10712-016-9394-y

Narama, C., Kääb, A., Duishonakunov, M., and Abdrakhmatov, K. (2010). Spatial variability of recent glacier area changes in the Tien Shan Mountains, Central Asia, using Corona (∼1970), Landsat (∼2000), and ALOS (∼2007) satellite data. *Glob. Planet. Change* 71, 42–54. doi: 10.1016/j.gloplacha.2009.08.002

Nuth, C., and Kääb, A. (2011). Co-registration and bias corrections of satellite elevation data sets for quantifying glacier thickness change. *Cryosphere* 5, 271–290. doi: 10.5194/tc-5-271-2011

Pieczonka, T., and Bolch, T. (2015). Region-wide glacier mass budgets and area changes for the Central Tien Shan between ˜1975 and 1999 using Hexagon KH-9 imagery. *Glob. Planet. Change* 128, 1–13. doi: 10.1016/j.gloplacha.2014.11.014

Pieczonka, T., Bolch, T., and Buchroithner, M. (2011). Generation and evaluation of multitemporal digital terrain models of the Mt. Everest area from different optical sensors. *ISPRS J. Photogr. Remote Sens.* 66, 927–940. doi: 10.1016/j.isprsjprs.2011.07.003

Pritchard, H. D. (2019). Asia's shrinking glaciers protect large populations from drought stress. *Nature* 569, 649–654. doi: 10.1038/s41586-019-1240-1

Severskiy, I., Vilesov, E., Armstrong, R., Kokarev, A., Kogutenko, L., and Usmanova, Z. (2016). Changes in Glaciation of the Balkhash - Alakol basin over the past decades. *Ann. Glaciol.* 57, 382–394. doi: 10.3189/2016AoG71A575

Severskiy, I. V., Kokarev, A. L., Severskiy, S. I., Tokmagambetov, T. G., Shagarova, L. B., and Shesterova, I. N. (2006). *Contemporary and Prognostic Changes of Glaciation in Balkhash Lake Basin*. Almaty: Institute of Geography.

Shahgedanova, M., Afzal, M., Hagg, W., Kapitsa, V., Kasatkin, N., Mayr, E., et al. (2020). Emptying water towers? Impacts of future climate and glacier change on river discharge in the Northern Tien Shan, Central Asia. *Water* 12:627. doi: 10.3390/w12030627

Shahgedanova, M., Afzal, M., Severskiy, I., Usmanova, Z., Saidaliyeva, Z., Kapitsa, V., et al. (2018). Changes in the mountain river discharge in the northern Tien Shan since the mid-20th Century: results from the analysis of a homogeneous daily streamflow data set from seven catchments. *J. Hydrol.* 564, 1133–1152. doi: 10.1016/j.jhydrol.2018.08.001

Shean, D. (2017). *High Mountain Asia 8-meter DEMs Derived from Cross-track Optical Imagery, Verson 1*.

Simon, M., Töppler, J., and Pillewizer, W. (1961). Zur kartographischen aufnahme des gletschergebietes tujuksu. *Petermanns Geogr. Mitt.* 105, 309–316.

Unger-Shayesteh, K., Vorogushyn, S., Farinotti, D., Gafurov, A., Duethmann, D., Mandychev, A., et al. (2013). What do we know about past changes in the water cycle of Central Asian headwaters? A review. *Glob. Planet. Change* 110, 4–25. doi: 10.1016/j.gloplacha.2013.02.004

Vilesov, E. I., and Uvarov, V. N. (2001). *Evolution of Contemporary Glaciation of the Ile Alatau in the XX Century (Evolyutsiya Sovremennogo Oledeneniya Zailijskogo Alatau v XX Veke)*. Amaty: Kazakh State University.

Zemp, M., Hoelzle, M., and Haeberli, W. (2009). Six decades of glacier mass-balance observations: a review of the worldwide monitoring network. *Ann. Glaciol.* 50, 101–111. doi: 10.3189/172756409787769591

Zemp, M., Huss, M., Thibert, E., Eckert, N., McNabb, R., Huber, J., et al. (2019). Global glacier mass changes and their contributions to sea-level rise from 1961 to 2016. *Nature* 568, 382–386. doi: 10.1038/s41586-019-1071-0

Zemp, M., Thibert, E., Huss, M., Stumm, D., Denby, C. R., Nuth, C., et al. (2013). The Cryosphere Reanalysing glacier mass balance measurement series. *Cryosphere* 7, 1227–1245. doi: 10.5194/tc-7-1227-2013

Conflict of Interest: The authors declare that the research was conducted in the absence of any commercial or financial relationships that could be construed as a potential conflict of interest.

frontiers in Earth Science

ORIGINAL RESEARCH
published: 11 August 2020
doi: 10.3389/feart.2020.00302

Regional Geography of Glacier Mass Balance Variability Over Seven Decades 1946–2015

Roger J. Braithwaite and Philip D. Hughes*

Department of Geography, School of Environment, Education and Development, The University of Manchester, Manchester, United Kingdom

Despite much progress with remote sensing, on-site measurements of glacier mass balance (with stakes and snow pits) still have advantages for resolution of interannual and seasonal changes of mass balance. Understanding these changes may help to identify the types of glaciers most sensitive to climate change. The standard deviation of mass balance data series for a few years describes the interannual variability, and balance amplitude, defined as half the difference between winter and summer balances, describes the seasonal variability. Interannual variability increases with seasonal variability, and seasonal variability increases with annual precipitation and summer temperature available from a half-degree gridded climatology. Measured glaciers have higher mean and median precipitation than average for all glaciers in the Randolph Glacier Inventory (version 6). High balance amplitudes are associated with warm/wet (maritime) environments and low amplitudes with cold/dry (continental) environments, as shown in previous studies of climate at the equilibrium line altitude. Balance amplitude can be modelled for half-degree grid squares in the glacier inventory using multiple regression of measured balance amplitude on the climate data. The resulting modelled balance amplitude is relatively low for Arctic Islands and Central Asia, but high for Western North America, Iceland, Scandinavia, Alps, and Caucasus.

Keywords: glacier mass balance, balance amplitude, climate at equilibrium line altitude, Randolph Glacier Inventory, Climatic Research Unit/University of East Anglia gridded climatology

OPEN ACCESS

Edited by:
Michael Zemp,
University of Zurich, Switzerland

Reviewed by:
Tómas Jóhannesson,
Icelandic Meteorological Office, Iceland
Pascal Buri,
University of Alaska Fairbanks, United States

****Correspondence:***
Roger J. Braithwaite
r.braithwaite@manchester.ac.uk

Specialty section:
This article was submitted to Cryospheric Sciences, a section of the journal Frontiers in Earth Science

Received: *31 December 2019*
Accepted: *26 June 2020*
Published: *11 August 2020*

Citation:
Braithwaite RJ and Hughes PD (2020) Regional Geography of Glacier Mass Balance Variability Over Seven Decades 1946–2015. Front. Earth Sci. 8:302. doi: 10.3389/feart.2020.00302

INTRODUCTION

Glacier mass balance study is concerned with changes in glacier mass, especially changes from year to year (Paterson, 1994; Cogley et al., 2011). We need to understand glacier mass balance to explain phenomena like ice ages, sea level changes and paleo-glaciers and the local effects of glaciers on river flow in high mountain areas. Ahlmann (1948) developed the first coherent mass balance concepts for glaciers, although measurements have been made at a few points on some glaciers since the nineteenth century (Mercanton, 1916; Chen and Martin, 1990; Huss et al., 2008).

In Ahlmann's method, field-workers mark measurement sites with stakes drilled into the glacier surface layer, measure changes in ice and snow surfaces relative to the tops of the stakes and measure the changing density of snow in snow pits dug close to the stakes or in snow samples taken by corers. Seven decades after Ahlmann (1948), field glaciologists still drill stakes and dig snow pits in harsh and dangerous environments and, after all that effort, they must accept that their results are only

approximately correct. For example, the comparisons of multiyear mass balances from stakes and snow pits with results of remote sensing have shown substantial discrepancies (Zemp et al., 2013; Andreassen et al., 2016).

The Ahlmann (1948) method of measuring glacier mass balance is often termed the "direct" or "glaciological" method as distinct from the "geodetic" method where mass balance is determined by repeated mapping of the glacier surface elevation (Cogley et al., 2011). For most of the twentieth century, the latter had to use terrestrial and aerial platforms and was rather limited in geographical scope and temporal resolution (see data table for Alpine glaciers 1889–2000 in Haeberli et al., 2007). However, enormous progress has been made recently using satellite-based sensors (Bolch et al., 2008; Gardner et al., 2013; Wouters et al., 2014; Zemp et al., 2015, 2019; Bamber et al., 2018), greatly extending the geographical and temporal scope of mass balance study. The present paper discusses results from the glaciological method as it still has advantages over the geodetic method for resolving the interannual and seasonal changes in glacier mass balance that are the main topics of the present paper. The motivation is our belief that understanding the variability of glacier mass balance may help to identify the type, or types, of glaciers most sensitive to climate change, e.g., a glacier with high sensitivity to seasonal and interannual forcing may also have high sensitivity to longer-term forcing.

We set the agenda for the present paper by quoting the entry for balance amplitude in the *Glossary of Mass Balance and Related Terms* (Cogley et al., 2011, p. 64): "One half of the difference between winter and summer mass balance. The balance amplitude tends to be large in maritime climates, in which accumulation is large, and small in continental climates, in which accumulation is small. The mean balance amplitude is well-correlated with the interannual variability of annual mass balance, and, when it can be estimated from climatological information, has been used as an estimator of the magnitude of the annual mass balance itself." This entry cites no references, but Meier (1984, 1993) coined the term "balance amplitude" and suggested that changes in long-term balance are proportional to balance amplitude. Braithwaite and Zhang (1999b) modified this by saying "large net balances of either sign are likely to be associated with high mass balance amplitudes, and glaciers with low amplitudes are likely to have only small (negative or positive) net balances." Braithwaite and Zhang (1999a; Figure 3) and Braithwaite et al. (2002; Figure 7) plot the temperature sensitivity of mass balance against balance amplitude as do Ohmura et al. (1992) if we accept their "turnover" is the same as our "amplitude." Oerlemans and Fortuin (1992) and De Woul (2008), similarly, treat annual precipitation as a parameter controlling the mass balance sensitivity.

We propose a simple theory for the correlation between balance amplitude and interannual variability of annual balance and test it with a much larger data set than available for previous exercises (Braithwaite, 1982; Braithwaite and Zhang, 1999b; Braithwaite, 2005). The balance amplitude, averaged over the whole glacier area, is closely related to accumulation and/or winter balance at the glacier equilibrium line altitude (ELA), so there is a connection here to discussions of "climate at the ELA" following Ahlmann (1924), e.g., by Krenke (1975), Ohmura et al. (1992), Ananicheva and Krenke (2005), Zemp et al. (2007), Braithwaite (2008), Hughes and Braithwaite (2008), and Ohmura and Boettcher (2018). These publications relate annual precipitation, accumulation, or winter balance to summer temperatures at the equilibrium line altitude using observed or extrapolated climate data.

A simplified glacier geography (**Figure 1**) shows the locations mentioned in this paper. The boxes in **Figure 1** show the half-degree latitude/longitude cells where glaciers are located according to the Randolph Glacier Inventory (Pfeffer et al., 2014; RGI Consortium, 2017). The grid squares in **Figure 1** are the same as in the Climatic Research Unit (CRU)/University of East Anglia (UEA) gridded climatology (New et al., 1999), so we can associate each grid cell with 1961–1990 averages for climate variables. Median altitudes for glaciers in the Randolph Glacier Inventory (RGI Consortium, 2017) allow extrapolation of temperatures from the gridded climatology to an estimate of glacier ELA (Braithwaite, 2015).

MEASURED MASS BALANCE

The longest continuing series of whole-glacier mass balance measurements is from 1946 on Storglaciären in northern Sweden (Schytt, 1962). Similar measurements started elsewhere from the late 1940s, so we now have stake and snow pit data from glaciers all over the world. With experience in different areas, the original ideas of Ahlmann (1948) were modified by Anonymous (1969), Østrem and Stanley (1969); Østrem and Brugman (1991), Kaser et al. (2003), and Cogley et al. (2011). In Ahlmann's method, field-workers measure mass balance at single points on the glacier surface and then average the results over the whole glacier. The balance at point j in year t is $b_{j,t}$, and the whole-glacier balance B_t is given by:

$$B_t = (1/S) \sum_{j=1}^{j=N} s_j b_{j,t} \quad (1)$$

In (1), s_j is the area of a polygon around stake j, assumed to be represented by $b_{j,t}$, and S is the total area of the glacier given by:

$$S = \sum_{j=1}^{j=N} s_j \quad (2)$$

If single-point balance is a linear function of altitude, the whole-glacier balance is equal to the single-point balance at the mean altitude of the glacier, which is close to the median altitude (listed for most of the world's glaciers in the Randolph Glacier Inventory) and to the balanced-budget ELA (Braithwaite, 2015). This linearity assumption is not exactly true (Rea, 2009) but suggests that whole-glacier balances should have generally similar characteristics to balances near the ELA.

Ahlmann (1948) originally proposed two annual visits to the glacier to measure winter accumulation and summer ablation, but Anonymous (1969) suggested that winter and summer balances are closer to what is actually measured in the field.

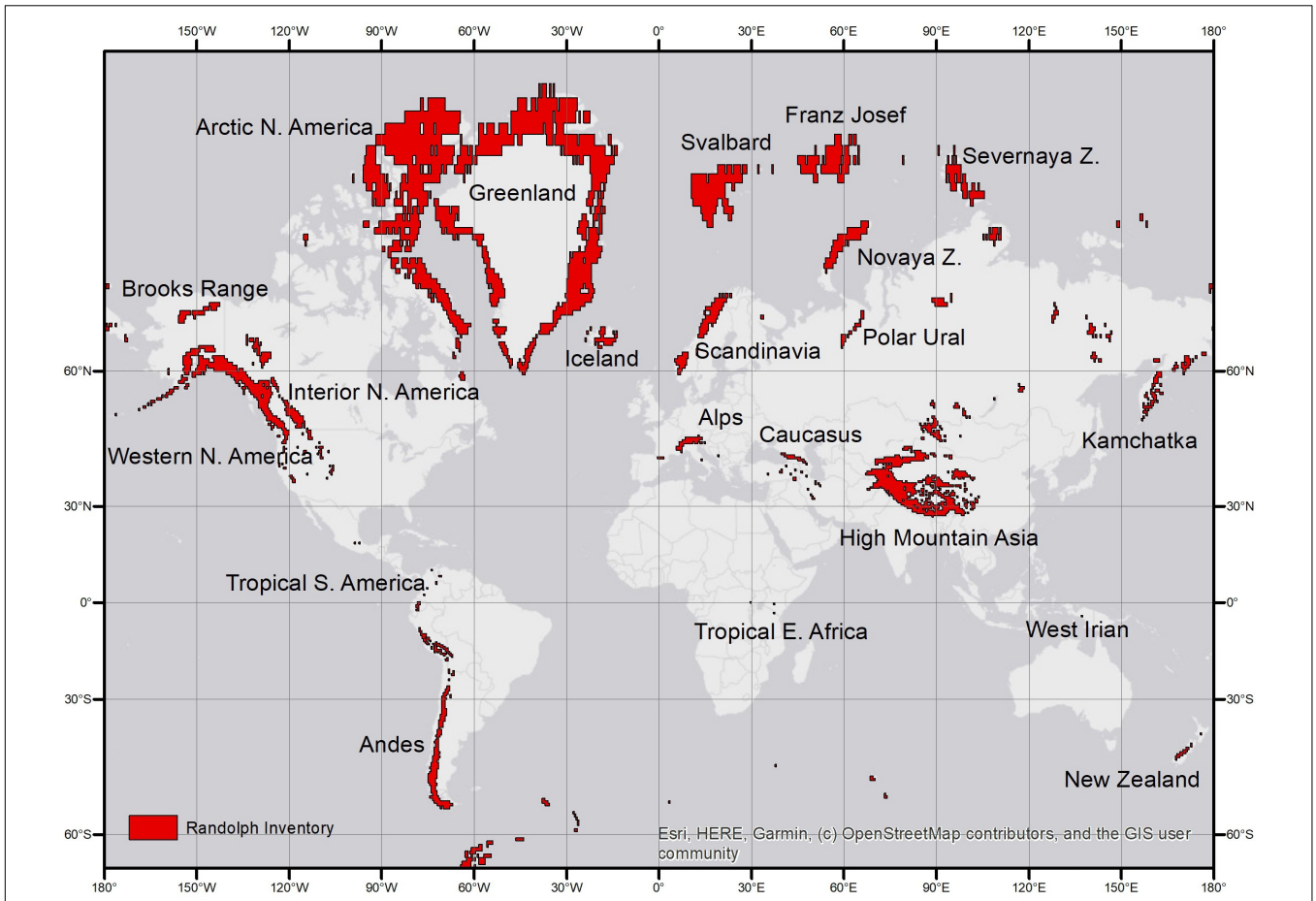

FIGURE 1 | Simplified geography of early twenty-first century glaciers. The highlighted half-degree latitude/longitude squares contain glaciers according to the Randolph Glacier Inventory (RGI Version 6) (Pfeffer et al., 2014; RGI Consortium, 2017).

Winter balance is the net change in mass since the late summer of the previous year, and summer balance is the net result of melting and snow fall during the summer. The whole-glacier annual balance is the sum of winter and summer balances:

$$B_{a,t} = B_{w,t} + B_{s,t} \quad (3)$$

Where point values of winter balance $b_{w,j,t}$ and summer balance $b_{s,j,t}$ are averaged over the whole glacier surface as in (1) to give the whole-glacier values in (3). By definition, summer balance values should be negative, although workers sometimes mistakenly report positive values. Winter and summer balances are applicable to glaciers with a clear seasonal variation in mass balance, e.g., the middle and high latitude glaciers that are well-represented in the modern mass balance data set (Cogley et al., 2011, p. 97). However, winter and summer balances cannot be defined in regions where there is little or no seasonal variability (Ageta, 1998; Kaser and Georges, 1999; Cogley et al., 2011, p. 22), and only annual balances are available for these regions.

Field-workers are encouraged to send their mass balance data to The World Glacier Monitoring Service (WGMS)[1] for storage and redistribution *via* the internet or in hard copy. Workers like Jania and Hagen(eds) (1996), Dyurgerov and Meier (1997), and Cogley and Adams (1998) were able to find much mass balance data that had until then escaped international compilation, but it is now very likely that all recent mass balance data are in the WGMS archive (WGMS, 2019). Note that previously distributed mass balance data are subject to amendments to take account of new methods and data sources. For example, average balances over a few years from stakes and snow pits may be adjusted to fit volume changes from remote sensing (Zemp et al., 2013; Andreassen et al., 2016).

We maintain our own copy of mass balance data (with 5,762 lines in September, 2019) that is analysed from time to time with a FORTRAN program to generate mass balance statistics. These statistics are now available for 1946–2015, and we discuss exactly seven decades of mass balance data in the present paper. The WGMS website offered some annual balance data up to 2018, but these did not include the winter and summer balances that we need. The latest Norwegian data report (Kjøllmoen et al., 2019) appeared in the final stages of writing our paper but its 2016–2018 data are not used here. There are mass balance data for 419 glaciers in our analysis, but winter and summer

[1]https://wgms.ch/data_submission/

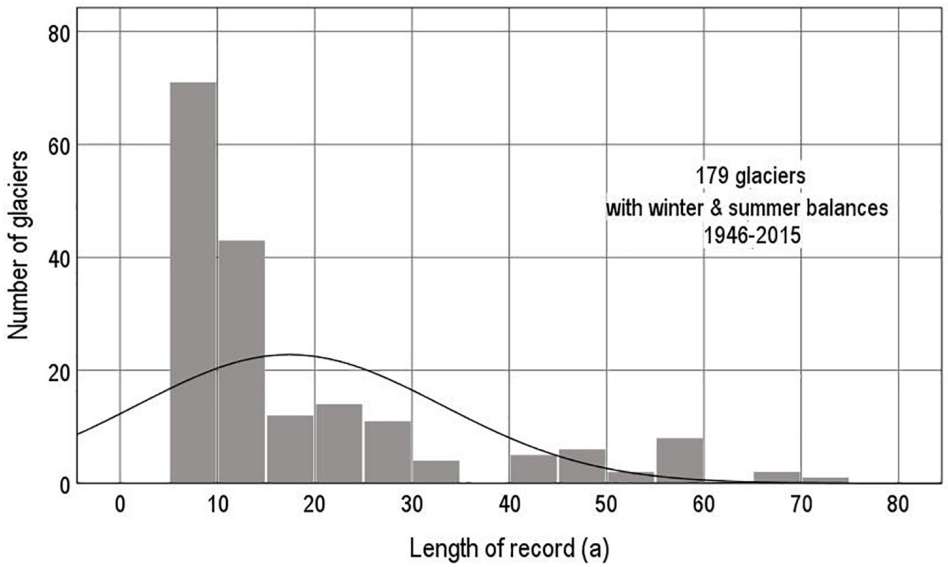

FIGURE 2 | Number of glaciers with measured annual, winter, and summer balances for different lengths of series in the years 1946–2015.

balances are only available for 270 of these glaciers (64% of the total). The barest minimum length of record for any statistical analysis is >4 years, and even this is debatable. This reduces the number of usable glaciers with winter and summer balances to only 179. The frequency distribution of these 179 glaciers (**Figure 2**) shows that most of the usable series are short, and that long series spanning many decades are relatively rare. If we only choose to analyse longer series >29 years of record, the number of glaciers falls to 28 and falls further to 13 glaciers with very long records >49 years. The available data are also highly biased in a geographical sense. For example, there are 10 or more measurement series (>4 years record) in only seven out of the 19 macro-regions (Regions 2, 6, 7, 8, 10, 11, and 13) in the Randolph Glacier Inventory (Pfeffer et al., 2014), and these regions only constitute 17% of global glacier area (for a breakdown of mass balance series within each macro-region, see **Table 1**).

The relatively few long mass balance series in **Figure 2** are interesting because they often include an earlier period (i) with relatively small negative balances, and a more recent period (ii) with increasingly negative balances. **Table 2** illustrates this by listing means of winter, summer and annual balances for the seven decades 1946–2015. There are too few data for 1946–1955 to say much beyond noting the prevalence of strongly negative balances, but the data set expands greatly in the following decades. For four decades, 1956–1995, average annual balances are negative but fairly small, i.e., only -9 to -20% of winter balance. In the most recent two decades, 1996–2015, annual balances are strongly negative, i.e., -42 to -47% of winter balance. The tendency towards increasingly negative annual balance with time is mainly "forced" by increasingly negative summer balance as the winter balance is fairly stable. The period 1961–1990 is usually identified as a 30-year reference period for assessing climate change, and **Table 2** does suggest that mass balances were generally small and negative in this reference period. The figures in **Table 2** are not homogeneous and do not necessarily describe any global trend, as there is a varying number of glaciers of different types in the database. The roughly constant number of records over four decades 1966–2005 masks the shifting nature of the data set with some series ending as others start.

Figure 3 shows locations with measured mass balance series >4 years for 287 glaciers in total, with full winter, summer

TABLE 1 | Glacier area within each RGI6 macro-region (RGI Consortium, 2017) compared with numbers of short (>4 years) and long (>29 years) series of winter, summer, and annual balances.

RGI6 Macro–region	Area (km^2)	%	Short series	%	Long series	%
01 – Alaska	86,725	12	5	3	2	7
02 – West Canada/United States	14,524	2	24	13	1	4
03 – Arctic Canada North	105,111	15	7	4	3	11
04 – Arctic Canada South	40,888	6	0	0	0	0
05 – Greenland periphery	89,717	13	3	2	0	0
06 – Iceland	11,060	2	12	7	0	0
07 – Svalbard	33,959	5	13	7	2	7
08 – Scandinavia	2,949	<1	38	21	10	36
09 – Russian Arctic	51,592	7	1	1	0	0
10 – North Asia	2,410	<1	10	6	1	4
11 – Central Europe	2,092	<1	34	19	4	14
12 – Caucasus + Middle East	1,307	<1	8	4	1	4
13 – Central Asia	49,303	7	17	10	3	11
14 – South Asia West	33,568	5	N/A	N/A	N/A	N/A
15 – South Asia East	14,734	2	N/A	N/A	N/A	N/A
16 – Low latitudes	2,341	<1	N/A	N/A	N/A	N/A
17 – South Andes	29,429	4	3	2	1	4
18 – New Zealand	1,162	<1	2	1	0	0
19 – Antarctic	132,867	19	2	1	0	0
Total	705,739	100	179	100	28	100

TABLE 2 | Inter-decadal variations in available data for winter, summer, and annual balances.

Records	Period	$\bar{B}_w$	$\bar{B}_s$	$\bar{B}_a$	$\bar{B}_a/\bar{B}_w$
(28)	1946–1955	(1.60)	(2.24)	(−0.64)	(−40%)
173	1956–1965	1.36	−1.53	−0.17	−13%
584	1966–1975	1.62	−1.77	−0.14	−9%
579	1976–1985	1.42	−1.7	−0.28	−20%
595	1986–1995	1.56	−1.74	−0.20	−13%
565	1996–2005	1.44	−2.05	−0.61	−42%
851	2006–2015	1.54	-2.27	-0.72	-47%
3,375	1946–2015	1.51	-1.90	-0.41	-27%

Units are m w.e. a^{-1}.

and annual balances for 179 of these. Logistics may explain the lack of full balance measurements at some northern locations that are notoriously expensive to access, but the lack of full balances in tropical South America and East Africa is due to lack of temperature seasonality (Kaser and Georges, 1999). Full balance measurements are also unavailable from the southern slopes of High Mountain Asia where summer accumulation-type glaciers (Ageta, 1998) are ubiquitous due to the influence of the Indian Ocean Monsoon. We discuss the role of precipitation as a control on mass balance in the section "Seasonal Variability of Mass Balance and Annual Precipitation," but **Figure 3** prepares the ground by plotting the locations of mass balance measurements onto contours of annual precipitation for 1961–1990 from the CRU/UEA climatology (New et al., 1999).

For statistical analysis of mass balance data, there is clearly a choice: one can either analyse relatively many short series, with greater statistical sampling errors (Yevjevich, 1972) but better coverage of different glacier types and regions, or analyse few series with more reliable data but less geographical coverage. Problems arise if there are interesting "anomalies" among shorter records that are ignored if one only considers longer records. After some experimentation, we decided to conduct data analysis in two parallel streams: (1) for 179 glaciers with >4 years record and (2) for 28 glaciers with >29 years record. This is an objective procedure and avoids arbitrary decisions about which glaciers to include or exclude in the study. Differences between (1) and (2) are discussed and illustrated in the **Supplementary Material**.

INTERANNUAL AND SEASONAL VARIABILITY OF MASS BALANCE

The effect of interannual variability of mass balance is shown in **Figure 4** where annual balance is plotted against year for those

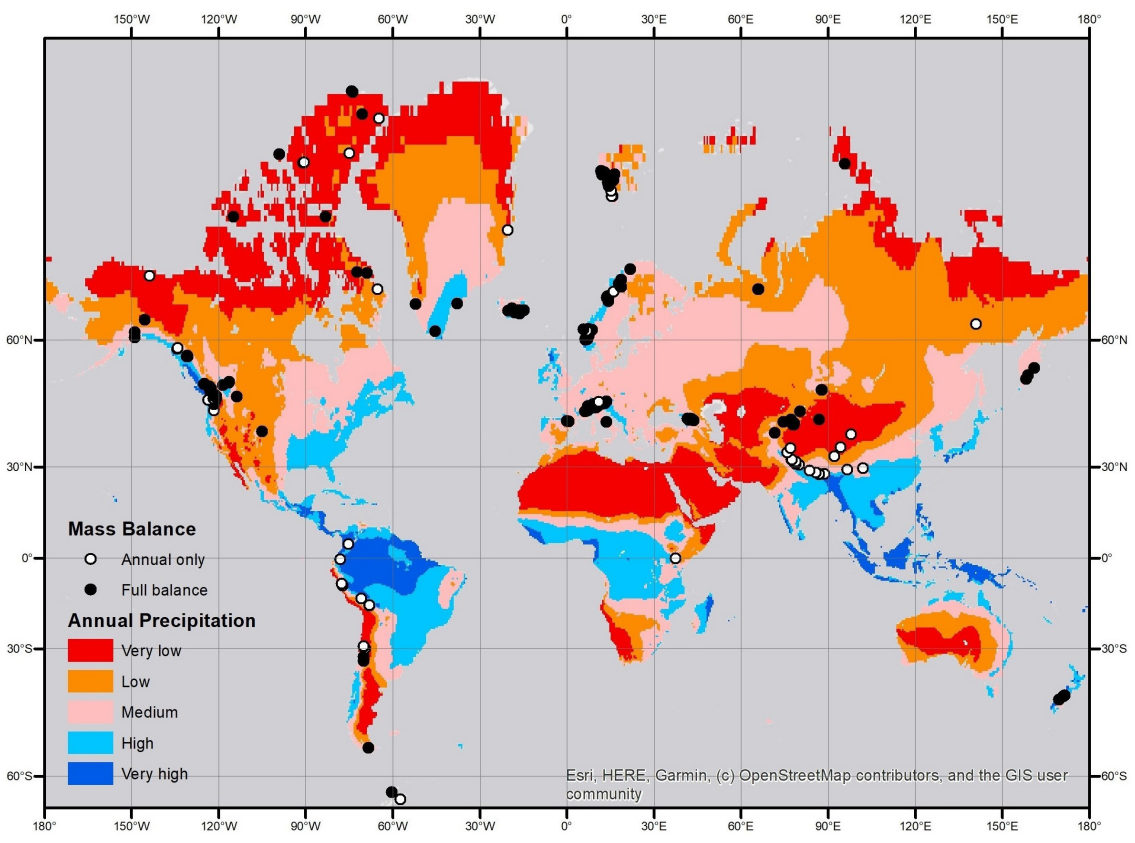

FIGURE 3 | Locations of mass balance studies >4 years of record for 1946–2015 plotted onto the global distribution of annual precipitation according to the Climatic Research Unit (CRU)/University of East Anglia (UEA) gridded climatology (New et al., 1999).

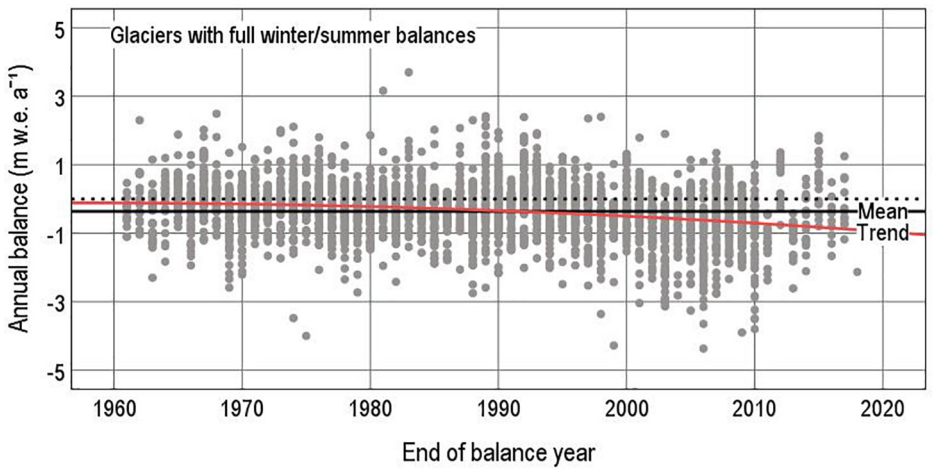

FIGURE 4 | Annual balances in the years 1961–2015 for glaciers with winter and summer balances. The solid black line denotes the mean value for all years, while the red curve denotes a quadratic year on year trend.

glaciers with winter and summer balances. The width of the cloud of points is due to interannual variations for individual glaciers and extends from about +4 to -5 m w.e. a^{-1}. The overall mean balance for the whole period (denoted by the solid black line in **Figure 4**) is negative, but there is a trend from very small in 1961 (the red curve in **Figure 4**) to very large negative balances in 2015. **Table 2** already documents this, but **Figure 4** shows the trend in mass balance is small compared with the interannual variations. If the trend in **Figure 4** is climate "signal," and the interannual variations are "noise," mass balance data have a very low signal-to-noise ratio. This shows that we need to understand the interannual variability of glacier mass balance if we want to detect or understand the effects of climate change.

The seasonal variability of annual balance is expressed by half the difference between winter and summer balances, which Meier (1984, 1993) terms the balance amplitude. He does not discuss the philosophy of using balance amplitude as a glacier–climate parameter, i.e., "quantity constant in the case considered but varying in different cases" (COD, 1981), but we assume it should be calculated ideally as a mean value over many years when the glacier is close to balance. As this is not always feasible, we simply calculate a time-averaged value of balance amplitude for whatever data are available:

$$\bar{\alpha} = \left(\bar{B}_w - \bar{B}_s\right)/2 \tag{4}$$

where $\bar{B}_w$ and $\bar{B}_s$ are time averages of winter and summer balances for N years of record.

The interannual variability of annual balance is expressed by the standard deviation of the mass balance series:

$$\sigma_a^2 = (1/(N-1)) \sum_{i=1}^{i=N} \left(B_{a,t} - \bar{B}_a\right)^2 \tag{5}$$

where $\bar{B}_a$ is the mean annual balance for N years. Standard deviations of winter and summer balances are defined in a similar way.

Expansion of (5) in terms of winter and summer balances gives:

$$\sigma_a^2 = \sigma_w^2 + \sigma_s^2 + 2\,\sigma_w \sigma_s r_{w,s} \tag{6}$$

where subscripts a, w and s denote annual, winter and summer balances, and $r_{w,s}$ is the product-moment correlation between winter and summer balances. Note that the statistics in (4) to (6) relate to the time series for individual glaciers, while later in the paper we discuss statistics for samples of many glaciers, i.e., 179 or 28. According to (6), the standard deviation of annual balance is approximately equal to the vector sum of standard deviations of winter and summer balances, increased or reduced by the winter–summer correlation term. We need two assumptions to develop a simple theory of mass balance variability, as first attempted by Braithwaite (1982). Firstly, we assume glaciers are in a balanced–budget state such that:

$$\bar{\alpha} = \bar{B}_w = -\bar{B}_s \tag{7}$$

This is not a bad assumption for the five decades 1956–1995 according to **Table 2**. Secondly, we assume that winter and summer balances have one-sided probability distributions (Yevjevich, 1972) such that their standard deviations are proportional to their mean values. Braithwaite (1982) assumed the same coefficient of variation β for both winter and summer balances:

$$\beta = \sigma_w/\bar{B}_w = -\sigma_s/\bar{B}_s \tag{8}$$

$$\sigma_a = \gamma \,.\, \bar{\alpha} \tag{9}$$

The coefficient γ in (9) is:

$$\gamma = \beta \left(2\left(1 - r_{w,s}\right)\right)^{0.5} \tag{10}$$

In other words, the standard deviation of the annual balance for a particular glacier should be proportional to the balance amplitude of that glacier. Depending on the strength of the correlation $r_{w,s}$,

which lies between -1 and +1, the proportionality coefficient γ varies between zero and $2^{0.5}.\beta$.

There is indeed a reasonable correlation ($r^2 = 0.61$, significant at less than 1% probability) between standard deviation of annual balance and balance amplitude (**Figure 5**) for series >4 years. **Table 3** shows that this correlation is intermediate between correlations for winter and summer balances, i.e., 0.78 and 0.61 (significant at 1% level). The regression equation in **Figure 5** does not pass close to the origin, and this falsifies our assumption of strict proportionality (Equation 10). The regression equations for winter and summer balances (**Table 3**) show how this happens: the regression line for winter balance passes close to the origin while that for summer balance does not. The pattern of correlation coefficients and regression lines in **Table 3** suggests that winter balances agree better with our simple theory than summer balances.

Points in **Figure 5** are coded according to a simplified glacier geography: Arctic Islands include Arctic Canada (regions 3 and 4 in the Randolph Glacier Inventory), Greenland (region 5), Svalbard (region 7) and Russian Arctic (region 9); Western North America (regions 1 and 2); Iceland (region 6); Scandinavia (region 8); North Asia (region 10); Europe and the Caucasus (regions 11 and 12); Central Asia (region 13); South Andes (region 17); New Zealand (region 18). Regions 14–16 (South Asia and Low latitudes; **Table 1**) are not included because balance amplitude is undefined and unmeasured in these regions. The same simplified geography is used for **Figures 6–9**.

Glaciers in Arctic Canada and Central Asia have lowest values of standard deviation for annual balances (**Figure 5**), while Western North America, Scandinavia, Europe and the Caucasus cover a wide range. Some North Asia glaciers have low standard deviations compared with relatively high balance amplitudes, and one South Andes glacier has the highest standard deviation in the whole data set but not the highest balance amplitude. It is important to note the location of glaciers from Arctic Islands and Central Asia in the lowest left-hand side of scatter plots like **Figure 5** because these two regions comprise 53% of the total area of glaciers in the Randolph Glacier Inventory (**Table 1**). So any regression line in a scatter plot that does not pass through these points is open to the criticism that it fails to represent more than half the glaciers in the world.

Each point in **Figure 5** represents the standard deviation of a series >4 years of record, and the sampling error of standard deviation is known to be high (Yevjevich, 1972) for very short series. We therefore repeated all calculations for the 28 glaciers with longer records >29 years. The resulting regression equations (**Supplementary Material**) are rather similar to those in **Table 3**, but the r^2 between standard deviation of annual balance and balance amplitude is increased to 0.82 (significant at 1% level). This shows that seasonal variability of mass balance strongly controls the interannual variability and suggests that it somehow typifies glaciers, e.g., some glaciers can have balanced budgets with low balance amplitudes and others with high balance amplitudes. The large-scale extension of conventional mass balance measurements to all glacial regions to achieve more even sampling (**Table 1**) would not be feasible financially or logistically. As an alternative, we can study the climatic controls on balance amplitude (sections "Seasonal Variability of Mass Balance" and "Annual Precipitation and Seasonal Variability of Mass Balance and Summer Temperature") and then extrapolate the results to all glacier regions (section "Regional Variations in Balance Amplitude").

TABLE 3 | Correlation coefficients and regression equations for standard deviations of winter, summer, and annual balances and means of balance amplitude.

Correlation coefficients				
	σ_w	σ_s	σ_a	$\bar{\alpha}$
σ_w	1.00	0.59	0.81	0.78
σ_s		1.00	0.75	0.61
σ_a			1.00	0.78
$\bar{\alpha}$				1.00

Regression equations				
Y variable	**X variable**	**Intercept**	**Slope**	**Correlation coefficient**
σ_w	$\bar{\alpha}$	−0.01	0.21	0.78
σ_s	$\bar{\alpha}$	0.26	0.15	0.61
σ_a	$\bar{\alpha}$	0.28	0.25	0.78

All variables are in units of m w.e. a^{-1}. Sample size is 179 glaciers for >4 years of record for each glacier.

SEASONAL VARIABILITY OF MASS BALANCE AND ANNUAL PRECIPITATION

Precipitation data from the CRU/UEA climatology (New et al., 1999) were interpolated to the central coordinates of each of the 179 glaciers with full annual, winter and summer balances for >4 years of record. In most cases, this interpolation involves the nearest four grid cells to the glacier, but there are six glaciers outside the topographic mask of the gridded climatology, so the 179 glaciers with >4 years record become 173 for further analysis.

Figure 6 illustrates the correlation between balance amplitude and annual precipitation. With $r^2 = 0.33$, the scatter plot accounts for about a third of the variance of balance amplitude. The correlation is statistically significant at less than 1% probability, although the high degree of scatter demonstrates the fundamental "noisiness" of the data. The r^2 values for the smaller data set with >28 years is slightly improved to 0.44 (see graphs in **Supplementary Material**), consistent with excluding data points with shorter records and presumably larger sampling errors. In **Figure 6**, for >4 years record and the corresponding figure for >29 years record in **Supplementary Material** (**Supplementary Figure SM1b**), the regression lines do not pass through the origin, i.e., the intercepts in the regression equation are substantially more than zero. This is because most data points in **Figure 6** have high precipitation, far from the origin, and "skew" the regression line away from the Arctic Islands and Central Asia that lie close to the origin. A substantial number of points including some from North Asia lie well above the regression line. These include two glaciers in the Polar

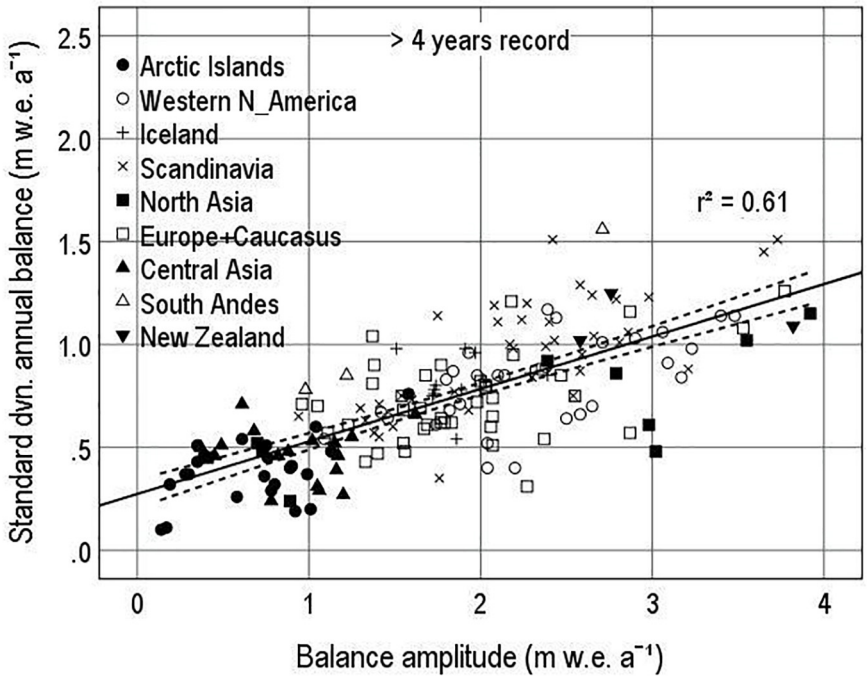

FIGURE 5 | Standard deviation of annual balance vs. balance amplitude for glaciers >4 years of record in 1946–2015.

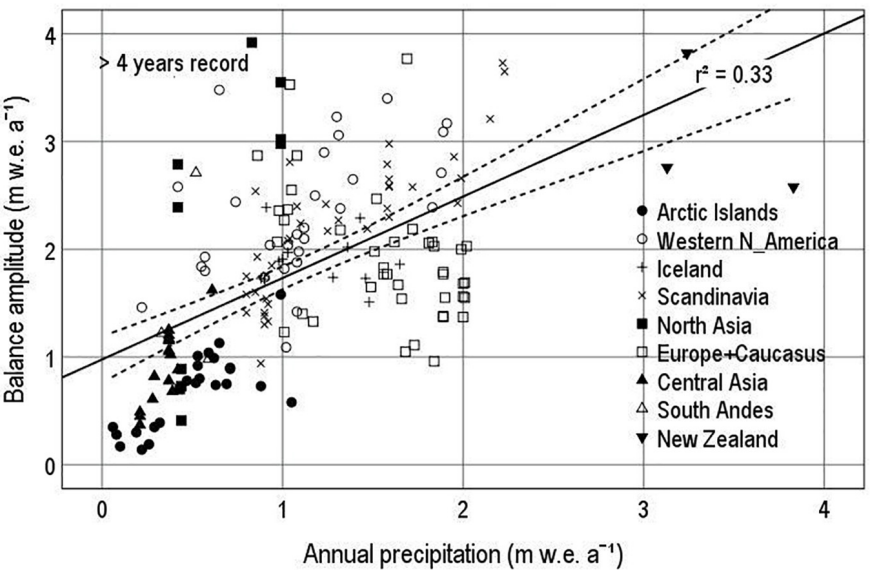

FIGURE 6 | Balance amplitude vs. annual precipitation from the Climatic Research Unit (CRU)/University of East Anglia (UEA) gridded climatology (New et al., 1999) for glaciers with >4 years of record in 1946–2015.

Ural known to have high accumulation in relation to regional precipitation (Voloshina, 1988), and Kamchatka glaciers seem similar. There are also many points below the regression line, including notably many from Europe and the Caucasus.

Figure 6 shows a high degree of scatter, and averages of balance amplitude and annual precipitation were therefore calculated for glaciers within each region to show the underlying relationship between balance amplitude and precipitation (**Figure 7**). For eight out of nine regions, average balance amplitude is much higher than regional average annual precipitation, consistent with precipitation increasing with altitude. There is only one group of glaciers (New Zealand) with an average well below the 1:1 line in **Figure 7**, but there are only three glaciers in that group. The scatter

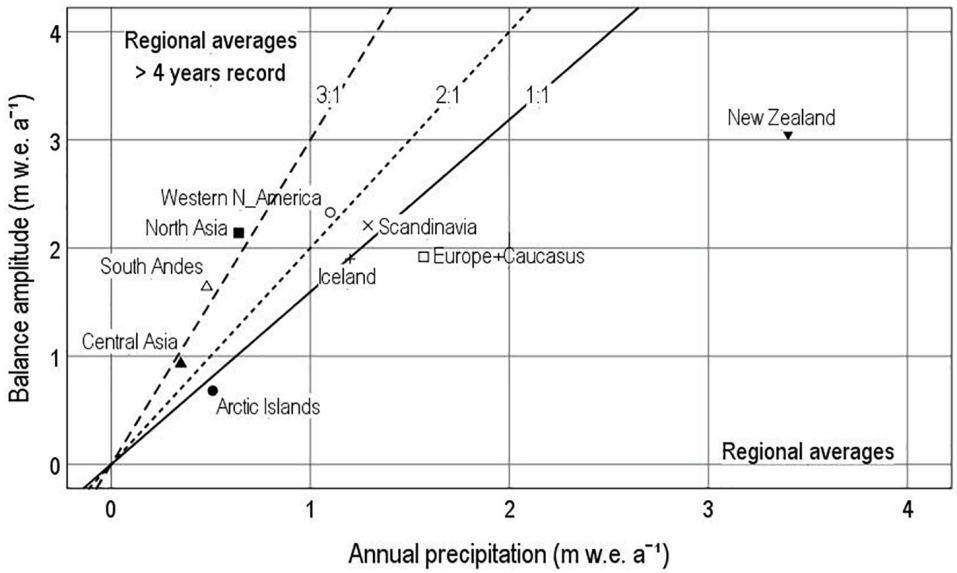

FIGURE 7 | Regional averages for balance amplitude and annual precipitation in nine regions. Balance amplitude data are for glaciers with >4 years record, and annual precipitation is from Climatic Research Unit (CRU)/University of East Anglia (UEA) gridded climatology (New et al., 1999).

of points in **Figure 7** suggests several balance-precipitation lines extending outward from the origin, e.g., the 1:1, 2:1 and 3:1 lines shown. A better understanding of precipitation processes in high mountain areas might explain these amplitude-precipitation relations.

Mean and median annual precipitation from the gridded climatology is shown in **Table 4** for three samples: (1) glaciers with >4 years of record, (2) glaciers with >29 years of record, and all glacier grid cells in the Randolph Glacier Inventory. The measured glaciers in (1) and (2) are clearly biased towards higher precipitation than for global glacier cover. According to **Table 4**, the global glacier average precipitation is 0.51 m water a^{-1}, which is roughly the same as regional average precipitation for the Arctic Islands and Central Asia in **Figure 7**, and all other regions have higher precipitation. This precipitation bias is partly caused by the geographical bias in selecting glaciers for mass balance study (**Table 1**). For example, the Western North America, Scandinavia and Europe and the Caucasus account for 63% of the measured glaciers with >4 years of record, and all have above average regional precipitation. By comparison, the drier glaciers of the Arctic Islands, Central and North Asia and South Andes are less accessible and less frequently measured. This bias may be a problem for assessing global changes solely on the basis of conventional mass balance measurements (Dyurgerov and Meier, 2005; Kaser et al., 2006), but it can be avoided by combining conventional mass balance data with other key indicators (Haeberli et al., 2007; Cogley, 2009; Zemp et al., 2019).

TABLE 4 | Mean and median annual precipitation from the Climatic Research Unit (CRU)/University of East Anglia (UEA) gridded climatology (New et al., 1999) for different glacier data sets.

Data set	Mean P_{ann} m w.e. a^{-1}	Median P_{ann} m w.e. a^{-1}	N
Glaciers >4 years record	1.11	1.03	173
Glaciers >29 years record	0.99	0.87	28
Grid cells in RGI6 inventory	0.51	0.38	4,483

Precipitation in mountain areas is difficult to measure accurately and depends on altitude and local exposure to prevailing winds (von Hahn, 1903), so one cannot expect a perfect correlation between balance amplitude and gridded precipitation. The balance amplitude will obviously depend on the glacier-level precipitation (generally unknown), but the correlation in **Figure 6** is large enough to assume that precipitation contours in **Figure 3** have some relevance to glacier-level precipitation. If this is correct, **Figure 3** suggests that glaciers occur in both wet and dry areas, e.g., Tropical South America and South Andes. Coastal North America, coastal Scandinavia and the southern slopes of High Mountain Asia may be rather wet, while their interiors are generally dry. Southwest Greenland appears wet, while northeast Greenland is dry. Although low, precipitation in Svalbard is higher than in Arctic North America because of the extratropical storms that also cause high precipitation in Iceland and southeast Greenland. The Alps and the Caucasus are associated with regional-scale precipitation maxima. Scotland and Montenegro are associated with similar precipitation maxima, but glaciers are absent today in Scotland although snow patches occasionally survive the summer (Manley, 1971), and only niche glaciers exist in Montenegro and neighbouring Albania (Hughes, 2007, 2009). In the Younger Dryas, there were many glaciers in Scotland and the western Balkans, which are both presently very wet, and also in the subtropical mountains of North Africa, which is presently very dry with occasional snow patches (Hughes et al., 2018, 2020).

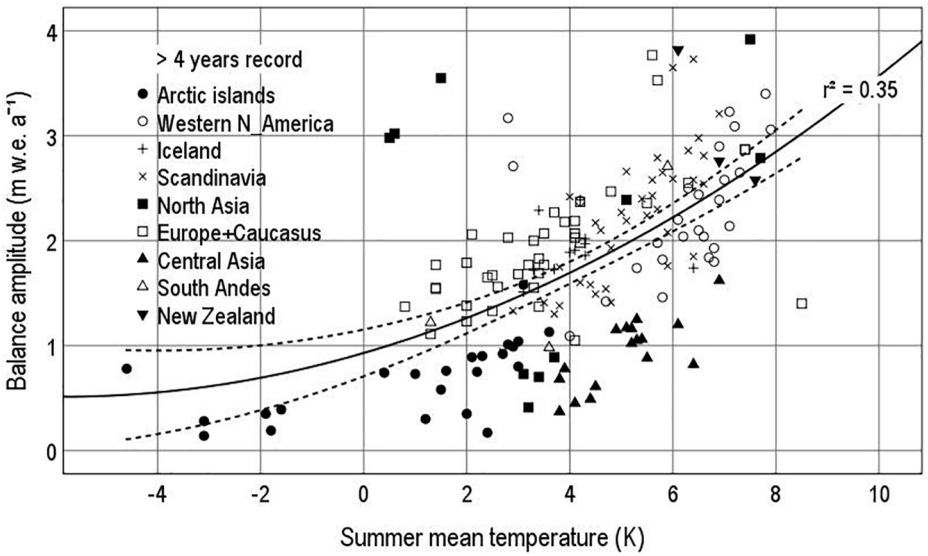

FIGURE 8 | Balance amplitude vs. summer mean temperature from the Climatic Research Unit (CRU)/University of East Anglia (UEA) gridded climatology (New et al., 1999) interpolated to glacier median altitude for glaciers with >4 years of record in 1946–2015.

SEASONAL VARIABILITY OF MASS BALANCE AND SUMMER TEMPERATURE

A series of papers on "climate at the ELA" (Ahlmann, 1924; Krenke, 1975; Ohmura et al., 1992; Ananicheva and Krenke, 2005; Zemp et al., 2007; Braithwaite, 2008; Hughes and Braithwaite, 2008; Ohmura and Boettcher, 2018) agree in suggesting a non-linear relation between some kind of precipitation variable (annual precipitation, annual accumulation, summer balance or balance amplitude) and summer temperature at the ELA. Our balance amplitude is approximately valid for the median altitude of the glacier (see argument in the section "Measured Mass Balance"), and we therefore plot it against summer mean temperature extrapolated from the gridded climatology to the glacier median altitude. Summer mean temperature is here defined as mean temperature for the warmest 3 months in the year: June–August for the Northern Hemisphere down to 27°N (RGI regions 1–15); undefined for lower latitudes (RGI region 16); December–February for the Southern Andes (RGI region 17); January–March for New Zealand (RGI region 18). The lack of definition for lower latitudes (RGI region 16) is no problem as there are no balance amplitude data for this region.

The distribution of points in **Figure 8** suggests a non-linear correlation, and we fit the data to a quadratic function of the summer temperature. With $r^2 = 0.35$, the scatter plot accounts for a little more than a third of the variance of balance amplitude. **Figure 8** is similar in scale of variation and form to figures reported by for "climate at the ELA" (Figure 3 in Ohmura et al., 1992; Figure 5 in Braithwaite, 2008), but the correlation is not as high. **Figure 8** supports the notion that balance amplitude can be typified on a spectrum of environments from cold/dry (lower left in **Figure 8**) to warm/wet (upper right of **Figure 8**) as already proposed for "climate at the ELA." This also fits the classification of climates as continental or maritime (von Hahn, 1903).

Figure 8 shows an implausible balance amplitude of around 0.5 m w.e. a^{-1} at low temperature (-5 K). This is another example of the "high intercept" problem from the section "Seasonal Variability of Mass Balance and Annual Precipitation" as the regression curve passes well above most of the points for Arctic Islands and Central Asia at low and medium temperatures. The correlation increases somewhat ($r^2 = 0.44$) if we only consider glaciers with >29 years of record (see **Supplementary Material**), but this is still not very good in predictive terms. However, the curve in the graph for these longer series (see **Supplementary Material**) does flatten out to give a balance amplitude plausibly close to zero at low temperature, which agrees reasonably well with results for "climate at the ELA."

As **Figure 8** shows a high degree of scatter, averages of balance amplitude and summer temperature were calculated for glaciers within each region to show the underlying relationship between balance amplitude and temperature (**Figure 9**). Eight out of the nine regions lie close to the gentle curve in **Figure 8**, and only Central Asia lies well below the curve. According to the curve, balance amplitude reaches zero for summer temperature well below zero. Despite the weak correlation in **Figure 8**, the regional averages in **Figure 9** strongly suggest an underlying relation between balance amplitude and summer temperature that is partly obscured by the scatter of points for single glaciers.

REGIONAL VARIATIONS IN BALANCE AMPLITUDE

The non-zero intercepts in the regression lines in **Figures 6**, **8** would be a problem if those equations were used to estimate

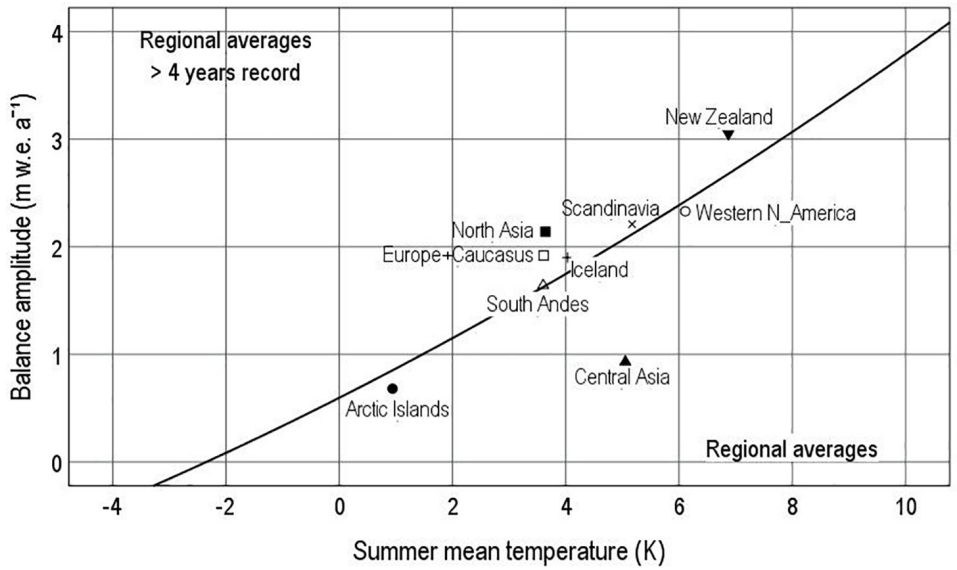

FIGURE 9 | Regional averages for balance amplitude and summer temperature in nine regions. Balance amplitude data are for glaciers with >4 years record, and summer temperature is from Climatic Research Unit (CRU)/University of East Anglia (UEA) gridded climatology (New et al., 1999).

balance amplitude for all glacier regions. This is because the calculation would give moderately large balance amplitudes for grid squares with extremely low precipitation and temperature. This might be plausible for glaciers located close to deserts like in South Andes or interior High Mountain Asia, where precipitation increases rapidly with elevation from the desert floor to glacier altitudes but is hardly plausible for high latitudes. However, balance amplitude depends on both precipitation (**Figure 6**) and summer temperature (**Figure 8**), so it is logical to use a multiple regression equation using both variables.

For 173 glaciers with >4 years record, the multiple correlation r^2 is only 0.57, which is not very impressive for predictive purposes, but the data set for 28 glaciers with >29 years record gives an impressively high $r^2 = 0.81$. The latter data set also avoids the "low intercept" problem as the regression line passes through the data points with the lowest measured balance amplitude (see discussion in **Supplementary Material**). The multiple regression model for >29 years record was therefore used to model balance amplitude in different regions in the Randolph Glacier Inventory using data from the gridded climatology. The root mean square error (RMSE) for calculating balance amplitude for a single grid cell is about ±0.4 m w.e. a^{-1}, which is reduced by averaging over the many grid cells within each region.

Means and standard deviations of modelled balance amplitude are shown in **Figure 10** for 17 out of the 19 macro-regions in the Randolph Glacier Inventory. There is a clear pattern of very low amplitudes for Arctic Islands and very high amplitudes for New Zealand. Mean balance amplitudes for other regions lie between these extremes, but the width of the bars around each point in **Figure 10** indicates large variations within each region. For example, both the West Canada/United States and Scandinavia regions contain larger balance amplitudes in the coastal mountains and lower values inland. This is illustrated in **Figure 11** for the six micro-regions within the macro-region Alaska. The lowest amplitude is for North Alaska (Brooks Range), which fits well with the Arctic Islands in **Figure 10**, but there are also high amplitudes in other subregions with substantial interregional variations.

From the correlation between interannual variability of annual balance and balance amplitude in **Figure 5**, we can infer high interannual variability in those macro-regions with high balance amplitudes in **Figure 10**. We think it plausible that mass balance sensitivity to climate change may follow a similar regional pattern (Braithwaite and Zhang, 1999a; Braithwaite et al., 2002). It is interesting to compare our **Figure 10** with Figure 1 in Zemp et al. (2019) that shows cumulative mass changes of global glaciers in 1961–2016 in units of both Gt and m w.e. a^{-1}. Zemp et al. (2019) shows very high changes (>0.5 m w.e. a^{-1}) for Alaska, Western North America and South Andes, which coincide with high amplitudes in our **Figure 10**. Zemp et al. (2019) also shows low (0 to -0.25 m w.e. a^{-1}) or medium (-0.25 to -0.5 m w.e. a^{-1}) changes for Arctic Canada (North and South), Svalbard and Russian Arctic which coincide with low amplitudes in **Figure 10**. For other regions, there is less agreement between **Figure 10** and Zemp et al., 2019), but that may be because we are not strictly comparing like with like. For example, the 1961–2016 period in Zemp et al. (2019) very probably combines periods with smaller/earlier and larger/later changes (Zemp et al., 2015), involving different degrees of climate forcing. If it were possible to reinterpret the 1961–2016 changes of Zemp et al. (2019) in terms of mass balance response to climate change (in m w.e. a^{-1} K^{-1}), we would expect our high-amplitude regions (Iceland, Scandinavia, Central Europe, Caucasus and New Zealand) to show a high mass balance sensitivity.

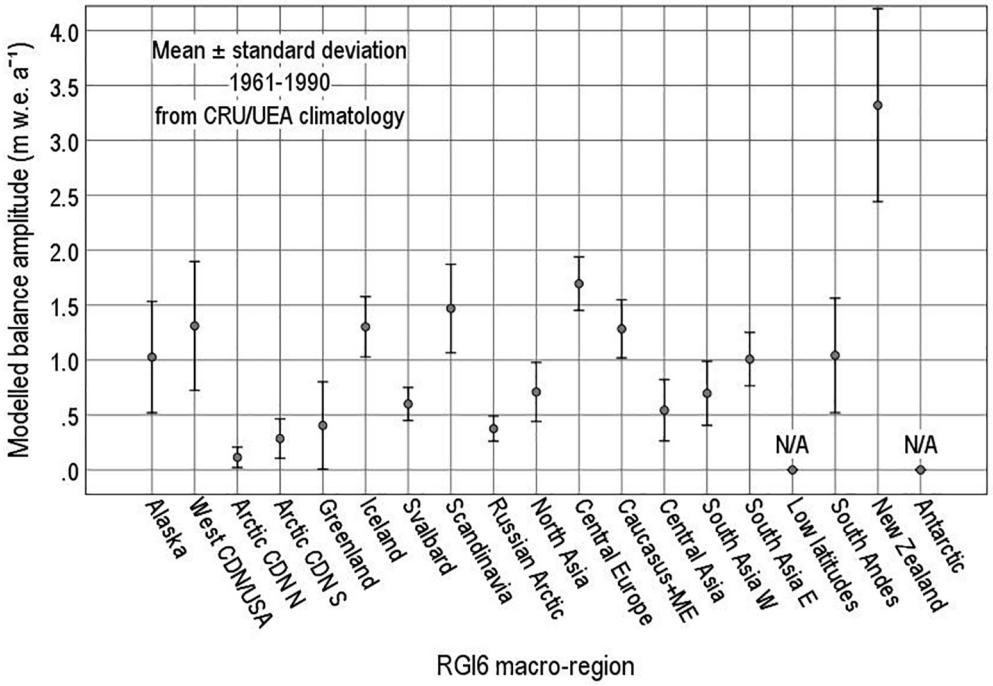

FIGURE 10 | Modelled balance amplitude for 17 macro-regions in the Randolph Glacier Inventory (RGI Consortium, 2017).

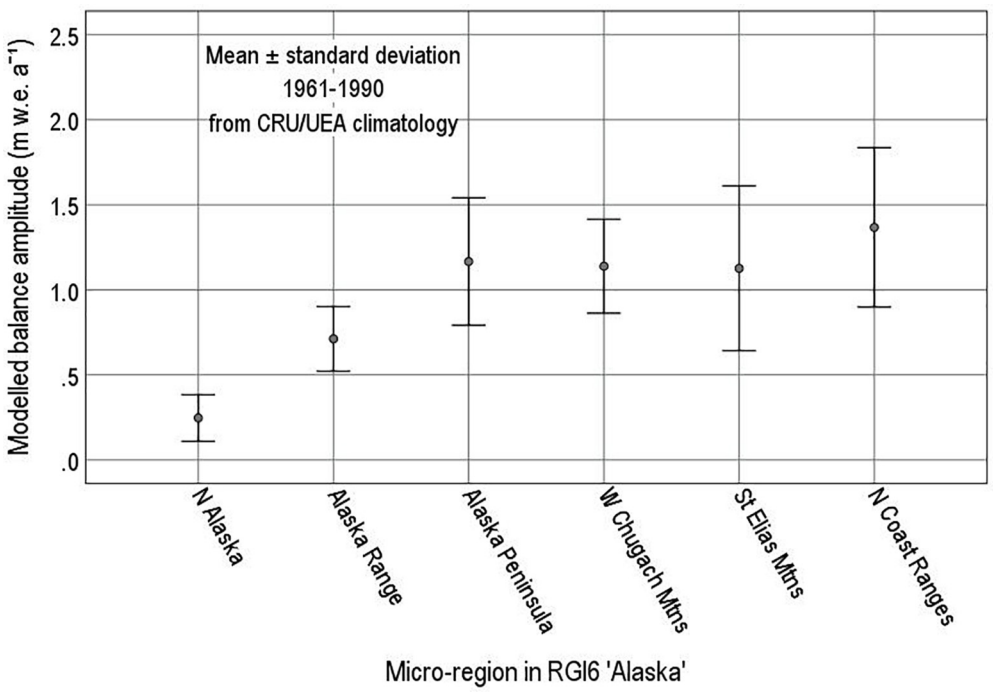

FIGURE 11 | Modelled balance amplitude for six micro-regions in the Randolph Glacier Inventory (RGI Consortium, 2017) for macro-region "Alaska."

CONCLUSION

Interannual variability of mass balance is proportional to the seasonal variability as expressed by the balance amplitude. In turn, balance amplitude depends on precipitation and summer temperature with lower amplitude for cold/dry glaciers and higher amplitude for warm/wet glaciers. Directly measured mass balance is biased to glaciers with generally higher precipitation than typical for the global average. Extrapolation of balance amplitude data to 17 macro-regions in the Randolph Glacier Inventory avoids this precipitation bias and shows substantial differences between different regions with generally low balance amplitude for Arctic Islands and very high amplitude for New Zealand.

DATA AVAILABILITY STATEMENT

The datasets generated for this study are available on request to the corresponding author.

AUTHOR CONTRIBUTIONS

RB and PH shared conception and design of the study. RB organised the database and performed the statistical analyses. Both authors contributed to the article and approved the submitted version.

ACKNOWLEDGMENTS

Interaction with the responsible editor (MZ) and two referees has greatly improved this manuscript. The University of Manchester has supported RB with an Honorary Research Fellowship since 2010. Many individual scientists and organisations collected the data used in this study and made them available to the international community through the archives of the World Glacier Monitoring Service (WGMS) in Zürich, Switzerland. Such openness and generosity with hard-won data are in the highest traditions of science. The staff of the WGMS have been energetic champions of mass balance study over several decades.

SUPPLEMENTARY MATERIAL

The Supplementary Material for this article can be found online at: https://www.frontiersin.org/articles/10.3389/feart.2020.00302/full#supplementary-material

REFERENCES

Ageta, Y. (1998). "Glaciers and the water cycle," in *Snow and Ice Science in Hydrology, the IHP Training Course on Snow Hydrology*, eds M. Nakawo, H. Hayakawa, and L. E. Goodrich (Nagoya: Nagoya University COOP).

Ahlmann, H. W. (1924). Le niveau de glaciation comme fonction de l'accumulation d'humidité sous forme solide. Méthode pour le calcul de l'humidité condensée dans la haute montagne et pour l'étude de la fréquence des glaciers. *Geogr. Ann.* 6, 223–272. doi: 10.1080/20014422.1924.11881098

Ahlmann, H. W. (1948). *Glaciological Research on the North Atlantic Coasts*. London: Royal Geographical Society.

Ananicheva, M. D., and Krenke, A. N. (2005). Evolution of climatic snowline and equilibrium line altitudes in the north– eastern Siberia Mountains (20th century). *Ice Clim. News* 6, 3–6.

Andreassen, L. M., Elvehøy, H., Kjøllmoen, B., and Engeset, R. V. (2016). Reanalysis of long– term series of glaciological and geodetic mass balance for 10 Norwegian glaciers. *Cryosphere* 10, 535–552. doi: 10.5194/tc-10-535-2016

Anonymous (1969). Mass balance terms. *J. Glaciol.* 52, 3–7. doi: 10.3189/s0022143000020736

Bamber, J., Westaway, R., Marzeion, B., and Wouters, B. (2018). The land ice contribution to sea level during the satellite era. *Environ. Res. Lett.* 13, 1–21. doi: 10.1088/1748-9326/aac2f0

Bolch, T., Buchroithner, M., Pieczonka, T., and Kunert, A. (2008). Planimetric and volumetric glacier changes in the Khumbu Himal, Nepal, since 1962 using Corona, Landsat TM and ASTER data. *J. Glaciol.* 54, 592–600. doi: 10.3189/002214308786570782

Braithwaite, R. J. (1982). A simple model of runoff from ungauged basins in West Greenland. *Rapport Grønlands Geol. Undersøgelse* 111, 1–26.

Braithwaite, R. J. (2005). Mass balance characteristics of arctic glaciers. *Ann. Glaciol.* 42, 225–229. doi: 10.3189/172756405781812899

Braithwaite, R. J. (2008). Temperature and precipitation climate at the equilibrium– line altitude of glaciers expressed by the degree–day factor for melting snow. *J. Glaciol.* 54, 437-444. doi: 10.3189/00221430878583 6968

Braithwaite, R. J. (2015). From Doktor Kurowski's Schneegrenze to our modern glacier equilibrium line altitude (ELA). *Cryosphere* 9, 2135–2148. doi: 10.5194/tc-9-2135-2015

Braithwaite, R. J., and Zhang, Y. (1999a). Modelling changes in glacier mass balance that might occur as a result of climate changes. *Geogr. Ann.* 81A, 489–496. doi: 10.1111/j.0435-3676.1999.00078.x

Braithwaite, R. J., and Zhang, Y. (1999b). Relationship between interannual variability of glacier mass balance and climate. *J. Glaciol.* 45, 456–462. doi: 10.3189/S0022143000001313

Braithwaite, R. J., Zhang, Y., and Raper, S. C. B. (2002). Temperature sensitivity of the mass balance of mountain glaciers and ice caps as a climatological characteristic. *Zeitschrift Gletscherkunde Glazialgeol.* 38, 35–61.

Chen, J., and Martin, F. (1990). Mass Balance of Rhonegletscher during 1882/83–1986/87. *J. Glaciol.* 36, 199–209. doi: 10.1017/s0022143000009448

COD (1981). *Concise Oxford Dictionary of Current English*, 6th Edn. Oxford: Oxford University Press.

Cogley, J. G. (2009). Geodetic and direct mass-balance measurements: comparison and joint analysis. *Ann Glaciol.* 50, 96–100. doi: 10.3189/172756409787769744

Cogley, J. G., and Adams, W. P. (1998). Mass balance of glaciers other than the ice sheets. *J. Glaciol.* 44, 315–325. doi: 10.3189/S0022143000002641

Cogley, J. G., Hock, R., Rasmussen, L. A., Arendt, A. A., Bauder, A., Braithwaite, R. J., et al. (2011). *Glossary of Glacier Mass Balance Terms and Related Terms (IHP– VII Technical Documents in Hydrology No. 86, IACS Contribution No. 2)*. Paris: UNESCO–International Hydrological Programme.

De Woul, M. (2008). *Response of Glaciers to Climate Change: Mass Balance Sensitivity, Sea Level Rise and Runoff*. Ph.D.Thesis, Stockholm University, Stockholm.

Dyurgerov, M. B., and Meier, M. F. (1997). Mass balance of mountain and subpolar glaciers: a new global assessment for 1961– 1990. *Arctic Alpine Res.* 29, 379–391. doi: 10.2307/1551986

Dyurgerov, M. B., and Meier, M. F. (2005). *Glaciers and the Changing Earth System: A 2004 Snapshot. Report INSTAAR/OP-58*. Boulder, CL: University of Colorado.

Gardner, A. S., Moholdt, G., Cogley, J. G., Wouters, B., Arendt, A. A., Wahr, J., et al. (2013). A reconciled estimate of glacier contributions to sea level rise: 2003 to 2009. *Science* 340, 852–885. doi: 10.1126/science.1234532

Haeberli, W., Hoelzle, M., Paul, F., and Zemp, M. (2007). Integrated monitoring of mountain glaciers as key indicators of global climate change: the European Alps. *Ann. Glaciol.* 46, 150–160. doi: 10.3189/172756407782871512

Hughes, P. D. (2007). Recent behaviour of the Debeli Namet glacier, Dumitor, Montenegro. *Earth Surf. Process. Landforms* 10, 1593–1602. doi: 10.1002/esp.1537

Hughes, P. D. (2009). Twenty–first Century glaciers in the Prokletje Mountains, Albania. *Arctic Antarctic Alpine Res.* 41, 455–459. doi: 10.1657/1938-4246-41.4.455

Hughes, P. D., and Braithwaite, R. J. (2008). Application of a degree–day model to reconstruct Pleistocene glacial conditions. *Quat. Res.* 69, 110–116. doi: 10.1016/j.yqres.2007.10.008

Hughes, P. D., Fink, D., Rodés, Á, Fenton, C. R., and Fujioka, T. (2018). 10Be and 36Cl exposure ages and palaeoclimatic significance of glaciations in the High Atlas, Morocco. *Quat. Sci. Rev.* 180, 193–213. doi: 10.1016/j.quascirev.2017.11.015

Hughes, P. D., Fletcher, W. J., Bell, B. A., Braithwaite, R. J., Cornelissen, H. L., Fink, D., et al. (2020). Late Pleistocene glaciers to present-day snowpatches: a review and research recommendations for the Marrakech High Atlas. *Mediter. Geosci. Rev.* 2, 163–184. doi: 10.1007/s42990-020-00027-4

Huss, M., Bauder, A., Funk, M., and Hock, R. (2008). Determination of the seasonal mass balance of four Alpine glaciers since 1865. *J. Geophys. Res.* 113:F01015. doi: 10.1029/2007JF000803

Jania, J., and Hagen, J. O. (eds) (1996). *Mass Balance of Arctic Glaciers. International Arctic Science Committee (IASC) Report 5*. Washington, DC: USGCRP.

Kaser, G., Cogley, J. G., Dyurgerov, M. B., Meier, M. F., and Ohmura, A. (2006). Mass balance of glaciers and ice caps: consensus estimates for 1961–2004. *Geophys. Res. Lett.* 33:L195011.

Kaser, G., Fountain, A. G., and Jansson, P. (2003). *A Manual for Monitoring the Mass Balance of Mountain Glaciers. Technical Documents in Hydrology 59*. Paris: UNESCO.

Kaser, G., and Georges, C. (1999). On the mass balance of low latitude glaciers with particular consideration of the Peruvian Cordillera Blanca. *Geogr. Ann.* 81A, 643–652.

Kjøllmoen, B., Andreassen, L. M., Elvehøy, H., and Jackson, M. (2019). *Glaciological investigations in Norway 2018. Rapport 46–2019*. Oslo: Norwegian Water Resources and Energy Directorate (NVE).

Krenke, A. N. (1975). Climatic conditions of present– day glaciation in Soviet Central Asia. *IAHS AISH Publ.* 104, 30–41.

Manley, G. (1971). Scotland's semi–permanent snows. *Weather* 26, 458–471. doi: 10.1002/j.1477-8696.1971.tb04145.x

Meier, M. F. (1984). Contributions of small glaciers to global sea level. *Science* 226, 1419-1421. doi: 10.1126/science.226.4681.1418

Meier, M. F. (1993). "Ice, climate, and sea level: do we know what is happening?," in *Ice in the Climate System*, ed. W. R. Peltier (Berlin and Heidelberg: Springer–Verlag).

Mercanton, P. L. (ed.) (1916). *Vermessungen am Rhonegletscher/Mensuration au glacier du Rhône: 1874–1915*. Zürich: Zücher and Furrer.

New, M., Hulme, M., and Jones, P. (1999). Representing twentieth century space–time climatic variability. I. Development of a 1961– 1990 mean monthly climatology. *J. Clim.* 12, 829-856. doi: 10.1175/1520-04421999012(0829:RTCSTC(2.0.CO;2

Oerlemans, J., and Fortuin, J. P. F. (1992). Sensitivity of glaciers and small ice caps to Greenhouse warming. *Nature* 258, 115–117. doi: 10.1126/science.258.5079.115

Ohmura, A., and Boettcher, M. (2018). Climate on the equilibrium line altitudes of glaciers: theoretical background behind Ahlmann's P/T diagram. *J. Glaciol.* 64, 489–505. doi: 10.1017/jog.2018.41

Ohmura, A., Kasser, P., and Funk, M. (1992). Climate at the equilibrium line of glaciers. *J. Glaciol.* 38, 397–411. doi: 10.3189/S0022143000002276

Østrem, G., and Brugman, M. (1991). *Glacier Mass Balance Measurements: A Manual of Field and Office Work*. Saskatoon: National Hydrology Research Institute.

Østrem, G., and Stanley, A. (1969). *Glacier Mass Balance Measurements: A Manual for Field and Office Work*. Ottawa: The Canadian Department of Energy.

Paterson, W. S. B. (1994). *The Physics of Glaciers*, 3rd Edn. Oxford: Pergamon.

Pfeffer, W. T., Arendt, A. A., Bliss, A., Bolch, T., Cogley, J. G., Gardner, A. S., et al. (2014). The Randolph Glacier Inventory: a globally complete inventory of glaciers. *J. Glaciol.* 60, 537–552. doi: 10.3189/2014JoG13J176

Rea, B. R. (2009). Defining modern day Area– Altitude Balance Ratios (AABRs) and their use in glacier– climate reconstructions. *Quat. Sci. Rev.* 28, 237–248. doi: 10.1016/j.quascirev.2008.10.011

RGI Consortium (2017). *Randolph Glacier Inventory (v.6.0): A Dataset of Global Glacier Outlines*. Boulder, CL: Global Land Ice Measurements from Space, doi: 10.7265/N5-RGI-60

Schytt, V. (1962). Mass balance studies in Kebnekasje. *J. Glaciol.* 33, 281–289.

Voloshina, A. P. (1988). Some results of glacier mass balance research on the glaciers of the Polar Urals. *Polar Geogr. Geol.* 12, 200–211. doi: 10.1080/10889378809377364

von Hahn, J. (1903). *Handbook of Climatology: Part I. General Climatology*. New York, NY: Macmillan.

WGMS (2019). *Fluctuations of Glaciers Database*. Zurich: World Glacier Monitoring Service, doi: 10.5904/wgms-fog-2019-12

Wouters, B., Bonin, J. A., Chambers, D. P., Riva, R. E. M., Sagen, I., and Wahr, J. (2014). GRACE, time–varying gravity, Earth system dynamics and climate change. *Report Progr. Phys.* 77:116801. doi: 10.1088/0034-4885/77/11/116801

Yevjevich, V. (1972). *Probability and Statistics in Hydrology*. Fort Collins, CL: Water Resources Publications.

Zemp, M., Thibert, E., Huss, M., Stumm, D., Denby, C. R., Nuth, C., et al. (2013). Reanalysing glacier mass balance measurement series. *Cryosphere* 7, 1227–1245. doi: 10.5194/tc-7-1227-2013

Zemp, M., Frey, H., Gärtner-Roer, I., Nussbaumer, S., Hoelzle, M., Paul, F., et al. (2015). Historically unprecedented global glacier decline in the early 21st century. *J. Glaciol.* 61, 745–762. doi: 10.3189/2015JoG15J017

Zemp, M., Huss, M., Thibert, E., Eckert, N., McNabb, R., Huber, J., et al. (2019). Global glacier mass changes and their contributions to sea level rise from 1961 to 2016. *Nature* 568:2019. doi: 10.1038/s41586-019-1071-0

Zemp, M., Hoelzle, M., and Haeberli, W. (2007). Distributed modelling of the regional climatic equilibrium line altitude of glaciers in the European Alps. *Global Planet. Change* 56, 83-100. doi: 10.1016/j.gloplacha.2006.07.002

Conflict of Interest: The authors declare that the research was conducted in the absence of any commercial or financial relationships that could be construed as a potential conflict of interest.

frontiers in Earth Science

ORIGINAL RESEARCH
published: 26 November 2020
doi: 10.3389/feart.2020.523646

Glacier Changes in Iceland From ~1890 to 2019

Guðfinna Aðalgeirsdóttir[1], Eyjólfur Magnússon[1], Finnur Pálsson[1], Thorsteinn Thorsteinsson[2], Joaquín M. C. Belart[1,3,4], Tómas Jóhannesson[2], Hrafnhildur Hannesdóttir[2], Oddur Sigurðsson[2], Andri Gunnarsson[5], Bergur Einarsson[2], Etienne Berthier[6], Louise Steffensen Schmidt[1,6], Hannes H. Haraldsson[5] and Helgi Björnsson[1]*

[1]Institute of Earth Sciences, University of Iceland, Reykjavík, Iceland, [2]Icelandic Meteorological Office, Reykjavík, Iceland, [3]National Land Survey of Iceland, Akranes, Iceland, [4]Laboratoire d'Etudes en Géophysique et Océanographie Spatiales, Université de Toulouse, CNRS, Toulouse, France, [5]National Power Company of Iceland, Reykjavík, Iceland, [6]Department of Geosciences, University of Oslo, Oslo, Norway

OPEN ACCESS

Edited by:
Michael Zemp, University of Zurich, Switzerland

Reviewed by:
Tom Holt, Aberystwyth University, United Kingdom
Jon Ove Methlie Hagen, University of Oslo, Norway

***Correspondence:**
Guðfinna Aðalgeirsdóttir
gua@hi.is

Specialty section:
This article was submitted to Cryospheric Sciences, a section of the journal Frontiers in Earth Science

Received: *30 December 2019*
Accepted: *13 October 2020*
Published: *26 November 2020*

Citation:
Aðalgeirsdóttir G, Magnússon E, Pálsson F, Thorsteinsson T, Belart JMC, Jóhannesson T, Hannesdóttir H, Sigurðsson O, Gunnarsson A, Einarsson B, Berthier E, Schmidt LS, Haraldsson HH and Björnsson H (2020) Glacier Changes in Iceland From ~1890 to 2019. Front. Earth Sci. 8:523646. doi: 10.3389/feart.2020.523646

The volume of glaciers in Iceland (~3,400 km^3 in 2019) corresponds to about 9 mm of potential global sea level rise. In this study, observations from 98.7% of glacier covered areas in Iceland (in 2019) are used to construct a record of mass change of Icelandic glaciers since the end of the 19th century i.e. the end of the Little Ice Age (LIA) in Iceland. Glaciological (*in situ*) mass-balance measurements have been conducted on Vatnajökull, Langjökull, and Hofsjökull since the glaciological years 1991/92, 1996/97, and 1987/88, respectively. Geodetic mass balance for multiple glaciers and many periods has been estimated from reconstructed surface maps, published maps, aerial photographs, declassified spy satellite images, modern satellite stereo imagery, and airborne lidar. To estimate the maximum glacier volume at the end of the LIA, a volume–area scaling method is used based on the observed area and volume from the three largest ice caps (over 90% of total ice mass) at 5–7 different times each, in total 19 points. The combined record shows a total mass change of −540 ± 130 Gt (−4.2 ± 1.0 Gt a^{-1} on average) during the study period (1890/91 to 2018/19). This mass loss corresponds to 1.50 ± 0.36 mm sea level equivalent or 16 ± 4% of mass stored in Icelandic glaciers around 1890. Almost half of the total mass change occurred in 1994/95 to 2018/19, or −240 ± 20 Gt (−9.6 ± 0.8 Gt a^{-1} on average), with most rapid loss in 1994/95 to 2009/10 (mass change rate −11.6 ± 0.8 Gt a^{-1}). During the relatively warm period 1930/31–1949/50, mass loss rates were probably close to those observed since 1994, and in the colder period 1980/81–1993/94, the glaciers gained mass at a rate of 1.5 ± 1.0 Gt a^{-1}. For other periods of this study, the glaciers were either close to equilibrium or experienced mild loss rates. For the periods of AR6 IPCC, the mass change rates are −3.1 ± 1.1 Gt a^{-1} for 1900/01–1989/90, −4.3 ± 1.0 Gt a^{-1} for 1970/71–2017/18, −8.3 ± 0.8 Gt a^{-1} for 1992/93–2017/18, and −7.6 ± 0.8 Gt a^{-1} for 2005/06–2017/18.

Keywords: mass balance, glaciers, climate, Iceland, glacier–climate relationship

1. INTRODUCTION

Glaciers in most areas of the world are losing mass as global temperatures rise in response to increased greenhouse gas concentrations in the atmosphere (e.g., Vaughan et al., 2013; Hock et al., 2019; Meredith et al., 2019; Zemp et al., 2019). *In situ* mass-balance observations are sparse (e.g., Zemp et al., 2020a), but with the aid of satellite and other remote-sensing data, an increasingly clear picture of glacier mass loss around the world has been appearing (e.g., Brun et al., 2017; Wouters et al., 2019; Morris et al., 2020; Shean et al., 2020). Glacier mass loss is a global phenomenon, and the rates in the early 21st century are unprecedented for the observed period (Zemp et al., 2015). Reconstructions of glacier mass-change rates for the 20th century and the first decade of the 21st century show substantial temporal and spatial variations, but a global mass loss trend became clear toward the end of the 20th century (Leclercq et al., 2011; Marzeion et al., 2015; Marzeion et al., 2012).

Iceland is located in a region of maritime climate in the middle of the North Atlantic Ocean with relatively cool summers, mild winters, and high precipitation. Glaciers in Iceland are all temperate and cover about 10% of the area of the country (Björnsson and Pálsson, 2008), with the largest ice cap Vatnajökull (~7,700 km^2, ~2,870 km^3, in the year 2019) located near the southeast coast, two smaller ice caps Langjökull (~835 km^2, ~171 km^3, in the year 2019) and Hofsjökull (~810 km^2, ~170 km^3, in the year 2019) in the central highlands [area estimates are from Hannesdóttir et al. (2020) and volumes are calculated in this study], and Mýrdalsjökull [~598 km^2, ~140 km^3, in the year 1991 (Björnsson et al., 2000)], near the southern coast. Seven additional glaciers in Iceland are larger than 10 km^2, and there are presently around 250 smaller glaciers, many of them in the central north highlands (Tröllaskagi (Trö) in **Figure 1**). The inventory of Icelandic glaciers made around the year 2000 includes about 300 glaciers (Sigurðsson and Williams, 2008). An update of this inventory in 2017 showed that some tens of those had disappeared or were categorized as dead ice (Sigurðsson et al., 2017). Several glaciers had, during their retreat, split into two or more separate glaciers or ice patches. The area loss since the end of the Little Ice Age (LIA) is ~2,200 km^2 and ~750 km^2 since the year 2000, or about 40 km^2 (or 0.4%) per year (Hannesdóttir et al., 2020).

Glaciers in Iceland have received much attention through the centuries due to their proximity to inhabited regions (**Figure 1**). The retreat of many glacier tongues was noticed in the early 20th century and in 1930 a country-wide voluntary monitoring program was initiated (Eyþórsson, 1963; Sigurðsson, 2005). This program was later continued by the Icelandic Glaciological Society (founded in 1950) and continues to this day (Björnsson, 2017; Hannesdóttir et al., 2020). Thirty to forty terminus positions are measured annually and the observations are posted on the website spordakost.jorfi.is. The surface and bedrock topographies of the largest ice caps have been measured in radio-echo sounding campaigns carried out since 1977. Radio-echo sounding on the temperate ice caps in Iceland required a much longer electromagnetic wavelength than had been used on the cold polar ice caps (Björnsson and Pálsson, 2020). The pioneering measurements resulted in a good knowledge of the subglacial topography of the ice caps and their total volume

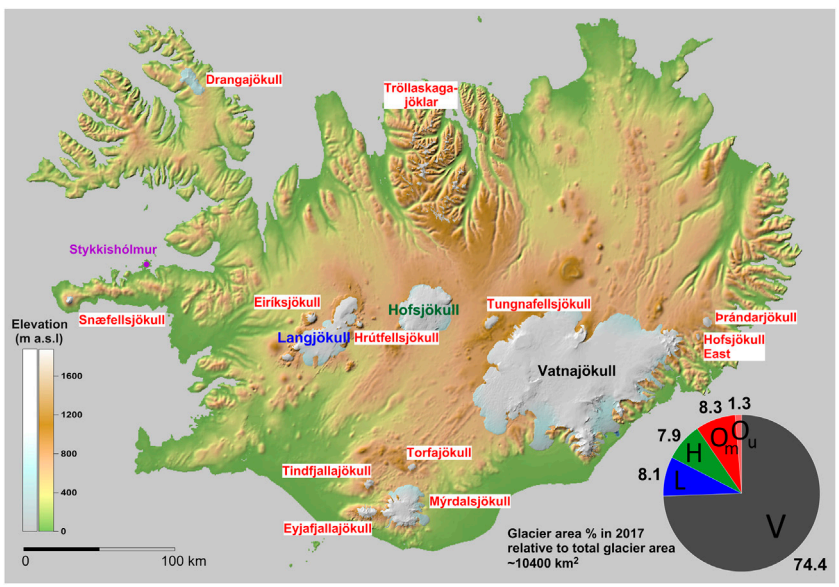

FIGURE 1 | Map of Iceland showing the glaciers considered in this study. The pie chart in the bottom right corner shows the relative sizes of the glaciers in 2017 (Hannesdóttir et al., 2020) in percentage; Vatnajökull (V), Langjökull (L), Hofsjökull (H), and the smaller glaciers grouped as O_m in pie chart: Drangajökull, Snæfellsjökull, Eyjafjallajökull, Tindfjallajökull, Torfajökull, Mýrdalsjökull, Þrándarjökull, Hofsjökull eystri, Tungnafellsjökull, Hrútfellsjökull, Eiríksjökull and Barkárdals- and Tungnahryggsjökull, considered as one glacier unit on Tröllaskagi. Unmeasured glaciers (O_u) corresponded to ~1.3% of the total area in 2019 (Hannesdóttir et al., 2020). The town Stykkishólmur is shown with a purple dot, from which a temperature record exists since the middle of the 19th century.

(Björnsson, 1986; Björnsson, 2017; Björnsson and Pálsson, 2020). Lidar measurements of the glacier surfaces were conducted in the period 2008–2013 (Jóhannesson et al., 2013). Annual glaciological mass-balance measurements started on Hofsjökull in the glaciological year 1987/88 (Thorsteinsson et al., 2017), in 1991/92 on Vatnajökull, and 1996/97 on Langjökull (Björnsson et al., 1998; Björnsson et al., 2002). Since 2001, mass-balance measurements have also been carried out on an irregular basis on Mýrdalsjökull (Ágústsson et al., 2013). Geodetic mass balance has been estimated for several glaciers, with an increasing coverage in recent years (Pálsson et al., 2012; Jóhannesson et al., 2013; Hannesdóttir et al., 2015a; Magnússon et al., 2016; Belart et al., 2019; Belart et al., 2020). Mass changes of the Icelandic glaciers have, furthermore, been estimated using ICESat (Nilsson et al., 2015), CryoSat2 (Foresta et al., 2016), and the GRACE satellites (von Hippel and Harig, 2019; Wouters et al., 2019; Ciracì et al., 2020), and Sørensen et al. (2017) showed that signal leakage due to mass changes of the neighboring Greenland Ice Sheet and the effect of glacial isostatic rebound need to be carefully taken into account.

Mass loss from Icelandic glaciers in the years 1994/5–2009/10 was reported as $9.5 \pm 1.5\,\mathrm{Gt\,a^{-1}}$ with a large interannual variability (Björnsson et al., 2013). In this article, we present an updated and extended record for the hydrological years 1890/91 to 2018/19. The main objective was to derive an estimate for the mass-change history of Icelandic glaciers for the 20th century and the first two decades of the 21st century. All recent studies and measurements with various methods are compiled and combined; a new estimate of the ~1890 volumes of the three largest ice caps is made using new data on their area at that time (Hannesdóttir et al., 2020) and volume–area scaling (Bahr et al., 2015), and the recently established non-surface mass balance of Icelandic glaciers, that takes into account energy dissipation caused by the flow of water and ice, geothermal melting, volcanic eruptions, and calving (Jóhannesson et al., 2020), is included to improve the estimate of the mass-balance history of all glaciers in Iceland since the end of the LIA.

2. METHODS AND DATA

The time steps in this study correspond to the glaciological year (Cogley et al., 2011) from autumn to autumn, using the floating-date mass-balance system (Østrem and Brugman, 1991; Björnsson et al., 2002; Cogley et al., 2011), that is, the end of the summer melt season marks the start of a new glaciological year. To construct the mass-balance history of Icelandic glaciers back to the year 1890/91 [assumed here to be the end of the LIA in Iceland (Thorarinsson, 1943; Sigurðsson, 2005)], we compile and combine different data sets and methods. These include the following:

(1) Record of the annual surface mass balance obtained with the glaciological method for the three largest ice caps, Vatnajökull (glaciological years 1991/92 to 2018/19), Hofsjökull (1987/88 to 2018/19), and Langjökull (1996/97 to 2018/19). The data records are shown in **Figures 2** and **3A,B,C**.

(2) Simulation of the surface mass balance of Vatnajökull for the years 1980/81 to 1991/92 from the HIRHAM5 snowpack model that uses MODIS albedo (Schmidt et al., 2017) and is forced with a ERA-Interim downscaling using the HARMONIE–AROME model at 2.5 km resolution (Schmidt et al., 2019) (see shaded area in **Figure 3A**). Data from automatic weather stations and glaciological surface mass balance, and runoff measurements were used to constrain the model (Schmidt et al., 2018).

(3) The non-surface mass-balance estimates from Jóhannesson et al. (2020) are taken into account and added to the glaciological and modeled surface mass balance listed above.

(4) Zero annual mass balance for Vatnajökull for the period 1970/71 to 1979/80 and for Hofsjökull from 1970/71 to 1986/87 is assumed (green boxes in **Figures 3A,B**). This is supported by the small area changes during these periods (Hannesdóttir et al., 2020), the relatively cold weather conditions (**Figure 3E**), the observations of limited terminus length changes (spordakost.jorfi.is), and the near–zero geodetic mass balances of several of the smaller glaciers in these periods (**Figure 3D**).

(5) Geodetic mass-balance records for Langjökull (Pálsson et al., 2012), from 1937/38 to 1996/97 (red lines with uncertainties in **Figure 3B**) and 12 smaller glaciers (**Figure 3D**) from 1945/46 to 2016/17 (Belart et al., 2020) that cover 8.3% of the glacier area in Iceland. The remaining 1.3% of glacier area that is not observed is assumed to have the same mass loss rate as the measured small glaciers. The geodetic results were also used to scale (Jóhannesson et al., 2013) and validate (Pálsson et al., 2012) the glaciological measurements.

(6) Estimates of the volumes of Vatnajökull and Hofsjökull in 1890 and 1945 as well as the volume of Langjökull in 1890 based on the volume–area scaling (Bahr et al., 1997; Bahr et al., 2015) (**Figure 4**). The glacier areas are derived from Hannesdóttir et al. (2020); we describe the method below and the resulting mass change rates calculated from the area and volume changes are shown with purple boxes in **Figures 3A,B,C**.

(7) To include an estimate of mass change for other glaciers than Vatnajökull, Langjökull, and Hofsjökull in the periods 1890/91–1944/45 and 2017/18–2018/19, the net mass change of those three is multiplied by $F = 1.130$, which is the ratio between mass change of all glaciers in Iceland in 1945/46–2016/17 and the mass change of the three large ice caps in the same period. Values for the ratio F are specifically calculated for the periods 1994/95–2003/04, 2004/5–2009/10, and 2010/11–2016/17 (1.176, 1.131, and 1.056, respectively), corresponding to the geodetic mass-balance periods of Belart et al. (2020). After 1994/95, an estimate of the annual variability of the mass change for other glaciers than the three largest is included by calculating the net mass change for each glaciological year, using the corresponding F value for each period. The net mass change during these periods, which is obtained with the geodetic method, is not altered by this.

The above records were combined to calculate the mass balance of all Icelandic glaciers from 1890/91 to 2018/19. The cumulative mass change of all the glaciers for each period was computed as the sum of the total mass balance of the all glaciers (the product of the specific mass balance and the time-dependent glacier area). Below we discuss i) how the surface mass balance from the glaciological method is combined with the non-surface mass-balance estimates, ii) the application of the volume–area scaling to estimate past volumes of the three largest ice caps, and iii) the uncertainty of the obtained total mass balance of the Icelandic glaciers.

2.1. Combining the Surface and Non-Surface Mass-Balance Records

The surface mass balance from the glaciological method is obtained by measuring the snow water equivalent (w.e.) thickness of the snowpack above last summer's surface in spring, and the summer ablation at the end of the summer melt season at ~60 survey sites on Vatnajökull and ~25 survey sites on Hofsjökull and Langjökull. These measurements, together with the HIRHAM5 snowpack model simulations, yield a detailed record of the winter, summer, and annual surface mass balance during the last three to four decades for these ice caps (**Figure 2**), constituting ~90% of the glacier area in Iceland. These records show rather large annual variability and the exceptional effect of the 2010 eruption in Eyjafjallajökull, which doubled the summer melt due to the deposition of volcanic tephra on the surface of the ice caps (Björnsson et al., 2013).

The non-surface mass balance is known to be a non-negligible component of the mass balance of glaciers in Iceland (e.g., Björnsson et al., 2013) but has so far not been included in mass-balance estimates. The previously published mass-balance record for the Icelandic glaciers has now been revised by including this component. The non-surface melting of glaciers in Iceland for the period 1995–2019 estimated by Jóhannesson et al. (2020) includes geothermal melting, energy dissipation caused by the flow of water and ice, volcanic eruptions, and calving.

For Hofsjökull and Langjökull, the non-surface mass balance due to volcanic eruptions and calving is negligible, but not for Vatnajökull. Rather than including the ice melt (~3.7 Gt) due to the Gjálp eruption in October 1996 (Guðmundsson et al., 2004), in the average rate over the period (1995/95–2018/19), it is subtracted and then added to the glaciological year 1996/97. This reduces the average mass balance due to geothermal melting and volcanic eruptions on Vatnajökull presented by Jóhannesson et al. (2020) from -0.075 m w.e. a^{-1} to -0.055 m w. e. a^{-1}. The mass loss due to energy dissipation in Vatnajökull, caused by the flow of water and ice as estimated by Jóhannesson et al. (2020), is assumed constant for the whole period: -0.085 m w.e. a^{-1}.

Mass loss due to calving is negligible for all outlets except for Breiðamerkurjökull on the south side of Vatnajökull, which calves into the terminal lake Jökulsárlón. We apply a variable calving rate as described by Jóhannesson et al. (2020) for the years 1996/97–2016/17, resulting in an average of -0.056 m w.e. a^{-1}. For the periods without observations, we assume a calving rate that changes linearly from 0 in 1950/51 [start of significant calving (Björnsson et al., 2001)] to -0.029 m w.e. a^{-1} in 1996/97 and use -0.067 m w.e. a^{-1} (value in 2016/17) for the last two years of the record.

The average non-surface mass-balance values for Langjökull and Hofsjökull, where calving is insignificant and no eruption has taken place during our study period, are -0.055 m w.e. a^{-1} and -0.067 m w.e. a^{-1}, respectively. In **Figures 3A,B,C**, the non-surface mass-balance estimates have been added to the annual surface mass-balance records.

Comparison of the glaciological surface mass-balance record of Hofsjökull with results from geodetic mass balance, derived by differencing digital elevation models (DEMs), revealed a bias between the two data sets. This bias has been corrected in the surface mass-balance record of Hofsjökull (Jóhannesson et al., 2013; Thorsteinsson et al., 2017) shown in **Figure 2**, taking into account the contribution of the non-surface mass balance.

2.2. Volume–Area Scaling

The volume of a glacier can be obtained by integrating the ice thickness, calculated as the difference between surface and

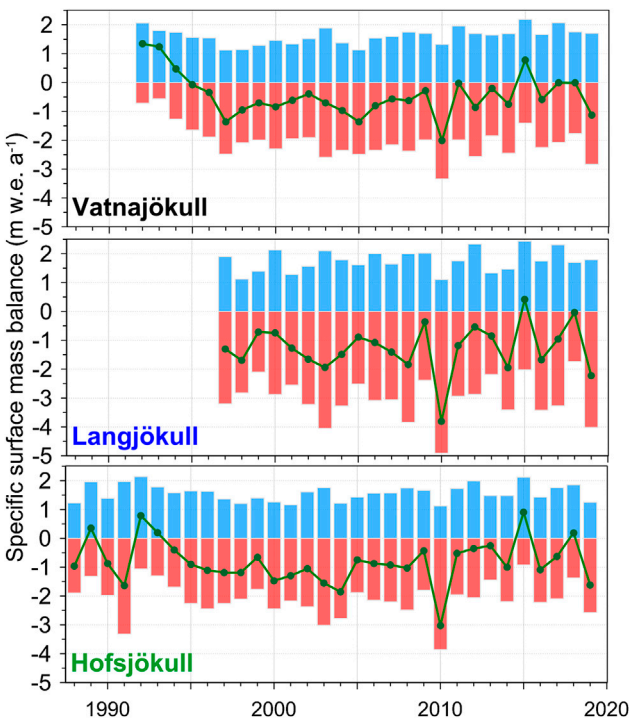

FIGURE 2 | Mean specific surface mass-balance records of the three largest glaciers in Iceland obtained with glaciological method (*in situ* surveys). The mass-balance measurements have been conducted at ~60, ~25, and ~25 locations since 1991/92, 1996/97, and 1987/88 for Vatnajökull, Langjökull, and Hofsjökull, respectively. Measurements by Institute of Earth Sciences, University of Iceland, and the National Power Company of Iceland (Langjökull and Vatnajökull) and the Icelandic Meteorological Office (Hofsjökull).

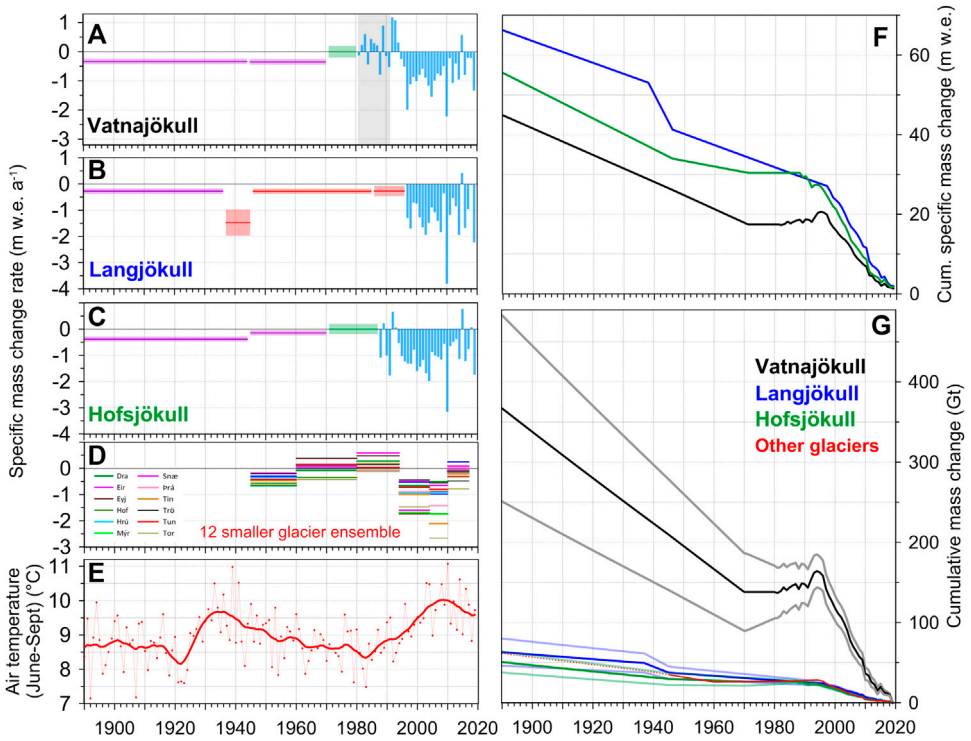

FIGURE 3 | Left: The specific mass balance of glaciers in Iceland as observed, modeled, and estimated with various methods. The gray area in **(A)** indicates a period of modeled surface mass balance for Vatnajökull (Schmidt et al., 2019), green boxes in **(A)** and **(C)** are estimates from various sources (see main text), red boxes in **(B)** and lines in **(D)** are from geodetic mass balance (Pálsson et al., 2012; Belart et al., 2020) (heights of the boxes indicate uncertainty of measurements), and purple boxes in **(A)**, **(B),** and **(C)** show estimated mass loss from volume–area scaling method (see. **Figure 4**). **(E)** The average summer (June through September) temperature at the meteorological station in Stykkishólmur (see **Figure 1** for location); the thick line shows the 11-year running average with triangular weight, a 5-year filter. Right: **(F)** Cumulative specific mass balance (m w.e.) for Vatnajökull (black), Langjökull (blue), and Hofsjökull (green). **(G)** Cumulative mass change (Gt) of the same ice caps and the sum of other glaciers in Iceland assuming that the mass-balance records of the glaciers shown in **(D)** are representative for the unmeasured glaciers. The red dotted line shows the extension of this record for the years 1890/91 to 1944/45 (see **Section 2**). [in **(G)** the mass change of Mýrdalsjökull for the years 1945/46–1959/60, not included in (Belart et al., 2020), is estimated from a linear fit (with R^2 = 0.98) between the mass balance of Mýrdalsjökull and the average mass balance of the neighboring glaciers, Eyjafjallajökull, Torfajökull, and Tindfjallajökull, during the other five periods shown in **(D)**].

bedrock DEMs. Bedrock DEMs for the three largest ice caps have been made from dense radio-echo sounding data (Björnsson and Pálsson, 2020) and are assumed stable over time. Their volumes have been calculated using the following surface DEMs: lidar surface DEM of Hofsjökull from 2008 (Jóhannesson et al., 2013), a SPOT5-HRS (Korona et al., 2009) surface DEM of Vatnajökull from 2010, and a SPOT5 surface DEM of Langjökull from 2004 (Korona et al., 2009; Pálsson et al., 2012). The areal extent at several times for all the glaciers has been estimated based on a data set of glacier outlines (Pálsson et al., 2012; Jóhannesson et al., 2013; Hannesdóttir et al., 2020). Ice-volume estimates at other times can be calculated by multiplying the annual specific mass balance (**Figure 3**) of each glacier by the corresponding glacier area, linearly interpolated with time between dates of area observations, converting the annual mass change into ice volume [assuming the conversion factor 0.85 (Huss, 2013); note that mass-balance records previously published that used conversion factor 0.9 (Pálsson et al., 2012; Jóhannesson et al., 2013) have been adjusted accordingly (Thorsteinsson et al., 2017)] and integrating the volume change relative to the date of the surface DEMs listed above. This calculation gives the area and volume for several times back to 1970 for Hofsjökull and Vatnajökull and to 1937 for Langjökull. The results for the three ice caps for dates of observed areas and corresponding glacier volumes are shown with filled circles on the volume–area scatter plot in **Figure 4**.

Volume–area scaling, as described by Bahr et al. (1997), Bahr et al. (2015), gives an empirical relation between glacier volume (V) and area (A) of the form:

$$V = cA^{\gamma}. \quad (1)$$

This relationship was already applied to estimate the ~1890 volume of Langjökull by Pálsson et al. (2012). Here, we assume that the relationship between area and volume is the same for the three largest glaciers in Iceland, Vatnajökull, Langjökull, and Hofsjökull, which is supported by the linear relationship shown in **Figure 4**. The available area and volume data for all of them are therefore combined to estimate the parameters for the volume–area scaling equation. We subtract the area of debris-covered moraines and dead-ice fields with little surface-elevation change in the GLIMS glacier outlines (Hannesdóttir et al., 2020) (in total 27 km^2 in the year 2019),

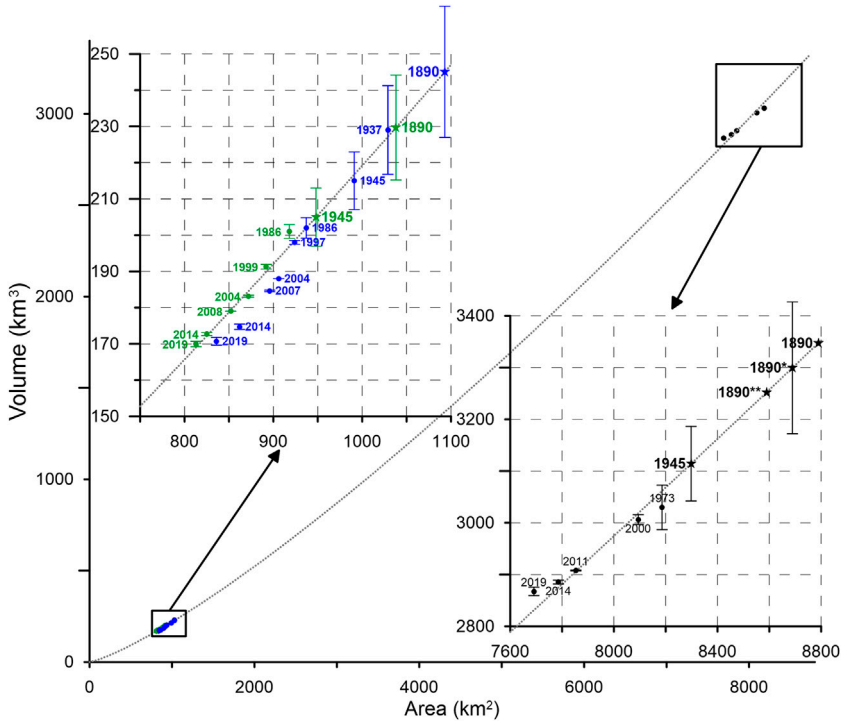

FIGURE 4 | Volume–area scatter plot for the three largest ice caps in Iceland at various times since 1890. The blue markers are for Langjökull, green markers for Hofsjökull, and the black for Vatnajökull. The dotted gray line shows the least square fit of **Eq. 1** through all volume–area points for these ice caps. Inset figures show a zoom in of the plot for the clusters with data from Hofsjökull and Langjökull **(upper left corner)** and Vatnajökull **(lower right corner)**. Labels by the filled circles indicate dates when both area (Hannesdóttir et al., 2020) and volume are well established, while labels beside stars indicate dates of well-known area, with volume estimated from the deduced volume–area relation (dotted gray line). The 1890 values are obtained using area based on geomorphological evidence of the Little Ice Age maximum extent (Hannesdóttir et al., 2020). The 1890* and 1890** for Vatnajökull show the volume estimates with the reduced area to compensate for the large portion of surging outlets from Vatnajökull (see main text).

in order to base our volume–area relationship on the area of the active glacier where substantial ice-thickness changes take place (these debris-covered areas are specified as polygons in our GLIMS data set). Using the least-squares fitting method, we found $c = 0.0379$ and $\gamma = 1.25$; the value of the exponent γ is the same as obtained independently by Bahr et al. (1997) for ice caps.

Volume–area scaling has been widely used to estimate the volume of glaciers with an unknown subglacial topography/ice thickness (e.g., Radić and Hock, 2010), and changes in ice volume associated with variations in glacier extent when multi-temporal DEMs of the glacier surface are not available (e.g., Pálsson et al., 2012). The method is found to be uncertain by tens of per cent, up to even a factor 2–3, for estimating the volume of ice caps with an unknown subglacial topography (Gärtner-Roer et al., 2014), and methods that include information on glacier mass balance and glacier-surface geometry using ice-flow dynamics (Huss and Farinotti, 2012; Farinotti et al., 2019) are preferred for this purpose. Using volume–area scaling to estimate changes in the volume of glaciers with a well-known subglacial topography, from variations in glacier area over decadal time spans, may be expected to be more accurate because this mainly relies on the assumption that the glacier maintains a similar shape as it responds to mass-balance variations with changes in its area and volume. Timescales for redistribution of ice volume to maintain the characteristic shape of a glacier are expected to be much shorter than the response time of the glacier to mass-balance changes (Jóhannesson et al., 1989; Harrison et al., 2001). This approach has its limitations for surge-type glaciers but may be expected to provide reasonable volume-change estimates over long time periods with substantial changes in volume, even for ice caps with many outlet glaciers that may surge at irregular intervals. In case the glacier surface and subglacial topographies are well known at one point in time, the computation of volume changes can be based on an accurate estimate of the glacier volume at that time and the method mainly relies on the assumption that there is a statistical relationship between volume and area changes (see **Figure 4**). Thus, uncertainty about the overall magnitude of the volume of the glacier in question does not affect the accuracy of the estimated volume changes in this case. We note that over the time periods considered in this article, repeated surface mapping and surface reconstructions of the glaciers, where available, have shown elevation changes that are small in the interior of the glacier and amplified toward the ice margin, as expected if the glacier maintains a geometrically similar shape as it adjusts toward a new geometry during variations in the climate (Hannesdóttir et al., 2015b; Thorsteinsson et al., 2017).

The volumes of Hofsjökull and Vatnajökull in 1945 and 1890 and for Langjökull in 1890 were calculated based on the derived fit (shown with stars in **Figure 4**). The area of the glaciers in ~1890 is based on geomorphological evidence of the maximum LIA extent in Iceland (Hannesdóttir et al., 2020). About half of Vatnajökull's glacier margin is substantially affected by surges (Björnsson et al., 2003). The geomorphological evidence indicating the maximum LIA extent in front of these surge-type outlets is due to an advance during a surge that increased the area of the glacier without much effect on the glacier volume. Using this area as input for the volume–area relationship (**Eq. 1**) is likely to result in an overestimate of the glacier volume in ~1890 for two reasons. First, Vatnajökull did not at any one time reach the determined maximum LIA extent because the surges responsible for the geomorphological evidence of maximum extent did not occur simultaneously. Second, right after a surge, the glacier spreads over a larger area than before without any increase in volume, resulting in a thinner glacier with smaller volume than indicated by the volume–area relationship (**Eq. 1**). To take this into account, we reduced the area so it represents the likely ice-cap area when the surge-type outlets are on average near their mid-quiescent-period size. This corresponds to ~500 m retreat from the determined LIA extent of Vatnajökull's surge-type outlets. Most of these advance between a few hundred meters and several kilometers during surges (Björnsson et al., 2003), the average probably being close to 1 km. The volume–area point marked 1890* for Vatnajökull in **Figure 4** includes an area correction that corresponds to a 500 m retreat (area reduction by 100 km^2), and the point marked 1890** includes double this area correction (the point marked 1890 corresponds to data that have not been adjusted to reflect the impact of the surges on the area). The effect of surges on Hofsjökull and Langjökull is much smaller than on Vatnajökull and therefore not taken into account in this study.

From the estimated ~1890 volume for the three ice caps and the 1945 volume for Vatnajökull and Hofsjökull, it is possible to estimate the mean specific mass balance for the periods between the volume estimates. The determined values for mean specific mass balance for two periods for Hofsjökull and Vatnajökull (1890/91 to 1944/45 and 1945/46 to 1969/70) and one period for Langjökull (1890/91 to 1936/37) are shown with purple lines in **Figures 3A,B,C**. They are computed to be the value which, multiplied by glacier area (linearly interpolated in time), converted to ice volumes [again assuming a conversion factor of 0.85 based on Huss (2013)] and summed over the periods, results in the volume determined with the volume–area scaling shown with stars in **Figure 4**.

2.3. Uncertainties of the Presented Mass-Balance Records

It is not straightforward to estimate the uncertainty of the mass-balance estimates derived from the different observations and methods described above. A thorough consideration results in an

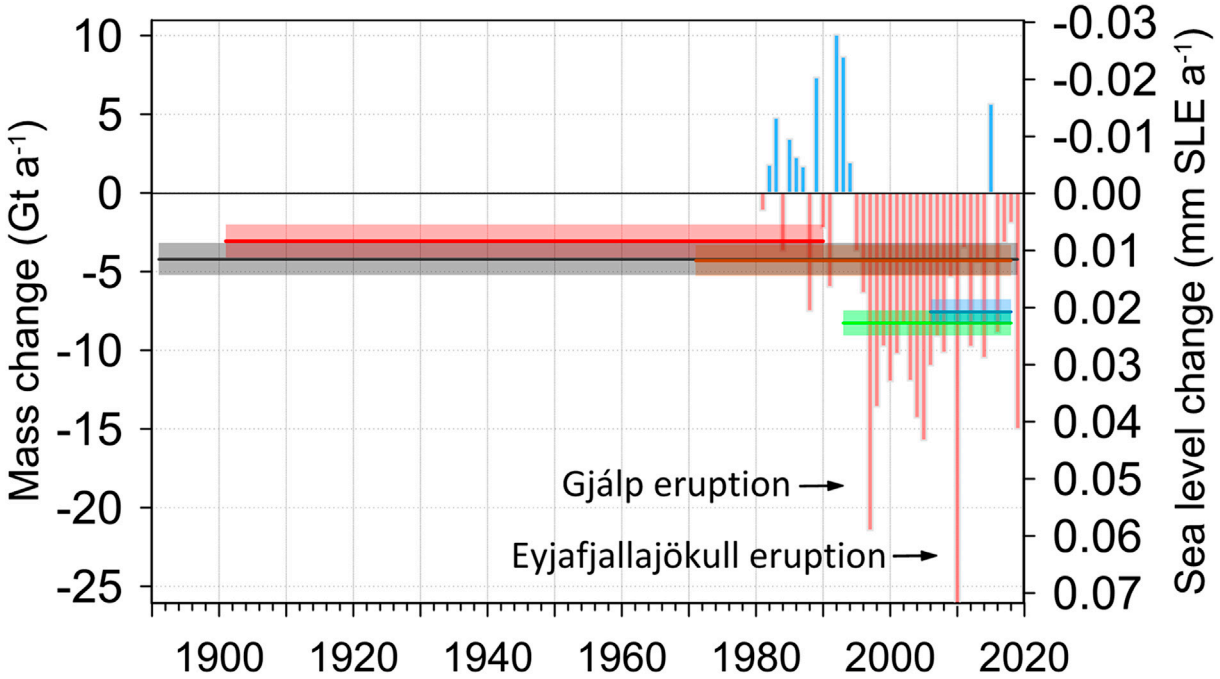

FIGURE 5 | The mass changes of all glaciers in Iceland as estimated from the data presented in **Figure 3**, showing annual values for the period 1980/81 to 2018/19 and average mass loss rates for the five periods; 1890/91–2018/19 (black), 1900/01–1989/90 (red), 1970/71–2017/18 (orange), 1992/93–2017/18 (green), and 2005/06–2017/18 (blue). The two pronounced extremes in 1996/97 and 2009/10 show the melting of ~3.7 Gt of ice due to the Gjálp eruption (mid-Vatnajökull) in October 1996 and the enhanced melting in summer 2010 caused by the deposition of a thin layer of volcanic tephra on the ice cap surfaces during the Eyjafjallajökull eruption in April–May 2010.

uncertainty of 0.10 m w.e. a^{-1} for Vatnajökull and 0.07 m w.e. a^{-1} for Hofsjökull and Langjökull, during the periods of observed/modeled surface mass balance and for the mean values obtained with volume–area scaling (see below for a justification of these values). For the periods of assumed zero mass balance of Vatnajökull in 1970/71 to 1979/80 and Hofsjökull in 1970/71 to 1986/87, the assigned uncertainty is 0.20 m w.e. a^{-1}. The uncertainty of the geodetic results of Langjökull in 1937/38 to 1996/97 varies between 0.10 and 0.50 m w.e. a^{-1} (Pálsson et al., 2012). A single value of 0.10 m w.e. a^{-1} is adopted for the smaller glaciers in 1945/46 to 2016/17. This corresponds to uncertainty values typically given for 10–20 year periods (Belart et al., 2020), while for periods exceeding 30 years, the uncertainty estimates are typically on the order of a few cm w.e. a^{-1}. The above uncertainties should be considered as possible biases and applicable for longer periods, exceeding decades. They neither reflect random annual errors in those records, nor annual deviation from long-term means for the geodetic and volume–area scaling results. When calculating the uncertainty of each time series shown in **Figure 3G**, the uncertainty for each contribution ΔC_V, ΔC_L, ΔC_H, and ΔC_O (corresponding to Vatnajökull, Langjökull, Hofsjökull, and "others", respectively) is derived by cumulating the assigned annual uncertainties. When calculating the uncertainty of the mass change of all Icelandic glaciers for the four IPCC periods (shown as horizontal lines in **Figure 5**), the uncertainties of the different contributions are considered independent. The uncertainty of the total mass change for 1970/71 to 2017/18, 1992/93 to 2017/18, and 2005/06 to 2017/18 is therefore

$$\Delta C_{VLHO} = \sqrt{\Delta C_V^2 + \Delta C_L^2 + \Delta C_H^2 + \Delta C_O^2}. \quad (2)$$

For 1900/01 to 1989/90, the total uncertainty is

$$\Delta C_{VLHO} = F\sqrt{\Delta C_V^2 + \Delta C_L^2 + \Delta C_H^2} \quad (3)$$

due to how C_O is calculated in 1890/91 to 1944/45 with the ratio F (as described above). Below we justify the above uncertainties and this approach.

In previous studies, we have assumed the uncertainty for a point measurement of the surface mass balance to be ~0.30 m w.e, while the uncertainty of the specific annual mass-balance values is expected to be smaller due to the good coverage of the survey sites and the number of measurement stakes (Björnsson et al., 2013). The surface mass-balance record obtained with the glaciological method for Langjökull (in 1997/98–2003/04) has been compared with volume changes derived from geodetic mass-balance estimates (Pálsson et al., 2012). This comparison revealed ~0.05 m w.e. a^{-1} higher mass loss from the glaciological method compared with the geodetic method. When adding the non-surface mass-balance component from Jóhannesson et al. (2020) of 0.055 m w.e. a^{-1}, the difference becomes ~0.10 m w.e. a^{-1}. It is unfortunate that the more recent DEM [from 2004 used in Pálsson et al. (2012)] was obtained in mid-August so the surface melting until the end of the melt season (late September) was not accounted for. Therefore, the observed difference may partly be due to the lack of seasonal correction (that could be 5–20% of typical summer melt) when estimating the geodetic mass balance.

Thorough validation of the glaciological mass-balance record for Vatnajökull has not yet been carried out, but comparison between geodetic and glaciological surface mass balance for limited periods and areas has suggested differences that are comparable to the non-surface melt included here (Zamolo, 2019). Based on these comparsions, the uncertainties for the decadal averages for specific mass balance of Vatnajökull during the observed and modeled periods is determined to be 0.1 m w.e. a^{-1}, while the corresponding number for Hofsjökull and Langjökull is determined to be 0.07 m w.e. a^{-1}. These values are supposed to reflect the uncertainty of the average mass-balance rate over a decade or longer period. For individual years, the uncertainty is assumed to be double this value, due to errors changing randomly from year to year.

The uncertainty of 0.1 m w.e. a^{-1} for the long periods obtained with volume–area scaling is supported by **Figure 4**. This value includes both the uncertainty of the volume used as input for the volume–area scaling and the uncertainty of the output values (shown with stars in **Figure 4**). This specific mass-balance uncertainty results in volume uncertainty of 127 km^3 and 72 km^3 for the Vatnajökull volumes in 1890 and 1945, respectively, when the uncertainties are cumulated from the date of the surface DEM (autumn 2010) used to calculate the volume (see **Section 2.2**). The corresponding minimum and maximum volume estimates for Vatnajökull in 1945 and 1890 (shown with error bars in **Figure 4**) are larger than the volumes estimated for the LIA maximum area (1890 star in **Figure 4**) and the doubled area correction due to surges (1890^{**} star in **Figure 4**). We therefore consider the uncertainties of the specific mass balance for the period of volume–area scaling as a generous estimate. The same applies for the uncertainty of the specific mass balance for Hofsjökull and Langjökull.

The choice of the year 1890 as the time of maximum LIA extent of glaciers in Iceland for our analysis leads to some uncertainty in the mass-balance estimate for the first period after 1890, as the glaciers in fact reached the LIA maximum extent at different times. Most glaciers in Iceland reached their greatest historical extent during the LIA, with a maximum recorded in the late 19th century, although some glaciers reached a similar extent already during the 18th century (e.g., Thorarinsson, 1943; Geirsdóttir et al., 2009; Björnsson, 2017; Hannesdóttir et al., 2020, and references therein). Many glaciers started retreating from an advanced position near their LIA terminal moraines in the last decades of the 19th century, even if they reached the absolute maximum extent somewhat earlier. The volume of the glaciers will therefore have been close to the LIA maximum near the end of the 19th century, which we choose to represent with the year 1890, even for glaciers that reached their maximum earlier. We do not quantify the contribution of this uncertainty about the timing of the LIA maximum to the uncertainty of our mass-balance estimates as this can only be done on a glacier-by-glacier basis.

The mass change record of each glacier is constructed from three to four methods. Each method may have a constant bias, of a similar magnitude to the estimated uncertainties; the probability of the minimum mass change occurring for all periods (or alternatively maximum mass change for all

periods) is, however, smaller. By cumulating the uncertainties independent of the method, we assume this is possible. This generous uncertainty estimate is applied because of the partial dependency between methods, for example, the input data for the volume–area scaling is from both geodetic and glaciological data. Treating the methods as independent would therefore lead to underestimation of the uncertainties. The uncertainties for each of the contributions, ΔC_V, ΔC_L, ΔC_H, and ΔC_O, are assumed to be independent and therefore ΔC_{VLHO} is calculated as the square root of a quadratic sum (**Eqs 2 and 3**). The more unrealistic assumption of full dependence between uncertainties, which would yield a direct sum of the uncertainties instead, would result in only ~25% higher uncertainties. This is because ΔC_V is by far the largest single contributor to the total uncertainty.

3. RESULTS

The mass change record of all glaciers in Iceland is shown in **Figure 5**. Before the glaciological year 1980/81, the observations do not allow the estimation of annual or decadal variability. The glaciological observations started on Hofsjökull in 1987/88 and annual variabilty in the period 1980/81 to 1987/88 is obtained from simulations from the HIRHAM5 snowpack model (Schmidt et al., 2019, see the **Section 2**). The annual variability is large: for the Vatnajökull record, the standard deviation of the observations is 0.75 m w.e. a^{-1} and for Langjökull and Hofsjökull 0.85 m w.e. a^{-1} and 0.78 m w.e. a^{-1}, respectively, during the period of glaciological observations on each glacier (see **Figure 2**).

Average mass change rates are computed for several selected periods (the reporting periods of the forthcoming IPCC AR6 assessment; see colored horizontal lines in **Figure 5**): 1900/01–1989/90: −3.1 ± 1.1 Gt a^{-1}, 1970/71–2017/18: −4.3 ± 1.0 Gt a^{-1}, 1992/93–2017/18: −8.3 ± 0.8 Gt a^{-1}, and 2005/06–2017/18: −7.6 ± 0.8 Gt a^{-1}. The rate in the rapid downwasting period 1994/95–2018/19 is −9.6 ± 0.8 Gt a^{-1}. For the whole 129-year period, 1890–2019, we estimate the average rate of mass change to be −4.2±1.0 Gt a^{-1}. Cumulating the specific mass-balance values for this period (**Figure 3F**) shows that Vatnajökull has lost about 45 m w.e. from 1890 to 2019, and Langjökull and Hofsjökull 66 m w.e. and 56 m w.e, respectively. **Figure 3F** shows that the cumulative mass change is primarily from Vatnajökull (365 ± 115 Gt) and that Langjökull and Hofsjökull have lost 63 ± 17 and 51 ± 13 Gt, respectively.

In the cold period 1980–1994 (see **Figure 3E**), 9 out of the 14 years show mass gain, but only 1 year after that (the mass-balance year 2014/15). The high mass losses of 1996/97 and 2009/10 are conspicuous. The large mass loss in 1996/97 is due to the melting of ~3.7 Gt of ice due to the subglacial Gjálp volcanic eruption in October 1996 (Guðmundsson et al., 2004), followed by a warm and sunny summer with low surface albedo due to dust precipitating onto the glacier surface. Both tephra and dust blown onto the surface of the glaciers enhance the surface melt due to lowering of the albedo (e.g., Möller et al., 2016; Wittmann et al., 2017). In the summer of 2010, a thin layer of volcanic tephra was distributed onto almost all Icelandic glaciers in the final phase of the Eyjafjallajökull eruption in April–May 2010 (Gudmundsson et al., 2012; Gascoin et al., 2017; Möller et al., 2019). Followed by an unusually warm and sunny summer, the tephra greatly enhanced melting (Björnsson et al., 2013; Belart et al., 2019), especially in the accumulation zones of the glaciers, except on Eyjafjallajökull and large portions of Mýrdalsjökull, where the tephra layer became thick enough to insulate the snow and ice, reducing the melt rates (Dragosics et al., 2016).

The mass balance year 2014/15 was characterized by a long sequence of low-pressure systems arriving one after another through the winter, bringing large amounts of precipitation, followed by a cool summer with little melt, resulting in positive mass balance on all the glaciers. In the following three years, the mass loss rate was less negative than in the previous years, but the glaciological year 2018/19 was one of the most negative mass-balance years on record, due to the persistence of anticyclonic conditions during the summer of 2019 (Tedesco and Fettweis, 2020), which resulted in warm and sunny conditions from early spring. This led to early melting of a relatively thin winter snow layer, which in turn led to early exposure of low-albedo regions in the ablation areas (Gunnarsson et al., 2020).

4. DISCUSSION

Although the glaciers in Iceland are located in a highly active volcanic region, they are useful monitors of climate variations. The detailed mass-balance record presented here is combined from glaciological observations, geodetic measurements, simulation with the HIRHAM5 snowpack model, estimates of non-surface mass balance, and results from an empirical volume–area scaling that are used to extend the record back to the time of maximum LIA extent of the glaciers as recorded by geomorphological evidence. The record spans 129 years, although the annual variability is not available until the last two decades of the 20th century. The record shows variability on decadal timescales with a period of near-zero mass balance in the 1980s and early 1990s before the onset of consistently negative mass balance on the order of −1 m a^{-1} that has prevailed since then. Close to half (−240 ± 20 Gt) of the total mass change (−540 ± 130 Gt) during the 129-year period occurred in 1994/95–2018/19, reflecting higher temperatures in this period (see **Figure 3E**) and is synchronous with glacier decline elsewhere in the world (Zemp et al., 2015). The record is valuable for studies of climate–glacier interactions and can be useful for validation of mass-balance models used to study glacier changes in other areas of the world where less data are available.

In the light of the limited geodetic observations (**Figures 3B,D**) (Pálsson et al., 2012; Belart et al., 2020), the length-change observations back to 1930 (Eyþórsson, 1963; Sigurðsson et al., 2005), the glaciological measurements carried out on southeast outlets of Vatnajökull in the 1930s (Thorarinsson, 1940; Björnsson et al., 2013), modeling of the Vatnajökull SE outlet glacier Hoffellsjökull (Aðalgeirsdóttir et al., 2011), and the temperature evolution in Iceland during our study period (**Figure 3E**), it is likely that a large proportion of the 20th-century mass loss occurred during the ~30 year period from the late 1920s to the late 1950s. For other time periods of the 20th

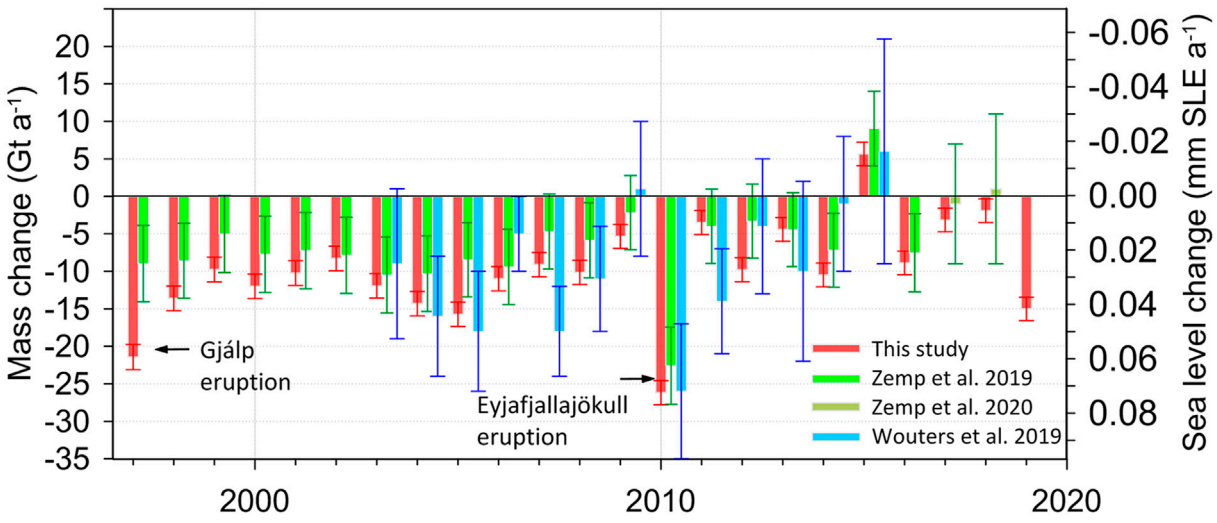

FIGURE 6 | Comparison of mass change rates estimated in this study and studies based on glaciological observations provided to the WGMS database (Zemp et al., 2019; Zemp et al., 2020b) and the GRACE observations (Wouters et al., 2019), with the respective estimated uncertainties. The figure shows only the period when Vatnajökull, Hofsjökull, and Langjökull have all been monitored with glaciological observations. The contribution of other glaciers is from geodetic results (Belart et al., 2020), including an estimated annual variability (see **Section 2**).

century, Icelandic glaciers were probably close to equilibrium on a decadal timescale. On those timescales, this study does not clearly indicate periods of substantially positive mass balance. In the period 1980/81–1993/94, which is probably the period with the most positive mass balance since the early 1920s, given the temperature history (**Figure 3E**), the average mass gain only corresponds to 0.23±0.1 m w.e. a^{-1} for Vatnajökull, which is responsible for most of the 1.5 ± 1.0 Gt a^{-1} mass gain of Icelandic glaciers during that period.

Mass change records for Icelandic glaciers have been made from the glaciological observations provided to the World Glacier Monitoring Service (WGMS) database (Zemp et al., 2019) (a subset of the observations presented in **Figure 3**), from ICESat data (Nilsson et al., 2015) (−10 ± 3 Gt a^{-1} for 2003–2009), CryoSat2 data (Foresta et al., 2016) (−5.8 ± 0.7 Gt a^{-1} for October 2010–September 2015), and the GRACE observations (von Hippel and Harig, 2019; Wouters et al., 2019; Ciracì et al., 2020). The results of von Hippel and Harig (2019) are not corrected for isostatic rebound and the mass loss rate of Ciracì et al. (2020) (−15.9 ± 4 Gt a^{-1} for 2002–2019) is almost twice as large as our estimate, possibly due to signal leakage from mass changes of the neighboring Greenland Ice Sheet or an overcompensation for the effect of glacial isostatic rebound (e.g., Sørensen et al., 2017). A comparison of our results to the annual mass change rates of Zemp et al. (2019) and Wouters et al. (2019) is shown in **Figure 6**. This comparison shows that the interannual variability is generally well captured by both data sets, but some details are not; for example, the large ice melt due to the Gjálp eruption in October 1996 and the non-surface mass balance are not included by Zemp et al. (2019). The GRACE record (Wouters et al., 2019) has some years (e.g., 2006/07 and 2010/11) with more negative mass change, and others (e.g., 2005/06, 2011/12, and 2013/14) are less negative than our estimates, although the data points from our record are within the large uncertainty range of the GRACE values.

As discussed above, annual mass-balance data are not available prior to 1980/81, so we have used geodetic observations and the volume–area scaling to extend the record to the end of the 19th century. Zemp et al. (2019) extend the record for Icelandic glaciers back to 1950 using mass-balance observations from Storglaciären in Sweden and Storbreen in Norway. The obtained mass change rate for the period 1950–1990 in their record is about double the rate that we find here (−4.0 vs. −1.7 Gt a^{-1}). Looking at decadal averages within this period, it appears that the difference is greatest in the period during which we assume near-zero balance, based on the temperature record (**Figure 3E**), glacier length observations, and geodetic observations of the smaller glaciers (Belart et al., 2020). Our study thus shows that Scandinavian glaciers are not representative of glacier mass change in Iceland. Our results emphasize the importance of direct observations from glaciers located in Iceland for evaluation of global glacier variations.

The mass-balance record presented here includes the non-surface mass balance due to geothermal melting, energy dissipation in the flow of water and ice, volcanic eruptions, and calving from the study of Jóhannesson et al. (2020). The previously estimated mass change rate of −9.5 ± 1.5 Gt a^{-1} for the period 1994/95–2009/10 (Björnsson et al., 2013), which included 0.5 Gt a^{-1} from geothermal melting (~3% of typical ablation of the survey period), is less negative than the current estimate for the same period: −11.6 ± 0.8 Gt a^{-1}, now including the recent improved estimate of the contribution from other glaciers than the three largest, the non-surface melt, and calving in Jökulsárlón. As a fraction of the typical magnitude of the surface mass balance (~−1 m w.e. a^{-1} on average for the glaciers in Iceland since 1995), the non-surface mass balance ranges from 5 to 38%, largest for

Mýrdalsjökull (31%) and the southern part of Vatnajökull (38%), and is therefore a non-negligible component of the mass balance. Assuming that the geothermal melting and energy dissipation of water and ice flow were constant during the entire study period, the non-surface mass balance, excluding volcanic eruptions, contributed 1.5 Gt a^{-1} on average to glacier runoff during the period 1890/91 to 1994/95 and increased to 2.0 Gt a^{-1} on average after that (2.1 Gt a^{-1} if the Gjálp eruption in October 1996 is included). The time-averaged non-surface mass balance, therefore, explains ~40% of the mass loss during the entire study period and ~20% of the mass loss after 1994/95.

There are strong similarities in the response of glaciers around the North Atlantic Ocean to atmospheric conditions, in particular at a multi-decadal time scale. This is illustrated by strongly negative mass balances and considerable retreat of glaciers in the 1930–1950s in Iceland (this study), on the east coast of Greenland (Bjørk et al., 2012), in Svalbard (Möller and Kohler, 2018) and for Hardangerjøkulen in Norway (Weber et al., 2019). More recently, the ocean around Iceland warmed after 1995 which correlates with the enhanced mass loss after 1995 in Iceland (Björnsson et al., 2013, this study) and Norway (Andreassen et al., 2020). The glaciers in Svalbard also shifted from a positive to a negative regime around 1990 (Østby et al., 2017; Schuler et al., 2020). The cooler oceanic conditions after 2010 (ICES, 2018) cooled the atmosphere and thereby reduced the mass loss in Iceland and Norway, and in Greenland the mass loss slowed down after a record mass-loss year in 2012 (Shepherd et al., 2019; Velicogna et al., 2020). The glaciological year 2018/19 shows one of the largest annual mass losses in our record. The Greenland Ice Sheet experienced a record mass loss in the same year (Sasgen et al., 2020) due to the persistence of anticyclonic conditions during the summer of 2019 (Tedesco and Fettweis, 2020).

With increased global temperatures, the summers in Iceland are warmer, resulting in longer ablation seasons, and in winter less precipitation falls as snow. With less snowfall on the glaciers, dirty ice appears earlier from beneath the snow in spring, which enhances the glacier ablation (Björnsson et al., 2013; Gunnarsson et al., 2020). There is, however, a large variability in the melting due to several factors. In some years, the spring is cool, so glacier ice appears later from beneath the snow. There can be snowfall on glaciers during the summer months that rapidly raises albedo and reduces melt. Dust and tephra from volcanic eruptions are blown around in the highlands in dry periods and are often deposited on the glaciers, enhancing the melt (Wittmann et al., 2017).

With more detailed information about the past mass changes of Icelandic glaciers, models for projecting their future evolution can be improved. The mass loss from glaciers in Iceland has been projected to continue in the coming decades (Flowers et al., 2005; Marshall et al., 2005; Aðalgeirsdóttir et al., 2006; Guðmundsson et al., 2009; Aðalgeirsdóttir et al., 2011; Schmidt et al., 2019). Mass-balance models have been coupled with ice-flow models, and scenarios for future climate have been applied to simulate past and future mass changes. Hofsjökull and Langjökull, which currently have more negative specific mass balance than Vatnajökull and are both smaller in area and with less ice thickness, are likely to lose about 60 and 80% of their mass, respectively, until the year 2100 (Guðmundsson et al., 2009; Thorsteinsson et al., 2013). The larger ice cap Vatnajökull will survive longer; it is projected to lose 20–30% of its mass until the end of the century. Its future after that will depend on how much warming will be realized (Schmidt et al., 2019). These studies are based on mass-balance models that do not take non-surface mass balance into account and they therefore have a tendency to underestimate the future glacier decline. The projected mass losses toward the end of the 21st century are more rapid and persistent than the observations presented here. In the period 1890–2019, Vatnajökull, Langjökull, and Hofsjökull lost 12 ± 4, 29 ± 8, and 25 ± 6%, respectively, relative to their estimated mass in 1890. The future mass loss will both be due to the already realized temperature increase (Mernild et al., 2013; Vaughan et al., 2013; Marzeion et al., 2018) and the projected continued warming. The glaciers are now in disequilibrium with the already realized warming (Christian et al., 2018), because of their several-decades-long response times (Jóhannesson et al., 1989; Harrison et al., 2001), and would continue to lose mass even if temperatures could be stabilized in the near future. The continued mass loss is dependent on future greenhouse gas emissions and whether, and if so how rapidly, they will be reduced.

5. CONCLUSION

Glaciers in Iceland are useful indicators of climate conditions in the middle of the North Atlantic Ocean. The results presented here add valuable information to global estimates of the response of glaciers to climate change in the past several decades. The study shows a total mass change of −540 ± 130 Gt (−4.2 ± 1.0 Gt a^{-1} on average) since the end of the LIA (~1890), which corresponds to a 16 ± 4% loss of the LIA maximum ice mass. Almost half of the total mass loss has occurred since 1994/95 (240 ± 20 Gt, corresponding to 9.6 ± 0.8 Gt a^{-1} on average). The most rapid loss is observed in the period 1994/95 to 2009/10 (mass change rate −11.6 ± 0.8 Gt a^{-1}). Since 2010, the mass loss rate has on average been ~50% lower, with the exception of 2018/19, when one of the highest annual mass losses was observed (mass change rate −15.0 ± 1.6 Gt a^{-1}). In 1930/31 to 1949/50, the average loss rates were probably close to the ones observed since 1994, while in 1980/81–1993/94, Icelandic glaciers had a period of small but significant surplus (1.5 ± 1.0 Gt a^{-1}). For other periods of the study, the glaciers were either close to equilibrium or experiencing mild loss rates. This pattern of glacier evolution is similar across the North Atlantic region as shown by records from glaciers in Greenland (Bjørk et al., 2012), Svalbard (Möller and Kohler, 2018), and Norway (Weber et al., 2019; Andreassen et al., 2020).

After 1995, we have detailed glaciological observations, made on ~60 survey sites on Vatnajökull and ~25 survey sites on each of Hofsjökull and Langjökull, which show mass loss every year until 2014. In 2014/15, high winter precipitation and reduced melt during a short and cold summer caused a single anomalous year with positive mass balance. There is large interannual variability that often is impacted by volcanic eruptions enhancing the melt and dust or volcanic tephra blown onto the glacier surface from

their sediment-rich vicinity. The glaciological year 2018/19 was among the most negative mass-balance years that were not significantly impacted by volcanic eruptions but by dust blown onto the glacier surface.

The non-surface mass balance of glaciers in Iceland, as estimated by Jóhannesson et al. (2020), is non-negligible, accounting for about one-fifth of the mass loss since 1994. A part of this non-surface mass balance is caused by calving activity, which was insignificant in the first half of the 20th century, but has been gradually increasing with the ongoing retreat of the outlet glaciers located in over-deepened troughs (Guðmundsson et al., 2019). The calving will continue to increase as the glaciers retreat, and should, along with other non-surface mass-balance components, be taken into account in future projections of mass loss of glaciers in Iceland.

DATA AVAILABILITY STATEMENT

The regional mass-balance record constructed here is provided in **Supplementary Tables S1, S2**, together with mass-change rates for various periods. A subset of the mass-balance observations from Vatnajökull, Hofsjökull, and Langjökull is submitted to the WGMS database on annual basis. The geodetic mass balance estimates from Belart et al. (2020) are in the last version of the WGMS database (10.5904/wgms-fog-2020-08). The outlines of glaciers in Iceland published by Hannesdóttir et al. (2020) are submitted to the GLIMS database. Glacier length changes measured by members of the Icelandic Glaciological Society are available at spordakost.jorfi.is.

AUTHOR CONTRIBUTIONS

GA, FP, and EM designed the study, wrote the paper, and made the figures. HB and HHH designed, initiated, and led the Vatnajökull mass-balance work for decades and AG has facilitated the continuation of the mass-balance studies reported here. FP, EM, TT, TJ, AG, BE, HB, HH, HHH, and OS have conducted the *in situ* mass-balance measurements on the three main ice caps. HH, OS, EM, and JB contributed the area estimates at different times. JB, EM, EB, and TJ processed and contributed the geodetic estimates. LS contributed the simulations from HARMONIE–AROME. TJ contributed the non-surface mass-balance estimates. All authors contributed to discussions at various stages of the work and during the revisions of the manuscript.

FUNDING

This work and collection of data on which this work is based has been supported financially by and with the participation of the University of Iceland Research Fund; the National Power Company of Iceland; the Icelandic Public Road Administration; Iceland Glaciological Society; Reykjavík Energy Environmental and Energy Research Fund; three multinational European Union research projects TEMBA, ICEMASS, and SPICE; two projects supported by Nordic Energy Research: Climate and Energy (CE) and Climate and Energy Systems (CES); the Nordic Centre of Excellence SVALI (Stability and Variations of Arctic Land Ice), funded by the Nordic Top-level Research Initiative (TRI); and the Icelandic Ministry for the Environment and Natural Resources through the cooperative project Melting glaciers. SPOT6/7 data were obtained thanks to public funds received in the framework of GEOSUD, a project (ANR-10-EQPX-20) of the program "Investissements d'Avenir" managed by the French National Research Agency. EB acknoweldges support from the French Space Agency (CNES).

ACKNOWLEDGMENTS

We express our gratitude to Þorsteinn Jónsson, Hlynur Skagfjörð Pálsson, Sveinbjörn Steinþórsson, Vilhjálmur Kjartansson, members of the Iceland Glaciological Society, and many others for their important contributions during decades of mass-balance measurements in the field. We thank three reviewers and the scientific editor Michael Zemp for constructive comments on the manuscript.

SUPPLEMENTARY MATERIAL

The Supplementary Material for this article can be found online at: https://www.frontiersin.org/articles/10.3389/feart.2020.523646/full#supplementary-material

REFERENCES

Aðalgeirsdóttir, G., Jóhannesson, T., Björnsson, H., Pálsson, F., and Sigurðsson, O. (2006). The response of Hofsjökull and southern Vatnajökull, Iceland, to climate change. *J. Geophys. Res.* 111, F03001. doi:10.1029/2005JF000388

Aðalgeirsdóttir, G., Guðmundsson, S., Björnsson, H., Pálsson, F., Jóhannesson, T., Hannesdóttir, H., et al. (2011). Modelling the 20th and 21st century evolution of Hoffellsjökull glacier, SE-Vatnajökull, Iceland. *Cryosphere* 5, 961–975. doi:10.5194/tc-5-961-2011

Ágústsson, H., Hannesdóttir, H., Thorsteinsson, T., Pálsson, F., and Oddsson, B. (2013). Mass balance of Mýrdalsjökull ice cap accumulation area and comparison of observed winter balance with simulated precipitation. *Jökull* 63, 91–104

Andreassen, L. M., Elvehøy, H., Kjøllmoen, B., and Belart, J. M. C. (2020). Glacier change in Norway since the 1960s—an overview of mass balance, area, length and surface elevation changes. *J. Glaciol.* 66, 313–328. doi:10.1017/jog.2020.10

Bahr, D. B., Meier, M. F., and Peckham, S. D. (1997). The physical basis of glacier volume–area scaling. *J. Geophys. Res.* 102 (B9), 20355–20362. doi:10.1029/97JB01696

Bahr, D. B., Pfeffer, W., and Kaser, G. (2015). A review of volume–area scaling of glaciers. *Rev. Geophys.* 63, 95–140. doi:10.1002/2014RG000470

Belart, J. M. C., Magnússon, E., Berthier, E., Pálsson, F., Aðalgeirsdóttir, G., and Jóhannesson, T. (2019). The geodetic mass balance of Eyjafjallajökull ice cap for

1945–2014: processing guidelines and relation to climate. *J. Glaciol.* 65, 395–409. doi:10.1017/jog.2019.16

Belart, J. M. C., Magnússon, E., Berthier, E., Gunnlaugsson, Á. Þ., Pálsson, F., Aðalgeirsdóttir, G., et al. (2020). Mass balance of 14 Icelandic glaciers, 1945–2017: spatial variations and links with climate. *Front. Earth Sci.* 8, 163. doi:10.3389/feart.2020.00163

Bjørk, A. A., Kjær, K. H., Korsgaard, N. J., Khan, S. A., Kjeldsen, K. K., Andresen, C. S., et al. (2012). An aerial view of 80 years of climate-related glacier fluctuations in southeast Greenland. *Nat. Geosci.* 5, 427–432. doi:10.1038/ngeo1481

Björnsson, H. (1986). Surface and bedrock topography of ice caps in Iceland, mapped by radio echo-sounding. *Ann. Glaciol.* 8, 11–18. doi:10.3189/S026030550000104X

Björnsson, H. (2017). *The glaciers of Iceland*. Paris, France: Atlantis Press, 2, 613.

Björnsson, H., and Pálsson, F. (2008). Icelandic glaciers. *Jökull* 58, 365–386.

Björnsson, H., and Pálsson, F. (2020). Radio-echo soundings on Icelandic temperate glaciers: history of techniques and findings. *Ann. Glaciol.* 61, 25–34. doi:10.1017/aog.2020.10

Björnsson, H., Pálsson, F., and Guðmundsson, M. T. (2000). Surface and bedrock topography of the Mýrdalsjökull ice cap, Iceland: the Katla caldera, eruption sites and routes of jökulhlaups. *Jökull* 49, 29–46.

Björnsson, H., Pálsson, F., and Guðmundsson, S. (2001). Jökulsárlón at Breiðamerkursandur, Vatnajökull, Iceland: 20th century changes and future outlook. *Jökull* 50, 1–18.

Björnsson, H., Pálsson, F., Guðmundsson, M. T., and Haraldsson, H. H. (1998). Mass balance of western and northern Vatnajökull, Iceland, 1991–1995. *Jökull* 45, 35–38.

Björnsson, H., Pálsson, F., Guðmundsson, M. T., and Haraldsson, H. H. (2002). Mass balance of Vatnajökull (1991–2001) and Langjökull (1996–2001), Iceland. *Jökull* 51, 75–78.

Björnsson, H., Pálsson, F., Guðmundsson, S., Magnússon, E., Aðalgeirsdóttir, G., Jóhannesson, T., et al. (2013). Contribution of Icelandic ice caps to sea level rise: trends and variability since the Little Ice Age. *Geophys. Res. Lett.* 40, 1–5. doi:10.1002/grl.50278

Björnsson, H., Pálsson, F., Sigurðsson, O., and Flowers, G. E. (2003). Surges of glaciers in Iceland. *Ann. Glaciol.* 36, 82–90. doi:10.3189/172756403781816365

Brun, F., Berthier, E., Wagnon, P., Kääb, A., and Treichler, D. (2017). A spatially resolved estimate of High Mountain Asia glacier mass balances from 2000 to 2016. *Nat. Geosci.* 10, 668–673. doi:10.1038/NGEO2999

Christian, J. E., Koutnik, M., and Roe, G. (2018). Committed retreat: controls on glacier disequilibrium in a warming climate. *J. Glaciol.* 64, 675–688. doi:10.1017/jog.2018.57

Ciracì, E., Velicogna, I., and Swenson, S. (2020). Continuity of the mass loss of the world's glaciers and ice caps from the grace and grace follow-on missions. *Geophys. Res. Lett.* 47, GL086926. doi:10.1029/2019GL086926

Cogley, J., Hock, R., Rasmussen, L., Arendt, A., Bauder, A., Braithwaite, R., et al. (2011). *Glossary of glacier mass balance and related terms (IHP-VII technical documents in hydrology No. 86, IACS contribution No. 2)*. Paris, France: UNESCO–IHP, 114.

Dragosics, M., Meinander, O., Jónsdóttir, T., Dürig, T., De Leeuw, G., Pálsson, F., et al. (2016). Insulation effects of Icelandic dust and volcanic ash on snow and ice. *Arab. J. Geosci.* 9, 126. doi:10.1007/s12517-015-2224-6

Eyþórsson, J. (1963). Variations of Iceland glaciers 1931–1960. *Jökull* 13, 31–33.

Farinotti, D., Huss, M., Fürst, J. J., Landmann, J., Machguth, H., Maussion, F., et al. (2019). A consensus estimate for the ice thickness distribution of all glaciers on Earth. *Nat. Geosci.* 12, 168–173. doi:10.1038/s41561-019-0300-3

Flowers, G., Marshall, S., Björnsson, H., and Clarke, G. (2005). Sensitivity of Vatnajökull ice cap hydrology and dynamics to climate warming over the next 2 centuries. *J. Geophys. Res.* 110, F02011. doi:10.1029/2004JF000200

Foresta, L., Gourmelen, N., Pálsson, F., Nienow, P., Björnsson, H., and Shepherd, A. (2016). Surface elevation change and mass balance of Icelandic ice caps derived from swath mode CryoSat-2 altimetry. *Geophys. Res. Lett.* 43, 12138–12145. doi:10.1002/2016GL071485

Gärtner-Roer, I., Naegeli, K., Huss, M., Knecht, T., Machguth, H., and Zemp, M. (2014). A database of worldwide glacier thickness observations. *Glob. Planet. Change.* 122, 330–344. doi:10.1016/j.gloplacha.2014.09.003

Gascoin, S., Guðmundsson, S., Aðalgeirsdóttir, G., Pálsson, F., Schmidt, L., Berthier, E., et al. (2017). Evaluation of MODIS albedo product over ice caps in Iceland and impact of volcanic eruptions on their albedo. *Rem. Sens.* 9 (5), 399. doi:10.3390/rs9050399

Geirsdóttir, Á., Miller, G. H., Axford, Y., and Ólafsdóttir, S. (2009). Holocene and latest Pleistocene climate and glacier fluctuations in Iceland. *Quat. Sci. Rev.* 28, 2107–2118. doi:10.1016/j.quascirev.2009.03.013

Guðmundsson, M. T., Sigmundsson, F., Björnsson, H., and Högnadóttir, Þ. (2004). The 1996 eruption at Gjálp, Vatnajökull ice cap, Iceland: course of events, efficiency of heat tranfer, ice deformation and subglacial water pressure. *Bull. Volcanol.* 66, 46–65. doi:10.1007/s00445-003-0295-9

Gudmundsson, M. T., Thordarson, T., Höskuldsson, A., Larsen, G., Björnsson, H., Prata, F. J., et al. (2012). Ash generation and distribution from the April–May 2010 eruption of Eyjafjallajökull, Iceland. *Sci. Rep.* 08, 572. doi:10.1038/srep00572

Guðmundsson, S., Björnsson, H., Aðalgeirsdóttir, G., Jóhannesson, T., Pálsson, F., and Sigurðsson, O. (2009). Similarities and differences in the response of two ice caps in Iceland to climate warming. *Hydrol. Res.* 40, 495–502. doi:10.2166/nh.2009.210

Guðmundsson, S., Björnsson, H., Pálsson, F., Magnússon, E., Sæmundsson, Þ., and Jóhannesson, T. (2019). Terminus lakes on the south side of Vatnajökull ice cap, SE-Iceland. *Jökull* 69, 1–34.

Gunnarsson, A., Gardarsson, S. M., Pálsson, F., Jóhannesson, T., and Sveinsson, O. G. B. (2020). Annual and interannual variability and trends of albedo for Icelandic glaciers. *Cryosphere Discuss.* 2020, 1–32. doi:10.5194/tc-2019-328

Hannesdóttir, H., Björnsson, H., Pálsson, F., Aðalgeirsdóttir, G., and Guðmundsson, S. (2015a). Changes in the southeast Vatnajökull ice cap, Iceland, between ~1890 and 2010. *Cryosphere* 9, 565–585. doi:10.5194/tc-9-565-2015

Hannesdóttir, H., Björnsson, H., Pálsson, F., Aðalgeirsdóttir, G., and Guðmundsson, S. (2015b). Variations of southeast Vatnajökull ice cap (Iceland) 1650–1900 and reconstruction of the glacier surface geometry at the Little Ice Age maximum. *Geogr. Ann. Phys. Geogr.* 97, 237–264. doi:10.1111/geoa.12064

Hannesdóttir, H., Sigurðsson, O., Þrastarson, R. H., Guðmundsson, S., Belart, J. M. C., Pálsson, F., et al. (2020). Variations in glacier extent in Iceland since the end of the Little Ice Age. *Jökull* 639, 200929. doi:10.33799/jokull2020.70.001

Harrison, W. D., Elsberg, D. H., Echelmeyer, K. A., and Krimmel, R. M. (2001). On the characterization of glacier response by a single time-scale. *J. Glaciol.* 47, 659–664. doi:10.3189/172756501781831837

Hock, R., Rasul, G., Adler, C., Cáceres, B., Gruber, S., Hirabayashi, Y., et al. (2019). IPCC special report on the ocean and cryosphere in a changing climate. high mountain areas. IPCC. Available at: https://www.ipcc.ch/srocc/chapter/chapter-2/ (Accessed September 25, 2019).

Huss, M. (2013). Density assumptions for converting geodetic glacier volume change to mass change. *Cryosphere* 7, 877–887. doi:10.5194/tc-7-877-2013

Huss, M., and Farinotti, D. (2012). Distributed ice thickness and volume of all glaciers around the globe. *J. Geophys. Res. Earth Surface.* 117, F04010. doi:10.1029/2012JF002523

ICES (2018). Report No.: #331. ICES report on ocean climate. International council for the exploration of the sea area 3—Icelandic waters. Available at: doi:10.17895/ices.pub.4625 (Accessed March 21, 2018).

Jóhannesson, T., Björnsson, H., Magnússon, E., Guðmundsson, S., Pálsson, F., Sigurðsson, O., et al. (2013). Ice-volume changes, bias estimation of mass-balance measurements and changes in subglacial lakes derived by lidar mapping of the surface of Icelandic glaciers. *Ann. Glaciol.* 54, 63–74. doi:10.3189/2013AoG63A422

Jóhannesson, T., Pálmason, B., Hjartarson, Á., Jarosch, A., Magnússon, E., Belart, J., et al. (2020). Non-surface mass balance of glaciers in Iceland. *J. Glaciol.* 66, 685–697. doi:10.1017/jog.2020.37

Jóhannesson, T., Raymond, C., and Waddington, E. (1989). Time–scale for adjustment of glaciers to changes in mass balance. *J. Glaciol.* 35, 355–369. doi:10.3189/S002214300000928X

Korona, J., Berthier, E., Bernard, M., Remy, F., and Thouvenot, E. (2009). SPIRIT. SPOT 5 stereoscopic survey of polar ice: reference images and topographies during the fourth international polar year (2007–2009). *ISPRS J. Photogramm. Remote Sens.* 64, 204–212. doi:10.1016/j.isprsjprs.2008.10.005

Leclercq, P. W., Oerlemans, J., and Cogley, J. G. (2011). Estimating the glacier contribution to sea-level rise for the period 1800–2005. *Surv. Geophys.* 32, 519. doi:10.1007/s10712-011-9121-7

Magnússon, E., Belart, J., Pálsson, F., Ágústsson, H., and Crochet, P. (2016). Geodetic mass balance record with rigorous uncertainty estimates deduced from aerial photographs and lidar data – case study from Drangajökull ice cap, NW Iceland. *Cryosphere* 10, 159–177. doi:10.5194/tc-10-159-2016

Marshall, S. J., Björnsson, H., Flowers, G. E., and Clarke, G. K. C. (2005). Simulation of vatnajökull ice cap dynamics. *J. Geophys. Res. Earth Surface.* 110, F03009. doi:10.1029/2004JF000262

Marzeion, B., Jarosch, A. H., and Hofer, M. (2012). Past and future sea-level change from the surface mass balance of glaciers. *Cryosphere* 6, 1295–1322. doi:10.5194/tc-6-1295-2012

Marzeion, B., Leclercq, P. W., Cogley, J. G., and Jarosch, A. H. (2015). Brief communication: global reconstructions of glacier mass change during the 20th century are consistent. *Cryosphere* 9, 2399–2404. doi:10.5194/tc-9-2399-2015

Marzeion, B., Kaser, G., and Maussion, F. (2018). Limited influence of climate change mitigation on short-term glacier mass loss. *Nat. Clim. Change.* 8, 305–308. doi:10.1038/s41558-018-0093-1

Meredith, M., Sommerkorn, M., Cassotta, S., Derksen, C., Ekaykin, A., Hollowed, A., et al. (2019). IPCC special report on the oceans and cryosphere in a changing climate. polar regions. Available at: https://www.ipcc.ch/srocc/chapter/chapter-3-2/ (Accessed September 25, 2019).

Mernild, S. H., Lipscomb, W. H., Bahr, D. B., Radić, V., and Zemp, M. (2013). Global glacier changes: a revised assessment of committed mass losses and sampling uncertainties. *Cryosphere* 7, 1565–1577. doi:10.5194/tc-7-1565-2013

Möller, M., and Kohler, J. (2018). Differing climatic mass balance evolution across Svalbard glacier regions over 1900–2010. *Front. Earth Sci.* 6, 128. doi:10.3389/feart.2018.00128

Möller, R., Dagsson-Waldhauserova, P., Möller, M., Kukla, P. A., Schneider, C., and Gudmundsson, M. T. (2019). Persistent albedo reduction on southern Icelandic glaciers due to ashfall from the 2010 Eyjafjallajökull eruption. *Remote Sens. Environ.* 233, 111396. doi:10.1016/j.rse.2019.111396

Möller, R., Möller, M., Kukla, P. A., and Schneider, C. (2016). Impact of supraglacial deposits of tephra from Grímsvötn volcano, Iceland, on glacier ablation. *J. Glaciol.* 62, 933–943. doi:10.1017/jog.2016.82

Morris, A., Moholdt, G., and Gray, L. (2020). Spread of Svalbard glacier mass loss to Barents Sea margins revealed by CryoSat-2. *J. Geophys. Res.: Earth Surface.* 125, e2019jf005357. doi:10.1029/2019JF005357

Nilsson, J., Sandberg Sørensen, L., Barletta, V. R., and Forsberg, R. (2015). Mass changes in Arctic ice caps and glaciers: implications of regionalizing elevation changes. *Cryosphere* 9, 139–150. doi:10.5194/tc-9-139-2015

Østby, T. I., Schuler, T. V., Hagen, J. O., Hock, R., Kohler, J., and Reijmer, C. H. (2017). Diagnosing the decline in climatic mass balance of glaciers in Svalbard over 1957–2014. *Cryosphere* 11, 191–215. doi:10.5194/tc-11-191-2017

Østrem, G., and Brugman, M. (1991). Report No.: 4. glacier mass-balance measurements: a Manual for Field and Office work. 234 (Oslo, Norwegian water resources and energy administration, and Saskatoon, Canada, national hydrology research institute. NHRI science. Available at: https://wgms.ch/downloads/Oestrem_Brugman_GlacierMassBalanceMeasurements_1991.pdf (Accessed March, 1996).

Pálsson, F., Guðmundsson, S., Björnsson, H., Berthier, E., Magnússon, E., Guðmundsson, S., et al. (2012). Mass and volume changes of Langjökull ice cap, Iceland, ~1890 to 2009, deduced from old maps, satellite images and *in situ* mass balance measurements. *Jökull* 62, 81–96.

Radić, V., and Hock, R. (2010). Regional and global volumes of glaciers derived from statistical upscaling of glacier inventory data. *J. Geophys. Res.: Earth Surface.* 115, F01010. doi:10.1029/2009JF001373

Sasgen, I., Wouters, B., Gardner, A. S., King, M., Tedesco, M., Landerer, F. W., et al. (2020). Return to rapid ice loss in Greenland and record loss in 2019 detected by the GRACE-FO satellites. *Commun. Earth Environ.* 1, 8. doi:10.1038/s43247-020-0010-1

Schmidt, L. S., Aðalgeirsdóttir, G., Guðmundsson, S., Langen, P. L., Pálsson, F., Mottram, R., et al. (2017). The importance of accurate glacier albedo for estimates of surface mass balance on Vatnajökull: evaluating the surface energy budget in a regional climate model with automatic weather station observations. *Cryosphere* 11, 1665–1684. doi:10.5194/tc-11-1665-2017

Schmidt, L. S., Aðalgeirsdóttir, G., Pálsson, F., Langen, P. L., Guðmundsson, S., and Björnsson, H. (2019). Dynamic simulations of Vatnajökull ice cap from 1980 to 2300. *J. Glaciol.* 66, 97–112. doi:10.1017/jog.2019.90

Schmidt, L. S., Langen, P. L., Aðalgeirsdóttir, G., Pálsson, F., Guðmundsson, S., and Gunnarsson, A. (2018). Sensitivity of glacier runoff to winter snow thickness investigated for Vatnajökull ice cap, Iceland, using numerical models and observations. *Atmosphere* 9, 450. doi:10.3390/atmos9110450

Schuler, T. V., Kohler, J., Elagina, N., Hagen, J. O. M., Hodson, A. J., Jania, J. A., et al. (2020). Reconciling Svalbard glacier mass balance. *Front. Earth Sci.* 8, 156. doi:10.3389/feart.2020.00156

Shean, D. E., Bhushan, S., Montesano, P., Rounce, D. R., Arendt, A., and Osmanoglu, B. (2020). A systematic, regional assessment of High Mountain Asia glacier mass balance. *Front. Earth Sci.* 7, 363. doi:10.3389/feart.2019.00363

Shepherd, A., Ivins, E., Rignot, E., Smith, B., van den Broeke, M., Velicogna, I., et al. (2019). Mass balance of the Greenland ice Sheet from 1992 to 2018. *Nature* 579, 233–239. doi:10.1038/s41586-019-1855-2

Sigurðsson, O. (2005). "Variations of termini of glaciers in Iceland in recent centuries and their connection with climate," in *Iceland—modern processes and past environment*. Editors C. Caseldine, A. Russell, J. Harðardóttir, and O. Knudsen (Amsterdam, Netherlands:Elsevier), 241–255.

Sigurðsson, O., and Williams, R. (2008). "Geographic names of Iceland's glaciers," in *Historic and modern* (Washington: U.S. Geological Survey Professional Paper), 1746.

Sigurðsson, O., Williams, R. S., and Víkingsson, S. (2017). *Jöklakort af íslandi/map of the glaciers of Iceland. scale 1:500,000, with two inset maps of 1:250,000, Tröllaskagi and Kerlingarfjöll, with accompanying illustrated pamphlet, and list of glacier place-names*. 2nd Edn. Reykjavík, Veðurstofa Íslands: National Energy Authority, 6. [Dataset].

Sørensen, L. S., Jarosch, A. H., Aðalgeirsdóttir, G., Barletta, V. R., Forsberg, R., Pálsson, F., et al. (2017). The effect of signal leakage and glacial isostatic rebound on GRACE-derived ice mass changes in Iceland. *Geophys. J. Int.* 209, 226–233. doi:10.1093/gji/ggx008

Tedesco, M., and Fettweis, X. (2020). Unprecedented atmospheric conditions (1948–2019) drive the 2019 exceptional melting season over the Greenland ice sheet. *Cryosphere* 14, 1209–1223. doi:10.5194/tc-14-1209-2020

Thorarinsson, S. (1940). Present glacier shrinkage, and eustatic changes of sea-level. *Geogr. Ann.* 22, 131–159. doi:10.1080/20014422.1940.11880686

Thorarinsson, S. (1943). Chapter XI. Oscillations of the Iceland glaciers in the last 250 years. *Geogr. Ann.* 25, 1–54. doi:10.1080/20014422.1943.11880716

Thorsteinsson, T., Jóhannesson, T., and Snorrason, Á. (2013). Glaciers and ice caps: vulnerable water resources in a warming climate. *Curr. Opin. Env. Sust.* 5, 590–598. doi:10.1016/j.cosust.2013.11.003

Thorsteinsson, T., Jóhannesson, T., Sigurðsson, O., and Einarsson, B. (2017). Tech. Rep., ví 2017-016. Afkomumælingar á Hofsjökli 1988–2017 (mass balance Measurements on Hofsjökull 1988–2017). Reykjavík, Iceland: Icelandic Meteorological Office, 84.

Vaughan, D., Comiso, J., Allison, I., Carrasco, J., Kaser, G., Kwok, R., et al. (2013). *Climate change 2013: the physical science basis. Contribution of working group I to the fifth assessment report of the intergovernmental panel on climate change*. Cambridge, United Kingdom: Cambridge University Press.

Velicogna, I., Mohajerani, Y., Geruo, A., Landerer, F., Mouginot, J., Noel, B., et al. (2020). Continuity of ice sheet mass loss in Greenland and Antarctica from the grace and grace follow-on missions. *Geophys. Res. Lett.* 47, GL087291. doi:10.1029/2020GL087291

von Hippel, M., and Harig, C. (2019). Long-term and inter-annual mass changes in the Iceland ice cap determined from GRACE gravity using Slepian functions. *Front. Earth Sci.* 7, 171. doi:10.3389/feart.2019.00171

Weber, P., Boston, C. M., Lovell, H., and Andreassen, L. M. (2019). Evolution of the Norwegian plateau icefield Hardangerjøkulen since the "little ice age". *Holocene* 29, 1885–1905. doi:10.1177/0959683619865601

Wittmann, M., Zwaaftink, C. D. G., Schmidt, L., Guðmundsson, S., Pálsson, F., Arnalds, O., et al. (2017). Impact of dust deposition on the albedo of Vatnajökull ice cap, Iceland. *Cryosphere* 11, 741–754. doi:10.5194/tc-11-741-2017

Wouters, B., Gardner, A. S., and Moholdt, G. (2019). Global glacier mass loss during the GRACE satellite mission (2002–2016). *Front. Earth Sci.* 7, 96. doi:10.3389/feart.2019.00096

Zamolo, A. (2019). Glacier mass balance and ice-volcano interactions of the Vatnajökull Ice Cap (Iceland) from SPOT 6/7 and LiDAR DEM differencing. Master's thesis. Talence, France: Bordeaux INP ENSEGID.

Zemp, M., Frey, H., Gärtner-Roer, I., Nussbaumer, S. U., Hoelzle, M., Paul, F., et al. (2015). Historically unprecedented global glacier decline in the early 21st century. *J. Glaciol.* 61, 745–762. doi:10.3189/2015JoG15J017

Zemp, M., Huss, M., Thibert, E., Eckert, N., McNabb, R., Huber, J., et al. (2019). Global glacier mass changes and their contributions to sea-level rise from 1961 to 2016. *Nature* 568, 382–386. doi:10.1038/s41586-019-1071-0

Zemp, M., Gärtner-Roer, I., Nussbaumer, S. U., Bannwart, J., Rastner, P., Paul, F., et al. (Editors) (2020a). *WGMS 2020. Global glacier change bulletin No. 3 (2016–2017)*. Zurich, Switzerland: CSU(WDS)/IUGG(IACS)/UNEP/UNESCO/WMO, World Glacier Monitoring Service, 274. [Dataset].

Zemp, M., Huss, M., Eckert, N., Thibert, E., Paul, F., Nussbaumer, S. U., et al. (2020b). Brief communication: ad hoc estimation of glacier contributions to sea-level rise from the latest glaciological observations. *Cryosphere* 14, 1043–1050. doi:10.5194/tc-14-1043-2020

Conflict of Interest: The authors declare that the research was conducted in the absence of any commercial or financial relationships that could be constructed as a potential conflict of interest.

The handling editor declared a past co-authorship with one of the authors HH

frontiers in Earth Science

ORIGINAL RESEARCH
published: 03 December 2020
doi: 10.3389/feart.2020.530997

Ice Mass Loss in the Central Andes of Argentina Between 2000 and 2018 Derived From a New Glacier Inventory and Satellite Stereo-Imagery

Lidia Ferri[1], Inés Dussaillant[2,3], Laura Zalazar[1], Mariano H. Masiokas[1], Lucas Ruiz[1], Pierre Pitte[1], Hernán Gargantini[1], Mariano Castro[1], Etienne Berthier[2] and Ricardo Villalba[1]*

[1]Instituto Argentino de Nivología, Glaciología y Ciencias Ambientales (IANIGLA), CONICET CCT Mendoza, Mendoza, Argentina, [2]LEGOS/OMP, Université de Toulouse, CNES, Centre National de la Recherche Scientifique, IRD, UPS, Toulouse, France, [3]Department of Geography, University of Zurich, Zurich, Switzerland

Based on the recently released National Glacier Inventory (NGI), we analyzed the characteristics and the mass balance rates of ice masses in the Argentinean Central Andes (ca. 30°–37° S). The NGI provides unprecedented information on area, number and distribution of different ice masses, including debris-covered glaciers and rock glaciers. In the Central Andes, a number of 8,076 ice masses were identified covering a total area of 1767 km^2. For the period 2000–2018, a general lowering of the ice surface was observed with a region-wide mass balance rate of –0.18 ± 0.19 m w.e. yr^{-1}. Clear differences depending on the debris coverage of the different ice masses were identified, with mass balance rates ranging from –0.36 ± 0.19 m w.e. yr^{-1} for partly debris-covered glaciers to –0.02 ± 0.19 m w.e. yr^{-1} for rock glaciers. Considering different sub-periods, the region-wide mass balance rate was slightly positive (+0.12 ± 0.23 m w. e. yr^{-1}) from 2000 to 2009 and negative (–0.21 ± 0.30 m w.e. yr^{-1}) from 2009 to 2018. A comparison with the Randolph Glacier Inventory (RGI version 6.0) indicates that the NGI provides more detailed information regarding different type of ice masses whereas region-wide mass balance rates show limited sensitivity to the choice of the inventory. The inclusion of rock glaciers and "debris-covered ice with rock glacier" in the NGI causes mass balance rates to be slightly less negative than when using the RGI. Since the Central Andes are experiencing an unprecedented decade-long drought, our study provides crucial information to estimate current and future hydrological contribution of the different type of ice masses to river discharge in the arid subtropical Andes.

Keywords: glacier inventory, Central Andes, debris-covered glaciers, rock glaciers, mass loss

OPEN ACCESS

Edited by:
Matthias Holger Braun, University of Erlangen Nuremberg, Germany

Reviewed by:
Fabien Gillet-Chaulet, UMR5001 Institut des Géosciences de l'Environnement (IGE), France
Samuel Nussbaumer, University of Zurich, Switzerland

****Correspondence:***
Lidia Ferri
lferri@mendoza-conicet.gob.ar

Specialty section:
This article was submitted to Cryospheric Sciences, a section of the journal Frontiers in Earth Science

Received: *30 January 2020*
Accepted: *09 November 2020*
Published: *03 December 2020*

Citation:
Ferri L, Dussaillant I, Zalazar L, Masiokas MH, Ruiz L, Pitte P, Gargantini H, Castro M, Berthier E and Villalba R (2020) Ice Mass Loss in the Central Andes of Argentina Between 2000 and 2018 Derived From a New Glacier Inventory and Satellite Stereo-Imagery. Front. Earth Sci. 8:530997. doi: 10.3389/feart.2020.530997

INTRODUCTION

Comprehensive and detailed glacier inventories provide important reference datasets for assessing the current status and estimating the recent and future glacier changes (Paul et al., 2013; Vaughan et al., 2013). In recent decades, with the development of satellite remote sensing techniques, more precise and standardized glacier outlines have been produced from optical satellite imagery, permitting the mapping of glaciers at a regional scale with high accuracy (Nagai et al., 2016; Meier et al., 2018; Mölg et al., 2018). Argentina is the second country in the Southern Andes with the

largest glacierized area (WGMS, 2020). Previous inventories for the Argentinean Andes were mostly local (Pitte et al., 2010; WGMS, 2012; Masiokas et al., 2015; Falaschi et al., 2016). The recent National Glacier Inventory of Argentina (hereafter NGI), conducted by IANIGLA-CONICET in accordance with the National Law 26,639 for glacier protection in Argentina, provides a comprehensive dataset and detailed outlines of all Argentinean ice masses (Zalazar et al., 2020). The NGI, developed following international standards (UNESCO-IASH, 1970; Raup et al., 2007; Kargel, 2014), identified 16,078 ice masses covering a total area of 5,769 km^2 in the Andes of Argentina. Until the publication of the NGI (Zalazar et al., 2020), the Randolph Glacier Inventory (RGI; Pfeffer et al., 2014) was the only glacier inventory considering the entire Argentinean Andes; still, some debris-covered glaciers and rock glaciers were not classified as this was not part of the RGI objectives.

In the Central Andes of Chile and Argentina ice masses play an important hydrological role providing meltwater during the dry season (austral summer) and during droughts periods (Gascoin et al., 2011; Ayala et al., 2016; Rivera et al., 2017). Since 2010 this region has experienced an unprecedented drought (commonly known as the "mega-drought") that has severely affected the water supply at both sides of the Andes (Rivera et al., 2017; Garreaud et al., 2019; Masiokas et al., 2019). Regional glacier melt contributed to mitigate the negative impacts of this unprecedented long dry period (Dussaillant et al., 2019).

As observed elsewhere in the Andes, most glaciers in the Central Andes of Chile and Argentina, have experienced a generalized retreating pattern during the last decades (Masiokas et al., 2009; Barcaza et al., 2017). For example, in the Aconcagua river basin (Chile), the total glacier area reduction was ca. 20% between 1955 and 2003 (Bown et al., 2008). Similarly, Malmros et al. (2016), detected a ca. 30% glacier reduction between 1955 and 2013/14 in the Central Andes of Chile and Argentina. Continuous measurements at the Echaurren Norte glacier in Chile provide the longest (>30 years) record of glacier variations including a complete *in-situ* mass balance time series (Masiokas et al., 2016; Farías-Barahona et al., 2019). The Echaurren Norte glacier experienced a significant downwasting from 1955 to 2015, with a total cumulative glacier-wide mass balance of −40.64 m w.e. (Farías-Barahona et al., 2019). The cumulative glaciological mass balance for the Piloto Este glacier during 1979–2003 amounted −10.5 m w.e. (Leiva et al., 2007). Besides these two mass balance series, *in-situ* observations of glacier mass balance still remain scarce for the region, with most of the records starting after 2010 (Kinnard et al., 2018; Pitte et al., 2018). More recently, geodetic mass balance observations have been used to estimate changes in glacier volumes over large glaciated regions (Falaschi et al., 2018b; Braun et al., 2019; Burger et al., 2019; Dussaillant et al., 2019). Two recent Andes-wide geodetic mass balance assessments identified continuous mass loss along the entire Andes after the year 2000, showing a marked latitudinal pattern of glacier mass change rates (Braun et al., 2019; Dussaillant et al., 2019). In this study, we combine the glacier elevation change rates obtained by Dussaillant et al. (2019) with the recently released NGI to calculate the mass balance of all the ice masses of the Central Andes of Argentina over the 2000–2018 period, and the 2 decades within, 2000–2009 and 2009–2018 sub-periods.

The goals of the present study are three-fold: 1) Analyze the main characteristics of the different ice masses identified in the NGI of the Central Andes of Argentina, focusing especially on the presence of debris coverage and rock glaciers, and compare these results with those provided by the RGI version 6.0 for the same region; 2) revise the geodetic mass balance estimates from Dussaillant et al. (2019) using the improved NGI; and 3) compare the mass balance rates of the different NGI ice masses in relation to their percentage of debris coverage.

REGIONAL SETTING

Following Lliboutry (1998), the Argentinean NGI was divided into five glaciological regions. The Central Andes of Argentina are located between ca. 30°S and 37°S and can be characterized by a semi-arid climate with precipitation largely concentrated during the austral winter season. Precipitation events are associated with passing fronts embedded in the mid-latitude Westerly flow and enhanced by the orographic effect of the Andes Mountains (Garreaud et al., 2009; Viale et al., 2019). Overall environmental conditions in this region can be considered as transitional between those in the Desert Andes to the north, and the northern Patagonian Andes to the south. Surging glaciers have been detected in the Central Andes (Pitte et al., 2016; Falaschi et al., 2018a) as well as glaciers on both extinct (e.g., Tupungato, 6,635 m a.s.l) and extremely active volcanoes (e.g., Peteroa, 4,113 m a.s.l).

According to Sagredo and Lowell (2012), ice masses in the Central Andes of Chile and Argentina can be climatically arranged in two latitudinal-distributed groups. A first northern group located around 30°–31°S with precipitation (~300 mm/yr) evenly distributed throughout the year (slightly higher during the winter months) and with the coldest mean annual temperatures reported for the Andes (ca. −4.5°C). In the second group of glaciers, located between ca. 32° and 37°S, precipitation is concentrated during the austral winter months (~700 mm/yr) and mean annual temperatures are around 0°C (Sagredo and Lowell, 2012). The snowline along the Andes decreases from ~5,000 to ~3,200 m a.s.l. from north to south (Nogami, 1972). South of 35°S, the mean elevation of the Cordillera decreases with latitude, and the glacier area is comparatively smaller than further north (Zalazar et al., 2020).

A total of seven large hydrological basins were delimited in the Central Andes of Argentina. From north to south they are: the San Juan, Mendoza, Tunuyán, Diamante, Atuel, Llancanelo and Colorado rivers basins (**Figure 1**). The San Juan basin is the northernmost catchment (30–32°S) with one of the highest summits in the region, the Cerro Mercedario (6,770 m a.s.l). Further south, the Mendoza river basin (32–33°S), contain the highest peak of the Americas, the Cerro Aconcagua (6,961 m a.s.l.). The two better studied surging glaciers in Argentina, the Horcones Inferior and Grande del Nevado glaciers, are also located in this basin (Pitte et al., 2016). The Tunuyán river basin (33–34°S), contains the San Jose volcano (6,070 m a.s.l.)

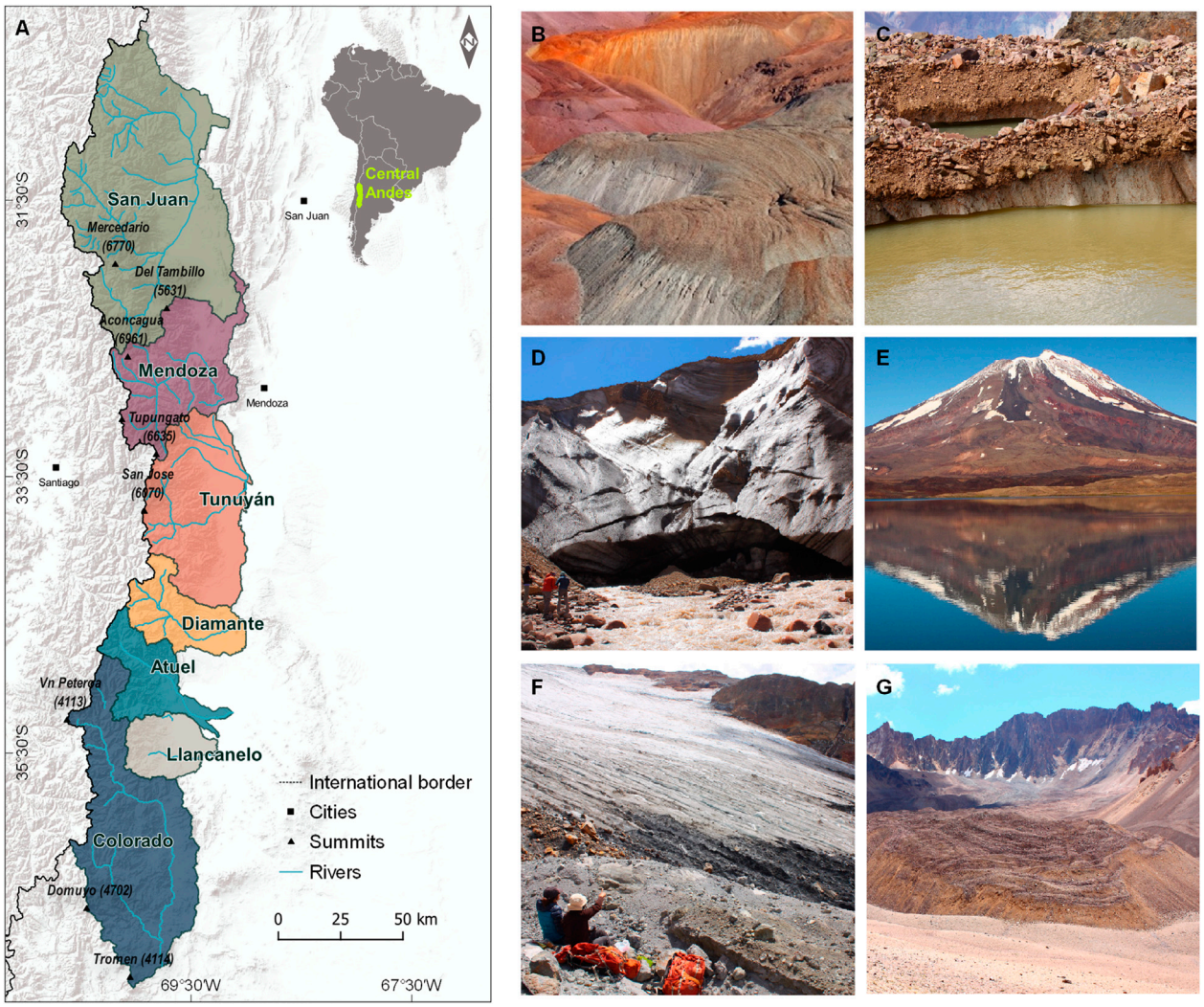

FIGURE 1 | (A) Map of the main river basins in the Central Andes of Argentina. **(B–G)** Some examples of the ice masses that can be found in this region **(B)** The Calingasta rock glacier, San Juan basin. **(C)** Thermokarst in a debris-covered glacier, Mendoza basin. **(D)** Proglacial stream and ice front of the Tunuyán glacier, the largest glacier in the Central Andes of Argentina. Note the debris cover at the glacier surface, Tunuyán basin. **(E)** Clean ice glaciers and perennial snowfields in the Maipo volcano area, Diamante basin. **(F)** The Azufre glacier, Colorado basin. Since 2010 the glacier is partially covered by a thin layer of ash due to the eruption of the neighboring Peteroa volcano. **(G)** Debris-covered ice with rock glacier, Llancanelo basin. (Photos: M. Castro, IANIGLA).

and, together with the Mendoza basin, contain the two of the most important irrigated "oases" and the largest population centers east of the Central Andes in Argentina. The Diamante river basin (around 34°S) contains the Maipo volcano (5,318 m a.s.l.) and a large high elevation lagoon at its base. Further south, in the Atuel river basin (34–35°S), historical documents indicate that the Humo glacier retreated approximately 3.2 km between 1914 and 1947 (Cobos and Boninsegna, 1983), showing one of the largest glacial retreats documented during the first half of the 20th century in the region. The headwaters of the Llancanelo basin (35°S) are situated along a small mountain range to the east of the main Cordillera. In the Colorado river basin (34–37°S), the mass balance of the Azufre glacier has been monitored since 2017 using the glaciological method (Pitte et al., 2018). South of 35°S in the Colorado river basin the presence of ice masses is mostly associated with volcanoes such as the Tromen (4,114 m a.s.l.) and the Domuyo (4,702 m a.s.l.).

DATA AND METHODS

Glacier Inventory Datasets

National Glacier Inventory of Argentina

The NGI of Argentina targeted different ice masses that represent strategic water reserves according to the National Law 26,639 (Zalazar et al., 2020) and includes: glaciers (both clean ice and debris-covered ice), glacierets or perennial snowfields and rock glaciers (active and inactive). Following international guidelines,

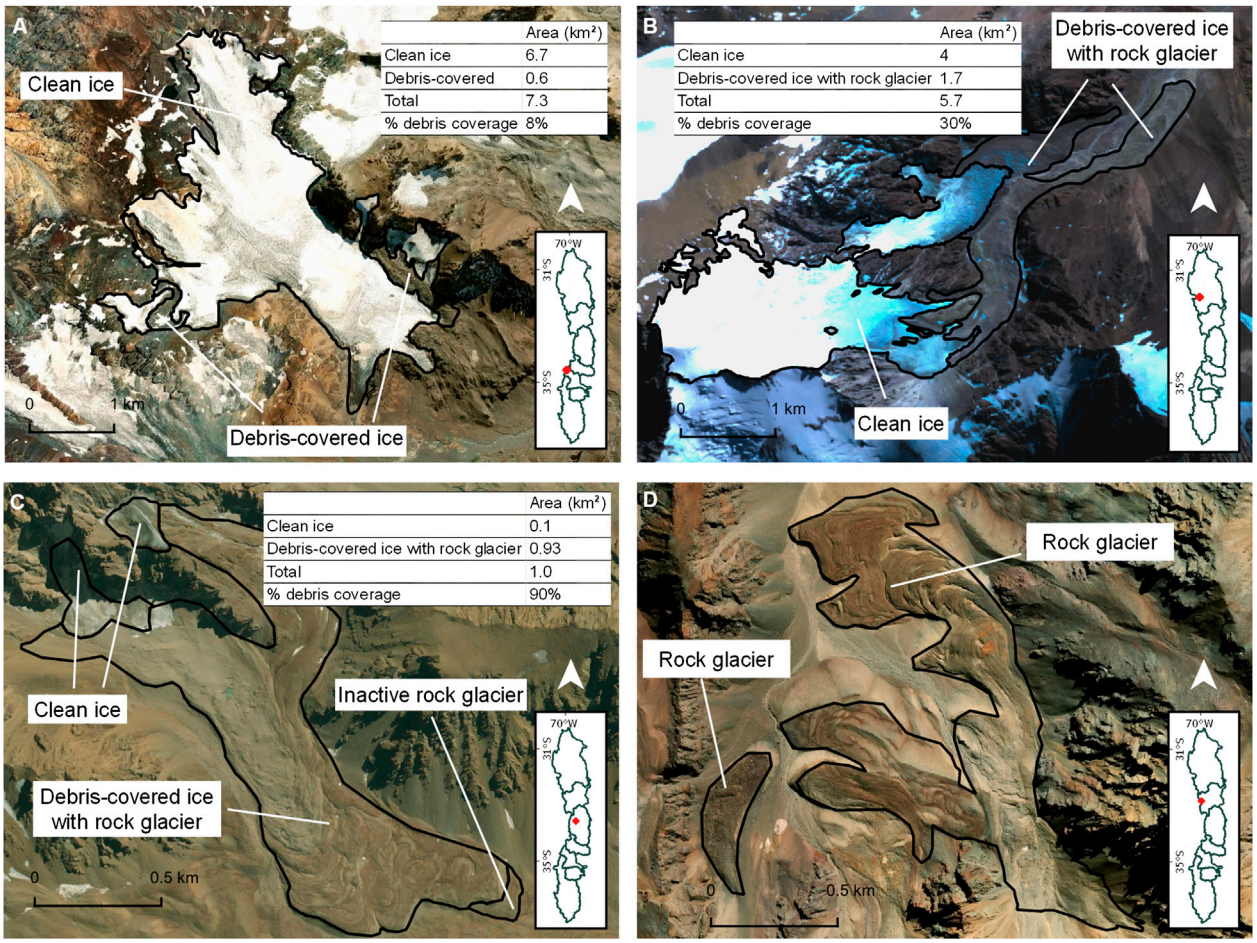

FIGURE 2 | Examples of ice masses showing the wide range of debris coverage that can be found in the study area. **(A)** Partly debris-covered glacier (8%) in the Atuel basin. **(B)** Partly debris-covered ice with rock glacier (30% debris coverage) in the San Juan basin. **(C)** Completely debris-covered ice with rock glacier (90% debris) in the Tunuyán basin. **(D)** Rock glacier (considered 100% covered by debris) in the Mendoza basin.fx.

the minimum area for an ice mass to be included in the NGI was 0.01 km^2 (Paul et al., 2009; RGI Consortium, 2017b). In the Central Andes of Argentina, the NGI was based on medium spatial resolution satellite images such as ASTER (28 scenes), ALOS-AVNIR (20 scenes) and LANDSAT 5 (1 scene) acquired between 2007 and 2011. A supervised classification was applied to the selected images to detect and delineate clean ice and perennial snowfields. Debris-covered ice and rock glaciers were delimited by visual interpretation and manual digitization. High resolution images were also used to improve the delineations (e.g. ALOS-PRISM, CBERS-HRC and Google Earth). The classification and morphological parameters of each ice mass are included into a database with a total of 38 attributes following international guidelines (UNESCO-IASH, 1970; Rau et al., 2005). The NGI includes an additional category termed "debris-covered ice with rock glacier" that represents a transitional phase where debris-covered ice gradually transforms into rock glaciers with no clear boundary between these surfaces (Zalazar et al., 2020). Additional fields were added to classify rock glaciers considering their origin, activity, form and structure. To improve the mapping quality and assess the activity of rock glaciers, a total of 598 ice masses where directly surveyed in the field during austral summers from 2012 to 2015. See Zalazar et al. (2020) for more details on materials and methods used in the NGI.

In this study, an additional field was included in the dataset to account for the percentage of debris-cover. This classification ranges from 0% for debris free glaciers, 10–50% for partly debris-covered ice (**Figure 2A**), 50–90% for mostly debris-covered ice and >90% for completely debris-covered ice. The same classification was used for "debris-covered ice with rock glacier" category (**Figures 2B,C**). Rock glaciers are considered as an independent category, completely covered by debris with no visible ice on the surface (**Figure 2D**).

Randoph Glacier Inventory

The RGI data were obtained from the GLIMS's website https://www.glims.org/. We used the RGI version 6.0 (hereafter RGI) to compare with the NGI outlines. According to the RGI documentation, the glacier outlines for the Central Andes were created from Landsat seven ETM + imagery acquired between

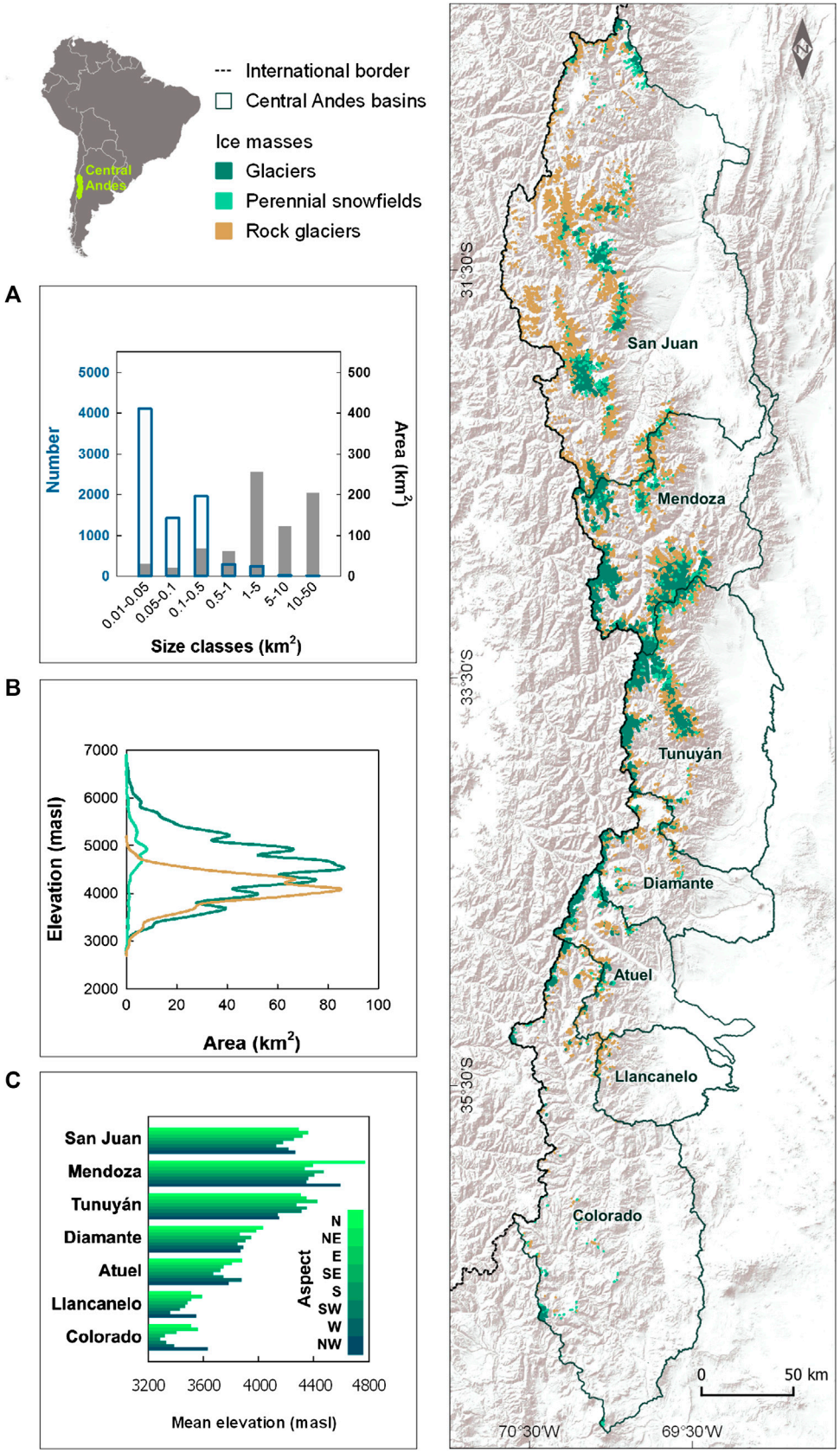

FIGURE 3 | Inventory of ice masses in the Central Andes of Argentina. **(A)** Distribution and number of ice masses according to their size. **(B)** Hypsometry of the different types of ice masses. **(C)** Mean elevation and aspect of the ice masses in the different river basins.

2000 and 2003. Version 6.0 includes some upgrades such as images of better quality to reduce the presence of seasonal snow. However, the ice cover for this region may still be overestimated (RGI Consortium, 2017). It is also important to note that rock glaciers are not explicitly included in this dataset as the main focus of the RGI is to provide a near global picture of glaciers for large-scale assessments.

Geodetic Mass Balance Dataset

Ice mass changes for the periods 2000–2018, 2000–2009 and 2009–2018, were calculated using the "ASTER monitoring of Ice towards eXtinction" geodetic method (hereafter the ASTERIX method, Dussaillant et al., 2019), for both the NGI and the RGI inventories. Individual glacier mass balance rates reported here for the RGI are the same as those reported by Dussaillant et al. (2019). Results for the NGI inventory were calculated from the original ASTERIX elevation change grids using the newer outlines. The ASTERIX method calculates surface elevation changes using times series of digital elevation models (DEMs) obtained from Advanced Spaceborne Thermal Emission and Reflection Radiometer (ASTER) stereo images (Wang and Kääb, 2015; Berthier et al., 2016). This methodology has been validated in different glaciated regions of the world with different climatic contexts and glacier types (Brun et al., 2017; Berthier et al., 2018; Menounos et al., 2019) including the Andes (Dussaillant et al., 2018). ASTERIX elevation changes rates in the Central Andes were derived from a mean for 26 DEMs, with 92% of the total glacierized area covered with valid elevation change measurements. Mass balance rates were estimated for every individual ice mass using the local hypsometric approach (McNabb et al., 2019) over 100 m elevation bands. Data gaps in the elevation change grids were filled on an individual ice mass basis using the mean rate of elevation change of the corresponding elevation bin. Elevation change outliers were also excluded and replaced by the mean elevation change of every bin. The glacier-wide volume change rate was calculated as the sum of the mean elevation changes multiplied by the area of each elevation band. The corresponding mass balance rates were computed assuming a volume to mass conversion factor of 850 ± 60 kg m^{-3} (Huss, 2013). Uncertainty on the glacier mass balance is calculated as a random error derived from three independent sources: the uncertainties in the rate of elevation change, the volume-to-mass-conversion factor and the glacierized area (Rolstad et al., 2009; Fischer et al., 2015). For larger regions (e.g., basin-wide or region-wide), the mass balance rates were calculated as the area weighted sum of all ice masses contained in the basin/region. The few ice masses with no valid elevation change rates, and thus presenting no mass balance rate estimate (5% of glacier covering only 1% of the total glacier surface), were assumed to respond with the regional mean mass balance rate. As in Dussaillant et al. (2019), the regional uncertainty was calculated as the quadratic sum of the regional random and triangulation uncertainty, both calculated considering all glaciers as one ice body. For more details in the methodology and uncertainty assessment of the ASTERIX elevation change grids used here we refer the reader to Dussaillant et al. (2019).

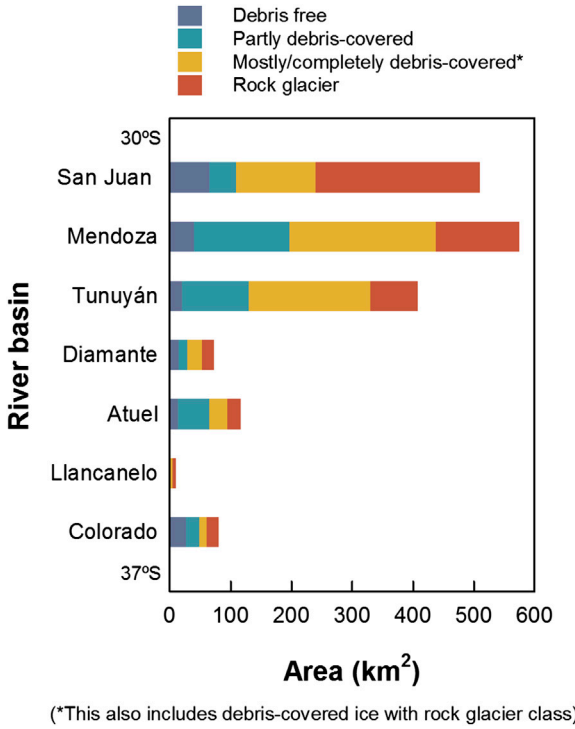

FIGURE 4 | Different debris coverage in glaciers and rock glaciers in the Central Andes basins of Argentina. "Debris-covered ice with rock glacier" corresponds to the new category included in the NGI of Argentina.

RESULTS

Characteristics of Ice Masses in the Central Andes

The NGI in the Central Andes of Argentina includes a total of 8,076 ice masses covering 1767 km^2 (**Figure 3**). This is the largest number of ice masses per region in the Argentinean Andes, and the second largest area covered by glaciers after the Southern Patagonia Andes (Zalazar et al., 2020). In terms of numbers, the most abundant type of ice masses are rock glaciers (68%). This region constitutes one of the places where rock glaciers are most abundant worldwide (Brenning, 2005; Blöthe et al., 2019). The majority (86%) of these rock glaciers were classified as active and 14% as inactive. The second most abundant category are perennial snowfields (20%) followed by glaciers (includes mountain and valley type glaciers) with a 12%. In terms of area, however, glaciers occupy 65% of the total, followed by rock glaciers (31%) and perennial snowfields (4%).

Most of the ice masses presented in this region are smaller than 1 km^2 (96%), half of them with areas between 0.01 and 0.05 km^2. The number of ice masses decreases markedly as size increases; only 14 ice masses cover 16% of the total inventoried area (**Figure 3A**). The largest ice masses correspond to valley glaciers that in some cases can reach areas of 10–60 km^2,

TABLE 1 | Glacier area for different types and debris coverage in the main river basins of the Central Andes of Argentina. Percentages refer to total glacier area (all types) in each basin.

Ice mass type	San Juan		Mendoza		Tunuyán		Diamante		Atuel		Llancanelo		Colorado		Total (all basins)	
	Area km^2	%	Area km^2	%	Area km^2	%	Area km^2	%	Area km^2	%	Area km^2	%	Area km^2	%	Area km^2	%
Debris free[a]	65	13	39	7	20	5	14	20	13	12	0	1	26	32	177	10
10–50% debris-covered	44	9	158	28	110	27	14	19	52	45	0	0	22	28	400	23
50–90% debris-covered	5	1	65	11	67	16	12	16	4	3	0	0	0	0	153	9
>90% debris-covered	0	0	17	3	3	1	1	1	1	0	0	0	1	1	23	1
10–50% debris-covered[b]	80	16	42	7	42	10	3	4	8	7	0	1	0	0	175	10
50–90% debris-covered[b]	35	7	91	16	62	15	7	10	9	8	0	0	9	12	213	12
>90% debris-covered[b]	11	2	25	4	26	6	1	2	7	6	4	39	2	2	76	4
Rock glacier	270	53	134	23	78	19	20	27	22	19	6	59	20	25	550	31
Total (all ice masses)	510	100	571	100	408	100	73	100	116	100	10	100	80	100	1767	100

[a]*Includes clean ice glaciers and perennial snowfields.*
[b]*Ice masses classified as "debris-covered ice with rock glacier".*

lengths of 10–18 km, and a vertical gradient of up to 2,500 m. Most of the tongues of the valley glaciers are debris-covered, or "debris-covered with rock glacier." The largest rock glaciers in Argentina were identified in this region, reaching in some cases over 2 km^2. The ice masses in the study region range between 2,600–2,800 and 6,700–6,800 m a.s.l., but the largest amount of ice is concentrated around 4,500 m a.s.l (**Figure 3B**). This wide altitudinal range is related to the high elevation of the Andes at these latitudes. The region hosts the highest ice bodies in the Americas (6,700–6,800 m a.s.l.), i.e. the hanging glaciers on the south face of Cerro Aconcagua. Some perennial snowfields and the accumulation areas of valley glaciers also reach high altitudes. In general, the northernmost basins (San Juan, Mendoza and Tunuyán) contain the highest glaciers and rock glaciers (**Figure 3C**). The ice masses with the lowest elevations (2,600–2,800 m a.s.l.) correspond to inactive rock glaciers and some perennial snowfields. These low elevations are recorded at the southernmost part of the region, where the Andes gradually decrease in elevation but receive larger amounts of precipitation. The San Juan, Mendoza and Tunuyán river basins also contain the largest ice masses and the greatest concentration of rock glaciers in this region. Similar to other Andean regions, ice masses are usually more frequent on the south and south-east facing slopes, where snow persistence is favored by the lower insolation compared to those facing to the north. The ice masses mean elevation in relation to the aspect indicates that northeast and northwest oriented ice masses show the highest elevations, while those on the southern and southeastern slopes reach the lowest altitudes (**Figure 3C**).

Debris-covered ice is an important characteristic of this region: 59% of the total inventoried area presents some degree of debris coverage (**Figure 4**; **Table 1**). Only 10% of the inventoried area corresponds to clean ice or perennial snowfields with no debris coverage. The remaining 31% corresponds to rock glaciers. It is interesting to note that the most common type of ice mass and the percentage of debris coverage also change with latitude (**Table 1**; **Figure 4**). The percentage of area covered by debris and by rock glaciers show a generalized decrease from north to south, with the exception of Llancanelo basin. The highest percentage of rock glaciers (53%) occurs at the northernmost San Juan basin (between ca. 30° and 32°S). Further south in the Mendoza, Tunuyán and Diamante basins (ca. 32°–34°), debris-covered ice and rock glaciers are still dominant, but the percentages of clean ice glaciers (including glaciers and perennial snowfields) increases in comparison with the northern San Juan basin. From the Atuel basin to the south (ca. 34°-35°S), the proportions of clean ice glaciers and snowfields increase markedly. This is also true for the southernmost Colorado basin (34°–37°S) which limits with the northern Patagonian Andes. Located in a drier environment east of the Colorado basin, the Llancanelo basin does not fit this regional pattern (**Figure 1**). The lowest elevation and the lowest humidity from the west that reaches this basin result in a much larger proportion of rock glaciers and "debris-covered ice with rock glacier" category, which represents the 98% of the total inventoried area. This basin presents characteristics more similar to those recorded in the northern part of the study area, where rock glaciers are also predominant.

Ice Mass Loss in the Central Andes of Argentina

Based on the ASTERIX methodology and the NGI dataset we found a thinning trend of the ice surface in the Central Andes during the period 2000–2018, with a regional mean mass balance rate of −0.18 ± 0.19 m w.e. yr^{-1}. From all ice masses, partly debris-covered glaciers

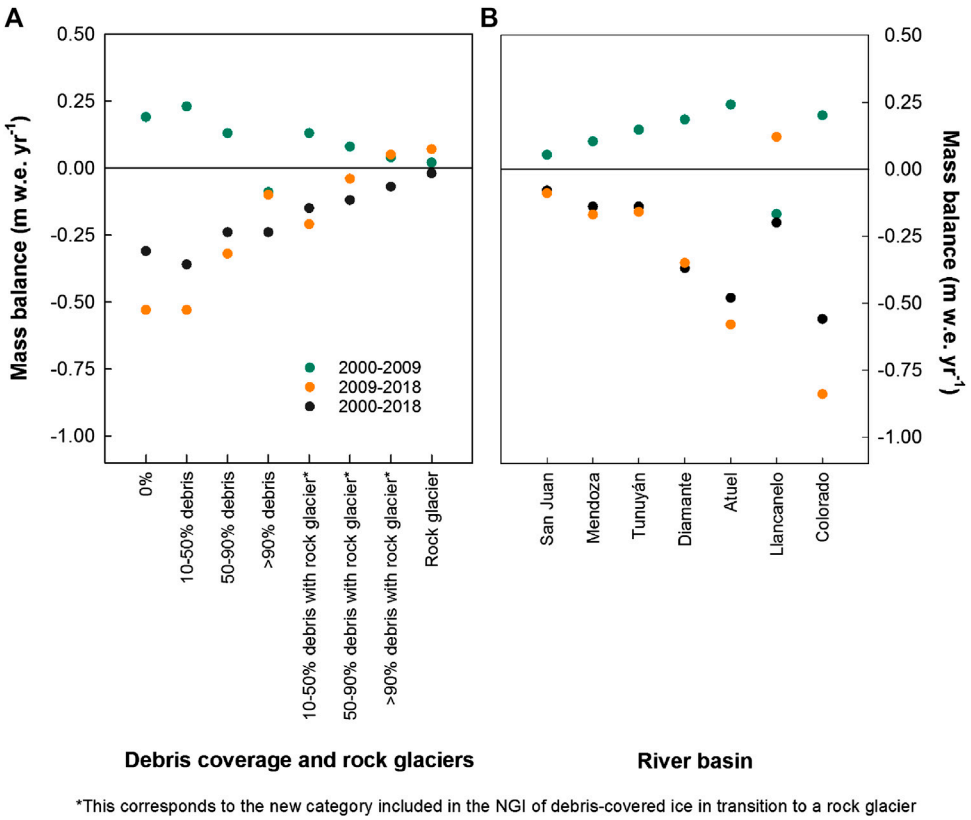

FIGURE 5 | (A) Mass balance rates for different ice masses based on the percentage of debris coverage for the period 2000–2018 and for the sub-periods 2000–2009 and 2009–2018. **(B)** Mass balance rates averaged for the main river basins in the study area.

and clean ice glaciers exhibited the most negative mass balance rates (−0.36 ± 0.19 and −0.31 ± 0.19 m w.e. yr^{-1}, respectively). Contrarily, mostly debris-covered glaciers, completely debris-covered and rock glaciers, underwent considerably lower mass losses and slightly negative or stable mass balances rates (−0.12 ± 0.18, −0.07 ± 0.19 and −0.02 ± 0.19 m w.e. yr^{-1}, respectively; **Figure 5A**). The strongest negative mass balance rates of −0.56 ± 0.20 m w.e. yr^{-1} resulted in the Colorado basin. In contrast, the less negative mass balance rates of −0.08 ± 0.18 m w.e. yr^{-1} were registered in the San Juan river basin. This suggest a general latitudinal pattern with a southern increase in ice mass loss, mirroring the increase of clean ice surface. The Llancanelo basin is the only exception to this latitudinal pattern, probably a consequence of the predominance of debris-covered glaciers and rock glaciers at this location (**Figure 5B**).

An evident inter-decadal shift in mass balance rates was recorded for the region (**Figure 5**). During the 2000–2009 decade, regional mass balance rates were slightly positive, reaching +0.12 ± 0.23 m w.e. yr^{-1}. Positive mass balance rates are consistent for all basins except for Llancanelo (−0.17 ± 0.25 m w. e. yr^{-1}, **Figure 5B**). Similarly, almost all the independent ice mass types experienced positive mass balance rates during this period, except for the completely debris-covered glaciers, registering a close to zero mass balance rate of −0.09 ± 0.22 m w.e. yr^{-1} (**Figure 5A**).

A notable change in this pattern was observed for the 2009–2018 decade, with all ice masses shifting towards more negative mass balance rates (**Figure 5**), and a mean regional mass loss of −0.21 ± 0.30 m w.e. yr^{-1}. Clean ice glaciers and partly debris-covered glaciers experienced the largest mass losses, amounting to −0.53 ± 0.26 and −0.53 ± 0.21 m w.e. yr^{-1} respectively. Conversely, completely debris-covered with rock glaciers and rock glaciers showed slightly positive mass balance rates of +0.05 ± 0.22 and +0.07 ± 0.21 m w.e. yr^{-1}, respectively. During this period nearly all basins in the Argentinean Central Andes showed consistent negative glacier mass balance rates, again with the exception of the Llancanelo basin, presenting positive rates of +0.12 ± 0.26 m w.e. yr^{-1} (**Figure 5B**). Examples of the changes in elevation maps for the long period 2000–2018 and the two sub-periods can be observed in **Figure 6** for three different glacier subsets located in different basins. A clear trend from positive to negative changes in elevation rates between decades can be readily observed for the three subsets.

The mass balances of some prominent glaciers in the Central Andes of Argentina are shown in **Table 2**. The list includes some of the ice masses with the largest overall lowering rates in the region as the Azufre, Peñón and Grande del Nevado glaciers. During the complete period 2000–2018, the Azufre

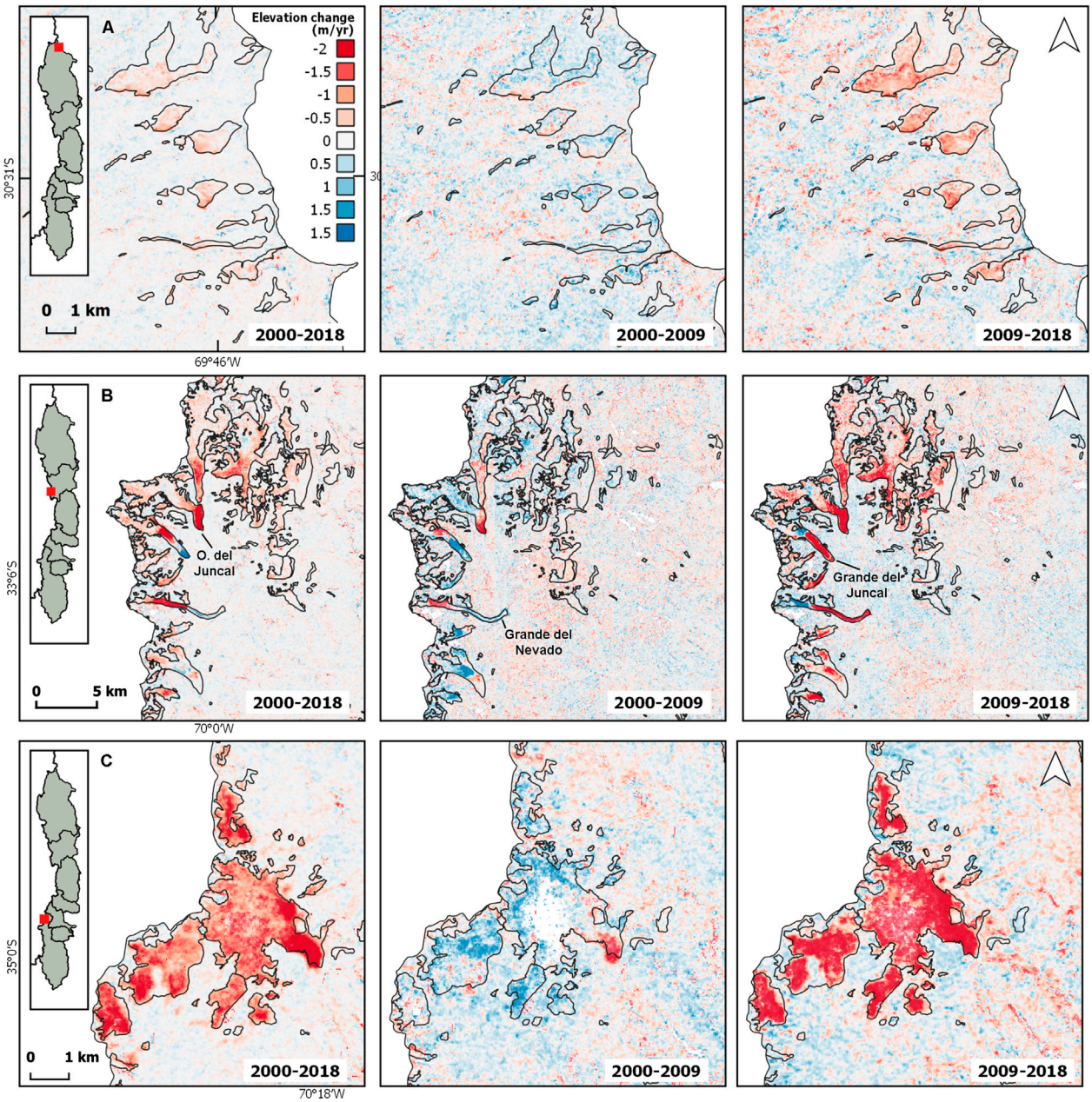

FIGURE 6 | Examples of elevation changes in different areas of the Central Andes for different sub-periods. NGI glacier outlines are shown in black lines. **(A)** Small mountain glaciers and perennial snowfields in San Juan basin. **(B)** Large valley glaciers in Mendoza basin, some of them classify as surging glaciers. **(C)** Mountain and valley glaciers in Atuel basin.

and Peñón glaciers lost −1.5 ± 0.15 and −1.4 ± 0.13 m w.e. yr^{-1}, respectively (**Table 2**). The Grande del Nevado glacier, a well-documented surging glacier (Helbling, 1935; Pitte et al., 2016), also experienced a strong negative mass balance. Its last surging event was registered during 2006-2007, concurrent with the decade (2000–2009) of positive mass balances across the Central Andes. Afterwards, a general down-wasting was observed during the 2009–2018 period (−0.97 ± 0.16 m w.e. yr^{-1}), related to a quiescent phase of this glacier (Pitte et al., 2016). The mass balance rates for the surging glaciers in this region during the period 2000–2018 was −0.30 ± 0.19 m w.e. yr^{-1}. This mean value is more negative but not statistically different than the mean recorded for the non-surging glaciers (−0.17 ± 0.19 m w. e. yr^{-1}) over the same period in this region. Elevation changes for several of the surging glaciers listed in **Table 2** are depicted in **Figure 6B**.

TABLE 2 | Mass balance rates calculated for particular ice masses with different percentages of debris coverage.

Basin	Glacier name	Lon	Lat	Area (km^2)	Debris coverage (%)	Mass balance rate (m w.e. yr^{-1})			Observations
						2000–2018	2000–2009	2009–2018	
San Juan	Del Caballito	−70.10	−31.98	5.70	31	−0.13 ± 0.05	0.19 ± 0.13	−0.29 ± 0.10	—
San Juan	Italia	−70.06	−32.05	8.31	4	−0.24 ± 0.05	0.30 ± 0.12	−0.46 ± 0.10	—
Mendoza	De las Vacas	−69.98	−32.56	18.35	6	−0.36 ± 0.04	0.23 ± 0.06	−0.55 ± 0.08	—
Mendoza	Güssfeldt	−70.01	−32.59	11.91	10	−0.49 ± 0.05	−0.10 ± 0.07	−0.70 ± 0.09	—
Mendoza	Horcones inferior	−70.00	−32.66	7.39	94	−0.45 ± 0.05	−0.50 ± 0.10	−0.13 ± 0.08	Surging glacier
Mendoza	Alto del Plomo	−70.01	−32.98	16.97	10	−0.30 ± 0.04	0.16 ± 0.06	−0.50 ± 0.07	—
Mendoza	Bajo del Plomo	−69.98	−33.00	18.66	7	−0.36 ± 0.04	0.18 ± 0.06	−0.55 ± 0.07	—
Mendoza	Grande del Juncal	−70.05	−33.05	7.43	23	−0.37 ± 0.06	0.37 ± 0.10	−0.48 ± 0.10	Surging glacier
Mendoza	Oriental del Juncal	−70.01	−33.06	10.67	10	−0.51 ± 0.06	0.35 ± 0.08	−0.90 ± 0.11	—
Mendoza	Beta	−70.06	−33.09	2.28	0	−0.29 ± 0.09	0.16 ± 0.16	−0.36 ± 0.17	—
Mendoza	Gama	−70.03	−33.10	1.84	29	−0.46 ± 0.10	0.45 ± 0.20	−0.62 ± 0.20	—
Mendoza	Grande del Nevado	−70.02	−33.13	3.38	60	−1.11 ± 0.12	−0.07 ± 0.14	−0.97 ± 0.16	Surging glacier
Mendoza	Pequeño del Nevado	−70.04	−33.14	1.57	57	−0.26 ± 0.11	0.20 ± 0.14	−0.48 ± 0.21	—
Tunuyán	Tunuyán	−69.78	−33.46	56.88	50	−0.31 ± 0.03	0.06 ± 0.04	−0.41 ± 0.05	Surging glacier
Atuel	De La Laguna	−70.10	−34.50	6.30	7	−0.50 ± 0.06	0.52 ± 0.15	−0.77 ± 0.11	Surging glacier
Atuel	Del Humo	−70.16	−34.57	8.88	6	−0.85 ± 0.08	0.55 ± 0.11	−1.03 ± 0.12	—
Atuel	Fiero	−70.16	−34.60	7.34	9	−0.95 ± 0.10	0.22 ± 0.09	−1.27 ± 0.14	—
Atuel	Corto	−70.03	−34.61	2.93	39	−0.77 ± 0.10	0.22 ± 0.09	−0.92 ± 0.16	—
Colorado	Peñón	−70.56	−35.27	3.48	0	−1.40 ± 0.14	0.30 ± 0.14	−2.07 ± 0.22	Presence of volcanic ash since 2010
Colorado	Azufre	−70.56	−35.29	3.94	0	−1.51 ± 0.15	0.14 ± 0.13	−1.96 ± 0.21	Presence of volcanic ash since 2010

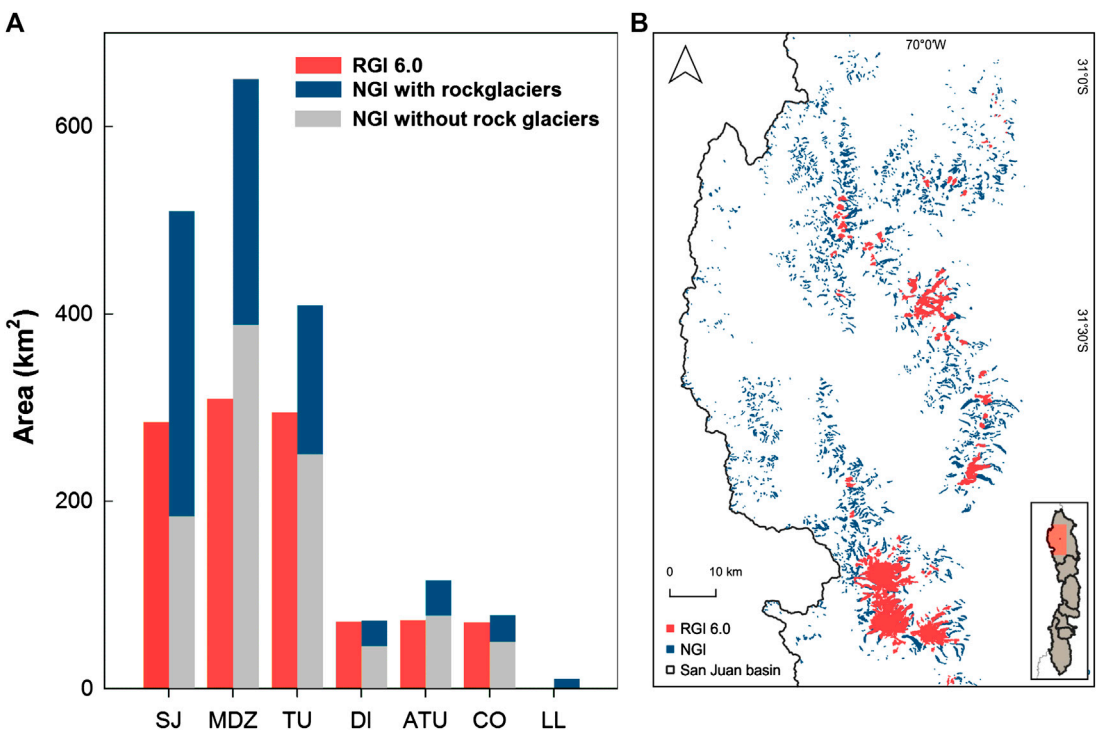

FIGURE 7 | (A) Comparison of results from the RGI version 6.0 and NGI for the main river basins in the study area: San Juan (SJ), Mendoza (MDZ), Tunuyán (TU), Diamante (DI), Atuel (ATU), Colorado (CO) and Llancanelo (LL). **(B)** Example from the San Juan river basin showing the differences in glacier outlines between the RGI and the NGI.

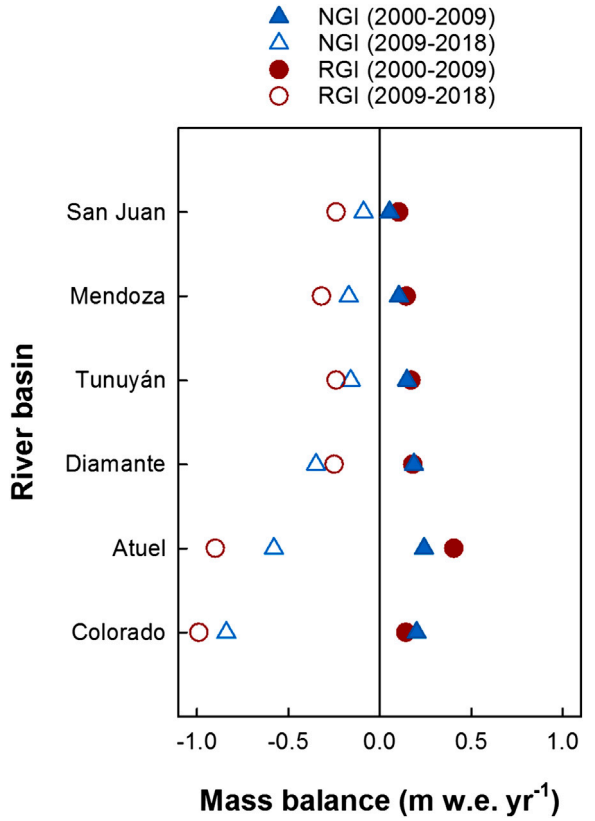

FIGURE 8 | Different mass balance rates in the Central Andes ice masses based on the NGI and RGI version 6.0 inventories.

Differences between the National Glacier Inventory and Randolph Glacier Inventory Datasets

In the Central Andes of Argentina, the RGI version 6.0 contains 1,135 glaciers covering a total area of 1,085 km^2. In total, 6,941 more ice masses and 682 km^2 of inventoried area were identified in the NGI (**Figure 7A**). For example, in the San Juan river basin alone, the NGI recorded 3,810 ice masses (i.e., 47% of the total number of units in the entire region), almost three times more units than those represented in the RGI (**Figure 7B**). As for the glacierized area, the RGI seems to have overestimated the glacier surface in some particular locations probably due to the use of scenes with presence of seasonal snow and the inclusion of some outcrops and avalanche contributing areas. Most of the glacier areas that were not included in the RGI correspond mostly to rock glaciers (69% of the area). The remaining 31% of the areal discrepancies between the NGI and the RGI corresponds to the lower tongues of valley glaciers, mainly the category "debris-covered ice with rock glacier," and some mountain glaciers and perennial snowfields. Comparing the inventoried areas for each basin, the larger differences occur in the San Juan and Mendoza basins, where rock glaciers are more frequent (**Figure 7B**). Further south, debris-covered ice and rock glaciers are less extensive and the differences between the inventoried areas in the RGI and NGI are smaller. As mentioned above, 98% of the area inventoried in the Llancanelo basin corresponds to rock glaciers and "debris-covered ice with rock glacier" category, and the RGI does not include ice masses in this basin.

Despite the differences in area and number of ice masses recorded in the RGI and NGI datasets, the geodetic mass balances calculated for both inventories are in good agreement (**Figure 8** and **Table 2**). The regional mass balance rate for the period 2000–2018 for the RGI (−0.26 ± 0.16 m w.e. yr^{-1}) is only slightly more negative than the regional mass balance obtained with the NGI (−0.18 ± 0.19 m w.e. yr^{-1}). Similarly as reported for the NGI a moderate positive regional mass balance rate is observed for the RGI (+0.16 ± 0.23 m w.e. yr^{-1}) during the 2000–2009 decade, with a marked shift towards more negative mass balance rates for the next decade 2009–2018 (−0.35 ± 0.21 m w.e. yr^{-1}).

Since glaciers in the RGI are not classified by ice mass type (i.e., debris coverage, rock glaciers, etc.) it is not possible to compare the changes in ice surface elevations using these parameters. At the watershed level, mass losses in the RGI show a general agreement with those recorded in the NGI (**Figure 8**), with an increase in thinning rates from north to south, and with the southernmost basins showing the most negative mass balance rates. Differently to the NGI inventory, the most negative mass balance rates over the period 2000–2018 correspond to the Atuel basin with −0.70 ± 0.19 m w.e. yr^{-1}. Inter-decadal mass balance rates for both inventories are presented in **Figure 8**. As expected, the main discrepancies between estimates occur in the basins where the differences in the total inventoried areas are larger. In the San Juan and Mendoza basins, where inventoried area in the NGI is more than two times larger than in the RGI, most of the differences correspond to the rock glacier and "debris-covered ice with rock glacier" category (**Table 3**).

DISCUSSION

Debris-Covered Ice

In the Argentinean Central Andes, the NGI confirms the presence of a high number of ice masses with a significant percentage of debris coverage (59% of the total inventoried area). The NGI also includes a new category for complex ice masses that represents a transition between debris-covered ice and rock glaciers (Zalazar et al., 2020). Although other studies identifying these complex forms are available (Janke et al., 2015; Monnier and Kinnard, 2015), the discussion on the delineation and classification of these interesting yet complex ice masses is still poorly documented and more detailed investigations are required. Nonetheless, the inclusion of different types of ice masses in the NGI allows for new analyses and studies that consider their particular characteristics and can facilitate our understanding of how they have reacted and may probably react to the ongoing climate changes.

TABLE 3 | Mass balance rates calculated for the main river basins using the RGI version 6.0 and NGI datasets and different time periods.

Basins	Area (km^2)		Mass balance rate 2000–2018 (m w.e. yr^{-1})		Mass balance rate 2000–2009 (m w.e. yr^{-1})		Mass balance rate 2009–2018 (m w.e. yr^{-1})	
	NGI	RGI	NGI	RGI	NGI	RGI	NGI	RGI
San Juan	491	270	−0.08 ± 0.18	−0.13 ± 0.19	0.05 ± 0.23	0.1 ± 0.23	−0.09 ± 0.21	−0.24 ± 0.21
Mendoza	571	306	−0.14 ± 0.18	−0.24 ± 0.18	0.10 ± 0.22	0.14 ± 0.22	−0.17 ± 0.20	−0.32 ± 0.21
Tunuyán	408	300	−0.14 ± 0.19	−0.17 ± 0.19	0.15 ± 0.23	0.17 ± 0.23	−0.16 ± 0.22	−0.24 ± 0.22
Diamante	73	68	−0.37 ± 0.20	−0.35 ± 0.20	0.18 ± 0.23	0.18 ± 0.23	−0.35 ± 0.22	−0.25 ± 0.22
Atuel	114	72	−0.48 ± 0.19	−0.70 ± 0.19	0.24 ± 0.23	0.4 ± 0.23	−0.58 ± 0.21	−0.9 ± 0.22
Llancanelo	8	NO DATA	−0.20 ± 0.22	NO DATA	−0.17 ± 0.25	NO DATA	0.12 ± 0.26	NO DATA
Colorado	79	72	−0.56 ± 0.20	−0.70 ± 0.21	0.20 ± 0.23	0.14 ± 0.23	−0.84 ± 0.23	−0.99 ± 0.31
Total	1744	1,088	−0.17 ± 0.19	−0.26 ± 0.16	0.12 ± 0.23	0.16 ± 0.23	−0.21 ± 0.30	−0.35 ± 0.21

Mass Balance Rate Vs. Debris Coverage

In the Central Andes of Argentina the different types of ice masses experienced dissimilar mass balance rates that are largely dependent on their degree of debris coverage. Partly debris-covered ice underwent the most significant downwasting in all basins, followed by clean ice glaciers and perennial snowfields. This behavior is consistent with that observed by Fyffe et al. (2019) over glaciers in the Italian Alps, where debris-covered glaciers showed the highest melt rates compared to clean and dirty-ice glaciers. El Peñón and Azufre glaciers recorded the greatest mass losses of the studied region, (**Table 2**). Both glaciers are located in the vicinity of the active Peteroa volcano crater (4,133 m a.s.l.), which has emitted fine particulates throughout the surrounding area in repeated occasions since 2010 (Haller and Risso, 2011; Aguilera et al., 2015). The thin layer of ash from this volcano has probably decreased the albedo of the ice surfaces, favoring the pronounced ablation recorded in these glaciers.

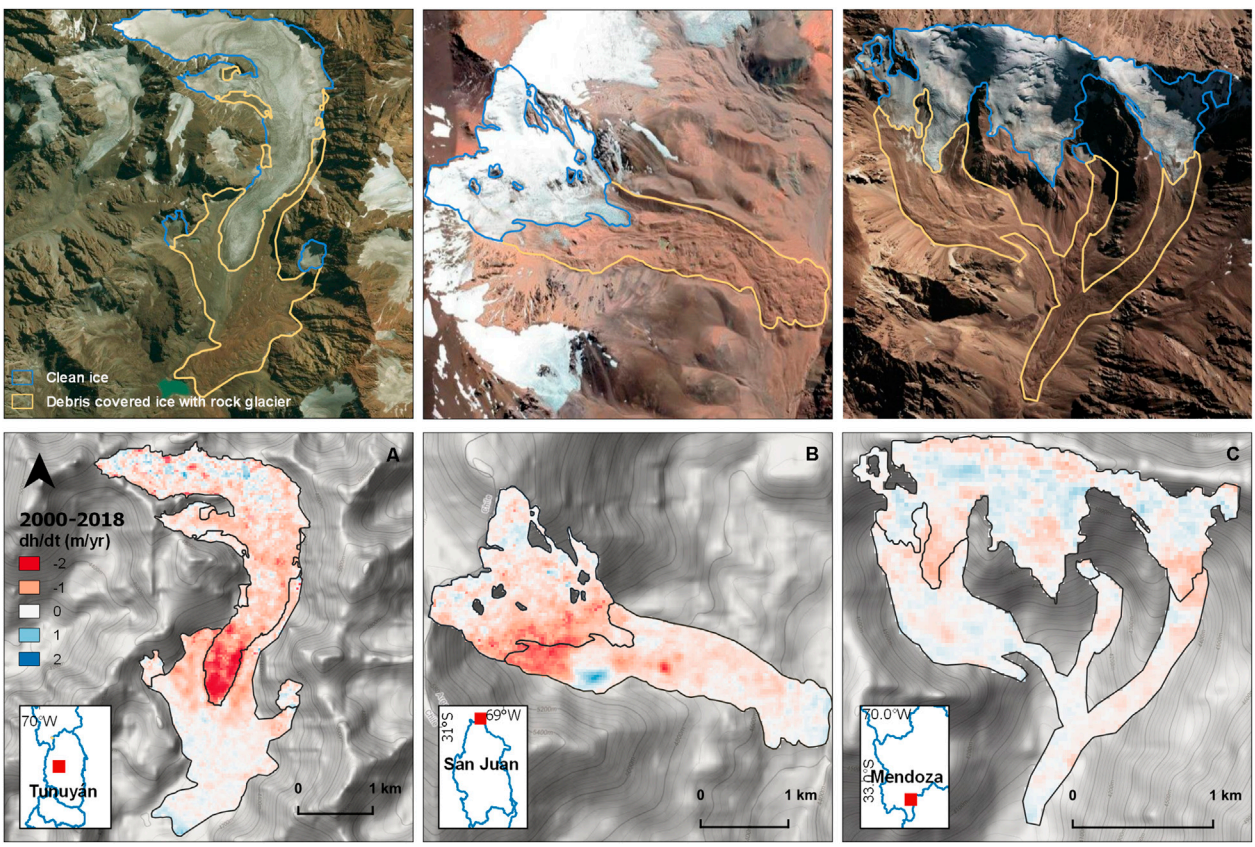

FIGURE 9 | Different examples of "debris-covered ice with rock glacier" category (upper row) in **(A)** Tunuyán, **(B)** San Juan and **(C)** Mendoza basins and the corresponding rate of elevation changes from 2000 to 2018 (lower row).

For glacier complexes in transition from debris-covered ice to rock glacier and rock glaciers, changes in volume were minor or stable over the study periods. Both categories are assumed to have a thicker debris layer that protect ice from ablation. Three different complex ice masses are shown in **Figure 9**. In their upper parts, they present clean ice evolving into debris-covered ice and rock glaciers (where characteristic features as furrows and ridges are visible on the lowermost reaches). From inspection of satellite images, they look similar to others debris-covered ice masses where debris increases in thickness toward their snouts (Rounce et al., 2018). For these particular cases, little or no change was observed in mass balance rates at their fronts during the period 2000–2018 (**Figures 9A–C**). However, we observe that the highest thinning rates (up to −2 m/year) were concentrated in areas with a thin layer of supraglacial till or dirty ice. This thinning can be observed in the three examples, although it is more remarkable in the glacier located at the Tunuyán basin (**Figure 9A**). This behavior is similar to that previously observed over ice masses in the Tien Shan, were most of the surface lowering also occurred in the transitional zone or "ice-debris complexes" (Bolch et al., 2019). This last study also evidences more stable mass balance rates in areas with thick debris coverage in transition to rock glaciers.

Our results show a clear temporal difference in mass balance rates over the last 2 decades. During the first decade of the 21st century (2000–2009) most of the ice masses showed relatively stable and even positive mass balance rates markedly changing to overall negative mass balance rates after 2009. The direct mass balance measurements at the Echaurren Norte glacier in Central Chile are consistent with this regional pattern, showing almost balanced conditions during the first decade of the 21st century and consistently negative balances after 2009 (Masiokas et al., 2016; Farías-Barahona et al., 2019; WGMS, 2020). Other glaciers in the region showed minor re-advances and increased surging activity during the wetter and colder first decade of the 21st century (Masiokas et al., 2009; Pitte et al., 2016; Falaschi et al., 2018a). The marked increase in ice mass loss that occurred afterwards has been related to the decrease in snow accumulation over the Andes, a phenomenon that started around 2010 as is still affecting the ice masses and water resources in this semiarid region (Garreaud et al., 2017; Rivera et al., 2017; Masiokas et al., 2019).

All ice masses play an important role in Central Andes hydrology, contributing to streamflow especially during the driest years (Schaffer et al., 2019). According to our results, the ice masses that most contributed to the runoff of the main rivers of the Central Andes during the period 2009–2018 were clean ice glaciers (-0.53 ± 0.26 m w.e. yr^{-1}) and partly debris-covered glaciers (-0.53 ± 0.21 m w.e. yr^{-1}). Conversely, most of the "debris-covered ice with rock glacier" and rock glaciers, underwent an almost zero mass balance rate ($+0.05 \pm 0.22$ and $+0.07 \pm 0.21$ m w.e. yr^{-1}) during the same period. Rock glaciers constitute an important long-term water reservoir in semiarid regions, with a large buffer capacity (Halla et al., 2020). Given their inherent characteristics, rock glaciers and completely debris-covered glaciers appear to be climatically more resilient than clean ice glaciers, suggesting that their importance as water storages will increase as climate warming continues in the Central Andes (Jones et al., 2018; Jones et al., 2019). This aspect is particularly important for the Central Andes of Argentina, because of the great variety and abundance of rock glaciers. Studies quantifying the role of the different ice masses are increasing rapidly, however, direct quantitative estimations of ice content and hydrological contribution of rock glaciers are still scarce in this region. Given the persistent drought conditions in the Central Andes, further research is clearly and urgently needed on this issue (Schaffer et al., 2019).

Understanding the correlation between debris coverage and mass balance changes is still a topic of active research and discussion. Indeed, Brun et al. (2019) did not observe systematic differences between clean ice glaciers and debris-covered glaciers in terms of glacier mass balances rates over High Mountain Asia glaciers. However, they suggest that the influence of debris-cover on glacier mass balances should be tested on a large number of glaciers and in different regions of the world. Our study represents a first attempt to address this issue in the Central Andes of Argentina, providing evidence for a discernible reduction in ice mass loss with increasing percentages of debris coverage in the different ice masses.

Differences in Geodetic Mass Balance Depending on the Inventory

Our study detected notable differences in the number of ice masses and the total area covered by the NGI and the RGI version 6.0. However, the differences in mass balance rates over the period 2000–2018 between the two products are negligible (i.e., −0.08 m w.e. yr^{-1}, which is within our uncertainty level). Nonetheless, a tendency towards comparatively more negative mass balance rates could be discerned in the RGI estimates. This pattern appears to be related to the fact that the RGI includes mostly clean ice glaciers, which represent one of the categories with the highest surface lowering over the period 2000–2018. As mentioned above, most of non-mapped units in the RGI correspond to the rock glaciers and "debris-covered ice with rock glacier" categories, which are the ones with the lowest thinning rates in the region. The different acquisition dates of the satellite imagery used to create the inventories may also account for the differences observed between the RGI and the NGI. The RGI used satellite imagery acquired between 2000 and 2003, prior to the acquisition of the images used in the NGI (images from 2007 to 2011). Despite these differences, it should also be noted that for basins with similar inventoried areas, the differences in mass balance between the NGI and RGI are minimal. The absence of successive inventories for this region hamper to account for area changes in the mass balance rate estimation. We estimate the area change impact on mass balance using a 0.5% annual area change rate estimated for the Andes (Vaughan et al., 2013). The corresponding sensitivity to mass balance rates was smaller than 0.01 m w.e. yr^{-1}, a value far below our uncertainty estimates. Therefore, we assume that area changes are negligible for regional assessment of glacier mass balance in this region during the studied period. Nevertheless, successive inventories of ice masses in this region are needed to

improve these first rough estimations and better account for areal changes in the mass balance changes in this region.

CONCLUSIONS

The Central Andes of Argentina host a vast number and diversity of glaciers, rock glaciers and perennial snowfields. The results discussed above are largely based on the recently published National Glacier Inventory of Argentina (NGI), which identified 8,076 ice masses covering 1767 km^2 in this region. More than half (59%) of the inventoried area presents some degree of debris coverage and the region also records an abundant number and variety of rock glaciers (68% of the total number).

A general surface lowering of the ice masses was observed during the period 2000–2018 (mass balance rate: −0.18 ± 0.19 m w.e. yr^{-1}). From 2000 to 2009 the mean regional mass balance rates were +0.12 ± 0.23 m w.e. yr^{-1}, switching to negative rates (−0.21 ± 0.30 m w.e. yr^{-1}) during the next decade 2009–2018. In general, the ice masses that experienced the most negative mass balance rates from 2000 to 2018 were partly debris-covered glaciers (−0.36 ± 0.19 m w.e. yr^{-1}) and clean ice glaciers (−0.31 ± 0.19 m w.e. yr^{-1}). On the other hand, completely debris-covered glaciers and rock glaciers showed almost zero mass balance rates (−0.07 ± 0.19 and −0.02 ± 0.19 m w.e. yr^{-1}, respectively). The basins with the most negative mass balance rates are those located further south in the Central Andes, which is consistent with the lowest percentage of debris-covered ice and/or rock glaciers. Despite these findings, there is still a need for studies that quantify the ice content of rock glaciers and their hydrological contribution to streamflows.

Compared to global inventories such as the RGI, the NGI provides more detailed information regarding different type of ice masses ("debris-covered ice with rock glacier" and rock glaciers). Due to the inclusion of these ice masses in the NGI, the mass balance rates were slightly less negative than when using the RGI. In view of these findings, the ongoing updating activities of the NGI will allow the analysis of the temporal changes in the ice surface and also the evolution of the different types of debris-covered glaciers in this region in response to the recent climate changes.

More frequent long-term droughts such as the current mega-drought are predicted for the future in the Central Andes of Argentina and Chile. Understanding the climatic response of all the different ice masses and quantify their hydrological contributions to streamflows will be crucial for determining the availability of water reserves for the populations adjacent to the Central Andes.

DATA AVAILABILITY STATEMENT

The complete NGI is available at http://www.glaciaresargentinos.gob.ar and at the GLIMS website (http://www.glims.org/maps/glims). The ASTERIX elevation change maps for the Andes are available in the PANGAEA repository (https://doi.org/10.1594/PANGAEA.903618). Individual glacier mass balance rates for the RGI glaciers in region 17 (Southern Andes) were published in the WGMS database (Dussaillant et al., 2019). The new mass balance estimates for the NGI ice masses in the Central Andes of Argentina are available upon request from the corresponding author, and will also be published in the WGMS database.

AUTHOR CONTRIBUTIONS

LF designed the study and led the writing of the paper. LF, LZ and MC generated the glacier inventory for the Central Andes and also participated in the fieldtrips. ID performed all the mass balance calculations. All authors contributed with the manuscript revision, and read and approved the final submitted version.

ACKNOWLEDGMENTS

This study was conducted within the framework of the National Glacier Inventory of Argentina (NGI) and was supported by CONICET and the National Ministry of Environment and Sustainable Development. We would like to thank Argentina's National Commission of Space Activities (CONAE), Global Land Ice Measurements from Space (GLIMS) and the Japan International Cooperation Agency (JICA) for providing some of the satellite images used to develop the NGI. This research was partially funded by project PICT-2018-03211. Etienne Berthier acknowledges support from the French Space Agency (CNES) through the TOSCA and ISIS programs. We thank Rachel Smedley for English proofreading of a preliminary version of the paper.

REFERENCES

Aguilera, F., Benavente, O., Gutiérrez, F., Romero, J., Saltori, O., González, R., et al. (2015). Eruptive activity of planchón-Peteroa volcano for period 2010-2011, southern andean volcanic zone, Chile. *Andgeo* 43, 20–46. doi:10.5027/andgeoV43n1-a02

Ayala, A., Pellicciotti, F., MacDonell, S., McPhee, J., Vivero, S., Campos, C., et al. (2016). Modelling the hydrological response of debris-free and debris-covered glaciers to present climatic conditions in the semiarid andes of central chile. *Hydrol. Process.* 30, 4036–4058. doi:10.1002/hyp.10971

Barcaza, G., Nussbaumer, S. U., Tapia, G., Valdés, J., García, J.-L., Videla, Y., et al. (2017). Glacier inventory and recent glacier variations in the andes of chile, south america. *Ann. Glaciol.* 58, 166–180. doi:10.1017/aog.2017.28

Berthier, E., Cabot, V., Vincent, C., and Six, D. (2016). Decadal region-wide and glacier-wide mass balances derived from multi-temporal ASTER satellite digital elevation models. validation over the mont-blanc area. *Front. Earth Sci.* 4, 63. doi:10.3389/feart.2016.00063

Berthier, E., Larsen, C., Durkin, W. J., Willis, M. J., and Pritchard, M. E. (2018). Brief communication: unabated wastage of the Juneau and Stikine icefields (southeast Alaska) in the early 21st century. *Cryosphere* 12, 1523–1530. doi:10.5194/tc-12-1523-2018

Blöthe, J. H., Rosenwinkel, S., Höser, T., and Korup, O. (2019). Rock-glacier dams in high asia. *Earth Surf. Process. Landforms* 44, 808–824. doi:10.1002/esp.4532

Bolch, T., Rohrbach, N., Kutuzov, S., Robson, B. A., and Osmonov, A. (2019). Occurrence, evolution and ice content of ice-debris complexes in the Ak-Shiirak, Central Tien Shan revealed by geophysical and remotely-sensed investigations. *Earth Surf. Process. Landforms* 44, 129–143. doi:10.1002/esp.4487

Bown, F., Rivera, A., and Acuña, C. (2008). Recent glacier variations at the aconcagua basin, central chilean andes. *Ann. Glaciol.* 48, 43–48. doi:10.3189/172756408784700572

Braun, M. H., Malz, P., Sommer, C., Farías-Barahona, D., Sauter, T., Casassa, G., et al. (2019). Constraining glacier elevation and mass changes in South America. *Nat. Clim. Change* 9, 130–136. doi:10.1038/s41558-018-0375-7

Brenning, A. (2005). Geomorphological, hydrological and climatic significance of rock glaciers in the andes of central chile (33–35°S). *Permafr. Periglac. Process.* 16, 231–240. doi:10.1002/ppp.528

Brun, F., Berthier, E., Wagnon, P., Kääb, A., and Treichler, D. (2017). A spatially resolved estimate of high mountain asia glacier mass balances from 2000 to 2016. *Nat. Geosci.* 10, 668–673. doi:10.1038/ngeo2999

Brun, F., Wagnon, P., Berthier, E., Jomelli, V., Maharjan, S. B., Shrestha, F., et al. (2019). Heterogeneous influence of glacier morphology on the mass balance variability in high mountain asia. *J. Geophys. Res. Earth Surf.* 124, 1331–1345. doi:10.1029/2018JF004838

Burger, F., Ayala, A., Farias, D., Shaw, T. E., MacDonell, S., Brock, B., et al. (2019). Interannual variability in glacier contribution to runoff from a high-elevation Andean catchment: understanding the role of debris cover in glacier hydrology. *Hydrol. Process.* 33, 214–229. doi:10.1002/hyp.13354

Cobos, D. and Boninsegna, J. (1983). "Fluctuations of some glaciers in the upper atuel river basin, mendoza, argentina,," in *Quaternary of south america and antarctic peninsula glacier fluctuations—andes centrales*. Editor J. Rabassa (Rotterdam, The Netherlands: A. A. Balkema), 61–82.

Dussaillant, I., Berthier, E., and Brun, F. (2018). Geodetic mass balance of the northern patagonian icefield from 2000 to 2012 using two independent methods. *Front. Earth Sci.* 6, 8. doi:10.3389/feart.2018.00008

Dussaillant, I., Berthier, E., Brun, F., Masiokas, M., Hugonnet, R., Favier, V., et al. (2019). Two decades of glacier mass loss along the Andes. *Nat. Geosci.* 12, 802–808. doi:10.1038/s41561-019-0432-5

Falaschi, D., Bolch, T., Lenzano, M. G., Tadono, T., Lo Vecchio, A., and Lenzano, L. (2018a). New evidence of glacier surges in the central andes of argentina and chile. *Prog. Phys. Geogr.: Earth Environ.* 42, 792–825. doi:10.1177/0309133318803014

Falaschi, D., Lenzano, M. G., Tadono, T., Vich, A. I., and Lenzano, E. (2018b). *Balance de masa geodésico 2000–2011 de los glaciares de la cuenca del río Atuel*. Mendoza, Argentina: Andes Centrales de Mendoza.

Falaschi, D., Masiokas, M., Tadono, T., and Couvreux, F. (2016). ALOS-derived glacier and rock glacier inventory of the volcán domuyo region (~36°S), southernmost central andes, argentina. *Z. Geomorphol.* 60 (14), 195–208. doi:10.1127/zfg/2016/0319

Farías-Barahona, D., Vivero, S., Casassa, G., Schaefer, M., Burger, F., Seehaus, T., et al. (2019). Geodetic mass balances and area changes of echaurren norte glacier (central andes, chile) between 1955 and 2015. *Rem. Sens.* 11, 260. doi:10.3390/rs11030260

Fischer, M., Huss, M., and Hoelzle, M. (2015). Surface elevation and mass changes of all swiss glaciers 1980–2010. *Cryosphere* 9, 525–540. doi:10.5194/tc-9-525-2015

Fyffe, C. L., Brock, B. W., Kirkbride, M. P., Mair, D. W. F., Arnold, N. S., Smiraglia, C., et al. (2019). Do debris-covered glaciers demonstrate distinctive hydrological behaviour compared to clean glaciers? *J. Hydrol.* 570, 584–597. doi:10.1016/j.jhydrol.2018.12.069

Garreaud, R. D., Alvarez-Garreton, C., Barichivich, J., Boisier, J. P., Christie, D., Galleguillos, M., et al. (2017). The 2010–2015 megadrought in central chile: impacts on regional hydroclimate and vegetation. *Hydrol. Earth Syst. Sci.* 21, 6307–6327. doi:10.5194/hess-21-6307-2017

Garreaud, R. D., Boisier, J. P., Rondanelli, R., Montecinos, A., Sepúlveda, H. H., and Veloso-Aguila, D. (2019). The central chile mega drought (2010–2018): a climate dynamics perspective. *Int. J. Climatol.* 40, 421. doi:10.1002/joc.6219

Garreaud, R. D., Vuille, M., Compagnucci, R., and Marengo, J. (2009). Present-day south american climate. *Palaeogeogr. Palaeoclimatol. Palaeoecol.* 281, 180–195. doi:10.1016/j.palaeo.2007.10.032

Gascoin, S., Kinnard, C., Ponce, R., Lhermitte, S., MacDonell, S., and Rabatel, A. (2011). Glacier contribution to streamflow in two headwaters of the huasco river, dry Andes of Chile. *Cryosphere* 5, 1099–1113. doi:10.5194/tc-5-1099-2011

Halla, C., Blöthe, J. H., Tapia Baldis, C., Trombotto, D., Hilbich, C., Hauck, C., et al. (2020). Ice content and interannual water storage changes of an active rock glacier in the dry Andes of Argentina. *The Cryosphere Discuss*. doi:10.5194/tc-2020-29

Haller, M. J. and Risso, C. (2011). La erupcion del volcán Peteroa (35°15′S, 70°18′o) del 4 de septiembre de 2010. *Rev. Asoc. Geol. Argent.* 68, 295–305.

Helbling, R. (1935). The origin of the rio plomo ice-dam. *Geogr. J.* 85, 41. doi:10.2307/1787035

Huss, M. (2013). Density assumptions for converting geodetic glacier volume change to mass change. *Cryosphere* 7, 877–887. doi:10.5194/tc-7-877-2013

Janke, J. R., Bellisario, A. C., and Ferrando, F. A. (2015). Classification of debris-covered glaciers and rock glaciers in the andes of central chile. *Geomorphology* 241, 98–121. doi:10.1016/j.geomorph.2015.03.034

Jones, D. B., Harrison, S., Anderson, K., and Betts, R. A. (2018). Mountain rock glaciers contain globally significant water stores. *Sci. Rep.* 8, 2834. doi:10.1038/s41598-018-21244-w

Jones, D. B., Harrison, S., Anderson, K., and Whalley, W. B. (2019). Rock glaciers and mountain hydrology: a review. *Earth Sci. Rev.* 193, 66–90. doi:10.1016/j.earscirev.2019.04.001

Kargel, J. S. (2014). *Global land ice measurements from space*. Berlin, Germany: Springer.

Kinnard, C., MacDonell, S., Petlicki, M., Mendoza Martinez, C., Abermann, J., and Urrutia, R. (2018). "Mass balance and meteorological conditions at universidad glacier, Central Chile," in *andean hydrology*. Editors D. A. Rivera, A. Godoy-Faundez, and M. Lillo-Saavedra (Boca Raton, FL: CRC Press), 102–123.

Leiva, J. C., Cabrera, G. A., and Lenzano, L. E. (2007). 20 years of mass balances on the piloto glacier, las cuevas river basin, mendoza, argentina. *Global Planet. Change* 59 (1–4), 10–16. doi:10.1016/j.gloplacha.2006.11.018

Lliboutry, L. (1998). "Glaciers of chile and argentina," in *Satellite image atlas of glaciers of the world. glacier Inventory—Andes*. Editors R. S. Williams and J. G. Ferrigno (Denver, CO: South America USGS).

Malmros, J. K., Mernild, S. H., Wilson, R., Yde, J. C., and Fensholt, R. (2016). Glacier area changes in the central chilean and argentinean Andes 1955–2013/14. *J. Glaciol.* 62, 391–401. doi:10.1017/jog.2016.43

Masiokas, M. H., Christie, D. A., Le Quesne, C., Pitte, P., Ruiz, L., Villalba, R., et al. (2016). Reconstructing the annual mass balance of the echaurren norte glacier (central andes, 33.5° S) using local and regional hydroclimatic data. *Cryosphere* 10, 927–940. doi:10.5194/tc-10-927-2016

Masiokas, M. H., Cara, L., Villalba, R., Pitte, P., Luckman, B. H., Toum, E., et al. (2019). Streamflow variations across the Andes (18°–55°S) during the instrumental era. *Sci. Rep.* 9. doi:10.1038/s41598-019-53981-x

Masiokas, M. H., Delgado, S., Pitte, P., Berthier, E., Villalba, R., Skvarca, P., et al. (2015). Inventory and recent changes of small glaciers on the northeast margin of the southern patagonia Icefield, argentina. *J. Glaciol.* 61, 511–523. doi:10.3189/2015jog14j094

Masiokas, M. H., Rivera, A., Espizua, L. E., Villalba, R., Delgado, S., and Aravena, J. C. (2009). Glacier fluctuations in extratropical south america during the past 1000 years. *Palaeogeogr. Palaeoclimatol. Palaeoecol.* 281, 242–268. doi:10.1016/j.palaeo.2009.08.006

McNabb, R., Nuth, C., Kääb, A., and Girod, L. (2019). Sensitivity of glacier volume change estimation to DEM void interpolation. *Cryosphere* 13, 895–910. doi:10.5194/tc-13-895-2019

Meier, W. J.-H., Grießinger, J., Hochreuther, P., and Braun, M. H. (2018). An updated multi-temporal glacier inventory for the patagonian Andes with changes between the little ice age and 2016. *Front. Earth Sci.* 6, 62. doi:10.3389/feart.2018.00062

Menounos, B., Hugonnet, R., Shean, D., Gardner, A., Howat, I., Berthier, E., et al. (2019). Heterogeneous changes in western north American glaciers linked to decadal variability in zonal wind strength. *Geophys. Res. Lett.* 46, 200–209. doi:10.1029/2018GL080942

Mölg, N., Bolch, T., Rastner, P., Strozzi, T., and Paul, F. (2018). A consistent glacier inventory for karakoram and Pamir derived from Landsat data: distribution of debris cover and mapping challenges. *Earth Syst. Sci. Data* 10, 1807–1827. doi:10.5194/essd-10-1807-2018

Monnier, S. and Kinnard, C. (2015). Reconsidering the glacier to rock glacier transformation problem: new insights from the central andes of chile. *Geomorphology* 238, 47–55. doi:10.1016/j.geomorph.2015.02.025

Nagai, H., Fujita, K., Sakai, A., Nuimura, T., and Tadono, T. (2016). Comparison of multiple glacier inventories with a new inventory derived from high-resolution ALOS imagery in the bhutan himalaya. *Cryosphere* 10, 65–85. doi:10.5194/tc-10-65-2016

Nogami, M. (1972). The snow line and climate during the last glacial period in the andes mountains. *Daiyonki Kenkyu* 11, 71–80. doi:10.4116/jaqua.11.71

Paul, F., Barrand, N. E., Baumann, S., Berthier, E., Bolch, T., Casey, K., et al. (2013). On the accuracy of glacier outlines derived from remote-sensing data. *Ann. Glaciol.* 54, 171–182. doi:10.3189/2013AoG63A296

Paul, F., Barry, R. G., Cogley, J. G., Frey, H., Haeberli, W., Ohmura, A., et al. (2009). Recommendations for the compilation of glacier inventory data from digital sources. *Ann. Glaciol.* 50, 119–126. doi:10.3189/172756410790595778

Pfeffer, W. T., Arendt, A. A., Bliss, A., Bolch, T., Cogley, J. G., Gardner, A. S., et al. (2014). The Randolph Glacier Inventory: a globally complete inventory of glaciers. *J. Glaciol.* 60, 537. doi:10.3189/2014JoG13J176

Pitte, P., Berthier, E., Masiokas, M. H., Cabot, V., Ruiz, L., Ferri Hidalgo, L., et al. (2016). Geometric evolution of the horcones inferior glacier (mount aconcagua, central andes) during the 2002–2006 surge: horcones inferior glacier surge. *J. Geophys. Res. Earth Surf.* 121, 111–127. doi:10.1002/2015JF003522

Pitte, P., Espizua, L. E., and Ferri Hidalgo, L. (2010). "glacier Inventory in the desert andes of san juan, argentina (29°20′S)," in *Glacier inventory* (Kolkata, India: CECS), 55.

Pitte, P., Hidalgo, L. F., Ruiz, L., Masiokas, M., Villalba, R., and Berthier, E. (2018). "¿Qué está pasando con los glaciares del complejo volcánico Planchón-Peteroa?," in Proceedings of the 13 Encuentro del Centro Internacional de Ciencias de la Tierra E-ICES-13, Mendoza, Argentina, December 2018.

Rau, F., Mauz, F., Mogt, S., Singh Khalsa, S. J., and Raup, B. (2005). *Illustrated GLIMS glacier classification*. Freiburg, Germany: GLIMS regional center "antarctic peninsula".

Raup, B., Racoviteanu, A., Khalsa, S. J. S., Helm, C., Armstrong, R., and Arnaud, Y. (2007). The GLIMS geospatial glacier database: a new tool for studying glacier change. *Global Planet. Change* 56, 101–110. doi:10.1016/j.gloplacha.2006.07.018

RGI Consortium (2017a). Version 6.0: Technical Report. Randolph Glacier inventory (RGI)—a dataset of global glacier outlines. Available at: https://www.glims.org/RGI/00_rgi60_TechnicalNote.pdf (Accessed January, 2020).

RGI Consortium (2017b). Version 6.0: Technical report. Randolph Glacier inventory (RGI) – a dataset of global glacier outlines: global Land ice measurements from Space. Available at: https://doi.org/10.7265/N5-RGI-60 (Accessed January, 2020).

Rivera, J., Penalba, O., Villalba, R., and Araneo, D. (2017). Spatio-temporal patterns of the 2010–2015 extreme hydrological drought across the central andes, argentina. *Water* 9, 652. doi:10.3390/w9090652

Rolstad, C., Haug, T., and Denby, B. (2009). Spatially integrated geodetic glacier mass balance and its uncertainty based on geostatistical analysis: application to the western svartisen ice cap, norway. *J. Glaciol.* 55, 666–680. doi:10.3189/002214309789470950

Rounce, D. R., King, O., McCarthy, M., Shean, D. E., and Salerno, F. (2018). Quantifying debris thickness of debris-covered glaciers in the everest region of Nepal through inversion of a subdebris melt model. *J. Geophys. Res. Earth Surf.* 123, 1094–1115. doi:10.1029/2017JF004395

Sagredo, E. A. and Lowell, T. V. (2012). Climatology of Andean glaciers: a framework to understand glacier response to climate change. *Global Planet. Change* 86-87 (87), 101–109. doi:10.1016/j.gloplacha.2012.02.010

Schaffer, N., MacDonell, S., Réveillet, M., Yáñez, E., and Valois, R. (2019). Rock glaciers as a water resource in a changing climate in the semiarid chilean andes. *Reg. Environ. Change* 19, 1263. doi:10.1007/s10113-018-01459-3

UNESCO-IASH (1970). *Perennial ice and snow masses*. Paris, France: UNESCO-IASH, Vol. 56.

Vaughan, D. G., Comiso, J. C., Allison, I., Carrasco, J., Kaser, G., Kwok, R., et al. (2013). *Climate change 2013: the physical science basis. Contribution of working group I to the fifth assessment report of the intergovernmental panel on climate*, Cambridge, UK: Cambridge University Press, Vol. 66.

Viale, M., Bianchi, E., Cara, L., Ruiz, L. E., Villalba, R., Pitte, P., et al. (2019). Contrasting climates at both sides of the Andes in Argentina and Chile. *Front. Environ. Sci.* 7, 69. doi:10.3389/fenvs.2019.00069

Wang, D. and Kääb, A. (2015). Modeling glacier elevation change from DEM time series. *Rem. Sens.* 7, 10117–10142. doi:10.3390/rs70810117

WGMS (2020). *Global glacier change bulletin No. 3 (2016–2017)*. Editors M. Zemp, I. Gärtner-Roer, S. U. Nussbaumer, J. Bannwart, P. Rastner, F. Paul, et al. (Zurich, Switzerland: ISC(WDS)/IUGG(IACS)/UNEP/UNESCO/WMO, World Glacier Monitoring Service), 274.

WGMS (2012). *Fluctuations of glaciers 2005–2010*, Editors M. Zemp, H. Frey, I. Gärtner-Roer, S. U. Nussbaumer, M. Hoelzle, et al. (Zurich, Switzerland: ICSU(WDS)/IUGG(IACS)/UNEP/UNESCO/WMO, World Glacier Monitoring Service).

Zalazar, L., Ferri, L., Castro, M., Gargantini, H., Gimenez, M., Pitte, P., et al. (2020). Spatial distribution and characteristics of andean ice masses in argentina: results from the first national glacier inventory. *J. Glaciol.* 66 (260), 1–12. doi:10.1017/jog.2020.55

Conflict of Interest: The authors declare that the research was conducted in the absence of any commercial or financial relationships that could be construed as a potential conflict of interest.

The reviewer FG-C declared a past co-authorship with several of the authors ID and EB to the handling editor.

Advantages of publishing in Frontiers

OPEN ACCESS
Articles are free to read for greatest visibility and readership

FAST PUBLICATION
Around 90 days from submission to decision

HIGH QUALITY PEER-REVIEW
Rigorous, collaborative, and constructive peer-review

TRANSPARENT PEER-REVIEW
Editors and reviewers acknowledged by name on published articles

Frontiers
Avenue du Tribunal-Fédéral 34
1005 Lausanne | Switzerland

Visit us: www.frontiersin.org
Contact us: frontiersin.org/about/contact

REPRODUCIBILITY OF RESEARCH
Support open data and methods to enhance research reproducibility

DIGITAL PUBLISHING
Articles designed for optimal readership across devices

FOLLOW US
@frontiersin

IMPACT METRICS
Advanced article metrics track visibility across digital media

EXTENSIVE PROMOTION
Marketing and promotion of impactful research

LOOP RESEARCH NETWORK
Our network increases your article's readership